Forging Asteroid-Meteorite Relationships through Reflectance Spectroscopy

by

Thomas H. Burbine Jr.

B.S. Physics
Rensselaer Polytechnic Institute, 1988

M.S. Geology and Planetary Science
University of Pittsburgh, 1991

SUBMITTED TO THE DEPARTMENT OF EARTH, ATMOSPHERIC, AND PLANETARY SCIENCES IN PARTIAL FULFILLMENT OF THE REQUIREMENTS FOR THE DEGREE OF

DOCTOR OF PHILOSOPHY IN PLANETARY SCIENCES
AT THE
MASSACHUSETTS INSTITUTE OF TECHNOLOGY

FEBRUARY 2000

© 2000 Massachusetts Institute of Technology. All rights reserved.

Signature of Author: _____
Department of Earth, Atmospheric, and Planetary Sciences
December 30, 1999

Certified by: _____
Richard P. Binzel
Professor of Earth, Atmospheric, and Planetary Sciences
Thesis Supervisor

Accepted by: _____
Ronald G. Prinn
Professor of Earth, Atmospheric, and Planetary Sciences
Department Head

MASSACHUSETTS INSTITUTE OF TECHNOLOGY
JAN 0 1 2000
LIBRARIES
ARCHIVES

Forging Asteroid-Meteorite Relationships through Reflectance Spectroscopy

by

Thomas H. Burbine Jr.

Submitted to the Department of Earth, Atmospheric, and Planetary Sciences
on December 30, 1999 in Partial Fulfillment of the
Requirements for the Degree of Doctor of Philosophy in
Planetary Sciences

ABSTRACT

Near-infrared spectra (~0.90 to ~1.65 microns) were obtained for 196 main-belt and near-Earth asteroids to determine plausible meteorite parent bodies. These spectra, when coupled with previously obtained visible data, allow for a better determination of asteroid mineralogies. Over half of the observed objects have estimated diameters less than 20 km.

Many important results were obtained concerning the compositional structure of the asteroid belt. A number of small objects near asteroid 4 Vesta were found to have near-infrared spectra similar to the eucrite and howardite meteorites, which are believed to be derived from Vesta. These asteroids appear almost certainly to be fragments of Vesta. Spectral variations between these objects are consistent with being primarily due to differences in particle size. These asteroids also tend to have stronger band depths with increasing ejection velocity from Vesta.

Objects with distinctive olivine bands appear to provide definitive evidence that spectral alteration is occurring in the asteroid belt. These objects have similar band depths but appear significantly reddened relative to measured olivine samples due to their significantly higher reflectance values with increasing wavelength. The only laboratory-simulated "weathering" process that reddens the spectra but does not significantly suppress the bands is alteration by laser irradiation, which is hoped to duplicate the effects of micrometeorite bombardment.

A number of plausible main-belt parent bodies were identified. These include 19 Fortuna and the CM chondrites, Eos family members with the CO chondrites and 599 Luisa with the CV chondrites.

A significant fraction of S asteroids have spectral properties that range from similar to ordinary chondrites to much redder with weaker absorption bands. These objects tend to have spectra consistent with a mixture of ordinary chondrite material and metallic iron. However, other alteration processes cannot be ruled out.

Asteroids with distinctive olivine bands are relatively rare. The available evidence is consistent with a scenario where, with the exception of Vesta, all differentiated bodies were either disrupted or had their mantles stripped very early in the age of the solar system. Olivine-rich metal-free fragments were then continually broken down until they almost all now fall below our current astronomical measurement limits.

Thesis Supervisor: Richard P. Binzel
Title: Professor of Earth, Atmospheric, and Planetary Sciences

This work is dedicated

to my Mother,
who never thought I would get into MIT,

to my Father
(1941-1995),
who thcught I would get in,

and

to Roger Burns
(1937-1994),
who got me into MIT.

Acknowledgements

I would first like to thank my advisor Rick Binzel. He was the best advisor a person could ever have and a very good friend. He also designed the "asteroid" grism system for the Infrared Telescope Facility (IRTF) that was used to obtain the asteroid spectra in this thesis. I would also like to thank my first advisor, Roger Burns, who supported my initial research at MIT. There are so many questions that arose during this thesis that I wish I could have asked him. I would also like to thank Jim Elliot, Tim Grove and Carlé Pieters for being on my thesis committee.

My family supported (personally and financially) all my decisions that allowed me to go to MIT. Special thanks to my mother who did everything possible to help me. It is also a slightly sad time because every day I do wish that my father was still alive to see me graduate. I would also like to thank the Kamekas (LaLa and Art), who have been my friends for as long as I can remember.

Numerous students, professors and staff at MIT have been very helpful during this project. Bobby Bus and Shui Xu supplied me with all their asteroid spectra from their Small Main-Belt Asteroid Spectroscopic Survey (SMASS). Sam Bowring and Mark Schmitz allowed me the use of their clean room to prepare meteorite samples. The staff at the Lindgren Library, especially Anne, Gareth, Kathy and Joe, were very helpful in my numerous searches for journals and books. The administrative assistants (Allison and Ginny) helped me considerably in travel arrangements. Courses taught by Professors Rick Binzel, Sam Bowring, Jim Elliot, Fred Frey and Tim Grove were invaluable for giving me the scientific background to work on this thesis.

Many different agencies and people supported this project. NASA supplied the grant money that supported me and this research. The Meteorite Working Group loaned me numerous American Antarctic samples and the National Institute of Polar Research loaned me some Japanese ones. Joe Boesenberg at the American Museum of Natural History also loaned a number of meteorite samples. Reflectance spectra were run at the RELAB facility at Brown University by Taki Hiroi and at the Planetary Geosciences/HIGP (Hawaii Institute of Geophysics and Planetology) spectrometer facility at the University of Hawai`i by John Hinrichs and Anders Meibom. Taki also supplied me with numerous unpublished spectra. Compositional analyses of the Antarctic samples were done by Paul Buchanan at the Instrumental Neutron Activation Analysis Laboratory at Johnson Space Center using the Cameca SX-100 electron microprobe at the NASA Johnson Space Center. Paul also supplied the Macibini sample for spectral analysis. The IRTF approved our group's requests for a significant amount of observing time for SMASSIR (SMASS in the near-infrared). Mike Hicks and Dave Rabinowitz supplied me with

broad-band visible data for 7889 1994 LX. Mike Gaffey supplied me with his spectra of 6 Hebe and 349 Dembowska.

A lot of lucky events occurred on my path to and through MIT. I met Mike Gaffey, who got me interested in asteroids, after seeing his picture in a RPI (Rensselaer Polytechnic Institute) newsletter. I picked the University of Pittsburgh as my first graduate school because of its late application deadline. Bruce Hapke allowed me to work on my own project for my Masters' thesis analyzing Jeff Bell's 52-color survey. When I wanted to leave Pittsburgh, Brian Marsden hired me part-time at the Center for Astrophysics in Cambridge to put labels on envelopes when his student worker went off mountain-climbing. Dale Graessle then gave me a full-time job there working on AXAF (Advanced X-Ray Astronomical Facility) so I could have enough money to eat and pay the rent. Roger Burns was able to then get me into MIT even though my undergraduate grades were rather low. I luckily picked Ashdown House to live, where I made almost all my friends at MIT. Tim McCoy gave me a reason to leave by helping to get me a postdoc at the Smithsonian Institution in Washington, D.C.

I have made too many friends here to count. I always get into trouble when I rank people, but my three best friends here were Kevin O'Brien, Benjie Sun and Fyllio Katsavounidou. I will remember hanging out with Kevin in the Ashdown lobby, driving all around Boston with Benjie on his little adventures and going to concerts with Fyllio. Each of them in their own ways have made a considerable difference to my life here at MIT.

I need to list the other good friends that I have made here. Some of these people I have lost touch with, but they were all good friends at one time. They include Ronak Bhatt, Brian Bowers, Juan Bruno, Emy Chen, Doug Crawford, Mario De Caro, Jenny Farver, Jennifer Han, Jennifer Healey, Jesse Hong, Rob Jagnow, Judy Kim, Dhaya Lakshminarayanan, Tom Lee, Francois Le Sellier, Bill Liteplo, Kathy Liu, Christina Manolatou, John Matz, Chi Nguyen, Lynn Qu, Vandana Sareen, Chris Spohr, Andy Tsai, Neda Vukmirovic, Rada Vukmirovic, Pat Walton, Ben Williams, Richard "Mouser" Williams, Rebecca Xiong, Lee Yang and Ruilin Zhao.

I have also made numerous friends at conferences with many of them helping considerably with my thesis. These people include Tomoko Arai, Erik Asphaug, Dave Blewett, Paul Buchanan, John Hinrichs, Taki Hiroi, Dante Lauretta, Tim McCoy, Anders Meibom, Ljuba Moroz, Andy Rivkin, Jessica Sunshine and Kees Welten. Paul suggested extensive revisions for the chapter on the Vesta family. Clark Chapman, Mike Gaffey, Faith Vilas and John Wasson reviewed published papers that were incorporated into this thesis. John needs to be especially thanked for suggesting the name "Battered to Bits" for the grinding down of mantle material in the main belt. Alberto Cellino, Don Davis and Paolo Farinella were very helpful in answering specific questions that I had during this study.

I would like to thank everybody who I met at Ashdown House, who made my time here so enjoyable. I would especially like to thank Beth and Vernon Ingram, who do so much for the dorm. I would also like to thank all the staff at Ashdown: Carmen, Christine, Joe, Lee, Lenny and John.

While here, I have done almost everything I wanted to do. I was chairperson of my dorm. I saw Bill Clinton, Salmon Rushdie and Kevin Spacey. I met Jackie "the Jokeman" and "Baba Booey" from the *Howard Stern Show*. I saw a Red Sox playoff game (Red Sox 23-7 over the Indians in Game 4 of the 1999 Division Series). I bench-pressed 225 pounds. I hit softball home runs. I watched every episode of *Seinfeld*, *Friends* and *X-Files*. I was an extra in a movie (*Civil Action*) and a Chinese miniseries. I saw Alcatraz, the Eiffel Tower and the remnants of the Berlin Wall. I saw Blue Oyster Cult, Lenny Kravitz, Alannis Morrisette and REM in concert. I have been on top of one of the MIT domes. I have dated very pretty girls. The only thing left for me to do is graduate.

Table of Contents

Chapter 1
Introduction

1.1 Background

Asteroids are relatively small objects, with diameters less than 1000 km, that are found throughout the solar system. They are generally concentrated between the orbits of Mars and Jupiter in what is called the asteroid belt. The orbits of these objects can be very accurately determined and are given in terms of semi-major axis (a, which is the distance from the sun in astronomical units or AU), proper sine of inclination (i') (measured from the ecliptic) and proper eccentricity (e'). These proper elements have had the effects of planetary perturbations removed and are stable over long periods of time (Knezevic and Milani, 1994). A plot (Figure 1.1) of the distribution of objects in the belt shows that this region of the solar system has been affected by numerous dynamical processes.

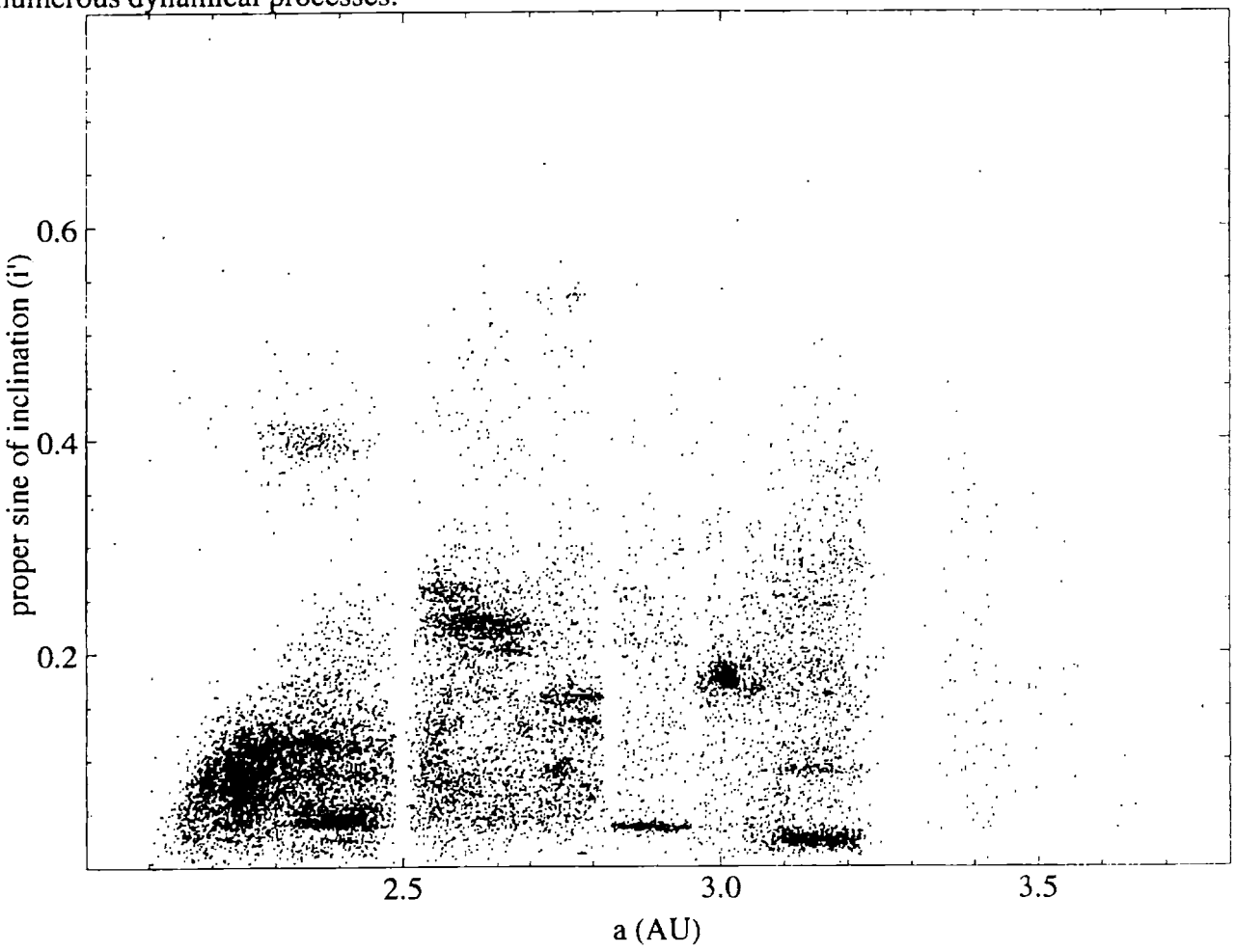

Figure 1.1. Plot of semi-major axis (a) (in AU) versus proper sine of inclination (i') for main-belt asteroids. Proper elements for low-inclination objects are from Milani and Knezevic (1994) and high-inclination objects are from LeMaitre (personal communication).

Gaps such as the ones at ~2.5 AU and ~2.8 AU are due to mean motion resonances with Jupiter while ones such as the arcing gap (ν_6) that bounds the inner main belt are due to secular resonances with Saturn. These resonances, due to their ability to generate chaotic orbits (e.g., Wisdom, 1983, 1985; Scholl and Froeschlé, 1991), have been noted as likely source regions of near-Earth asteroids (NEAs) and, therefore, meteorites. Over 800 NEAs have been identified to date. Clusterings are asteroid families, which are statistically significant groupings of objects. Families are believed to be the result of the break-up of a precursor body or the formation of large craters on an object.

Meteorites are smaller objects, with diameters of less than a millimeter to over three meters, which are seen to fall or have been found on Earth that have chemical compositions that indicate that they formed elsewhere in the Solar System. Meteorites sample bodies that range (Table 1.1) from those with elemental compositions very similar to the Sun (and, presumably, to the solar nebula) to those that have been extensively heated. Asteroids are the most likely source of most meteorites since collisions among these objects and their relatively low escape velocities should be able to produce more than enough fragments to explain the flux of material hitting the Earth (e.g., Wasson and Wetherill, 1979). Our meteorite collection also includes a few fragments from the Moon and Mars. Meteorites from Mercury (Love and Keil, 1995) and comets (Campins and Swindle, 1998; Lodders and Osborne, 1999) appear theoretically possible, but none are conclusively known to date. The formation ages of minerals in meteorites tend to cluster around 4.55 billion years (e.g., Allègre *et al.*, 1995) so by studying them, insight hopefully can be gained on the chemical and physical processes in the early solar system.

The most common meteorites to land on Earth today are the ordinary chondrites (Table 1.2), which make up ~80% of all known falls. There are over 20,000 meteorites in our collections with over 90% of them discovered in Antarctica (Meibom and Clark, 1999). A large number of unique objects (e.g., lunar meteorites, naturally heated carbonaceous chondrites) have also been discovered in Antarctica (Zolensky, 1998). Over 90% of the meteorites found in Antarctica are ordinary chondrites (Lindstrom and Score, 1994); however, many of these samples are paired with one another, meaning they are fragments of single falls. Normalizing the Antarctic find frequency by mass produces roughly similar fall distributions for Antarctic and non-Antarctic ordinary chondrites (e.g., Cassidy and Harvey, 1991; Lindstrom and Score, 1994). Since the Antarctic meteorite population samples a much longer time frame (hundreds of thousands of years) (e.g., Nishiizumi *et al.*, 1989; Welten *et al.*, 1999) compared to the period (last ~200 years) of objects known to fall, the percentage of ordinary chondrites falling to Earth appears to have been roughly constant, at least over the last few hundred thousand years.

Table 1.1. A listing of major meteorite classes and their mineralogy. This table is revised from tables and descriptions in Pieters and McFadden (1994), Rubin (1997), Mittlefehldt *et al.* (1998) and Meibom and Clark (1999).

Class			Major Mineralogy
chondrites (usually contains chondrules)			
	carbonaceous		roughly solar composition
		CI	phyllosilicates; chondrules absent
		CM	phyllosilicates; no metallic iron
		CO	mafic minerals; small chondrules, minor metal
		CV	mafic minerals; calcium-aluminum inclusions (CAIs), minor phyllosilicates
		CR	mafic minerals; phyllosilicates, minor metal
		CK	80 vol.% olivine; mostly matrix
		CH	mafic minerals; metal
	ordinary*		olivine, low-Ca pyroxene, feldspar, metal
		H	high in total Fe; greater than 50 vol.% metal
		L	low in total Fe; ~1/3 vol.% metal
		LL	low in total Fe; most oxidized ordinary chondrite
	enstatite*		enstatite, metal
		EH	most reduced type of enstatite chondrite; mostly metal
		EL	less reduced type of enstatite chondrite; mostly metal
	other		
		K	mafic silicate compositions intermediate between H and E chondrites
		R	more oxidized than ordinary chondrites; ~70 vol.% olivine
achondrites (melted; differentiated)			
	eucrites		low-Ca pyroxene, plagioclase
	diogenites		orthopyroxene
	howardites		breccias of eucritic and diogenitic material
	ureilites		carbon-rich; olivine, pyroxene
	aubrites		enstatite
	angrites		Al-Ti-diopside, plagioclase, olivine
	SNC†		basaltic, olivine
	lunar		anorthositic breccia
	primitive		achondritic texture, but a chondritic elemental composition
		acapulcoites, lodranites	olivine, pyroxene, metal ± troilite ± plagioclase
		brachinites	primarily olivine
stony-irons (metal + silicates)			
	mesosiderites		metal, basaltic achondritic material
	pallasites		network of FeNi and olivine
irons‡			FeNi (kamacite and taenite) + troilite

* The ordinary and enstatite chondrites are given number designations (3 through 7), which refers to increasing degree of thermal metamorphism that they have experienced. Increasing number indicates increasing degree of thermal alteration.
† SNC meteorites include shergottites, nakhlites and chassignites. These meteorites appear to be derived from Mars.
‡ Irons are usually classified into 12 main groups according to trace element abundances of Ga, Ge, Ni and Ir. A classification system (hexahedrites, octahedrites and ataxites) also exists using structural properties of iron meteorites.

Table 1.2. Meteorite classes and fall frequencies (Sears and Dodd, 1988). Only meteorite classes with fall frequencies above 1% are given.

Meteorite Classes	Fall Frequency (%)
L chondrites	38.3
H chondrites	33.2
LL chondrites	7.9
howardites, eucrites, diogenites	6.3
CM chondrites	2.2
IIIAB irons	1.4
aubrites	1.1

However, the fall percentages are probably not accurately representing the distribution of material striking the Earth's atmosphere. Sears (1998) argues that fall statistics are heavily biased against CI (0.06% of all falls) and CM chondrites since these objects are more fragile than other meteorites. Baldwin and Sheaffer (1971) have shown that carbonaceous chondrites should have a decrease in mass by a factor of ~1000 as they pass through the atmosphere compared to the stronger ordinary chondrites. Since the likelihood of recovery is proportional to mass, the fall statistics need to be adjusted by multiplying the number of CI and CM meteorites found by ~1000, which would make these meteorites ~97% of all objects hitting the Earth's atmosphere.

To determine the surface composition of an asteroid, reflectances at different wavelengths are measured at a telescope and compared to meteorite and mineral reflectance spectra measured in a laboratory. Many minerals (e.g., olivine, pyroxene) (Figure 1.2) commonly found in meteorites have characteristic spectral absorption bands in the visible and near-infrared due primarily to the absorption of radiation by electrons of Fe^{2+}, which is a constituent of many different minerals.

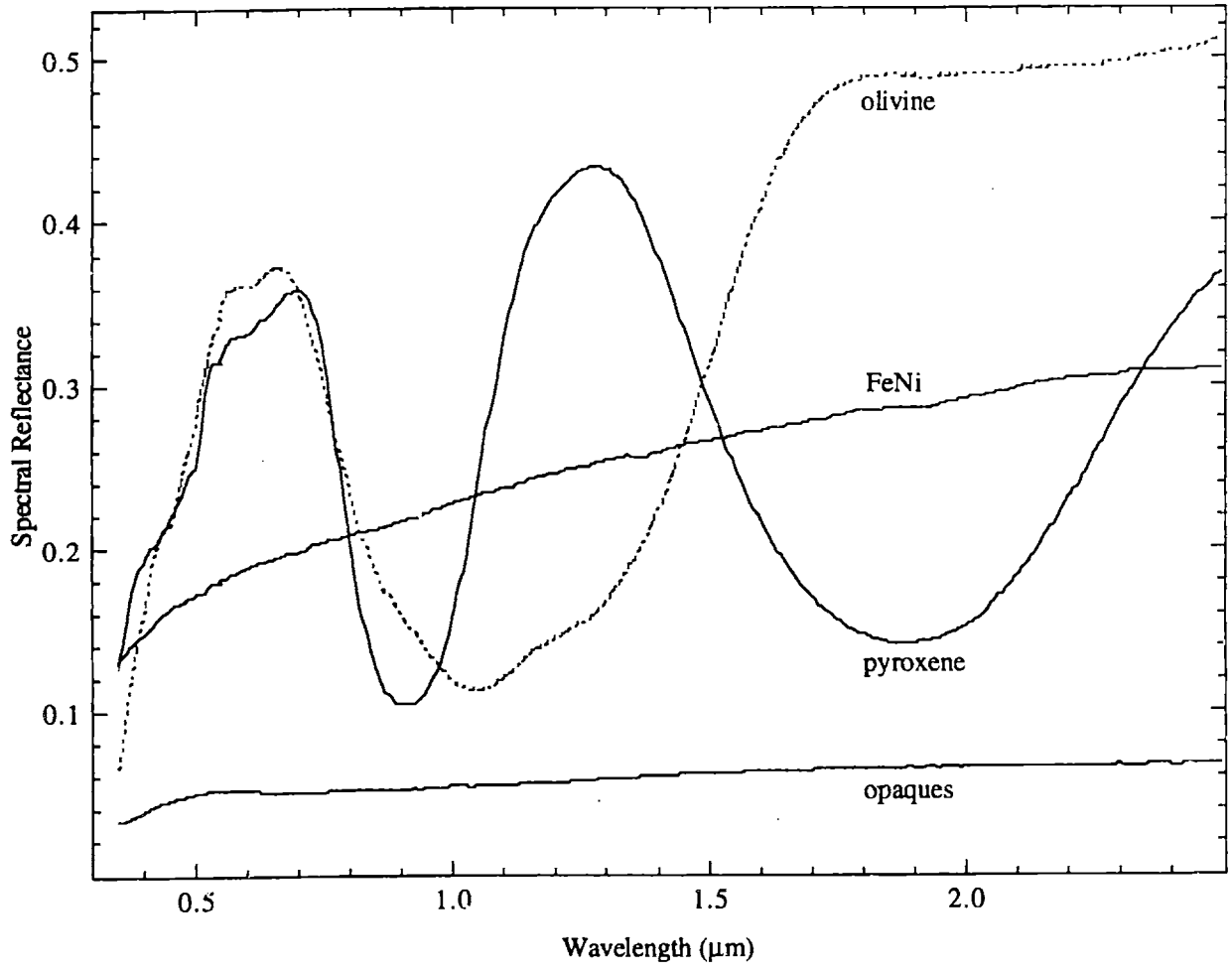

Figure 1.2. Reflectance spectra of olivine (Chassigny) (dashed line), FeNi (octahedrite Chulafinee), pyroxene (diogenite Johnstown) and opaques (CM chondrite Murchison). All spectra are from Gaffey (1976).

Examples of absorption features due to Fe^{2+} include the distinctive asymmetric feature centered at ~1 μm due to olivine and the two distinctive symmetric features centered at ~0.9 μm and ~2.0 μm due to pyroxene. These features due to olivine and/or pyroxene are usually called the 1 and 2 μm features. Olivine and pyroxene also have a strong absorption band shortwards of ~0.7 μm called the UV (ultraviolet) feature. FeNi (metallic iron) has no characteristic absorption features in the visible and near-infrared. Also important for determining the surface composition of an asteroid is albedo, which is the percentage of light reflected in the visible (usually at 0.55 μm) and gives insight on how dark or light the surface is. The low albedo spectrum (CM chondrite Murchison) has its spectral characteristics dominated by opaques (e.g., carbon), which suppresses the absorption bands of other minerals that compose this meteorite.

Asteroids are grouped into a variety of classes according to their reflectance properties, primarily in the visible wavelength region. Each asteroid class is hoped to group asteroids with similar compositions. As discussed by Bell *et al.* (1989), "the true value of a classification can only be realized if a class name can be firmly linked with a surface chemical composition." The most widely used asteroid taxonomy is the one developed by Tholen (1984) (Figure 1.3 and Table 1.3), which grouped objects into fourteen classes according to clusterings in their reflectance properties using colors from seven broad-band filters and visual albedo (when available).

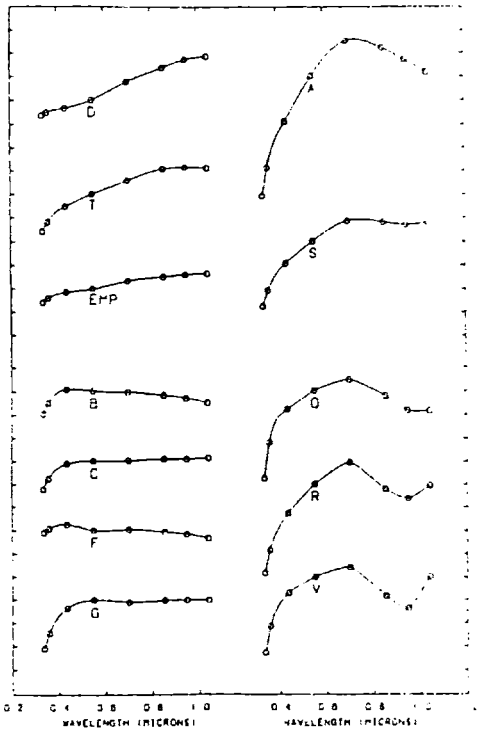

Figure 1.3. Reflectance characteristics of the Tholen (1984) classes. Figure is taken from Tholen and Barucci (1989).

Table 1.3. A listing of asteroid classes and their reflectance properties. This table is revised from tables in Wetherill and Chapman (1988), Tholen and Barucci (1989) and Pieters and McFadden (1994). IRAS (Infrared Astronomical Satellite) albedos (Tedesco, 1994) are derived from thermal fluxes measured at four different infrared wavelengths. The term "red" refers to reflectances increasing with increasing wavelength and the term "blue" refers to reflectances decreasing with increasing wavelength.

Class (Tholen)	IRAS Albedo	Reflectance Properties (0.3 to 1.0 μm)
P	0.02-0.07	flat to slightly red, featureless spectrum
C	0.03-0.20	weak UV feature, flat to reddish past 0.4 μm
B	0.06-0.16	weak UV feature, blue past 0.4 μm, subclass of C class
F	0.03-0.10	very weak UV feature, flat to bluish past 0.4 μm, subclass of C class
D	0.03-0.08	very red spectrum
G	0.05-0.11	strong UV feature, flat past 0.4 μm, subclass of C class
T	0.05-0.10	weak UV feature, reddish past 0.4 μm
M	0.11-0.30	flat to slightly red, featureless spectrum
S	0.05 0.50	strong UV feature, usually has 1 μm feature
A	0.17-0.60	very strong UV feature, strong 1 μm feature
Q	(0.21)*	strong UV and 1 μm feature
R	0.38	strong UV and 1 μm feature
V	0.42	strong UV and 1 μm feature
E	0.50-0.55	flat to slightly red, featureless spectrum
Class (Other)		
K (Bell, 1988)	0.14	spectrum intermediate between S and C asteroids
J (Binzel and Xu, 1993)	?	spectrum have deeper 1 μm features than V types
O (Binzel *et al.*, 1993)	?	weak UV feature out to 0.44 μm, very strong 1 μm feature
W (Rivkin *et al.*, 1995)	0.16-0.25	M asteroid with 3 μm feature

* The albedo for 1862 Apollo is from Lebofsky *et al.* (1981b).

The asteroids that were classified by Tholen (1984) were almost all over 20 km in diameter. A number of other classes have also been proposed (Table 1.3) by a variety of other authors (e.g., Bell, 1988; Binzel and Xu, 1993; Binzel *et al.*, 1993; Rivkin *et al.*, 1995).

Over 1500 asteroids (e.g., Xu *et al.*, 1995; Bus, 1999) have been characterized by CCD (charge-coupled device) measurements of their visible (~0.4 to ~1.0 μm) reflectance spectra as part of the Small Main-Belt Asteroid Spectroscopic Survey (SMASS) undertaken at MIT. Over half of the SMASS objects had estimated diameters of less than 20 km, which is a population of asteroids that very little spectral information was previously available on.

Bus (1999) used a variety of techniques to group asteroids into twenty-six classes on the basis of his CCD spectra between 0.44 and 0.92 μm. The taxonomy includes the A, B, C, D, K, O, Q, R, S, T, V and X classes plus the newly created L class and a number of intermediate classes. The spectral characteristics of each class are shown in Figure 1.4.

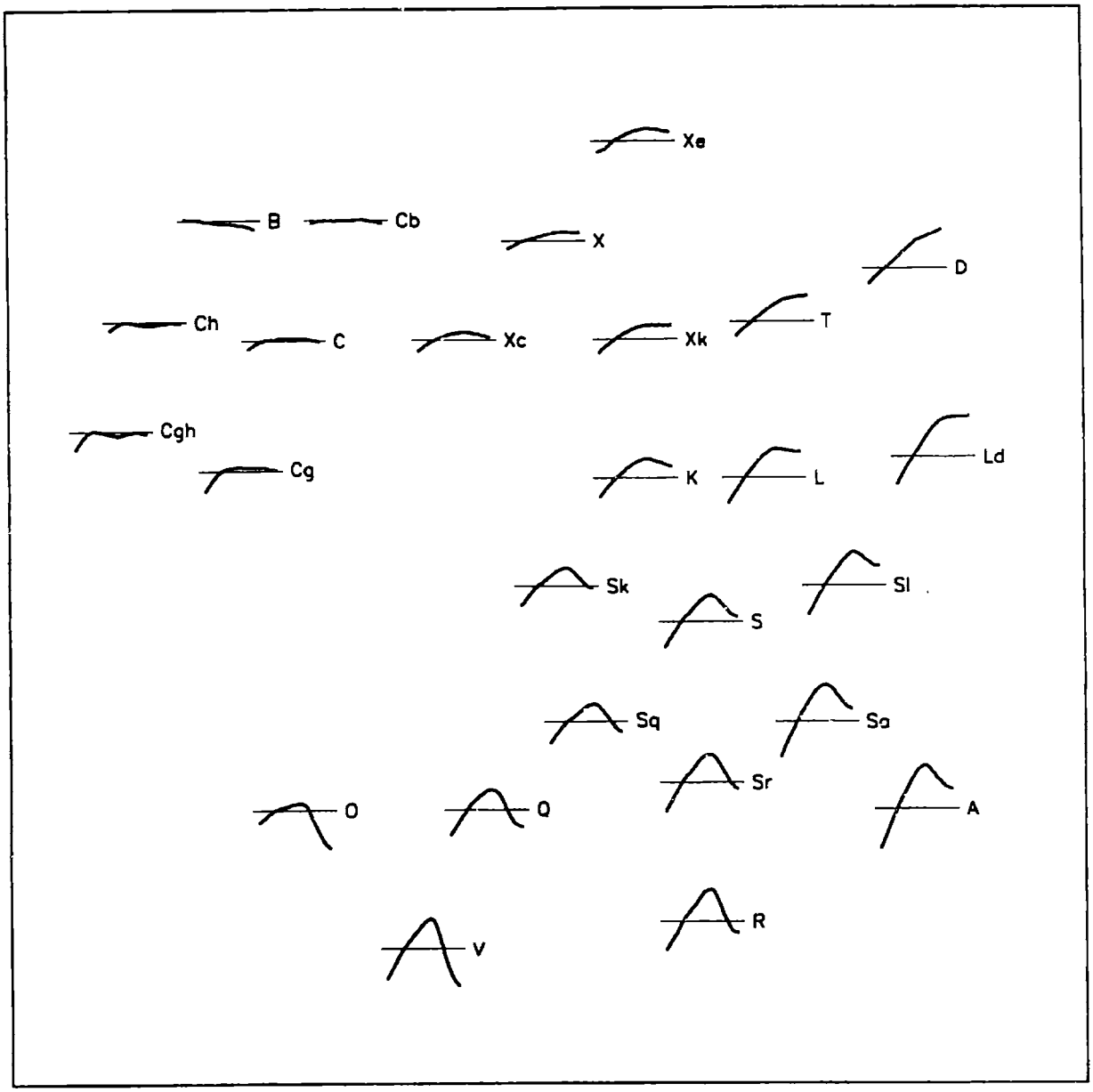

Figure 1.4. Plot of spectral characteristics of 26 classes proposed by Bus (1999), where the figure is taken from. Each spectrum plots the reflectance versus wavelength (0.44 to 0.92 μm) and are normalized to unity (horizontal straight lines) at 0.55 μm. The depth of the 1 μm feature generally increases from top to bottom and the continuum slope generally increases from left to right.

If an asteroid can be linked with a particular meteorite type, considerable insight can be gained on the petrological, thermal and collisional history of the asteroid from detailed laboratory analyses of those meteorites. Since the orbital position of the asteroid is known,

insight can also be gained on mechanisms for delivering meteorites to Earth. Spectroscopic studies have allowed researchers to propose relationships between a number of particular asteroids and types of meteorites. Two of the most widely discussed linkages are 4 Vesta with the howardites, eucrites and diogenites (abbreviated as HEDs) (e.g., McCord *et al.*, 1970; Larson and Fink, 1975; Binzel and Xu, 1993) and NEA 3103 Eger with the aubrites (enstatite achondrites) (Gaffey *et al.*, 1992). Both proposed links appear highly probable due to spectral similarities and plausible dynamical mechanisms for delivering fragments of these bodies to Earth. Other asteroid and meteorite relationships that have been suggested include the K-type asteroids in the Eos family and the CO/CV chondrites (Bell, 1988), some C, G, B and F asteroids with CI/CM chondrites that have undergone late-stage thermal metamorphism (Hiroi *et al.*, 1993c), 6 Hebe and the H chondrites (Farinella *et al.*, 1993; Gaffey, 1996; Gaffey and Gilbert, 1998), 3628 Boznemcová with the LL6 chondrites (Binzel *et al.*, 1993) and some near-Earth objects with ordinary chondrites (Binzel *et al.*, 1996a). Meibom and Clark (1999) estimate that our meteorite collections have evidence for at least 135 different parent bodies, which is primarily due to the large number (~90) (Wasson, 1995) of different iron meteorite groups (containing 5 or more members), grouplets (2 to 4 members) and anomalous objects.

One unknown quantity in comparing asteroid and meteorite spectra is how much alteration ("space weathering") is occurring on asteroid surfaces. The spectrum of an asteroid may not be representative of the actual composition since light only interacts with the top surface layer, which may could be altered by processes such as micrometeorite impacts or solar wind irradiation. Laboratory studies have tended to use pulse lasers (e.g., Moroz *et al.*, 1986; Yamada *et al.*, 1999) to try to duplicate these effects. "Space weathering" has tended to be invoked to explain the spectral differences between the most common classified asteroids (S types) and the most common meteorites found on Earth (ordinary chondrites). Both types of objects tend to have spectral features due to olivine and pyroxene, but the S asteroids have redder spectra and shallower features than the ordinary chondrites. A spectrum is redder than another if its reflectances increase in value at a faster rate (larger spectral slope) with increasing wavelength.

1.2 Meteorite Delivery Mechanisms

Farinella *et al.* (1993) performed a dynamical study of ~2400 numbered main-belt asteroids to identify the objects with the highest probability of injecting fragments into the 3:1 mean motion and the ν_6 secular resonances. Both the 3:1 (Wisdom, 1983, 1985) and ν_6 (Scholl and Froeschlé, 1991) resonances have been noted as likely source regions of Earth-approaching asteroids. These resonances increase the eccentricity of an object, which causes interactions (gravitational and collisional) with the body and the terrestrial planets. Farinella *et al.* (1993) estimated each asteroid's relative fragment production rate (the fragment delivery efficiency) to

these resonances to determine which asteroids are theoretically supplying large numbers of fragments to the 3:1 and ν_6 resonances from cratering and breakup events. Their results showed that a significant percentage of the near-Earth asteroids and, therefore, meteorites could be generated by a small (~1%) and possibly non-representative fraction of the known asteroid population that is mostly made up of large bodies located near these resonances. However, their study is highly model dependent and uses many critical parameters (e.g., the width of the secular resonance, the mass versus velocity distribution of the fragments) that are not well known.

Farinella *et al.* (1993) noted twenty-eight asteroids (Table 1.4) that could be injecting relatively large numbers of fragments into the resonances. The asteroids are ordered according to decreasing total fragment delivery efficiencies (E_1 plus E_2). However, it is unknown if both resonances are ultimately producing Earth-crossing asteroids with comparable rates.

Table 1.4. Asteroid numbers, names, classes (Tholen, 1989; Xu *et al.*, 1995; Bus, 1999; Gaffey *et al.*, 1993) and proper elements (Milani and Knezevic, 1994; LeMaitre, personal communication) for fragment delivery efficiencies (E_1 to the 3:1 resonance and E_2 to the ν_6 resonance) (Farinella *et al.*, 1993) for objects with E_1 or E_2 greater than 0.5. The asteroids are ordered from highest to lowest sums of E_1 and E_2.

		SMASS						
Asteroid	Tholen	I	II	Gaffey	a (AU)	E_1	E_2	Near-Infrared Data
6 Hebe	S	S	S	S(IV)	2.425	0.947	34.553	52-color, SMASSIR
46 Hestia	P		Xc		2.526	7.158	0.054	
19 Fortuna	G		Ch		2.442	3.258	0.093	52-color, SMASSIR
335 Roberta	FP		B		2.475	2.683	0.085	SMASSIR
4 Vesta	V	V	V		2.361	2.029	0.676	52-color, SMASSIR
304 Olga	C		Xc		2.404	0.021	2.427	SMASSIR
89 Julia	S		K	----	2.552	2.090	0.032	
29 Amphitrite	S	S	S	S(IV)	2.554	2.091	0.000	52-color
17 Thetis	S		SI		2.471	1.982	0.104	
1 Ceres	G		C		2.767	1.460	0.398	52-color, SMASSIR
13 Egeria	G		Ch		2.576	1.614	0.090	52-color
11 Parthenope	S		Sk	S(IV)	2.452	1.531	0.068	52-color, SMASSIR
907 Rhoda	C		Xk		2.576	0.000	1.593	
751 Faina	C		Ch		2.551	1.132	0.110	
631 Philippina	S	S	S		2.793	0.000	1.150	
409 Aspasia	CX		Xc		2.576	0.931	0.075	
449 Hamburga	C				2.554	0.879	0.000	
329 Svea	C				2.476	0.764	0.100	
759 Vinifera			X		2.618	0.007	0.849	
5 Astraea	S		S		2.576	0.688	0.000	52-color, SMASSIR
42 Isis	S	S	L	S(I)	2.441	0.637	0.029	52-color, SMASSIR
405 Thia	C		Ch		2.583	0.618	0.017	
344 Desiderata	C				2.595	0.589	0.021	
14 Irene	S	S	S		2.588	0.596	0.000	
712 Boliviana	C		X		2.575	0.552	0.018	
134 Sophrosyne	C	C	Ch		2.564	0.523	0.029	
7 Iris	S	S	S	S(IV)	2.386	0.515	0.000	52-color, SMASSIR
419 Aurelia	F				2.594	0.508	0.000	

The given fragment delivery efficiencies are useful for comparing two asteroid's relative number of fragments theoretically being supplied to each resonance. Asteroid 6 Hebe, the postulated parent body of the H chondrites, has a fragment delivery efficiency that is approximately five times higher than the asteroid (46 Hestia) with the next highest efficiency and makes Hebe a likely candidate as a meteorite source body. Vesta, the proposed HED parent body, has the fifth highest theoretical total fragment delivery efficiency. Intriguingly, H chondrites have the second highest fall frequency of all meteorite classes (Table 1.2) and HEDs have the fourth highest.

Other dynamical processes have been proposed for delivering meteorites to Earth. Recent work (e.g., Rubincam, 1995; Farinella *et al.*, 1998; Farinella and Vokrouhlicky, 1999; Bottke *et al.*, 1999; Hartmann *et al.*, 1999) has argued that the Yarkovsky effect may be very important. The Yarkovsky effect is due to the absorption of solar radiation by a body, which heats the body and then is reradiated after a time lag. Since there is an asymmetry between the direction of absorption of sunlight and the direction of reradiated thermal radiation, there is a net force (due to the momentum of the infrared photons which give a "kick" to the asteroid) that will cause a body to spiral inward for retrograde motion or outward for prograde motion. This is called the "diurnal" Yarkovsky effect. The "seasonal" Yarkovsky effect is due to the differing temperatures for different hemispheres for asteroids whose obliquity (angle between the polar axis and orbital plane), which causes the amount of thermal radiation that is reradiated to be different. The net force, averaged around an orbit, causes the object to spiral inward. The Yarkovsky effect appears to be most effective for bodies between 10 and 100 m in diameter.

The Yarkovsky effect apparently explains the relatively long cosmic ray exposure ages (ranging from ~2 to ~50 million years for ordinary chondrites) (Marti and Graf, 1992) compared to the estimated dynamical lifetimes of asteroids (a few million years) (Gladman *et al.*, 1997) delivered by Earth-supplying resonances. Cosmic ray exposure ages measure the time interval in space that a meteoroid spent exposed within a meter of the surface on its parent body or as a meter-sized object and its subsequent landing on Earth by measuring the abundance of radioactive nuclei produced by galactic cosmic rays (Marti and Graf, 1992). Researchers (e.g., Burns *et al.*, 1999) have found that most meteoroids reach Earth-crossing orbits via the 3:1 and ν_6 resonances after drifting in the main belt for tens of millions of years, consistent with cosmic ray exposure ages of ordinary chondrites and not consistent with the injection of fragments immediately into the 3:1 and the ν_6 resonances. They also found that nearly any body in the main belt could be supplying fragments to Earth.

Researchers (e.g., Nesvorny and Morbidelli, 1998) have also found a large number of resonances scattered throughout the belt. The lowest order mean motion resonances (e.g., 3:1, 5:2) tend to produce planet crossers on a much shorter timescale (a few million years) compared to higher order resonances (e.g., 7:2, 9:4) (timescales of tens of millions of years to a billion years).

1.3 Motivation

A number of factors have hampered attempts to link asteroids with particular meteorite types. Most asteroids have only been observed in the visible wavelength region, which allows for only part of the absorption feature usually due to olivine and/or pyroxene (Figure 1.1.2) to be characterized. Many meteorites with different compositions and thermal histories (e.g., ordinary chondrites and HEDs) have very similar reflectance properties in this limited wavelength range (Britt *et al.*, 1992). However, these objects can be distinguished (Figure 1.5) easily with spectral data in the near-infrared (Burbine, 1991).

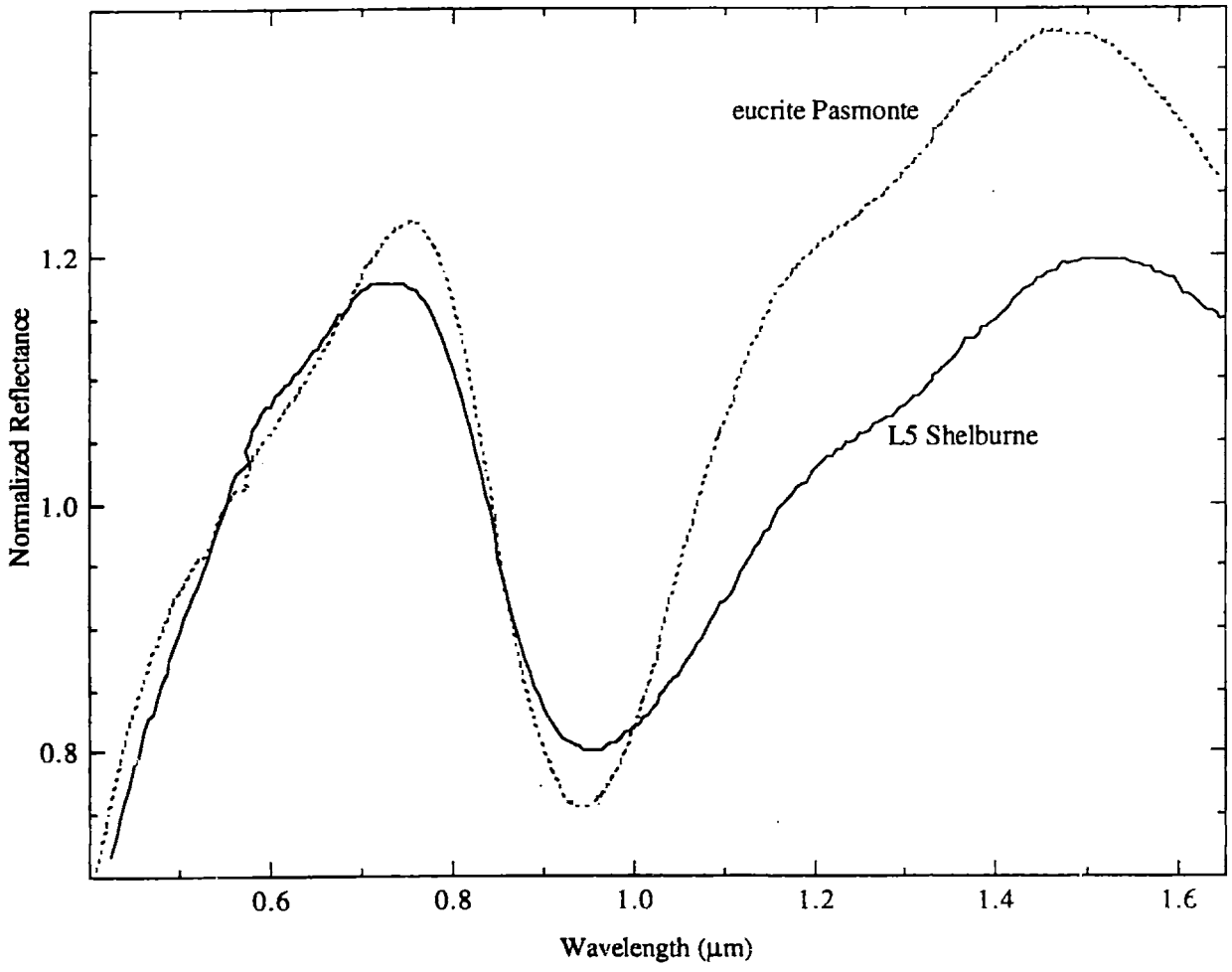

Figure 1.5. Reflectance spectra of the eucrite Pasamonte (dashed line) and L5 chondrite Shelburne (dark line). All spectra are from Gaffey (1976). All spectra are normalized to unity at 0.55 μm.

Besides scientific curiosity, studying the composition of main-belt and near-Earth asteroids gives information on a set of bodies that could have both destructive and beneficial effects on mankind. Asteroids have the capability of wiping out life as we know it, as seen by the evidence indicating an impact at the Cretaceous-Tertiary (K-T) boundary when the dinosaurs became extinct. Currently, asteroid discovery programs can identify possible Earth-impacting objects (none known to date), which would need to be destroyed or have their orbit changed by missile or spacecraft if they were found to threaten Earth. It would be vital to know the composition of such an object, since the material characteristics of the asteroid would be an important factor in the planning of any mission to avert an object's impact with Earth.

Metal-rich meteorites are abundant in precious metals such as Au, Pt, Ir, Os, Pd, Rh and Ru, which are vital to present-day technology in pure form or as part of alloys (Kargel, 1994). Their uses include being catalysts and electrodes in the automotive and chemical industries and as part of alloys, which are used in the electronics and computer industries. These metals are rare since ~99.8% of them in the Earth would be found in the metal-rich core. High-grade ores on Earth contain 10 to 50 ppm (parts per million) of precious metals, while the FeNi in LL chondrites contain 50-220 ppm of these metals with the richest iron meteorites containing over 300 ppm. Kargel (1994) estimates that a 1 km metallic asteroid that contains 100 ppm of precious metals would be worth ~5 trillion dollars at current market values (and ~320 billion at collapsed prices due to oversaturation of the market). Technological advances are needed to mine any asteroid, but compositional studies would be a vital part of any mission to identify possible iron-rich objects.

To increase our spectroscopic knowledge of asteroids, a near-infrared (~0.90 to ~1.65 μm) spectroscopic survey called SMASSIR (SMASS in the Infrared) has been undertaken, which has observed objects in the near-Earth and main-belt population with diameters ranging from a few hundred meters to hundreds of kilometers. In combination with SMASS data, this work will allow the compositional characteristics of small (diameters less than 20 km) objects that have been previously unobserved in the near-infrared to be analyzed and compared to the compositions of larger main-belt objects.

Almost all asteroid classes were surveyed in SMASSIR to try to get as much spectral information on as many different types of objects as possible. An emphasis was placed on observing asteroids in the near-infrared that had visible spectra similar to those of HEDs, ordinary chondrites and olivine since these meteorites have characteristic absorption features that can be analyzed. Over half of the observed objects in SMASSIR have estimated diameters of 20 km or less. One goal of this study is to identify plausible meteorite parent bodies and to use this information to gain insight on the processes of meteorite delivery to Earth and the compositional

structure of the asteroid belt. Another goal is to test how well the Bus taxonomy (1999) is grouping objects with similar surface compositions since asteroid mineralogies can be better determined using near-infrared spectra. A third goal is to understand the compositional differences between large and small objects in the main belt and near-Earth population.

The compositions of the asteroids will be determined by analyzing a combination of the SMASS and SMASSIR spectra. But to see if an asteroid can be a plausible parent body for a particular type of meteorite, a wide variety of different data sets for the asteroid (e.g., reflectance spectra, albedo, orbital characteristics) and the meteorites (e.g., reflectance spectra, albedo, compositional analyses, fall statistics, cosmic ray exposure ages) must be looked at. The suggested parent body for any type of meteorite should have orbits that are consistent with models for producing the fall frequencies and cosmic ray exposure ages of the linked meteorites. Inconsistencies may indicate that the asteroid is not a probable parent body or that the model is wrong. Only a few other studies (e.g., Gaffey *et al.*, 1992; Binzel and Xu, 1993) have tried to meld together a wide variety of asteroid and meteorite analyses to form a coherent picture of meteorite delivery from an object that agrees with all available evidence.

This thesis is broken up into a number of chapters. Chapter 2 gives a background on mineral and meteorite spectroscopy and then discusses previous asteroid spectroscopic surveys. Chapter 3 focuses on the observations and data reduction of the SMASSIR survey. V asteroids and the Vesta family will be discussed in Chapter 4. Chapter 5 is an analysis of the mineralogical characteristics for each of the asteroid classes (except the V class) observed in SMASSIR. Chapter 6 analyzes the rarity of mantle material (metal-free olivine dominated objects) in our meteorite collections and in the main belt. Chapter 7 discusses conclusions of this study and future work.

Chapter 2
Spectroscopy

2.1 Mineral Spectroscopy

Absorption bands in asteroid spectra are due to the interaction of solar electromagnetic radiation with minerals on the surface. Minerals have a large number of features from the far-ultraviolet through the infrared; however, the most studied features in asteroid spectroscopy are in the ultraviolet, visible and near-infrared since this region is rich in diagnostic absorption bands for many minerals. Also, the solar flux (and, therefore, the flux from the asteroid) peaks in the visible and the atmosphere is relatively transparent at these wavelengths.

As light strikes a mineral grain, some photons are reflected from the grain surface, some pass through the grain and some are absorbed (Clark, 1999). The photons that are reflected from grains or pass through them are said to be scattered. These scattered photons can encounter another grain or be scattered back to an observer, where they can be detected and measured. The absorption of photons by a material is governed by Beers Law ($I = I_0 e^{-kx}$) where I is the observed intensity, I_0 is the original light intensity, k is the absorption coefficient and x is the distance traveled through the medium by the photon.

Spectral features arise from a variety of electronic and vibrational transitions within mineral phases. Electronic transitions mainly come from absorptions due to transition metal elements (e.g., iron, nickel, cobalt, titanium) found within different minerals (Burns, 1993a, 1993b). The first series transition metal elements are characterized by having partially filled 3d shells. The 3d shell can have a maximum of 10 electrons, which are split into five orbitals. An orbital can be expressed as a wave function, which gives the spatial distribution of the electron density around the nucleus. Each orbital can contain two electrons, which, according to the Pauli exclusion principle, must be spinning in opposite directions. The d orbitals each have a crossed dumb-bell shape and are split into two groups: one where the lobes project between the cartesian axes and another where the lobes are directed along the axes. Electrons in isolated transition metal ions will have an equal probability of being located in any of the five d orbitals since they have identical (or degenerate) energy levels. However, when the transition metal cation is in a crystal structure, the effect of a non-spherical electrostatic field from surrounding anions removes some of the degeneracy and the d orbitals are split into different energy levels.

Electrons can be excited from one orbital to another by absorbing a photon equal to the energy difference of the orbitals. The energy separations between 3d orbital levels correspond to visible and infrared wavelengths. The energy states of the orbitals will be therefore be affected by the coordination state and dimensions of the crystallographic sites that the transition metal

element lies within, so different mineral species will tend to have absorption features at different wavelengths.

Iron is the most important of these transition metal elements due to its relatively high abundance in minerals and the characteristic absorptions it produces. Fe^{2+} has six valence electrons and is the primary source of most electronic absorption features for minerals important in meteorites such as olivine and pyroxene.

Olivine is usually found as part of the forsterite-fayalite [$(Mg,Fe)_2SiO_4$] solid solution. Within olivine, Fe^{2+} is found in two distinctly different distorted octahedral sites (M1 and M2). Olivine is an orthorhombic mineral since the crystal cell is defined by three crystallographic axes at different lengths, which are perpendicular to each other. Since olivine is orthorhombic, three different spectra are produced when polarized light is transmitted through each of the crystallographic directions (perpendicular axes α, β and γ), where the axes have different lengths ($\alpha > \beta > \gamma$), through oriented single crystals and can be attributed to different sites. The α and β directions both have broad absorption bands near 0.9 and 1.25 μm, which have been attributed to absorptions by the valence electrons of iron in the M1 site. The γ direction has a band near 1.1 μm, which has been attributed to iron in the M2 site. (In silicates, M1 and M2 sites are used to represent the positions of cations and neighboring oxygens.) Increasing the iron content of the olivine tends to move each of the absorptions to longer wavelengths (Burns, 1970). This is due to decreasing bond lengths in the crystal structure as the larger Fe^{2+} ions substitute for the smaller Mg^{2+} ones (Burns, 1993a). This leads to a decrease in the energy separations between the 3d orbital levels, which causes an increase in the wavelength of the absorptions.

The most common way to subdivide pyroxenes uses the chemical systems $CaSiO_3$ (wollastonite), $MgSiO_3$ (enstatite) and $FeSiO_3$ (ferrosilite) (e.g., Klein and Hurlbut, 1993). Structurally pyroxenes are divided into orthorhombic (orthopyroxene) and monoclinic (clinopyroxene) types. In monoclinic systems, the crystal cell is defined by three crystallographic axes of different lengths with two of the axes inclined to each other at an oblique angle and the third perpendicular to the plane of the other two. Iron in the M2 sites of pyroxenes tends to dominate the spectrum.

Orthopyroxenes are found as an enstatite-ferrosilite solid solution [$(Mg, Fe)_2Si_2O_6$] and contain virtually no calcium, which can substitute for Mg or Fe. The positions of the 1 and 2 μm band centers moves to longer wavelengths for increasing iron content (e.g., Adams, 1974). Pure enstatite will not have 1 or 2 μm absorption features due to the absence of iron in the pyroxene. Pigeonite is a calcium-poor monoclinic pyroxene, containing 5 to 15 mol.% Ca. As the Ca content is increased in pigeonite, the 1 μm band center moves to longer wavelengths. High calcium pyroxenes include diopside [$(Ca, Mg)_2Si_2O_6$] and augite [$(Ca, Na)(Mg, Fe,Al)(Si, Al)_2O_6$]. Increasing the calcium content of calcic pyroxenes moves the 1 and 2 μm band centers

to longer wavelengths (e.g., Adams, 1974).

Charge transfer transitions involve electronic transitions between different shells in a particular cation or between adjacent cations or cation-anion pairs (Gaffey *et al.*, 1989). These features are generally at shorter wavelengths and stronger than the crystal-field transitions. The overlapping series of these transitions (primarily due to interactions between oxygen and Fe^{2+}) produces the strong ultraviolet (UV) absorption edge found in silicate minerals (Figure 1.2).

Vibrational transitions arise from absorptions at vibrational (and combination and overtone) frequencies due to bound molecules. For asteroid spectroscopy, the most important vibrational transitions are due to bound water or structural OH, which can be found in a variety of hydrated silicates or oxides. Water (if visualized as a V with oxygen at the apex and hydrogen at the ends of the arms) can undergo three types of vibrations (Gaffey *et al.*, 1989). One is a bend (where the V opens and closes), which has a fundamental frequency of 6.08 μm. Another is a symmetric stretch (where both arms lengthen or shorten), which has a fundamental frequency of 3.05 μm. The third is an asymmetric stretch (one arm lengthens or shortens), which has a fundamental frequency of 2.87 μm. An OH^- can only undergo the asymmetric stretch. The 3.05 and 2.87 μm fundamentals and the first overtone (twice the frequency) of the bend fundamental at 3.04 μm combine to produce a broad and intense feature in the 3 μm region in the spectra of hydrated silicates. Combination and overtone features of these water fundamentals are also present at shorter wavelengths (e.g., 1.4 μm, 1.9 μm). Absorption features due to water are also present in the atmosphere, which cause problems for any Earth-based telescopic observations.

The relative abundance of the mineral phases does not correlate directly with the apparent spectral abundance for intimate mixtures. As shown by the spectral reflectance model derived by Hapke (1981), the reflectance of a mixture is a function of viewing geometry and properties of the particles such as single scattering albedo (efficiency of an average particle to scatter and not absorb light), porosity, diameters and mass fractions. The spectrum of a mixture will tend to be dominated by the species that is most absorbing at that wavelength. A very small abundance of opaques will tend to dominate the spectrum and suppress all absorption features due to its ability to absorb radiation. In mixtures of pyroxene and olivine, pyroxene tends to more absorbing and to dominate the spectral properties.

2.2 Meteorite Spectroscopy

The largest spectral survey of meteorites was done by Gaffey (1974, 1976), who measured more than 150 specimens of almost all types and subtypes known at that time from 0.3 to 2.5 μm. A correction factor of +0.025 μm is added to the original wavelengths of Gaffey to compensate for a later-discovered calibration offset (Gaffey, 1984). Spectra of L4 chondrite

Saratov measured by Gaffey (1976), with the calibration offset added, and recently measured at the Brown University Reflectance Experiment Laboratory (RELAB) facility showed no noticeable offset in the position of its 1 and 2 μm features; however, the 0.505 μm feature due to Fe^{2+} in pyroxenes appears offset by ~0.015 μm in the Gaffey (1976) eucrite spectra compared to those measured at RELAB showing that the correction may not be entirely linear over the entire wavelength range.

Gaffey found that the spectral characteristics of members of a particular meteorite class did not differ significantly. He also found that there were significant differences between the spectra of different meteorite types (such as those plotted in Figure 1.2) and that these spectral variations were understandable in terms of the composition, abundance and distribution of mineral phases in the meteorites.

The meteorite samples that Gaffey used were chosen to be as unaltered as possible and were taken from interior fragments that showed no discernible alteration. The powdered samples were crushed to particle sizes in the fine (~30 μm) to coarse (~300 μm) size ranges, but spectra were usually taken of a combination of these different particle sizes. A few meteorite samples (the irons and a mesosiderite) were only measured as whole rocks due to the difficulty in producing a powder out of metal without producing a significant amount of alteration. Later researchers (e.g., Hiroi and Takeda, 1991; Hiroi *et al.*, 1993a) who have measured meteorite spectra have tended to focus on samples found in Antarctica.

One possible problem with measuring the reflectance properties of any meteorite is the effects of terrestrial weathering. Salisbury *et al.* (1991) has shown that almost all anhydrous meteorites (including falls) have been terrestrially altered as seen by the presence of a 3 μm absorption feature in their reflectance spectra. This alteration can apparently just be due to exposure of the meteorite to water vapor in the air. Salisbury and Hunt (1974) have shown that weathering also induces a slight spectral slope between 0.5 and 0.6 μm for anhydrous meteorites, but appears not to noticeably affect the 1 μm feature for small amounts of weathering.

Another possible problem is that almost all meteorite spectra (e.g., Gaffey, 1976) have been measured at room temperature, while main-belt asteroid surfaces are at much lower temperatures (~125 to ~225 K) (Hinrichs *et al.*, 1999). Singer and Roush (1985) and Roush and Singer (1987) showed that minerals such as olivine (Figure 2.1) and pyroxene have spectral properties that are a function of temperature. They found that absorption bands tended to narrow for lower temperatures. They also found that the position of the 1 μm band minimum did not noticeably change. The position of the 2 μm band minimum was noticeably affected with the minima going to shorter wavelengths for low temperature orthopyroxene spectra and to longer wavelengths for low temperature clinopyroxene spectra. Crystal field theory predicts that absorption bands should narrow for decreasing temperature since the thermal motions of atoms should decrease for lower temperatures and, therefore, fewer vibrational modes are available (Burns, 1993a).

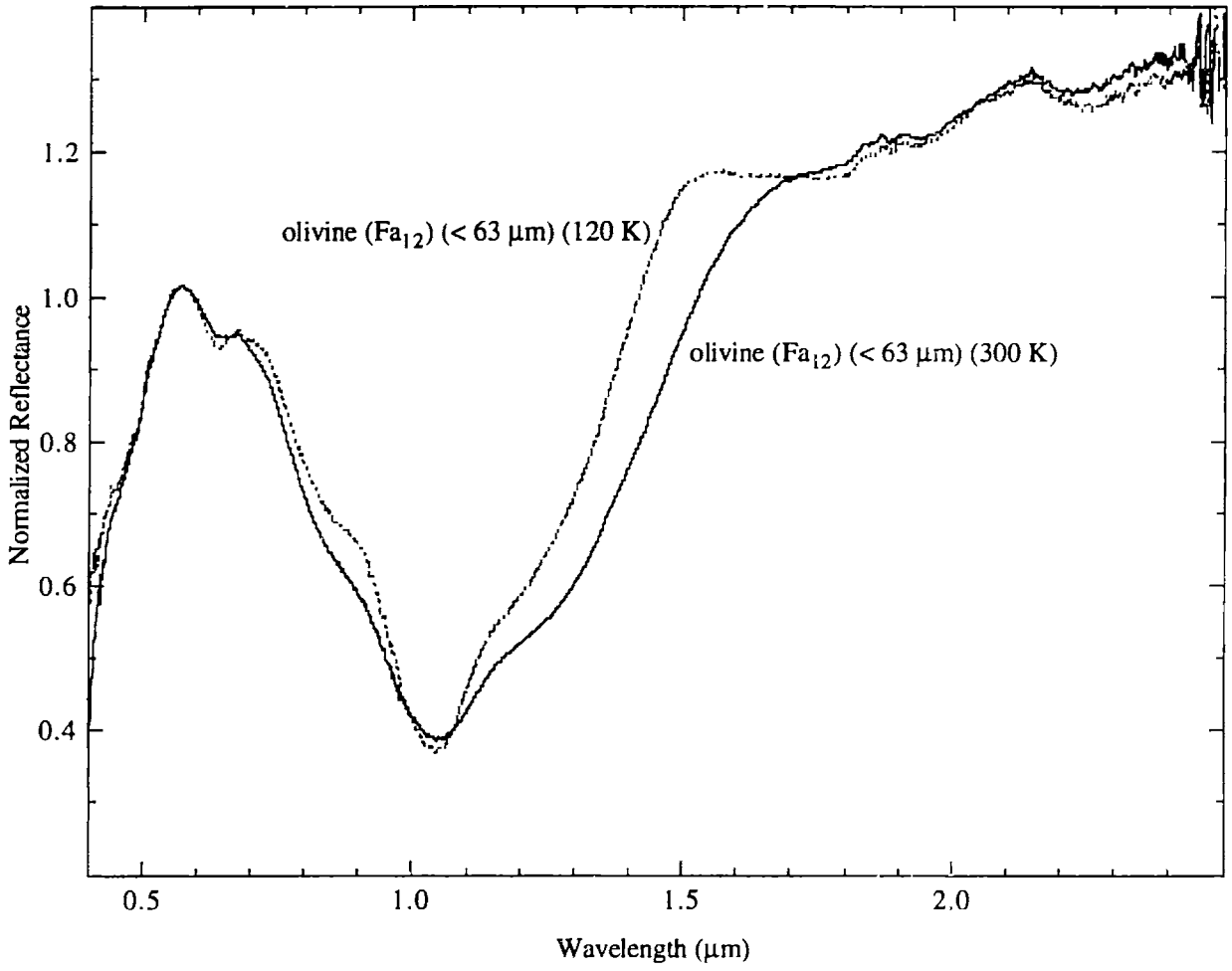

Figure 2.1. Reflectance spectra for olivine (Fa_{12}) at 300K (dark line) and 120 K (dashed line). Spectra are from Hinrichs *et al.* (1999). All spectra are normalized to unity at 0.55 μm.

Another factor that affects meteorite spectra is particle size. For material with features due to olivine and/or pyroxene, the absorption bands (Figure 2.2) tend to decrease in width for decreasing particle size (e.g., Hiroi *et al.*, 1994) and to redden. Reddening a spectrum refers to increasing the reflectance values at a particular wavelength, which can be seen in the higher reflectances and steeper spectral slope for the finer-grained howardite. Larger grains have larger internal path lengths so photons are more likely to be absorbed in the material than be scattered (Clark, 1999). The positions of absorption features do not appear to be noticeably affected by changing the particle size. The visual albedo also tends to increase as the size of the grains decreases. The finer-grained howardite in Figure 2.2 has an albedo of 0.25 while the larger-grained sample has an albedo of 0.18. Ordinary chondrites tend not redden as significantly as HEDs, with decreasing grain size, which is probably due to the higher abundance of opaques and metallic iron in ordinary chondrites.

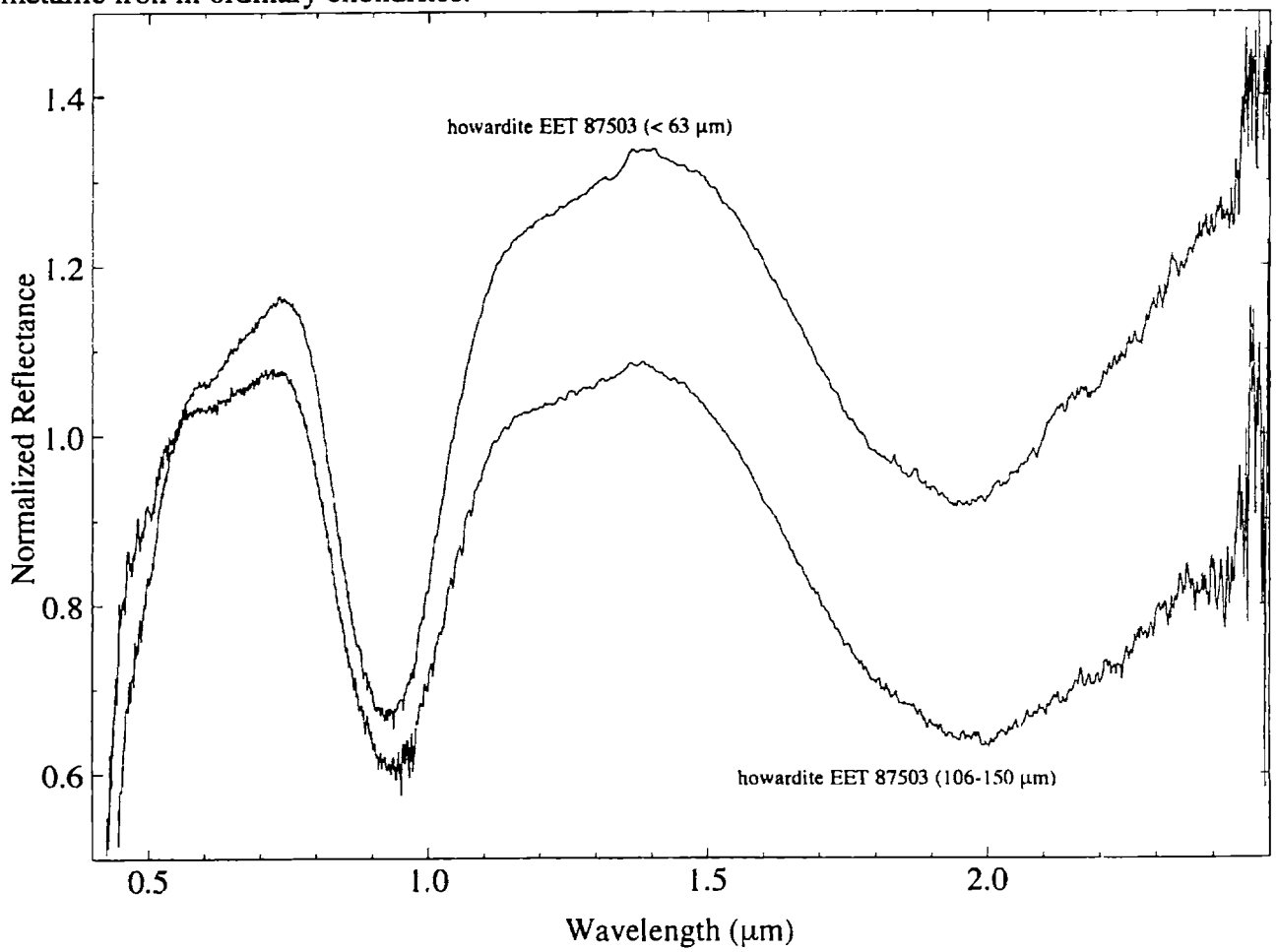

Figure 2.2. Reflectance spectra of howardite EET 87503 for two different particle sizes. The top line is for sizes less than 63 μm while the bottom line is for sizes between 106 and 150 μm. Th e Meteorite Working Group supplied the sample of EET 83251. The spectrum is from Hinrichs (personal communication) and was taken at the Planetary Geosciences/HIGP spectrometer facility at the University of Hawai'i. All spectra are normalized to unity at 0.55 μm.

For carbonaceous chondrites, the UV feature tends to weaken in strength for larger particle sizes (Johnson and Fanale, 1973). However, increasing the amounts of opaque material (Johnson and Fanale, 1973) and/or lowering iron contents in the silicates (Feierberg *et al.*, 1981) will also weaken the UV feature. Spectra of carbonaceous chondrites tend to have relatively red continuum slopes for small particle sizes (less than 100 μm) and flatter slopes for larger particle sizes. The 3 μm feature tends to decrease in intensity for increasing grain size and/or increasing amounts of non-hydrated material (Jones, 1988).

2.3 Lunar Analogy

The only extra-terrestrial object that we have physically retrieved samples from is the Moon. Telescopic reflectance spectra of the landing sites have been found to be very good spectral matches for typical bulk soil (regolith) samples from these sites (e.g., Adams and McCord, 1970, 1973).

The returned lunar soil samples have been found to be crucial for understanding the "weathering" effects on the Moon (Pieters, 1999). Many researchers (e.g., Adams and McCord, 1973) noticed that lunar soil is darker and had redder continuum slopes with weaker absorption features than particulate samples of rocks that they were derived. "Space weathering" on the Moon appears to be due to a number of factors such as exposure to solar wind irradiation, micrometeorite impacts and particle segregation in the regolith (Chapman, 1996). Pieters *et al.* (1993) has found that the finest fraction (less than 25 μm) of lunar soil dominates the spectral properties of the bulk soil. However, the spectral properties of the finest fraction cannot be duplicated simply by grinding down larger agglutinate-rich soil. (Agglutinates are glass-welded aggregates that tend to be very dark.) Pieters *et al.* (1993) believes that the development of fine-grained (less than 300 angstroms) Fe^{o} on the surface of the grains may be causing the spectral alteration effects on the lunar surface. This conjecture is consistent with the experiments of Allen *et al.* (1995). They found that the spectral changes in lunar soil is consistent with the formation of metallic iron blebs by reduction in a reducing (hydrogen-rich) environment.

It is very unclear how well the better-understood spectral processes occurring on the Moon can be applied to asteroidal bodies. Alteration on both types of bodies occur in a relative vacuum. However, the regolith on asteroids would be considered to be less mature (processed) than that of the Moon due its higher gravity (~5 times stronger than the largest asteroid Ceres and ~10,000 times stronger than a 20 km object). Asteroids also would be expected to experience decreased solar wind irradiation and lower impact velocities from micrometeorites.

2.4 Previous Asteroid Spectroscopic Surveys

To understand the spectral properties of asteroids, a number of comprehensive asteroid spectroscopic surveys have been instituted including the Eight-Color Asteroid Survey (ECAS) (Zellner *et al.*, 1985), SMASS (Xu *et al.*, 1995; Bus, 1999), the 52-color survey (Bell *et al.*, 1988; Howell *et al.*, 1994) and the Seven-Color Asteroid survey (SCAS) (Clark *et al.*, 1995). A reflectance spectrum for an asteroid is produced by dividing the asteroid spectrum by the spectrum of a solar analog star. Since the chosen standard stars have colors analogous to the sun, the resulting reflectance spectrum will be relative to the sun as shown by the equation (Chapman and Gaffey, 1979b)

$$\frac{asteroid}{sun} = \frac{asteroid}{standard\ star} \times \frac{standard\ star.}{sun}$$

ECAS observed 589 asteroids with eight broad-band filters from 0.3 to 1.1 μm that produced seven colors normalized to the visual filter. ECAS observations were mainly done on large (diameters greater than 20 km) asteroids. To make the colors relative to the sun, solar-type stars were also measured to produce zero points for each color. The ECAS colors were used as the basis of the asteroid taxonomy developed by Tholen (1984), which grouped objects into fourteen classes according to clusterings in their reflectance properties and visual albedo (when available) (Table 1.1.2).

SMASS I (Xu *et al.*, 1995) and II (Bus, 1999) observations were taken at the 2.4 and 1.3 meter telescopes at the Michigan-Dartmouth-MIT (MDM) observatory at Kitt Peak in Arizona with data acquisition procedures and data reduction techniques described in Xu *et al.* (1995) and Bus (1999). Each asteroid reflectance spectrum is produced by dividing the asteroid spectrum by the spectrum of a solar-analog (standard) star. An extinction correction, which compensates for the reddening of spectra as you go to higher airmass, is applied to each spectrum since the asteroid and standard star are usually observed at slightly different airmasses (usually differences of less than 0.1 airmasses). (Extinction is the dimming of light as it passes through the atmosphere. The longer the path length through the atmosphere, the more the light is dimmed. One airmass is defined as the shortest path length through the atmosphere, which is directly straight above the observer or the zenith. The airmass of an object is the secant of its angle from the zenith.) The extinction correction in SMASS uses a mean extinction model (Hayes and Latham, 1975) for Kitt Peak. Extinction increases as you go to shorter wavelengths and is a function of observing location and weather conditions. In the visible, extinction is mainly due to scattering by molecules (Rayleigh scattering) and dust (Mie scattering) (e.g., Young, 1989).

SMASS I spectrally observed 316 asteroids, mainly in the inner main belt, using a CCD with usable wavelength coverage ~0.48 to ~1.0 μm. SMASS I observations have no plotted error bars, but have estimated overall uncertainties typically in the range of 1-2%. Approximately half of the objects observed had estimated diameters less than 20 km and approximately two-thirds of these objects were classified for the first time. The biggest discovery from SMASS I was the identification of approximately twenty small asteroids with "Vesta-like" spectra that were located near Vesta (Binzel and Xu, 1993).

SMASS II has observed over 1400 asteroids with most of these objects listed in Bus (1999). A slightly different CCD from SMASS I was used. The SMASS II CCD was more responsive at lower wavelengths, but less at higher wavelengths. The usable wavelength coverage of SMASS II are from ~0.44 to ~0.92 μm. The data cut off at the telluric water band, which is centered at ~ 0.94 μm. However, the SMASS I spectra past ~0.92 μm may also be affected by the same atmospheric absorption feature. SMASS II data also have one-sigma error bars for individual points. SMASS II focused on small families to test how spectrally "similar" their members are. Bus (1999) found that all examined families were found to be spectrally homogeneous and tended to be distinct from the background (non-family) objects.

The 52-color survey observed over 100 asteroids from 0.8 to 2.5 μm over fifty-two wavelengths. The 52-color survey observed at least one asteroid for all asteroid classes (except Q), but the asteroids observed in the survey were mainly S types. All of the asteroids observed had diameters greater than 20 km with an average diameter of ~100 km (Clark *et al.*, 1995). Each 52-color spectrum was normalized to ECAS data (when available). Atmospheric absorption features are still present (e.g., Gaffey *et al.*, 1993; Cloutis and Gaffey, 1993a) in many of the 52-color spectra at ~1.4 and ~1.9 μm. The 52-color survey allowed Gaffey *et al.* (1993) to mineralogically characterize the S-asteroid class and they were able to divide them into numerous subgroups.

SCAS observed 126 asteroids using seven broad band filters between 0.91 and 2.3 μm, producing six colors normalized to the 0.91 μm filter. Only six of the objects observed in SCAS had estimated diameters less than 20 km with an average diameter of ~50 km. Clark *et al.* (1995) identified a number of K-type asteroids and a few objects with spectral characteristics similar to ordinary chondrites.

2.5 Reproducibility of Asteroid Spectra

Since the SMASSIR spectra need to be normalized to visible data and the visible spectra will be taken from three different surveys (ECAS, SMASS I and SMASS II), it is important to understand how comparable asteroid spectra are of the same object but taken by different observers at different times. Xu *et al.* (1995) compared his SMASS spectra to ECAS data of the

same objects (82 asteroids). The two sets of observations tended to match very well in most cases with an average reflectance difference between the two data sets (~80 asteroids had data that covered all overlapping wavelengths from 0.701 to 0.948 μm) of between 0.02 and 0.03. These differences are consistent with the work of other researchers such as Chapman and Gaffey (1979a) who state that in their 26-color survey (0.33-1.06 μm) of 277 asteroids, the error bars are never less than 0.03 due to possible systematic errors in the calibrations of their standard stars. Between the ECAS and SMASS I data, the differences were not systematically positive or negative with an average offset near zero (-.002). However, a few objects (most notably 14 Irene, 339 Dorothea and 416 Vaticana) tended to have very different spectral properties at the long wavelength part of the spectrum.

Other researchers have noticed spectral differences between their spectra and previous data. Sawyer (1991) noted a number of slope differences (e.g., 1 Ceres, 87 Sylvia) between his CCD data and previous measurements, plus a few objects (e.g., 148 Gallia) that looked completely different in multiple data sets. NEAR spacecraft data (Clark *et al.*, 1999) of 253 Mathilde differ significantly (~10%) from ground-based observations (Binzel *et al.*, 1996a).

Over 90 objects were observed in both SMASS I and II. The average reflectance difference for the two ends of the overlapping wavelength region was 0.02 at 0.44 μm and 0.06 at 0.92 μm. Disturbingly, the SMASS II data tend to have lower reflectance values at 0.92 μm with an average offset of -0.04 from the SMASS I data for the same object, which indicates a strongly systematic difference. These differences are higher than the uncertainties (less than ±0.02) in spectral slope that Bus (1999) estimates may arise from using the mean extinction model for objects observed at the highest airmass. These differences make it very difficult to apply the Bus (1999) classification system to the SMASS I data.

Twenty-one asteroids were observed in both the 52-color survey and SCAS. The average reflectance difference (excluding the very noisy objects 69 Hesperia and 584 Semiramis, which had distinctively different spectra in the two data sets) was 0.06 at both 1.65 and 2.3 μm. Approximately three-quarters of these objects tended to have 52-color spectra with higher reflectances than SCAS data at these two wavelengths. One possible source of spectral variation for photometric measurements, such as the 52-color survey and SCAS, is due to these observations not measuring all wavelengths simultaneously. Lightcurve effects, where the flux from the asteroid varies over time due to rotation of the object, can cause false color or slope variations in a reflectance spectrum since the asteroid may become brighter or fainter over a sequence of filter or color measurements (Gaffey, 1997).

However, some asteroids also are known to exhibit rotational variations. One of the most studied asteroids, 4 Vesta, is known to have spectral variations across its surface from Earth-based (e.g., Gaffey, 1997) and spacecraft observations (Binzel *et al.*, 1997) with some data sets

(e.g., McFadden *et al.*, 1981) showing spectral differences of ~7% in the strength of the 1 μm feature. Gaffey and Gilbert (1998) have shown that 6 Hebe exhibits rotational variations of ~4% in the strength of its 1 μm feature. Howell (1995) has noted that 20% of 52-color objects that were observed on two different occasions have distinct spectral differences, which she attributes to rotational variations.

Approximately 40% of the objects that were observed in SMASSIR had at least two sets of visible observations (ECAS, SMASS I and/or SMASS II). The spectral repeatability (Figure 2.3) varied from "perfect" matches (e.g., 5 Astraea, 42 Isis, 44 Nysa) to differences of over 10% at some wavelengths (e.g., 33 Polyhymnia, 113 Amalthea, 1929 Kollaa). SMASS II observations tend to have deeper 1 μm features than SMASS I (and ECAS) observations when there is a spectral difference. The deeper 1 μm features of SMASS II argue for a systematic effect; however, Bus (personal communication) could not find any problems in his reduction process that would cause systematically stronger features.

There are a number of factors that may cause these spectral differences. One is that extinction is known to vary over time and location in the sky. This means that extinction cannot be accurately modeled by a mean extinction model or observations of only a few standard stars during the night. High-precision spectra such as those of Vesta by Gaffey (1997) are done by taking a pair of standard star observations (within a few degrees of the asteroid) before and after the asteroid observations. Solar-calibrated standard stars are also observed each night to derive solar calibrations for these standards, which are usually not solar analogs. However in spectral surveys, the goal is to observe a large number of asteroids, which can not be done if a large number of standard stars also have to be observed.

Bus (1999) has also found sporadic changes in spectral slope of his SMASS II objects of up to ±0.05 in reflectance between observations of the same asteroid. He attributes these slope differences as being due to preferential loss of blue or red light through the spectroscopic slit. This loss of light may be due to observations taken in cloudy skies where the clouds do not act like a completely neutral filter and/or the slit size being used was not sufficient to collect all the light during poor seeing. Lazzaro *et al.* (personal communication) noted in her visible spectroscopic data that the proximity of the Moon to an observed object tended to increase the slope of the spectrum. The spectral differences between an object observed with the Moon present and without were as much as 10%.

Asteroid spectra taken by different observers at different times under good circumstances are expected to match with 2-3%. Although most observations appear reliable to better than 5%, worst case scenarios can lead to discrepancies of ~10%. These differences may be due to observational problems and/or compositional variations on the surface of the asteroid. The only way to know the true spectral characteristics of an asteroid is to observe it numerous times.

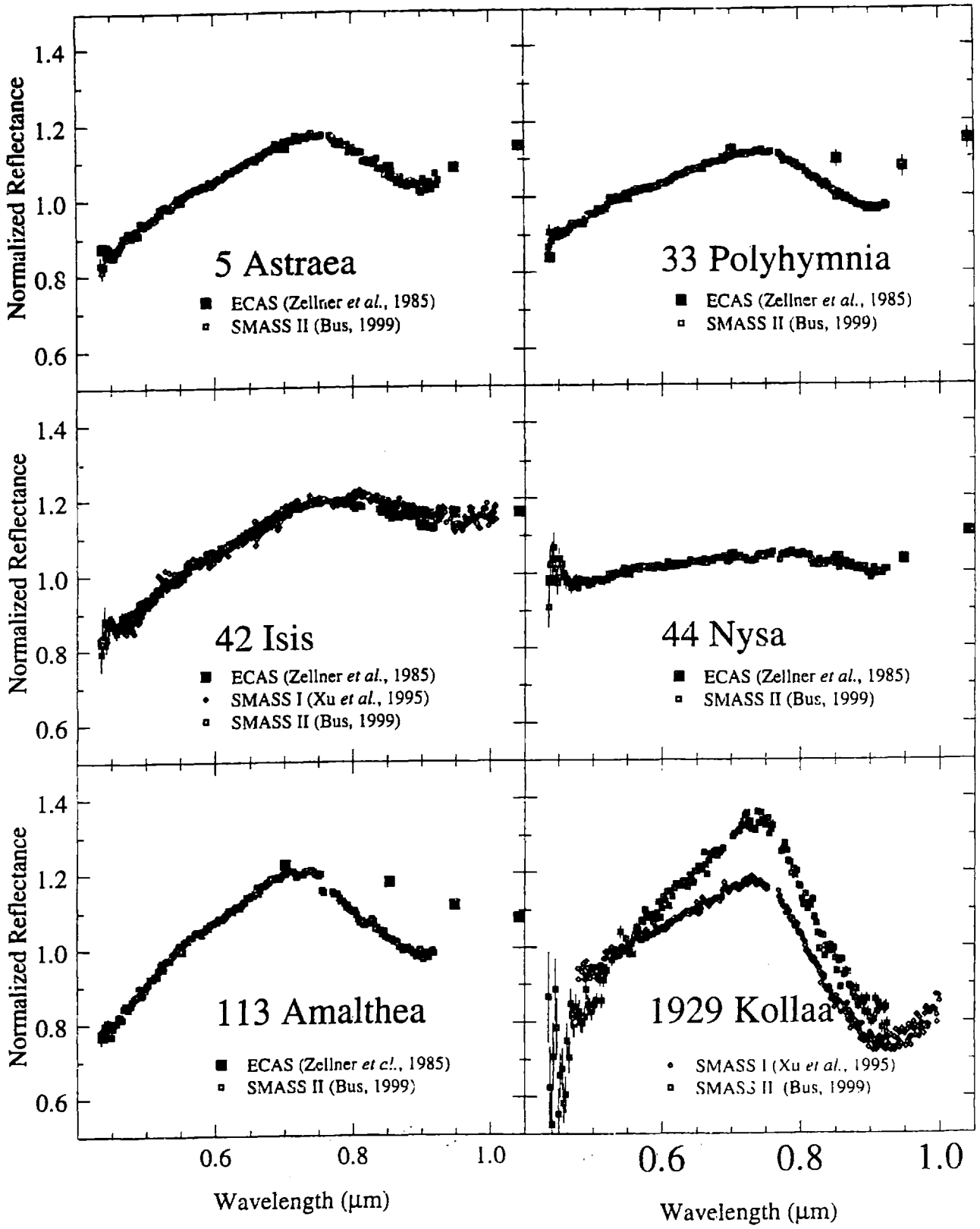

Figure 2.3. Reflectance spectra of 5 Astraea, 33 Polyhymnia, 42 Isis, 44 Nysa, 113 Amalthea and 1929 Kollaa for different spectral surveys. Error bars are $\pm 1\sigma$.

Chapter 3
SMASSIR

3.1 Observations and Data Reduction

To obtain near-infrared data on small (diameters less than 20 km) objects in the main belt, the SMASSIR observing program has been instituted at the NASA Infrared Telescope Facility (IRTF) on Mauna Kea using the NSFCAM InSb array. After a series of testing observations, there were nine observing runs (ir6 through ir14) with usable data. A low-resolution "asteroid" grism with appropriate blocking filters is used to record a simultaneous first-order spectrum from ~0.90 to ~1.65 μm with a dispersion of ~0.015 μm per pixel. A typical asteroid spectrum is shown in Figure 3.1. Atmospheric water features can be seen at ~1.15 and ~1.4 μm. The SMASSIR wavelengths overlaps the visible CCD coverage (~0.44 to ~0.92 μm) of SMASS. Spectral coverage past ~1.65 μm is not possible due to the overlap of a second order spectrum.

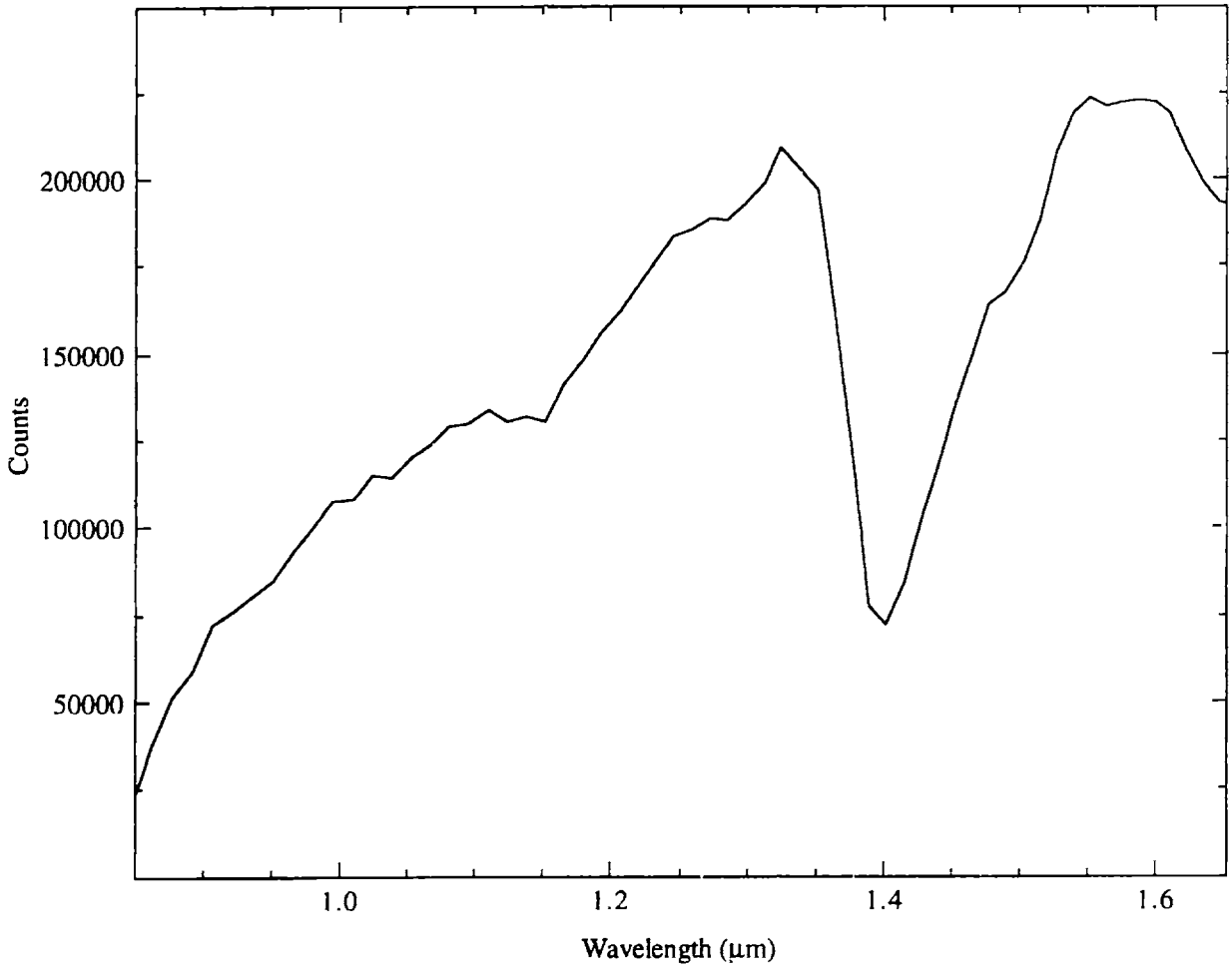

Figure 3.1. Plot of sky-subtracted counts versus wavelength (μm) for a single spectrum of 289 Nenetta.

Each image is obtained in pairs (images "A" and "B") where the spectra fall on alternating parts of the CCD chip. As much as possible, the "A" spectrum is repeatedly placed on the same column (and similarly for the "B" beam). Image "A" is subtracted by "B" and vice versa to remove background counts from the sky in the image. Spectral data reduction was done using the Image Reduction and Analysis Facility (IRAF), developed by the National Optical Astronomical Observatories. The IRAF package *apall* was used to sum the pixel values within a specified aperture at each point along the dispersion axis and to subtract any remaining background level. Since the different parts of the CCD chip may have different sensitivities, asteroid spectra from the "A" side of the chip are only divided by the spectra of the standard star from the "A" side of the chip, and similarly for the "B" side. The "A" and "B" reflectance spectra are combined to produce the final spectrum.

A large number of different standard stars were observed. Standard stars that were found to best reduce the asteroid spectra were the widely-used solar analog Hyades 64 (e.g., Xu *et al.*, 1995; Bus, 1999; Howell, 1995) and G-class Landolt standard stars (93-101, 98-978, 102-1081, 107-998 and 112-1333) (Landolt, 1973). All of these standard stars were found to produce asteroid spectra that reproduced previous 52-color spectra very well. At least two different standard stars were observed each night. Hyades 64 was the preferred standard star for all reductions; however, it was not always available each night.

In the near-infrared, extinction is dominated by molecular absorption (Young, 1989). At Mauna Kea, median values for the extinction coefficient at 1.2 μm (J filter) and 1.6 μm (H filter), respectively, are 0.101 and 0.051 magnitudes/airmass (Krisciunas *et al.*, 1987). (The wavelength position and passband width of these broadband filters are chosen to avoid molecular absorptions in the near-infrared, primarily due to water.) For airmass differences of less than 0.2, reflectance differences between two sets of spectra should be, on average, less than 1% for those two wavelengths.

However during this study, the extinction was found to be more variable. Figure 3.2 plots the strength of the incompletely removed absorption feature at ~1.4 μm versus the slope difference (in percent) from ~0.92 to 1.65 μm for standard stars observed in the study. A slope difference of 0% indicates two standard stars have the same spectral slope. Each point is for a standard star divided by another standard star of a lower airmass taken on the same evening. The average slope is approximately zero (0.3 ± 6.6%) and the average difference in slope from unity is approximately 5% (4.9 ± 4.4%). The reddening can be seen to get worse for increasing airmass difference.

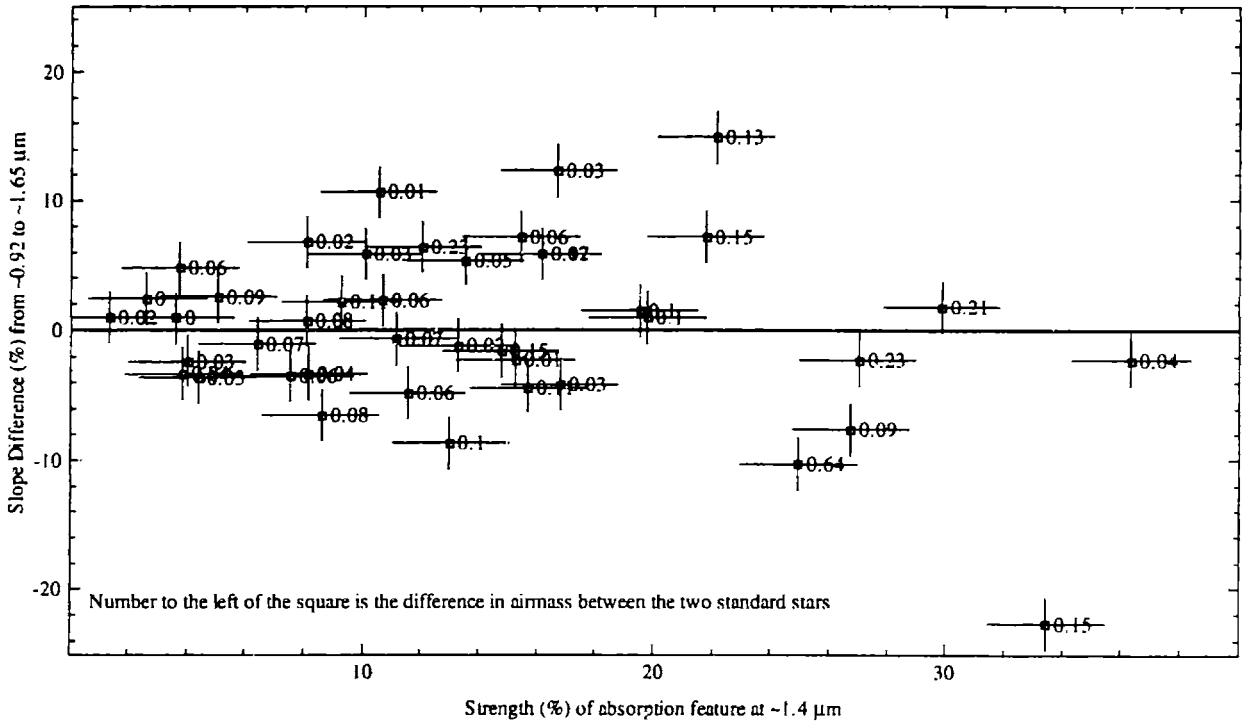

Figure 3.2. The strength of the incompletely removed absorption feature at ~1.4 μm versus the slope difference (in percent) from ~0.92 to 1.65 μm for standard stars. Each point is for a standard star divided by another standard star of a lower airmass taken on the same evening. Error bars are ±2% and are for the range of possible reasonable values for the calculated slope or strength.

No correction for extinction was made to the asteroid data since the extinction did not always vary in a systematic way. The average uncertainty in the slope at the SMASSIR wavelengths is on the order of 5%, which is comparable to slope uncertainties in the visible. To check for any problem with the standard stars for each set of observations, a few asteroids that were previously observed as part of the 52-color survey were re-observed and reduced with each solar analog star during each night.

Examples of spectral matches are shown in Figure 3.3. Asteroids from previous SMASSIR runs were also observed to see how they repeated. The standard star for each asteroid was then chosen using a variety of factors that included the standard star's ability to reproduce a 52-color spectrum, ability to reduce the strength of the atmospheric absorption features, similarity in airmass and similarity in time of observation. The choice of a standard star affected only the continuum slope of the spectra and the strength of the residual atmospheric absorption features, but not the shape of any absorption features due to minerals (e.g., olivine, pyroxene).

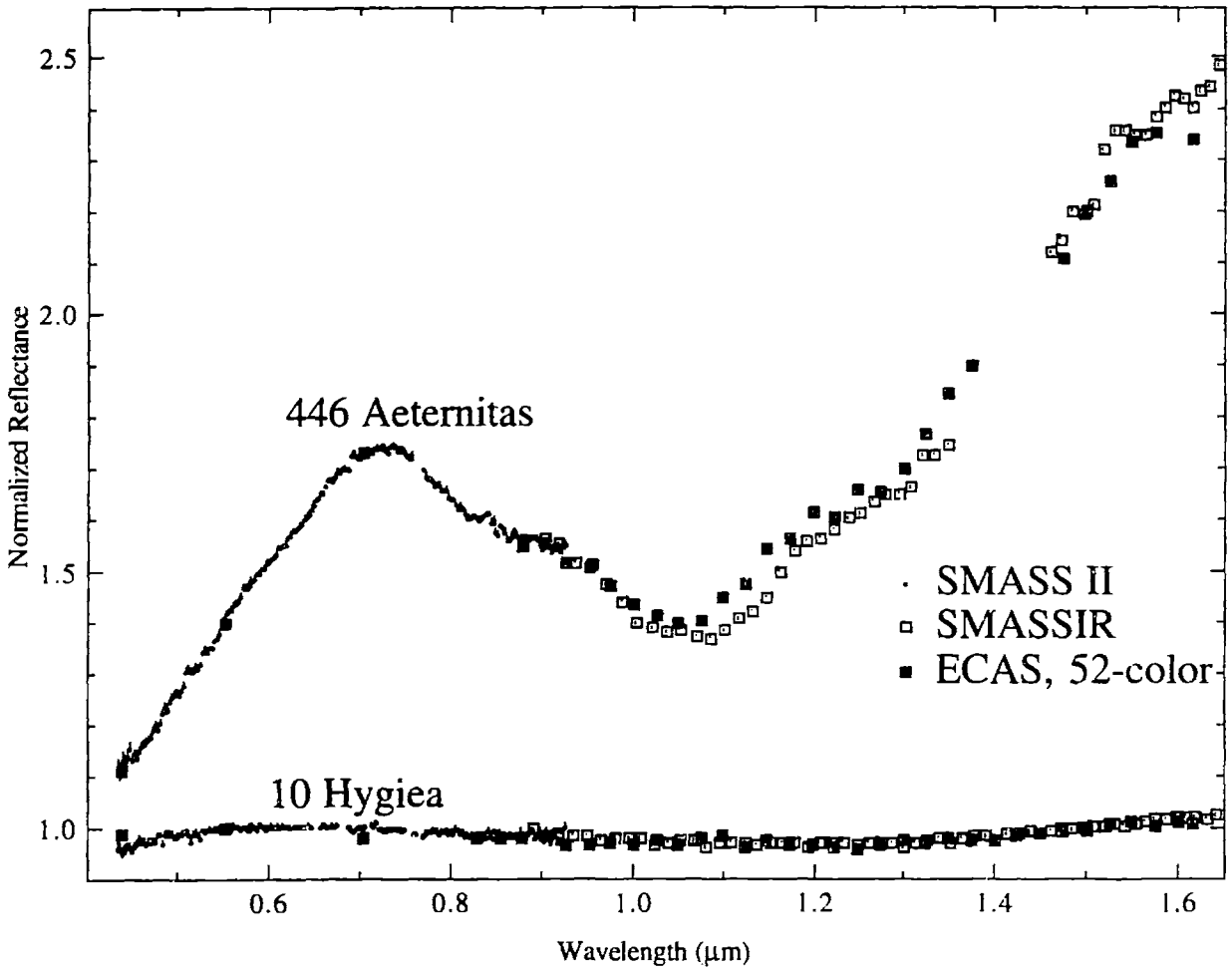

Figure 3.3. Reflectance spectra for 10 Hygiea and 446 Aeternitas. Small dots are from SMASS II (Bus, 1999), open circles are from SMASSIR and dark squares are ECAS data from Zellner *et al.* (1985) and 52-color data from Bell *et al.* (1988). All spectra are normalized to unity at 0.55 μm. The asteroid spectra are offset by 0.4 in reflectance from each other. Error bars are $\pm 1\sigma$. Error bars for the 52-color data are smaller than the symbols.

The wavelength calibration was obtained by taking spectral images of the flatly-illuminated dome through narrow band filters (1.083 μm, 1.094 μm, 1.282 μm, 1.58 μm, 1.70 μm). A quadratic function was then fit to the pixel position of the first order line for each filter, excluding the 1.094 μm filter since it is so close in wavelength position to the 1.083 μm filter.

The error bars for the wavelength positions are approximately one pixel (±0.015 μm) since the difference in the number of counts between the peak position and one pixel one either side of the peak were sometimes very slight. The wavelength calibration repeated very consistently for all runs. In ir12, the 1.083 μm filter was not available so the wavelength position of the 1.094 μm filter was used in the wavelength calibration. During ir13 and ir14, only the 1.58 and 1.70 μm filters were available so the wavelength calibration from ir12 was used for both of these runs since the wavelength positions for the available filters did not change.

Error bars for the reflectance values were calculated using Poisson statistics. The signal-to-noise ratio for each image was calculated by dividing the signal (the summed pixel values with the remaining background level removed from the subtracted images) by the noise (the square root of the summed pixel values with no remaining background level removed from the unsubtracted images). The inverse of the signal-to-noise is the fractional error for each image. The fractional errors for each image (standard star and asteroid) could be propagated to produce the one-sigma error bars for the final composite spectra. Since the error bars from Poisson statistics go as the square root of the number of counts, most calculated error bars are very small (less than 1%) due to the high number of counts measured (usually greater than 2000, as seen in Figure 3.1). However, the "real" uncertainty in the slope of all the SMASSIR spectra are ±5%, which is due to the problems in accurately correcting for extinction.

The atmospheric water band centered at ~1.4 μm (Figure 3.1) causes the points between 1.35 and 1.5 μm to be very suspect and not usable for most asteroids. Due to the problems in correcting for atmospheric water, as seen by the atmospheric features still present in many of the 52-color spectra at ~1.4 and ~1.9 μm, no atmospheric corrections have been made and points that appear to have been affected significantly have been deleted. Weaker atmospheric effects are also sometimes present in the spectra at ~0.94 and ~1.15 μm.

Observational parameters for the SMASSIR objects are given in Appendix A. For objects with multiple observations, an asterisk is used to indicate which spectrum is deemed the "highest-quality," which included factors such as visual inspection of the scatter in the points, fit to the visible data, strength of the residual atmospheric absorption feature and match to previous 52-color data.

Each SMASSIR spectrum was normalized to a visible spectrum (when available). When an object had spectra from both SMASS I and II, the SMASS II spectrum was generally used. The normalization to the visible spectrum was done by first fitting the SMASSIR spectrum with errors using a cubic spline program (Reinsch, 1967) that was adapted by Schleicher (personal communication) and has been previously used by Bus (1999). Points that appeared significantly affected by atmospheric water features were not used. The SMASSIR spectra were fit from 0.92 to 1.65 μm at 0.01 μm intervals. The 0.92 μm endpoint was chosen since the SMASS II spectra

were fit from 0.44 to 0.92 μm (Bus, 1999) and the two fits could be directly overlapped. Also, the number of counts measured shortward of 0.92 μm (Figure 3.1) in SMASSIR is rapidly decreasing, which increases the uncertainty in the value of those points. When a SMASS II spectrum was not available, a SMASS I or ECAS spectrum was fit from 0.44 to 0.92 μm. The SMASSIR fit was then normalized to the fitted visible spectrum. The actual SMASSIR spectrum was multiplied by this normalization factor and then overlaid on the visible spectrum to get the best continuous spectrum from ~0.44 to ~1.65 μm. SMASSIR spectra that were deemed too noisy to fit with a cubic spline were normalized visually to the visible data. SMASSIR spectra that had no corresponding visible spectra were normalized to unity at ~0.92 μm.

Spectra for the 196 SMASSIR objects are shown in Appendix B. For objects with multiple observations, only the "best" spectrum is plotted in Appendix B. To show how repeatable the SMASSIR measurements are, all of the observations for the 28 asteroids that were observed multiple times are plotted in their entirety (including points affected by atmospheric absorption features) in Appendix C.

Classes, albedos and diameters for each of the 196 SMASSIR objects are given in Appendix D. Fifty objects were NEAs (Aten, Apollo or Amor objects). Atens have semimajor axes less than 1.0 AU, Apollos have perihelion (closest approach to the sun) distances less than 1.0 AU and Amors have perihelion distances less than 1.3 AU. Fifty-five of the objects also had 52-color observations. Two objects (243 Ida and 253 Mathilde) have been visited by spacecraft.

3.2 Mineralogical Analysis of SMASS and SMASSIR Data

Mineralogical analysis of the asteroid spectra in the following chapters will be done by identifying the presence or absence of particular absorption bands. The usefulness of the SMASSIR spectra are that they allow, in conjunction with SMASS data, a better mineralogical characterization of the 1 μm absorption feature. Meteorites such as ordinary chondrites and HEDs can have very similar spectral properties in the visible wavelength region (Figure 1.5), but can be distinguished much better in the near-infrared. At the SMASSIR wavelengths, the HEDS show narrower 1 μm bands and the position of the maximum between the 1 and 2 μm feature is at longer wavelengths for ordinary chondrites than for the HEDs.

The drawback of SMASSIR spectra, compared to 52-color data, is that it can not fully characterize the 2 μm feature, which is primarily due to pyroxene. Spinel also has been found to have a 2 μm feature (Rajan and Gaffey, 1984) with no apparent 1 μm feature; however, spinel is only found as an abundant mineral in meteorites in calcium aluminum inclusions (CAIs). The 2 μm feature is vitally important for determining the approximate mineralogy for olivine-pyroxene mixtures. By ratioing the areas of the 2 and 1 μm features, the relative abundance of olivine to pyroxene can be determined (Cloutis *et al.*, 1986). The iron content of the pyroxene can be

estimated from the position of the 2 μm band (Adams, 1974) and will not change in position with increasing olivine content since olivine does not have a 2 μm feature. In contrast, the position of the 1 μm band minimum increases in wavelength with increasing olivine content.

Another possible problem is due to the overlapping at ~0.92 μm of visible and near-infrared data taken at separate times. Near the overlap region, there is an atmospheric absorption band centered at ~0.94 μm plus the SMASSIR spectrum is getting noisier for smaller wavelengths as the number of counts are decreasing. There is also a possibility that different hemispheres with slightly different mineralogies could be observed in SMASS and SMASSIR, respectively, so spectra with slightly different spectral properties could be overlapped. These factors could all lead to possible problems in analyzing an object's 1 μm feature. All band positions from fits at 0.01 μm resolution to the SMASSIR data have error bars of ±0.02 μm.

It appears difficult to use fitting programs to analyze asteroid spectra. One type of modeling (e.g., Hiroi *et al.*, 1993a; Clark, 1995) inputs spectra for different minerals and combines them using Hapke theory (or some other spectral modeling algorithm) until the best fit to the asteroid spectrum is produced. However, these models tend to be constrained by that fact that they tend to input spectra for minerals (usually called endmembers) of only one particular composition even though minerals such as olivine and pyroxene have a continuum of spectral properties that vary with composition (e.g., iron content in the silicates). Results from this kind of modeling also seem to have compositions that do not appear realistic. For example, the derived compositions from Clark (1995) for S asteroids tended to have clinopyroxene abundances much higher than anything found in our meteorite collections.

Another type of fitting program models specific absorption features using Gaussians and then matches the band positions of these curves with fits to laboratory spectra of known compositions. The most widely used one was developed by Sunshine (1994) and is called the Modified Gaussian Model (MGM). MGM deconvolves a spectrum into a series of absorption bands superimposed on a continuum. However, this type of modeling can not easily handle the spectra of assemblages with unknown compositions of more than one mineral (Gaffey, 1999a) since the number of Gaussians that will need to be fit to the spectrum is then unknown. Also, asteroid spectra tend to be noisier and have decreased spectral resolution compared to laboratory data, which can lead to non-unique solutions.

Mineralogical analysis will primarily be done by comparing absorption bands that are present in the asteroid spectra with features in the meteorite spectra. All meteorite and mineral spectra that are plotted in this thesis are listed in Appendix E. Due to the problems in determining spectral slopes for the asteroids and the large slope changes that can be obtained in the meteorite spectra by changing particle size, slope differences of ~5% or less will not be considered significant. Spectral matches with specific absorption features imply similar

compositional characteristics between the meteorite sample and the surface of the asteroid. The absence of any absorption features implies a surface with either abundant opaques, metallic iron or a spectrally featureless mineral such as enstatite. For featureless objects, albedo information (usually from IRAS) is crucial for identifying possible surface compositions. IRAS albedos and visual albedos of meteorites (reflectances at 0.55 μm) will be assumed to be directly comparable even though these albedos are determined in entirely different ways. IRAS albedos are calculated from the modeling of thermal fluxes while albedos of meteorites are measured directly in the laboratory.

It should always be remembered that the meteorite spectra are taken of samples containing ~50 mg to a few grams of material while the asteroid spectra are hemispherical averages of objects having diameters ranging from a few hundred meters to hundreds of kilometers. This large difference in scale makes "perfect" matches unlikely so the extent of any spectral discrepancies must be judged. Slight spectral differences may be due to factors such as composition, particle size and/or temperature. Relatively large spectral differences should mainly be due to composition.

Chapter 4
V Asteroids and the Vesta Family

4.1 Introduction

Asteroid 4 Vesta has been linked to the howardite, eucrite and diogenite (abbreviated as HED) meteorites due to Vesta's distinctive basaltic spectrum from 0.3 to 2.5 μm (McCord *et al.*, 1970; Larson and Fink, 1975), which has absorption features similar to the HEDs (Figure 4.1). As a group, the HEDs make up the largest suite of crustal igneous rocks found in the solar system after the Earth and Moon (Mittlefehldt *et al.*, 1998). Approximately 6% (Table 1.3) of all meteorites that fall to Earth are classified as HEDs (Sears and Dodd, 1988).

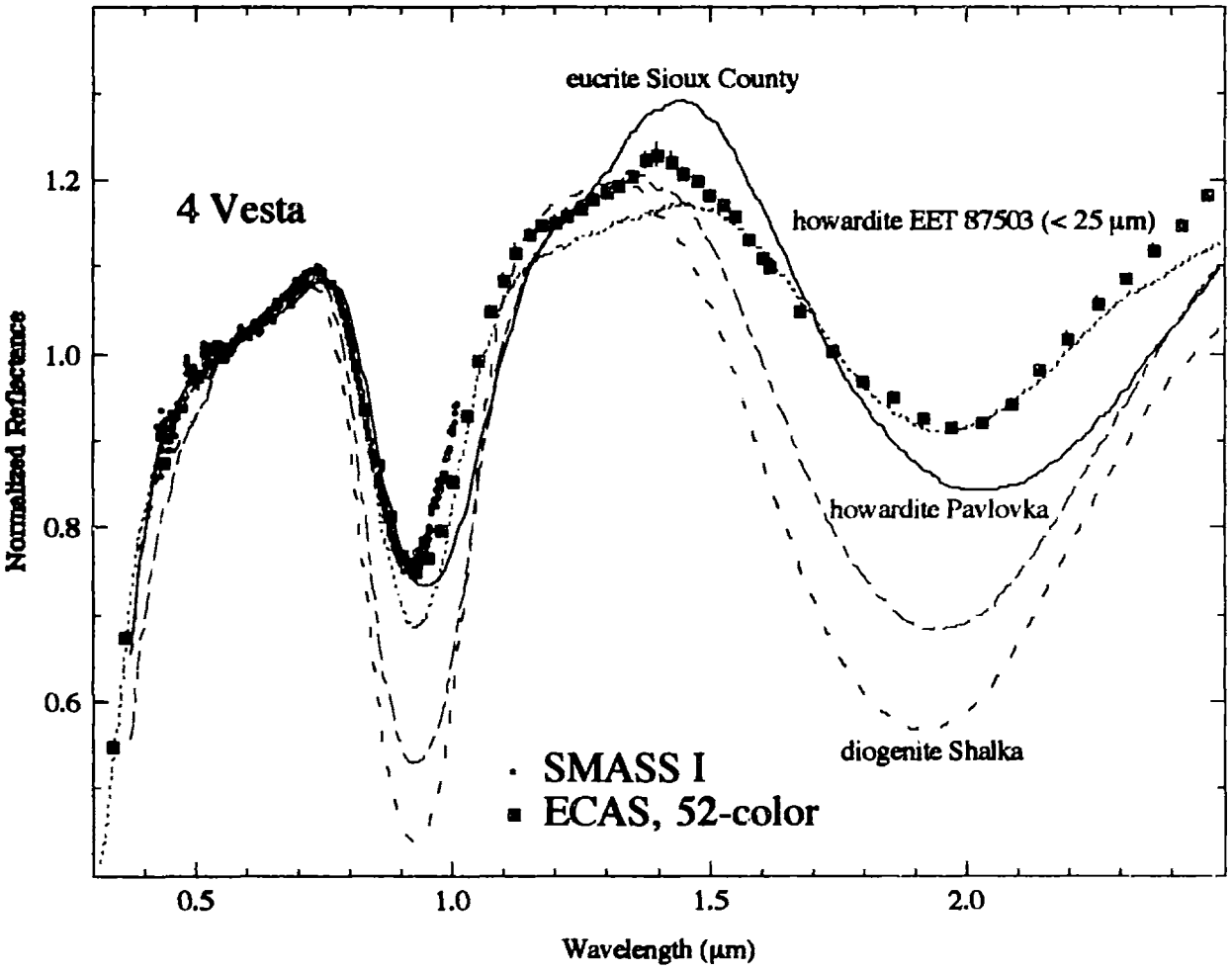

Figure 4.1. Reflectance spectrum of V asteroid 4 Vesta versus spectra of eucrite Sioux County (dark line), howardite Pavlovka (red broken line), howardite EET 87503 (particle size < 25 μm) (blue broken line) and diogenite Shalka (dashed line). Small dots are from SMASS I (Xu *et al.*, 1995) and dark squares are a combination of ECAS (Zellner *et al.*, 1985) and 52-color data (Bell *et al.*, 1988). The meteorite spectra are from Gaffey (1976) except for EET 87503, which is from Hiroi *et al.* (1994). All spectra are normalized to unity at 0.55 μm. Error bars are ±1σ.

The howardite, eucrite and diogenite meteorites form a related series of igneous/volcanic rocks distinguished by continuous variations in mineralogy and chemistry and apparently formed on the same parent body or related parent bodies (e.g., Dodd, 1981; Ruzicka *et al.*, 1997; Takeda, 1997; Mittlefehldt *et al.*, 1998). The simplest model for explaining the compositional characteristics of the HEDs is fractional crystallization (e.g., Takeda, 1997), where precipitated crystals fall out of a cooling magma. The minerals that precipitate will be a function of the composition of the melt, which is constantly changing as minerals of different compositions are formed and removed from the melt. Other factors such as pressure also affect which minerals form. For assumed chondritic compositions of Vesta, metallic iron formed first and segregated into the core. The evidence for this is the depletion of siderophile elements (ones that tend to go into the metallic iron phase) in HEDs relative to chondritic assemblages. For the remaining melt, fractional crystallization will first form olivine and then pyroxenes that become increasingly iron- and calcium-rich as the crystallization continues.

Most of the HED meteorites are breccias, which are rocks composed of fragments from previous generations of rocks. Monomict breccias are composed of materials that are derived from rocks that are similar in texture, mineralogy and composition whereas polymict breccias contain material derived from different types of rocks. The diogenites are primarily coarse-grained breccias that are predominately orthopyroxene [$(Mg, Fe)_2Si_2O_6$]. Eucrites contain primarily pyroxene (mainly pigeonite, a low-calcium pyroxene) and plagioclase feldspar and are broken into a number of subclasses, such as the cumulate, non-cumulate and polymict eucrites. Cumulate eucrites are believed to have formed by the settling of crystals to a magma floor as shown by the preferred orientations of their coarse-grained crystals and complex exsolution textures (inverted pigeonite), which imply slow cooling. Exsolution refers to the process where an initially homogenous solid solution separates into two or more distinct crystalline minerals (Klein and Hurlbut, 1993). Non-cumulate eucrites have a fine to medium grain-size. Howardites (e.g., Bunch, 1975) are polymict breccias of diogenitic and eucritic material with greater than 10 vol.% orthopyroxene. This dividing line is used to differentiate the howardites from polymict eucrites, which can contain minor diogenitic material. The eucrites, due to their higher calcium and iron contents in their pyroxenes, are assumed to have formed at shallower depths than the more magnesium-rich diogenites.

All HEDs are generally assumed to have originated on the same asteroid; however, ALH 84001 was originally classified as a diogenite before a Martian origin was proposed (Mittlefehldt, 1994) due to a number of anomalous petrologic features such as the presence of pyrite and calcite and similar oxygen isotope (^{18}O versus ^{17}O, normalized to ^{16}O) values with other "Martian" meteorites. HEDs all have similar oxygen isotope compositions (Clayton and

Mayeda, 1978), which is also consistent with the HEDs all originating from the same parent body or related parent bodies.

Both Vesta and the HEDs have two features centered near 0.9-1 μm and 1.9-2 μm due to pyroxene. The positions of these features (Figure 4.1) are a function of composition with eucrites having band minima that are shifted to longer wavelengths than the diogenites due to the different composition of their pyroxenes (Gaffey, 1976). The pyroxenes in eucrites tending to be more calcium- and iron-rich than those in diogenites (e.g., Takeda, 1997). As can be seen in the figure, the band minimum shift is much more pronounced for the 2 μm feature. The inflection in the eucrite spectra centered at about 1.25 μm has been attributed to feldspar (e.g., Gaffey, 1976). The positions of Vesta's absorption bands appears to be best matched by some combination of eucritic and diogenitic material (possibly analogous to a howardite) (Hiroi *et al.*, 1994; Gaffey, 1997). As can be seen in Figure 4.1, the strengths of the absorption bands between Vesta and HEDs from Gaffey (1976) do not match very well, which can be accounted for by differences in particle size. Decreasing the particle size for HEDs tends to decrease the strength of the 1 and 2 μm features. A much better spectral match (Figure 4.1) for Vesta has been found to be a fine-grained (< 25 μm) howardite (EET 87503) (Hiroi *et al.*, 1994). But as can be seen in the figure, EET 87503 is not a perfect spectral match for Vesta with a slight mismatch between 0.9 and 1.5 μm.

Vesta, with a mean diameter of 506 km (Thomas *et al.*, 1997a), is the only large (> 20 km) object with this distinctive spectrum. Vesta is also the largest body in a family of asteroids. Williams (1979, 1989, 1992) was the first to propose a Vesta family. Williams (1992) defined a family of eight objects from a sample of 2823 asteroids.

Zappalà *et al.* (1990, 1994, 1995) using different statistical clustering methods on much larger databases (12,487 objects in their 1995 study) of asteroid proper orbital elements and found much bigger Vesta families (over 200 members). Zappalà *et al.* (1995) used two different clustering techniques, the hierarchical clustering method (HCM) and the wavelet analysis method (WAM), with the "exact" size of the family depending on which clustering algorithm they used. HCM connects objects using a dendrogram (minimal tree that connects different objects) at increasing relative distances (meters/second), which are related to the velocities needed for orbital change. This dendrogram is compared to one computed for a quasi-random distribution of proper elements to determine the distance threshold needed to produce statistically significant clusters of objects. WAM uses a density analysis technique in three-dimensional proper element space to locate statistically significant clumps within the data. Almost all Vesta family members have estimated diameters less than 10 km and most of them are unnumbered. The original Zappalà *et al.* (1995) HCM family defines a distance metric between nearest neighbors of 120 m/s. However, Marzari *et al.* (1996) feel that a velocity of

~140 m/s may be more suitable, which produces a family of over 300 members. Zappalà *et al.* (1995) believe that the WAM method tends to be more "liberal" than the HCM method by tending to find broader groupings

Objections have been raised with linking Vesta with the HEDs. Some researchers (e.g., Wetherill, 1987) pointed out that ejection velocities from Vesta were unlikely to be high enough (> 600 m/s) for a significant number of fragments to reach the 3:1 Jovian and υ_6 secular resonances, which are known mechanisms for supplying objects into Earth-crossing orbits. Wasson (1995) notes that oxygen-isotope data for IIIAB irons, the main-group pallasites, the HEDs and the mesosiderites are consistent with all of these meteorites originating from the same disrupted parent body and not the still-intact Vesta. However, their oxygen isotopes are also consistent with all of these meteorites being derived from different bodies that had similar oxygen isotope abundances (Clayton and Mayeda, 1978).

Several studies (Farinella *et al.*, 1993; Marzari *et al.*, 1996; Asphaug, 1997) have shown that fragments from Vesta could be ejected with high enough velocities to reach the 3:1 resonance. The identification of the same distinctive type of spectrum in the visible (0.4-1.0 μm) (Figure 4.2) (Binzel and Xu, 1993) among a number of small asteroids (called Vestoids due to their "Vesta-like" spectra) in the Vesta family and between Vesta and these meteorite-supplying resonances lends support to the argument that fragments from Vesta could be ejected from the surface and subsequently reach Earth (Binzel, 1995). However, the Vestoids are not perfect spectral matches for Vesta and tend to have visible spectra that are redder than Vesta (e.g., Hiroi and Pieters, 1997, 1998).

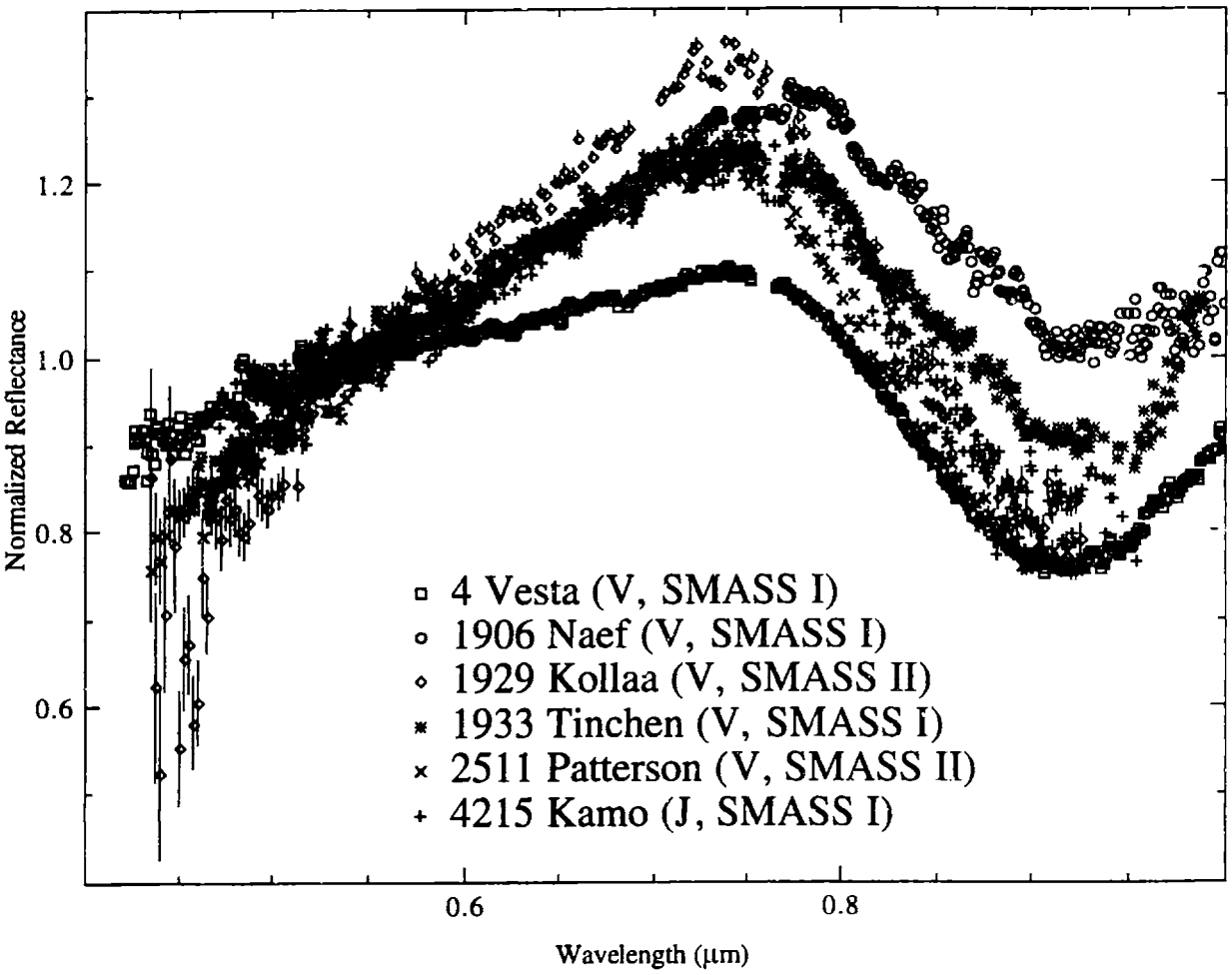

Figure 4.2. Reflectance spectra of V and J asteroids in the visible. The spectra of Vesta, Naef, Tinchen and Kamo are from SMASS I (Xu *et al.*, 1995). The spectra of Kollaa and Patterson are from SMASS II (Bus, 1999). All spectra are normalized to unity at 0.55 μm. Error bars are $\pm 1\sigma$.

Twenty-one 'Vesta-like" objects (excluding Vesta) observed originally in SMASS were originally classified visually (Binzel and Xu, 1993) and then by principal component analysis (Xu *et al.*, 1995). These objects were broken into two classes, V and J. The V class had spectra

roughly similar to Vesta with band centers near 0.94 μm, while the J class (e.g., 4215 Kamo) had deeper 1 μm features and band centers at shorter wavelengths. J asteroids were interpreted by Binzel and Xu (1993) as being closer in spectral properties to diogenites. Bus (1999) identified eighteen new "Vesta-like" objects. These objects were only placed into a V class since no spectral information is used past 0.92 μm, which is needed to identify J-class objects. A number of near-Earth asteroids (NEAs) have also been identified with this distinctive spectrum (Cruikshank *et al.*, 1991).

The visible spectra of the "Vesta-like" objects tend to be consistent with HED spectra. However, in the visible wavelength region, many ordinary chondrites, since their absorption features are also primarily due to pyroxene, do have absorption bands with similar strengths to some eucrites (Britt *et al.*, 1992) and some of the Vestoids. The spectral differences between the ordinary chondrites and HEDs are much more pronounced in the near-infrared where these two types of objects can be easily distinguished (Figure 3.4).

Objections have also been raised in linking Vesta with the Vesta family members. Wasson *et al.* (1996) invoked a scenario where fragments of a projectile that had a grazing impact with Vesta are coated with "Vesta dust" and, thus, appear "Vesta-like." Bell (1998) has proposed that many to all of the Vestoids are background S asteroids with deeper 1 μm features since near-infrared measurements (Burbine and Binzel, 1997; Burbine *et al.*, 1998) of these objects shows them to be significantly redder (higher reflectance values) than Vesta.

4.2 Investigation of the Vesta Family and V Asteroids

To see if any of these objections have any merit, twenty-four Vestoids were observed in the near-infrared. Fifteen of these objects are in the HCM Vesta family (Table 4.1). The goal of this study is to understand how mineralogically similar these Vestoids are to Vesta and to the HEDs and to see what can be concluded about the origin of these objects. The spectra of Vestoids in the Vesta family will also be compared to the spectra of "Vesta-like" objects that fall outside the Vesta family (Table 4.2). To understand the effects of grain size and temperature on the spectra of the Vestoids, a number of Antarctic HEDs had their spectra measured for different grain sizes and at room and low temperatures. Spectra from SMASS I (Xu *et al.*, 1995) and II (Bus, 1999; Binzel and Bus, personal communication) will be directly compared; however, as discussed in Section 2.5, the SMASS II observations tend to have deeper 1 μm features than SMASS I spectra.

Table 4.1. Asteroids in the HCM Vesta family that have been observed in SMASS I or SMASS II. Proper elements (a, e', sin i') are from Milani and Knezevic (1994). Vesta's diameter is from Thomas *et al.* (1997a) while the rest of the diameters that are not in parentheses are IRAS diameters from Tedesco (1994). Diameters in parentheses are calculated using the H magnitude (see Appendix D for details) with estimated albedos of 0.25 for A, R, S and X objects, 0.05 for C and T objects and 0.42 (Vesta's IRAS albedo) for V and J objects. Family memberships includes members at a slightly higher distance level than those of Zappalà *et al.* (1995). SMASS I classifications are from Xu *et al.* (1995) and SMASS II are from Bus (1999).

				Diameter	Family Membership		SMASS		
Asteroid	a (AU)	e'	sin i'	(km)	HCM	WAM	I	II	Near-Infrared Data
4 Vesta	2.362	0.099	0.111	506	Vesta	Vesta	V	V	52-color, SMASSIR
306 Unitas	2.358	0.118	0.117	47	Vesta			S	
442 Eichsfeldia	2.345	0.100	0.098	66	Vesta			Ch	
1697 Koskenniemi	2.374	0.115	0.106	(18)	Vesta		TX		
1781 Van Biesbroeck	2.395	0.083	0.108	(8)	Vesta		XS		
1906 Naef	2.374	0.100	0.112	(6)	Vesta	Vesta	V		SMASSIR
1929 Kollaa	2.363	0.114	0.123	(8)	Vesta	Vesta	V	V	SMASSIR
1933 Tinchen	2.353	0.094	0.119	(5)	Vesta	Vesta	V		SMASSIR
2011 Veteraniya	2.387	0.111	0.111	(5)	Vesta		J		
2024 McLaughlin	2.325	0.095	0.114	(7)	Vesta	Vesta	S		
2029 Binomi	2.350	0.085	0.112	(5)	Vesta	Vesta		S	
2045 Peking	2.380	0.090	0.116	(8)	Vesta	Vesta		V	SMASSIR
2086 Newell	2.401	0.115	0.105	(9)		Vesta		Xc	
2346 Lilio	2.371	0.113	0.120	(25)	Vesta	Vesta		C	
2468 Repin	2.327	0.116	0.112	(7)		Vesta		V	
2508 Alupka	2.368	0.094	0.112	(4)	Vesta	Vesta		V	
2511 Patterson	2.299	0.094	0.126	(7)	Vesta			V	
2547 Hubei	2.385	0.093	0.109	(3)	Vesta	Vesta		V	
2590 Mourao	2.343	0.097	0.117	(6)	Vesta	Vesta	V		SMASSIR
3007 Reaves	2.368	0.093	0.132	(9)	Vesta			X	
3155 Lee	2.343	0.098	0.117	(6)	Vesta	Vesta	J	V	
3265 Fletcher	2.411	0.107	0.106	(5)	Vesta	Vesta		V	
3268 De Sanctis	2.347	0.100	0.122	(4)	Vesta	Vesta	V		SMASSIR
3354 McNair	2.325	0.079	0.118	(7)	Vesta		S		
3376 Armandhammer	2.349	0.097	0.123	(9)	Vesta	Vesta		Sq	SMASSIR
3494 Purple Mountain	2.350	0.098	0.115	(6)	Vesta	Vesta	V		
3498 Belton	2.355	0.099	0.120	(4)	Vesta	Vesta		V	
3536 Schleicher	2.343	0.077	0.116	(4)	Vesta			V	
3657 Ermolova	2.313	0.088	0.115	(6)	Vesta		J		SMASSIR
3782 Celle	2.415	0.108	0.106	(7)	Vesta	Vesta		V	
3865 1988 AY_4	2.398	0.094	0.123	(8)	Vesta			Xc	
3900 Knezevic	2.371	0.114	0.122	(4)	Vesta	Vesta		V	
3944 Halliday	2.369	0.109	0.118	(5)	Vesta	Vesta	V		SMASSIR
3968 Koptelov	2.322	0.091	0.116	(5)	Vesta	Vesta	V		SMASSIR
4005 Dyagilev	2.452	0.113	0.105	(6)	Vesta		J		SMASSIR
4038 Kristina	2.366	0.100	0.110	(5)	Vesta	Vesta	V		
4147 Lennon	2.362	0.102	0.113	(5)	Vesta	Vesta	V		SMASSIR
4215 Kamo	2.417	0.098	0.115	(7)	Vesta		J		SMASSIR
4311 Zguridi	2.442	0.110	0.109	(4)	Vesta	Vesta		V	
4510 Shawna	2.360	0.098	0.119	(6)	Vesta	Vesta	S		
4546 Franck	2.356	0.090	0.114	(4)	Vesta	Vesta	V		
4548 Wielen	2.285	0.097	0.135	(5)	Vesta			Xc	
4900 Maymelou	2.380	0.102	0.114	(5)	Vesta	Vesta		V	SMASSIR
4977 Rauthgundis	2.292	0.093	0.104	(4)	Vesta			V	
4993 1983 GR	2.369	0.091	0.111	(5)	Vesta	Vesta		V	
5051 1984 SM	2.294	0.099	0.115	(6)	Vesta			Sr	
5108 Lübeck	2.305	0.099	0.117	(5)	Vesta	Vesta		S	
5111 Jacliff	2.354	0.083	0.117	(6)	Vesta	Vesta		R	
5240 Kwasan	2.383	0.105	0.111	(7)	Vesta	Vesta		V	

Table 4.2. Vestoids (not in the Vesta family) observed in SMASSIR. Osculating elements are given for the NEAs, which are from the *Ephemerides of Minor Planets* (1999). Diameters in parentheses are calculated using the H magnitude with estimated albedos of 0.42. SMASS I classifications are from Xu *et al.* (1995) and SMASS II are from Bus (1999).

Asteroid	a (AU)	e'	sin i'	Diameter (km)	HCM Family	SMASS I	SMASS II	NEA
1273 Anchises	2.394	0.123	0.109	(6)		V		
1981 Midas	1.776	0.650	0.641	(2)		V		Apollo
2442 Corbett	2.388	0.097	0.095	(6)		J		
2579 Spartacus	2.210	0.081	0.103	(5)			V	
2653 Principia	2.444	0.114	0.089	(8)			V	
2851 Harbin	2.478	0.119	0.136	(7)			V	
3908 Nyx	1.926	0.459	0.038	1$			V	Amor
4188 Shulnazaria	2.335	0.112	0.098	(6)			V	
7889 1994 LX	1.261	0.346	0.641	(2)			(V)∞	Apollo

$ Diameter for 3908 Nyx is from Cruikshank *et al.* (1991).
∞ Asteroids 1981 Midas and 7889 194 LX are classified as V types from their SMASSIR spectra.

4.3 Vesta Family

Thirty-two Vesta-family asteroids have been identified with V or J designations, while seventeen objects were given other classifications. Of the four objects with diameters between 15 and 70 km, three asteroids have relatively featureless spectra (Figure 4.3) not consistent with any relationship with Vesta. One S-asteroid, 306 Unitas, has visible spectra that could be consistent with a relationship to Vesta; however, its diameter (47 km) is much larger than all other objects with "Vesta-like" spectra (diameters less than 10 km), excluding Vesta.

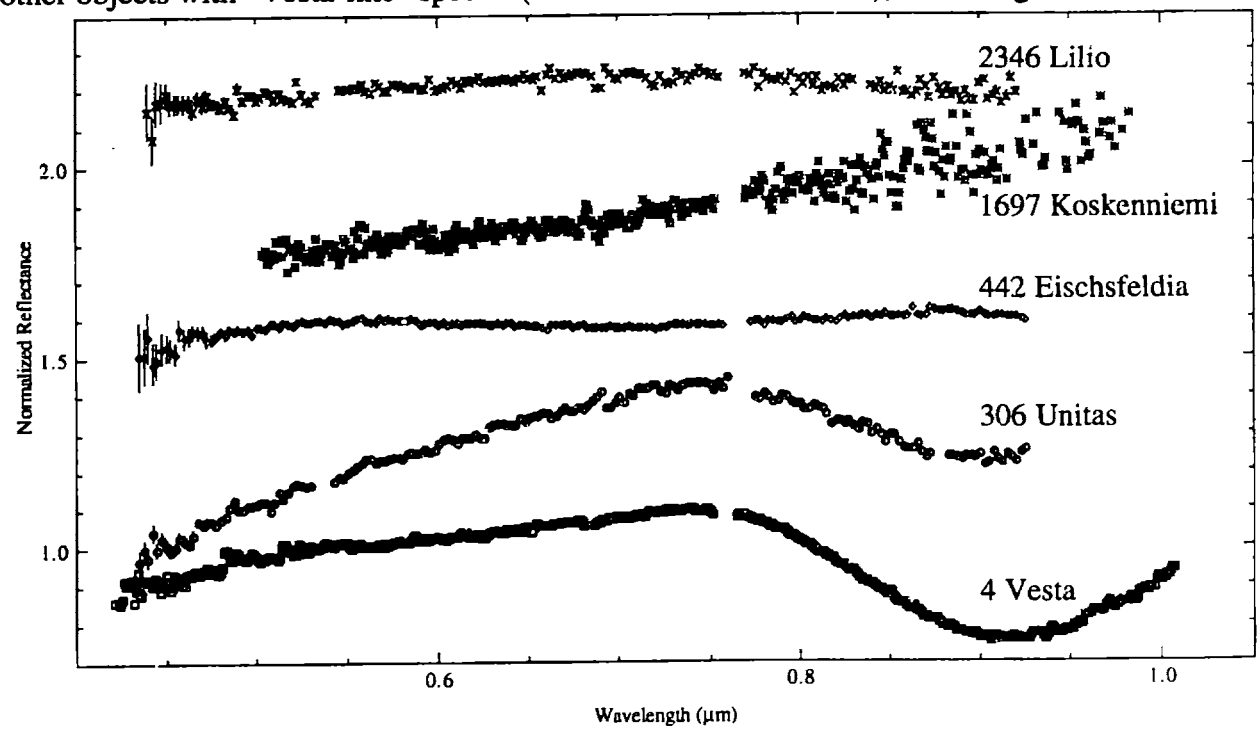

Figure 4.3. Reflectance spectra of large asteroids (diameters greater than 20 km) in the Vesta family. The spectra of Vesta, Naef, Tinchen and Kamo are from SMASS I (Xu *et al.*, 1995) and the spectra of Kollaa and Patterson are from SMASS II (Bus, 1999). All spectra are normalized to unity at 0.55 μm. Error bars are $\pm 1\sigma$.

All of the remaining objects have estimated diameters under ~10 km. (Lowering the estimated albedos of the V-class objects to 0.25 from 0.42 raises the diameters by ~2 km.) Thirteen asteroids with diameters less than 10 km were not classified as a V or a J. One object (Sq asteroid 3376 Armandhammer) was observed in the near-infrared and has spectra similar to other Vestoids. Other objects (e.g., Sr asteroid 5051 1984 SM, S asteroid 5108 Lübeck, R asteroid 5111 Jacliff) (Figure 4.4) have visible spectra similar to the Vestoids and eucrites showing that objects with "Vesta-like" spectra may be falling in a variety of different Bus (1999) classes.

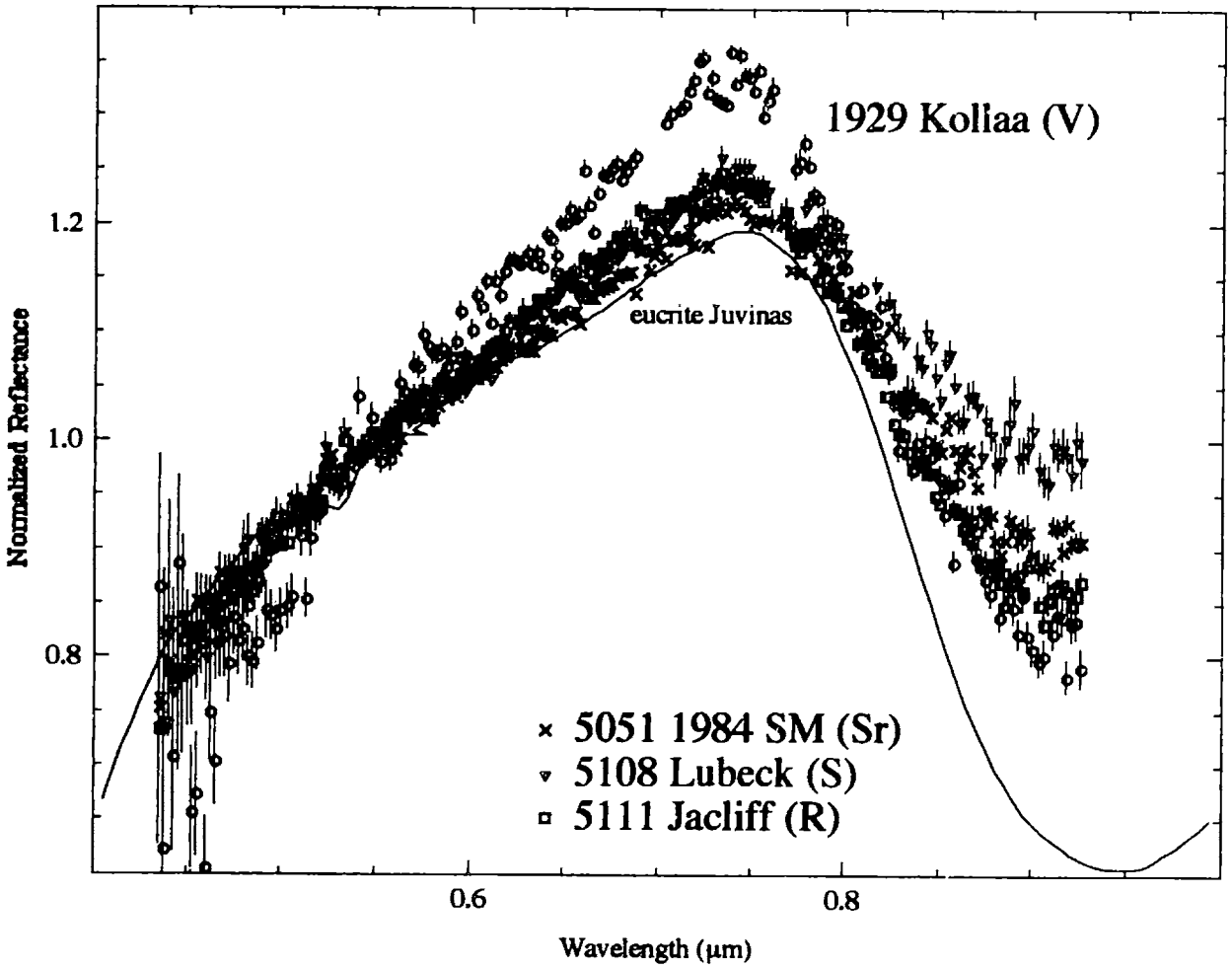

Figure 4.4. Reflectance spectra of Vesta family asteroids 1929 Kollaa (blue diamonds), 5051 1984 SM (black crosses), 5108 Lübeck (red upside-down triangles) and 5111 Jacliff (black squares) versus the spectrum of the eucrite Juvinas (Gaffey, 1976). The spectra are from SMASS II (Bus, 1999). All spectra are normalized to unity at 0.55 μm. Error bars are $\pm 1\sigma$.

Migliorini *et al.* (1995) has estimated the number of interlopers (which are not fragments of the original parent body) in families by modeling the density of background objects that should occupy the volume of the family in proper orbital element space. From their work, Marzari *et al.* (1996) concluded that the Vesta family should contain a fairly low number of

interlopers with ~10 up to 10 km in size and a few for larger sizes. Examination of visible spectra of Vesta family members indicates that ~15% of the observed objects under 10 km could be interlopers. If this percentage can be extrapolated to the whole Vesta family, the number of interlopers in the family would be estimated to be ~30 objects, which is higher than the number (~10) calculated by Marzari *et al.* (1996).

4.4 HED Spectra

4.4.1 Grain Size

To understand the spectral differences among the Vestoids and Vesta, the spectral diversity among the HEDs needs to be analyzed. Even though a large number of HED samples have had their spectra measured and samples of these meteorites are available for detailed chemical and spectral analyses, there has been little work on understanding the diversity of HED spectra. Figure 4.5 plots the range of HED spectra from Gaffey (1976).

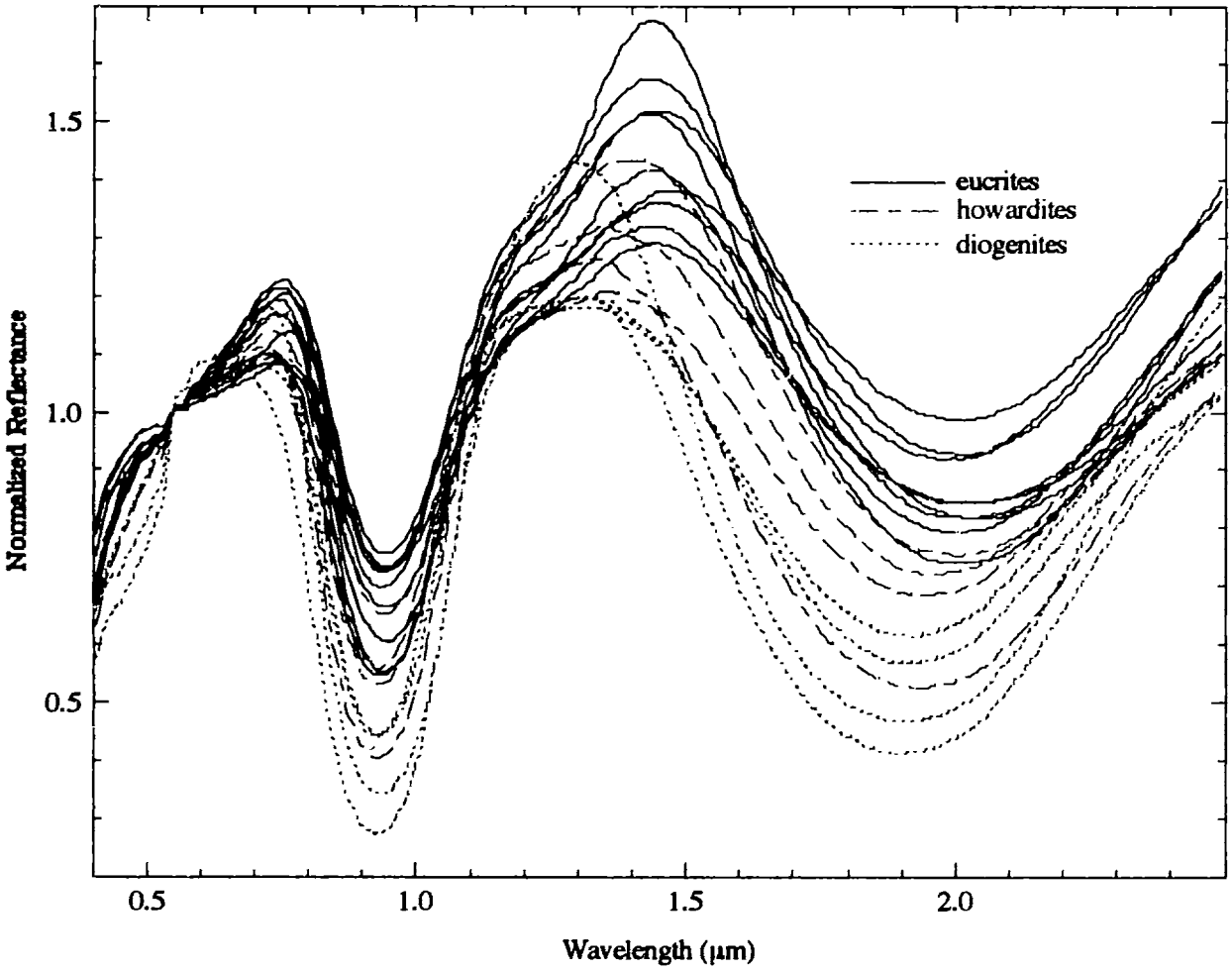

Figure 4.5. Reflectance spectra of eucrites (dark lines), howardites (red broken lines) and diogenites (blue dashed lines). All spectra are from Gaffey (1976). All spectra are normalized to unity at 0.55 μm.

As can be seen in the figure, there is a huge variety of spectral slopes and in the strength of the 1 and 2 μm features with the largest spread among the eucrites. There is also a substantial range in the strength of the UV features. These HED spectra were all measured for particle sizes somewhere between 30 and 300 μm at room temperature. Gaffey (1976) suggested that spectral differences among the eucrites could be due to a shock effect since one of the eucrites (Padvarninkai) with weak UV features and relatively flat spectral slopes had significant amounts of maskelynite (shock-produced glass), which forms from plagioclase.

Some eucrites from Gaffey (1976) with very similar compositions have very different spectral properties. For example, Juvinas (Figure 4.6) has a much stronger UV feature and a much redder spectral slope than Sioux County.

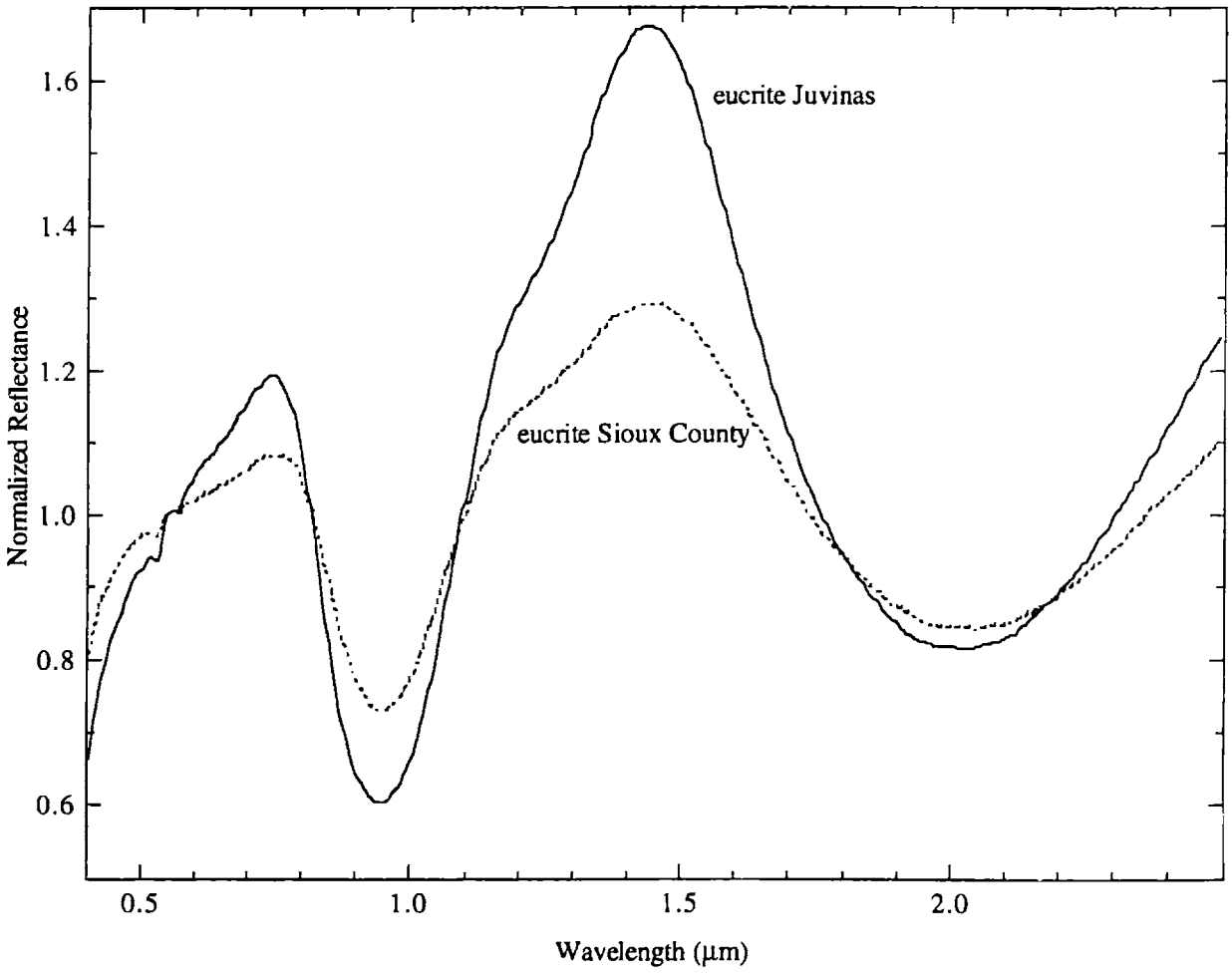

Figure 4.6. Reflectance spectra of eucrites Juvinas (black line) and Sioux County (dashed line). All spectra are from Gaffey (1976). All spectra are normalized to unity at 0.55 μm.

Compositionally, Sioux County and Juvinas are both brecciated, monomict, non-cumulate eucrites and have almost identical mineralogies (Table 4.3) (Kitts and Lodders, 1998). They are also believed to have similar cooling and reheating histories (Takeda and Graham, 1991). This implies that grain size, which were only roughly measured for these two meteorites, could be causing these spectral differences.

Table 4.3. Normative mineralogies of eucrites Juvinas and Sioux County from Kitts and Lodders (1998).

Vol.%	Juvinas	Sioux County
Pyroxene	52.1	51.5
Olivine	0	0
Plagioclase	43.6	44.2
Ilmenite	0.8	0.7
Chromite	0.2	0.3
Apatite	0.2	0.2
Quartz	3.1	3.0
Mineral composition (mol.%)		
Pyroxene	$En_{36}Fs_{49}Ws_{14}$	$En_{37}Fs_{50}Ws_{12}$
Plagioclase	$An_{89}Ab_{10}Or_{1}$	$An_{90}Ab_{9}Or_{1}$

Table 4.4 lists the HEDs that had spectra measured for this study. All of the Antarctic meteorites were chosen to be as unaltered as possible (weathering classes of A or A/B). Bulk particulate samples, where the samples were just crushed to a powder with particle sizes that could be as large as a millimeter, were measured to gain information on a size range that was not normally analyzed for most HEDs. INAA (instrumental neutron activation analysis) measurements were done on powdered samples to gain information on bulk chemical compositions. INAA involves exposing the sample to a flux of neutrons, which causes most of the elements within the sample to become radioactive. The energy of the radioactive emission allows identification of the element and the intensity of the emission is proportional to the mass of that element. A large number of elements were measured by INAA; however, only the major elements iron and calcium are given in Table 4.4. The iron abundances will primarily be from the pyroxene, plus a few other minor phases (e.g., iron sulfides, ilmenite, FeNi metal). The calcium abundance will be from both the feldspar and the pyroxenes.

Table 4.4. HEDs that had spectra measured for this study. The type, weathering indicator and ferrosilite (Fs) percentage for American Antarctic meteorites are from Grossman (1994). The type, weathering indicator and ferrosilite (Fs) percentage for Japanese Antarctic meteorites are from the *Catalog of the Antarctic Meteorites* (1995). Weathering class of "A" indicate minor rustiness, "B" indicates moderate rustiness, "C" indicates severe rustiness and "e" indicates evaporite minerals visible to the naked eye. Weight percents of FeO (error bars of approximately ±0.2) and CaO (error bars of approximately ±0.5) were calculated from INAA (instrumental neutron activation analysis) measurements of powdered samples at the Instrumental Neutron Activation Analysis Laboratory at Johnson Space Center. Bulk samples were just crushed to a powder with particle sizes that could be as large as a millimeter. INAA measurements were not done on Bouvante, EET 87503 and Macibini clast 3 samples. The American Antarctic samples were supplied by the Meteorite Working Group. The Japanese Antarctic samples were supplied by the National Institute of Polar Research.

				wt.%		Spectra Measured	
Meteorite	Type	Weathering	Fs %	FeO	CaO	Particle Sizes	temperature
ALHA76005	eucrite, polymict	A	37-57	18.5	9.8	< 250 μm, bulk	room
ALHA81001	eucrite, polymict	Ae	33-60	17.9	9.9	bulk	room
ALH 85001	eucrite, Mg-rich	A/B	32	14.3	7.6	bulk	room
Bouvante	eucrite, dimict		31-64			< 63 μm, < 250 μm, bulk	room
EETA79005	eucrite, polymict	A	30-61	16.6	9.3	< 250 μm, bulk	room
EET 83251	eucrite, polymict	B	14-58	18.1	8.3	< 63 μm, bulk	80-400 K
EET 87503	howardite	A	20-56			< 63 μm, 106-150 μm	80-400 K
EET 87542	eucrite, brecciated	A	24-55	20.7	10.2	bulk	room
EET 90020	eucrite, unbrecciated	A	40-55	20.7	10.0	bulk	room
LAP 91900	diogenite	A/B	23	15.4	9.0	bulk	room
LEW 87004	eucrite, polymict	A	31-56	18.8	8.9	bulk	room
Macibini clast 3	eucrite, polymict		30-60			< 63 μm	room
PCA 82501	eucrite, unbrecciated	A	41-57	18.6	10.4	bulk	room
PCA 82502	eucrite, unbrecciated	A	36-61	18.5	10.5	bulk	room
PCA 91007	eucrite, brecciated	A/Be	33-56	18.7	10.2	bulk	room
Y-75011	eucrite, polymict	A	27-48	19.0	9.7	bulk	room
Y-791186	eucrite, monomict		56-62	18.9	9.4	bulk	room
Y-792510	eucrite, monomict		60-64	21.3	8.9	bulk	room

Figure 4.7 plots the spectral characteristics of bulk-powder eucrite samples except for EET 90020, whose spectrum appears heavily weathered and will be discussed later. As can be seen in the figure, there is a huge range in spectral properties for the eucrites from spectrally blue (reflectance tends to decrease for increasing wavelength) to very red. Since meteorites with very similar compositions (e.g., unbrecciated eucrites PCA 82501 and PCA 82502, which are the two green lines in Figure 4.7) have very different spectral properties, the most likely cause of these spectral differences is grain size, which was not constrained very well in the preparation of these bulk-powder samples.

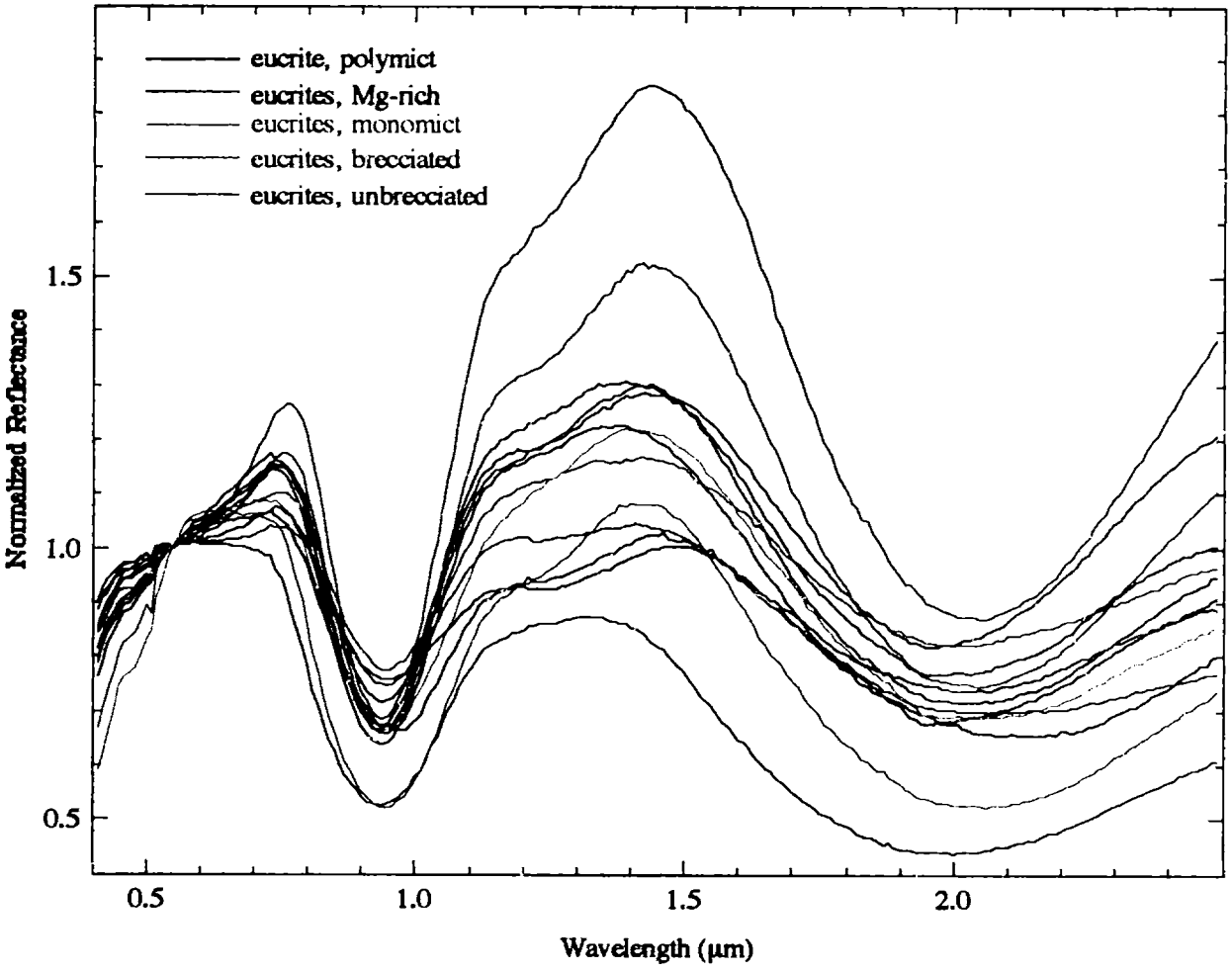

Figure 4.7. Reflectance spectra of bulk-powder eucrite samples from Antarctica. Polymict eucrites are plotted with black lines, the Mg-rich eucrite is plotted with a blue line, monomict eucrites are plotted with purple lines, brecciated eucrites are plotted with red lines and unbrecciated eucrites are plotted with green lines. The Meteorite Working Group supplied the American Antarctic eucrite samples. The Japanese Antarctic eucrite samples were supplied by the National Institute Polar Research. The spectra were measured at RELAB. All spectra are normalized to unity at 0.55 μm.

Figure 4.8 shows the difference in spectral characteristics for the bulk-powder samples and samples that were sieved to grain sizes less than 250 μm. For decreasing grain size, the UV features tend to become slightly stronger and the spectra tend to become redder. For these grain sizes, the spectra become redder by ~15%. The width of the 1 μm features does not significantly change for these grain sizes.

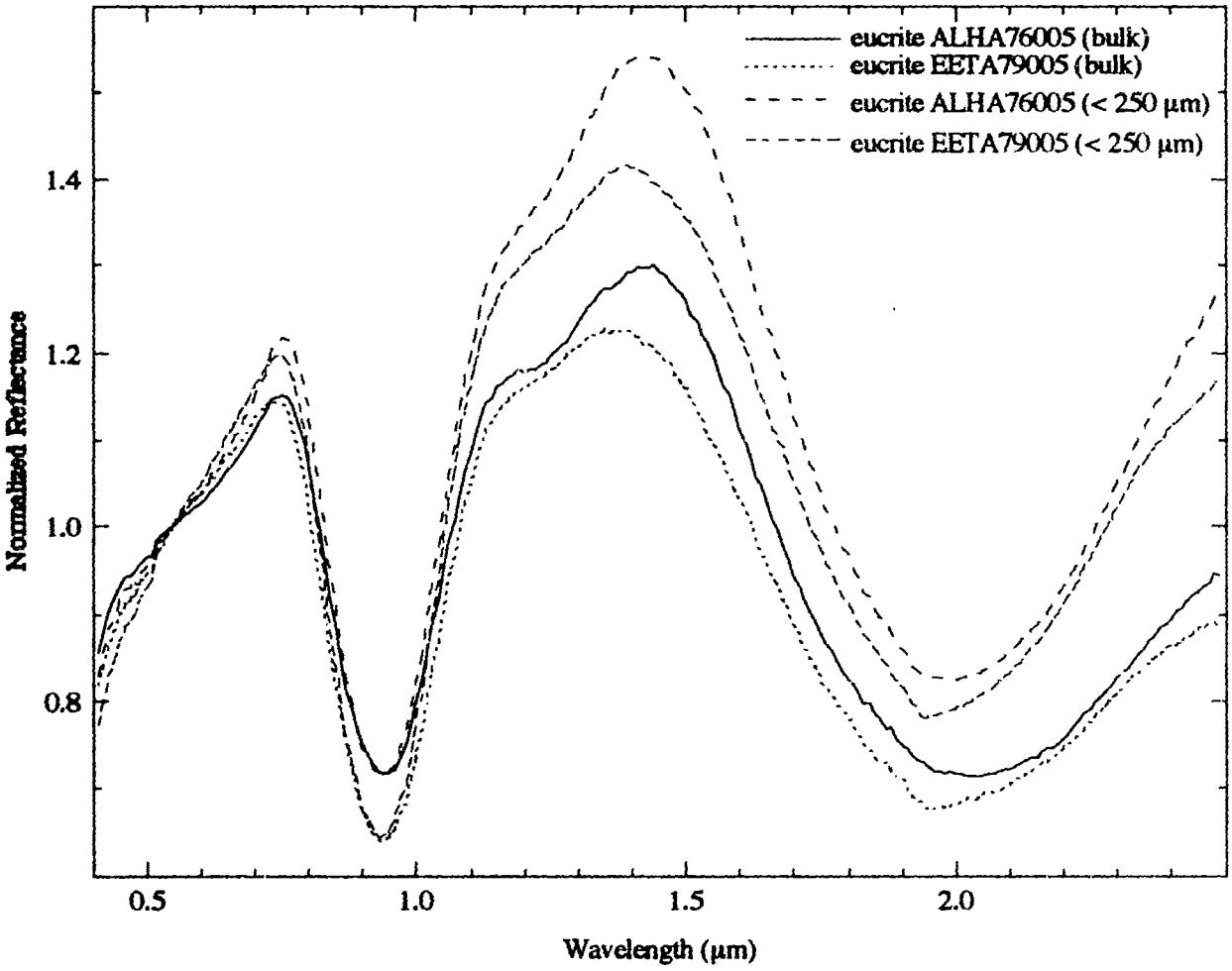

Figure 4.8. Reflectance spectra of different particle sizes (bulk powder and less than 250 μm) of eucrites ALHA76005 and EETA79005. The Meteorite Working Group supplied the eucrite samples. The spectra were measured at RELAB. All spectra are normalized to unity at 0.55 μm.

Figure 4.9 plots three different grain sizes for the eucrite Bouvante. The Bouvante spectrum for the particle size less than 25 μm (Hiroi, personal communication) has the reddest continuum slope of any measured HED with a normalized reflectance peaking at a value of almost 2.0. The width of the 1 μm feature becomes much narrower for the smallest particle size. The feature centered at 0.65 μm appears to be due to ilmenite ($FeTiO_3$) (Clark *et al.*, 1993), which is found as relatively coarse-grained (a few hundred microns) inclusions in Bouvante.

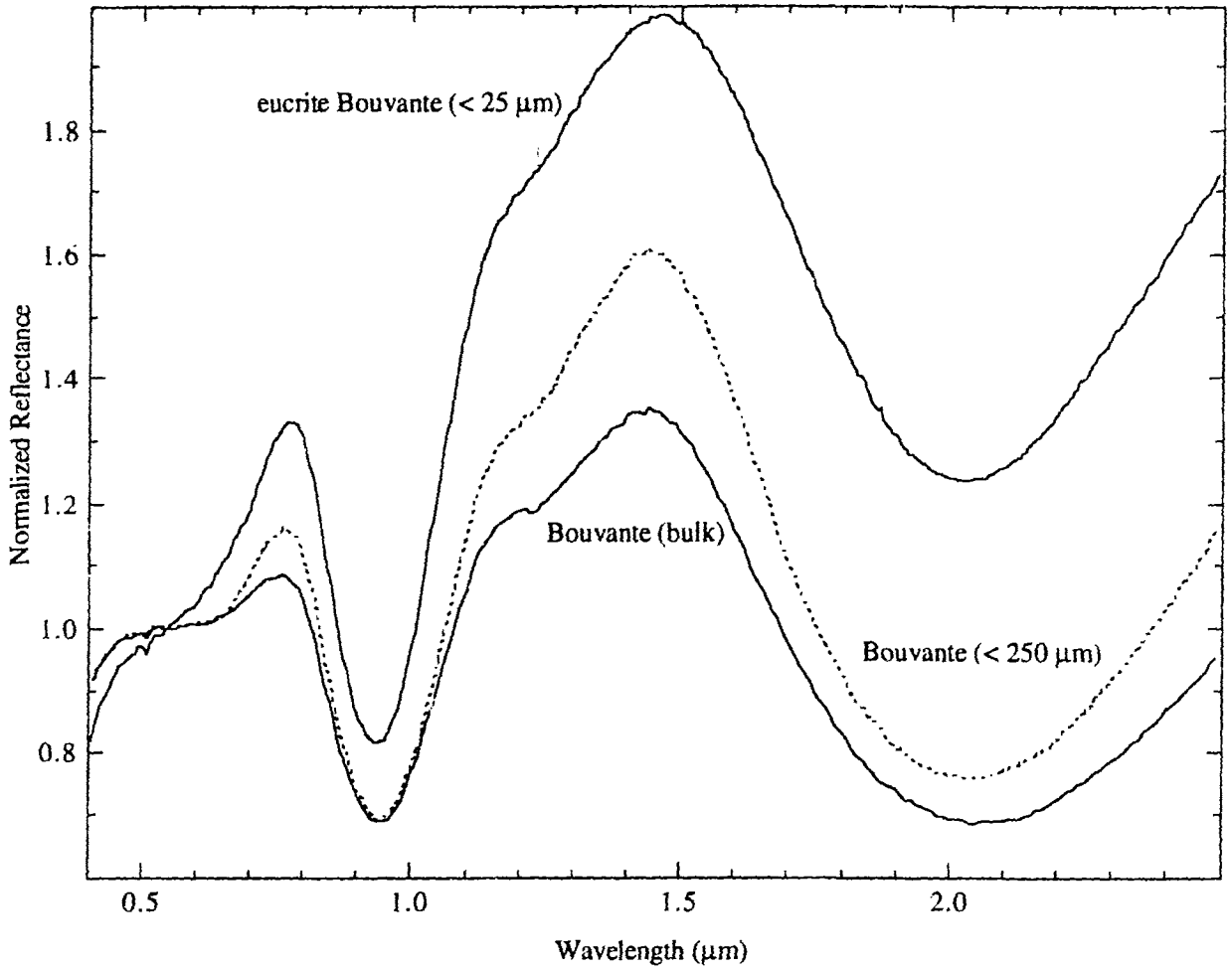

Figure 4.9. Reflectance spectra of different particle sizes (bulk powder, less than 250 μm and less than 25 μm) of eucrite Bouvante. The American Museum of Natural History supplied the sample where the two largest size samples of Bouvante were taken from. These spectra were measured at RELAB. The spectrum of the smallest size sample of Bouvante is from Hiroi (personal communication) for a sample borrowed from the Paris Museum of Natural History and was measured at RELAB. All spectra are normalized to unity at 0.55 μm.

The normative composition of Bouvante is 56 vol.% pyroxene, 36% plagioclase, 1% ilmenite and 6% quartz (glass) (Kitts and Lodders, 1998). The average pyroxene composition from a thin section of Bouvante was found to be $En_{32.8}Fs_{54.8}Wo_{12.4}$ (Buchanan, personal communication). Bouvante is a brecciated, dimict, noncumulate meteorite (Delaney *et al.*, 1984; Kitts and Lodders, 1998). (A dimict eucrite contains material derived from two different types

of rocks.) The pyroxenes in Bouvante fall at the Fe-rich end of the eucritic range (Christophe Michel-Levy *et al.*, 1987). Bouvante does have one of the highest abundances (two to three times the average eucrite) of incompatible trace elements of any known eucrite (Palme and Rammensee, 1981; Christophe Michel-Levy *et al.*, 1987). Incompatible elements tend to be abundant in the liquid phase. This high abundance of incompatible trace elements indicates a very low degree of partial melting of a primitive achondritic source relative to other eucrites since the first melt will be enriched in these elements relative to later ones. However, these trace elements (e.g., La, Sm, Ta, W) should not have any effect on the spectral properties of pyroxene since the spectra of pyroxenes tend to be controlled by the major elements such as iron, calcium and pyroxene.

4.4.2 Glass

Wasson *et al.* (1997) have shown that the formation of glass in HEDs, through laser impulse irradiation, can redden (by ~30%) HED spectra (Figure 4.10). Yamada *et al.* (1999) obtained similar results for his laser experiments on terrestrial pyroxenes at lower energies and shorter timescales for the pulse. Irradiation by a laser is used to duplicate the energy supplied by the impact of micrometeorites on the surface of an asteroid. Work by Bell *et al.* (1976) has shown that the spectral properties of glass are a function of composition.

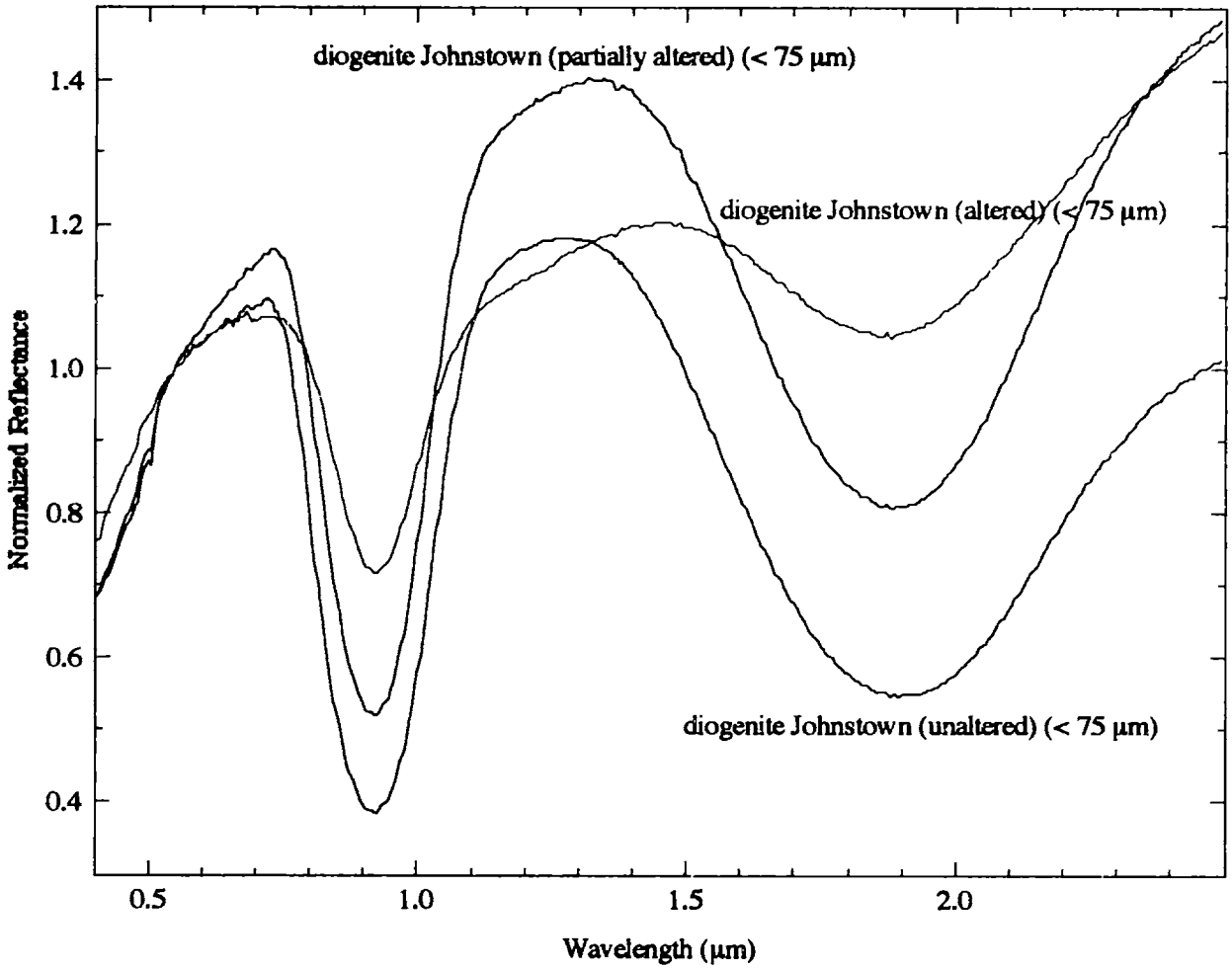

Figure 4.10. Reflectance spectra of diogenite Johnstown (particle size less than 75 μm) for unaltered (lower black line), partially altered (red line) and altered samples (top black line). The spectra are from Wasson *et al.* (1997). All spectra are normalized to unity at 0.55 μm.

The altered sample contains more altered material (glass) than the partially altered sample. It is unclear why the spectra reddens and then becomes less red as more glass is produced during the Wasson *et al.* (1997) experiments. The altered diogenite sample also has a much weaker 1 μm feature. The turnover between the 1 and 2 μm feature also moves to longer wavelengths (becoming more "eucrite-like", as the sample becomes more altered.

To see the effects of naturally-formed glass, samples of glass-rich HEDs had their spectra measured (Figure 4.11). These samples included a clast from Macibini (Buchanan *et al.*, 2000) and the eucrite Padvarninkai (Gaffey, 1976; Hiroi *et al.*, 1995). (A clast is a multi-grained fragment of rock, which hopefully provides a representative sample of the texture and composition of the original material.)

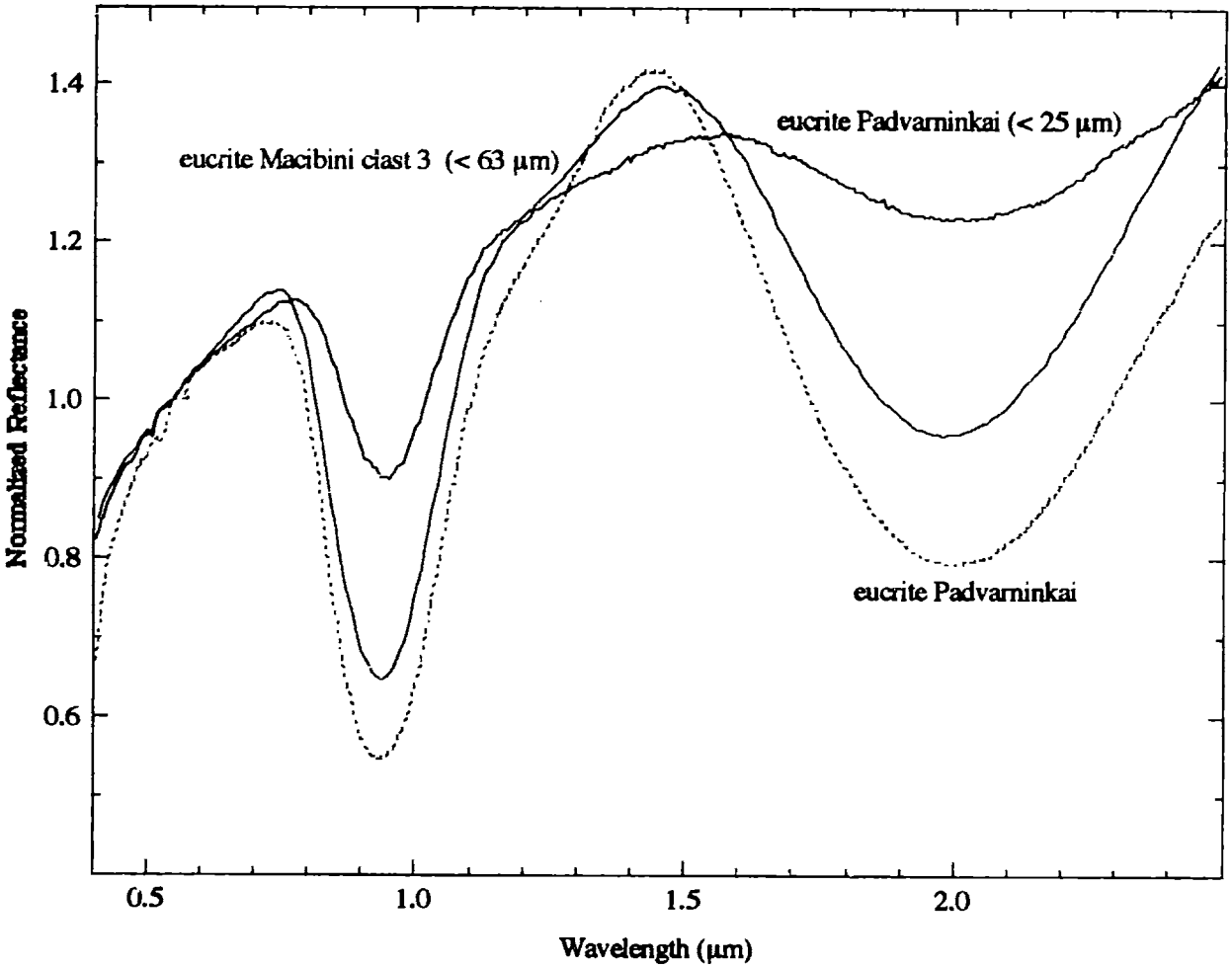

Figure 4.11. Reflectance spectra of eucrite Padvarninkai (dark and dashed lines) and eucrite Macibini clast 3 (particle size less than 63 μm) (red line). The Padvarninkai spectrum for particle sizes less than 63 μm is from Hiroi *et al.* (1995) and the other Padvarninkai spectrum is from Gaffey (1976). The Macibini sample is from the Transvaal Museum in South Africa. Buchanan (personal communication) supplied the sample. The spectrum was measured at RELAB. All spectra are normalized to unity at 0.55 μm.

The Macibini clast is approximately 50% glassy material and 50% silicates (Buchanan, personal communication). Padvarninkai is the most highly shocked eucrite known (Yamaguchi *et al.*, 1993) with most plagioclase converted to maskelynite. Padvarninkai also contains a significant amount of glass. The very fine-grained Padvarninkai has a much narrower 1 μm feature, a much weaker band depth and a turnover between the 1 and 2 μm features at a longer wavelength than the coarser-grained sample. These spectral differences could be due to a higher

glass component in the finer-grained sample. These meteorites are not noticeably reddened compared to other HEDs.

4.4.3 Terrestrial Weathering

Terrestrial weathering does not appear to be causing the reddening. One spectrum (EET 90020) (Figure 4.12) has an intense UV feature, which is not apparent in other eucrite spectra. Visual inspection of the meteorites showed them to have the characteristic grayish color of eucrites except for EET 90020, which was reddish-brown. All Antarctic HED spectra have 3 μm features, indicating some terrestrial alteration due to water has taken place, but the alteration does not appear to be significantly affecting their reflectance spectra in most cases.

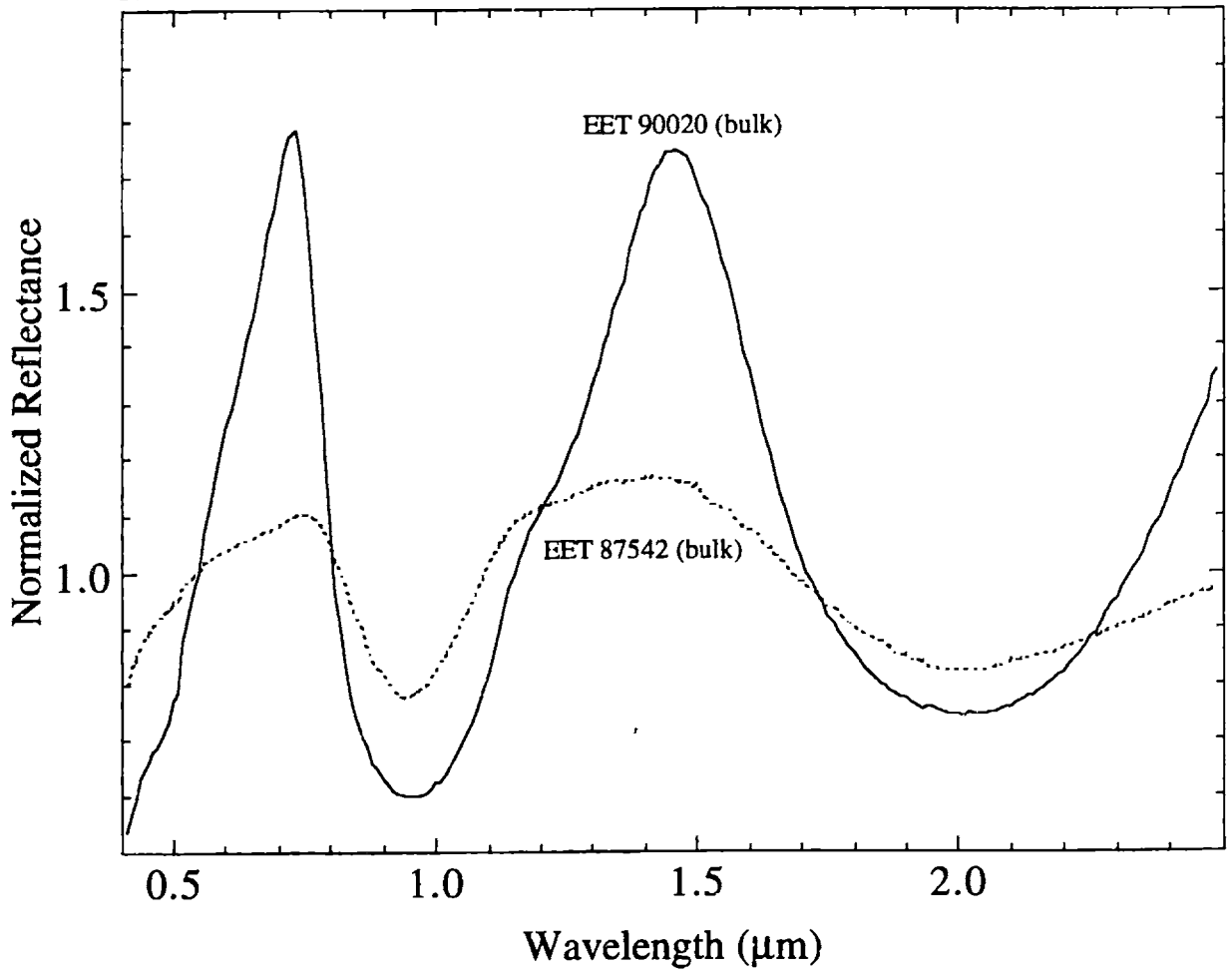

Figure 4.12. Reflectance spectra of eucrites EET 90020 (bulk powder) (black line) and EET 87542 (bulk powder) (dashed line). The Meteorite Working Group supplied the eucrite samples. Their spectra were measured at RELAB. All spectra are normalized to unity at 0.55 μm.

4.4.4 Temperature

Figure 4.13 plots reflectance spectra for room (300 K) and low (120 K) temperature spectra of an eucrite. At low temperatures, there is a narrowing of the width of the 1 μm band by ~15%. There is no significant reddening or change in the strength of the UV feature. The considerable amount of noise at ~0.9 and ~2.4 μm is due to low counting statistics.

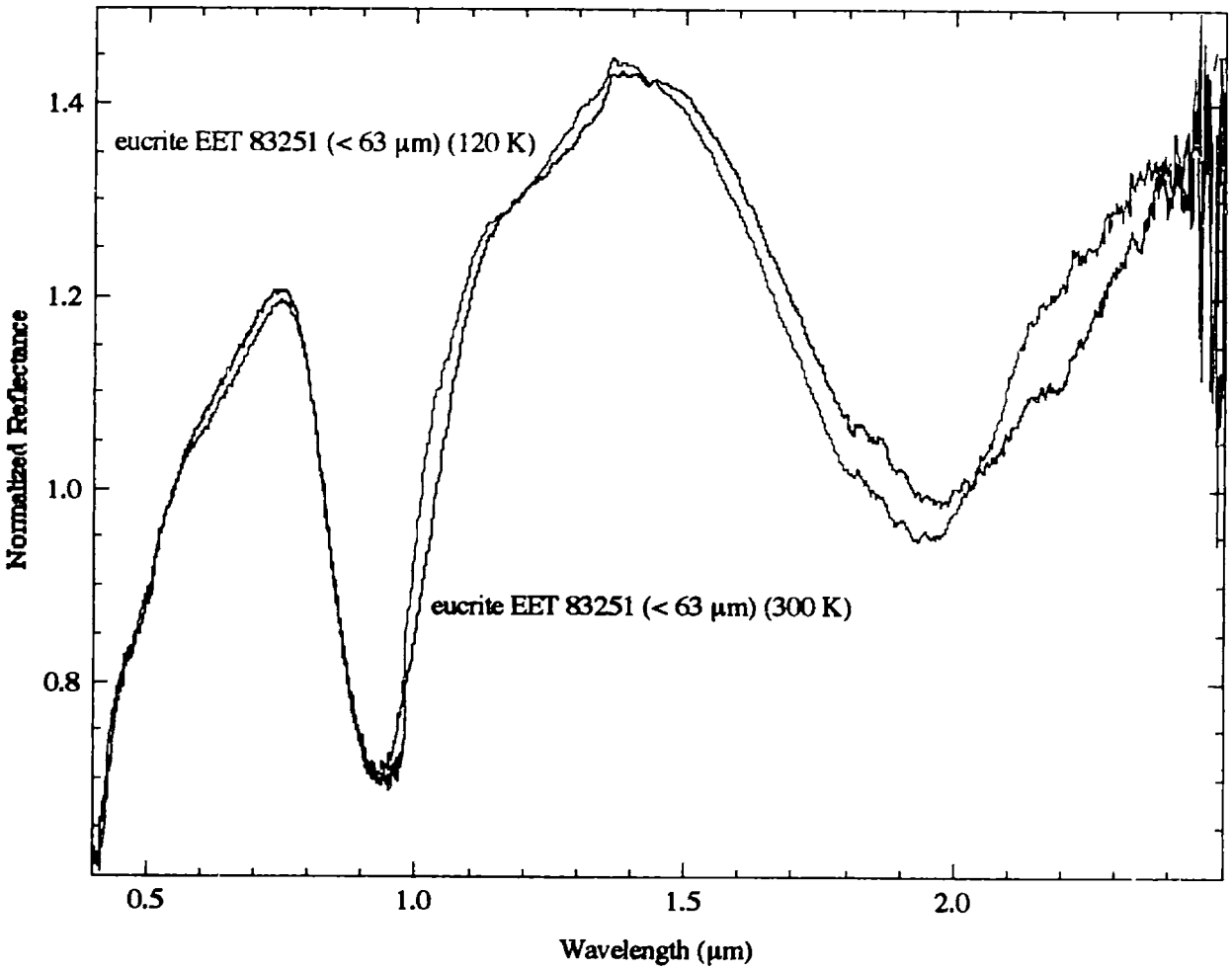

Figure 4.13. Reflectance spectra of eucrite EET 83251 (particle size less than 63 μm) at room (300 K) (black line) and low (120 K) (blue line) low temperatures. The Meteorite Working Group supplied the sample of EET 83251. The spectrum is from Hinrichs (personal communication) and taken at the Planetary Geosciences/HIGP spectrometer facility at the University of Hawai'i. All spectra are normalized to unity at 0.55 μm.

Figure 4.14 plots room (300 K) and low (120 K) temperature reflectance spectra of a howardite for different grain sizes. For the howardite samples, decreasing the temperature weakens the strength of the UV feature. For the smaller particle sizes, there is a slight decrease in the reflectance value of the ~1.4 μm peak at the lower temperature. As can be seen in the figure, the spectral differences due to grain size are much larger than those due to temperature changes. The smaller grain size samples have much stronger UV features and much redder spectral slopes.

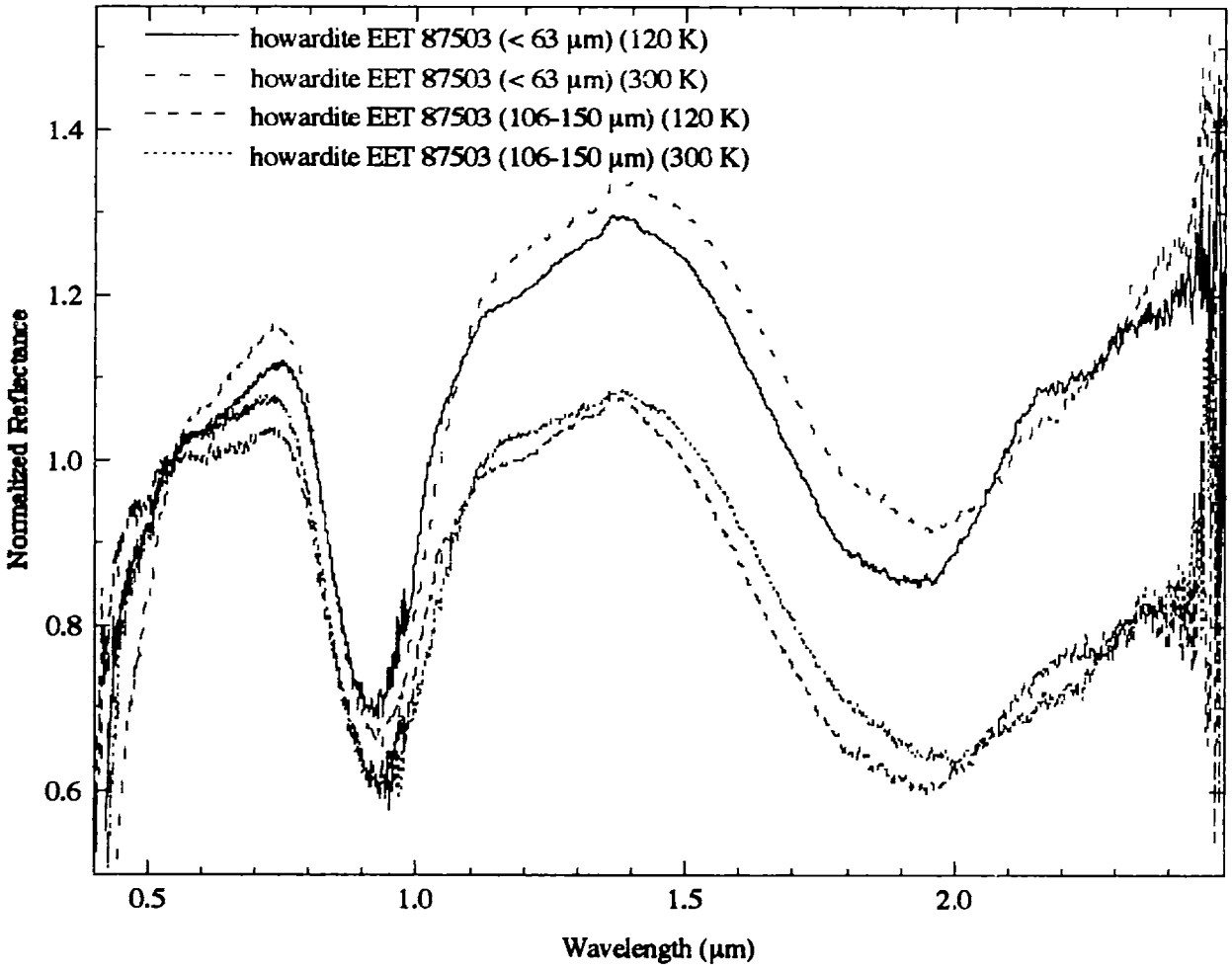

Figure 4.14. Reflectance spectra of howardite EET 87503 (particle size less than 63 μm and between 106 and 150 μm) at room (300 K) and low (120 K) temperatures. The Meteorite Working Group supplied the sample of EET 83251. The meteorite spectra are from Hinrichs (personal communication) and taken at the Planetary Geosciences/HIGP spectrometer facility at the University of Hawai'i. All spectra are normalized to unity at 0.55 μm.

4.4.5 Conclusions from HED Spectra

The preceding discussion shows that most of the spectral diversity among the HEDs in the strength of the UV feature and spectral slope can be explained by differences in grain size. Small grain sizes and low temperatures will also tend to narrow the width of the 1 μm feature.

Low temperatures do not noticeably change the spectral slope or the strength of the UV feature. The glass found naturally in HEDs does not seem to noticeably redden their spectra; however, laboratory experiments have shown that glass formed by irradiation by lasers can also redden HED spectra.

4.5 Vesta

Figure 4.15 plots the SMASSIR spectrum of Vesta versus the 52-color spectrum (Bell *et al.*, 1988). The SMASS I spectrum (Xu *et al.*, 1995) is used because it is a better match to the ECAS and 52-color data than the SMASS II spectrum. The SMASSIR spectrum matches the 52-color spectrum very well out to ~1.35 μm, but is offset by ~5% from the 52-color data past 1.5 μm. It is unclear if this offset is real since the rest of the spectrum matches so well.

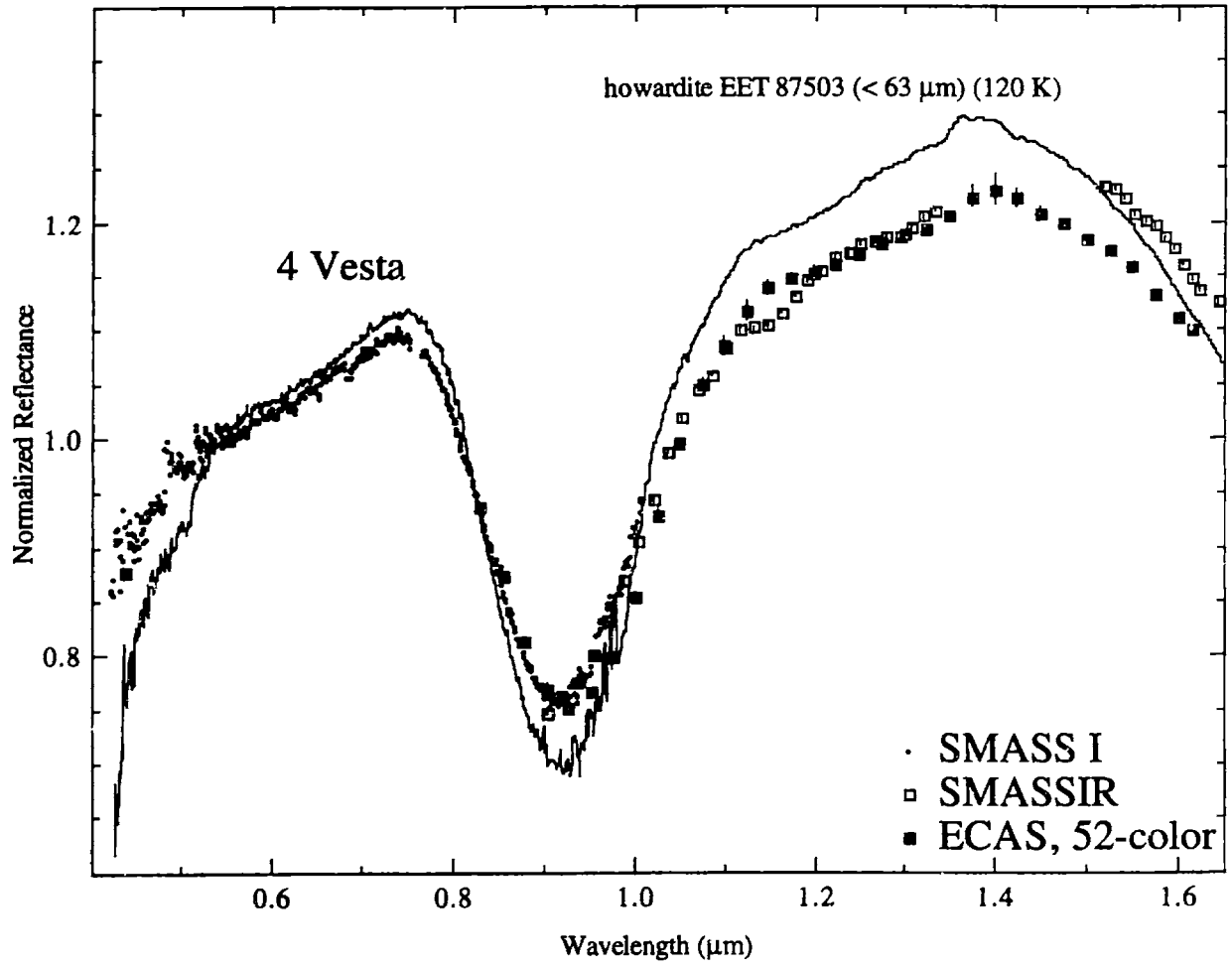

Figure 4.15. Reflectance spectra of 4 Vesta versus howardite EET 87503 (< 63 μm) (120 K). Small dots are from SMASS I (Xu *et al.*, 1995) and open squares are from SMASSIR. The dark squares are a combination of ECAS (Zellner *et al.*, 1985) and 52-color data (Bell *et al.*, 1988). All spectra are normalized to unity at 0.55 μm. Error bars are ±1σ.

Due to Vesta's brightness, the telescope had to be defocused to obtain a usable spectrum and a defocused Hyades 64 was used as the standard star. No other objects were observed in this manner, so it is unclear if problems in the spectral slope could arise from this procedure. Vesta is also known to have rotational variations (Gaffey, 1997). The low-temperature spectrum of howardite EET 87503 matches the UV feature strength and the width and depth of Vesta's 1 μm feature moderately well, but is slightly redder than Vesta past 1.1 μm. Increasing slightly the particle size of the howardite would result in a better match by slightly reducing the spectral slope.

4.6 Vestoids in the Vesta Family

Vesta and fourteen Vestoids (including 3376 Armandhammer) in the Vesta family were all observed in SMASSIR (Figure 4.16). All of the measured objects had the distinctive 1 and 2 μm features due to pyroxene.

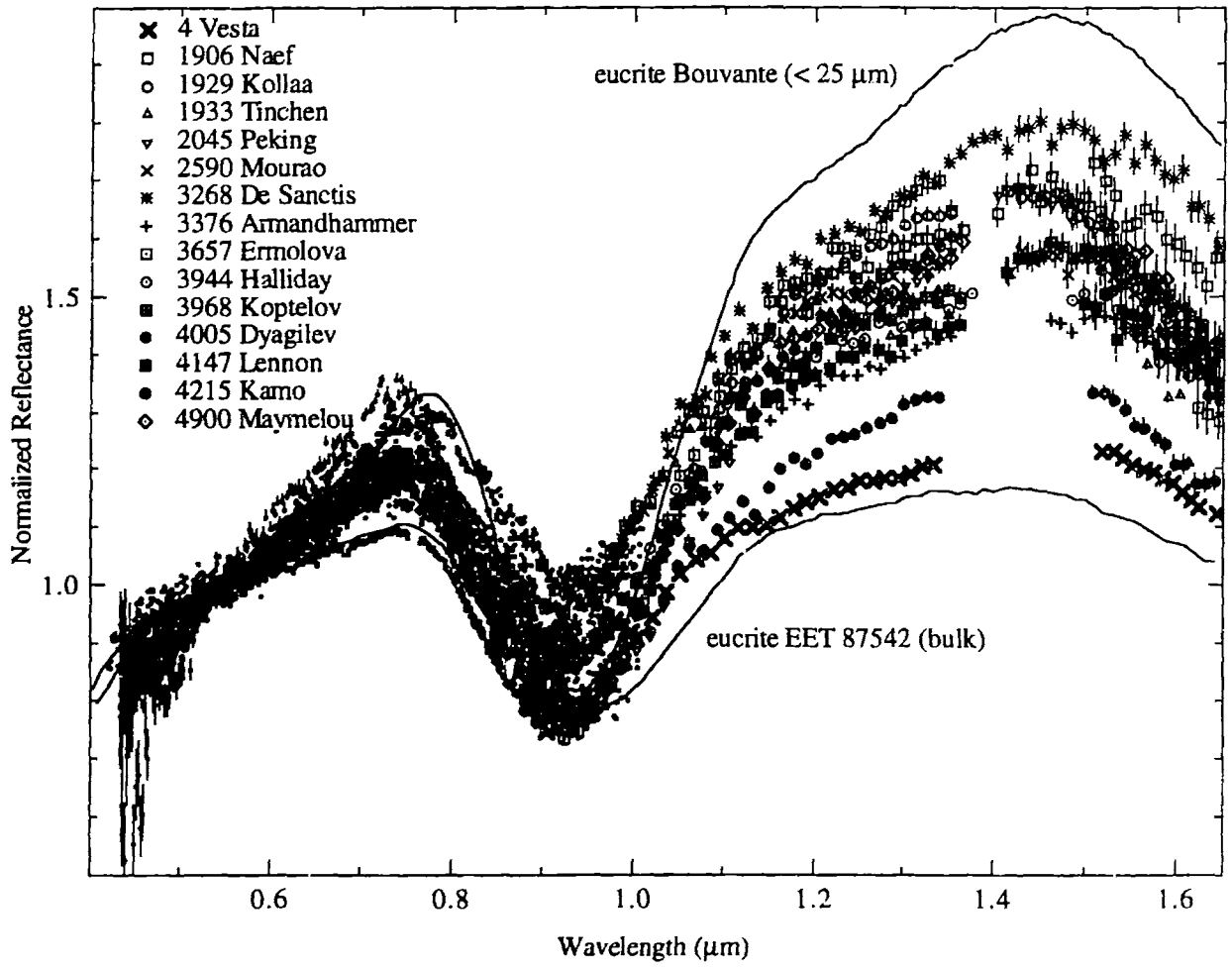

Figure 4.16. Reflectance spectra of Vesta and the smaller Vestoids in the Vesta family versus the spectra of eucrites Bouvante (particle size less than 25 μm) and EET 87542 (bulk powder). Small dots are from SMASS I (Xu *et al.*, 1995) and open squares are from SMASSIR. All spectra are normalized to unity at 0.55 μm. Error bars are ±1σ.

These objects can be seen to be much redder than Vesta; however, their spectra tend to fall intermediate between the spectra of eucrites Bouvante (particle size < 25 μm) and EET 87542 (bulk powder). Except for 4 Vesta and 4215 Kamo (the least red-sloped objects), all of the objects have a very continuous range of spectral properties. All of these objects have band minima between 0.91 and 0.93 μm (error bars of ±0.02 μm), which are consistent with the minima for the HEDs (0.92 to 0.94 μm).

The distinctive pyroxene features of these measured Vesta family members appears to be almost certain evidence that these objects are fragments of Vesta. The spectral differences (strength of their UV features and continuum slopes) between different objects could be primarily due to particle size; however, it is appears very difficult to completely rule out other effects such as slight differences in mineralogy or glass abundances.

One important question is "Why are the small Vestoids so much redder than Vesta?" Vesta's surface would be expected to be much older than those of the Vestoids and, therefore, much finer-grained since it would have experienced a much larger degree of micrometeorite impacts. However, the redder spectra of the Vestoids would argue that they have finer-grained surfaces. One possibility is that the higher degree of impact-related effects have caused Vesta's surface to be much glassier than the surfaces of the Vesta family members. Vesta's surface would be like the glass-rich samples measured in Figure 4.11, which are not as red as the fine-grained samples in Figure 4.9.

The two asteroids (3268 De Sanctis and 4215 Kamo) at the extremes of the spectral range of the Vestoids are plotted in Figure 4.17. Besides a large difference in spectral slope, there is an approximately 30% difference between the band widths of these objects. (The band width is the length of a line from the middle of the short wavelength side of the 1 μm feature.) For eucrites, the band width should decrease and the spectral slope should increase as you go to the finest particle sizes, such as the fine-grained (less than 63 μm) sample of Bouvante in Figure 4.9. However, excluding De Sanctis and Kamo, there was no correlation between the band widths and spectral slopes among the Vestoids. This could indicate that other factors (such as the amount of opaques and glass on the surface) are also affecting the band widths and spectral slopes.

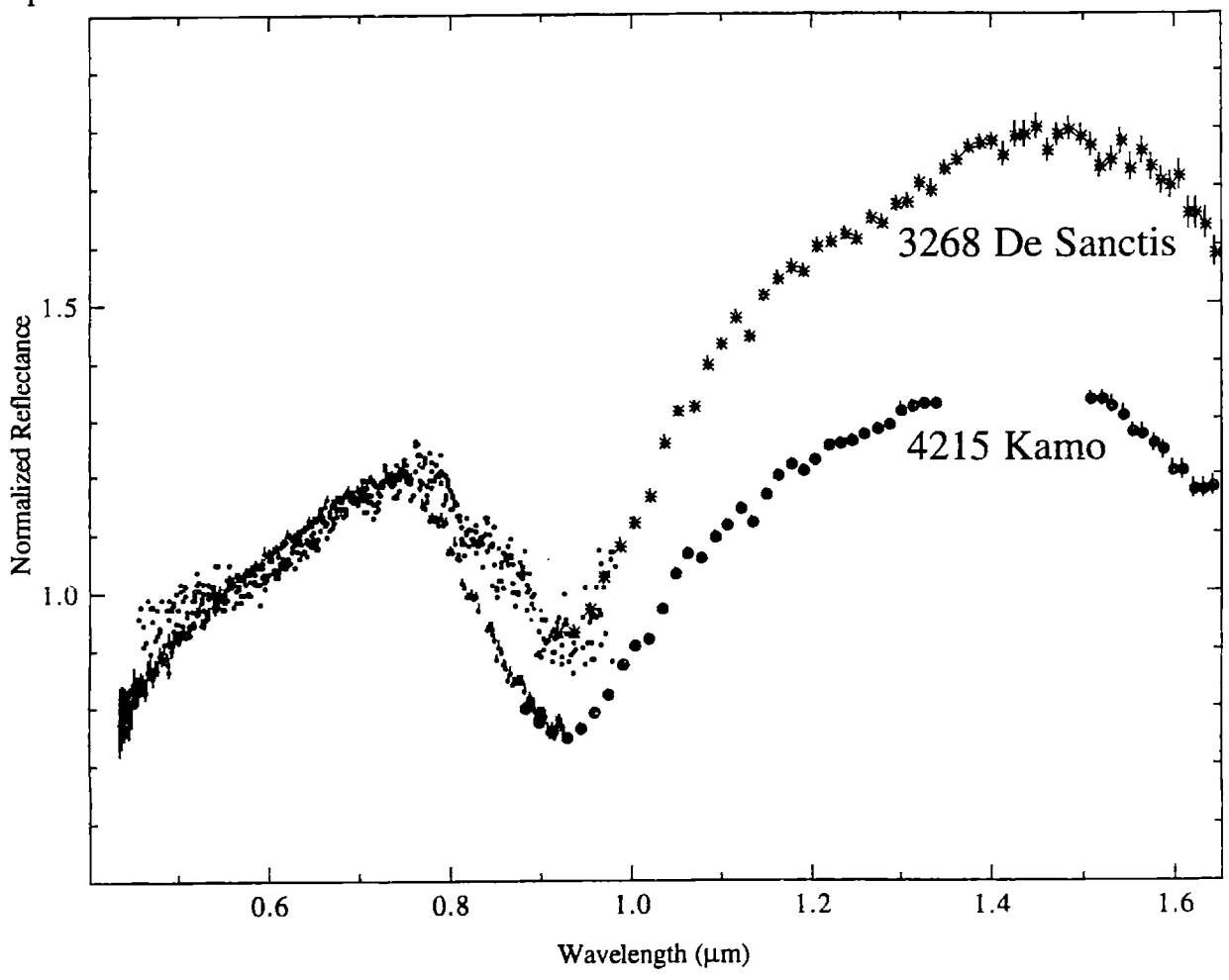

Figure 4.17. Reflectance spectra of Vestoids 3268 De Sanctis and 4215 Kamo. Small dots are from SMASS I (Xu *et al.*, 1995) and open squares are from SMASSIR. All spectra are normalized to unity at 0.55 μm. Error bars are ±1σ.

The asteroids classified as J objects in SMASS I and observed in SMASSIR are plotted in Figure 4.18. As can be seen in the figure, these three objects bear more resemblance to eucrites than diogenites with turnovers between the 1 and 2 μm features at much higher wavelengths (by

at least 0.1 μm) than the diogenite turnover. None of the Vestoids have surfaces that resemble diogenites. It may be much easier to eject 10-km fragments with eucrite/howardite surface compositions than objects with predominately diogenite surfaces. Impacts may not be able to penetrate to depths where the ejected 10-km objects are composed almost entirely of diogenite fragments. It may be much easier to eject smaller diogenite samples, which would land on earth as meteorites. Estimates for the formation region of the diogenites on Vesta vary from depths of ~23 to ~42 km (Ruzicka *et al.*, 1997) to ~130 km (Grove and Bartels, 1992), depending on the fractional crystallization model and pressures needed to produce the diogenites from assumed initial compositions. Impacts on Vesta, such as the one that produced the 460-km diameter basin on Vesta (Thomas *et al.*, 1997b), are expected to sample depths of ~30-40 km (Asphaug, personal communication).

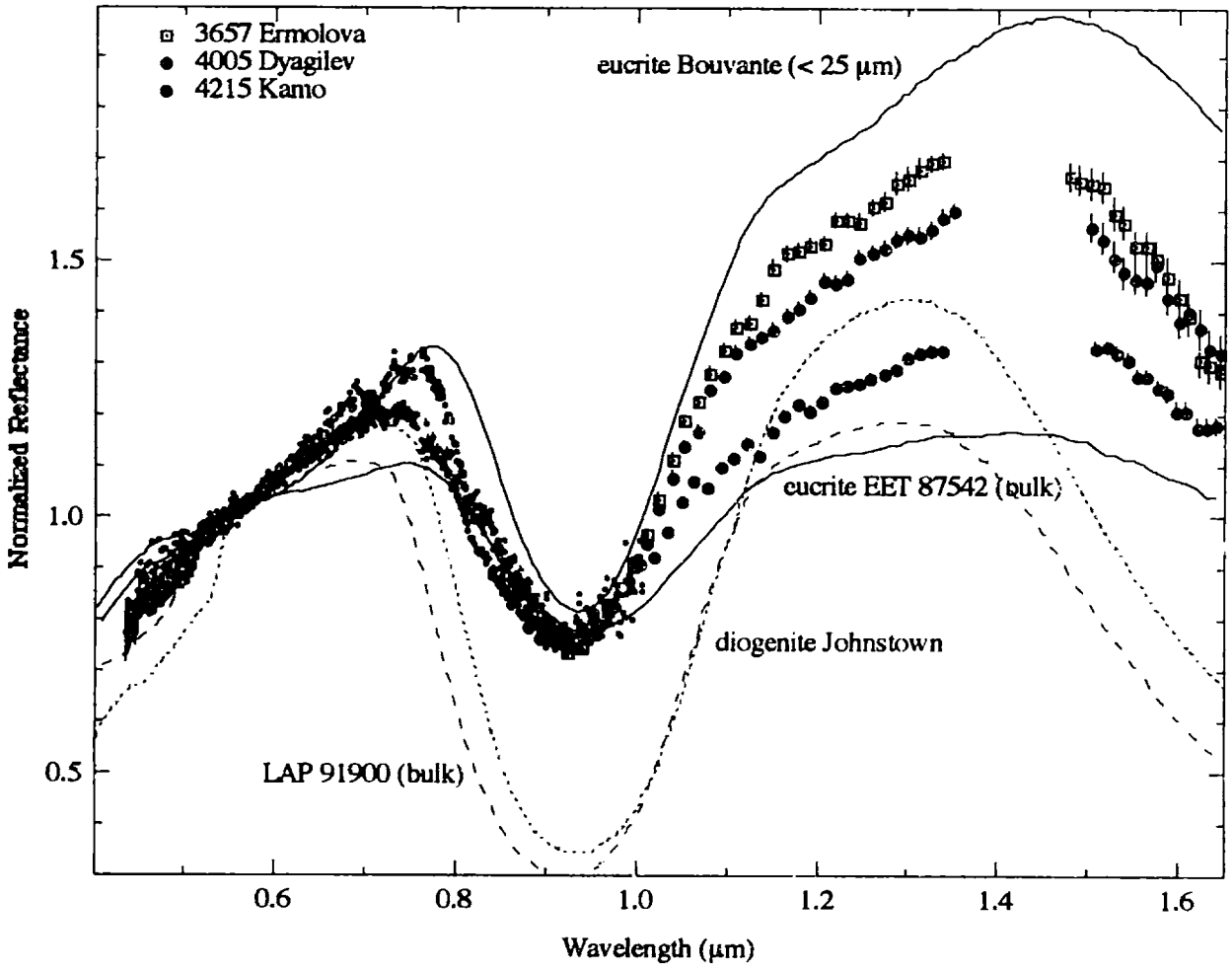

Figure 4.18. Reflectance spectra of J asteroids 3657 Ermolova, 4005 Dyagilev and 4215 Kamo versus the spectra of eucrites Bouvante (particle size less than 25 μm) and EET 87542 (bulk powder) and also diogenites Johnstown (blue dashed line) (Gaffey, 1976) and LAP 91900 (bulk powder) (red dashed line). Small dots are from SMASS I (Xu *et al.*, 1995) and open squares are from SMASSIR. All spectra are normalized to unity at 0.55 μm. Error bars are $\pm 1\sigma$.

4.7 Vestoids Outside the Vesta Family

Six main-belt Vestoids were observed in SMASSIR with the spectra shown in Figure 4.19. Except for 2579 Spartacus, their spectra also tend to fall intermediate between the spectra of eucrites Bouvante (particle size < 25 μm) and EET 87542 (bulk powder). Except for Spartacus (2.21 AU), these observed non-family main-belt Vesta-like objects (~2.34 to ~2.48 AU) are all located relatively near the Vesta family (~2.30 to ~2.45 AU) and just fall out of the "defined" Vesta family in at least one of the proper elements.

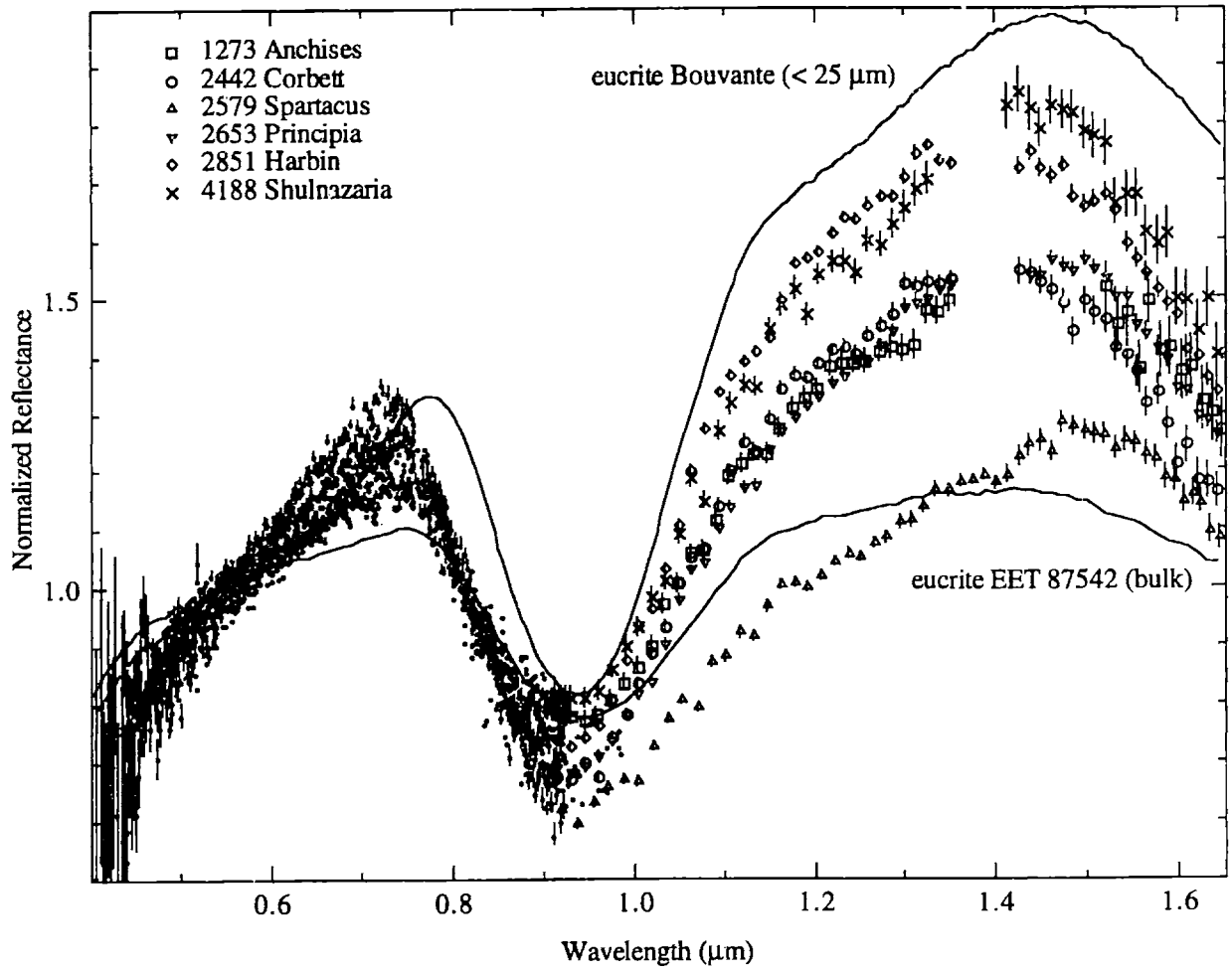

Figure 4.19. Reflectance spectra of V asteroids outside the Vesta family versus the spectra of eucrites Bouvante (particle size less than 25 μm) and EET 87542 (powder). Small dots are from SMASS I (Xu *et al.*, 1995) and open squares are from SMASSIR. All spectra are normalized to unity at 0.55 μm. Error bars are ±1σ.

The longer wavelength position (~1.5 μm) of the turnover between the 1 and 2 μm features in Spartacus' spectrum compared to the other Vestoids (~1.4 μm) implies a phase such as olivine or clinopyroxene, which would drive the turnover to a longer wavelength. The broader 1 μm feature implies that it is olivine. Spartacus is plotted (Figure 4.20) versus eucrite ALHA76005 and lodranite MAC 88177. MAC 88177 has a normative mineralogy of 39%

olivine, 44% orthopyroxene, 6% clinopyroxene and 11% metal and opaques (Hiroi *et al.*, 1993a). The spectrum of MAC 88177 bears some resemblance in structure to Spartacus; however, their UV features have different strengths and Spartacus' 1 μm band is deeper while its 2 μm band appears to be deeper. It is unclear if these spectral differences are just due to a smaller grain size on Spartacus or due to differences in mineralogy. Spartacus' unusual spectrum indicates that not all V asteroids have near-infrared spectra similar to measured HEDs. Spartacus could also be an olivine-rich HED; however, its far location from the Vesta family (~0.1 AU) lessens any argument that this asteroid has to be a fragment of Vesta.

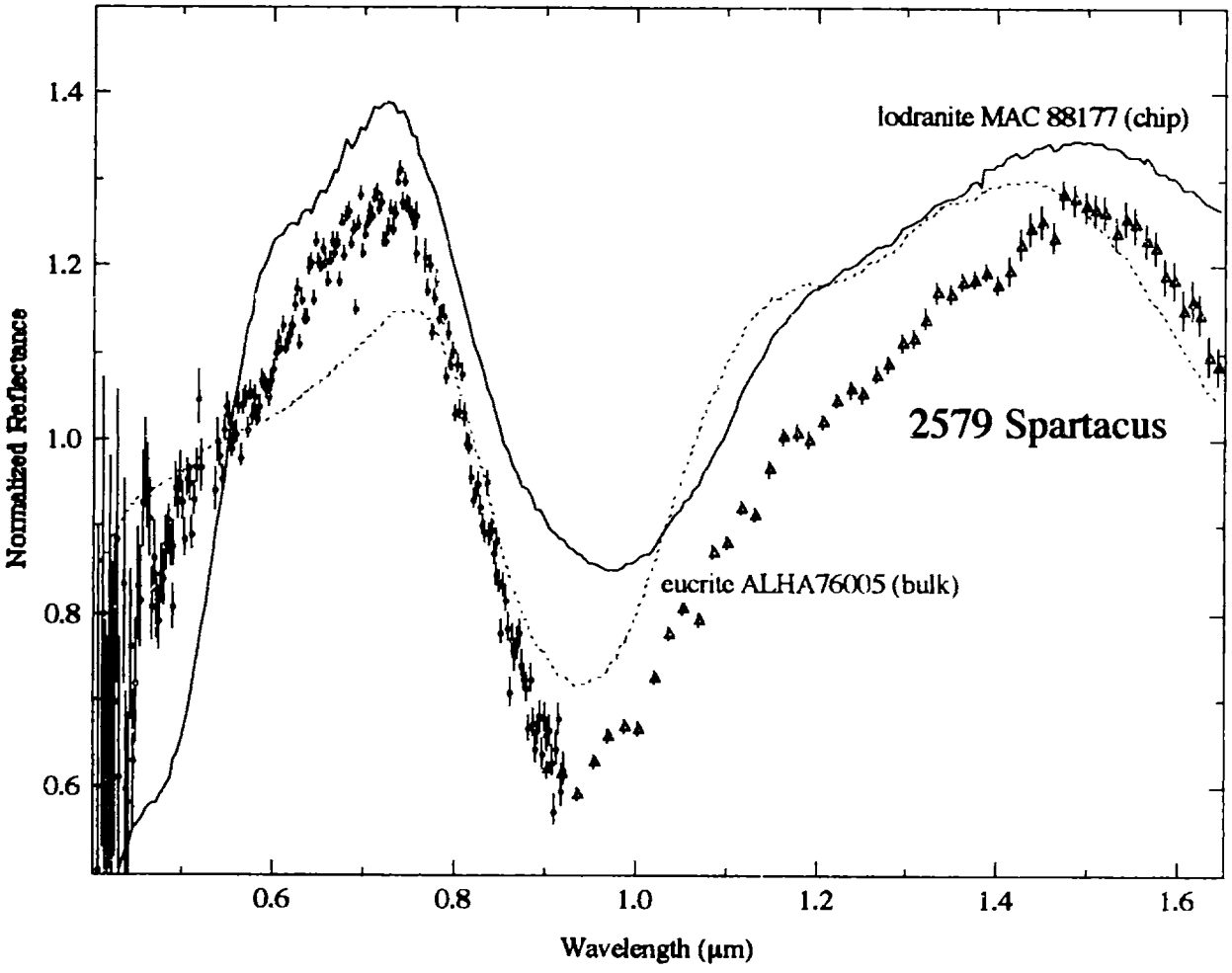

Figure 4.20. Reflectance spectrum of 2579 Spartacus versus the spectra of eucrite ALHA76005 (bulk powder) (dashed red line) and lodranite MAC 88177 (Hiroi *et al.*, 1993a) (dark line). Small dots are from SMASS I (Xu *et al.*, 1995) and open squares are from SMASSIR. All spectra are normalized to unity at 0.55 μm. Error bars are ±1σ.

The two V-type NEAS (3908 Nyx and 7889 1994 LX) with visible data that were observed in SMASSIR are plotted in Figure 4.21. (Another V type, 1981 Midas, had the distinctive near-infrared spectrum of a V type, but is only plotted in Appendix B since no visible data is available.) The SMASSIR observations for Nyx are slightly redder (less than 5%) than previous near-infrared observations by Cruikshank *et al.* (1991). For 1994 LX, only broad-band visible observations by Hicks and Rabinowitz (personal communication) are available. Assuming Nyx and 1994 LX have similar spectral properties from ~0.8 μm to ~0.92 μm, these objects also have very similar spectra in the near-infrared. Both of these objects have very similar spectral properties to howardites.

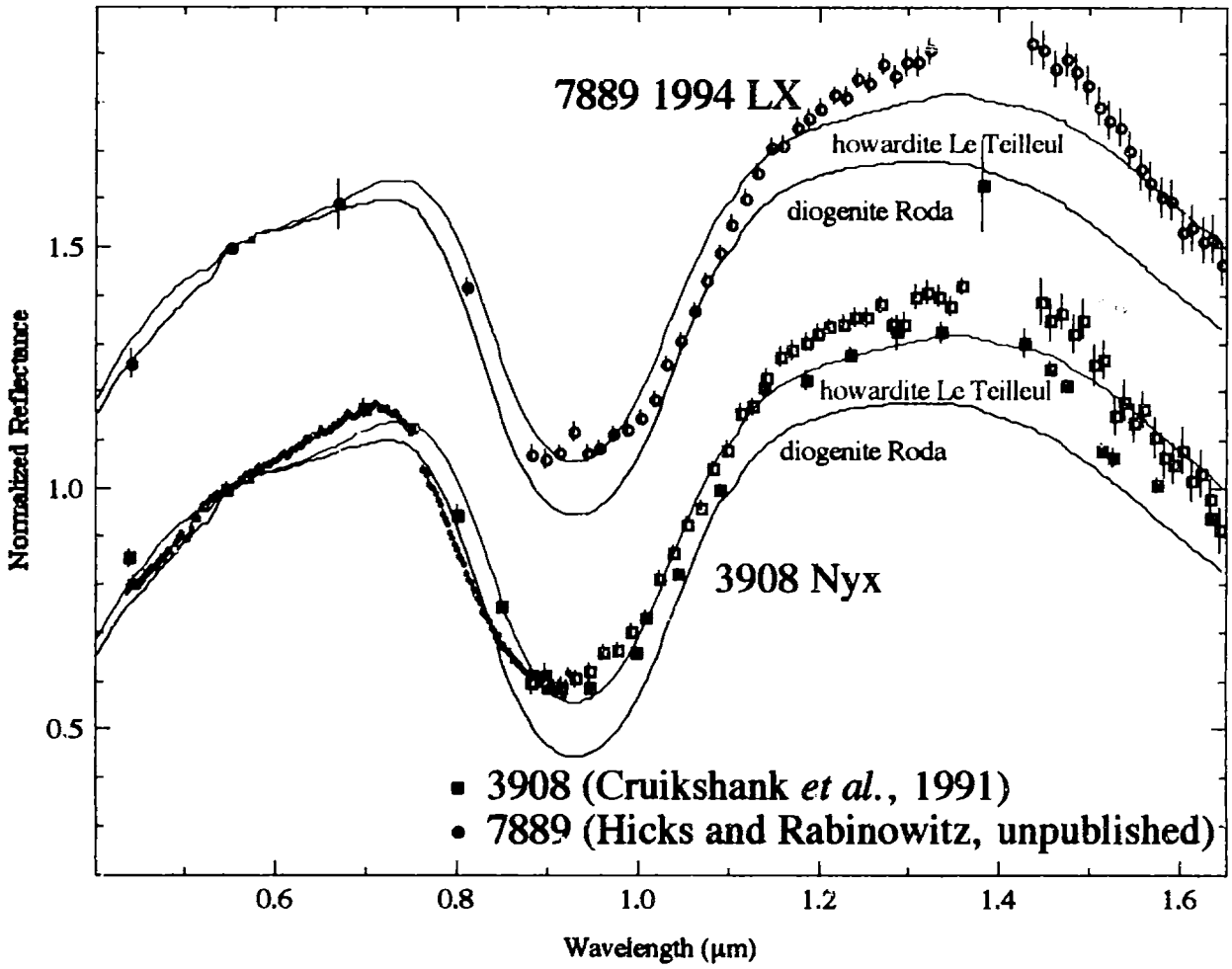

Figure 4.21. Reflectance spectra of NEAs 3908 Nyx and 7889 1994 LX versus howardite Le Teilleul and diogenite Roda. Small dots are from SMASS II (Bus, personal communication). Open symbols are from SMASSIR. The dark squares are from Cruikshank *et al.* (1991) and the dark circles are from Hicks and Rabinowitz (personal communication). The meteorite spectra are from Gaffey (1976). All spectra are normalized to unity at 0.55 μm. Error bars are ±1σ.

Figure 4.22 plots the band depth (in percent) versus the peak reflectance value for the Vestoids and eucrite and diogenite spectra. One interesting result is that the objects not in the Vesta family tend to have stronger band depths than Vesta family members. The two observed NEAS, which also have the smallest estimated sizes of 1 to 2 km, have the strongest band depths of the Vestoids.

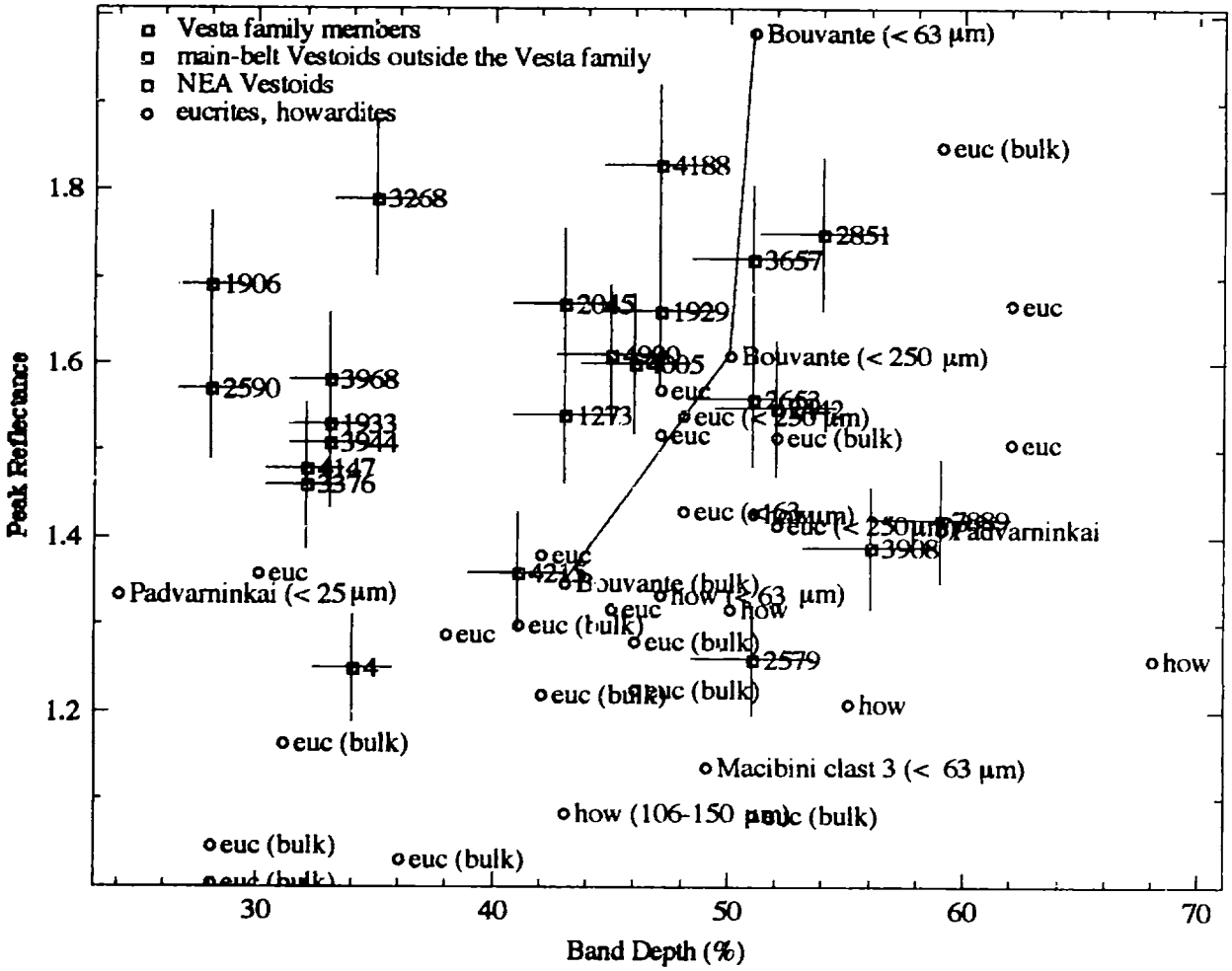

Figure 4.21. Bands depths (in percent) versus the peak reflectance values for Vesta family members (black squares), main-belt Vestoids outside the Vesta family (red squares), NEA Vestoids (blue squares) and eucrites and howardites (green circles). Meteorites without a listed particle size are from Gaffey (1976). Meteorites with a listed particle size are from Table 4.4 except for the diogenite LAP 91900, the heavily weathered EET 90020 and the eucrite ALH 85001, which has a peak reflectance less than 1.0. A line connects the three different grain sizes for Bouvante. The estimated error bars for the band depths are ±5% times the depth. The error bars for the peak reflectances are ±5%.

It should be noted that the observations of the Vesta family members are heavily biased towards SMASS I observations (Xu *et al.*, 1995) while the data for main-belt Vestoids outside the Vesta family and NEA Vestoids are all from SMASS II data (Bus, 1999; Binzel and Bus, unpublished). SMASS II data tend to have stronger 1 μm features than SMASSI observations by approximately 5%, as discussed in Section 2.5. Even if you assumed depths that were 5%

greater for the SMASS I observations, the objects outside the Vesta family still tend to have larger band depths.

One possibility is that the surfaces of the Vesta family members tend to have more glass-rich surfaces than the non-Vesta family Vestoids. The glass-rich Padvarninkai sample (particle size less than 25 μm) has the smallest band depth of the measured meteorites; however other glass-rich meteorites (such as Macibini clast 3) do not have such a suppressed feature.

Except for the NEAs and Vesta, all of the Vestoids have comparable estimated diameters (4 to 8 km). Figure 4.22 plots the maximum ejection velocity from Vesta needed to put these main-belt Vestoids into their orbits versus their band depths. The ejection velocity is calculated from the velocity needed to remove a fragment from Vesta's gravity (~300 m/s for the latest calculated diameter and mass of Vesta) plus the maximum velocity needed to change the Vestoid's proper elements (e.g., Zappalà *et al.*, 1990). As can be seen in the figure, there appears to be a definite increase in band depth with increasing ejection velocity. Higher velocity impacts would be expected to produce higher ejection velocities for the fragments. If the spectral difference is due to glass, more glass might be expected to be formed in higher-velocity impacts and band depth would be expected to decrease with ejection velocity. No correlation was found between peak reflectance and maximum ejection velocity.

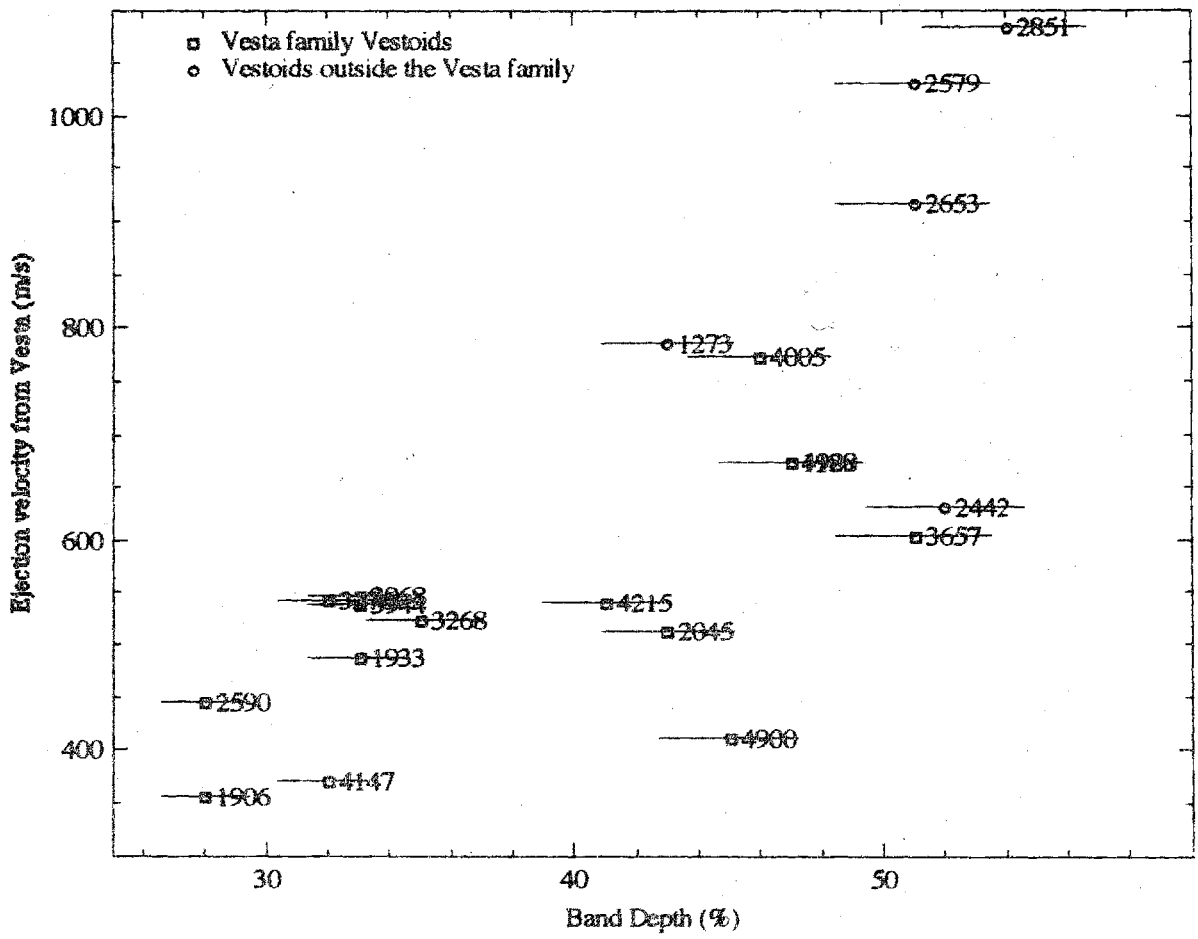

Figure 4.22. Bands depths (in percent) versus maximum ejection velocities for Vesta family members (black squares) and main-belt Vestoids outside the Vesta family (red squares). The estimated error bars for the band depths are ±5% times the depth. The error bars for the peak reflectances are ±5%. This figure does not include NEAs.

Higher velocity impacts would be expected to eject fragments from deeper into the interior of Vesta so the differences could be due to composition. Howardites (band depths of 53 ± 8%) tend to have larger average band depths than eucrites (45 ± 10%). Diogenites have the largest band depths (70 ± 10%). This is consistent with Vestoids that have higher ejection velocities also having surfaces containing more diogenite material mixed in with the eucritic fragments since deeper depths would be expected to be sampled. The Vestoids outside the Vesta family would also be expected to have a turnover between the 1 and 2 μm feature at a shorter wavelength since they would contain more orthopyroxene material; however, the water band at ~1.4 μm makes determining the wavelength of the turnover difficult.

4.8 Conclusions

Approximately 85% of the observed small (diameters less than 10 km) objects that have been placed in the Vesta family by the HCM clustering technique have visible spectra consistent with a pyroxene-rich assemblage similar to the HEDs; however, visible spectra alone can not rule out an ordinary chondrite-like assemblage. Near-infrared spectra of fourteen of these Vesta family members show that these asteroids have spectral properties very similar to the eucrites with its characteristic 1 μm feature due to pyroxene. None of these objects have spectra similar to ordinary chondrites. Besides Vesta, larger asteroids in the Vesta family (sizes greater than 15 km) do not have spectra that argue persuasively for any relationship with Vesta.

There appears to be a very continuous range of spectral properties for the observed Vestoids, which are all redder than Vesta. Examination of laboratory spectra of eucrites and howardites shows that decreasing the particle size to diameters as small as 25 μm can significantly redden their spectra. Glass formation by laser impulse irradiation can also slightly redden the spectra of a HED but appears not to able to redden to the extremes that decreasing the grain size can. All Vesta family members have spectra that tend to fall intermediate between the spectra of the very fine-grained (less than 25 μm) Bouvante and very coarse-grained eucrites. None of the objects have spectra similar to diogenites, which probably implies that it is very difficult to eject 10-km objects with only diogenite surfaces since the diogenites are located beneath the eucrite crust on Vesta. Observed non-family members also have spectra similar to eucrites except for one object (2579 Spartacus), which has an unusual spectrum and also is located (~0.1 AU) relatively far from the Vesta family region. Spartacus' spectrum appears more olivine-rich than a typical Vestoid spectrum due to its broader 1 μm feature and is probably not a fragment of Vesta. The two NEAs observed in SMASSIR have spectra similar to howardites.

Vestoids in the Vesta family (lower ejection velocities) tend to have smaller band depths than those not in the Vesta family. These differences in band depths may be due to composition

since howardites tend to have deeper band depths than eucrites. Higher velocity impacts would be expected to sample material from deeper in the interior and the fragments would be expected to contain more diogenite material and have deeper band depths. The two observed NEAs, diameters of 1 to 2 km and compositions similar to howardites, have the strongest band depths of the measured Vestoids.

Since Vesta appears to have a spectrum similar to howardites (e.g., Gaffey, 1997) and the observed asteroids in the Vesta family have spectra intermediate between eucrites of different grain sizes, it appears very difficult to argue for any scenario except the one where these small "Vestoids" are fragments of Vesta. Theoretical calculations (e.g., Marzari *et al.*, 1996; Asphaug, 1997) have no difficulty in modeling the ejection of fragments from Vesta and the creation of the Vesta family. The formation of the 460-km diameter impact basin on Vesta (Thomas *et al.*, 1997b) would have ejected ~10^6 km^3 of material, which is dramatically more than the volume of the over 200 asteroids that are located in the Vesta family.

Other possibilities appear very unlikely. A scenario (Wasson *et al.*, 1996) where fragments of a projectile that had a grazing impact with Vesta are coated with "Vesta dust" and, thus, appear "Vesta-like" may be possible, but the identification of the 460-km basin on Vesta argues very persuasively that material from Vesta has been excavated and ejected. The possibility that the Vesta family members are predominately background objects (Bell, 1997) with no relation to Vesta also appears improbable since the disruption of another basaltic body near Vesta would be expected to release many more mantle fragments than basaltic objects (e.g., Burbine *et al.*, 1996). This is not the case for the Vesta family, which is dominated by pyroxene-rich asteroids.

Chapter 5
Asteroid Classes

5.1 A Asteroids

5.1.1 Background

A-class asteroids have strong UV and 1 μm features that appear similar to those of olivine [$(Mg,Fe)_2SiO_4$]. Five asteroids were classified as A types by Tholen (1984). Approximately ten other objects have been classified as A asteroids (Bus, 1999). Near-infrared spectra of these objects (Figure 5.1.1) (Bell *et al.*, 1988) confirm that these surfaces contain significant amounts of olivine as seen by the three distinctive olivine bands that make up the 1 μm feature and band minima near ~1.07 μm.

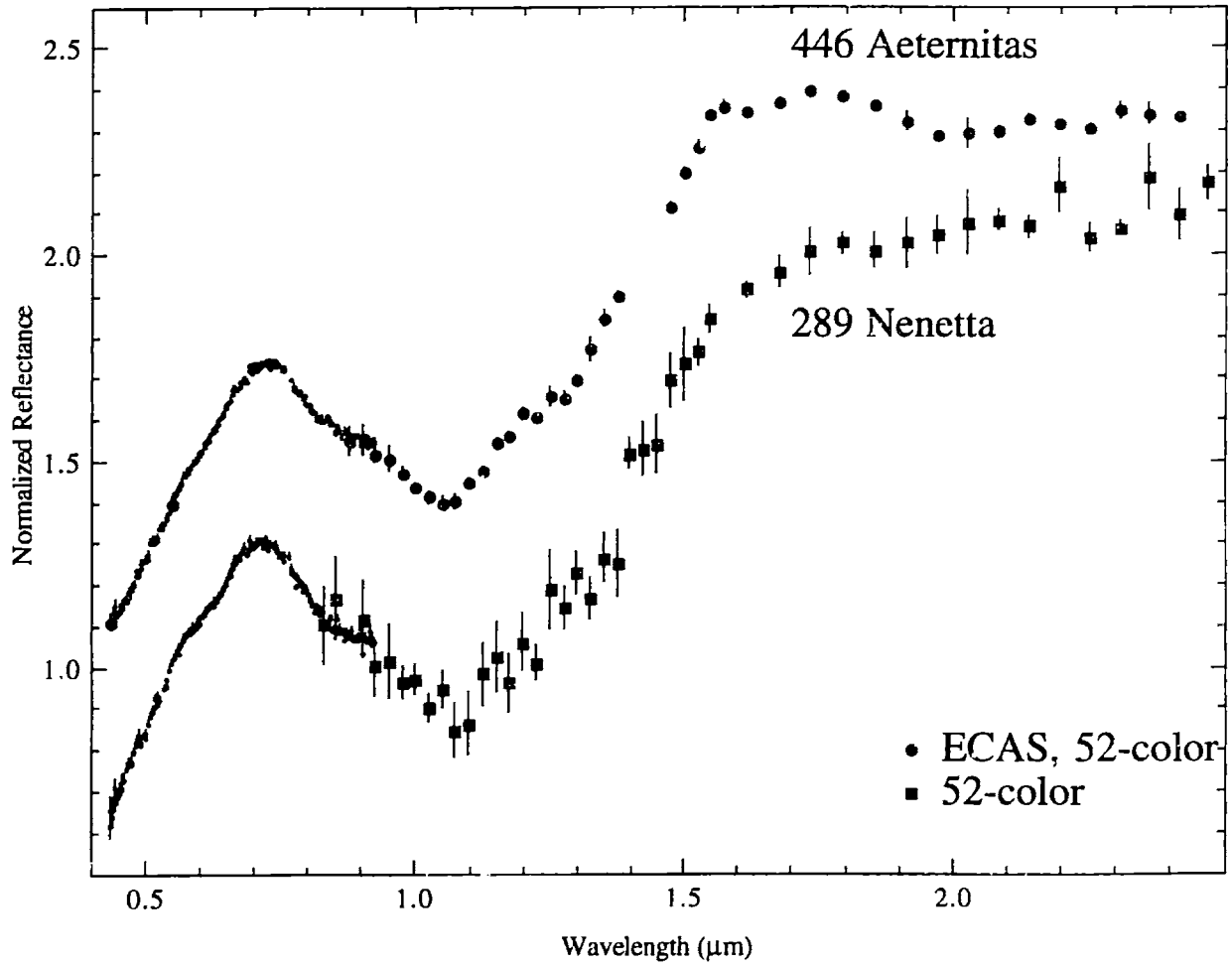

Figure 5.1.1. Reflectance spectra for A-asteroids 289 Nenetta and 446 Aeternitas. Small dots are from SMASS II (Bus, 1999). Dark squares for 289 Nenetta are from Bell *et al.* (1988). Dark circles for 446 Aeternitas are from Zellner *et al.* (1985) and Bell *et al.* (1988). All spectra are normalized to unity at 0.55 μm and are offset by 0.4 in reflectance from each other. Error bars are ±1σ.

Objects with these compositions apparently indicate that enough differentiation to accumulate silicates composed almost entirely of olivine took place on some objects in the main belt (Cruikshank and Hartmann, 1984). These asteroids could be the exposed mantle or core fragments of disrupted differentiated asteroids. Two types of meteorites (brachinites and pallasites) have silicate mineralogies dominated by olivine that have been postulated to have compositions similar to the A asteroids. (The spectral properties of brachinites and pallasites will be discussed in the next section.)

Brachinites are named after Brachina, a fine-grained achondrite containing predominately olivine (Fa_{30-35}) (80 mod.%) (Nehru *et al.*, 1983). Individual brachinites have between 79-93 mod.% olivine with fayalite compositions of Fa_{30-35} (Mittlefehldt *et al.*, 1998). The brachinites are labeled as primitive achondrites due to their near-chondritic bulk compositions, but textures that are igneous or metamorphic (Nehru *et al.*, 1992). Due to their high chalcophile (elements tend to go into the sulfide phase) and siderophile (elements tend to go into the metal phase) contents relative to other igneous meteorites (e.g., eucrites, Chassigny), Warren and Kallemeyn (1989) have proposed that brachinites formed on a small, slightly-differentiated asteroid (or asteroids) where sulfide and metal phases remained abundant in partially molten regions of the mantle and/or crust and did not segregate.

Pallasites are stony-iron meteorites containing predominately magnesian olivine and metallic iron. Olivine varies from about 35-85 vol.% in pallasites (Mittlefehldt *et al.*, 1998). The fayalite compositions of pallasites are between Fa_{10-20} (Mittlefehldt *et al.*, 1998). Wasson (1974) and Scott (1977b) classified twenty-two of twenty-eight pallasites into a main group (nineteen members) and the Eagle Station grouplet (three members) on the basis of trace element concentrations in the metal phase and classified six other pallasites as anomalous. Recently, a third pallasite grouplet (pyroxene-pallasites) have been defined on the basis of the identification of two members (Vermillion and Y-8451) (Boesenberg *et al.*, 1995). Pallasites in this grouplet contain relatively large (millimeter-sized) pyroxene grains while pyroxenes in main group and Eagle Station pallasites are much smaller (sizes on the order of microns to tens of microns) (Buseck, 1977; Davis and Olsen, 1991).

The evidence that pallasites are from the core-mantle boundaries of differentiated asteroids is that they contain the expected mineralogy (olivine and Ni-rich iron metal) of a material from such an interface and slow cooling rates (2-10 K/million years) (Haack *et al.*, 1990). However, Wood (1979) theorizes that pallasites could not have formed in bodies much larger than 20 km in diameter because the gravitational acceleration in larger bodies should have caused a much cleaner separation of the olivine and metal by squeezing the more-plastic and lower-density olivine out of the metallic iron.

Attempts have been made to estimate the fayalite content on A asteroids to determine if these objects have compositions more similar to brachinites or pallasites. Lucey *et al.* (1998) concluded that four A-asteroids 246 Asporina, 289 Nenetta, 446 Aeternitas and 863 Benkoela) had fayalite compositions (Fa_{5-15}) similar to pallasites on the basis of similarities of the bandwidths (full widths at half maximums) of their 52-color spectra to those of low-iron olivines at low temperatures. Sunshine *et al.* (1998) using MGM, which resolves olivine spectra into their three distinctive absorption bands, found 52-color spectra of Asporina and Benkoela to have fayalite compositions similar to pallasites, but 52-color and preliminary SMASSIR spectra of Nenetta to have an olivine composition ($\approx Fa_{30}$) similar to brachinites.

The main questions concerning the A asteroids is whether they are the core or metal fragments of disrupted differentiated bodies (similar to pallasites), are from partially-differentiated bodies (such as the brachinites) or have compositions unlike any known meteorite. The importance of this question is that one serious problem in our current understanding of the asteroid belt is the explanation for the apparent rarity of olivine-dominated metal-free silicate objects in the main belt and in our meteorite collection (Chapman, 1986; Bell *et al.*, 1989). The complete (or near complete) differentiation of a chondritic parent body is believed to result in an object with a iron-nickel core, a thick olivine-dominated mantle and a thin plagioclase/pyroxene crust. The meteoritical evidence for these differentiated bodies is the existence of iron meteorites, pallasites and basaltic achondrites (HEDs). However, mantle material from these differentiated bodies is apparently not present in our meteorite collection (Grady, 1995). Wasson (1995) believes that there is evidence for ~70 differentiated parent bodies; however, less than twenty A types have been identified by various spectral surveys. This topic will be discussed in more detail in Chapter 6.

5.1.2 Olivine Spectra

Spectra of olivine from a brachinite (Brachina) and pallasites (Brenham and Imilac) are shown in Figure 5.1.2. The composition of the Brachina olivine is Fa_{30-32} (Mittlefehldt *et al.*, 1998) while both pallasitic olivines have compositions of ~$Fa_{12.5}$ (Buseck, 1977). Of these olivines, the brachinite spectrum has the strongest feature at ~0.65 μm, but both pallasitic olivine spectra have much weaker features centered at this wavelength. Sunshine and Pieters (1998) and Sunshine *et al.* (1998) argue that this feature tends to be present in the more iron-rich olivine spectra (≈ $Fa_{>34}$). King and Ridley (1987) have previously argued that this feature is due to nickel, but Sunshine and Pieters (1998) have found no correlation with nickel abundance in olivine and the presence of the feature. The absorption feature centered at ~0.65 μm tends to decrease in intensity for smaller grain sizes (usually less than ~60 μm) (King and Ridley, 1987). The features past ~1.6 μm are due to weathering effects.

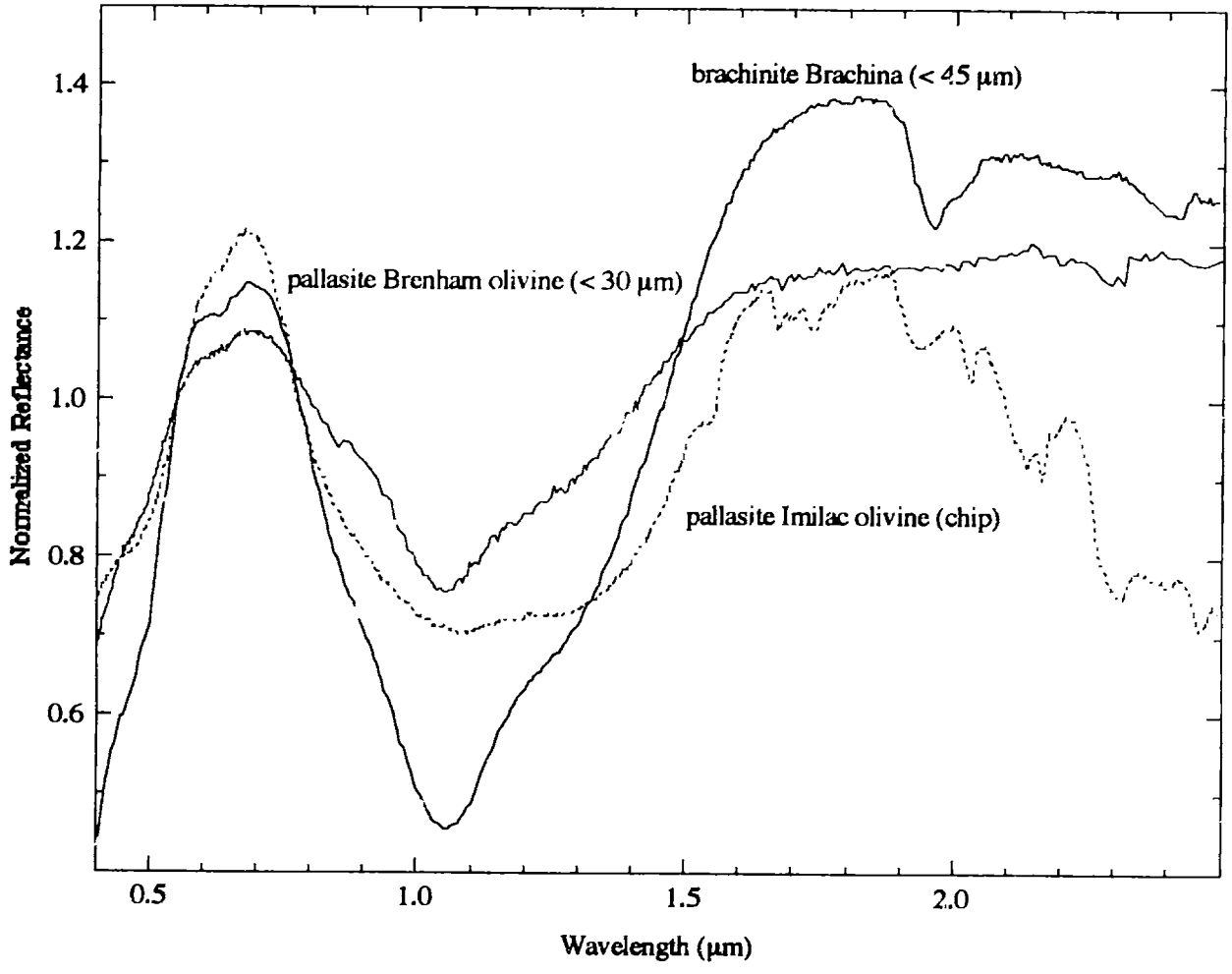

Figure 5.1.2. Reflectance spectra for brachinite Brachina (particle size less than 45 μm) (dark line), pallasite olivine from Imilac (chip) (dashed line) and pallasite olivine from Brenham (particle size less than 30 μm) (red line). The Brachina spectrum is a RELAB spectrum from Sunshine and Hiroi (personal communication) from a sample supplied by the South Australian Museum. The Imilac olivine spectrum is from Hiroi *et al.* (1993b). The Brenham olivine spectrum is from King and Ridley (1987). All spectra are normalized to unity at 0.55 μm.

Spectra of the powdered pallasitic olivine (King and Ridley, 1987) is very different from the spectrum of the pallasitic olivine chip (Hiroi *et al.*, 1993b), which has a much flatter 1 μm band. This flatness does not appear to be due to weathering since no distinctive sharp band is present, such as the features present past ~1.6 μm. Imilac's broad band is most likely due to the spectral properties of uncut silicate surfaces. The spectrum of the powdered pallasitic olivine is very similar in structure to the Brachina spectrum with both having an absorption minimum at ~1.05 μm. The albedo of Brachina is 0.29, the Imilac chip is 0.13 and Brenham olivine is 0.59.

Figure 5.1.3 shows the reflectance characteristics of intimate mixtures of olivine and meteoritic metal (45-90 μm) (Cloutis *et al.*, 1990a). The visual albedo values are 0.72 for the pure olivine mixture, 0.26 for the 75/25 wt.% olivine-metal mixture, 0.16 for the 50/50 mixture, 0.13 for the 25/75 wt.% olivine-metal mixture and 0.11 for the pure metal mixture. As the percentage of olivine decreases, the band depth decreases, the continuum slope increases and the albedo decreases. Also when 25% metal is added, the feature at ~0.65 μm disappears and the ~0.7 μm peak moves to longer wavelengths.

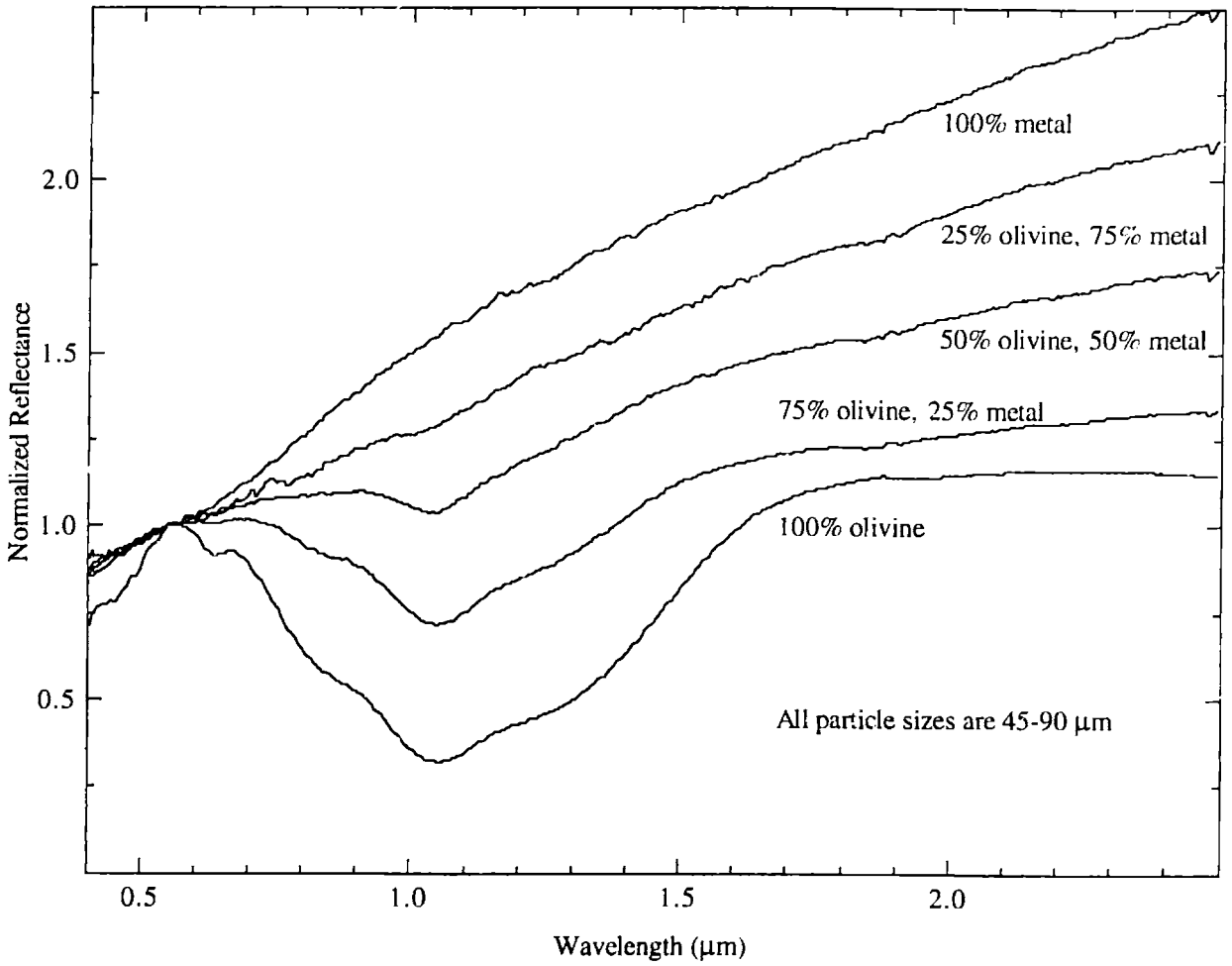

Figure 5.1.3. Reflectance spectra for mixtures of olivine and meteoritic metal (octahedrite Odessa) for grain sizes of 45 to 90 μm from Cloutis *et al.* (1990a). All percents are weight percents. All spectra are normalized to unity at 0.55 μm.

5.1.3 Investigation of A Asteroids

To try to answer the questions posed earlier concerning the composition of A asteroids, eleven A types (Table 5.1.1) were observed in SMASSIR. The A types that have only been observed in SMASSIR are relatively small (diameters less than 15 km) compared to previously observed A asteroids (diameters between 27 and 60 km).

Table 5.1.1. A asteroids observed in SMASSIR. Proper elements (a, e', sin i') are from Milani and Knezevic (1994) except for high-inclination objects, which are from LeMaitre (personal communication). Diameters and albedos are from IRAS (Tedesco, 1994) except for diameters in parentheses, which are calculated using the H magnitude with an estimated albedo of 0.25. Family memberships are from Zappalà *et al.* (1995).

Asteroid	a (AU)	e'	sin i'	IRAS Albedo	Diameter (km)	HCM Family	NEA	52-color
246 Asporina	2.695	0.106	0.267	0.17	60			yes
289 Nenetta	2.874	0.169	0.112	0.24	34			yes
446 Aeternitas	2.788	0.096	0.176	0.24	45			yes
863 Benkoela	3.199	0.040	0.415	0.60	27			yes
1126 Otero	2.272	0.199	0.110	0.18	12			
1600 Vyssotsky	1.849	0.026	0.338		(11)			
2715 Mielikki	2.735	0.114	0.124	0.18	13			
2732 Witt	2.760	0.030	0.101		(10)	Lydia		
3352 McAuliffe	1.879	0.369	0.083		(2)		Amor	
4142 Dersa-Uzala	1.912	0.133	0.424		(5)			
4713 Steel	1.926	0.104	0.334		(7)			

5.1.4 Deep-Featured A asteroids

Four of the objects (246 Asporina, 289 Nenetta, 446 Aeternitas and 863 Benkoela) (Figure 5.1.4) have the typical A-type spectrum. (The other A asteroids will be discussed in the next section.) These objects have the relatively deep absorption due to olivine with three bands at ~0.85, ~1.07 and ~1.28 μm. A few subtle differences do exist between their spectra. Asporina is relatively flat between ~0.7 and ~0.92 μm while the other A-types have more curvature in this wavelength region. Nenetta has a small absorption around 0.65 μm that appears absent in the other spectra. The 0.7 μm peak and the band minima and centers (continuum-removed) for all of the observed A types and a variety of olivine spectra are listed in Table 5.1.2. As can be seen in the table, the differences (0.02 to 0.03 μm) in band minimum and center positions for very different fayalite compositions and for different temperatures are very slight. For error bars of ±0.02 μm, the fayalite composition of the A asteroids can not be determined from their band positions.

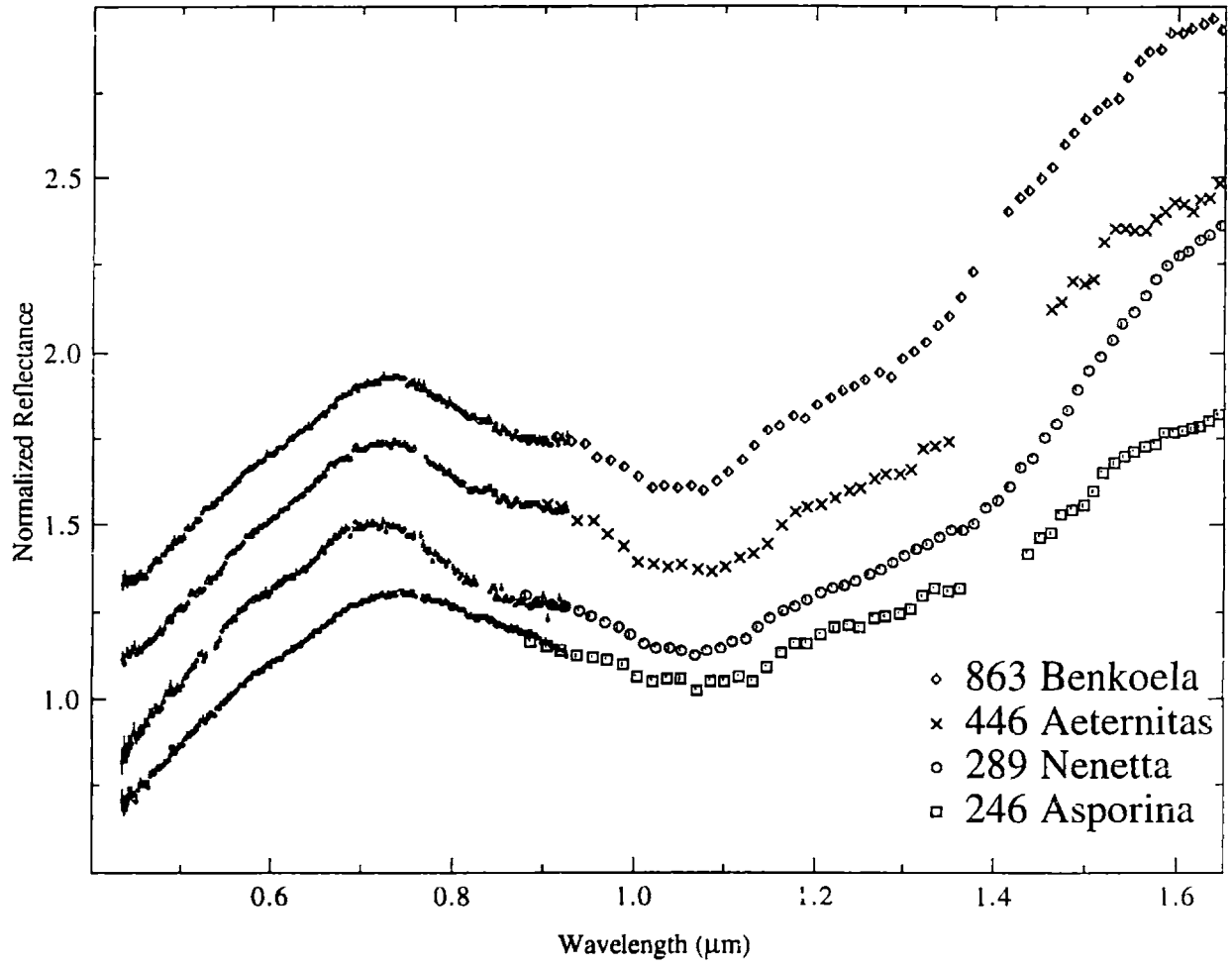

Figure 5.1.4. Reflectance spectra for A-asteroids 246 Asporina (squares), 289 Nenetta (circles), 446 Aeternitas (crosses) and 863 Benkoela (diamonds). Small dots are from SMASS II (Bus, 1999) and larger symbols are from SMASSIR. All spectra are normalized to unity at 0.55 μm and are offset by 0.2 in reflectance from each other. Error bars are ±1σ.

Table 5.1.2. Band positions and depths for 1 μm features for A type, olivine and olivine/metal mixtures. The error bars for the asteroid band positions are estimated to be ±0.01 μm for the ~0.7 μm peak and ±0.02 μm for the band minimas and centers (minima where a linear continuum has been removed). The estimated error bars for band positions from the olivine spectra are estimated to be ±0.01 μm. The estimated error bars for the band depths are ±5% times the depth. The band depth is calculated by dividing a linear continuum out of each spectrum. The error bars for the IRAS albedos are less than 10%. The error bars for the reflectances at 1.65 μm are ±5%. The olivines altered by Yamada *et al.* (1999) and Moroz *et al.* (1996) were altered by a laser with the (Yamada *et al.*, 1999) samples being altered at lower energies with shorter durations.

Asteroid	~0.7 μm Peak (μm)	Band Minimum (μm)	Band Center (μm)	Band Depth	Albedo	Reflectance at 1.65 μm
246 Asporina	0.74	1.07	1.10	35%	0.17	1.80
289 Nenetta	0.71	1.07	1.09	54%	0.24	2.14
446 Aeternitas	0.73	1.08	1.09	48%	0.24	2.05
863 Benkoela	0.73	1.07	1.08	54%	0.60	2.35
1126 Otero	0.74	0.94	1.07	17%	0.18	1.50
1600 Vyssotsky	0.74	0.91	1.04	16%		1.45
2715 Mielikki	0.75	1.02	1.06	18%	0.18	1.57
2732 Witt	0.74	0.89	(0.90)*	11%		1.55
3352 McAuliffe	0.75	0.92	(0.92)*	20%		1.57
4142 Dersa-Uzala	0.74	0.90	1.05	22%		1.85
4713 Steel	0.74	0.92	0.92	14%		1.67
Meteorites						
Brachina	0.68	1.05	1.06	67%	0.29	1.33
Brenham	0.68	1.05	1.05	32%	0.59	1.15
Imilac	0.68	1.08	1.08	40%	0.13	1.14
Olivine						
Fa_{12} (300 K)	0.57	1.05	1.06	67%	0.63	1.14
Fa_{12} (120 K)	0.57	1.05	1.05	70%	0.65	1.16
Fa_{34}	0.67	1.06	1.07	70%	0.44	1.19
Fa_{40}	0.67	1.06	1.08	66%	0.46	1.21
Fa_{49}	0.67	1.07	1.08	63%	0.38	1.22
Altered olivine by pulse laser irradiation (Yamada *et al.*, 1999)						
Fa_9 (unaltered)	0.57	1.06	1.06	37%	0.87	1.07
Fa_9 (15 mJ laser)	0.71	1.06	1.07	36%	0.59	1.43
Fa_9 (30 mJ laser)	0.73	1.05	1.07	34%	0.46	1.78
Melted and recrystallized olivine (Moroz *et al.*, 1996)						
Fa_{10} (unaltered)	0.56	1.06	1.06	47%	0.73	1.08
Fa_{10} (partially)	0.69	1.05	1.06	40%	0.49	1.35
Fa_{10} (altered)	0.75	1.07	1.06	14%	0.24	1.09
Olivine and metal (Cloutis *et al.*, 1990a)						
100% olivine	0.56	1.05	1.05	70%	0.72	1.07
75% olivine; 25% metal	0.69	1.05	1.05	36%	0.26	1.20
50% olivine; 50% metal	0.89	1.04	1.05	13%	0.16	1.49
100% metal	-	-	-	0%	0.11	2.00

* The relatively short wavelength for the band centers for Witt and McAuliffe appear to be due to problems in overlapping the SMASS and SMASSIR data at 0.92 μm and the scatter in the SMASSIR spectra.

The 1 μm band positions of these A types tend to occur at longer wavelengths than olivines with fayalite compositions similar to brachinites and pallasites. It is unclear what is causing this difference. Possibilities include a higher olivine content in the A-asteroid olivines and/or the presence of another phase (e.g., clinopyroxene). The 0.7 μm peak of the A types is also at a longer wavelength than the peaks found in olivine spectra. A pyroxene (peak at ~0.75 μm) and/or metallic iron component (due to its spectral redness) will tend to move this peak to longer wavelengths. Another spectral difference with olivine is that these four A types are much redder (Figure 5.1.5) than measured unaltered olivine samples with reflectances at 1.65 μm (1.80 to 2.35) that are much higher than measured olivine samples (1.14 to 1.33).

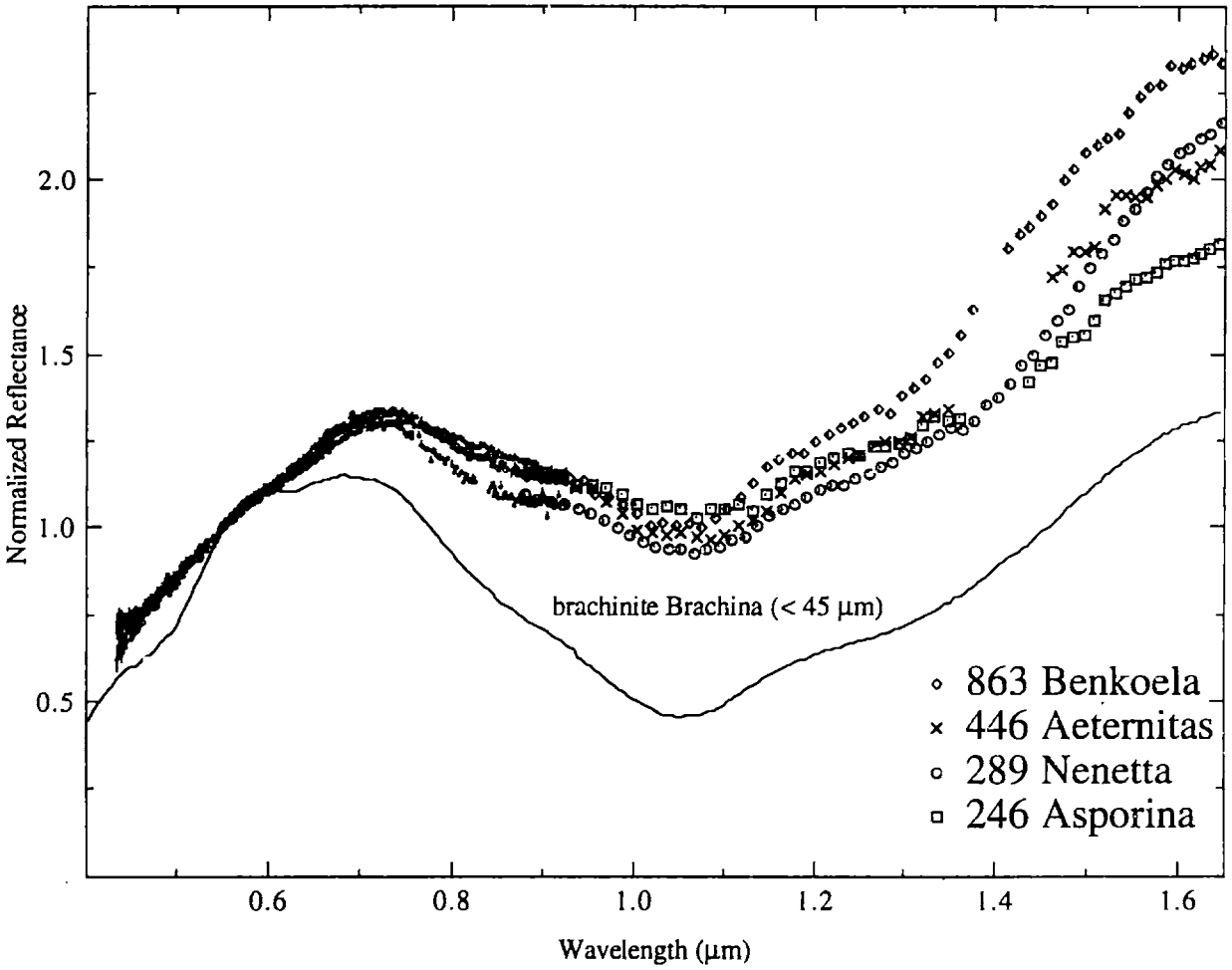

Figure 5.1.5. Reflectance spectra for A-asteroids 246 Asporina (squares), 289 Nenetta (circles), 446 Aeternitas (crosses) and 863 Benkoela (diamonds) versus the brachinite Brachina (particle size less than 45 μm). Small dots are from SMASS II (Bus, 1999) and larger symbols are from SMASSIR. All spectra are normalized to unity at 0.55 μm. Error bars are $\pm 1\sigma$.

The reddest olivine-metal mixtures (Figure 5.1.3) have very suppressed bands. The only mechanism that seems to redden A asteroids while keeping their distinctive olivine band is the pulse laser irradiation experiments of Yamada *et al.* (1999), which are hoped to be simulating impact heating through processes such as micrometeorite impacts (Hiroi and Sasaki, 2000). The pulse duration is 6 to 8 nanoseconds, which is hoped to be comparable to the duration of micrometeorite impacts. One possibility (Hiroi and Sasaki, personal communication) that has been proposed for the reddening is the formation of nanophase iron particles.

Figure 5.1.6 plots 246 Asporina versus unaltered and altered (laser energies of 15 and 30 mJ) olivine. As the energy of the laser increases, the UV feature increases in strength, the spectra reddens and the ~0.7 μm peak moves to longer wavelengths while keeping the distinctive three absorption bands due to olivine. The depth of their features (Table 5.1.2) stays relatively constant. The albedo of the unaltered olivine is 0.87, while the altered (30 mJ) olivine is 0.46.

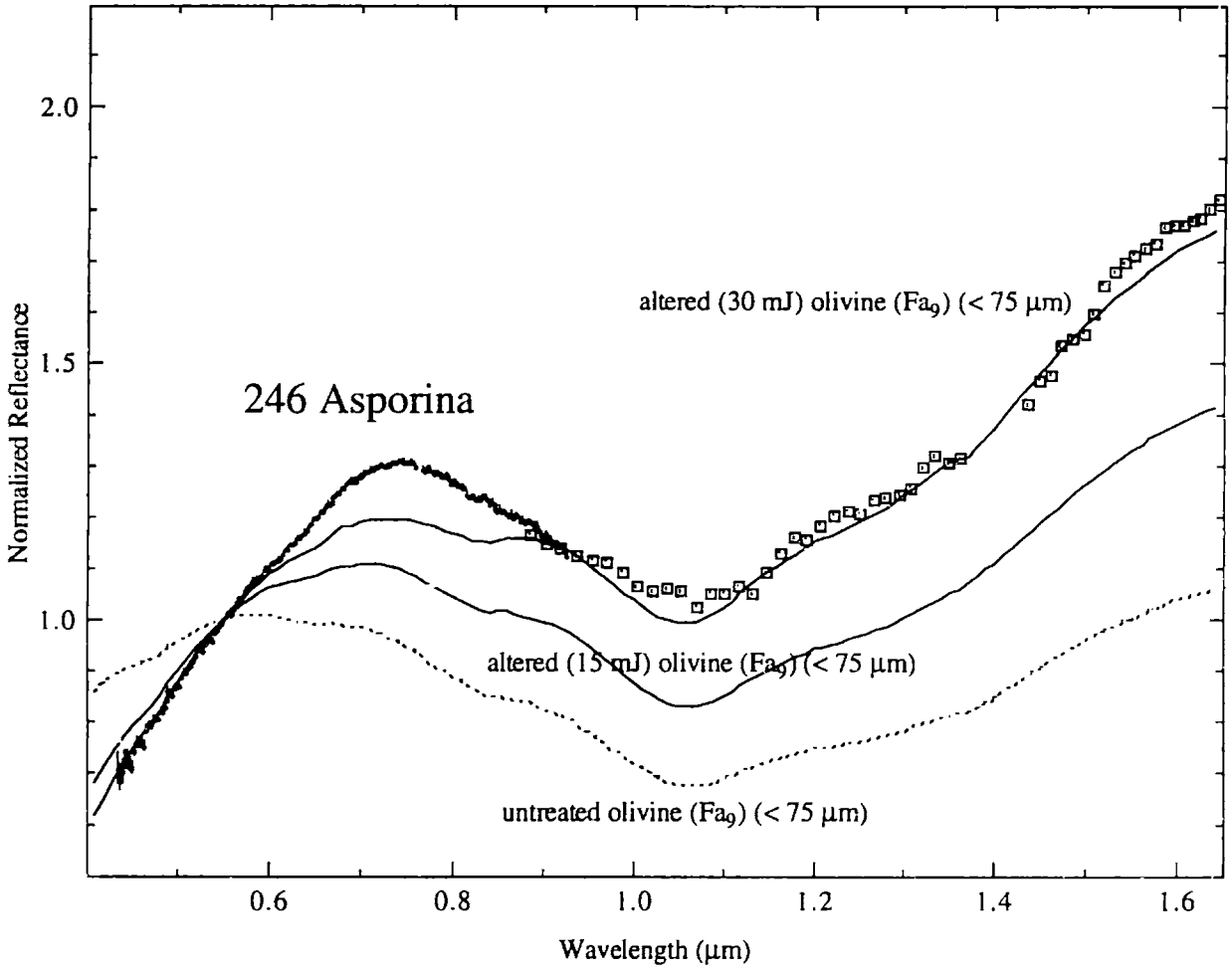

Figure 5.1.6. Reflectance spectrum for A-asteroid 246 Asporina (squares) versus spectra of unaltered olivine (dashed lines) and altered olivine (energies of 15 and 30 mJ) (dark lines). Small dots are from SMASS II (Bus, 1999) and larger symbols are from SMASSIR. Olivine spectra are from Yamada *et al.* (1999) and are for particles sizes less than 75 μm. All spectra are normalized to unity at 0.55 μm. Error bars are $\pm 1\sigma$.

Of these A types, only 863 Benkoela has a roughly comparable albedo (0.60 ± 0.07) to "pure" olivine. The other three deep-featured A asteroids are much darker (albedos of 0.17 to 0.24). Asporina has a slightly stronger UV feature than the 30 mJ-altered olivine sample, which could imply a slightly higher alteration energy on Asporina's surface.

Figure 5.1.7 plots the band depths versus the reflectances at 1.65 μm for the A asteroids and also olivine and olivine/metal samples listed in Table 5.1.2. As can be seen in the figure, the only process that reddens the spectra and does not decrease the band depth substantially is the laser alteration study of Yamada *et al.* (1999) (blue line). Laser alteration by Moroz *et al.* (1996) (green line), which altered olivine samples at a higher energy and longer duration than the Yamada *et al.* (1999) work, tends to decrease the band strength and does not substantially redden the spectrum. Increasing the metallic iron component reddens the spectra, but substantially decreases the band depth (red line).

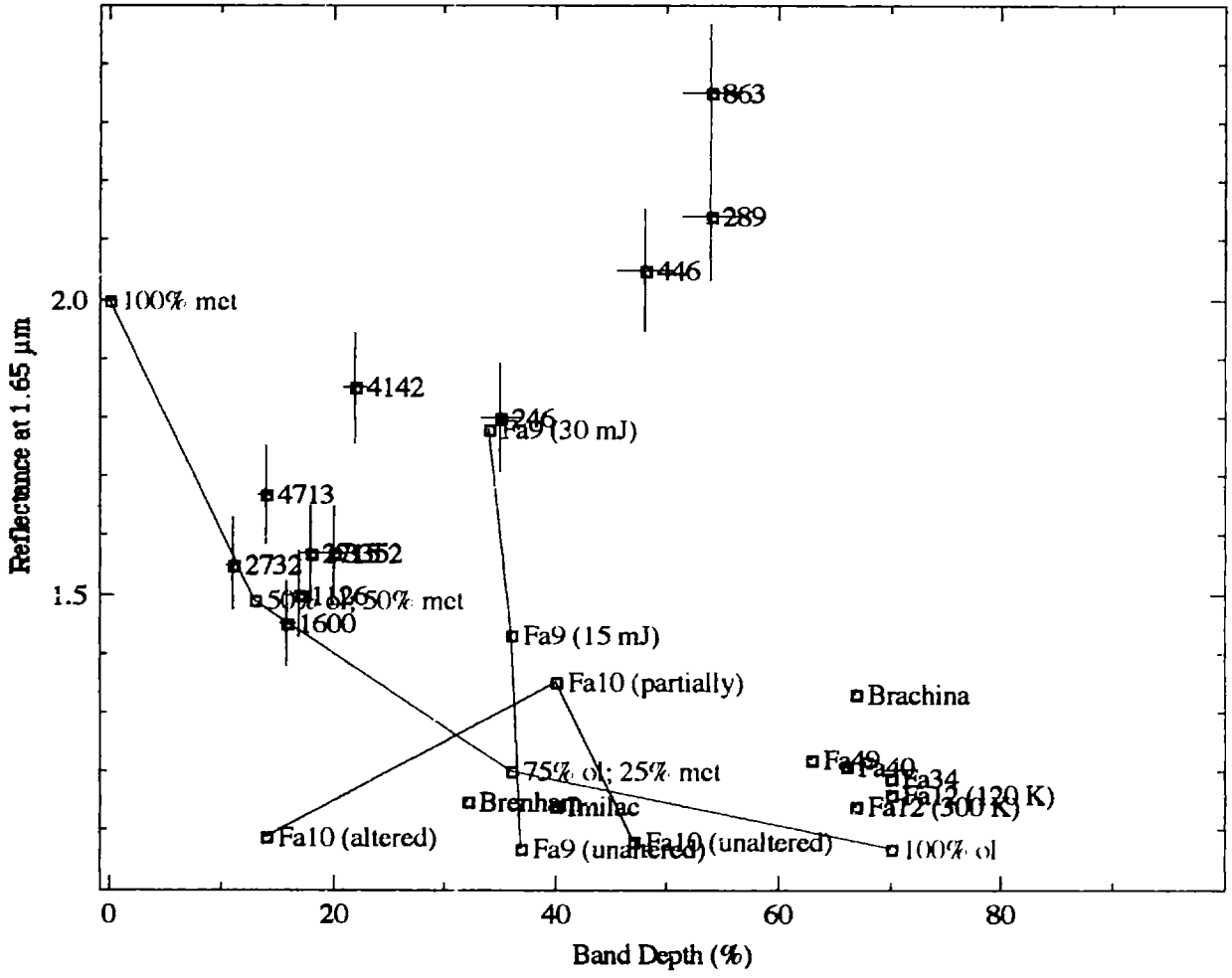

Figure 5.1.7. Band depths (%) versus reflectances at 1.65 μm for A asteroids, olivine and olivine/metal mixtures from Table 5.1.2. Blue symbols and lines are data from the alteration experiments of Yamada *et al.* (1999), red symbols and lines are from the olivine/metal mixtures of Cloutis *et al.* (1990a) and green symbols and lines are data from the alteration experiments of Moroz *et al.* (1996). The estimated error bars for the band depths are ±5% times the depth. The error bars for the reflectances at 1.65 μm are ±5%.

Asporina appears offset from the three other deep-featured A-types and plots very near the parameters derived for the 30 mJ-altered olivine sample. Interestingly, the laser-alteration line (blue) begins very near the parameters for the pallasite olivine and ends very near Asporina. A similar trend from Brachina would end up very near the other three deep-featured A types (Nenetta, Aeternitas and Benkoela). These trends appear consistent with Asporina having an olivine composition consistent with pallasites while Nenetta, Aeternitas and Benkoela would have olivine compositions similar to brachinites. Asporina could also have a brachinite composition that was more altered (e.g., slightly melted), which would give this object a weaker band depth and less-red spectral slope than the other deep-featured A types. Asporina has the lowest albedo (0.17 ± 0.03) of these objects. Nenetta and Aeternitis have albedos (0.24 ± 0.04) roughly similar to Brachina (0.29), while Benkoela's albedo (0.60 ± 0.07) is much higher.

5.1.5 Shallow-Featured A Asteroids

Six of the A asteroids (Figure 5.1.8) (1126 Otero, 1600 Vyssotsky, 2715 Mielikki, 2732 Witt, 3352 McAuliffe and 4713 Steel) have much shallower 1 μm features and are less red (as shown by reflectances at 1.65 μm from 1.45 to 1.67) (Table 5.1.2 and Figure 5.1.6). Asteroid 4142 Dersa-Uzala, which is redder than these objects, will be discussed later.

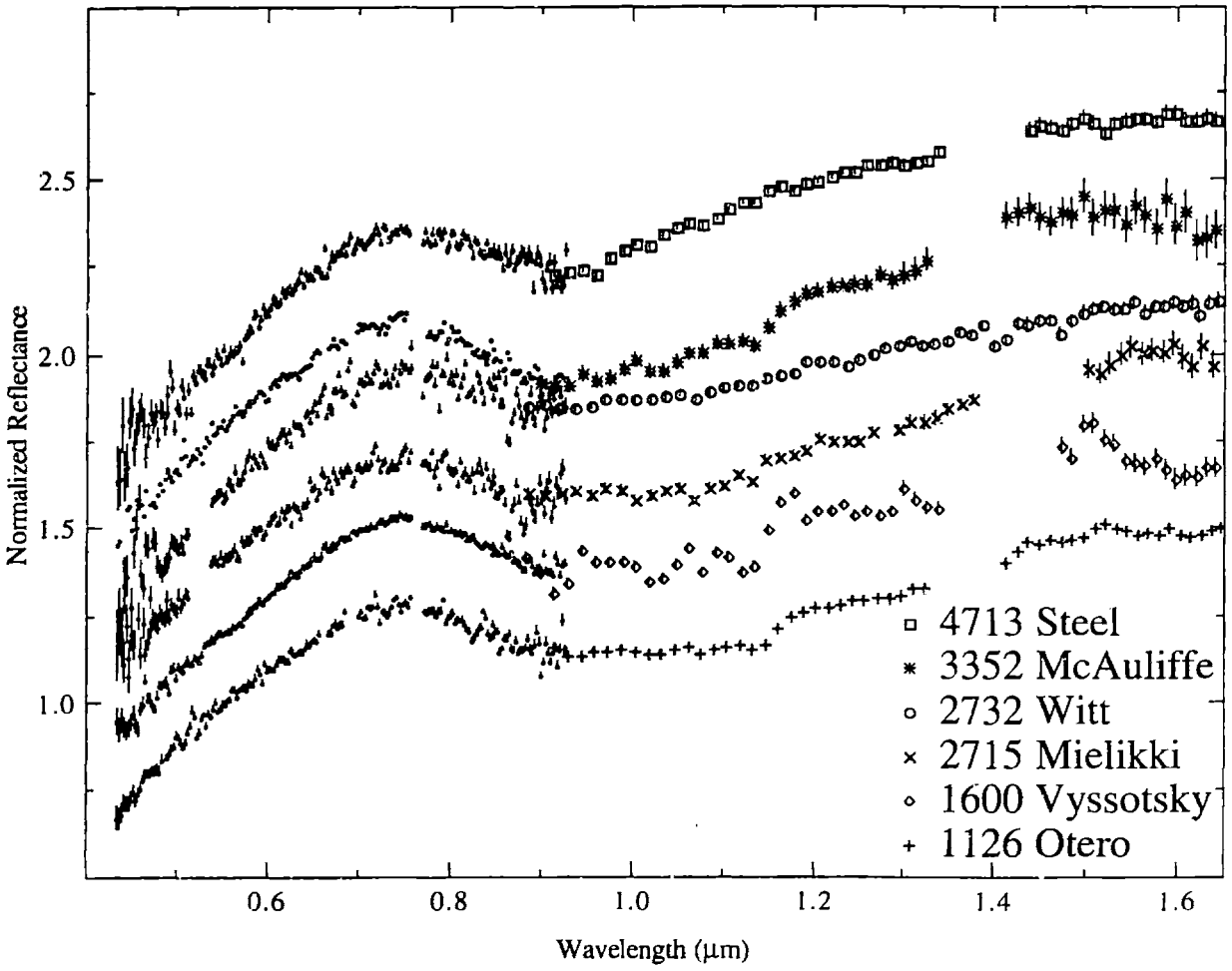

Figure 5.1.8. Reflectance spectra for A-asteroids 1126 Otero (pluses), 1600 Vyssotsky (diamonds), 2715 Mielikki (crosses), 2732 Witt (circles), 3352 McAuliffe (asterisks) and 4713 Steel (squares). Small dots are from SMASS II (Bus, 1999) and larger symbols are from SMASSIR. All spectra are normalized to unity at 0.55 μm and are offset by 0.2 in reflectance from each other. Error bars are $\pm 1\sigma$.

One object, Vyssotsky, has a very strong residual atmospheric absorption feature (~40%) at ~1.4 μm, indicative of telluric effects that cause the spectrum to be relatively noisy. The SMASS II spectrum of Mielikki has a slight turnup at ~0.89 μm, while the SMASSIR spectrum of Mielikki is relatively flat in the overlap region (~0.92 μm). It is unclear if this discontinuity is due to an observational problem with one of the spectra or some type of rotational variation. This object should be reobserved.

Except for Steel, these objects have very broad 1 μm features. The distinctive bands that are indicative of olivine are apparent, but are much weaker than those in the deep-feature A-asteroid spectra. The Steel spectrum is unusual compared to the other shallow-featured A-asteroids since it has a minimum at ~0.92 μm and appears not as flat between ~0.9 and ~1.15 μm, which is more characteristic of an orthopyroxene-rich assemblage.

Another asteroid (4142 Dersa-Uzala) (Figure 5.1.9) has spectral features that are somewhat intermediate between the strong- and shallow-featured A-types. As can be seen in this plot, A asteroids can have very similar strong UV features in the visible, but have very different spectral slopes and band depths in the near-infrared. Dersa-Uzala has a very red spectral slope like the strong-featured A-types, but has a very weak 1 μm feature like the shallow-featured ones. The band center is past 1.05 μm, which indicates an olivine-dominated assemblage. The slight feature at ~1.15 μm is probably due to incompletely removed atmospheric absorptions. Because of this object's suppressed feature, it will be grouped with the shallow-featured A-types.

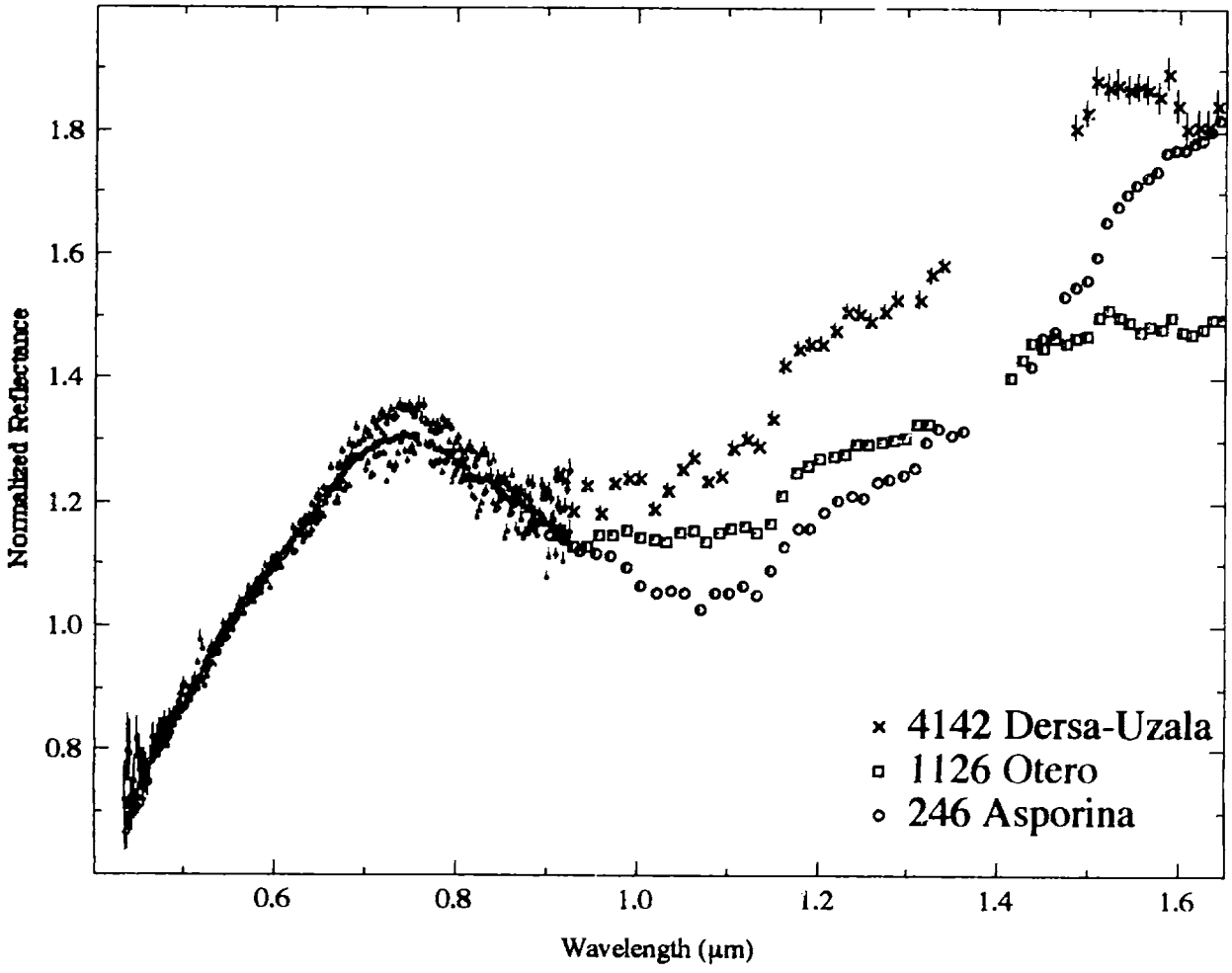

Figure 5.1.9. Reflectance spectra for A-asteroids 246 Asporina (blue diamonds), 1126 Otero (red squares) and 4142 Dersa-Uzala (black crosses). Small dots are from SMASS II (Bus, 1999) and larger symbols are from SMASSIR. All spectra are normalized to unity at 0.55 μm. Error bars are $\pm 1\sigma$.

The shallow-featured A-asteroids (using Otero as a representative object) are not very good spectral matches (Figure 5.1.10) for ordinary chondrites and ureilites, which also have relatively shallow 1 μm features. These A objects have stronger UV features and are spectrally redder than these meteorites. The spectra of the lodranite Y-74357 (normative mineralogy of 83% olivine, 6% orthopyroxene, 3% augite and 8% metal and opaques) (Hiroi *et al.*, 1993a) also does not match very well. In the lodranite spectrum, olivine produces the very broad 1 μm band. The lodranite sample does shows signs of rust, such as the feature at 0.5 μm. The albedo of the lodranite (0.09) is also lower than that of Otero (0.18 ± 0.03).

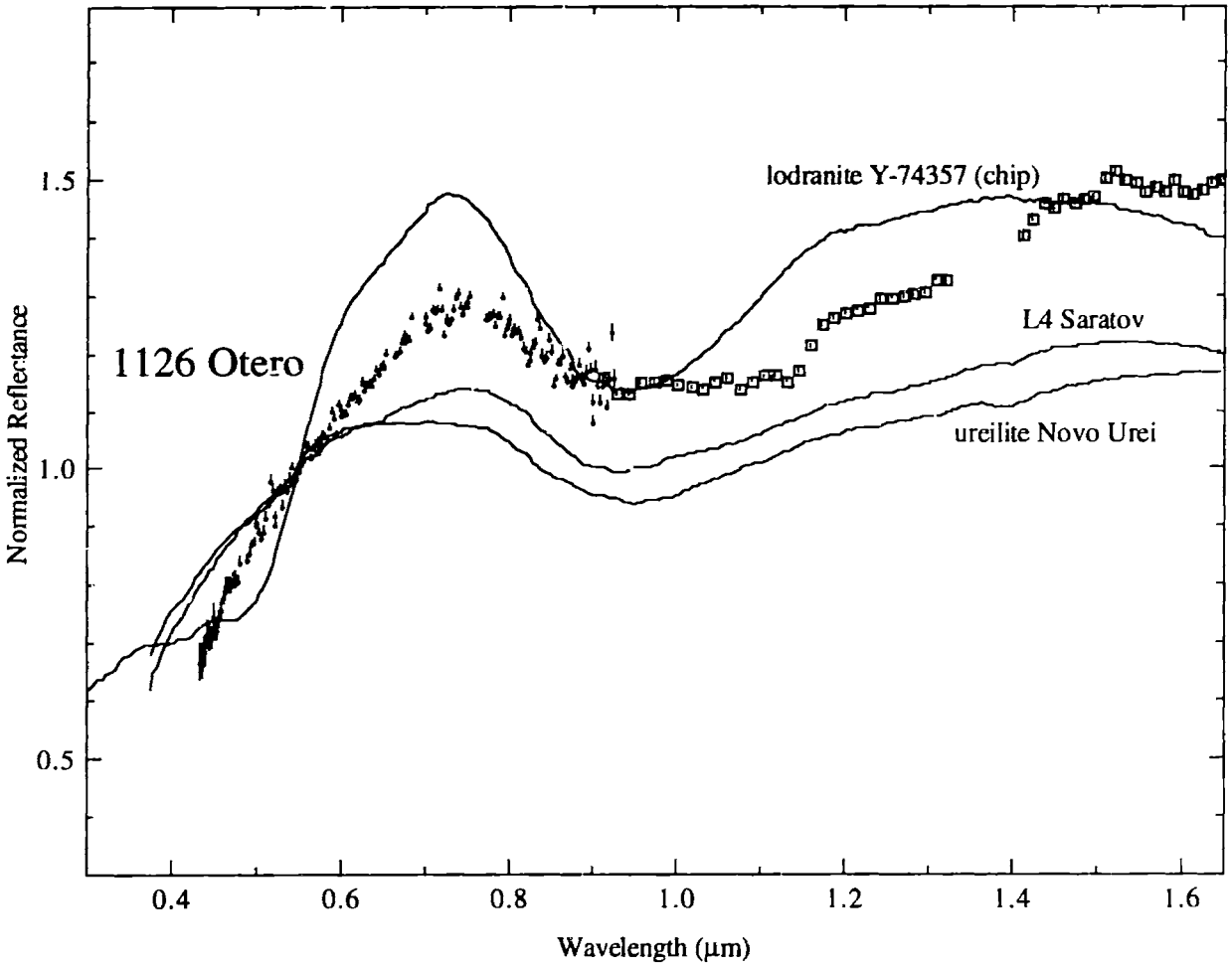

Figure 5.1.10. Reflectance spectrum for A-asteroid 1126 Otero versus lodranite Y-74357 (chip) (top line) (Hiroi *et al.*, 1993a), L4 chondrite Saratov (middle line) (Gaffey, 1976) and ureilite Novo Urei (bottom line) (Gaffey, 1976). Small dots are from SMASS II (Bus, 1999) and open squares are from SMASSIR. All spectra are normalized to unity at 0.55 μm. Error bars are ±1σ.

One possible explanation for the suppressed 1 μm bands of the shallow-featured A-asteroids is a relatively high abundance of metal on the surface. However, the shallow-featured A-asteroids tend to have much stronger UV features than these olivine-metal mixtures (Figure

5.1.11). The whole-rock sample of the Butler octahedrite measured by Gaffey (1976) has a much stronger UV feature than the pulverized Odessa sample. This is consistent with results of Britt and Pieters (1988), where the spectra of rougher metallic surfaces tended to have weaker UV features. Odessa's redder spectral slope is due to its lower Ni abundance than Butler (Buchwald, 1975), which Gaffey (1976) has found is inversely proportional to spectral slope.

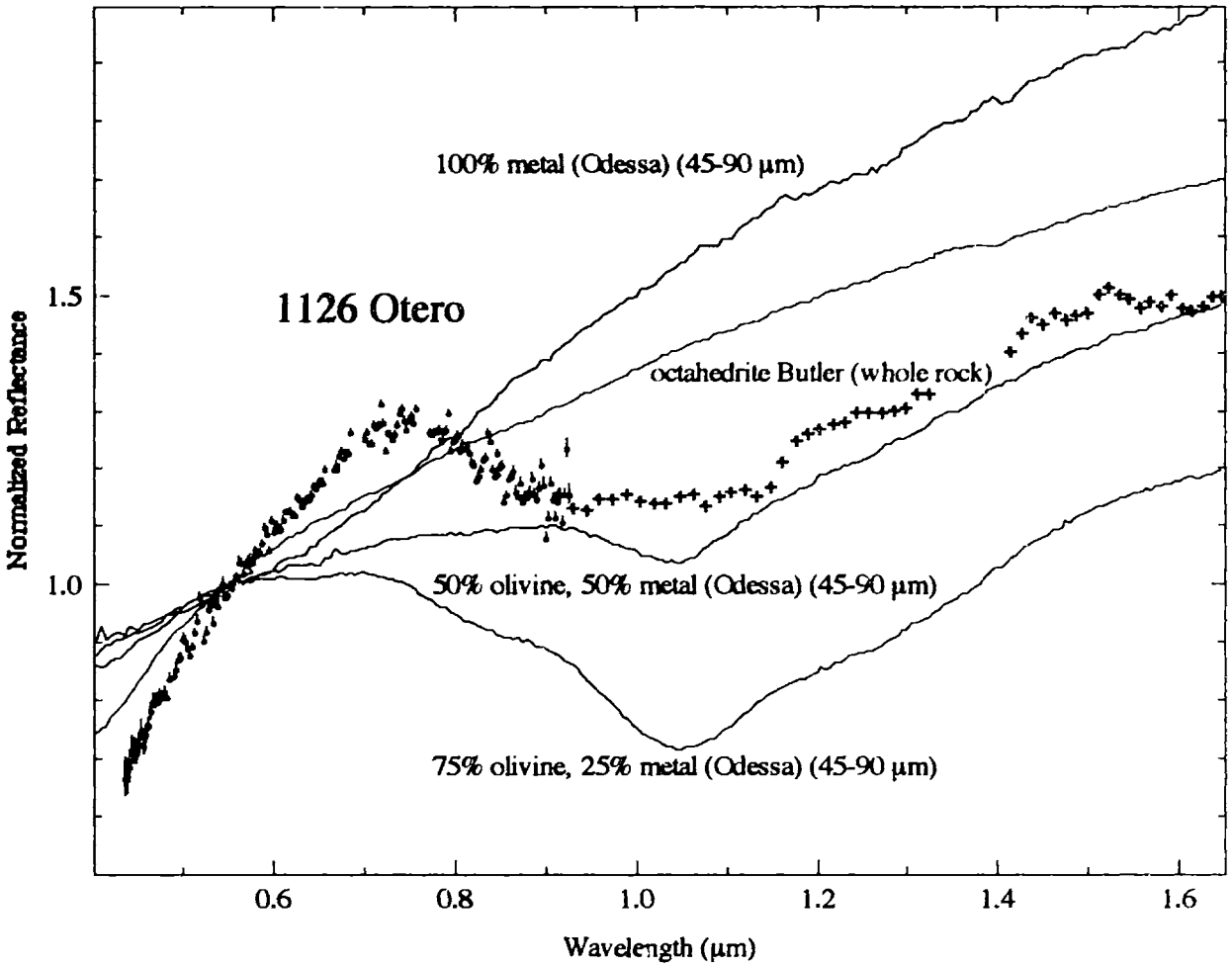

Figure 5.1.11. Reflectance spectrum for A-asteroid 1126 Otero versus spectra of mixtures (75% olivine, 25% metal; 50% olivine, 50% metal; 100% metal) of olivine and meteoritic metal (octahedrite Odessa) (black lines) for grain sizes of 45 to 90 μm from Cloutis *et al.* (1990a) and octahedrite Butler (whole rock) (blue line) from Gaffey (1976). All percents are weight percents. Small dots are from SMASS II (Bus, 1999) and larger symbols are from SMASSIR. All spectra are normalized to unity at 0.55 μm. Error bars are $\pm 1\sigma$.

Another possible way to suppress the strength of the 1 μm band would be to coat the surface with a small amount of carbonaceous material and/or some other types of opaques. Cloutis *et al.* (1990b) did a study where they mixed olivine with amorphous carbon and olivine with magnetite. Some of these mixtures are plotted versus Otero in Figure 5.1.12. As can be seen in the figure, the amount of the fine-grained carbon needed to suppress the bands is very small (0.5 wt.%). None of the spectra are a very good match for Otero and they all have UV features that are much weaker in strength than Otero. (It should be noted that CM chondrites do have stronger UV features than the amorphous carbon.) The albedos of these olivine-opaque mixtures are also lower (0.10-0.13) than Otero's albedo (0.18 ± 0.03). The original albedo of the olivine in the mixture was 0.73.

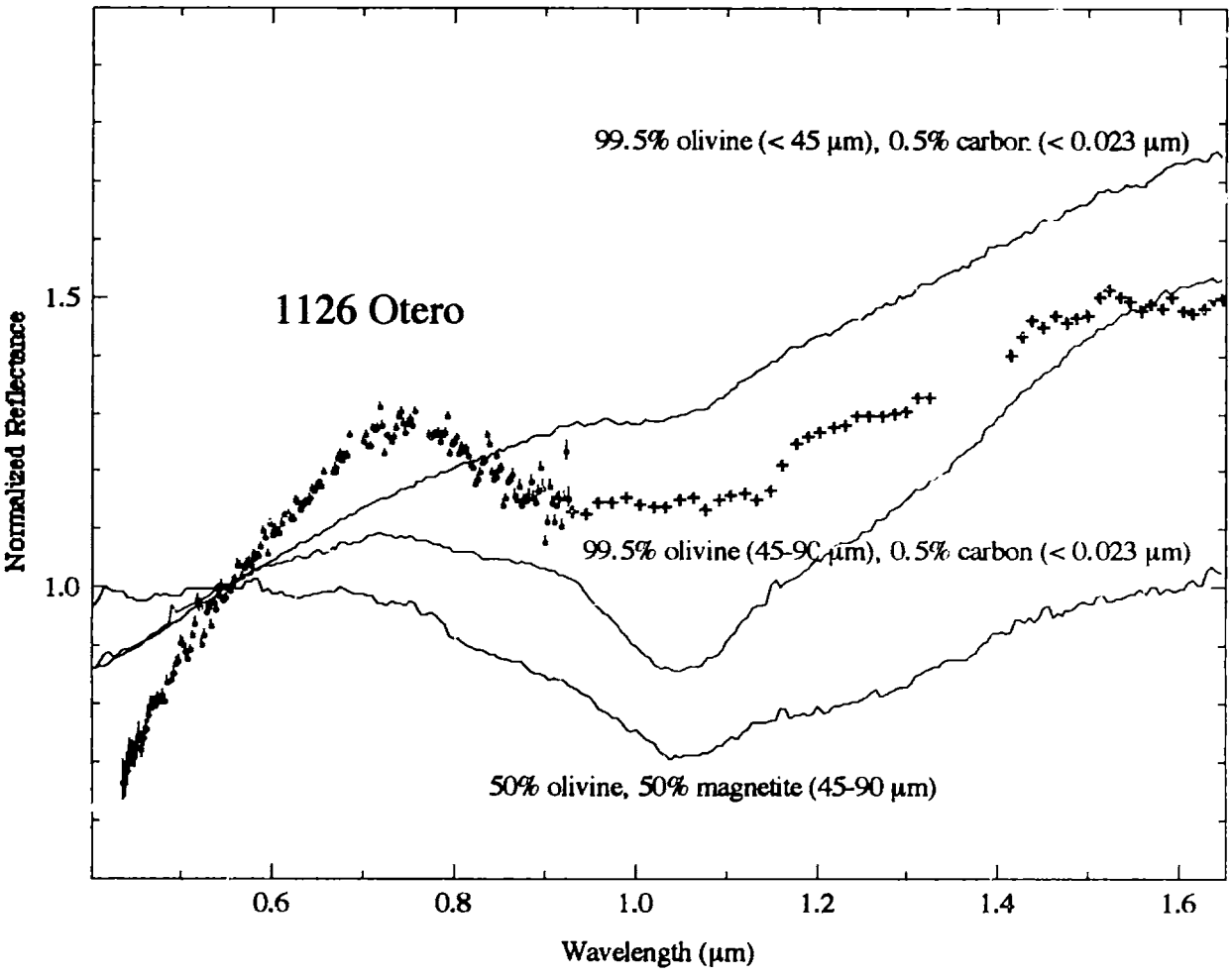

Figure 5.1.12. Reflectance spectrum for A-asteroid 1126 Otero versus spectra of mixtures of olivine (99.5%) and amorphous carbon (0.05%) (particle size less than 0.023 μm) for two different grain sizes of olivine (top black line for sizes less than 45 μm and blue line for sizes between 45 and 90 μm) and mixtures of olivine (50%) and magnetite (50%) (particle size between 45 and 90 μm) (lowest line). All mineral spectra are from Cloutis *et al.* (1990b). All percents are weight percents. Small dots are from SMASS II (Bus, 1999) and larger symbols are from SMASSIR. All spectra are normalized to unity at 0.55 μm. Error bars are $\pm 1\sigma$.

A third possible way to redden the spectra and to suppress the features is by quickly melting and crystallizing the surface material. As mentioned earlier, Moroz *et al.* (1996) used a laser to alter olivine samples at a higher energy and longer duration than the Yamada *et al.* (1999) work. Completely altering the olivine into a glassy material produces a suppressed band of similar strength; however, the altered olivine is still not as red as Otero (Figure 5.1.13).

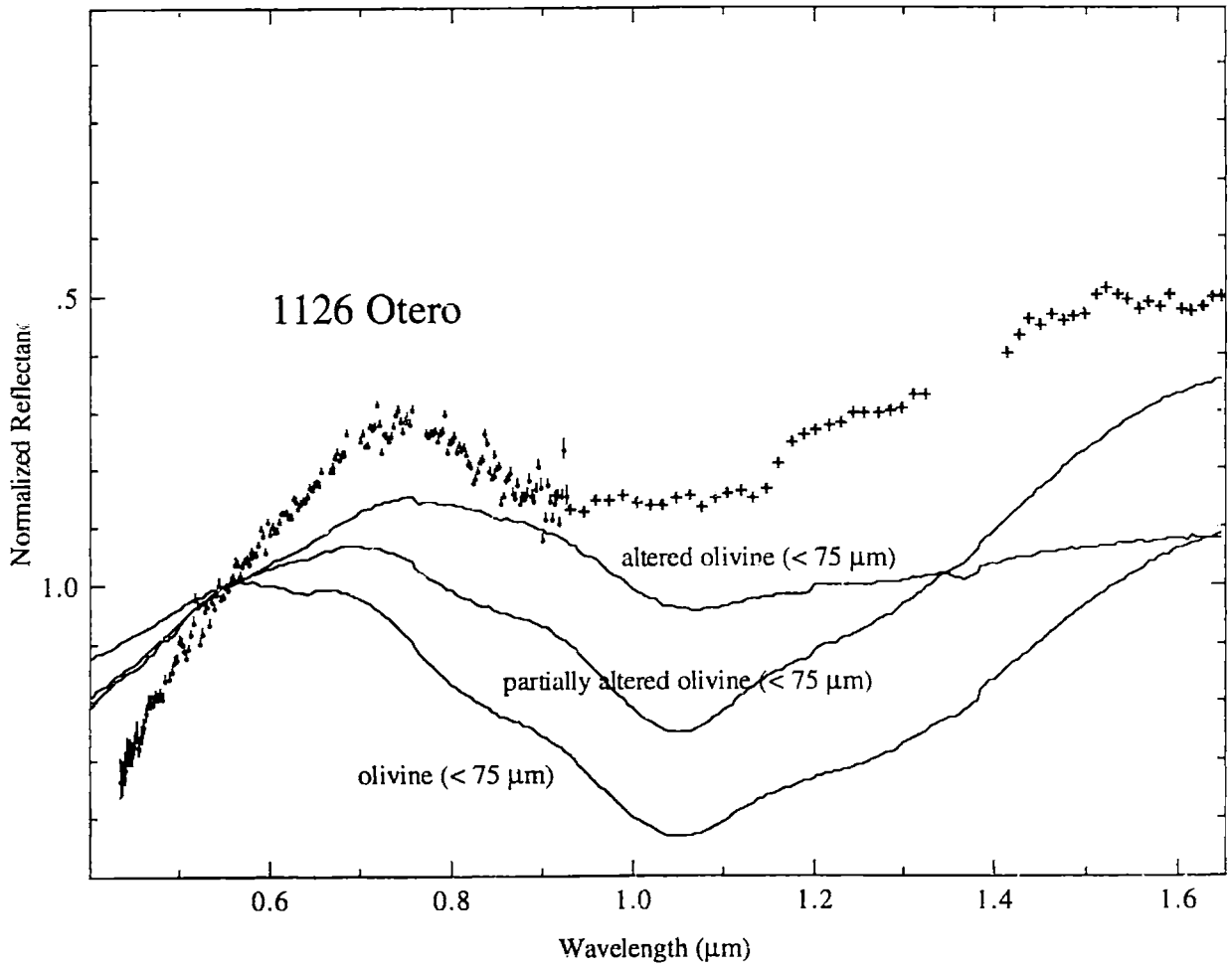

Figure 5.1.13. Reflectance spectra for A-asteroid 1126 Otero versus spectra of olivine, partially altered olivine and completely altered olivine (Moroz *et al.*, 1996). All particle sizes are less than 75 μm. Small dots are from SMASS II (Bus, 1999) and larger symbols are from SMASSIR. All spectra are normalized to unity at 0.55 μm. Error bars are ±1σ.

The advantage of having metallic iron suppress the bands on the shallow-featured A types instead of some type of opaque is that metal has a much higher albedo (usually between 0.15 and 0.30), which is more comparable to these object's albedos, than opaques (0.04 to 0.07). Also, a metallic iron component should also produce similar strength UV features with the shallow-featured A types. However, the spectra of the mixtures of olivine and metal in Figure 5.1.11 are also not very good spectral matches for Otero. One possible explanation may be that these objects have surfaces better represented by slabs than by mixtures of particles. Figure

5.1.14 plots Otero and Witt versus a spectrum of a whole-rock sample of the mesosiderite Veramin (albedo of 0.14) (Gaffey, 1976) and the linearly mixed spectrum of the Imilac olivine and the octahedrite Butler. (In a linear spectral mixture, the surface is assumed to have a checkerboard appearance with two different mineral compositions and a mineral's contribution to the spectra is linearly related to the area it covers.)

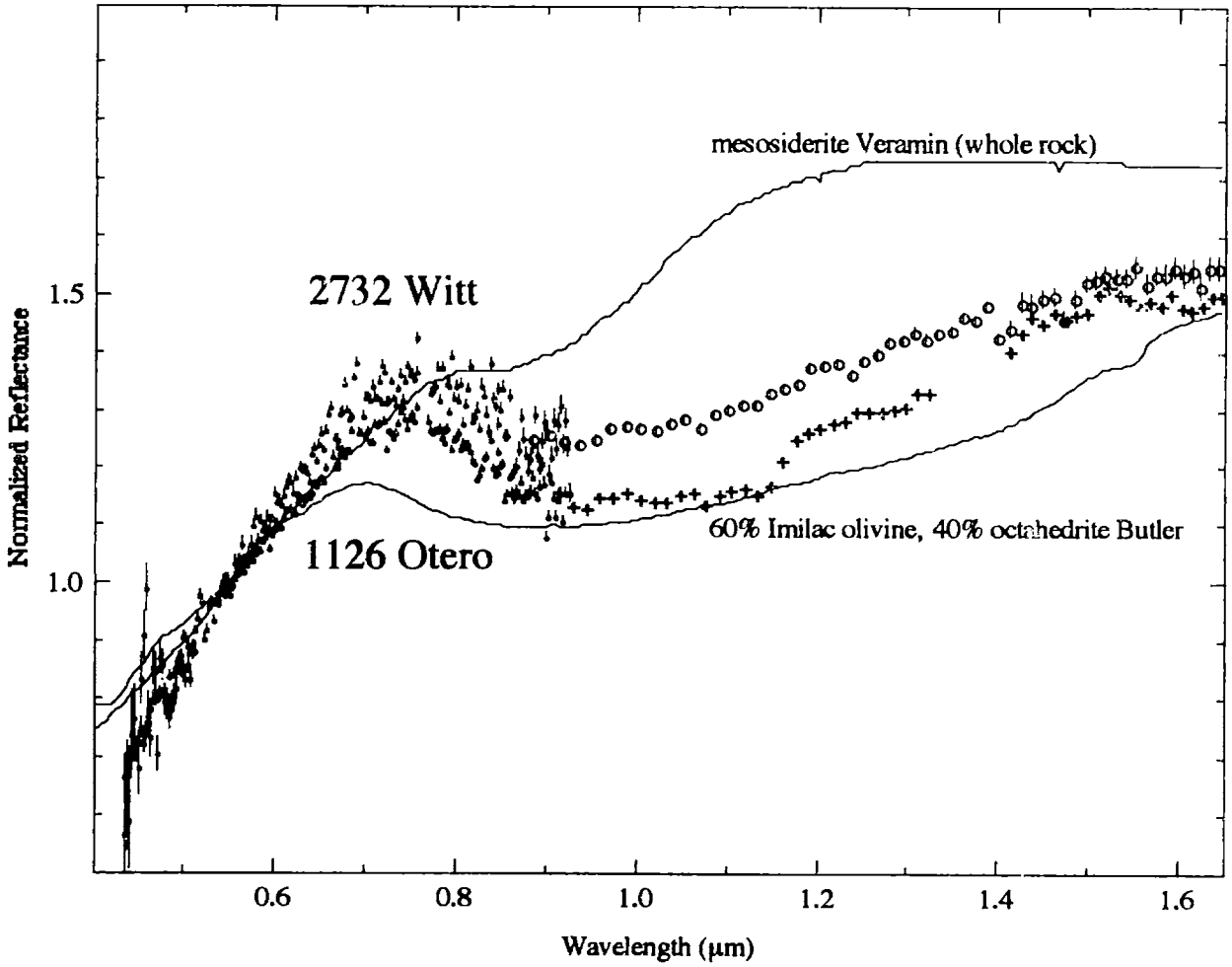

Figure 5.1.14. Reflectance spectra for A-asteroids 1126 Otero (black crosses) and 2732 Witt (red diamonds) versus a spectrum of Veramin (whole rock) (Gaffey, 1976) and spectra of linear mixtures of 60% Imilac olivine spectrum and 40% Butler octahedrite spectrum. Small dots are from SMASS II (Bus, 1999) and larger symbols are from SMASSIR. All spectra are normalized to unity at 0.55 μm. Error bars are ±1σ.

Mesosiderites are stony-iron meteorites containing Ni-rich iron metal and mafic silicates (Floran, 1978). Veramin is 49 wt.% metal and the silicates are primarily orthopyroxene (Powell, 1971). The Veramin sample matches much better the UV feature of these A objects. Veramin also has a very broad feature that does not appear very similar to the symmetric feature usually indicative of pyroxene. This is similar to what is seen in the chip spectrum of the Imilac olivine compared to ground-up olivine samples. The linearly mixed spectrum has an absorption feature

that is roughly similar in strength to these A-asteroid spectra; however, the ~0.7 μm peak is at a longer wavelength in the A asteroid spectra. The presence of pyroxene on these objects could be determined from spectral measurements out to 2.5 μm.

Another possible way to produce the spectral features of these A types would be some intermediate "weathering" process between the laser alteration of silicates by Yamada *et al.* (1999) (Figure 5.1.5) and the melting and crystallization of silicates (also by a laser) by Moroz *et al.* (1996) (Figure 5.1.13). The Yamada *et al.* (1999) altered material has a strong UV feature, is reddened and has a 1 μm band with distinctive features due to olivine. The Moroz *et al.* (1996) altered material has a weak UV feature, is not particularly reddened and has a suppressed 1 μm band. Some mixture of these two types of material would also probably mimic the spectral characteristics of the shallow-featured A asteroids.

5.1.6 Forging Spectroscopic Links to Brachinites

The proposed alteration trend (reddening the spectrum while keeping the band depth relatively constant) implies that Nenetta, Aeternitas and Benkoela, which have band depths stronger than measured pallasite olivine but slightly weaker than the measured brachinite, have olivine compositions similar to brachinites. The low cosmic ray exposure ages for some of the brachinites, ~3 million years for Brachina (Ott *et al.*, 1985) and ~10 million years for ALH 84025 (Ott *et al.*, 1987), argues for a source relatively near a low-order resonance, which would tend to deliver meteorites quickly to Earth. Aeternitas (heliocentric distance of 2.79 AU) is located very near the 5:2 resonance (~2.8 AU) while Nenetta is located slightly farther away (2.87 AU). Asporina, which has a weaker band depth than the other deep-featured A types, could have an olivine composition similar to pallasites that have been reddened without changing the band depth or one similar to a more heavily altered (e.g., slightly melted) brachinite.

5.1.7 Conclusions

The observed A asteroids are not spectrally similar to measured unaltered meteorite or mineral samples (Table 5.1.3). Two types of A asteroids are generally observed: deep- and shallow-featured objects. Larger objects (diameters greater than 25 km) tend to have deeper features with redder spectral slopes and smaller objects (diameters less than 15 km) tend to have shallower features with less red slopes. (One 9-km object, 3819 Robinson, with very distinctive olivine features is in the Sr class and will be discussed in Section 5.7.7.) The deep-featured objects tend to fall in the outer part of the belt (past ~2.7 AU) while most of the shallow-featured asteroids tend to fall in the inner part (~1.8 to ~2.3 AU).

Table 5.1.3. Mineralogic interpretations of A asteroids observed in SMASSIR. For NEAs, their orbital type is given instead of their semi-major axis (a). Quotation marks are used for meteoritic analogs that appear less certain.

Type	Asteroid	a (AU)	Meteoritic Analog	Mineralogic Interpretation
deep-featured A	246 Asporina	2.695	"reddened" pallasite or "altered" brachinite	olivine-dominated surface assemblages as indicated by strong UV features and the three distinctive olivine bands; spectra have similar strength 1 μm features with laboratory-measured samples, but are much redder; this indicates an alteration process such as the one proposed by Yamada *et al.* (1999) using laser impulse irradiation; surfaces can not contain significant amounts of metal since the 1 μm bands are not substantially suppressed
	289 Nenetta	2.874	"reddened" brachinite	
	446 Aeternitas	2.788	"reddened" brachinite	
	863 Benkoela	3.199	"reddened" brachinite	
shallow-featured A	1126 Otero	2.272	none readily apparent	silicate-dominated (primarily olivine) surface assemblages as indicated by strong UV features and 1 μm bands; the 1 μm features appear suppressed and reddened relative to laboratory samples, possibly indicating a metallic iron component and/or some type of alteration process that could include melting and recrystallization
	1600 Vyssotsky	1.849	none readily apparent	
	2715 Mielikki	2.735	none readily apparent	
	2732 Witt	2.760	none readily apparent	
	3352 McAuliffe	(Amor)	none readily apparent	
	4142 Dersa-Uzala	1.912	none readily apparent	
	4713 Steel	1.926	none readily apparent	

The deep-featured objects have the distinctive absorption bands due to olivine; however, these asteroids are much redder than known olivine from extraterrestrial or terrestrial sources. The only proposed way to alter their surfaces so as to keep these object's strong UV features and strong distinctive bands due to olivine while reddening the spectra is to use a pulse laser (Yamada *et al.*, 1999), which is hoped to duplicate the energy and duration of micrometeorite impacts. Their altered olivine samples appear more spectrally similar to A-asteroid spectra than any known samples.

The shallow-featured objects have weaker 1 μm bands that do not have the distinctive bands due to olivine and are less red than the deeper-featured A asteroids. One possibility is that they are mixtures of metal and silicates (olivine and/or pyroxene), which would have very broad, but shallow 1 μm bands. Another possibility is that they have been more heavily altered, which should tend to suppress the 1 μm feature, than the deep-featured A asteroids.

Even within the A-asteroid population, it appears that objects with the distinctive bands due to olivine are not abundant and tend to be prevalent at rather large diameters (27 to 60 km). Other smaller objects with A-type visible spectra have less distinctive olivine bands. The spectral differences between the large and small A asteroids could be due to composition and/or alteration effects. Larger objects would be expected to have older surfaces and be more altered than smaller asteroids, which would argue that the spectral differences are more likely due to composition.

5.2 C Types

5.2.1 Background

C-type asteroids have been generally linked to the type 1 and type 2 carbonaceous chondrite meteorites (CI, CM and CR) since these objects tend to have very low albedos (~0.03 to ~0.07) and relatively featureless spectra; however, some researchers (e.g., Lodders and Osborne, 1999) have postulated that CI and CM chondrites could be derived from extinct comets. C-type asteroids do tend to have weaker UV features (Figure 5.2.1) than carbonaceous chondrite meteorites. These meteorites contain abundant phyllosilicates (hydrated silicates) (e.g., Brearley and Jones, 1998). Phyllosilicates tend to have sheet-like structures and contain a hydroxyl (OH) group (Klein and Hurlbut, 1993). Type 1 carbonaceous chondrites tend to be more aqueously altered than Type 2 ones.

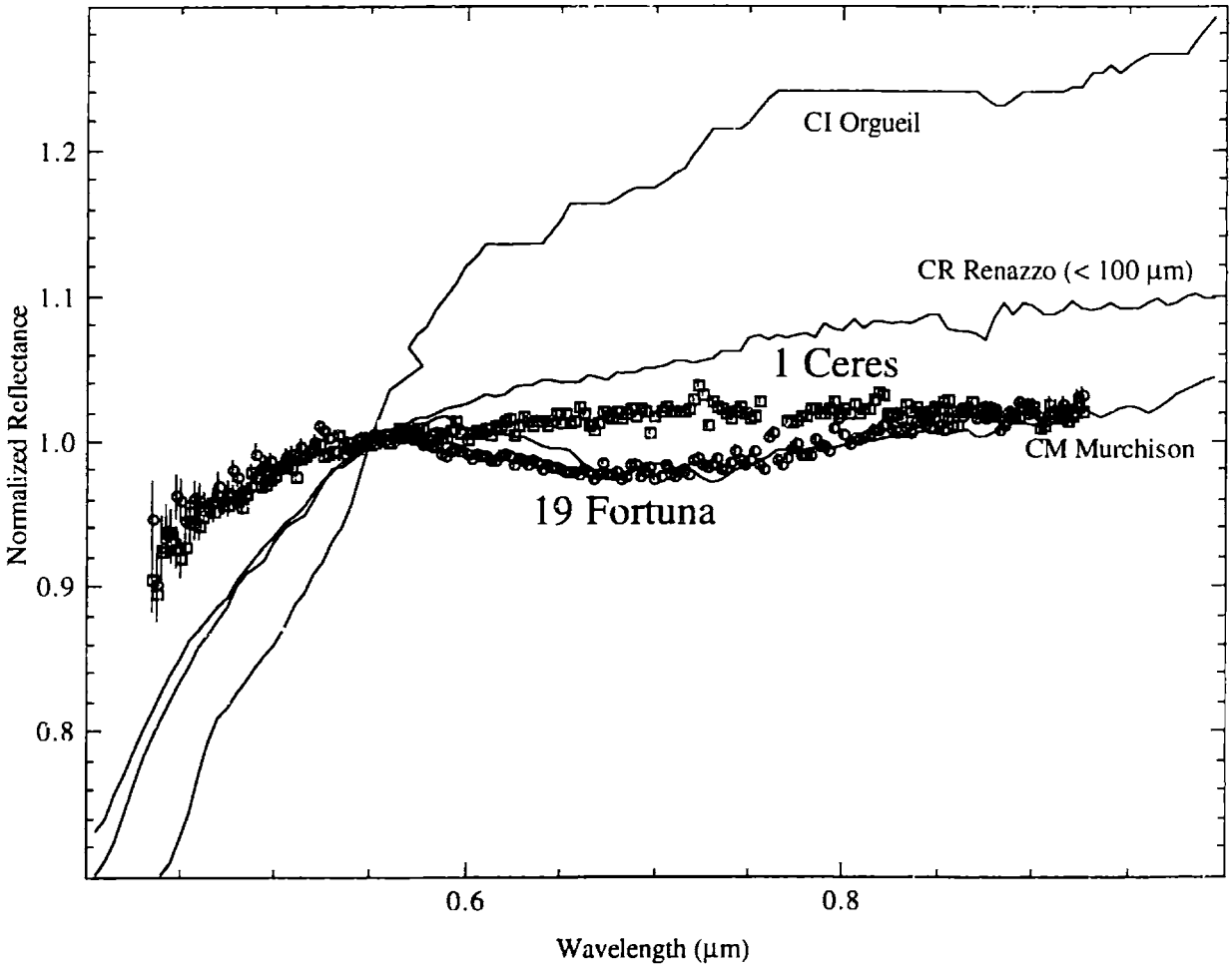

Figure 5.2.1. Reflectance spectra for 1 Ceres (squares) and 19 Fortuna (circles) versus CI chondrite Orgueil (top line) (Gaffey, 1976), CM chondrite Murchison (bottom line) (Gaffey, 1976) and CR chondrite Renazzo (middle line) (Hiroi *et al.*, 1993c). Asteroid spectra are from SMASS II (Bus, 1999). All spectra are normalized to unity at 0.55 μm. Error bars are $\pm 1\sigma$.

Tholen (1984) divided the C asteroids into a number of subtypes (B, C, F and G) based on differences in the strength of their UV features and spectral slopes in the visible. Bus (1999) later divided the C asteroids into a number of classes (B, C, Cb, Cgh and Ch) based on differences in the strength of their UV features, spectral slopes in the visible and the presence or absence of an absorption feature centered at 0.7 μm. Objects with this 0.7 μm feature are given an "h" designation. Objects with very strong UV features are given a "g" designation.

The CI, CM and CR chondrites tend to contain abundant matrix (fine-grained material). CI chondrites have matrices dominated by fine-grained phyllosilicates (e.g., serpentine [$Mg_3Si_2O_5(OH)_4$]) and do not contain chondrules. CI chondrites have elemental compositions similar to the sun, indicating similar compositions to the solar nebula. CM chondrites have matrices containing serpentines such as the Fe^{3+}-rich cronstedtite and chrysotile plus intergrowths of tochilinite and serpentine. Tochilinite is a composite mineral composed of alternating layers of an iron sulfide (FeS_{1-x}) and brucite [$Mg(OH)_2$] (Buseck and Hua, 1993). Zolensky *et al.* (1993) has shown that the Fe/(Fe + Mg) (wt.%) ratios for serpentines in different CM chondrites vary over a large range (~0.3 to ~1.0). CR chondrites contain matrices of fine-grained mixtures of hydrous and anhydrous silicates plus ~7 vol.% FeNi. A number of unusual carbonaceous chondrites found in Antarctica (e.g., Belgica 7904, Y-82162, Y-86720) appear to have been thermally metamorphosed at temperature of 500 to 700 °C (Lipschutz *et al.*, 1999), which tends to dehydrate the phyllosilicates. These meteorites and laboratory-heated CM material tend to have weaker UV features than the "normal" carbonaceous chondrites, which led Hiroi *et al.* (1993c, 1996) to link this type of heated carbonaceous material with C asteroids.

Observations of approximately two-thirds of all C-type asteroids indicate hydrated minerals on their surfaces with 3 μm features of varying strengths. The CI (band depths of ~55%), CM (~45%) and CR (~35%) chondrites all have relatively strong 3 μm features (e.g., Jones, 1988; Miyamoto and Zolensky, 1994). The 3 μm bands of these meteorites are due to bound water or structural OH in hydrated silicates. Heating of carbonaceous material to temperatures above ~700°C tends to dehydrate the silicates enough so that the 3 μm feature is not apparent.

Visible and near-infrared reflectance spectra of CI, CM and CR chondrites tend to be featureless except for their ultraviolet absorption features plus CM chondrites have a number of weak absorption features between 0.5 and 1 μm (Gaffey, 1976; Vilas and Gaffey, 1989). Simple linear combinations of the spectra of both Mg- and Fe-bearing phyllosilicates have been found to match many of the features found in carbonaceous chondrite spectra (Calvin and King, 1997). Many CM chondrites have a feature centered at approximately 0.7 μm, such as Murchison in Figure 5.2.1. Over half (e.g., Sawyer, 1991; Barucci *et al.*, 1998; Fornasier *et al.*, 1999) of measured C asteroids have this 0.7 μm feature, such as 19 Fortuna (Figure 5.2.1). This 0.7 μm

feature has been interpreted as being due to oxidized iron in hydrated silicates (e.g., cronstedtite, chlorite) (King, 1986; King and Clark, 1989). King and Clark (1997) have noted that a number of different types of minerals, including silicates, oxides, hydroxides and sulfides, have similar strength 0.7 μm; however, the only type of meteorite found with this spectral feature is the CM chondrites. Spectral surveys indicate that approximately one-half (Barucci *et al.*, 1998) to three-quarters (Sawyer, 1991) of measured C-type asteroid spectra have this 0.7 μm absorption band.

Two of the most studied C asteroids (Ceres and Pallas) are the largest objects (diameters of 848 and 498 km, respectively) in the belt and the two of the brightest (albedos of 0.11 ± 0.01 and 0.16 ± 0.01, respectively) C types. Gaffey (1978) and Feierberg *et al.* (1981) interpreted Ceres' weaker UV feature compared to CI and CM chondrites as showing that Ceres' surface assemblage was more iron-poor than studied meteorite samples. Their models for producing both Ceres' suppressed spectral features and relatively high albedo compared to carbonaceous chondrites are to extensively aqueously alter iron-bearing phyllosilicates on the surface. Iron would be leached from the phyllosilicates and would precipitate into relatively coarse-grained magnetite, which should decrease the intensity of the phyllosilicate absorption features and also raise the albedo. Pallas has been generally interpreted as also having a relatively iron-poor phyllosilicate composition, due to the weak strength of its UV feature (e.g., Feierberg *et al.*, 1982; Gaffey *et al.*, 1989). Sato *et al.* (1997) noted the spectral similarity of Pallas' (Jones *et al.*, 1990) and CR chondrite Renazzo's 3 μm feature due to the position and the similar strengths of their bands.

Another well-studied C asteroid is 253 Mathilde, which was a NEAR spacecraft target. From the spacecraft rendezvous (Veverka *et al.*, 1999), Mathilde has a visual albedo of 0.05 and a very low density of 1.3 ± 0.2 g/cm^3. Binzel *et al.* (1996a) found that visible spectra of Mathilde to be best matched by a shock-darkened ordinary chondrite and an anomalous CI-chondrite (Y-82162) that had been thermally metamorphosed. Observations in the 3 μm wavelength region by Rivkin *et al.* (1997) show that Mathilde does not appear to have a feature within error bars of ±10%. The absence of a 3 μm feature is not consistent with an anomalous CI-chondrite composition, which has a 3 μm band (Sato *et al.*, 1997), but is consistent with a shock-darkened ordinary chondrite one (Britt and Pieters, 1991). A heated (900 °C) sample of Murchison (Hiroi *et al.*, 1993c) was also suggested as a spectral analog for Mathilde by Rivkin *et al.* (1997).

As can be seen in the above discussion, the C asteroids appear to contain a number of different carbonaceous chondrite compositions. Possible parent bodies for the CM chondrites and the heated carbonaceous chondrites have been identified in the belt; however, it is unclear why the CM chondrites are more abundant (~60 objects known) relative to thermally metamorphosed carbonaceous chondrites, which are relatively rare (~4 known).

5.2.2 Investigation of C Asteroids

To investigate the compositions of C-type asteroids and understand the prevalence or rarity of different carbonaceous chondrite groups in the asteroid belt, eleven C-type asteroids (Table 5.2.1) were observed in SMASSIR. These objects represent four (B, C, Cb and Ch) of the Bus (1999) classes, which will be discussed in separate sections. These asteroids tend to have relatively large diameters (38 to 848 km) compared to other SMASSIR objects, except for the one observed NEA (1998 KU_2).

Table 5.2.1. C-type asteroids observed in SMASSIR. Proper elements (a, e', sin i') are from Milani and Knezevic (1994) except for high-inclination objects, which are from LeMaitre (personal communication). Diameters and albedos are from IRAS (Tedesco, 1994) except for diameters in parentheses, which are calculated using the H magnitude with an estimated albedo of 0.05. Family memberships are from Zappalà *et al.* (1995). The 3 μm band depths are the relative depth (given as a percentage) from the continuum (reflectance at either 2.2 or 2.5 μm).

Asteroid	a (AU)	e'	sin i'	SMASS II	IRAS Albedo	Diameter (km)	HCM Family	NEA	3 μm band depth
1 Ceres	2.767	0.115	0.168	C	0.11	848	Ceres		21 ± 1.3% (Jones *et al.*, 1990)
2 Pallas	2.769	0.276	0.535	B	0.16	498			18 ± 1.2% (Jones *et al.*, 1990)
10 Hygiea	3.142	0.135	0.088	C	0.07	407	Hygiea		12 ± 3.7% (Jones *et al.*, 1990)
19 Fortuna	2.442	0.135	0.039	Ch		225#			25 ± 6% (Jones *et al.*, 1990)
253 Mathilde	2.647	0.225	0.115	Cb	0.05!	53!			0 ± 10% (Rivkin *et al.*, 1997)
335 Roberta	2.475	0.162	0.082	B	0.06	89			
379 Huenna	3.136	0.157	0.031	C	0.06	92	Themis		
511 Davida	3.173	0.187	0.243	C	0.05	326			12 ± 4% (Jones *et al.*, 1990)
515 Athalia	3.121	0.156	0.018	Cb	0.04	38	Themis		
702 Alauda	3.195	0.017	0.369	B	0.06	195			
1998 KU_2	2.251	0.554	0.085	Cb		(1)		Amor	

The diameter for 19 Fortuna is from Hubble Space Telescope observations (Storrs *et al.*, 1999).
! The albedo and diameter for 253 Mathilde are from the NEAR spacecraft encounter (Veverka *et al.*, 1999).
@ The albedo and diameter for 2100 Ra-Shalom are from Harris *et al.* (1998).

5.2.3 Subgroup: B Asteroids

Three B asteroids (2 Pallas, 335 Roberta and 702 Alauda) were observed in SMASSIR (Figure 5.2.2). B asteroids tend to have very weak UV features and blue spectral slopes in the visible.

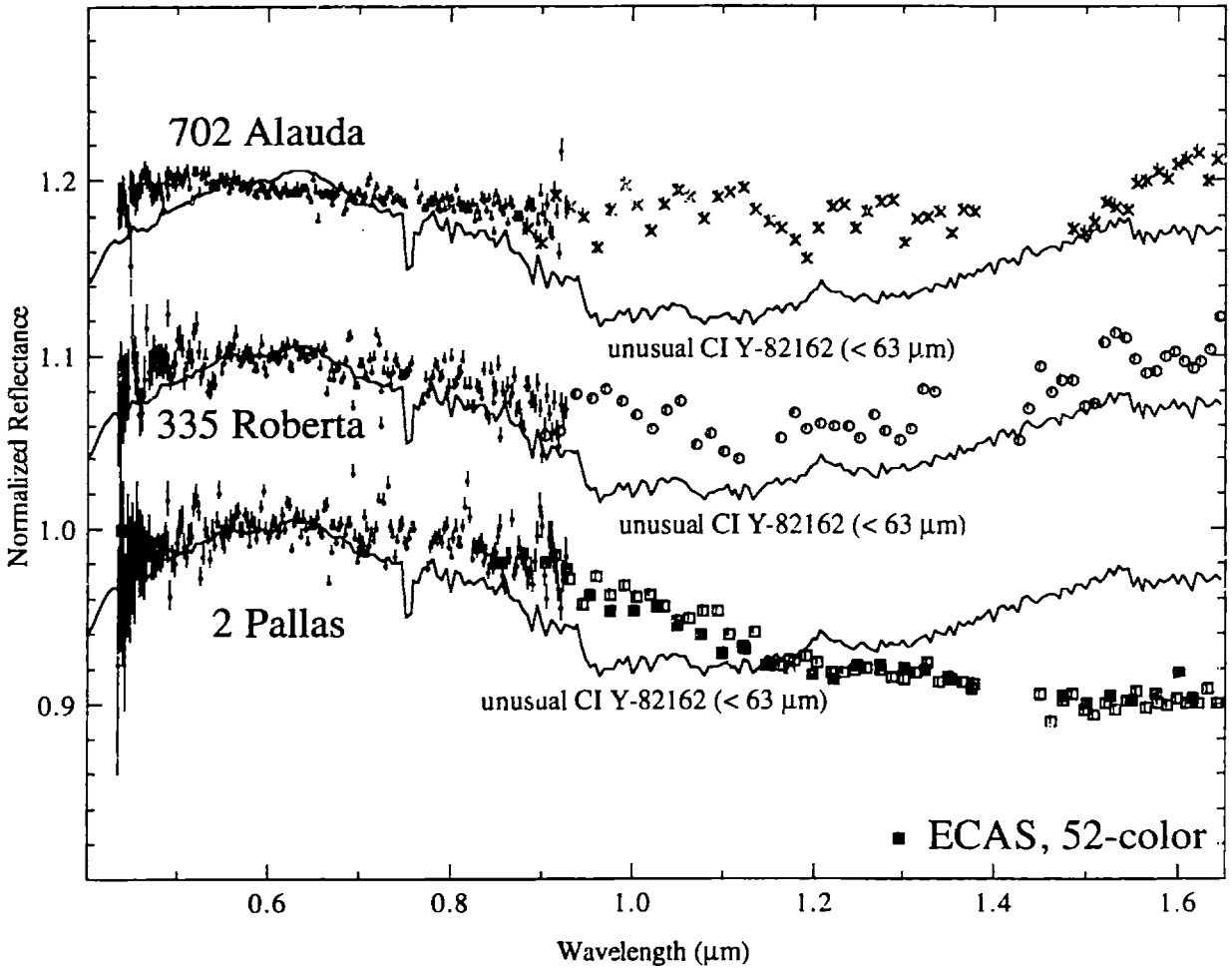

Figure 5.2.2. Reflectance spectra for B-asteroids 2 Pallas (squares), 335 Roberta (circles) and 702 Alauda (squares) versus unusual CI chondrite Y-82162 (particle size less than 63 μm). Small dots are from SMASS II (Bus, 1999) and large symbols are from SMASSIR. ECAS and 52-color data (dark symbols) are plotted for Pallas. All meteorite spectra are from Hiroi *et al.* (1993c). All spectra are normalized to unity at 0.55 μm with the spectra offset by 0.1 in reflectance from each other. Error bars are $\pm 1\sigma$.

Pallas' SMASSIR spectrum is an almost "perfect" match for its 52-color spectrum and is also plotted versus unusual CM chondrite (Y-86720). Pallas has a much weaker UV feature than Y-86720 and their albedos are very different (0.16 ± 0.01 for Pallas and 0.06 for Y-86720).

Roberta has a very high residual absorption feature (25%) in the 1.4 μm region and a relatively noisy spectrum. Roberta's spectrum is a relatively good match for unusual CI Y-82162 with both object's having very weak UV features. Y-82162 has a very broad feature in the near-infrared, which is weaker to not apparent in Roberta's spectrum. The weak UV feature

in the spectrum of Y-82162, compared to other CI chondrites and thermally metamorphosed carbonaceous chondrites is probably due to its relatively high abundance of sulfides (Tomeoka *et al.*, 1989). The albedos (0.04 for Roberta and 0.06 for Y-82162) of these two objects are also very similar. Alauda has a similar spectrum to Roberta with a relatively flat spectrum in the near-infrared. Roberta and Alauda appear spectrally similar to naturally-heated carbonaceous chondrites.

Pallas has an unusual reflectance spectrum out to 3.5 μm (Figure 5.2.3). This figure compares a number of different carbonaceous chondrite spectra with Pallas. Plotted versus Pallas are the spectra of CR chondrite Renazzo, CM LEW 90500 and unusual CM Y-86720. The 3 μm features of Renazzo, CM chondrite LEW 90500 and Pallas all have similar structures.

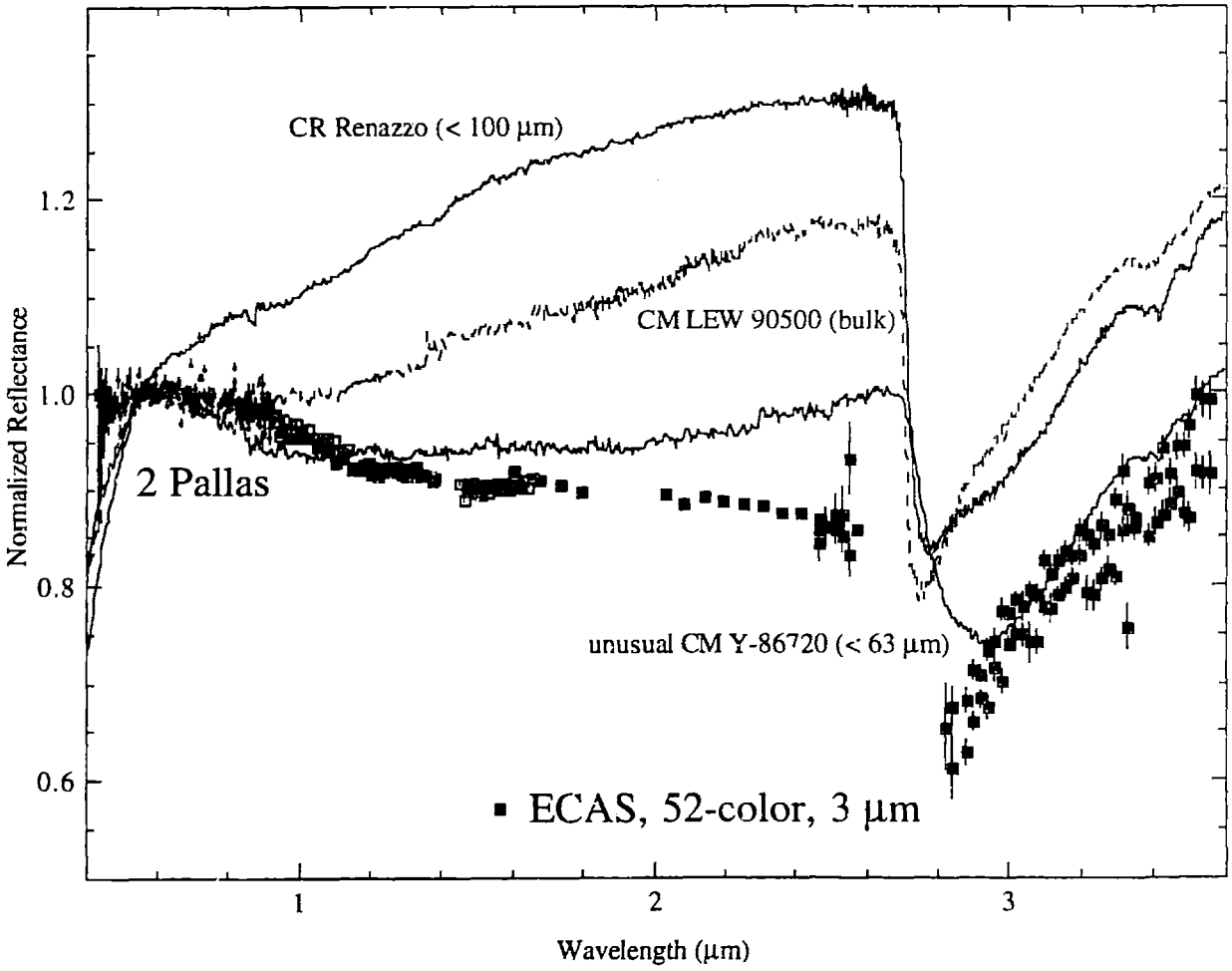

Figure 5.2.3. Reflectance spectrum for B-asteroid 2 Pallas versus spectra of CR chondrite Renazzo (particle size less than 100 μm) (top line) (Hiroi *et al.*, 1993c), unusual CM chondrite Y-86720 (bottom line) (particle size less than 63 μm) (Hiroi *et al.*, 1993c) and CM chondrite LEW 90500 (dashed intermediate line) (Burbine, 1998) (bulk particle). The Pallas spectrum includes SMASS II (Bus, 1999) (small dots), SMASSIR (open squares), 52-color (Bell *et al.*, 1988) (dark squares from ~0.83 to ~2.5 μm) and 3 μm data (dark squares from ~2.5 to 3.5 μm) (Jones *et al.*, 1990; 4/21/87). The 3 μm data are normalized to the 52-color data at ~2.5 μm. The LEW 90500 sample was supplied by the Meteorite Working Group and measured at RELAB. All spectra are normalized to unity at 0.55 μm. Error bars are $\pm 1\sigma$.

CR chondrites tend to be intergrowths of serpentine and saponite (a hydrous aluminum silicate that contains bound water) (e.g., Brearley and Jones, 1998), while CM chondrites tend to have serpentines that have compositions that range from cronstedtite (Fe^{2+}- and Fe^{3+}-bearing) to antigorite/chrysotile (Mg-bearing) (e.g., Buseck and Hua, 1993; Zolensky *et al.*, 1993). Since CM chondrites contain serpentines with Fe^{3+}, they have a 0.7 μm feature due to the charge transfer transition from Fe^{2+} to Fe^{3+}. The absence of a 0.7 μm feature in the Pallas spectrum and the similar shape of the 3 μm feature implies a phyllosilicate composition similar to the CR chondrites; however, there are a number of spectral differences between them. Renazzo is much redder than Pallas from 0.4 to 2.5 μm and darker (0.07) than Pallas (0.16). The weaker UV feature for Pallas could imply a surface with phyllosilicates with lower iron abundances than Renazzo. The thermally metamorphosed CM chondrite Y-86720 has a 3 μm band with a minimum at a slightly longer wavelength and appears not be a good spectral analog for Pallas. Pallas' relatively high albedo (0.16 ± 0.01) also implies a much lower abundance of opaques compared to CI, CM and CR chondrites. As can be seen by the spectral comparisons, Pallas' spectrum and albedo are not consistent with any of these meteorites.

One other possibility to suppress the UV features of these asteroids is some type of alteration process, such as the one proposed to redden the surfaces of the A asteroids by Yamada *et al.* (1999) and Hiroi and Sasaki (2000). These processes should be affecting all asteroids in the belt, with the magnitude of any spectral differences being a function of the compositions and lifetimes of their surfaces. For example, olivine appears more spectrally altered than pyroxene at the same laser energy. It appears plausible that processes such as micrometeorite impacts could be heating carbonaceous chondrite material on asteroid surfaces to temperatures (~500 to 700 °C) that are high enough to alter their spectral properties by tending to dehydrate their phyllosilicates.

5.2.4 Subgroup: C Asteroids

Four C-class asteroids were observed in SMASSIR. Of these objects, Ceres has been the most intensively studied due to its high apparent brightness, which allows for greater signal-to-noise telescopic observations. Visible spectra of Ceres is plotted in Figure 5.2.4.

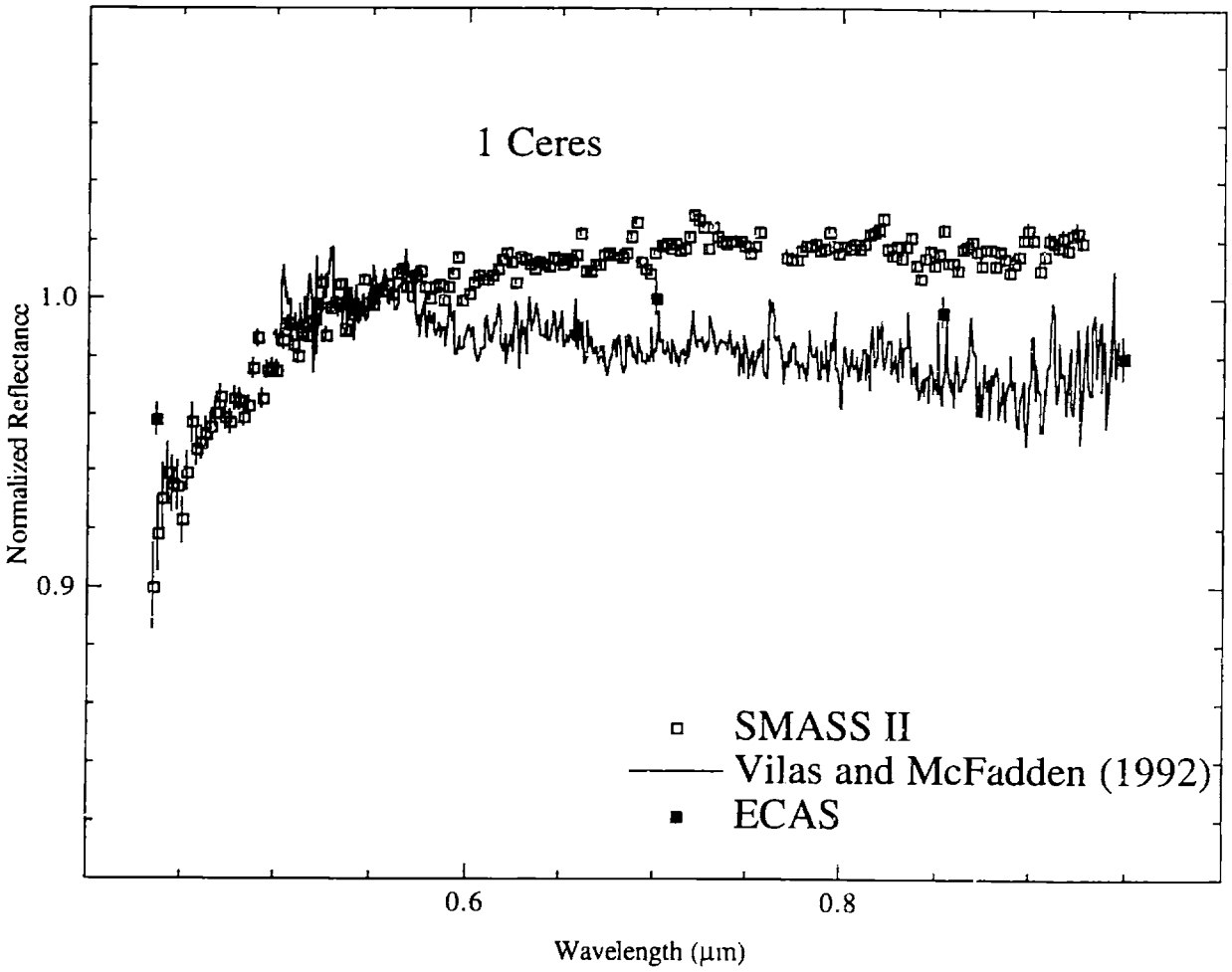

Figure 5.2.4. Reflectance spectra for C-asteroid 1 Ceres. Open squares are from SMASS II (Bus, 1999), line is from Vilas and McFadden (1992) and dark squares are from ECAS (Zellner *et al.*, 1985). Error bars are $\pm 1\sigma$.

Ceres was classified as a G asteroid by Tholen (1984). In the Bus (1999) classification, Ceres was labeled as a C because it did not have a strong-enough UV feature to be labeled a Cg, which is similar to Tholen's (1984) G class. CCD spectra (Figure 5.2.4) of Ceres shows that it does not have an absorption feature centered at 0.7 μm, but other weaker apparent features (e.g., 0.60, 0.67 μm) have been identified in Ceres' spectrum by Vilas and McFadden (1992). The Bus spectrum is slightly redder than the Vilas and McFadden spectrum with the ECAS data falling intermediate between the two spectra. The 0.60 μm feature does appear to be present in the Bus (1999) spectrum, but the 0.67 μm feature is not readily apparent.

The spectrum of Ceres is plotted versus unusual CM chondrite Y-86720 (particle size less than 63 μm) (albedo of 0.06) (Figure 5.2.5). The SMASSIR spectrum tends to be slightly redder than the 52-color data by ~2%. Both objects have ultraviolet features with similar strengths. However, the meteorite has a much broader feature than Ceres in the near-infrared that begins at a slightly shorter wavelength (~0.6 μm) than the band (beginning at ~0.8 μm) for Ceres. Their 3 μm absorption features also do not match in structure.

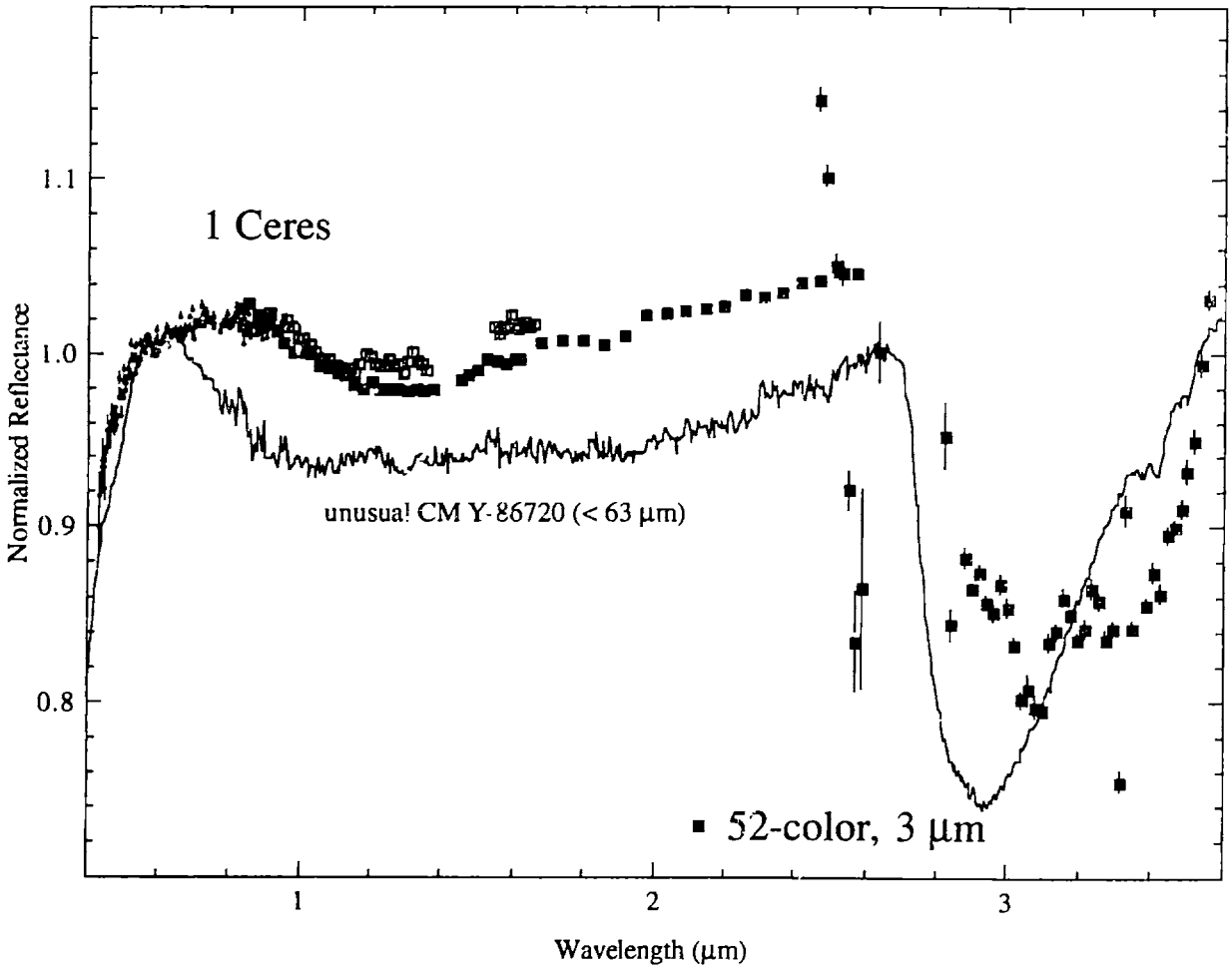

Figure 5.2.5. Reflectance spectra for C-asteroid 1 Ceres versus unusual CM chondrite Y-86720 (particle size less than 63 μm) (Hiroi *et al.*, 1993c). The Ceres spectrum includes SMASS II (Bus, 1999) (small dots), SMASSIR (open squares), 52-color (Bell *et al.*, 1988) (dark squares from ~0.83 to ~2.5 μm) and 3 μm data (dark squares from ~2.5 to 3.5 μm) (Jones *et al.*, 1990; 4/25/87). The 3 μm data are normalized to the 52-color data at ~2.5 μm. All spectra are normalized to unity at 0.55 μm. Error bars are ±1σ.

Ceres' 3 μm spectrum and high albedo (0.11 ± 0.01) is unlike that of any known carbonaceous chondrite (Jones, 1988; Hiroi *et al.*, 1996; Sato *et al.*, 1997). A narrow absorption feature at 3.07 μm, which was originally interpreted as H_2O frost (Lebofsky *et al.*, 1981a), has been interpreted by King *et al.* (1992) as indicating an ammonium-bearing mineral species, most likely ammoniated saponite, on the surface. Saponite has been found in CI, CR and CV

chondrites (Buseck and Hua, 1993), but has only been identified in one unusual CM chondrite (Bells) (Brearley, 1995).

As with Pallas, Ceres' spectrum from 0.3 to 3.5 μm is not consistent with any measured meteorite type. Either our meteorite collection contains no fragments of Ceres and/or some process has altered Ceres' surface so it is not spectrally representative of the material underneath. CM material with a relatively large particle size would have ultraviolet and 0.7 μm features with reduced strengths and a flatter spectral slope. But since the visual albedo would also be lowered (Johnson and Fanale, 1973), this is not a plausible mechanism for producing both Ceres' spectral features and its relatively high albedo. Also changing the particle size will not change the position of Ceres' 3 μm feature, which does not match measured meteorite samples.

Three other main-belt C-asteroids (10 Hygiea, 379 Huenna and 511 Davida) were also observed in SMASSIR (Figure 5.2.6). These C asteroids have slightly stronger UV features than the B types mentioned earlier, but slightly weaker UV features than Ceres. The SMASSIR spectrum of Hygiea is a "perfect" match for its 52-color data. The SMASSIR spectrum of Davida is not as red as its 52-color spectrum; however, the difference is very small (5%) and could possibly be due to extinction.

Hygiea and Huenna have UV features with similar strengths with unusual CI Y-82162. These asteroids also have similarly shaped spectral curves from 0.8 to 1.65 μm. Y-82162 has a roughly similar albedo (0.04) with these asteroids (0.05-0.07). Davida tends to be slightly redder in the visible than Hygiea and Huenna. Y-82162 has a similar strength UV feature with Davida but is not as red in the infrared. Unusual CM Belgica 7904 has a stronger UV feature than Davida. Hiroi *et al.* (1996) originally noted the spectral similarities (0.3 and 3.6 μm) between Hygiea and Y-82162 and also Davida and Belgica 7904.

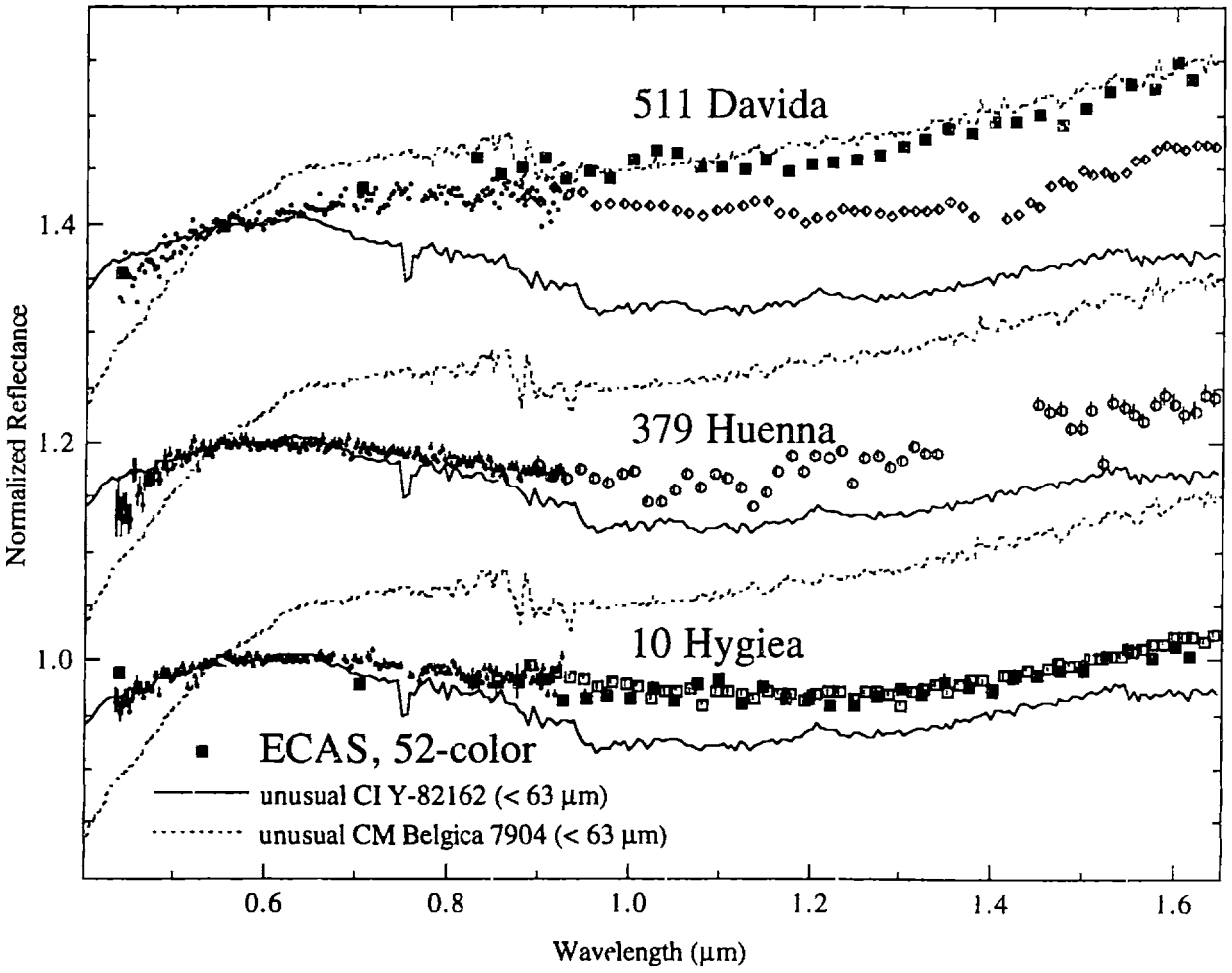

Figure 5.2.6. Reflectance spectra for C-asteroids 10 Hygiea, 379 Huenna and 511 Davida versus unusual CI chondrite Y-82162 (dark lines) (particle size less than 63 μm) and unusual CM chondrite Belgica 7904 (dashed lines) (particle size less than 63 μm). Small dots are from SMASS II (Bus, 1999) and large symbols are from SMASSIR. ECAS and 52-color data (dark squares) are plotted for Hygiea and Davida. The meteorite spectra are from Hiroi *et al.* (1993c). All spectra are normalized to unity at 0.55 μm and are offset by 0.2 in reflectance from each other. Error bars are $\pm 1\sigma$.

These C asteroids are spectrally very similar in the near-infrared from measured B asteroids (excluding Pallas). C-asteroid Hygiea is plotted versus B-asteroid Alauda in Figure 5.2.7. The only apparent spectral difference between these two objects is that Hygiea's UV feature is stronger by ~2%. This spectral difference could be due to a higher abundance of opaques on Alauda's surface; however, this spectral difference is within any realistic uncertainties in the spectral slopes (~5%) for these objects.

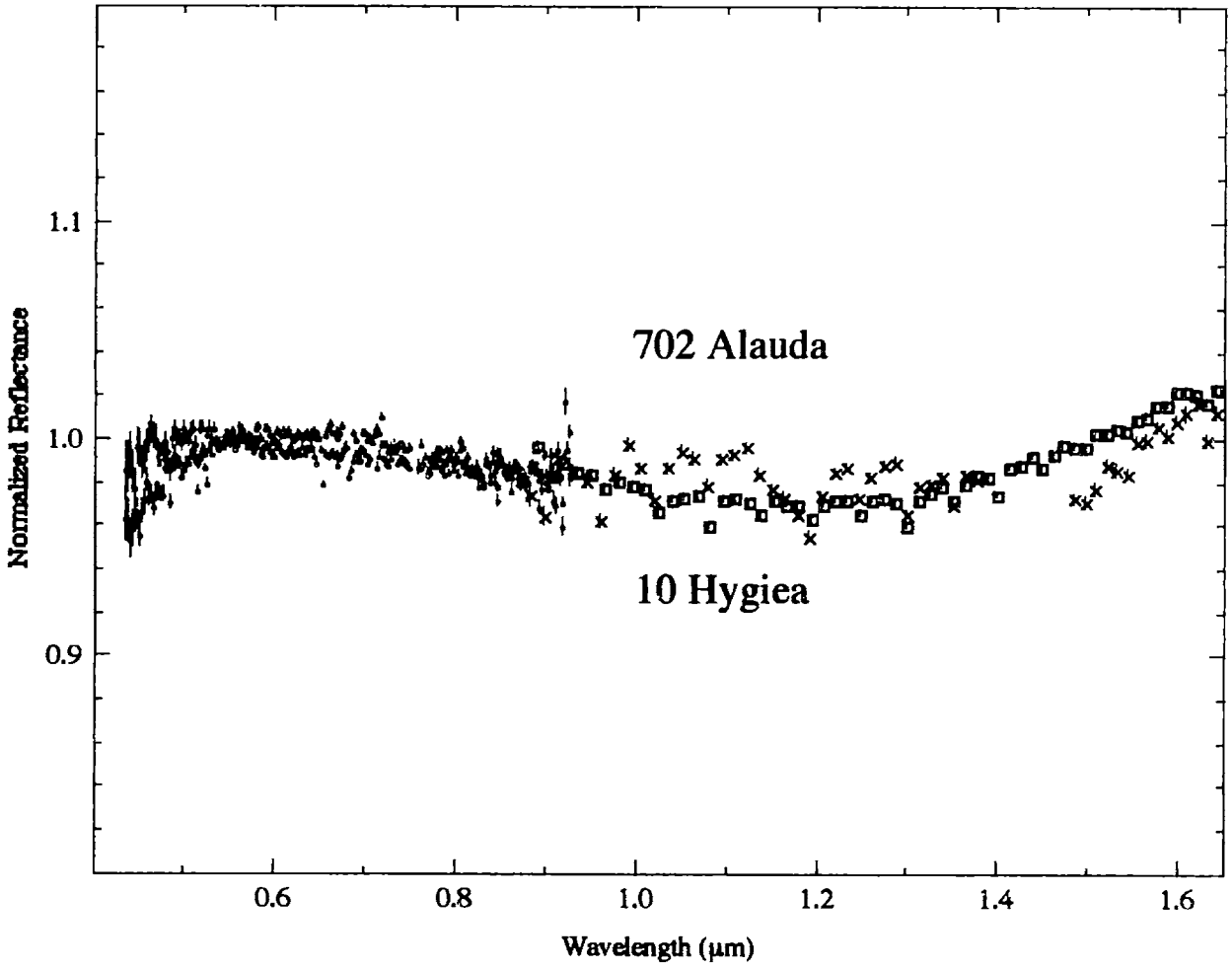

Figure 5.2.7. Reflectance spectra for C-asteroid 10 Hygiea and B-asteroid 702 Alauda. Small dots are from SMASS II (Bus, 1999) and large symbols are from SMASSIR. All spectra are normalized to unity at 0.55 μm. Error bars are ±1σ.

5.2.5 Subgroup: Cb Asteroids

Three Cb asteroids (253 Mathilde, 515 Athalia and 1998 KU_2) were observed in SMASSIR. Cb asteroids have spectra intermediate between B and C asteroids. Athalia was originally classified as a U (Tholen, 1984) and then as an I (Tholen, 1989) due to its S-like spectrum, but low albedo (0.04 ± 0.01). Asteroid 1998 KU_2 is a NEA.

The SMASSIR spectra of these three Cb asteroids indicate two types of objects. One type (253 Mathilde and 1998 KU_2) (Figure 5.2.8) have a broad absorption feature in the near-

infrared with a band depth of ~5%. These asteroids have similar features in this extended wavelength region to both the heated (900 °C) Murchison sample and the thermally metamorphosed CI Y-82162. The asteroid spectra are not similar to shock-darkened Gorlovka, which has an upturn at a shorter wavelength than the Mathilde and 1998 KU_2 spectra. This feature in Gorlovka's spectrum is due primarily to a suppressed pyroxene band. The best spectral match in the near-infrared to these two objects is the heated (900 °C) sample of Murchison.

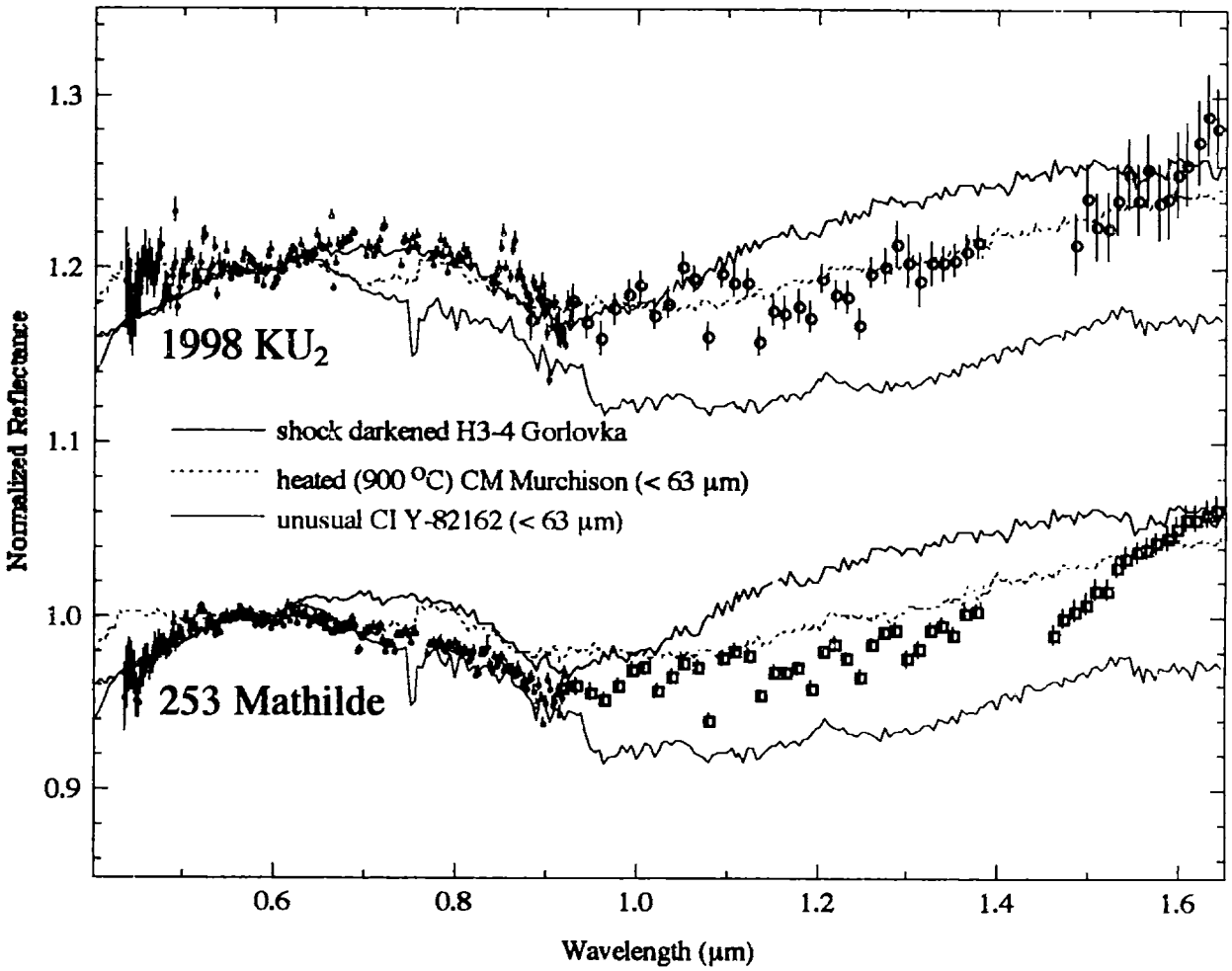

Figure 5.2.8. Reflectance spectra for Cb-asteroids 253 Mathilde and 1998 KU_2 versus shock darkened H3-4 chondrite Gorlovka (dark line) (Britt and Pieters, 1989), heated (900 °C) CM chondrite Murchison (dashed line) (Hiroi *et al.*, 1993c) and unusual CI chondrite Y-82162 (red line) (Hiroi *et al.*, 1993c). The Mathilde and 1998 KU_2 spectra are a combination of SMASS II (Bus, 1999) (small dots) and SMASSIR (open symbols). All spectra are normalized to unity at 0.55 μm. The 1998 KU_2 spectrum and a set of the meteorite spectra are offset by 0.2 in reflectance. Error bars are $\pm 1\sigma$.

The spectrum of the third observed Cb asteroid, Athalia, is shown in Figure 5.2.9. As can be seen in the figure, the SMASS II spectrum is not consistent with the ECAS data. The SMASSIR data is consistent with the relatively featureless SMASS II spectrum. The Athalia spectrum is much flatter than the other two Cb spectra with no apparent absorption features, except for the telluric band at ~1.4 μm. This spectrum is unlike any measured meteorite due to the absence of any discernible UV feature and any other absorption band. The featureless spectrum and low albedo (0.04 ± 0.01) implies a surface composed primarily of some type of opaque. The apparent absence of meteorites like these in our collections may imply that they are too fragile to make it through the earth's atmosphere.

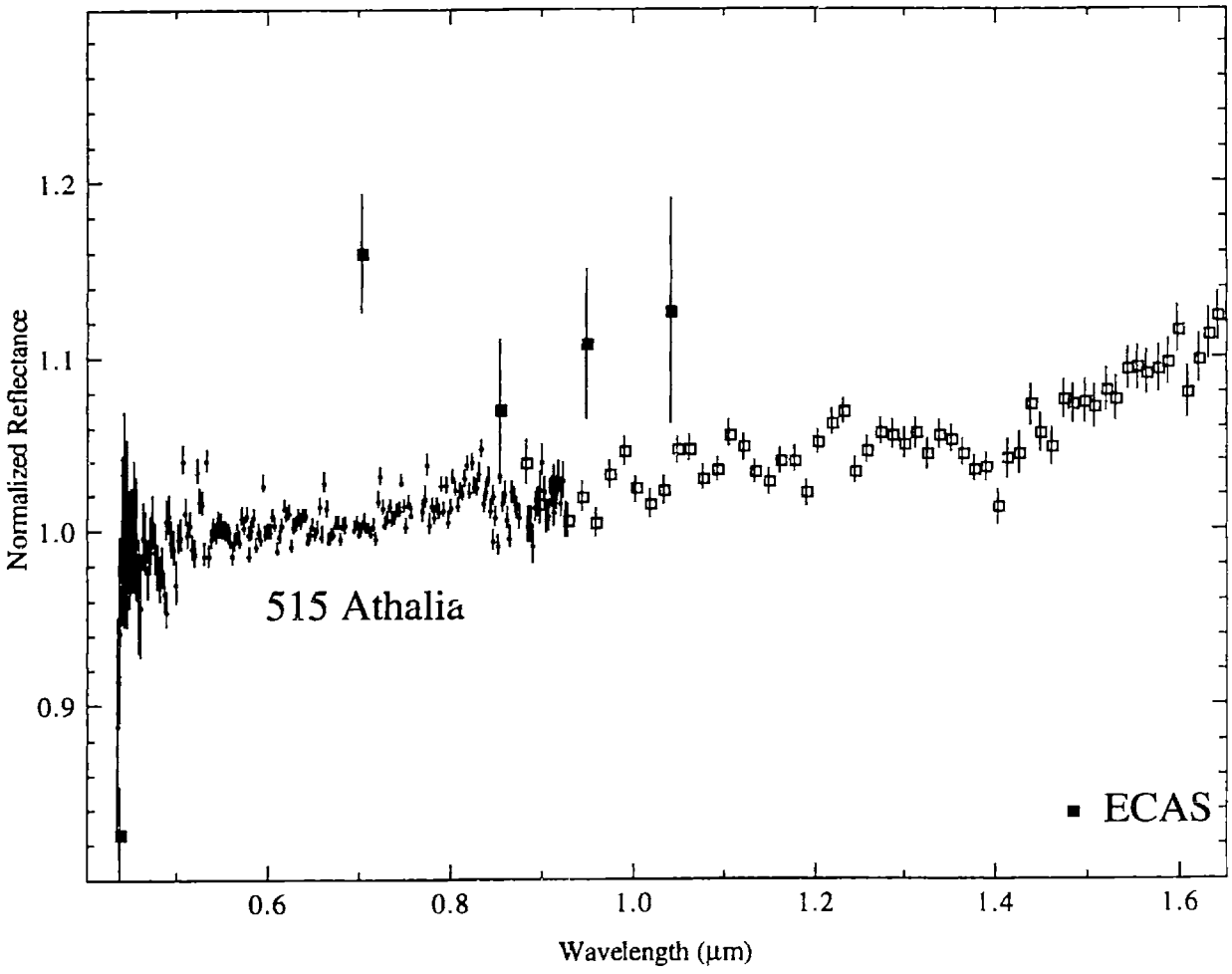

Figure 5.2.9. Reflectance spectra for Cb-asteroid 515 Athalia. All spectra are normalized to unity at 0.55 μm. Small dots are from SMASS II (Bus, 1999) and open squares are from SMASSIR. Dark squares are ECAS data (Zellner *et al.*, 1985). Error bars are ±1σ.

5.2.6 Subgroup: Ch asteroids

One Ch asteroid (19 Fortuna) was observed in SMASSIR. Ch asteroids have an absorption feature centered at ~0.7 μm. The visible and near-infrared spectrum (out to 2.5 μm) of Fortuna (Figure 5.2.10) matches very well the spectra of CM chondrite Murchison (bulk powder) (Gaffey, 1976) and LEW 90500 (particle size less than 100 μm) (Hiroi *et al.*, 1993c); however, the ultraviolet absorption feature is slightly weaker in Fortuna's spectrum. Burbine (1991) has noted that 19 Fortuna and the bulk-powder spectrum of Murchison have one of the best spectral matches (out to 2.5 μm) between asteroids with 52-color data (Bell *et al.*, 1988) and meteorites from Gaffey (1976). The SMASSIR spectrum for Fortuna tends not be as red (by ~3%) as the 52-color data

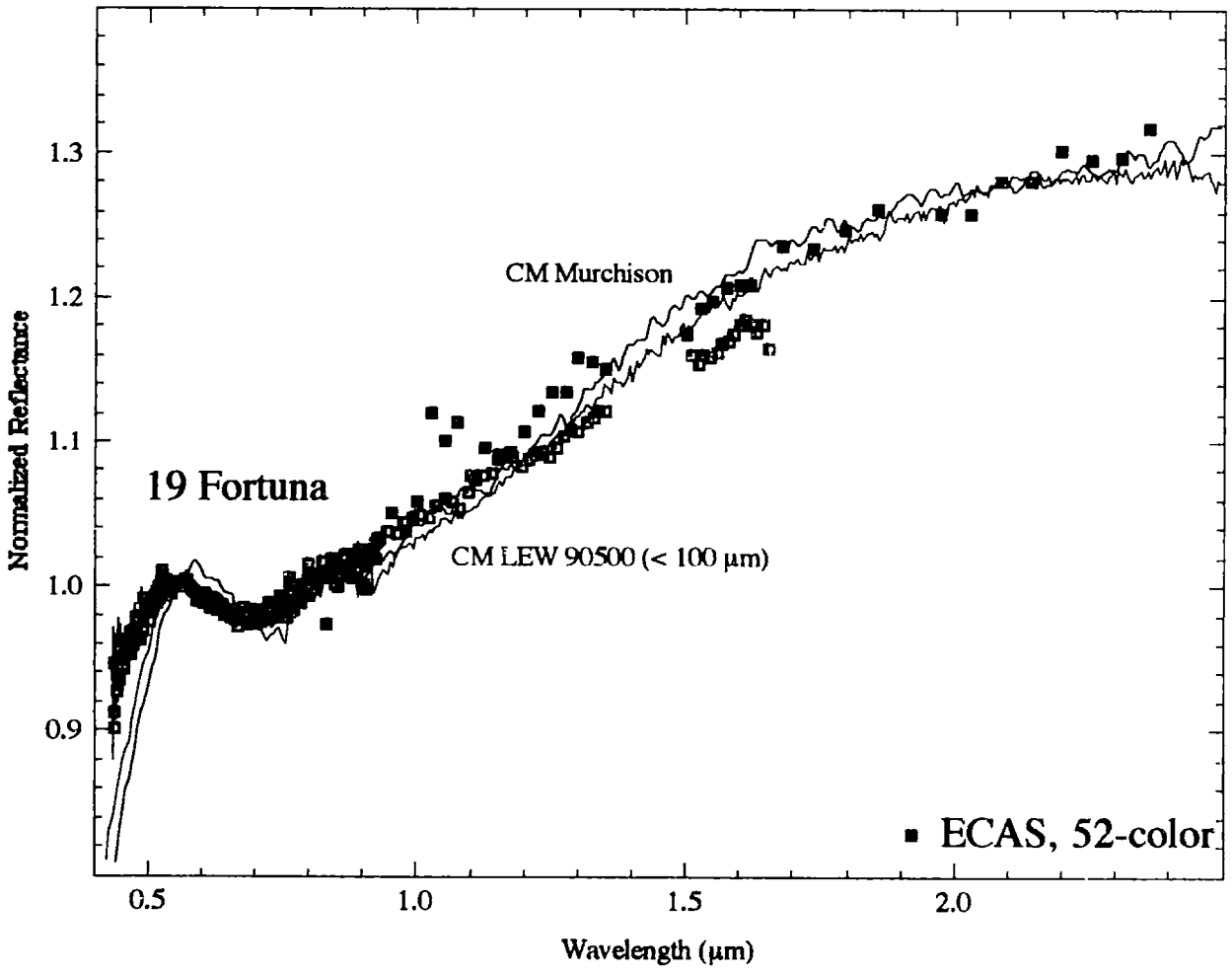

Figure 5.2.10. Reflectance spectra for Ch-asteroid 19 Fortuna versus Murchison (Gaffey, 1976) (black line) and LEW 90500 (particle size less than 100 μm) (blue line) (Hiroi *et al.*, 1993c). The small dots are SMASS II (Bus, 1999) data and open squares are SMASSIR data. The dark squares are a combination of ECAS (Zellner *et al.*, 1985) and 52-color data (Bell *et al.*, 1988). All of the spectra are normalized to unity at 0.55 μm. Error bars are ±1σ.

Fortuna has an absorption feature centered around 0.7 μm that is similar in shape and strength to those found in many CM chondrites. The SMASS II spectrum of Fortuna (Figure 5.2.11) is plotted versus spectra of Murchison (bulk powder) and LEW 90500 (particle size less than 100 μm). The fine-grained LEW 90500 appears to be the best match. The band center (where a linear continuum has been removed) of the 0.7 μm feature in LEW 90500 (particle size less than 100 μm) is at a slightly longer wavelength (~0.72 μm) than the band centers for Fortuna (~0.67 μm) (assumed error bars of ±0.01 μm), which may imply a slight compositional difference in their phyllosilicate compositions. It is also unclear what the effects of temperature are on the spectra of CM chondrites. Fornasier *et al.* (1999) also has found that a visible spectrum of LEW 90500 matches very well the spectra of Fortuna and other C type asteroids with 0.7 μm features.

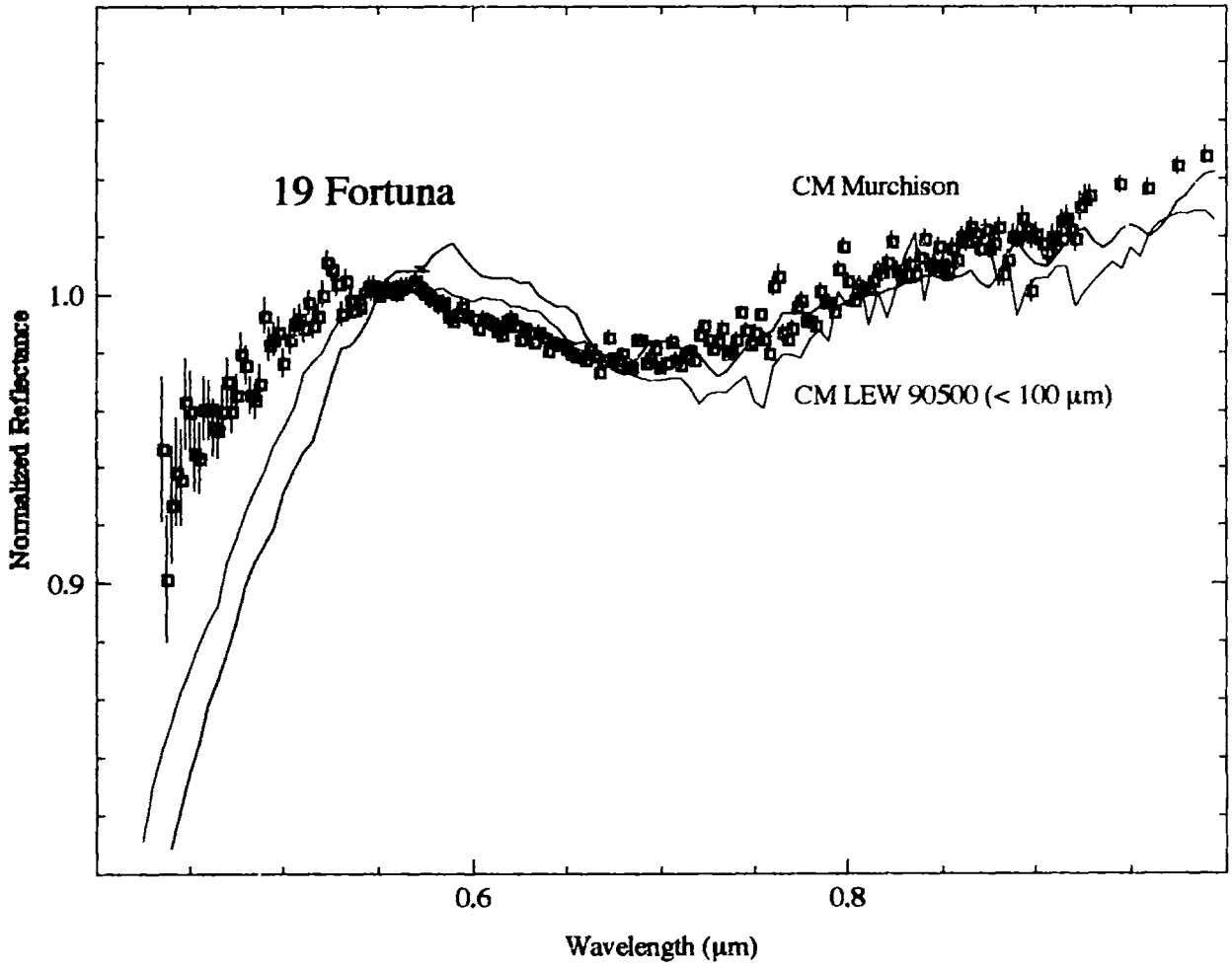

Figure 5.2.11. Reflectance spectra for Ch-asteroid 19 Fortuna versus Murchison (Gaffey, 1976) and LEW 90500 (particle size less than 100 μm) (Hiroi *et al.*, 1993c). The open squares are a combination of SMASS II (Bus, 1999) (shortwards of ~0.92 μm), SMASSIR (longwards of ~0.92 μm) data. All of the spectra are normalized to unity at 0.55 μm. Error bars are ±1σ.

Another Ch asteroid (13 Egeria) has also been noted as being spectrally similar to CM chondrites (Burbine, 1998). Egeria's ultraviolet absorption feature matches pretty well the spectrum of a bulk powder of LEW 90500 (Figure 5.2.12); however, the bulk powder spectrum of LEW 90500 is redder than Egeria in the near-infrared.

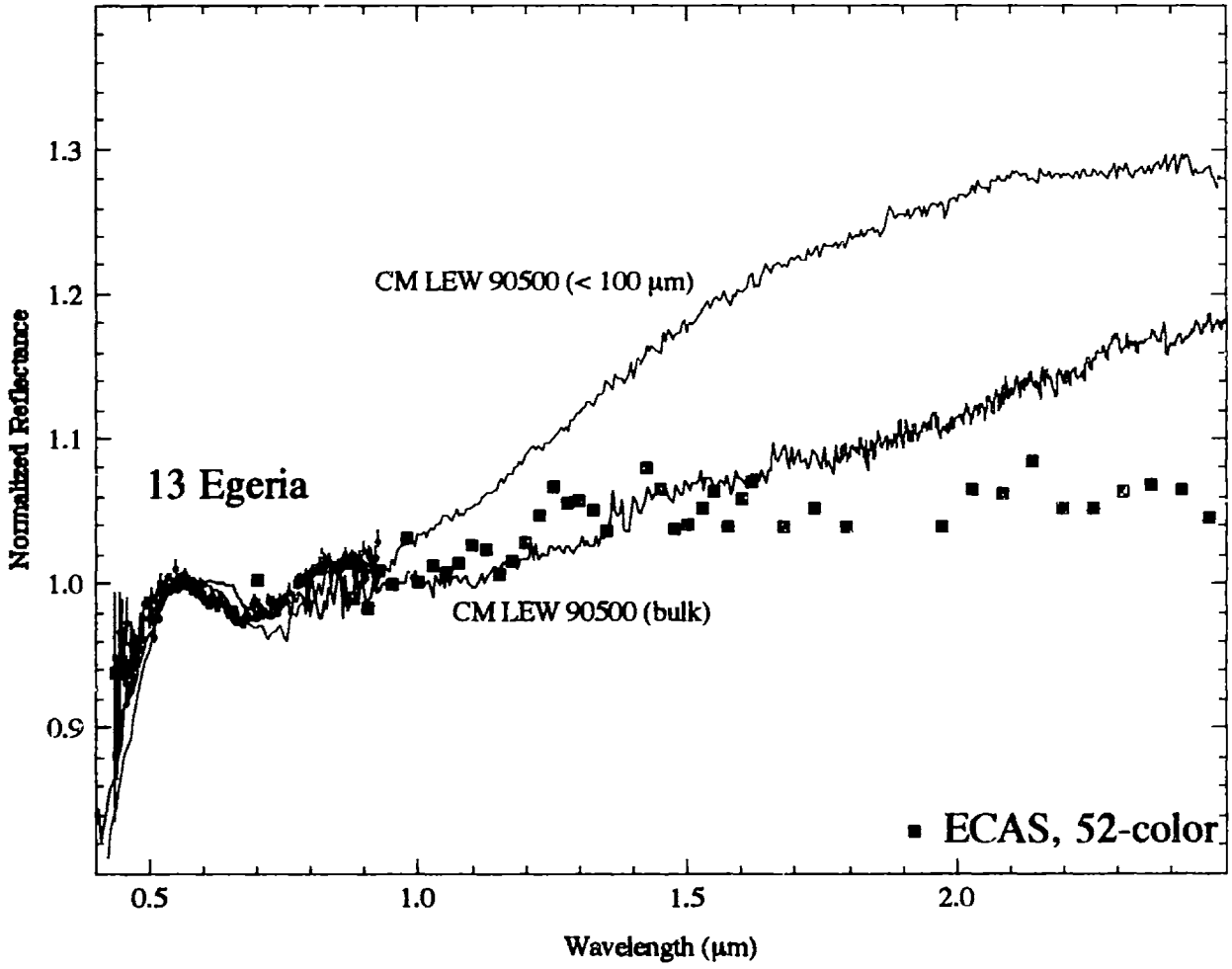

Figure 5.2.12. Reflectance spectra for Ch-asteroid 13 Egeria versus LEW 90500 (particle size less than 100 μm) (blue line) (Hiroi *et al.*, 1993c) and LEW 90500 (bulk powder) (Burbine, 1998) (black line). The bulk-powder LEW 90500 sample was supplied by the Meteorite Working Group and measured at RELAB. Small dots are from SMASS II (Bus, 1999). The dark squares are a combination of ECAS (Zellner *et al.*, 1985) and 52-color data (Bell *et al.*, 1988). All of the spectra are normalized to unity at 0.55 μm. Error bars are $\pm 1\sigma$.

In the visible, a CCD spectrum of Egeria (Figure 5.2.13) matches better with the spectrum of the finer-grained LEW 90500 than with the spectrum of the bulk powder of LEW 90500. The band center of the 0.7 μm feature in LEW 90500 (particle size less than 100 μm) is also at a slightly longer wavelength (~0.72 μm) than the band centers for Egeria (~0.67 μm). The strength of Egeria's 3 μm feature (40 ± 15%) is also similar to those of CM chondrites (~45%), but its IRAS albedo (0.08 ± 0.01) is slightly higher than these meteorites (~0.04). The scatter in the points shortwards of ~0.45 μm are due to the low number of counts in this wavelength region.

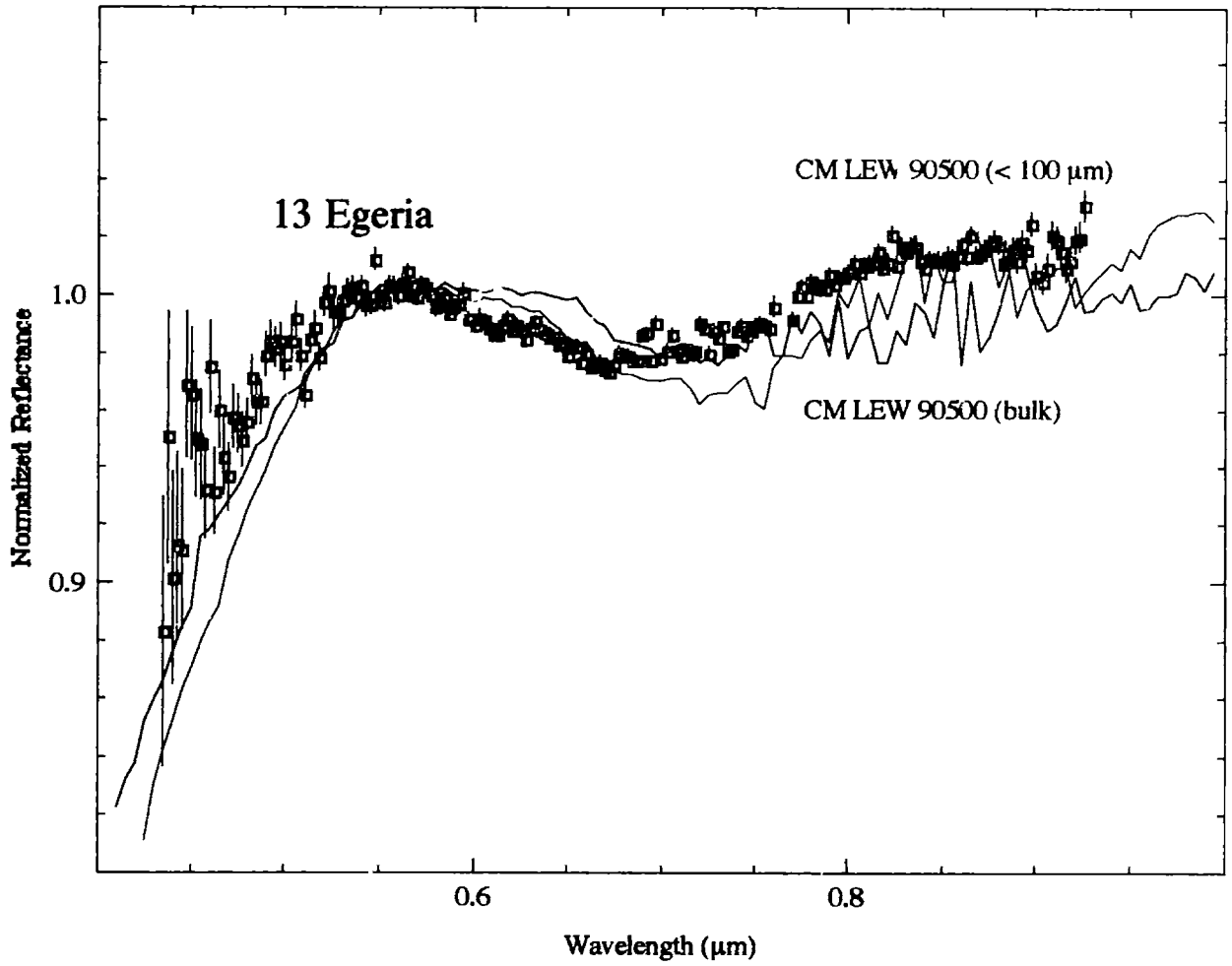

Figure 5.2.13. Reflectance spectra for Ch-asteroid 13 Egeria versus LEW 90500 (particle size less than 100 μm) (blue line) (Hiroi *et al.*, 1993c) and LEW 90500 (bulk powder) (Burbine, 1998) (black line). The bulk-powder LEW 90500 sample was supplied by the Meteorite Working Group and measured at RELAB. The open squares are from SMASS II (Bus, 1999). All of the spectra are normalized to unity at 0.55 μm. Error bars are ±1σ.

The difficulty in matching the spectral slope and the characteristics of the 0.7 μm absorption feature between Egeria and LEW 90500 could imply a slight compositional difference between their phyllosilicates. Particle size differences do not appear to be a likely cause since

increasing the particle size of the measured LEW 90500 sample to decrease the spectral slope would tend to decrease the strength of the 0.7 μm feature and make the feature look less like Egeria's feature. However, the presence of the 0.7 μm feature does imply a CM-like composition for Egeria. As mentioned earlier, it is unclear what the effects of temperature will be on CM chondrite spectra.

5.2.7 Forging Spectroscopic Links to Carbonaceous Chondrites

One interesting trend from Table 1.4 is that five Ch asteroids (19 Fortuna, 13 Egeria, 751 Faina and 405 Thia) are among the top twenty-six asteroids with the highest total fragment delivery efficiencies. The large number of CM chondrites in our meteorite collection may be due to the relatively large number of parent bodies (most likely Ch objects) located very-near resonances. Since "CM-like" material should be more fragile than stony or iron meteorites, the source bodies of the CM chondrites would need to be located very near a resonance to supply fragments to Earth without being destroyed. CM meteorites tend to have very short cosmic ray exposure ages (less than 6.5 million years) (Eugster *et al.*, 1998) with LEW 90500 having an exposure age of ~0.24 million years and Murchison having one of ~0.58 million years. Other carbonaceous chondrites (e.g., CO, CV, CK) tend to have much longer exposure ages (~1 to ~63.5 million years) (Scherer and Schultz, 2000), which is probably due to the less fragile nature of these meteorites. Fortuna is located relatively near (~0.04 AU) the edge of the 3:1 resonance while Egeria is near (~0.06 AU) the intersection of the 3:1 and ν_6 resonances. These locations near resonances appear consistent with the short exposure ages of the CM chondrites. The presence of a NEA with a CM composition could also produce the low cosmic ray exposure ages of CM chondrites since meteorites from this body would not be expected to reside long in space before hitting Earth (Scherer and Schultz, 2000); however, no Ch asteroids have been identified in the NEA population (Bus, personal communication).

Carbonaceous chondrite material may be too fragile to survive the long transit times from the higher-order resonances and may be coming preferentially from the lower order and the ν_6 resonances. Ceres is located far from the 5:2 resonance at ~2.8 AU (the closest low-order resonance) so fragments may not survive long enough to reach Earth. Ceres makes the Farinella *et al.* (1993) list of objects with the highest probability of injecting fragments into resonances due to its large surface area for producing fragments compared to other asteroids. Roberta, a plausible parent body for thermally metamorphosed carbonaceous chondrites, is located relatively near (~2.48 AU) the 3:1 resonance.

Since Fortuna and Egeria should be supplying a relatively large number of fragments into earth-crossing orbits, it is likely that samples of these asteroids do exist in our meteorite collection. If samples of Fortuna and Egeria have been found, they have probably been

classified as CM chondrites. But as mentioned earlier, observational surveys estimate approximately one-half (Barucci *et al.*, 1998) to three-quarters (Sawyer, 1991) of C-type asteroid spectra contain the 0.7 μm absorption feature. Fornasier *et al.* (1999) found that two-thirds of their studied C-type asteroids had 0.7 μm features. Vilas (1994) has estimated that this feature is found in the spectra of approximately one-half of C-type asteroids using an algorithm to predict the presence of the 0.7 μm feature in an asteroid's spectrum from ECAS data. Since this feature can be found in the spectra of a significant number of other asteroids, it is impossible to make any definitive conclusions between any proposed relationships between Fortuna and Egeria and the CM chondrites.

Of the asteroids with spectral similarities to the heated carbonaceous chondrites, Roberta, due to its location near the 3:1 resonance is and spectral similarity to anomalous CI Y-82162, is probably the most plausible parent body for some of these meteorites. Ceres and Pallas are very anomalous and do not match very well any measured meteorite sample, which may be due to their orbits falling very far from known meteorite-supplying resonances. However, if some process (e.g., micrometeorite bombardment) is altering the spectral properties of some of the A asteroids, the same process may be altering some of the carbonaceous chondrite parent bodies so they appear thermally altered. The asteroids that look like CM chondrites may just have surfaces with younger ages, which would mean that they would tend to be less altered.

5.2.8 Conclusions

Except for the very unusual objects Ceres and Pallas, observed C types tend to have spectral properties similar to known meteorites (Table 5.2.1). Some of these asteroids (e.g., 19 Fortuna) have spectral properties similar to CM chondrites, while a number of other observed objects (e.g., 253 Mathilde, 379 Huenna) appear spectrally similar (e.g., weak UV features; broad bands in the near-infrared) to thermally metamorphosed carbonaceous chondrites, which are relatively rare in our meteorite collections. This is consistent with the results of Hiroi *et al.* (1993c, 1996), who previously linked heated carbonaceous chondrites to C asteroids. The presence of spectral analogs to the CM chondrites in the main belt argues against the Lodders and Osborne (1999) scenario that CM chondrites are derived from comets.

Table 5.2.1. Mineralogic interpretation of C-type asteroids observed in SMASSIR. For NEAs, their orbital type is given instead of their semi-major axis (a). Quotation marks are used for meteoritic analogs that appear less certain.

Type	Asteroid	a (AU)	Meteoritic Analog	Mineralogic Interpretation
Low-albedo B or C	10 Hygiea	3.142	heated CI chondrite	weak UV feature; slightly bluish to flat spectral slopes in the near-infrared; albedos less than 0.07; spectral features appear consistent with heated carbonaceous chondrite
	335 Roberta	2.475	heated CI chondrite	
	379 Huenna	3.136	heated CI chondrite	
	511 Davida	3.173	"heated CI –CM chondrite"	
	702 Alauda	3.195	heated CI chondrite	
High-albedo B	2 Pallas	2.769	none readily apparent	weak UV feature; blue-sloped spectrum in the near-infrared; albedo of 0.16
High-albedo C	1 Ceres	2.767	none readily apparent	slightly stronger UV feature than other C types; blue spectral slope in near-infrared with slight absorption band; albedo of 0.11
Featured Cb	253 Mathilde	2.647	heated (900 °C) CM chondrite	weak UV feature; weak but broad feature in the near-infrared; spectral features appear consistent with heated carbonaceous chondrite material
	1998 KU_2(Amor)		heated CI or CM chondrite	
Featureless Cb	515 Athalia	3.121	none readily apparent	very weak UV feature; flat to slightly red in the near-infrared
Cb	19 Fortuna	2.442	Murchison (CM chondrite), LEW 90500 (CM chondrite)	slightly stronger UV feature than CM chondrites; feature at ~0.7 μm and red spectral slope in the near-infrared similar to those of CM chondrites

Fortuna has a similar 0.7 μm feature and spectral slope with CM chondrites Murchison (bulk powder) and LEW 90500 (particle size less than 100 μm). Egeria matches well with the bulk powder spectrum of LEW 90500, but their 0.7 μm features do not match very well in structure. Also, the band center of the 0.7 μm feature in the finer-grained LEW 90500's spectrum is at a slightly higher wavelength than Fortuna's and Egeria's minima. The presence of the 0.7 μm feature implies a CM composition for these objects, but the difference in wavelength positions of the centers implies that LEW 90500 is not a perfect spectral match for these asteroids.

The CM chondrites tend to have slightly stronger UV features than Egeria and Fortuna. Besides increasing the particle size, one possible way to reduce the strength of the ultraviolet feature in carbonaceous chondrite spectra is to heat the material (Hiroi *et al.*, 1993c). However, the 0.7 μm feature disappears in the spectra of CM material heated to temperatures above ~400 °C. Theoretical work (e.g., Love and Ahrens, 1996) has suggested that most asteroids are rubble piles. These are objects that have been shattered, but whose gravitational attraction has kept them intact. Vilas and Sykes (1996) have proposed that if the weaker ultraviolet feature in C-type asteroid spectra compared to carbonaceous chondrites is due to heating, then the presence of the 0.7 μm feature in the same spectrum may imply a rubble pile whose surface consists of metamorphosed material from the interior and relatively unheated CM material from the original body's exterior.

The CM chondrites are known to contain members with varying degrees of alteration; however, compositional trends among different alteration parameters suggest that the CM chondrites experienced similar processes (e.g., Browning *et al.*, 1996). The two CM chondrites (Murchison and LEW 90500), even though spectrally similar, have experienced different amounts of alteration (Hanowski and Brearley, 1997), implying different formation locations on the same parent body or in different parent bodies altogether.

Fortuna and Egeria are spectrally similar to measured CM chondrites, which implies some type of compositional similarity. But the chief problem with trying to link these asteroids with the CM chondrites is that these asteroids' spectral features are not unique. Fortuna and Egeria are located relatively near meteorite-supplying resonances with short timescales for delivery of fragments to Earth, so these objects appear to be the two most-likely parent bodies for the CM chondrites.

Most of the C asteroids observed in SMASSIR had spectral properties similar to thermally metamorphosed carbonaceous chondrites. The rareness of these meteorites in our collections could just be due to the relative absence of their parent bodies near low order resonances, which have short transit times to Earth. It is also possibly that some type of surface alteration process (e.g., micrometeorite bombardment) is changing the surface properties of bodies with carbonaceous chondrite compositions and their spectra are not really indicative of the material underneath. Laser irradiation experiments need to be done on carbonaceous chondrite material. Ceres and Pallas have spectra that are unlike any measured meteorite sample and it is possible that fragments of these objects have not reached Earth due to their distance from these low order resonances.

5.3 K Asteroids

5.3.1 Background

Bell (1988) first proposed the K-asteroid designation on the basis of near-infrared spectra (52-color data) of four Eos family members. Although the 52-color spectra were very noisy (Figure 5.3.1), K asteroids were provisionally defined as having albedos near 0.09, S-like spectral curvature at visual wavelengths, weak 1 μm features and relatively flat reflectances from 1.1 to 2.5 μm. The observed Eos family members were noted to have visible and near-infrared spectra similar to CO/CV chondrites (Figure 5.3.1); however, these asteroid's near-infrared spectra were relatively noisy. Eos family members have been known since the work of Gradie and Zellner (1977) to have spectra and albedos intermediate between C and S objects. The Eos family contains over 450 objects (Zappalà *et al.*, 1995).

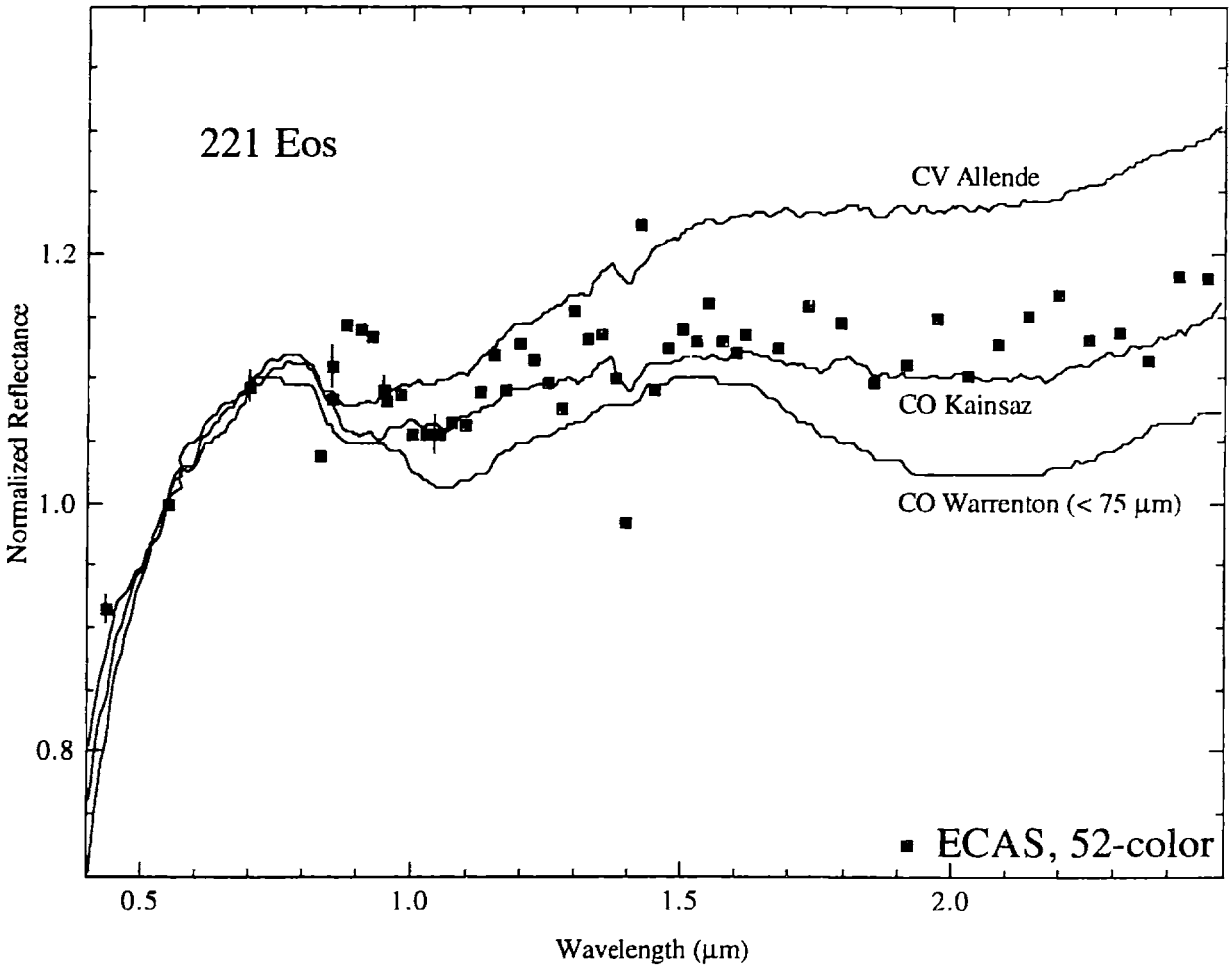

Figure 5.3.1. Reflectance spectrum of K-asteroid 221 Eos versus spectra of CO chondrite Kainsaz, CO chondrite Warrenton (particle size less than 75 μm) and CV chondrite Allende. All the meteorite spectra are from Gaffey (1976). The dark squares are a combination of ECAS (Zellner *et al.*, 1985) and 52-color data (Bell *et al.*, 1988). All spectra are normalized to unity at 0.55 μm. Error bars are $\pm 1\sigma$.

Visible spectra of 45 asteroids in the Eos family by Doressoundiram *et al.* (1998) show a continuum of spectral properties for almost all objects with only two observed asteroids seeming to be interlopers. They noted that the lower range of the distribution had spectral properties similar to CO/CV chondrites, but the upper range could not be satisfactorily linked with any known meteorite type.

CO and CV chondrites are both type 3 carbonaceous chondrites and are composed primarily of chondrules and matrices of olivine. Type 3 chondrites are the least thermally altered type of chondrite. Relative to CO chondrites, CV chondrites tend (McSween, 1977; Dodd, 1981) to have larger chondrules (0.5-2 mm versus sizes less than 0.5 mm in CO chondrites) and higher contents of dark matrix material. CV chondrites also have lower Fe/Si and higher Ca/Si, Al/Si and Ti/Si ratios, which are correlated with the higher abundance of CAIs in CV chondrites. CO chondrites are subdivided (Scott and Jones, 1990) into types 3.0 to 3.7 using primarily olivine compositions with fayalite content increasing with increasing grade. The CV chondrites also have been divided into a number of subgroups (McSween, 1977; Weisberg *et al.*, 1997; Krot *et al.*, 1998) using differences in opaque mineralogies and degrees of aqueous alteration.

The prevailing question concerning the K asteroids is whether they actually have compositions similar to CO/CV chondrites. Previous near-infrared studies of these objects have produced only very low-quality or low-resolution data, which makes any specific mineralogical interpretations difficult.

5.3.2 Investigation of K Asteroids

To help determine the composition of K asteroids, three of these objects (221 Eos, 599 Luisa and 653 Berenike) were observed in SMASSIR (Table 5.3.1). All of these asteroids have relatively large diameters (39 to 104 km). Eos and Berenike are both in the Eos family.

Table 5.3.1. K asteroids observed in SMASSIR. Proper elements (a, e', sin i') are from Milani and Knezevic (1994). Diameters and albedos are from IRAS (Tedesco, 1994). Family memberships are from Zappalà *et al.* (1995).

Asteroid	a (AU)	e'	sin i'	IRAS Albedo	Diameter (km)	HCM Family	NEA	52-color
221 Eos	3.012	0.077	0.173	0.14	104	Eos		yes
599 Luisa	2.773	0.228	0.288	0.14	65			
653 Berenike	3.014	0.080	0.181	0.24	39	Eos		yes

As can be seen in Figure 5.3.2, Eos and Berenike are almost perfect spectral matches in the visible and near-infrared. Both have similar strength UV features, plus an absorption feature centered around ~1.06-1.08 μm. The wavelength position of this feature plus the more subtle features at ~0.9 and ~1.3 μm indicates an olivine-rich assemblage.

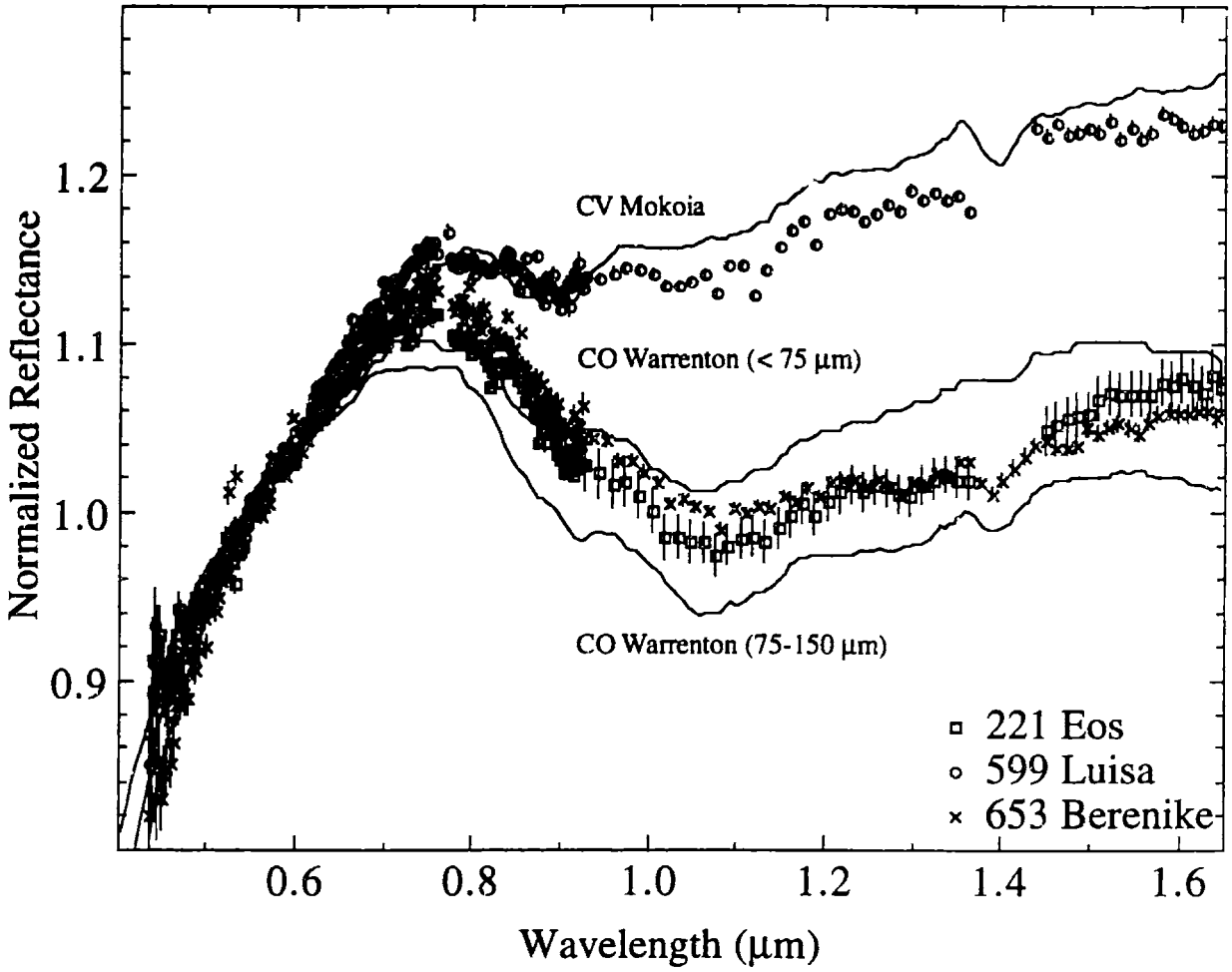

Figure 5.3.2. Reflectance spectra for K-asteroids 221 Eos (squares), 599 Luisa (circles) and 653 Berenike (crosses) versus spectra of CV chondrite Mokoia and CO chondrite Warrenton (particle sizes less than 75 μm and between 75 and 150 μm). Small points are from SMASS II (Bus, 1999) and larger symbols are from SMASSIR. All meteorite spectra are from Gaffey (1976). All spectra are normalized to unity at 0.55 μm. Error bars are ±1σ.

These two spectra are remarkably similar to spectra of CO chondrite Warrenton. The two Eos family members fall intermediate between a Warrenton spectrum for a particle size less than 75 μm and one between 75 and 150 μm. The Warrenton spectra have a similarly shaped absorption feature that is centered at 1.06 μm. This feature is due to olivine since Warrenton is ~75% olivine (and ~4% pyroxene) (Wahl, 1950) with an average fayalite composition of Fa_{27} (Scott and Jones, 1990) (and an average ferrosilite composition of Fs_3). Warrenton is a type 3.6 and relatively fayalite-rich compared to other CO chondrites. The feature at ~1.4 μm in the

spectrum of Berenike is most likely due to an incompletely removed atmospheric absorption feature. The feature at ~1.4 μm in the Warrenton spectra could be due to a terrestrial alteration product; however, CO chondrites are known to contain phyllosilicates (e.g., Buseck and Hua, 1993), which could also produce such a feature. The albedo of Eos (0.14 ± 0.01) falls intermediate between the albedos (0.10 and 0.16) of the Warrenton spectra, while Berenike is brighter (albedo of 0.24 ± 0.03).

Luisa is redder than the two other K types. The scatter in the points makes any interpretation difficult, but an absorption feature centered at ~1.1 μm, most likely due to olivine, is apparent in the spectrum. Luisa is spectrally similar to CV chondrite Mokoia with this meteorite also having a weak absorption feature centered at 1.1 μm and a similar strength UV feature. This feature is due to olivine since the mafic silicates in the matrix and chondrules in Mokoia are primarily olivine (Weisberg and Prinz, 1998). The composition of the olivine in CV matrices range from $Fa_{10\text{-}90}$ with most analyses varying between $Fa_{40\text{-}60}$. Luisa is slightly brighter (albedo of 0.14 ± 0.01) than the Mokoia sample (0.07). The albedos of other CV chondrites vary from 0.06 to 0.11.

5.2.3 Forging Spectroscopic Links to CO and CV chondrites

Luisa (found at 2.773 AU) is located near the 5:2 resonance at ~2.8 AU, which should be supplying fragments quickly into Earth-crossing orbits. The Eos family is cut by the 9:4 resonance (at ~3.03 AU) with Jupiter (Morbidelli *et al.*, 1995). Numerical simulations by Di Martino *et al.* (1997) found that ~92% of test particles that entered the 9:4 resonance were ejected from the solar system. However, they believe that ~2% of all CO/CV meteorites could be from the Eos family, due to the large amount of material that would enter the resonance during the event that created the family. Interestingly, Mokoia (the spectral analog to Luisa) has a relatively short cosmic ray exposure age (9.7 million years) while Warrenton (the spectral analog for Eos and Berenike) has a much longer age (34 million years) (Scherer and Schultz, 2000). These calculated ages (error bars estimated to be less than 20%) for these meteorites appear consistent with the 5:2 resonance (near Luisa) moving fragments (possibly Mokoia) into an Earth-approaching orbit much quicker than the 9:4 resonance (near the Eos family), where timescales for delivering fragments (possibly Warrenton) into Earth-crossing orbits are estimated to at least 50 million years (Di Martino *et al.*, 1997).

5.3.4 Conclusions

The three observed K asteroids are very good spectral matches (Table 5.3.2) for specific CO and CV chondrites, which is consistent with the interpretations of Bell (1988) and Doressoundiram *et al.* (1998). The two Eos family members observed in SMASSIR are almost

perfect spectral matches with each other. Their spectra have the same absorption features due to olivine as CO chondrite Warrenton and fall intermediate between spectra of two particle sizes of this meteorite. The other K chondrite measured (599 Luisa) is a very good spectral match for CV chondrite Mokoia. All of these objects have similar strength UV features with their meteorite counterpart.

Table 5.3.2. Mineralogic interpretation of K asteroids observed in SMASSIR.

Type	Asteroid	a (AU)	Meteoritic Analog	Mineralogic Interpretation
Featured K	221 Eos	3.012	Warrenton (CO chondrite)	strong UV feature; 1 μm feature due to olivine
	653 Berenike	3.014	Warrenton (CO chondrite)	with three distinctive bands and a band depth of ~10%
Flatter K	599 Luisa	2.773	Mokoia (CV chondrite)	strong UV feature; subdued olivine feature with band depth of ~5%; slightly red spectral slope

5.4 L and Ld Asteroids

5.4.1 Background

The L and Ld classes are newly defined by Bus (1999). Over 40 L and Ld asteroids were classified in SMASS II. L-class spectra have a very steep red slope shortward of 0.75 μm and a very weak 1 μm feature. The "L" designation was chosen to stress the apparent spectral continuum that these objects have with K asteroids, which have shallower UV features. Ld asteroids have spectra intermediate between L and D objects.

Two L-class members (387 Aquitania and 980 Anacostia, which were previously classified as S types) have been noted previously (Burbine *et al.*, 1992) to have unusual near-infrared spectra with moderately deep and broad 2 μm features and very weak 1 μm features (Figure 5.4.1).

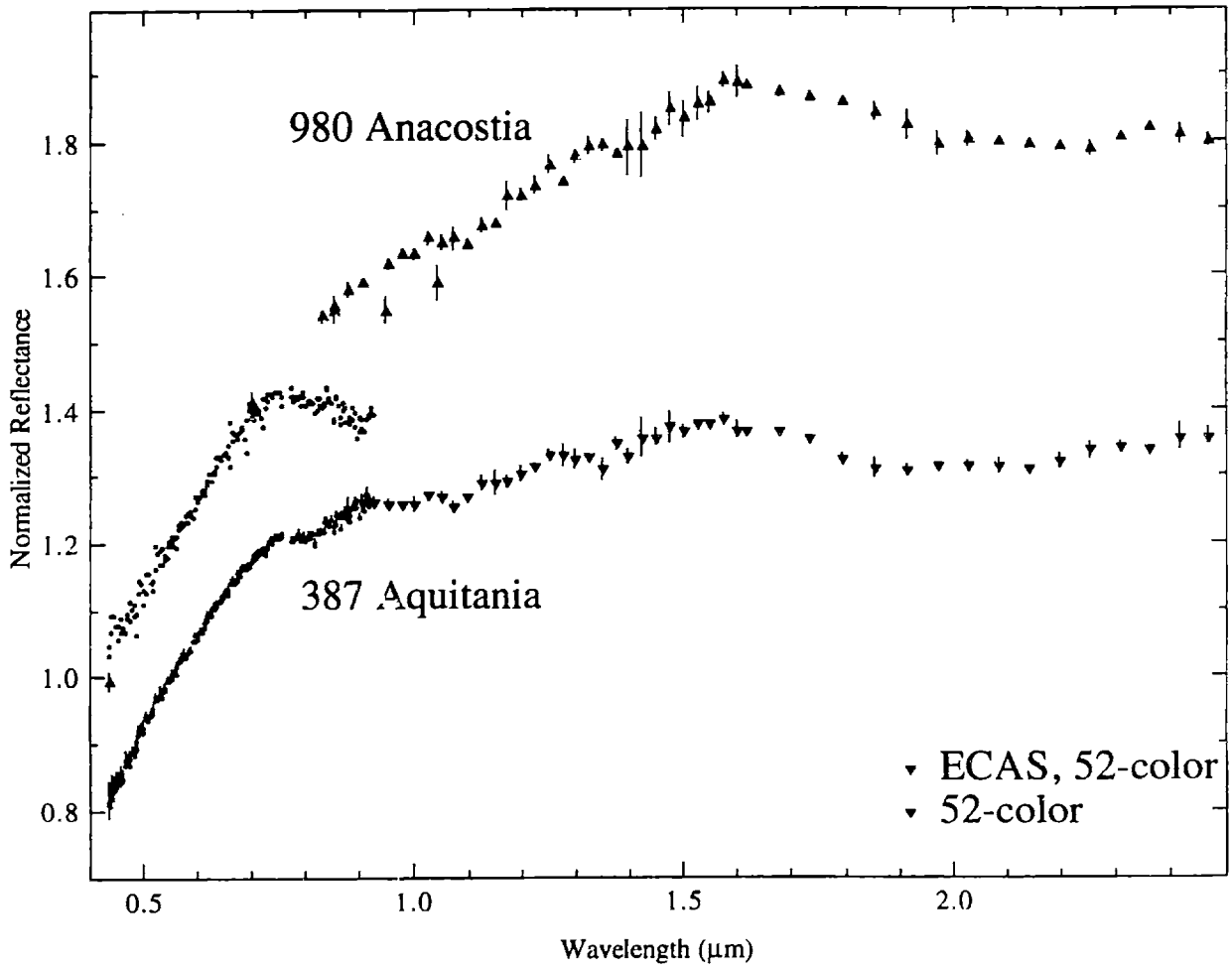

Figure 5.4.1. Reflectance spectra for L-asteroids 387 Aquitania and 980 Anacostia. Small dots are from SMASS II (Bus, 1999). Only 52-color data (upside-down triangles) for Aquitania are plotted while ECAS and 52-color data (triangles) are plotted for Anacostia. All spectra are normalized to unity at 0.55 μm with Anacostia offset by 0.2. Error bars are ±1σ.

But as can be seen in the figure, the SMASS spectrum (Bus, 1999) of Anacostia has a much deeper 1 μm feature than its ECAS spectrum (Zellner *et al.*, 1985), which has a very weak feature (as shown by the two dark triangle symbols that fall below the 52-color points). Aquitania and Anacostia were also noted to have very similar semi-major axes (2.739 and 2.741, respectively) and proper sines of inclination (0.284 and 0.298), but different eccentricities (0.228 and 0.132). Since the 1 μm feature is always stronger than the 2 μm feature in pyroxene spectra, the surface assemblage was interpreted to contain spinel, which has a discernible 2 μm feature but no corresponding 1 μm feature. Spinel is commonly found in CAIs, which are common constituents in CO and CV chondrites. However, an igneous origin for these objects could not be ruled out. Aquitania was also found to have a 3 μm absorption feature (Rivkin *et al.*, 1998), apparently indicating hydrated minerals on the surface. However, Anacostia was found not to have a 3 μm feature (Rivkin, personal communication).

Other objects (e.g., 12 Victoria, 42 Isis) classified by Bus (1999) as L types have also been previously classified as S types (Tholen, 1984). The 52-color observations of Victoria indicate an olivine-rich surface, but Gaffey *et al.* (1993) did note that the Victoria spectrum appeared anomalous compared to other S asteroids with similar band area ratios and 1 μm band minima. The 52-color observations of Isis indicate a monomineralogic olivine composition with no pyroxene component due to the absence of any apparent 2 μm band (Gaffey *et al.*, 1993).

The prevailing question concerning the newly defined L class is whether it refers to objects with compositions different from other classes. One type (e.g., Aquitania) does not have apparent 1 μm features while another kind (e.g., Isis) has a very distinctive 1 μm feature that is apparently due to olivine. No mineralogical interpretation has yet been given for the Ld objects.

5.4.2 Investigation of L Asteroids

To understand the compositions of the L class, two L (12 Victoria and 42 Isis) asteroids and one Ld (5840 1978 ON) asteroid were observed in SMASSIR (Table 5.4.1). Victoria and Isis are rather large (diameters of 113 and 100 km, respectively) while 1978 ON is rather small (10 km). Since SMASSIR spectra of Aquitania and Anacostia are not available, 52-color data will be used for these two objects for any spectral comparisons. Aquitania and Anacostia are located farther out (~2.74 AU) than Victoria and Isis, but relatively near 1978 ON (2.75 AU).

Table 5.4.1. L and Ld asteroids observed in SMASSIR. Proper elements (a, e', sin i') are from Milani and Knezevic (1994). Diameters and albedos are from IRAS (Tedesco, 1994) except for diameters in parentheses, which are calculated using the H magnitude with an estimated albedo of 0.05. Family memberships are from Zappalà *et al.* (1995).

Asteroid	a (AU)	e'	sin i'	SMASS II	IRAS Albedo	Diameter (km)	HCM Family	NEA	52-color
12 Victoria	2.334	0.175	0.162	L	0.18	113			yes
42 Isis	2.441	0.189	0.132	L	0.17	100			yes
5840 1978 ON	2.747	0.067	0.055	Ld		(10)	Henan		

The SMASSIR spectra of 12 Victoria and 42 Isis are shown in Figure 5.4.2. The Victoria SMASS II spectrum has an absorption feature centered at ~0.85 μm. The SMASSIR spectrum for Victoria does not overlap very well with the visible data since the SMASSIR data is turning down immediately at ~0.92 μm. A very shallow absorption band is apparent longwards of 0.92 μm in the 52-color and SMASSIR data. The SMASSIR points for Victoria also tend to have a relatively large scatter making any interpretation difficult.

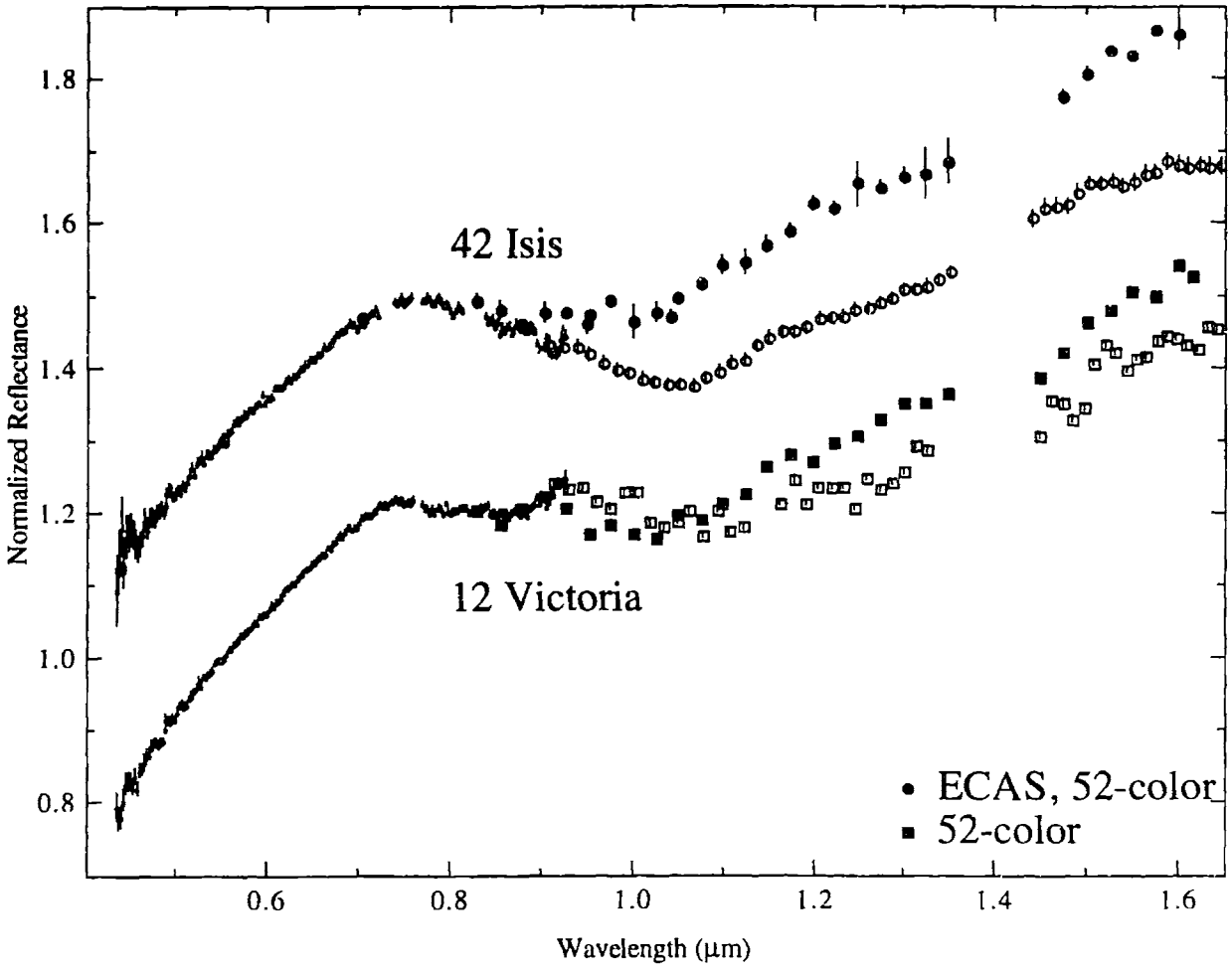

Figure 5.4.2. Reflectance spectra for L-asteroids 12 Victoria and 42 Isis. Small dots for Victoria and Isis are from SMASS II (Bus, 1999). Open symbols are SMASSIR data for Victoria and Isis. 52-color data (dark symbols) are plotted for Victoria and Isis. All spectra are normalized to unity at 0.55 μm. All spectra are offset by 0.3 from each other. Error bars are $\pm 1\sigma$.

The SMASSIR spectrum of Isis indicates a substantial olivine component with the characteristic olivine feature that has the three distinctive bands. However, the SMASSIR data (open squares) have a much deeper feature than the 52-color spectrum (dark circles).

The 52-color spectra of Aquitania and Anacostia do not show any discernible olivine feature or any substantial 1 μm band (Figure 5.4.2). However, Anacostia's SMASS II spectrum is similar to that of Isis' spectrum. Interestingly, Aquitania's SMASS II spectrum is similar to that of Victoria's spectrum except that Victoria has a slightly stronger feature at ~0.85 μm.

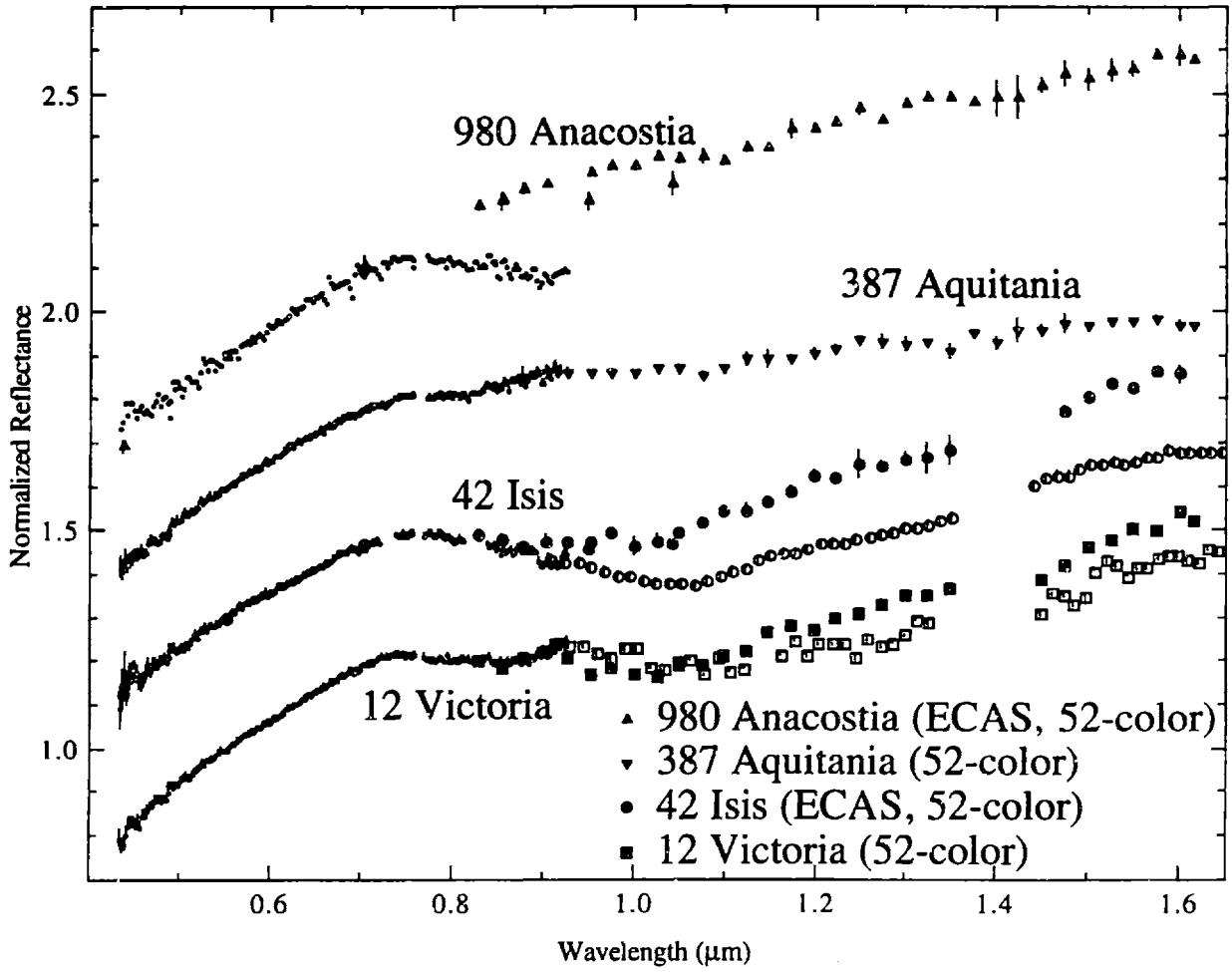

Figure 5.4.3. Reflectance spectra for L-asteroids 12 Victoria, 42 Isis, 387 Aquitania and 980 Anacostia. Small dots for Victoria, Isis, Aquitania and Anacostia are from SMASS II (Bus, 1999). Open symbols are SMASSIR data for Victoria and Isis. Only 52-color data (dark symbols) are plotted for Victoria, Isis and Aquitania wile ECAS and 52-color data are plotted for Anacostia. All spectra are normalized to unity at 0.55 μm. All spectra are offset by 0.3 from each other. Error bars are $\pm 1\sigma$.

The SMASS II spectrum for Victoria is different, due to the absence of the ~0.85 μm absorption feature, from its ECAS spectrum (Figure 5.4.4). The ECAS data for Victoria are closer to the spectral properties of the SMASS spectra of Isis and Anacostia. The three L objects that have been observed at separate times (Victoria, Isis and Anacostia) all have considerable spectral variations. It is unclear if this is just a coincidence and the differences are due to observational problems or these objects tend to have significant compositional differences on rotation.

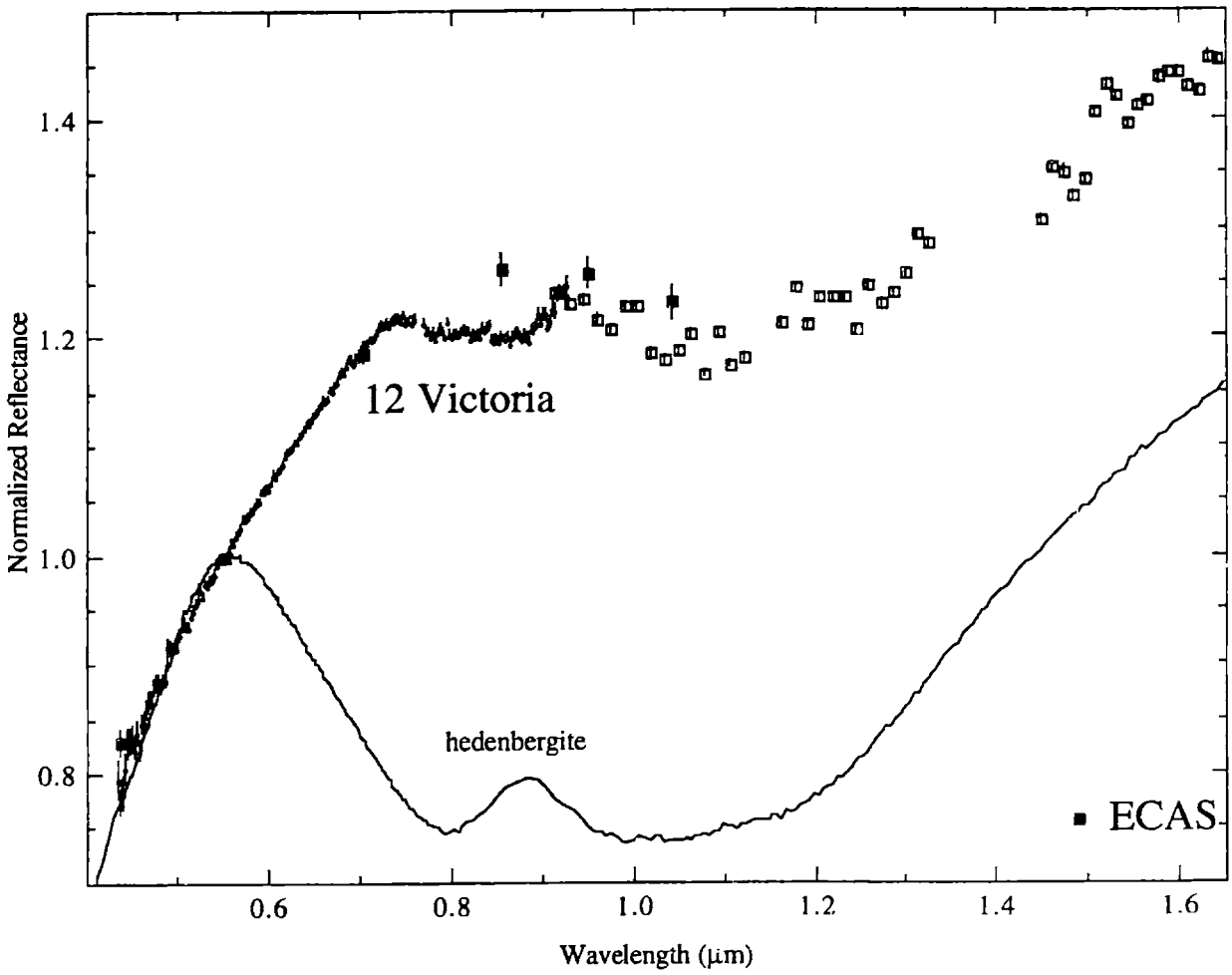

Figure 5.4.4. Reflectance spectrum for L-asteroid 12 Victoria versus spectrum of hedenbergite (Clark *et al.*, 1995). Small dots are from SMASS II (Bus, 1999) and larger symbols are from SMASSIR. The dark squares are ECAS data (Zellner *et al.*, 1985). All spectra are normalized to unity at 0.55 μm.

The structure of the SMASS II Victoria spectrum (Figure 5.4.4) bears some resemblance to the spectra of hedenbergite (Clark *et al.*, 1993) with both having two distinct absorption features; however, the wavelength of the first feature of hedenbergite is at a lower wavelength (~0.8 μm) than the Victoria feature (~0.85 μm). Hedenbergite is a calcic clinopyroxene ($CaFeSi_2O_6$) where other cations such as Fe^{3+} can substitute for Ca and/or Fe^{2+} (Klein and

Hurlbut, 1993). This feature in hedenbergite is due to a Fe^{2+} to Fe^{3+} transition. Hedenbergite is a very rare mineral in meteorites (Rubin, 1997) and has been only found in anhydrously altered Allende chondrules (Kimura and Ikeda, 1995). However, Fe^{3+} tends to be relatively rare in meteorites and tends to be found only in phyllosilicates in CM chondrites (Rubin, 1997).

Figure 5.4.5 plots Isis versus spectra of pallasitic olivine, a mixture of 50% olivine and 50% metal and altered (30 mJ) olivine (Fa_9). The band minimum for Isis is at 1.06 μm and the band center (continuum-removed) is 1.05 μm with estimated error bars for these positions of ±0.02 μm. These positions for Isis are similar to those of the plotted olivine samples. The 0.7 μm peak for Isis (0.75 μm) is at a higher wavelength than the usual peaks (0.68 μm) for olivine assemblages. The altered olivine sample (Yamada *et al.*, 1999) matches very well the spectrum of Isis out to ~0.9 μm; however, the altered olivine is redder and has a slightly deeper feature.

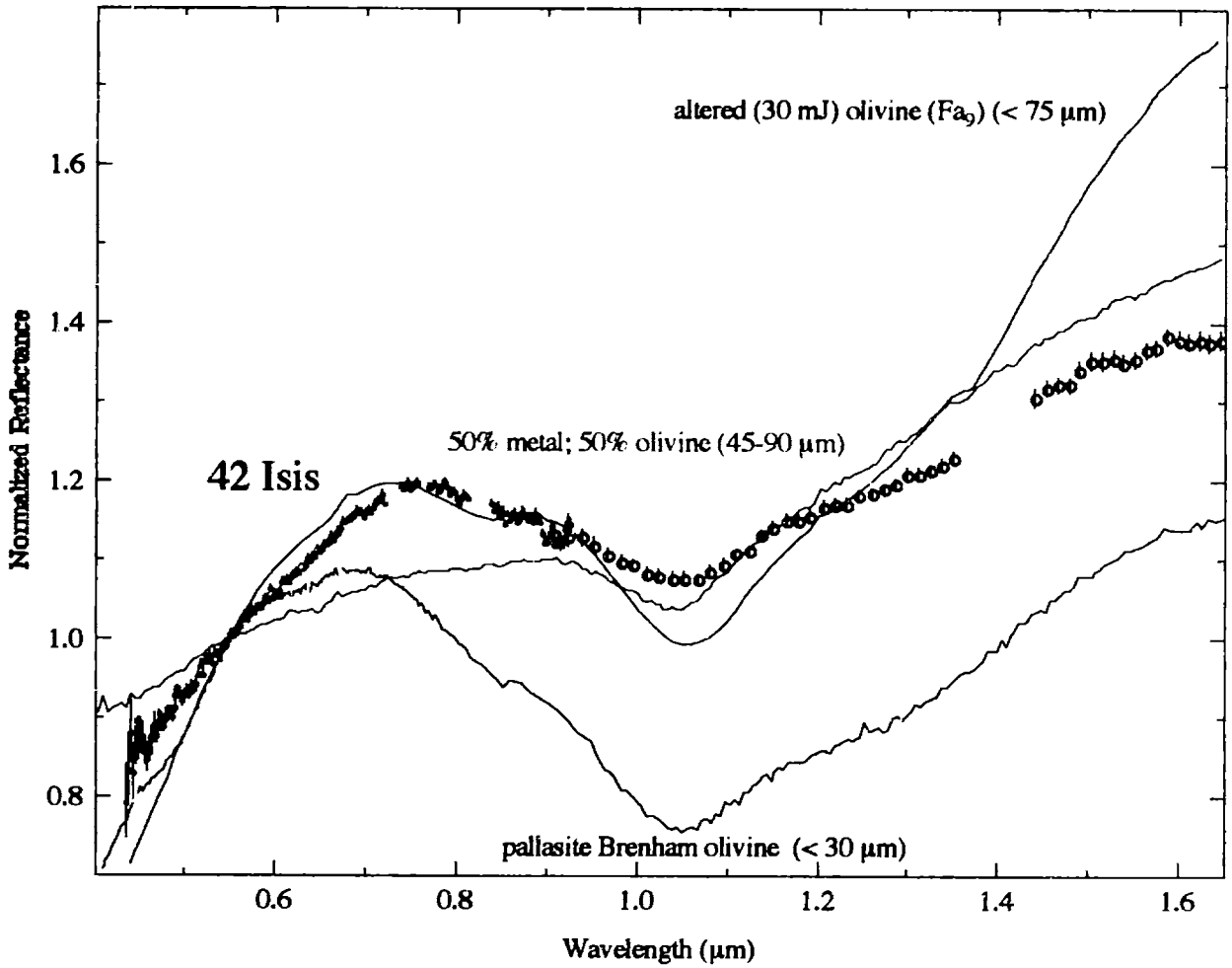

Figure 5.4.5. Reflectance spectrum for L-asteroid 42 Isis versus spectra of pallasite olivine from Brenham (particle size less than 30 μm) (black line), the mixture of 50 wt.% olivine and 50 wt.% metal (particle size between 45 to 90 μm) (red line) and the laser-altered (30 mJ) (Fa_9) (particle size less than 75 μm). Small dots are from SMASS II (Bus, 1999) and open circles are SMASSIR data. The Brachina spectrum is a RELAB spectrum from Sunshine and Hiroi (personal communication) from a sample supplied by the South Australian Museum. The Brenham spectrum is from King and Ridley (1987). The spectrum of the olivine and metal mixture is from Cloutis *et al.* (1990a). The laser altered olivine spectrum is from Yamada *et al.* (1999). All spectra are normalized to unity at 0.55 μm. Error bars are ±1σ.

Another possibility for the composition of Isis is a mixture of metallic iron and pallasite olivine, which would move the 0.7 μm peak to a longer wavelength, redden the bands and suppress the 1 μm feature so it was similar to the Isis spectrum. The olivine would probably need to be found as a powder to keep its distinctive absorption bands, but the iron would probably have to be found as a slab so as not to weaken the UV feature.

Figure 5.4.6 plots the band depths versus the reflectances at 1.65 μm for 42 Isis and other objects (believed to be olivine-rich) from Table 5.1.2. Isis is set off from the deep-featured A types and plot very near the shallow-featured ones. What sets Isis apart from the shallow-featured A-types is that Isis' 1 μm feature has better defined bands due to olivine. A mixture of olivine and metal or altered olivine plus some type of opaque could have similar spectral properties (UV feature, band depth, spectral slope and distinctive olivine band) with Isis.

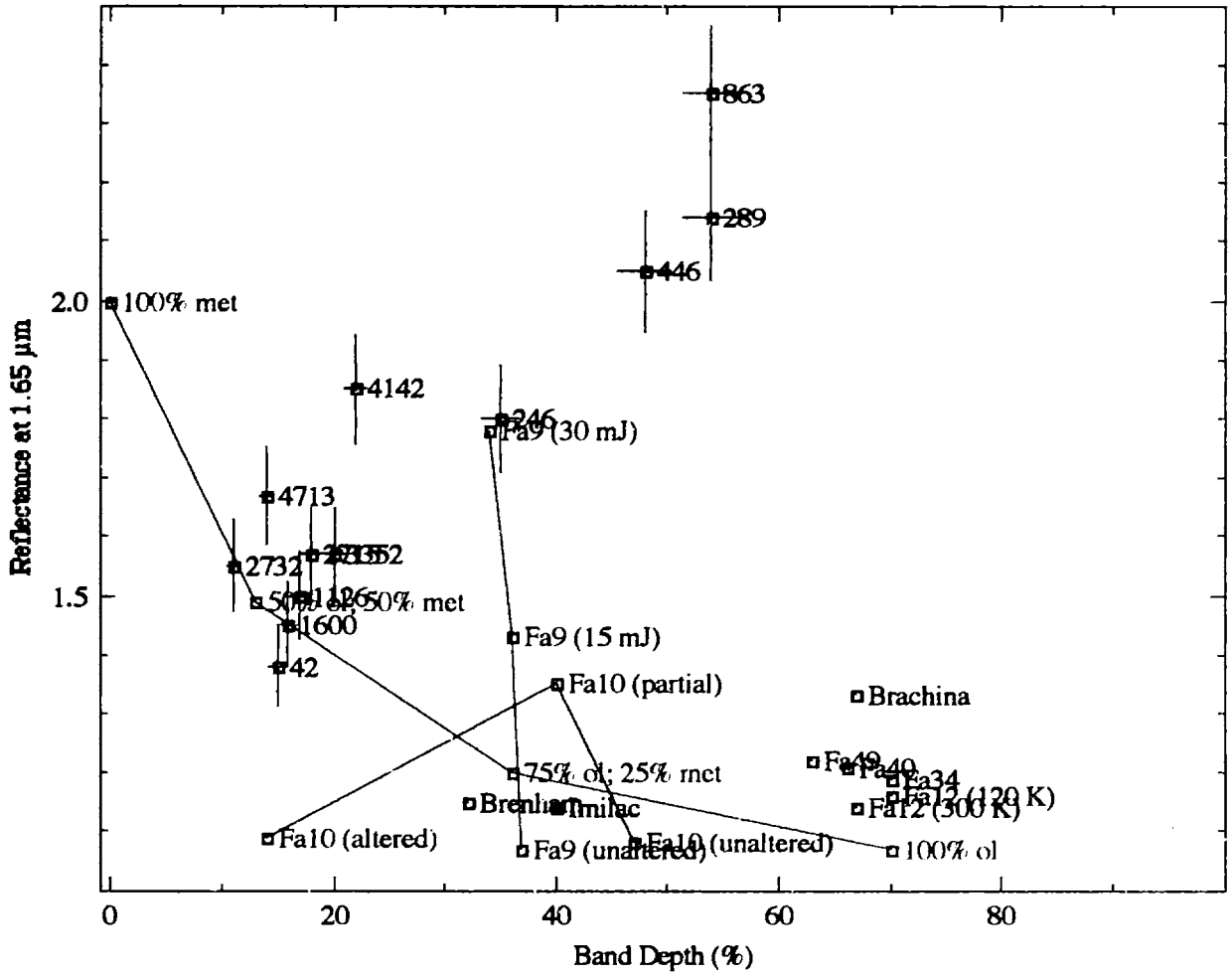

Figure 5.4.6. Band depths (%) versus reflectance at 1.65 μm for A asteroids, 42 Isis and olivine and olivine/metal mixtures from Table 5.1.2. Blue symbols and lines are data from Yamada *et al.* (1999), red symbols and lines are from the olivine/metal mixtures of Cloutis *et al.* (1990a) and green symbols and lines are data from Moroz *et al.* (1996). Error bars for the asteroids for the band depths and reflectances are estimated to be ±5%.

5.4.3 Investigation of the Ld Asteroid

The spectrum of 5840 1978 ON has a strong UV feature, but is relatively flat in the near-infrared (Figure 5.4.7). The spectrum is also very noisy from ~0.7 to ~0.9 μm. This object was observed twice in SMASSIR (Appendix C) and had a similar flat reflectance both times. CV chondrite Leoville and K chondrite Kakangari have similar flat near-infrared spectra; however, the spectrum of 1978 ON has a stronger UV feature than these two meteorites. K chondrites have matrix abundances similar to carbonaceous chondrites, metal abundances similar to H chondrites and mafic silicate compositions between H and E chondrites (Weisberg *et al.*, 1996). The UV features of the meteorites could be strengthened by decreasing their particle sizes, which would hopefully match the 1978 ON spectrum better.

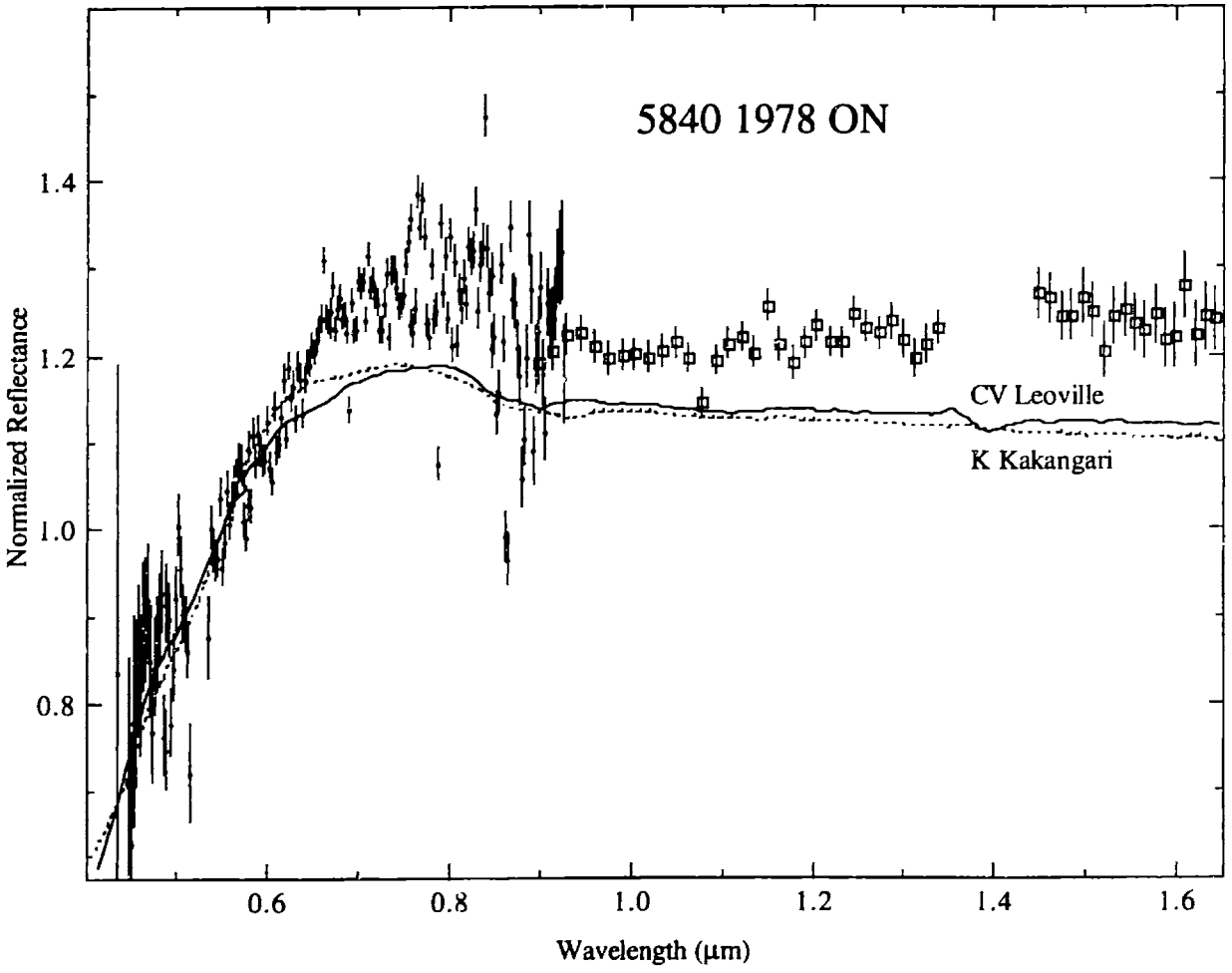

Figure 5.4.7. Reflectance spectrum of Ld-asteroid 5840 1978 ON versus CV chondrite Leoville (dark line) and K chondrite Kakangari (dashed line). Small dots are from SMASS II (Bus, 1999) and open squares are from SMASSIR. The Leoville spectrum is from Gaffey (1976) and the Kakangari spectrum is from Gaffey (personal communication). All spectra are normalized to unity at 0.55 μm. Error bars are ±1σ.

5.4.4. Conclusions

The L types observed in SMASSIR have some unusual spectral properties (Table 5.4.2). The SMASS spectrum of Victoria has an unusual feature (not present in the ECAS data) centered at ~0.85 μm and then a very broad feature in the near-infrared. Isis appears to be olivine-rich, which is consistent with both the 52-color and SMASSIR data; however, the near-infrared data do not match very well. The Isis spectrum appears roughly consistent with laser-altered olivine or some mixture of pallasitic olivine and metal. One thing that is unclear is why the L objects (e.g., Isis, Aquitania, Victoria) appear to have different spectral properties when observed at different times. It could simply be a coincidence or these objects could have very distinctive compositional differences on different hemispheres.

Table 5.4.2. Mineralogic interpretation of L and Ld asteroids observed in SMASSIR. Quotation marks are used for meteoritic analogs that appear less certain.

Type	Asteroid	a (AU)	Meteoritic Analog	Mineralogic Interpretation
Deep-featured L	42 Isis	2.441	"pallasite"	relatively strong UV feature; distinctive 1 μm absorption band due to olivine; 1 μm feature much weaker than those found in A-asteroid spectra
Unusual L	12 Victoria	2.334	none readily apparent	relatively strong UV feature; anomalous feature at ~0.85 present in some spectra; relatively weak 1 μm feature
Ld	5840 1978 ON	2.747	"fine-grained" CV or K chondrite	relatively strong UV feature; flat spectral slope in the near-infrared

The observed Ld object (1978 ON) has a very strong UV feature, but is relatively flat in the near-infrared. Possible meteoritic analogs include CV chondrites and K chondrites; however, these meteorites have weaker UV features. Decreasing the particle size of these meteorites should strengthen the UV feature and make a better spectral match with 1978 ON.

5.5 O and Q Asteroids

5.5.1 Background

The ordinary chondrites are the most common type of meteorite to fall (~80%) on Earth so identifying their parent bodies has been a major goal of asteroid spectroscopic surveys. The ordinary chondrites contain olivine, pyroxene, feldspar, FeNi and sulfides and have metamorphic features suggesting that these meteorites experienced temperatures ranging from at least ~400 °C (type 3) to greater than 950 °C (type 7) (Dodd, 1981). The ordinary chondrites are broken into the H, L and LL classes. Ordinary chondrites have spectral features due to olivine and pyroxene. There are differences between the spectra of different types of ordinary chondrites (Figure 5.5.1), which are functions of mineralogy.

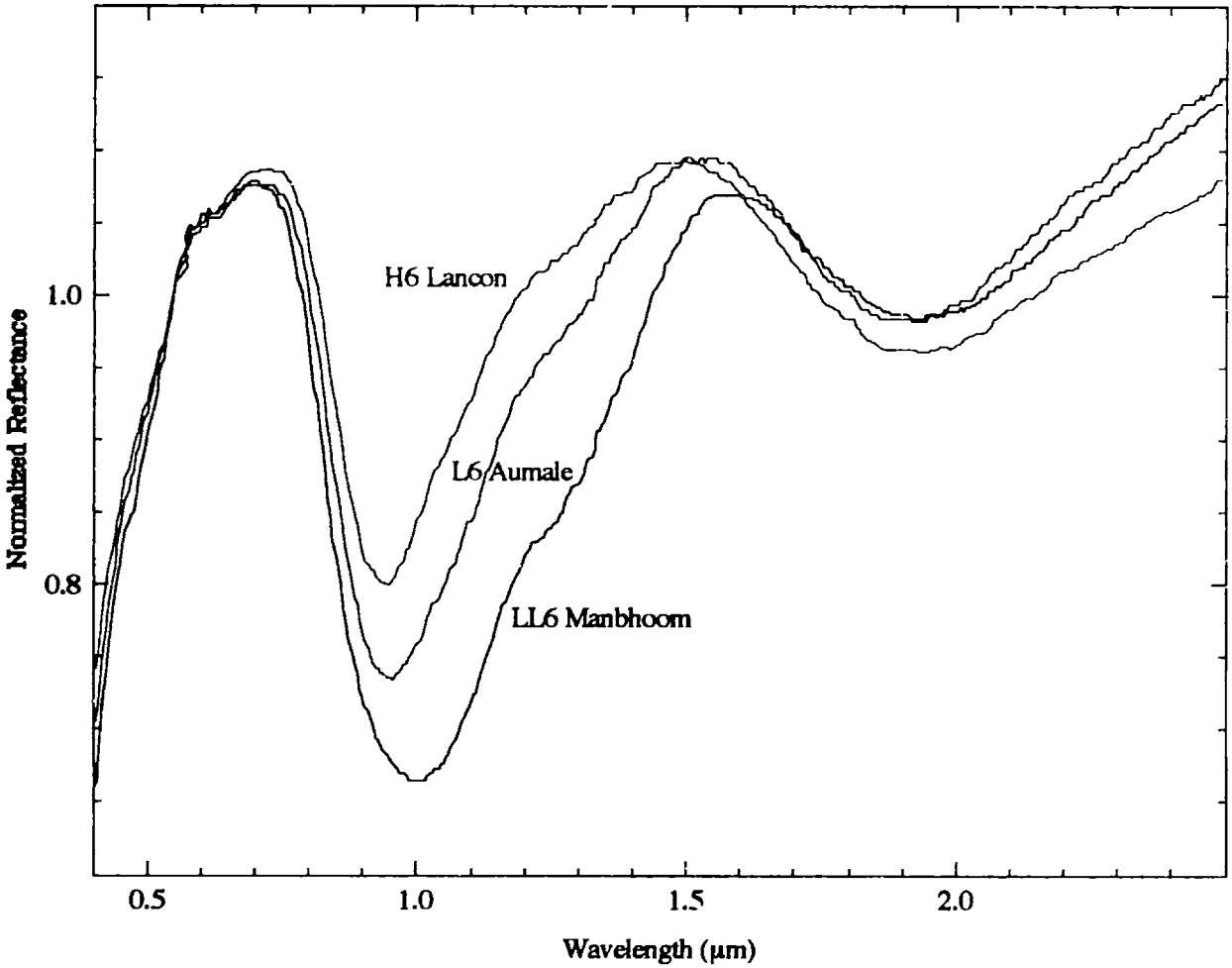

Figure 5.5.1. Reflectance spectra for H6 Lancon, L6 Aumale and LL6 Manbhoom. All meteorite spectra are from Gaffey (1976). All spectra are normalized to unity at 0.55 μm.

LL chondrites tend to have stronger 1 μm band strengths than L chondrites, which have stronger 1 μm bands than H chondrites. This effect is due to the decreasing metallic iron abundance in these meteorites. The 1 μm band positions tend to move to longer wavelengths from H to L to LL chondrites due to increasing olivine abundance in these meteorites. H chondrites have ~36% olivine and ~29% pyroxene, L chondrite have ~47% olivine and ~28% pyroxene and LL chondrites have ~52% olivine and ~27% pyroxene (Dodd, 1981, McSween *et al.*, 1981). The band strengths also tend to increase for higher metamorphic grade (Gaffey, 1976). Even though ordinary chondrites contain significant amounts of metallic iron, which would be expected to redden their spectra, they have flat spectral slopes. Gaffey (1986) has proposed that FeNi in ordinary chondrites is coated with an optically thick surface layer, which is suppressing the spectral properties of the metal. He believes that this layer is produced during the formation of the metallic iron on the original parent body and is not the result of terrestrial weathering.

The LL chondrites have the highest iron (fayalite and ferrosilite) contents in their silicates, the L chondrites have slightly lower abundances and the H chondrites have the lowest. The H chondrites also have higher normative abundances of metallic iron (~18%) than L (~8%) and LL (~4%) (McSween *et al.*, 1991). Rubin (1990) believes that there is evidence that there are more than three ordinary chondrite parent bodies exist due to some ordinary chondrites having intermediate compositions between groups.

Two relatively unusual asteroids have been linked with ordinary chondrites, particularly the LL types. Near-Earth asteroid 1862 Apollo has been known to be spectrally similar to the LL4 chondrites since the work of McFadden *et al.* (1985). Tholen (1984) classified Apollo as the only member of the Q class due to its spectral properties (strong UV and 1 μm features) that appear intermediate between the spectra of Vesta (V class) and Dembowska (R class). Apollo's 1 μm feature is not as strong as Vesta's feature and has a minimum at a longer wavelength than Dembowska. The visual albedo (0.21) (Lebofsky *et al.*, 1981b) of Apollo is also consistent with those of ordinary chondrites. A number of other Q types have been identified in the NEA population (Bus, personal communication). The Q class has become synonymous for describing objects that appear to have surface compositions consistent with ordinary chondrites.

Apollo is plotted in Figure 5.5.2 versus LL4 chondrite Soko Banja and can be seen to have similar visible spectra to this meteorite. Broadband near-infrared spectra (McFadden *et al.*, 1984) are also consistent with an ordinary chondrite composition.

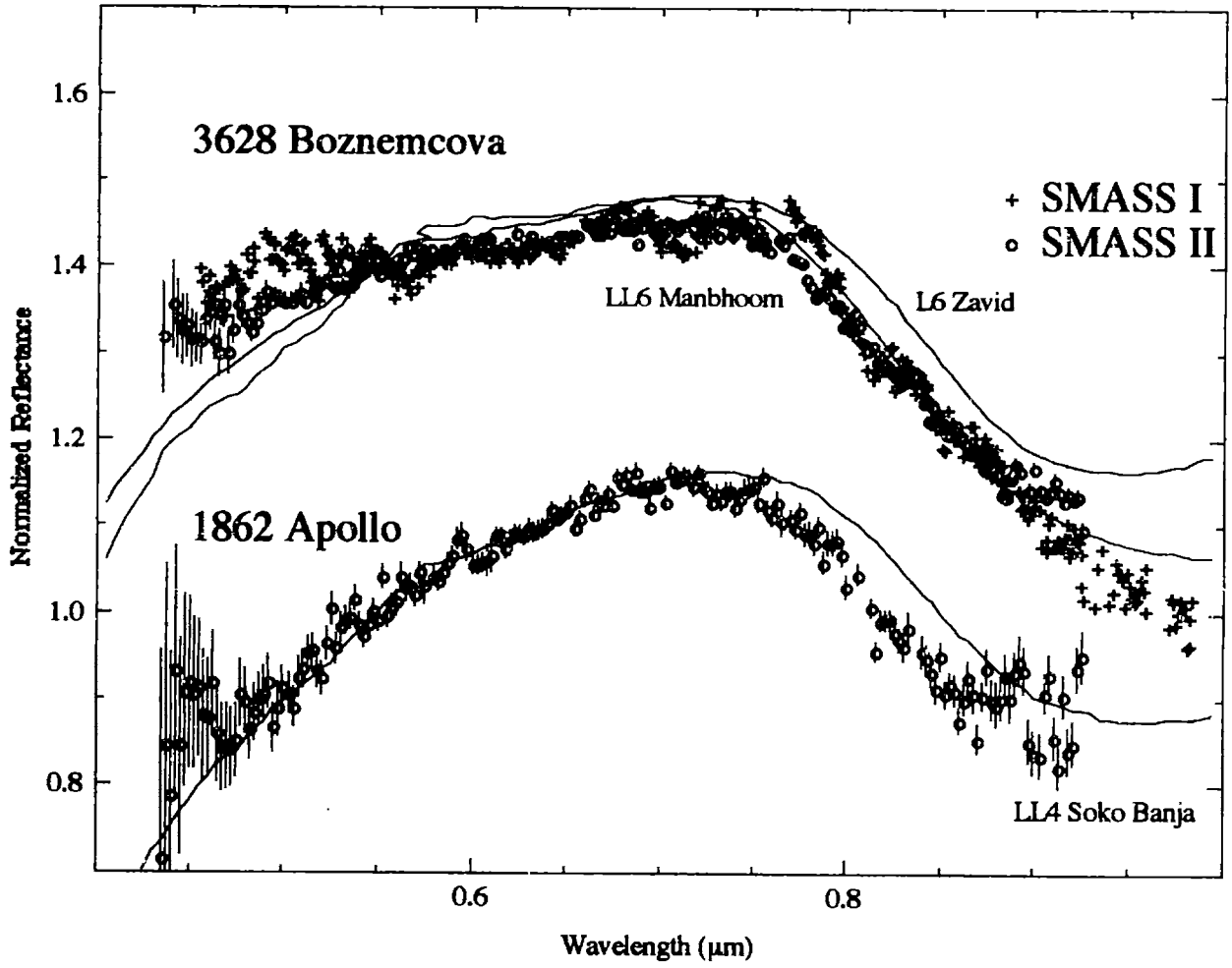

Figure 5.5.2. Reflectance spectra for Q-asteroid 1862 Apollo versus LL4 Soko Banja (black line) and O-asteroid 3628 Boznemcová versus L6 Zavid (black line) and LL6 Manbhoom (blue line). The Apollo spectrum is from Bus (personal communication). SMASS I (Xu *et al.*, 1995) (pluses) and SMASS II spectra (Bus, 1999) (circles) are plotted for Boznemcová. Only the SMASS I data out to ~0.984 μm are plotted. All meteorite spectra are from Gaffey (1976). The asteroid spectra are offset by 0.4 in reflectance from each other. All spectra are normalized to unity at 0.55 μm. Error bars are ±1σ.

Main-belt asteroid 3628 Boznemcová was identified by Binzel *et al.* (1993) as having an unusual visible spectrum different from all other observed asteroids. Its spectrum was noted as being similar (Figure 5.5.2) to those of L6 and LL6 chondrites due to its relatively strong 1 μm feature. Chapman (1996) disagreed with this interpretation due to differences with ordinary chondrites in the SMASS I spectrum at the short wavelength end (below ~0.5 μm) and at the longer wavelength end (past ~0.92 μm). No albedo information is available for Boznemcová. Boznemcová was classified as an O asteroid in SMASS I (Xu *et al.*, 1995) and II (Bus, 1999). Boznemcová has an estimated diameter of 8 km and is located at 2.54 AU near the 3:1

resonance. Three NEAs have recently been classified as O types (Bus, personal communication).

The main question concerning the O and Q types is whether they have compositions similar to ordinary chondrites. Binzel *et al.* (1996b) has found that there appears to be a continuum of spectral properties between the S asteroids and the ordinary chondrites among the NEAs, which is consistent with the beliefs of many researchers (e.g., Chapman, 1996) who think that the parent bodies of some of the ordinary chondrites are S asteroids. To support any linkage, it is important to understand if the objects with visible spectra similar to the ordinary chondrites maintain that similarity when measurements are extended into the near-infrared.

5.5.2 Investigation of O and Q Asteroids

To answer these questions, two O types and three Q types (Table 5.5.1) were observed in SMASSIR to see how well they match the spectra of ordinary chondrites in the near-infrared. The three Q types are all NEAs. They all have very different semimajor axes and sample the Aten, Apollo and Amor classes of NEAs. The calculated albedo (0.61 $\pm$ 0.03) (Mottola *et al.*, 1997) for Golevka from the phase curve (V magnitude versus phase angle) and thermal observations imply a very reflective surface. All of these objects are very small (diameters less than 10 km).

Table 5.5.1. O and Q types observed in SMASSIR. Proper elements (a, e', sin i') are from Milani and Knezevic (1994). Osculating elements are given for the NEAs, which are from the *Ephemerides of Minor Planets* (1999). Diameters and albedos are from IRAS (Tedesco, 1994) except for diameters in parentheses, which are calculated using the H magnitude with an estimated albedo of 0.25. These objects are not in any families as identified by Zappalà *et al.* (1995).

Asteroid	a (AU)	e'	sin i'	SMASS II	IRAS Albedo	Diameter (km)	HCM Family	NEA
1862 Apollo	1.471	0.606	0.111	Q	0.21§	1*f*		Apollo
3628 Boznemcová	2.536	0.255	0.106	O		(8)		
3753 Cruithne	0.998	0.515	0.339	Q		(3)		Aten
6489 Golevka	2.514	0.597	0.040	Q	0.61∂	0.3∂		Amor
1997 RT	2.247	0.524	0.115	Q		(0.3)		Amor

§ The albedo for 1862 Apollo is from Lebofsky *et al.* (1981b).
f The diameter for 1862 Apollo is from Goldstein (1981).
∂ The diameter and albedo for 6489 Golevka are from Mottola *et al.* (1997).

5.5.3 Investigation of O Asteroids

The SMASSIR spectrum of Boznemcová is shown in Figure 5.5.3. The large error bars are due to its faint magnitude of V17.1. As can be seen in the figure, Boznemcová matches very well the Manbhoom spectrum from 0.6 to 1.1 μm, but deviates from Manbhoom between 1.1 and 1.4 μm. One possibility is that atmospheric absorption features are affecting the spectrum between these wavelengths and causing the deviation. However, the atmospheric effect would need to happening at a much shorter wavelength (~1.30 μm) than what is normally found. Also, Boznemcová's spectrum is very smooth without significant scatter as would be expected for a substantial atmospheric effect.

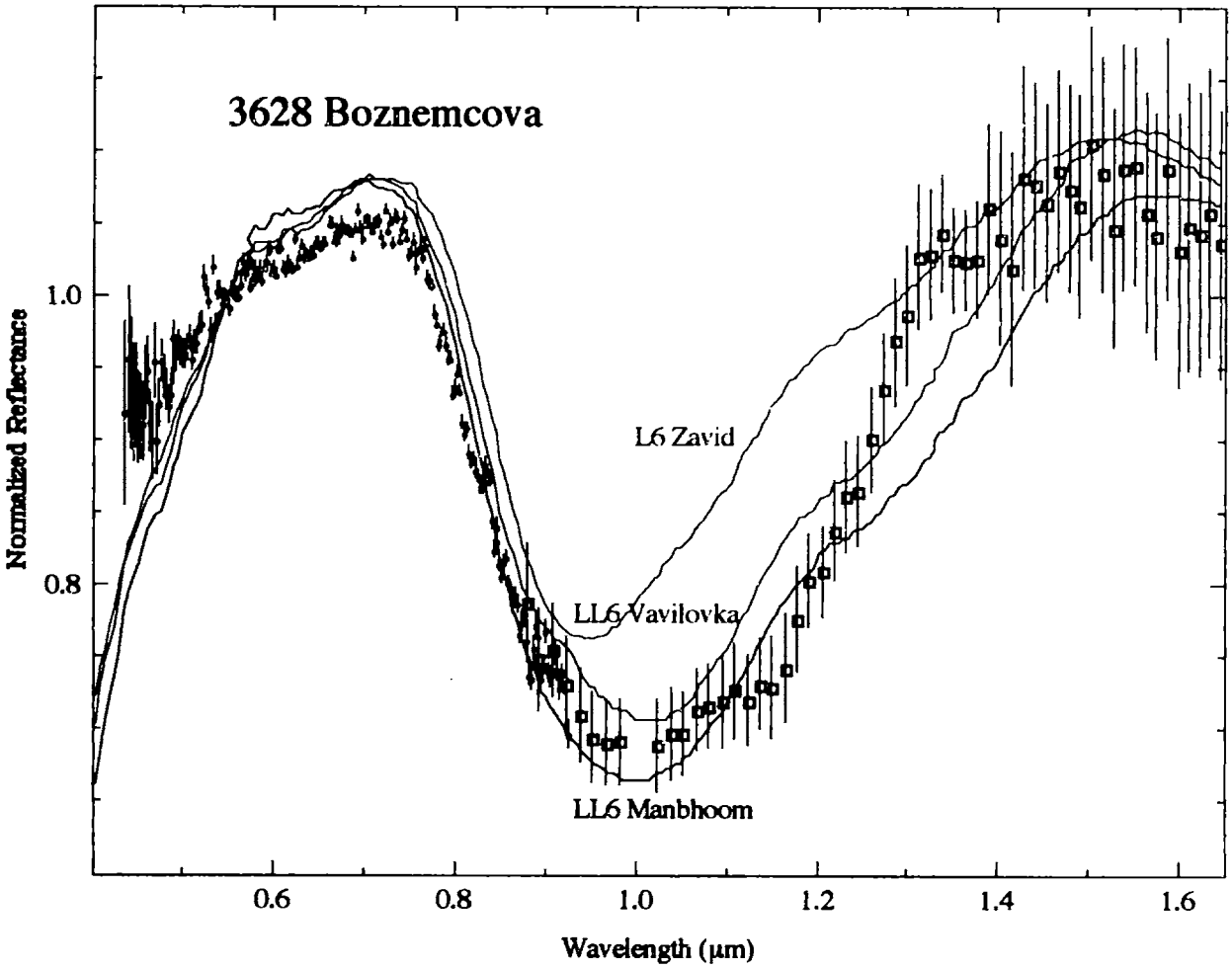

Figure 5.5.3. Reflectance spectrum for O-asteroid 3628 Boznemcová versus spectra of L6 chondrite Zavid (red line), LL6 chondrite Vavilovka (blue line) and LL6 chondrite Manbhoom (black line). Small dots are from SMASS II (Bus, 1999) and larger symbols are from SMASSIR. All meteorite spectra are from Gaffey (1976). All spectra are normalized to unity at 0.55 μm. Error bars are ±1σ.

Temperature does not seem to be causing the spectral difference between Boznemcová and Manbhoom. Low temperature (120 K) spectra (Figure 5.5.4) of Manbhoom is more of a mismatch for Boznemcová since the width of the 1 μm band becomes narrower and turns up at a shorter wavelength than the room temperature spectra. The width and depth of their 1 μm features are also smaller than those parameters from the Gaffey (1976) Manbhoom spectrum due to the smaller grain size for these samples.

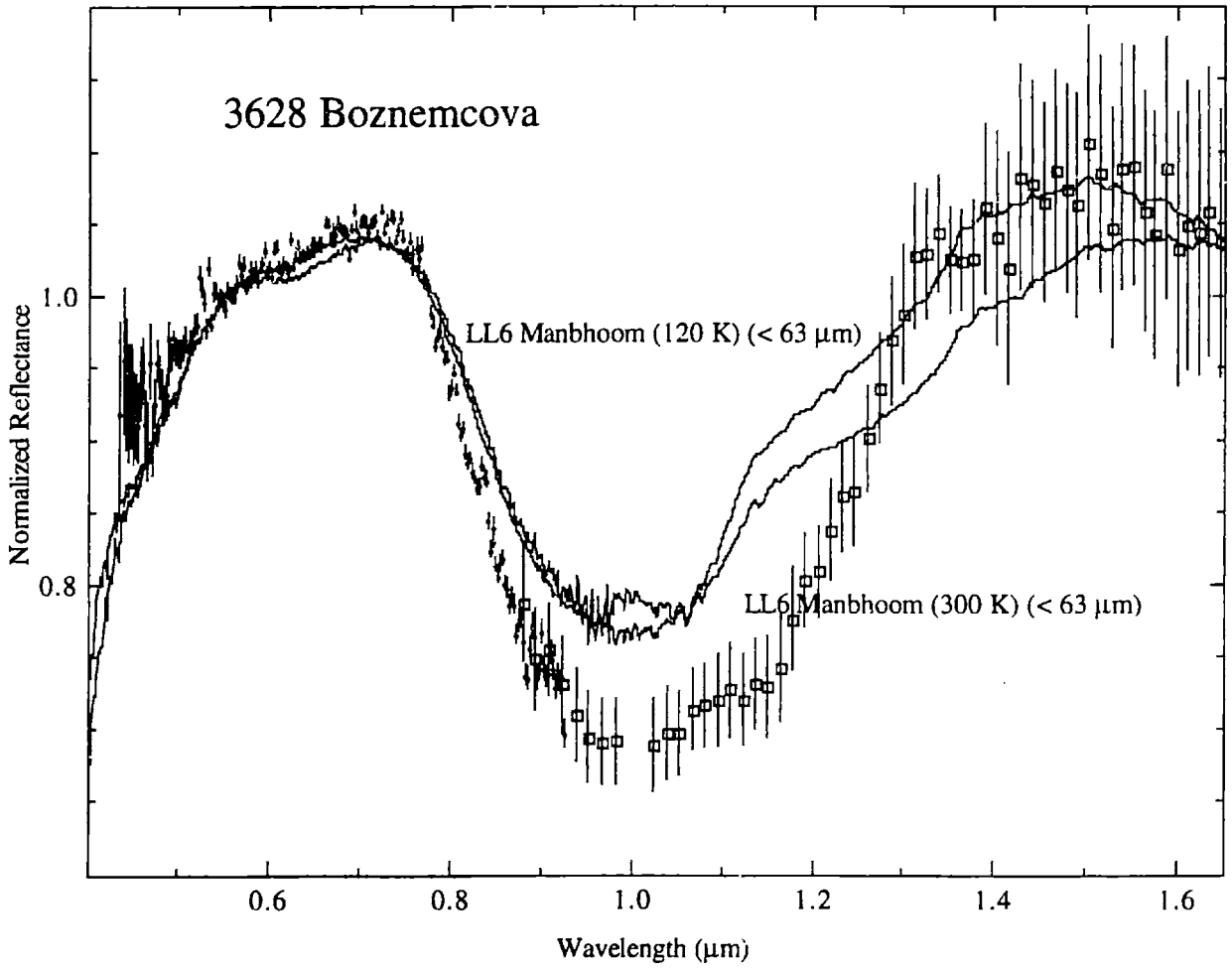

Figure 5.5.4. Reflectance spectrum of O-asteroid 3628 Boznemcová versus spectra of LL6 Manbhoom (particle size less than 63 μm) at room (300 K) (upper line) and low (120 K) (lower line) low temperatures. Small dots are from SMASS II (Bus, 1999) and larger symbols are from SMASSIR. The American Museum of Natural History supplied the Manbhoom sample. The meteorite spectra are from Hinrichs (personal communication) and taken at the Planetary Geosciences/HIGP spectrometer facility at the University of Hawai`i. All spectra are normalized to unity at 0.55 μm.

If this very symmetric bowl-shaped feature is due to some type of pyroxene, it is a pyroxene type that is not abundant in measured meteorite samples. Figure 5.5.5 plots Boznemcová against an augite, which also has a bowl-shaped feature. This broad-shaped 1 μm feature is due to Fe^{3+} (the feature at ~0.8 μm) and Fe^{2+} (the rest of the μm feature). Augite is a calcic clinopyroxene [(Ca, Na)(Mg, Fe, Al)(Si, $Al)_2O_6$] which is found as a solid solution with

aegirine ($NaFe^{3+}Si_2O_6$). However, the feature due to augite is much broader than the Boznemcová band due primarily to the Fe^{3+} to Fe^{2+} transition. As stated earlier, Fe^{3+} tends to be relatively rare in meteorites and found only in phyllosilicates in CM chondrites. Clinopyroxenes are not abundant in most meteorites. For example, they tend to be found in ordinary chondrites with abundances less than 5%. A few ureilites are known to contain large amounts of augite (Takeda *et al.*, 1989; Goodrich, 1992) with percentages up to ~50% (Goodrich, personal communication). Ureilites are essentially carbon-bearing ultramafic rocks consisting primarily of olivine and pyroxene (usually pigeonite). The plotted augite-rich ureilite (META78008) (Hiroi and McFadden, personal communication) in Figure 5.5.6 is not a good spectral match for Boznemcova; however, the sample has been heavily weathered, as seen by the strong UV feature and the absorption feature at ~0.5 μm.

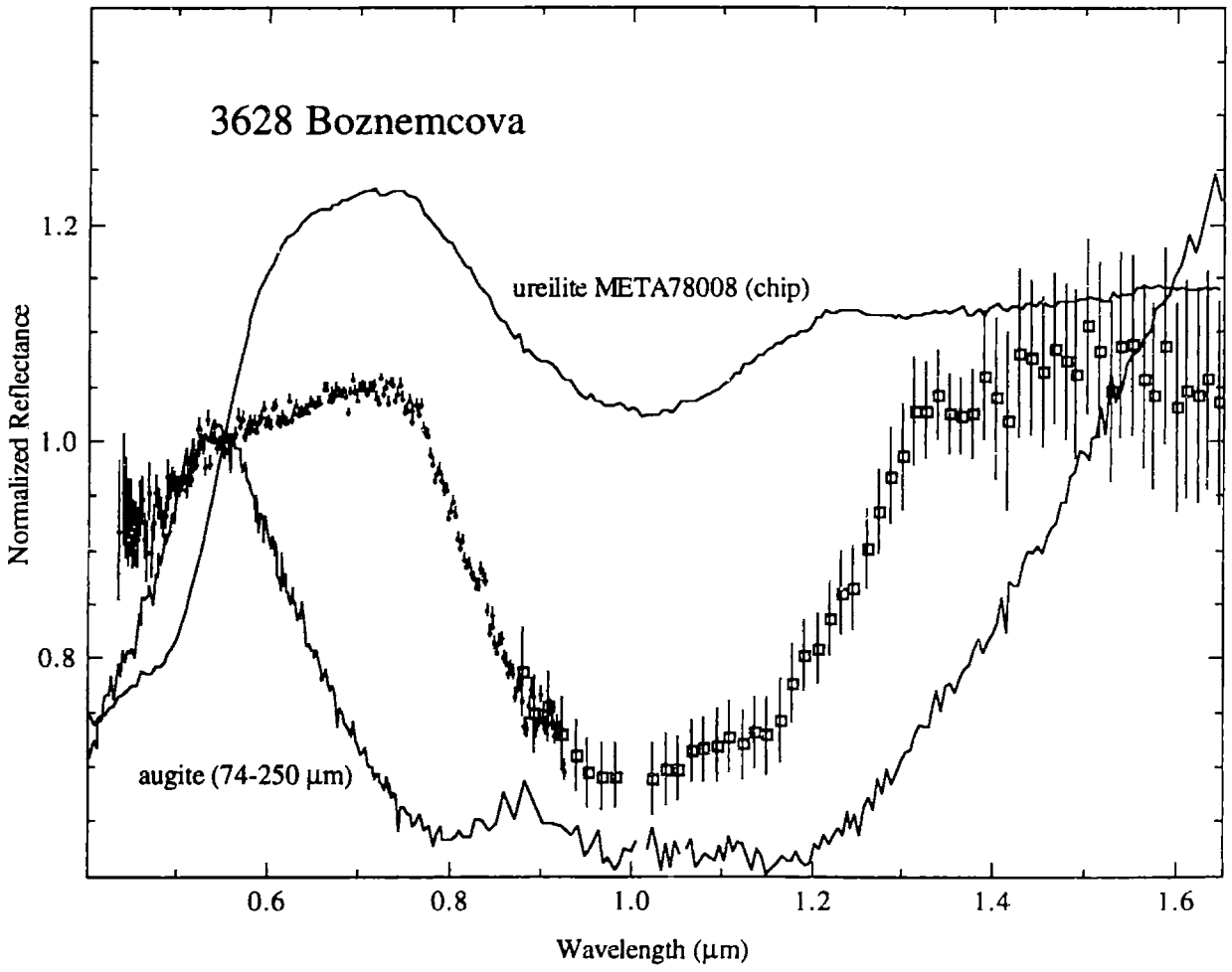

Figure 5.5.5. Reflectance spectrum for O-asteroid 3628 Boznemcová versus the spectra of augite (Clark *et al.*, 1993) and the ureilite META78008 (Hiroi and McFadden, personal communication). Small dots are from SMASS II (Bus, 1999) and larger symbols are from SMASSIR. The ureilite spectrum was measured at RELAB. All spectra are normalized to unity at 0.55 μm. Error bars are ±1σ.

The other observed O asteroid, NEA 1997 RT, has an extremely noisy spectrum (Figure 5.5.6) due to its faint magnitude of V17.7. There is significant scatter around all the atmospheric water bands. The spectrum is plotted versus LL6 Vavilovka, but the noisiness of the SMASSIR data makes any interpretation difficult.

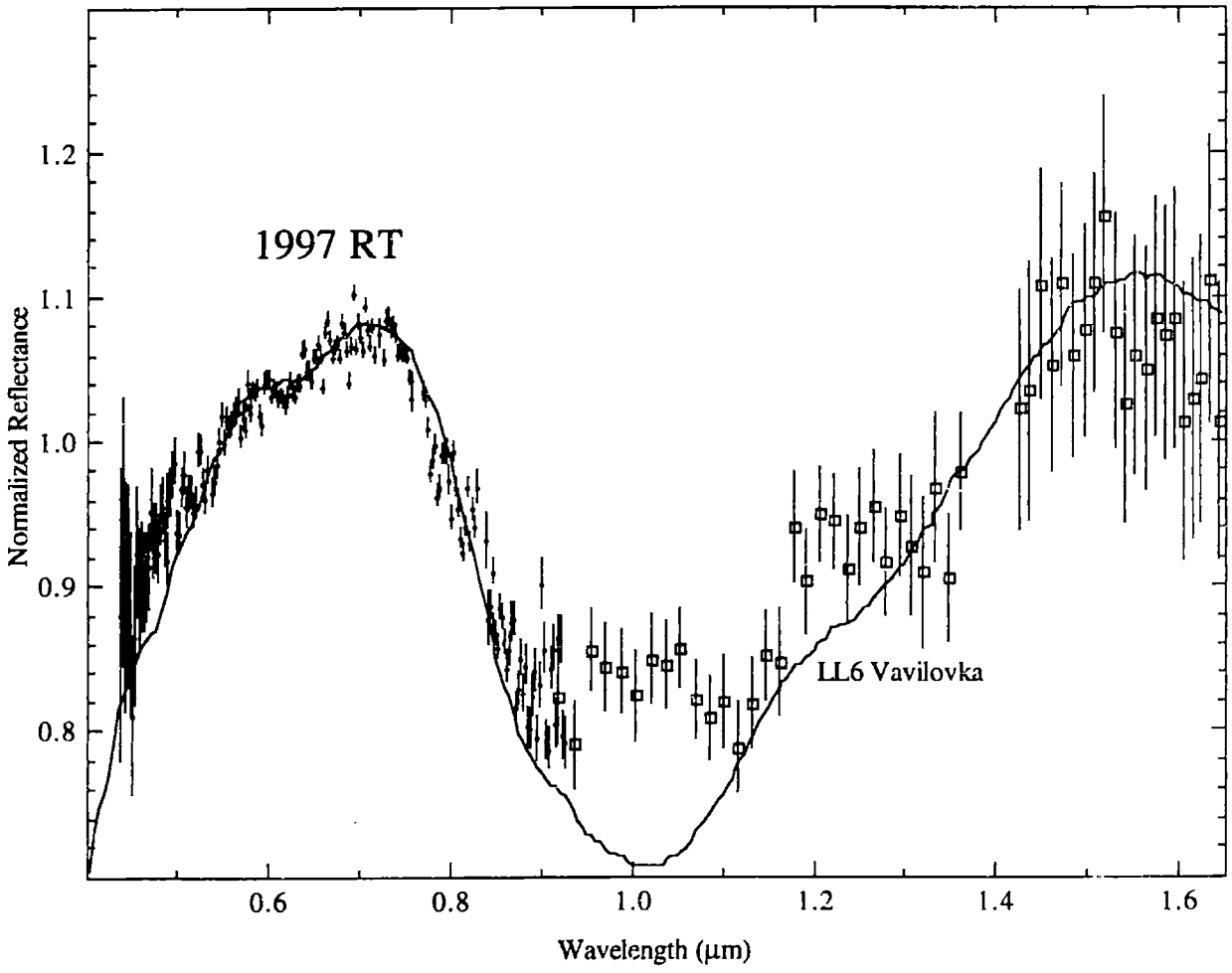

Figure 5.5.6. Reflectance spectrum for O-asteroid 1997 RT versus the spectrum of LL6 chondrite Vavilovka (Gaffey, 1976). Small dots are from SMASS II (Bus, 1999) and larger symbols are from SMASSIR. All spectra are normalized to unity at 0.55 μm. Error bars are $\pm 1\sigma$.

5.5.4 Investigation of Q Asteroids

The SMASSIR spectrum of Apollo versus an LL4 and LL5 chondrite is shown in Figure 5.5.7. LL chondrites contain ~50% olivine, ~20% orthopyroxene, ~5% clinopyroxene and ~5% FeNi (McSween *et al.*, 1991). The Apollo spectrum appears intermediate between the two ordinary chondrite spectra with a similarly-shaped 1 μm feature and a similar spectral slope; however, the Apollo spectrum is rather noisy with large error bars due to its faint magnitude (V17.9). Apollo's albedo (0.21 ± 0.02) is also similar to LL chondrites (0.23-0.35).

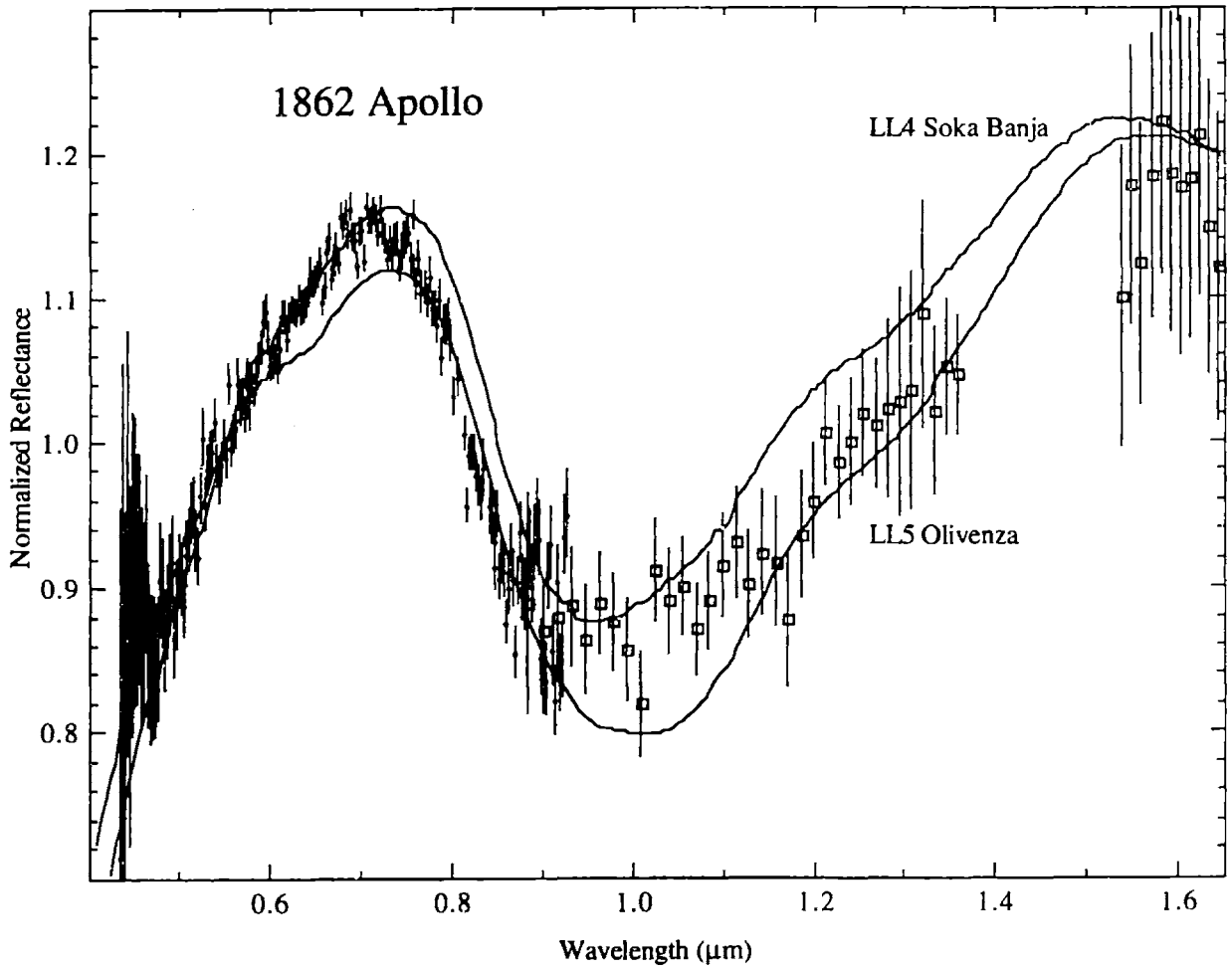

Figure 5.5.7. Reflectance spectrum for Q-asteroid 1862 Apollo versus spectra of LL4 chondrite Soko Banja and LL5 chondrite Olivenza. Small dots are from SMASS II (Bus, 1999) and larger symbols are from SMASSIR. All meteorite spectra are from Gaffey (1976). All spectra are normalized to unity at 0.55 μm. Error bars are ±1σ.

The SMASSIR spectra of 3753 Cruithne and 6489 Golevka are shown in Figure 5.5.8. Both of these objects have very broad 1 μm features but with minima below 1.0 μm. This spectral shape is characteristic of some type of mixture of olivine and pyroxene. Cruithne's slightly noisy spectrum is very similar to that of LL6 chondrite Jelica. Both have similar 1.0 μm band shapes, band strengths and spectral slopes. One noticeable difference is that Cruithne

appears to have a stronger 2 μm feature than LL6 Jelica; however, this may be due to just to the relatively large scatter among Cruithne's points from ~1.50 to ~1.65 μm. The Cruithne spectrum is similar in continuum slope to Apollo while Golevka has a much redder spectrum. Golevka also has a slightly stronger UV feature than Cruithne. The high albedo (0.61 ± 0.03) of Golevka implies that its surface is composed almost entirely of silicates and that an opaque (such as metal) is not reddening the surface. One possible alteration process to redden the spectrum and keep the high albedo is the laser experiments of Yamada *et al.* (1999).

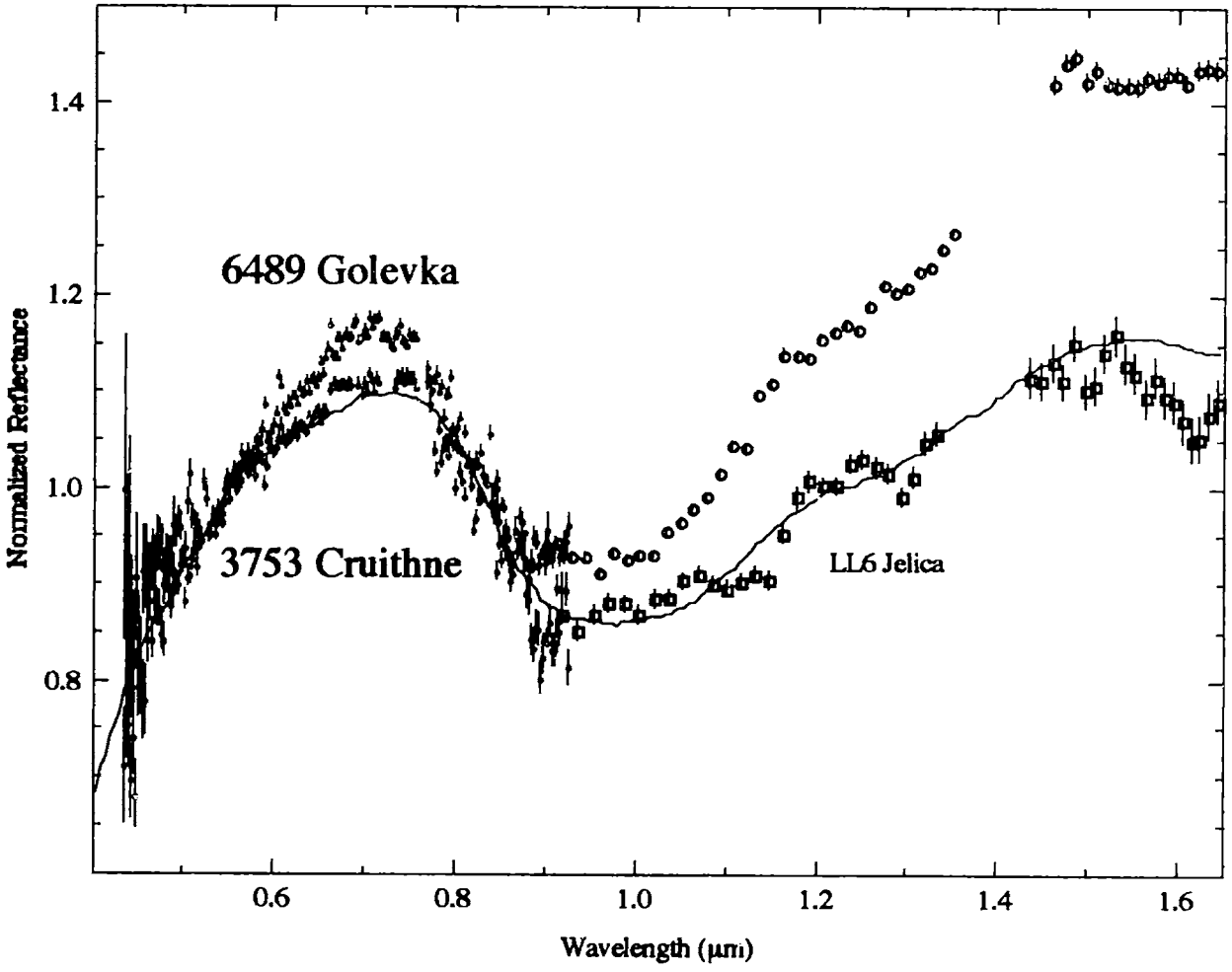

Figure 5.5.8. Reflectance spectra for Q-asteroids 3753 Cruithne (black symbols) and 6489 Golevka (red symbols) versus LL6 chondrite Jelica. Small dots are from SMASS II (Bus, 1999) and larger symbols are from SMASSIR. All meteorite spectra are from Gaffey (1976). All spectra are normalized to unity at 0.55 μm. Error bars are ±1σ.

5.5.4 Conclusions

Boznemcová has an unusual bowl-shaped near-infrared spectrum that is unlike any measured meteorite (Table 5.5.2). The SMASSIR spectrum deviates from the spectrum of an LL6 chondrite in the near-infrared, which it matches very well in the visible. The spectral dissimilarities in the near-infrared implies a compositional difference between Boznemcová and the LL6 chondrites. One possibility is a higher abundance of augite relative to ordinary chondrites. The other O asteroid that was observed (1997 RT) is too noisy to make any mineralogical interpretation.

Table 5.5.2. Mineralogic interpretation of Q and O asteroids observed in SMASSIR.

Type	Asteroid	a (AU)	Meteoritic Analog	Mineralogical Interpretation
O	3628 Boznemcová	2.536	none readily apparent	anomalous bowl-shaped 1 μm feature; best guess for these object's composition is some type of pyroxene that is not normally found in meteorites
	1997 RT	(Amor)	none apparent	
Flat-sloped Q	1862 Apollo	(Apollo)	LL4-5 chondrite	spectral features similar to LL chondrites with a distinctive broad 1 μm feature due primarily to olivine plus pyroxene
	3753 Cruithne	(Aten)	LL6 chondrite	
Red-sloped Q	6489 Golevka	(Amor)	none readily apparent	spectral features similar to LL chondrites with a distinctive broad 1 μm feature due primarily to olivine plus pyroxene; however, the spectra are reddened relative to ordinary chondrites; very high albedo (0.61) implies very few opaques on the surface

Two (1862 Apollo and 3753 Cruithne) of the three measured Q types have spectra similar to LL chondrites while the third (6489 Golevka) is much redder (Table 5.5.2). Apollo has a spectrum intermediate between an LL4 and LL5 chondrite, while Cruithne has a spectrum similar to an LL6 chondrite. Golevka's high albedo (0.61 ± 0.03) implies a silicate composition with virtually no opaques.

5.6 R Asteroids

5.6.1 Background

Asteroid 349 Dembowksa has long been known to have a unique visible spectrum (e.g., Tholen, 1984). Bus (1999) identified three other main-belt object asteroids with similar visible spectra. The visible and near-infrared spectrum of Dembowska has generally been interpreted as indicating a surface assemblage of approximately equal amounts of olivine and pyroxene (Gaffey *et al.*, 1989). The pyroxene composition has been interpreted as being calcium-poor and low-iron with a ferrosilite composition estimated to be 16-32% (Feierberg *et al.*, 1980; Abell and Gaffey, 1999) from the minimum of the 2 μm feature; however, there has been no correction in calculating the ferrosilite composition for any temperature effect in the position of the 2 μm band. Lower temperatures tend to move the 2 μm minimum to lower wavelengths, which would indicate a less iron-rich pyroxene than the actual composition. No spectral analog for Dembowska has been identified in our meteorite collection. Hiroi and Sasaki (2000) were able to duplicate Dembowska's spectrum with a theoretical mixture of laser-treated olivine and laser-treated pyroxene.

The question that can be answered in SMASSIR concerning these objects is how similar they are to Dembowska. Other questions concerning the exact compositions of these objects are difficult to answer due to the absence of a complete 2 μm feature in the SMASSIR spectra.

5.6.2 Investigation of R Asteroids

To try to understand the spectral similarity of R objects, two asteroids (Dembowska and Massevitch) were observed in SMASSIR (Table 5.6.1). Dembowska is much larger (diameter ≈ 140 km) than Massevitch (18 km) and also brighter (albedo of 0.38 ± 0.03 versus 0.16 ± 0.04). Dembowska is also located much farther out in the belt (2.93 AU) than Massevitch (2.74 AU).

Table 5.6.1. R asteroids observed in SMASSIR. Proper elements (a, e', sin i') are from Milani and Knezevic (1994). Diameters and albedos are from IRAS (Tedesco, 1994). These objects are not in any families as identified by Zappalà *et al.* (1995).

Asteroid	a (AU)	e'	sin i'	IRAS Albedo	Diameter (km)	HCM Family	52-color
349 Dembowska	2.925	0.055	0.135	0.38	140		yes
1904 Massevitch	2.744	0.039	0.205	0.16	18		

Dembowska and Massevitch are plotted in Figure 5.6.1. Each object has a relatively broad 1 μm band with a minimum at ~0.92 μm, indicating a mixture of olivine and pyroxene. The wavelength of the turnover between the 1 and 2 μm features is at a longer wavelength than the eucrite, also indicating a substantial olivine component. Dembowska is redder than previous

52-color observations and has a slightly stronger 2 μm feature. These two objects are almost perfect matches in the visible, but Dembowska is slightly redder in the near-infrared. The higher abundance of opaques on Massevitch (indicated by its lower albedo) may be causing this object to be less red. These asteroids have "identical" spectra out to 1.2 μm. The strengths of the 2 μm features appear similar; however, the residual atmospheric absorption feature at ~1.4 μm in Massevitch's spectrum makes any exact comparison difficult.

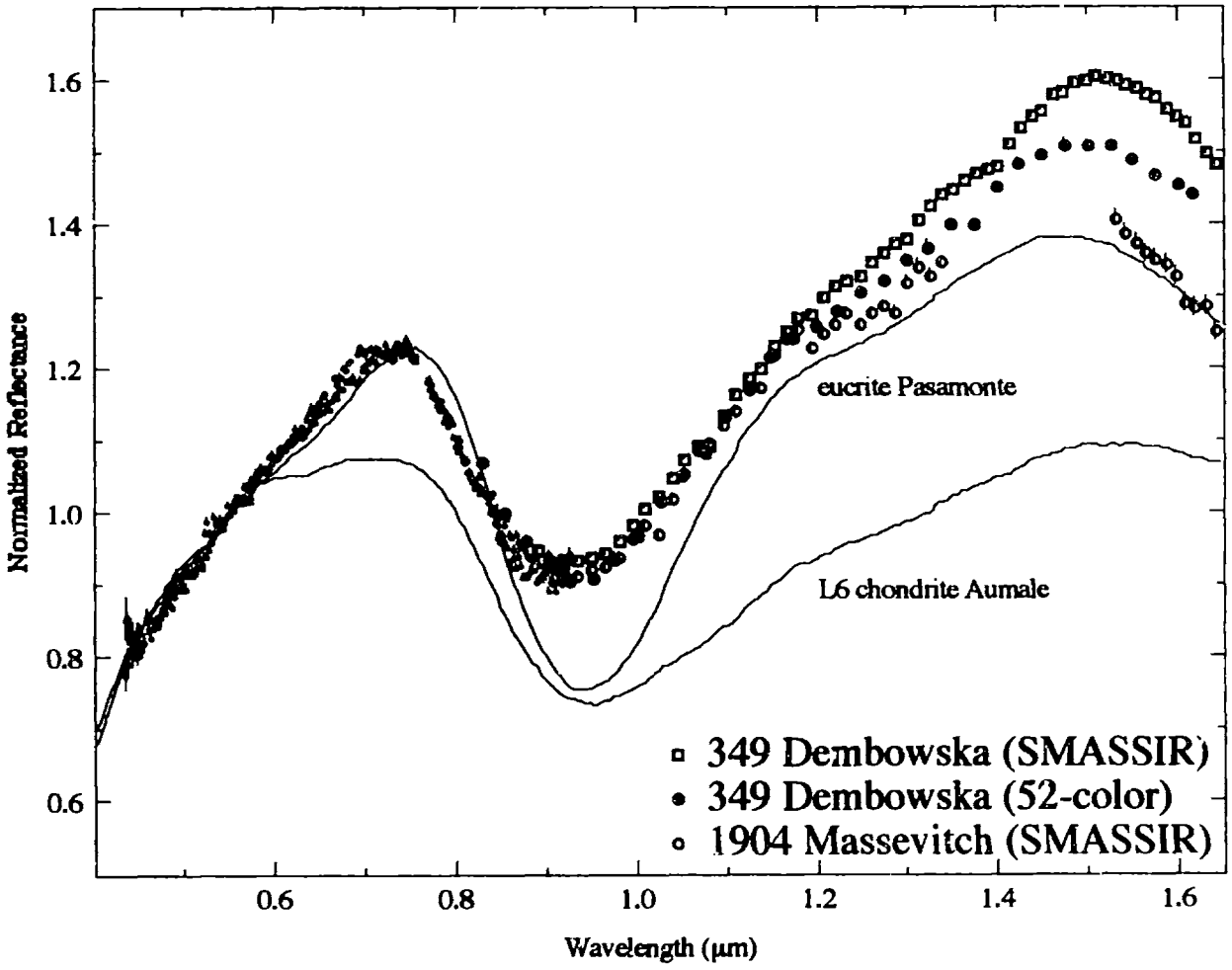

Figure 5.6.1. Reflectance spectra of R-asteroids 349 Dembowska (black symbols) and 1904 Massevitch (blue symbols). Small dots are from SMASS II (Bus, 1999) and larger symbols are from SMASSIR (open symbols) and the 52-color survey (dark circles). The meteorite spectra are from Gaffey (1976). All spectra are normalized to unity at 0.55 μm. Error bars are ±1σ.

5.6.3 Conclusions

Dembowska and Massevitch have spectra that indicate an olivine-pyroxene mixture, but no measured meteorites appear to be adequate spectral analogs for these objects (Table 5.6.2). Meteorites from these objects may not be present in our meteorite collection due to Dembowska's position in the outer part of the belt and due to Massevitch's small size, even though it is located relatively near the 5:2 resonance.

Table 5.6.2. Mineralogic interpretation of R asteroids observed in SMASSIR. Quotation marks are used for meteoritic analogs that appear less certain.

Type	Asteroid	a (AU)	Meteoritic Analog	Mineralogic Interpretation
R	349 Dembowska	2.925	none readily apparent	broad 1 μm feature due primarily to olivine and pyroxene; spectrally much redder than ordinary chondrites; broader 1 μm band than eucrites, which indicates an olivine component
	1904 Massevitch	2.744	none readily apparent	

5.7 S Asteroids

5.7.1 Background

S objects are the most abundant classified type of asteroid and are known (e.g., Gaffey *et al.*, 1993) from their visible and near-infrared reflectance spectra to have silicate compositions that tend to range from olivine-dominated to olivine-pyroxene mixtures to pyroxene-dominated. S asteroids have been linked to the ordinary chondrites (H, L and LL), since these meteorites have spectral features due to olivine and pyroxene and are the most abundant type of meteorite to land on Earth. However, the S asteroids tend to have redder spectra and shallower absorption features than the ordinary chondrites (Figure 5.7.1). These spectral differences have been recognized since the earliest days of asteroid-meteorite spectral comparisons (e.g., Chapman and Salisbury, 1973; McCord and Gaffey, 1974).

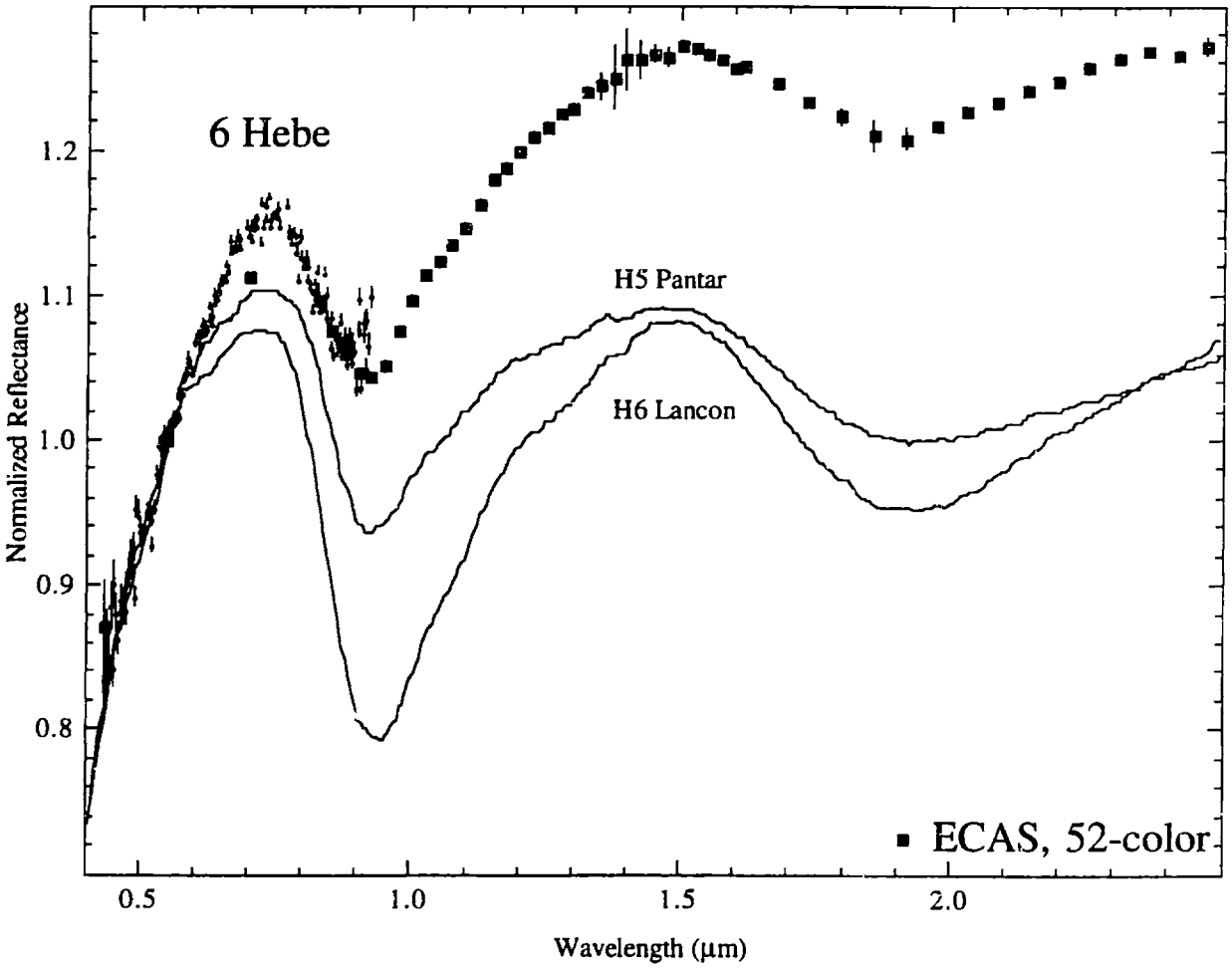

Figure 5.7.1. Reflectance spectrum of S-asteroid 6 Hebe versus spectra of H5 Pantar (top line) and H6 Lancon (bottom line). Small dots are from SMASS II (Bus, 1999) and dark squares are from the 52-color survey (dark circles). The meteorite spectra are from Gaffey (1976). All spectra are normalized to unity at 0.55 μm. Error bars are $\pm 1\sigma$.

There is considerable disagreement on the importance of these spectral mismatches, which are almost entirely in slope, and if they are caused by compositional differences and/or alteration effects. Some researchers argue that some percentage (between 5 to 50%) (Chapman, 1996) of the S asteroids have ordinary chondrite compositions, while others believe that the ordinary chondrite parent bodies tend to be found among small (diameters less than 10 km) objects and not among the S asteroids (Bell *et al.*, 1989), which they believe to be primarily differentiated or partially-differentiated bodies.

To try to understand the mineralogical diversity of the S class, Gaffey *et al.* (1993) divided the S types with high-quality 52-channel data into seven subclasses (Figure 5.7.2) based on the wavelength of their 1 μm band centers and the ratio of the areas of their 1 and 2 μm absorption features. (The band center has had the continuum slope divided out of the spectrum.) Cloutis *et al.* (1986) has shown that these two parameters are functions of the relative abundances of olivine and orthopyroxene for olivine-orthopyroxene mixtures. Spectra of pure olivine will have 1 μm band centers between ~1.05 and ~1.1 μm and band area ratios of zero, since olivine does not have a 2 μm feature. Spectra of pure orthopyroxene will have 1 μm band centers between ~0.90 and ~0.95 μm and band area ratios of ~2. One of the most interesting results from Gaffey *et al.* (1993) was that only the S(IV) asteroids have mineralogical parameters (band centers, band area ratios) that were consistent with the mineralogy of ordinary chondrites. S(I) objects have spectra consistent with "pure" olivine and S(VII) asteroids have spectra consistent with "pure" pyroxene. S(II) thr gh S(VI) asteroids have spectra consistent with some mixture of olivine and pyroxene. Some subtypes, such as the S(II) and S(III) classes, fell off the olivine-pyroxene mixing line and were interpreted as containing a clinopyroxene component.

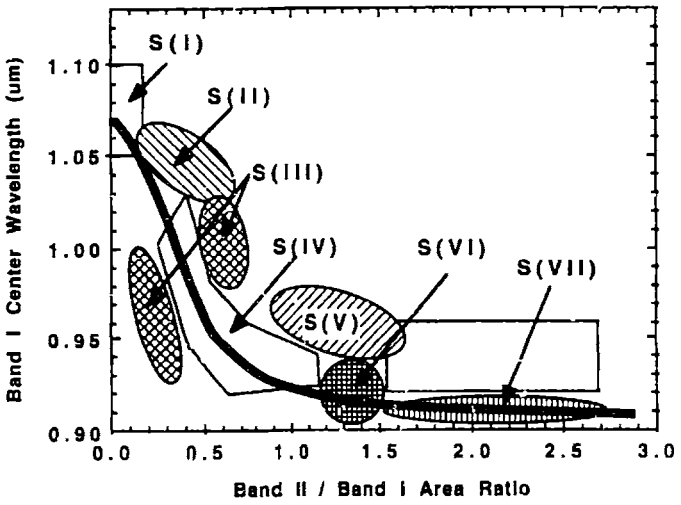

Figure 5.7.2. Plot of Band I (1 μm feature) center wavelength versus Band II (2 μm feature)/Band I area ratio. The Gaffey *et al.* (1993) subclasses from S(I) to S(VII) are labeled. The S(IV) region is defined by the area occupied by the parameters derived from the ordinary chondrites. The rectangular box above the S(VII) is the region occupied by the HEDs.

One of these S(IV) objects, 6 Hebe (Figure 5.7.1), has been proposed by a number of researchers (Farinella *et al.*, 1993; Gaffey, 1996; Gaffey and Gilbert, 1998) to be the parent body of the H chondrites. Hebe is located near both the 3:1 and ν_6 resonances and is believed to be supplying a relatively large number of fragments into Earth-crossing orbits (Table 1.4). Hebe also has a silicate mineralogy, derived from 1 μm band centers and band area ratios, that is consistent with the H chondrites. Gaffey (1996) and Gaffey and Gilbert (1998) propose that Hebe's redness compared to H chondrites is due to melt sheets of FeNi on the surface. These melt sheets would need to be spectrally red, unlike the relatively flat spectral characteristics of ordinary chondrite metal (Gaffey, 1986). H chondrites have been linked with the IIE iron meteorites due to the presence of silicate inclusions similar to H chondrites in these irons (e.g., Casanova *et al.*, 1995). Gaffey (1999b) believes that his interpretation is supported by the discovery of H6 chondrite Portales Valley (Kring *et al.*, 1999), which has an unusually large number of thick metallic veins running through it.

Differences between the Gaffey subtypes may not be entirely due to differences in composition. Moroz *et al.* (2000) believes that ignoring temperature effects in interpreting band area ratios and 1 μm band centers may lead to the misinterpretation of S-asteroid compositions. For example, they suggest that S(II) and S(III) asteroids may not necessarily be enriched in calcic pyroxene and their offset from the olivine-orthopyroxene mixing line may be due to an effect due to the low temperatures of their surfaces, which can affect the band positions of olivine-pyroxene mixtures.

Bus (1999) divided the S class into six separate groups: S, Sa, Sk, Sl, Sq and Sr classes. The S subclasses have spectra intermediate between the S class and the class indicated by the lower case letter. However, Bus (1999) found no definite breaks in spectral properties between the S class, intermediate classes (Sa, Sk, Sl, Sq and Sr) and other classes (A, K, L, Q and R), but instead found a continuum of spectra. This means that asteroids with different classifications may have only very subtle differences between their spectra since the dividing lines between classes are somewhat arbitrary.

There are many questions concerning the properties of the S asteroids. One question is what percentage of them have compositions similar to ordinary chondrites. As mentioned earlier, Binzel *et al.* (1996b) has found that there appears to be a continuum of spectral properties in the visible wavelength region between the S asteroids and the ordinary chondrites among the NEAs. Among observed S and Q objects, the 1 μm band depth tends to increase for decreasing diameter (Binzel *et al.*, 1998). This has been interpreted as showing that larger objects have been more altered than smaller ones. Another question that can be answered from this study is how well the Bus (1999) S subclasses are grouping objects with distinct differences in composition.

5.7.2 Investigation of S Asteroids

To answer the above questions, over 70 different S asteroids classified by Bus (1999) that were also observed in SMASSIR will be discussed. Objects had sizes ranging from a few hundred kilometers to a few hundred meters (NEAs). Mineralogic interpretations of the SMASSIR spectra are hampered by the absence of complete data on the 2 μm feature, which is essential for determining the relative contents of olivine and pyroxene on the surface. This can be seen in Figure 5.7.2 where objects (ordinary chondrite and HEDs) with widely different abundances of olivine can have similar values for their 1 μm band centers. The band area ratio, which can be determined from SMASSIR spectra, is needed to differentiate them in the figure.

Each of the Bus (1999) subtypes will be discussed in separate sections. Band minima, centers (minima for spectra where a linear continuum has been removed) and depths for the 1 μm feature will be calculated; however, problems in overlapping the SMASS and SMASSIR data at 0.92 μm and the scatter in the SMASSIR spectra sometimes cause the centers to occur at ~0.92 μm even though the feature appears to be very broad. Visual interpretation of the broadness of the 1 μm feature will be primarily used to determine if an object appears olivine- or pyroxene-rich. The terms "olivine-rich" "pyroxene-rich" will be used for asteroid spectra that appear spectrally dominated by their respective minerals.

5.7.3 Subgroup: Sa Asteroids

Thirteen Sa asteroids (Table 5.7.1) were observed in SMASSIR. One object, 244 Sita, has a very noisy spectrum (Appendix B) due to residual atmospheric water features and will not be discussed. These objects tended to rather small with all but one having diameters less than 30 km.

Table 5.7.1. Sa asteroids observed in SMASSIR. Diameters and albedos are from IRAS (Tedesco, 1994) except for diameters in parentheses, which are calculated using the H magnitude with an estimated albedo of 0.25. HCM family membership is from Zappalà *et al.* (1995). SMASS II classifications are from Bus (1999). The error bars for the asteroid band positions are estimated to be ±0.02 μm for the band minima and centers. The estimated error bars for the band depths are ±5% times the depth. The band depth is calculated by dividing a linear continuum out of each spectrum.

Asteroid	a (AU)	e'	sin i'	IRAS Albedo	Diameter (km)	HCM Family	NEA	Gaffey *et al.* (1993) subclass	Minimum (μm)	Center (μm)	Depth
63 Ausonia	2.395	0.120	0.108	0.16	103			S(II-III)	0.89	0.90	25%
244 Sita	2.174	0.110	0.061	0.19	11	Flora			0.90	-	-
625 Xenia	2.647	0.199	0.184	0.22	28				0.90	1.05	17%
913 Otila	2.198	0.133	0.085		(11)	Flora			0.94	1.04	18%
950 Ahrensa	2.371	0.203	0.388	0.18	15				0.92	0.92	16%
1350 Rosselia	2.858	0.052	0.039	0.16	23	Koronis			0.92	0.92	14%
1587 Kahrstedt	2.545	0.162	0.145		(16)				0.92	0.92	19%
2038 Bistro	2.435	0.096	0.238	0.13	13				0.89	0.91	12%
2396 Kochi	2.794	0.095	0.210		(13)				1.02	1.03	21%
3474 Linsley	2.558	0.215	0.105		(7)				0.93	0.94	16%
3545 Gaffey	2.870	0.042	0.038		(10)	Koronis			0.92	0.92	19%
3767 DiMaggio	2.603	0.172	0.226		(13)	Eunomia			1.04	1.09	18%
4512 Sinuhe	2.767	0.230	0.153		(11)				0.96	1.04	20%

5.7.3.1 Red-Sloped Sa Asteroids

Four of these Sa objects are relatively red-sloped (Figure 5.7.3) with reflectances at 1.65 μm of between 1.59 and 1.69. As can be seen by their very broad features, these objects contain significant amounts of olivine. Xenia has weak features at ~1.1 and ~1.3 μm, which is indicative of an olivine surface assmblage with essentially no pyroxene, since pyroxene tends to wipe out the distinctive structure of the olivine bands. For Ausonia and Otila, their spectra indicate the presence of a 2 μm feature, which would indicate a pyroxene component. Ausonia and Bistro appear to be more pyroxene-rich due to band minima at ~0.9 μm. All of these objects can be seen to much redder than LL4 chondrite Soko Banja. LL chondrites contain ~50% olivine, ~20% orthopyroxene, ~5% clinopyroxene and ~5% FeNi (McSween *et al.*, 1991).

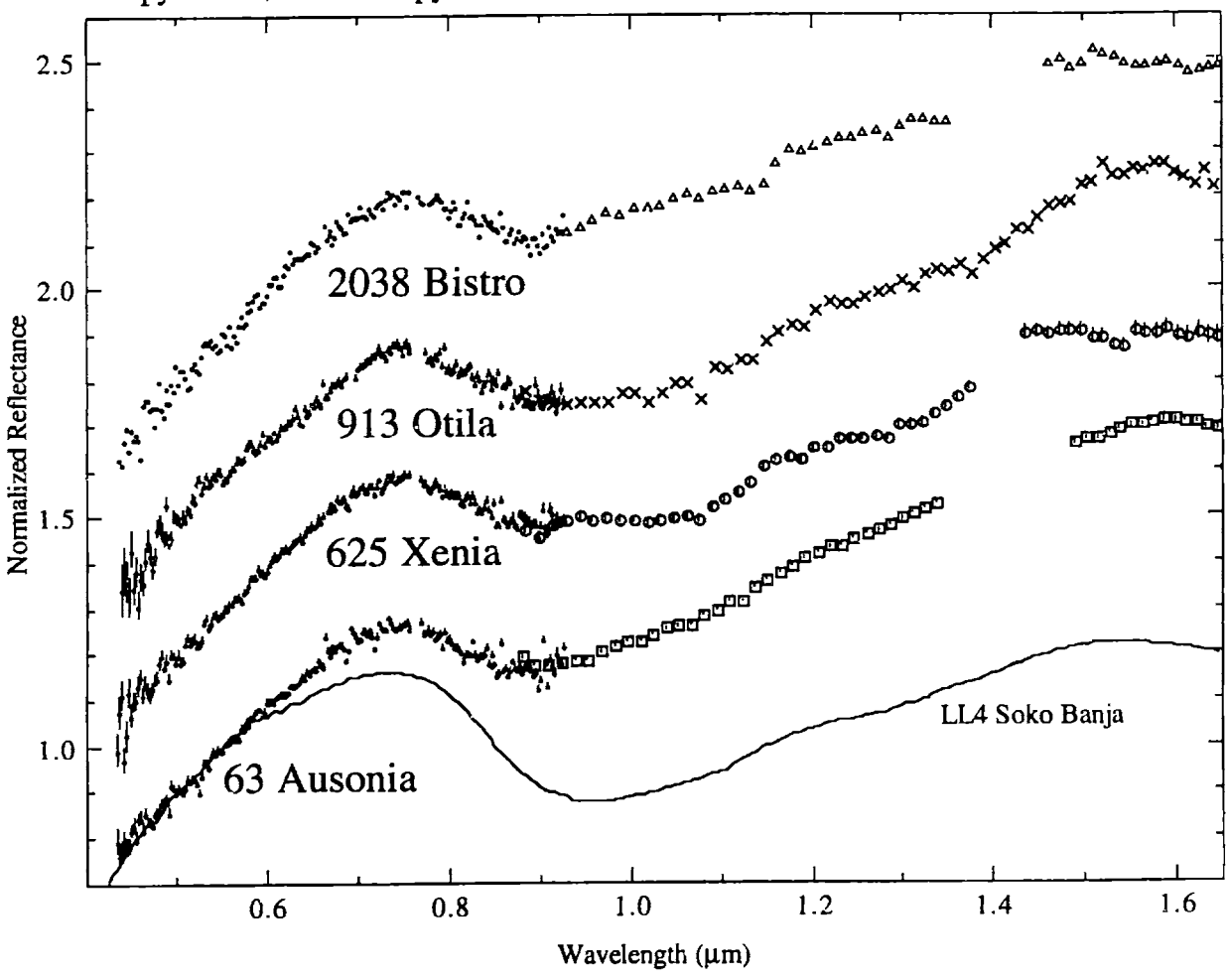

Figure 5.7.3. Reflectance spectra of Sa-asteroids 63 Ausonia (squares), 625 Xenia (circles), 913 Otila (crosses) and 2038 Bistro (triangles) versus a spectrum of LL4 chondrite Soko Banja (Gaffey, 1976). Small dots are from SMASS II (Bus, 1999) and larger symbols are from SMASSIR (open symbols) and the 52-color survey (dark circles). All spectra are normalized to unity at 0.55 μm. All asteroid spectra are offset by 0.3 in reflectance from each other. Error bars are ±1σ.

As can be seen in Figure 5.7.4, these Sa objects have virtually indistinguishable visible spectra with A asteroids. These Sa objects have very similar near-infrared spectral properties with the shallow-featured A types. As with the shallow-featured A types, the best guesses for these objects' compositions are some type of heavily-altered silicates and/or some type of mixture of metal and silicates. Like Xenia, Otero also has weak features at ~1.1 and ~1.3 μm, which is indicative of an olivine surface assemblage with essentially no pyroxene. The altered silicates could be some combination of the laser-altered material of Yamada *et al.* (1999) and Moroz *et al.* (1996) (which has been melted and recrystallized). Both types of compositions would be expected to redden the spectra and suppress the absorption bands. These spectra could also be consistent with some mixture of metallic iron and silicates.

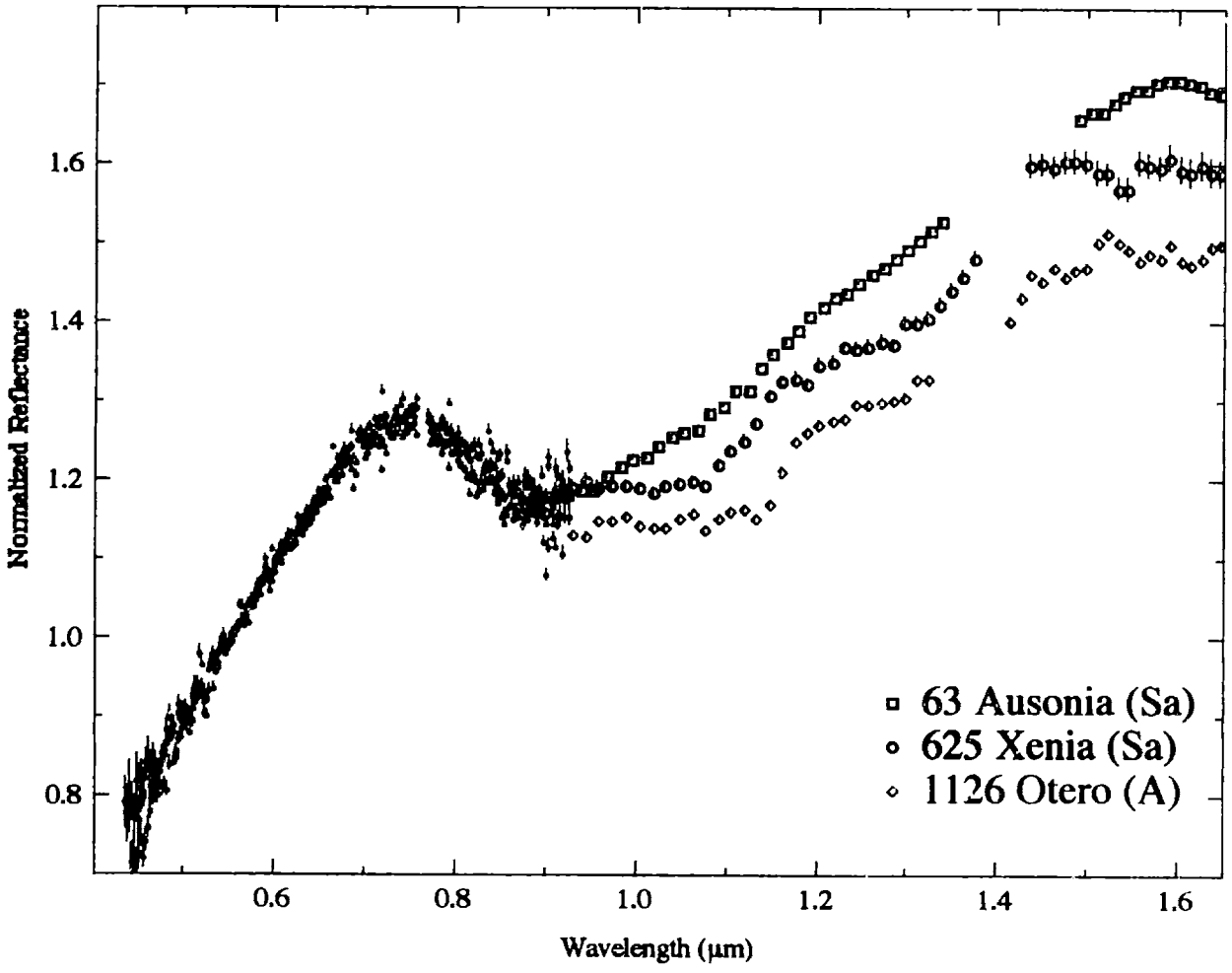

Figure 5.7.4. Reflectance spectra of Sa-asteroids 63 Ausonia (squares) and 625 Xenia (circles) versus a spectrum of A-asteroid 1126 Otero (diamonds). Small dots are from SMASS II (Bus, 1999) and larger symbols are from SMASSIR (open symbols) and the 52-color survey (dark circles). All spectra are normalized to unity at 0.55 μm. Error bars are ±1σ.

5.7.3.2 Less Red-Sloped Sa Asteroids

The other Sa asteroids are not as red-sloped with reflectances at 1.65 μm of between 1.29 and 1.46. Some of these asteroids (950 Ahrensa, 1587 Kahrstedt, 3545 Gaffey) appear to be more pyroxene-rich (Figure 5.7.5) than the others due to a slight upturn in the 1 μm feature at a shorter wavelength (~0.95 μm) than the other objects. All of the objects have slightly stronger UV features and redder spectral slopes than ordinary chondrites. These objects are also relatively small (diameters less than 16 km). The band depths of these objects (16-19%) are similar to the measured depth of H5 chondrite Castalia (depth of 17%)

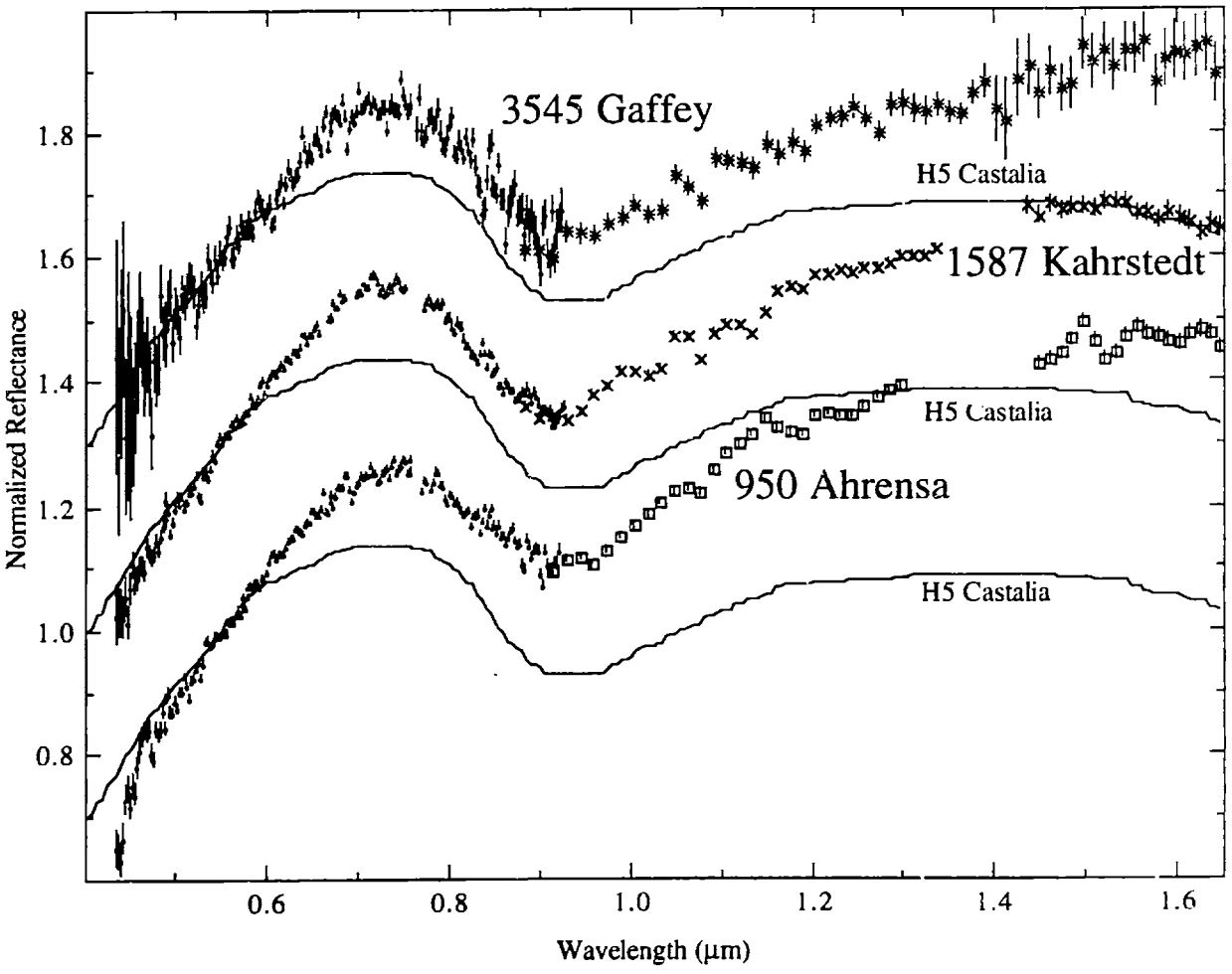

Figure 5.7.5. Reflectance spectra of the less-red pyroxene-rich Sa asteroids. Also plotted is the spectrum of H5 chondrite Castalia (Gaffey, 1976). Small dots are from SMASS II (Bus, 1999) and larger symbols are from SMASSIR (open symbols) and the 52-color survey (dark circles). All spectra are normalized to unity at 0.55 μm. All asteroid spectra are offset by 0.3 in reflectance from each other. Error bars are ±1σ.

The less-red olivine-rich Sa asteroids are plotted in Figure 5.7.6. These objects tend to have relatively broad 1 μm bands. These objects can all be seen to be redder (by ~10%) with shallower band depths (8% to 21%) than LL4 chondrites (depths of ~25-30%), which have similar 1 μm band structures to these asteroids. LL4 chondrites have band minima and centers at ~0.95 μm. The addition of a "red" metallic iron component (similar to iron meteorites) to an LL4 chondritic composition would be expected to redden the spectrum and suppress the band so it would appear more similar to these objects. This is consistent with the lower albedo of Rosselia (0.16 ± 0.03) versus Soko Banja (0.27). Since the finer-grained LL4 chondrite is not redder than the coarser-grained Soko Banja, lowering the particle size for a sample of Soko Banja would not be expected to significantly redden the spectrum.

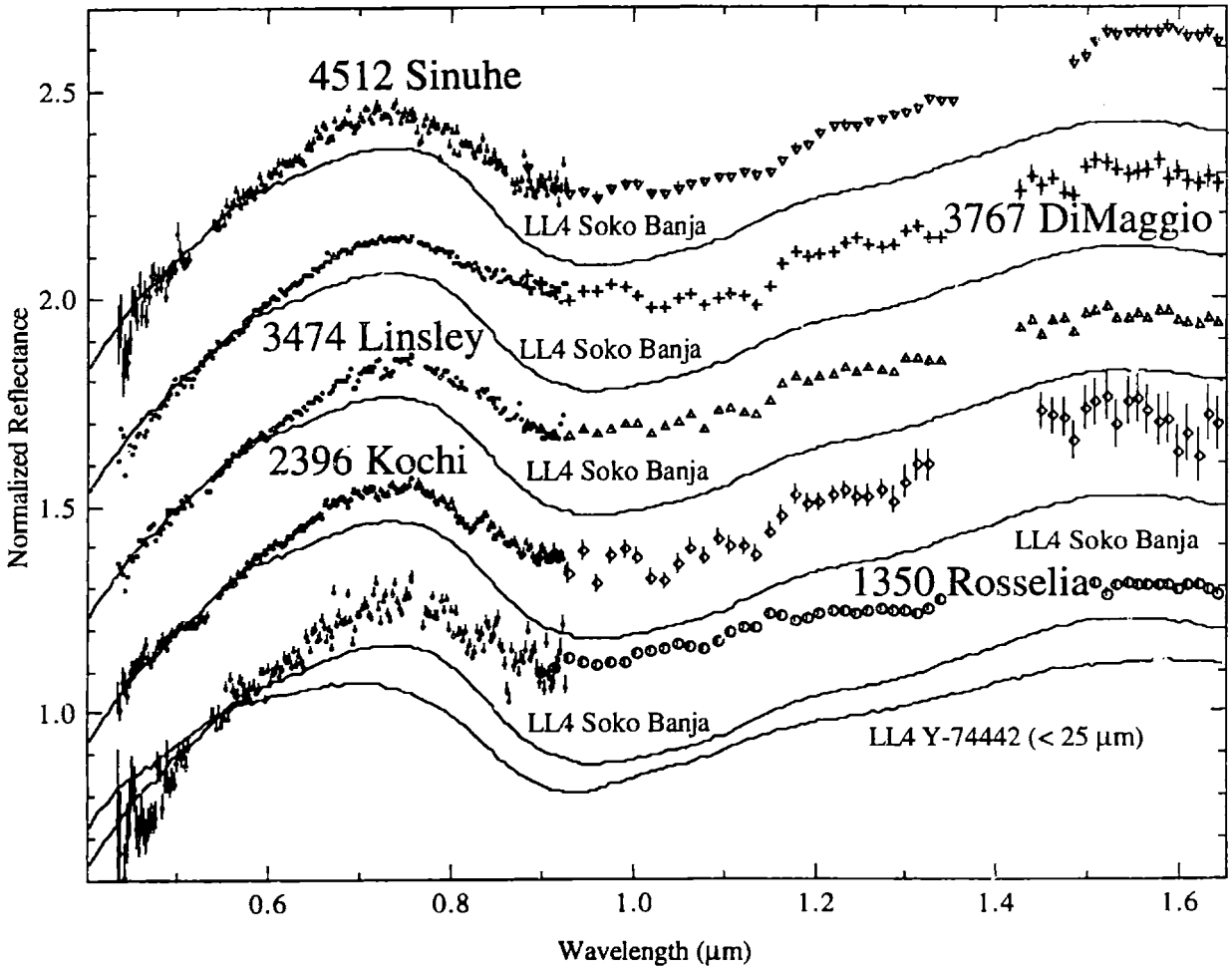

Figure 5.7.6. Reflectance spectra of the less-red olivine-rich Sa asteroids. Also plotted are the spectra of LL4 chondrites Soko Banja (Gaffey, 1976) and Y-74442 (particle size less than 25 μm) (Hiroi, personal communication). The spectrum of Y-74442 was measured at RELAB. Small dots are from SMASS II (Bus, 1999) and larger symbols are from SMASSIR (open symbols) and the 52-color survey (dark circles). All spectra are normalized to unity at 0.55 μm. All asteroid spectra are offset by 0.3 in reflectance from each other. Error bars are ±1σ.

5.7.4 Subgroup: Sk Asteroids

Five Sk objects (Table 5.7.2) were observed in SMASSIR. Except for the one observed NEA, these objects all tended to be very large with diameters ranging from 40 to 234 km. These asteroids have moderate albedos ((0.18 to 0.24).

Table 5.7.2. Sk asteroids observed in SMASSIR. Proper elements (a, e', sin i') are from Milani and Knezevic (1994). Osculating elements are given for the NEAs, which are from the *Ephemerides of Minor Planets* (1999). Diameters and albedos are from IRAS (Tedesco, 1994) except for diameters in parentheses, which are calculated using the H magnitude with an estimated albedo of 0.25. HCM family membership is from Zappalà *et al.* (1995). SMASS II classifications are from Bus (1999). The error bars for the asteroid band positions are estimated to be ±0.02 μm for the band minima and centers. The estimated error bars for the band depths are ±5% times the depth. The band depth is calculated by dividing a linear continuum out of each spectrum.

Asteroid	a (AU)	e'	sin i'	IRAS Albedo	Diameter (km)	HCM Family	NEA	Gaffey *et al.* (1993) subclass	Minimum (μm)	Center (μm)	Depth
3 Juno	2.669	0.232	0.231	0.24	234	Juno		S(IV)	0.92	0.93	12%
11 Parthenope	2.452	0.075	0.068	0.18	153			S(IV)	0.90	0.91	12%
43 Ariadne	2.203	0.140	0.070	0.27	66	Flora		S(III)	0.91	0.96	17%
167 Urda	2.854	0.043	0.037	0.22	40	Koronis			0.90	0.91	10%
1991 VH	1.137	0.444	0.240		(1)		Apollo		1.00	1.02	18%

These objects (Figure 5.7.7) are spectrally similar to the L4 chondrite Saratov, which is one of the reddest ordinary chondrites measured by Gaffey (1976). Saratov has a normative mineralogy of 39% olivine, 29% orthopyroxene, 5% clinopyroxene, 10% metal and 6% troilite (McSween *et al.*, 1991). It is unclear why Saratov tends to be redder than other ordinary chondrites since it is not distinct from other L chondrites compositionally (Rubin, 1990; McSween *et al.*, 1991). Reddening due to weathering can not be ruled, but no alteration features are apparent in the Saratov spectra. Except for the redder Ariadne, these asteroids have very similar spectral slopes (within ~10%) to Saratov. Urda appears to be the most pyroxene-rich with an upturn in its 1 μm feature at a shorter wavelength than the other objects. NEA 1991 VH appears to be the most olivine-rich with the broadest 1 μm band and a band mininimum and center past 1 μm.

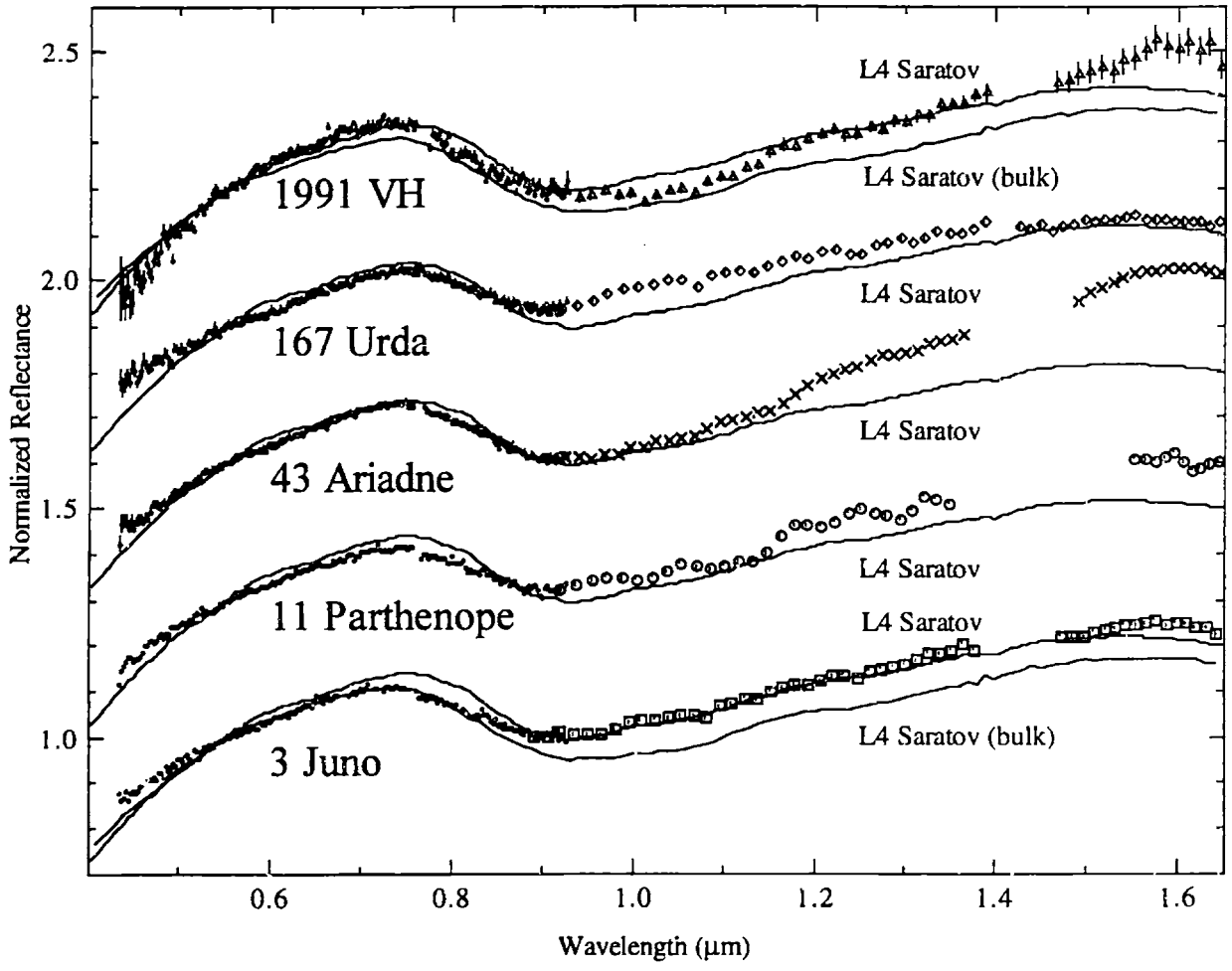

Figure 5.7.7. Reflectance spectra of Sk asteroids versus L4 chondrite Saratov. Small dots are from SMASS II (Bus, 1999) and larger symbols are from SMASSIR. The redder Saratov spectrum (plotted against all asteroids) is from Gaffey (1976). The other Saratov spectrum (plotted against Juno and 1991 VH) is for a bulk-powder sample. All spectra are normalized to unity at 0.55 μm. All spectra are offset by 0.3 in reflectance from each other. Error bars are ±1σ.

Data out to 2.5 μm are plotted in Figure 5.7.8 for objects with 52-color data. The SMASSIR data for Juno can be seen to be slightly redder than its 52-color data. Juno appears to be the best match to L4 chondrite Saratov in this extended wavelength range with both objects having broad 2 μm features with similar strengths and a spectrum that falls intermediate between the two Saratov spectra. Parthenope also has a 2 μm band that has a similar strength to Saratov's feature. Parthenope is located relatively near (2.45 AU) the 3:1 resonance while Juno (2.67 AU) is located relatively farther from the 5:2 and ν_6 resonances. Ariadne can still be seen to be much redder than Saratov.

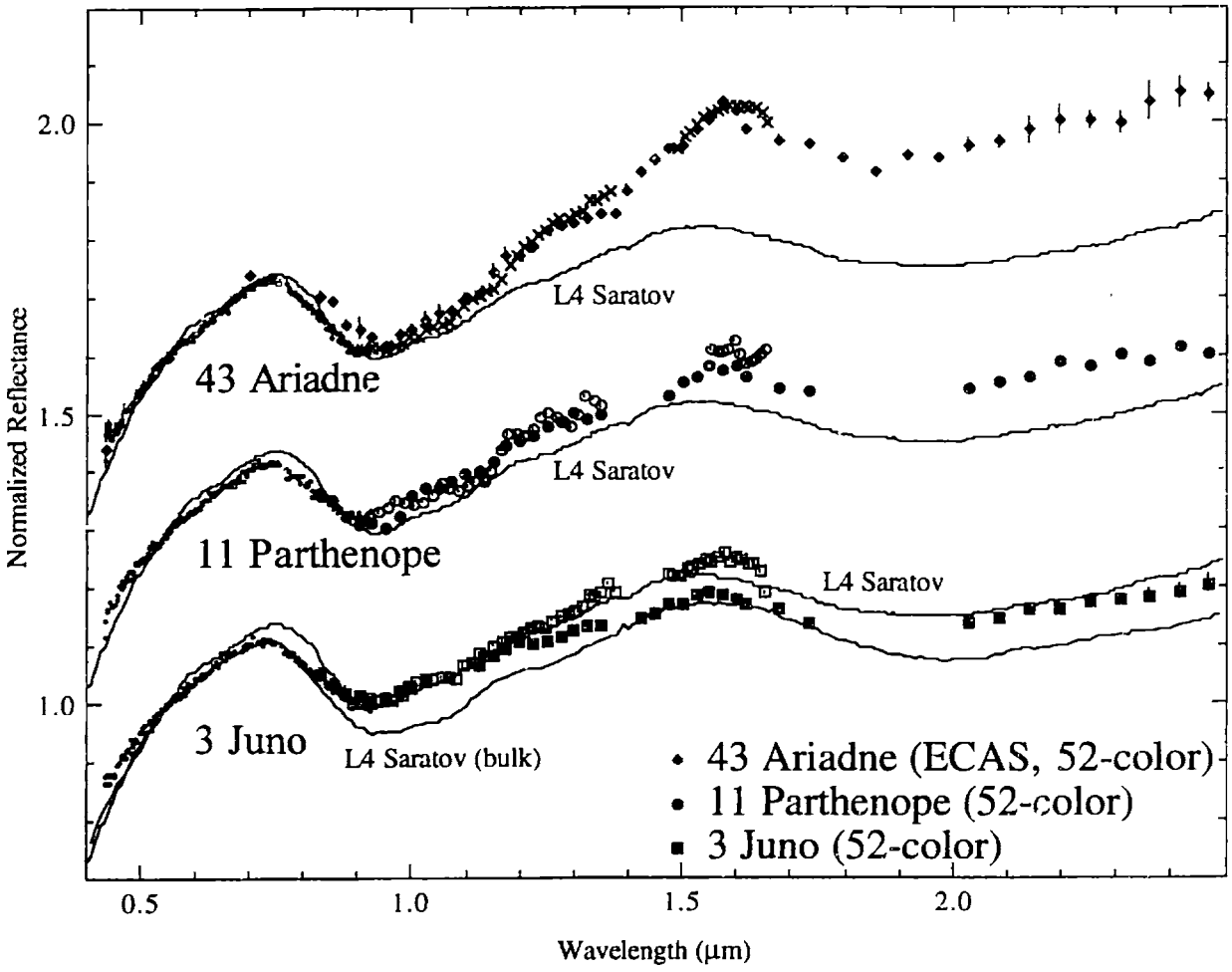

Figure 5.7.8. Reflectance spectra of Sk asteroids out to 2.5 μm versus L4 chondrite Saratov. Small dots are from SMASS II (Bus, 1999) and larger open symbols are from SMASSIR. Dark symbols are from ECAS and 52-color for Ariadne and only 52-color for Juno and Parthenope. The redder Saratov spectrum (plotted against all asteroids) is from Gaffey (1976). The other Saratov spectrum (plotted against Juno) is for a bulk-powder sample. All spectra are normalized to unity at 0.55 μm. All spectra are offset by 0.3 in reflectance from each other. Error bars are $\pm 1\sigma$.

5.7.5 Subgroup: Sl Asteroids

Six Sl asteroids (Table 5.7.3) were observed in SMASSIR. These objects tend to be relatively large (diameters greater than 20 km) except for NEA 1980 Tezcatlipoca. These asteroids all tend to have moderate albedos (0.17 to 0.23) except for the much brighter 352 Gisela (albedo of 0.43).

Table 5.7.3. Sl asteroids observed in SMASSIR. Proper elements (a, e', sin i') are from Milani and Knezevic (1994). Osculating elements are given for the NEAS, which are from the *Ephemerides of Minor Planets* (1999). Diameters in parentheses are calculated using the H magnitude with an estimated albedo of 0.25. HCM family membership is from Zappalà *et al.* (1995). SMASS II classifications are from Bus (1999). SMASS II classifications are from Bus (1999). The error bars for the asteroid band positions are estimated to be ±0.02 μm for the band minima and centers. The estimated error bars for the band depths are ±5% times the depth. The band depth is calculated by dividing a linear continuum out of each spectrum.

Asteroid	a (AU)	e'	sin i'	IRAS Albedo	Diameter (km)	HCM Family	NEA	Gaffey *et al.* (1993) subclass	Minimum (μm)	Center (μm)	Depth
169 Zelia	2.358	0.094	0.100	0.23	34				0.90	0.92	15%
352 Gisela	2.194	0.136	0.070	0.43	20	Flora			0.90	1.02	16%
354 Eleonora	2.798	0.179	0.292	0.19	155			S(I)	1.04	1.07	24%
416 Vaticana	2.788	0.253	0.197	0.17	85				0.92	0.94	13%
584 Semiramis	2.374	0.179	0.206	0.20	54			S(IV)	0.89	1.02	16%
1980 Tezcatlipoca	1.710	0.365	0.452	0.21	4		Amor		0.90	0.97	24%

Five of these objects are plotted in Figure 5.7.9. (The sixth SI asteroid, 354 Eleonora, will be discussed in the next paragraph.) These objects all have 1 μm features that are dominated by olivine due to their very broad features. Zelia and Vaticana appear to be slightly more pyroxene-rich than the others due to their 1 μm band centers occurring at shorter wavelengths. All of these objects can be seen to be significantly redder than LL4 chondrites. Their band depths vary from similar (24% for Tezcatlipoca) to smaller (13% to 16%) than those of LL4 chondrites (~25 to 30%). A "reddened" LL chondrite would appear to have similar spectral characteristics to these asteroids; however, other assemblages (e.g., some type of olivine-metal mixture) can not be ruled out.

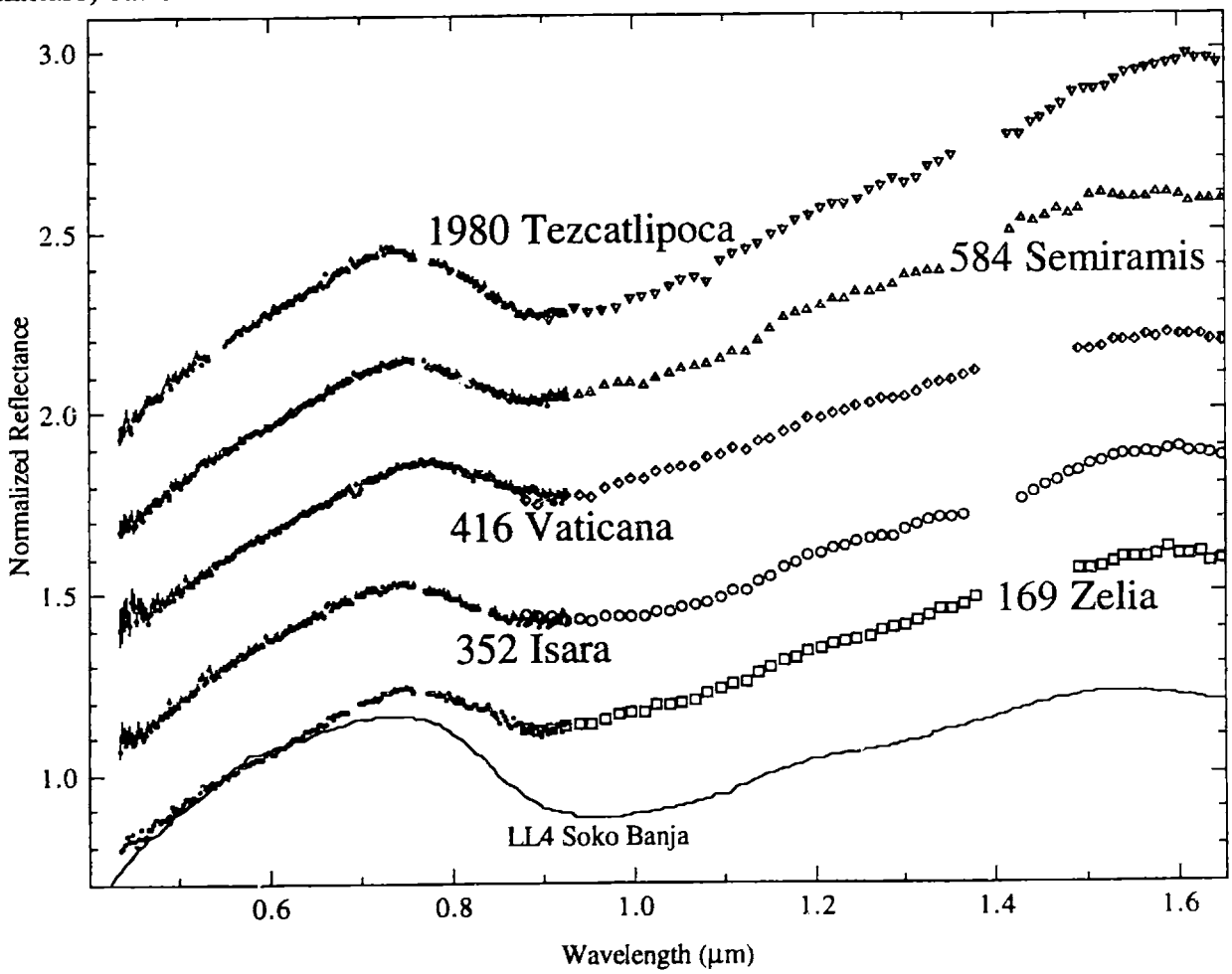

Figure 5.7.9. Reflectance spectra of SI asteroids (excluding 354 Eleonora) versus a spectrum of LL4 chondrite Soko Banja. Small dots are from SMASS II (Bus, 1999) and larger symbols are from SMASSIR. The meteorite spectrum is from Gaffey (1976). All spectra are normalized to unity at 0.55 μm. All spectra are offset by 0.3 in reflectance from each other. Error bars are $\pm 1\sigma$.

Asteroid 354 Eleonora (Figure 5.7.10) has an unusual spectrum compared to the other Sl asteroids. The SMASS II spectrum has a deep absorption at ~0.85 μm, which is not apparent in the other Sl objects. The SMASS I spectrum does not have this absorption feature. This unusual feature is similar to the one found in the Victoria spectrum (Figure 5.4.4). The SMASS I spectrum appears more consistent with the SMASSIR spectrum. Eleonora has more distinctive olivine bands than the other Sl asteroids and has spectra more similar in structure to the deep-featured A asteroids (e.g., 246 Asporina). The band minimum for Eleonora is at 1.04 ± 0.02 μm and the band center is at 1.07 ± 0.02 μm, which are at slightly lower wavelengths than the deep-featured A asteroids.

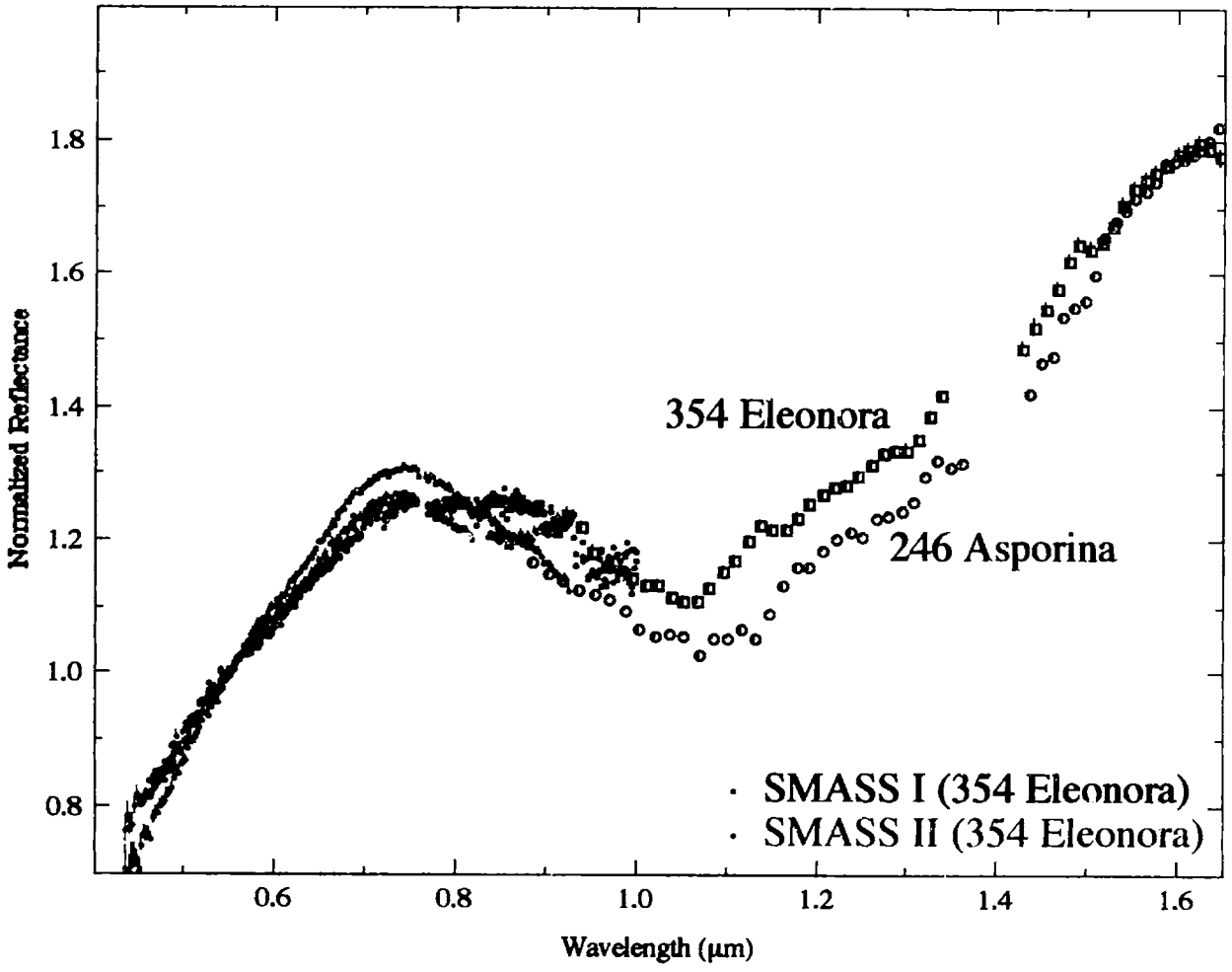

Figure 5.7.10. Reflectance spectra of Sl asteroid 354 Eleonora and A asteroid 246 Asporina. Red and blue small dots are from SMASS II (Bus, 1999), black dots are from SMASS I (Xu *et al.*, 1995) and larger symbols are from SMASSIR. All spectra are normalized to unity at 0.55 μm. Error bars are ±1σ.

5.7.6 Subgroup: Sq Asteroids

Fifteen Sq objects (Table 5.7.4) were observed in SMASSIR. Compared to other S subgroups, this subtype contains mainly objects with estimated diameters less than 20 km.

Table 5.7.4. Sq asteroids observed in SMASSIR. Proper elements (a, e', sin i') are from Milani and Knezevic (1994). Osculating elements are given for the NEAS, which are from the *Ephemerides of Minor Planets* (1999). Diameters and albedos tend to be from IRAS (Tedesco, 1994) except for diameters in parentheses, which are calculated using the H magnitude with an estimated albedo of 0.25. HCM family membership is from Zappalà *et al.* (1995). SMASS II classifications are from Bus (1999). The error bars for the asteroid band positions are estimated to be ±0.02 μm for the band minima and centers. The estimated error bars for the band depths are ±5% times the depth. The band depth is calculated by dividing a linear continuum out of each spectrum.

Asteroid	a (AU)	e'	sin i'	IRAS Albedo	Diameter (km)	HCM Family	NEA	Gaffey *et al.* (1993) subclass	Minimum (μm)	Center (μm)	Depth
33 Polyhymnia	2.867	0.300	0.035		(53)			S(IV)	0.90	0.91	16%
720 Bohlinia	2.887	0.051	0.036	0.20	33	Koronis			0.90	0.90	13%
808 Merxia	2.745	0.133	0.085	0.22	32	Merxia			0.91	0.91	20%
1324 Knysna	2.185	0.137	0.080		(8)	Flora			0.92	1.03	21%
1483 Hakoila	2.717	0.216	0.063		(14)				0.90	0.90	16%
2078 Nanking	2.369	0.301	0.393		(10)				0.90	0.90	15%
2873 Binzel	2.245	0.123	0.073		(7)	Flora			1.03	1.04	25%
3199 Nefertiti	1.574	0.284	0.544	0.26-0.41¿	2¿		Amor		1.08	1.13	23%
3376 Armandhammer	2.349	0.097	0.123		(9)	Vesta			0.91	0.92	32%
3903 Kliment Ohridski	2.930	0.086	0.036		(11)	Koronis			0.90	0.90	15%
4051 Hatanaka	2.790	0.072	0.066		(9)	Liberatrix			0.92	0.92	16%
7358 1995 YA_3	2.198	0.502	0.081		(5)		Amor		0.92	0.92	20%
1998 FX_2	2.152	0.494	0.173		(0.6)		Amor		0.95	1.01	17%
1998 PG	2.015	0.392	0.113		(1)		Amor		0.92	0.92	18%
1998 QR_{15}	2.755	0.565	0.168		(0.7)		Amor		0.93	0.92	14%

¿ The albedo and diameter for 3199 Nefertiti are from Veeder *et al.* (1989).

5.7.6.1 Pyroxene-Rich Sq Asteroids

A number of these asteroids appear pyroxene-rich with six of them plotted in Figure 5.7.11. The seventh, 3376 Armandhammer, will be discussed in the next paragraph. All of these pyroxene-rich objects tend to have very similar visible spectra to the H and L chondrites. In the near-infrared, some of these asteroids (720 Bohlinia, 3903 Kliment Ohridski, 7358 1995 YA_3) are pretty good spectral matches for these meteorites while other asteroids (33 Polyhymnia, 808 Merxia. 2078 Nanking) have 1 μm features that tend to turn up faster and have lower band minimums (0.89 to 0.91 μm) than the H and L chondrite spectra (minima of 0.92 to 0.94 μm), which indicates a higher orthopyroxene abundance than the H chondrites (~25% orthopyroxene, ~4% clinopyroxene, ~35% olivine). These asteroids tend to have spectral slopes that range from similar to the ordinary chondrites to slightly redder (~10%). This set of objects contains the three largest Sq asteroids (33 Polyhymnia, 720 Bohlinia and 808 Merxia).

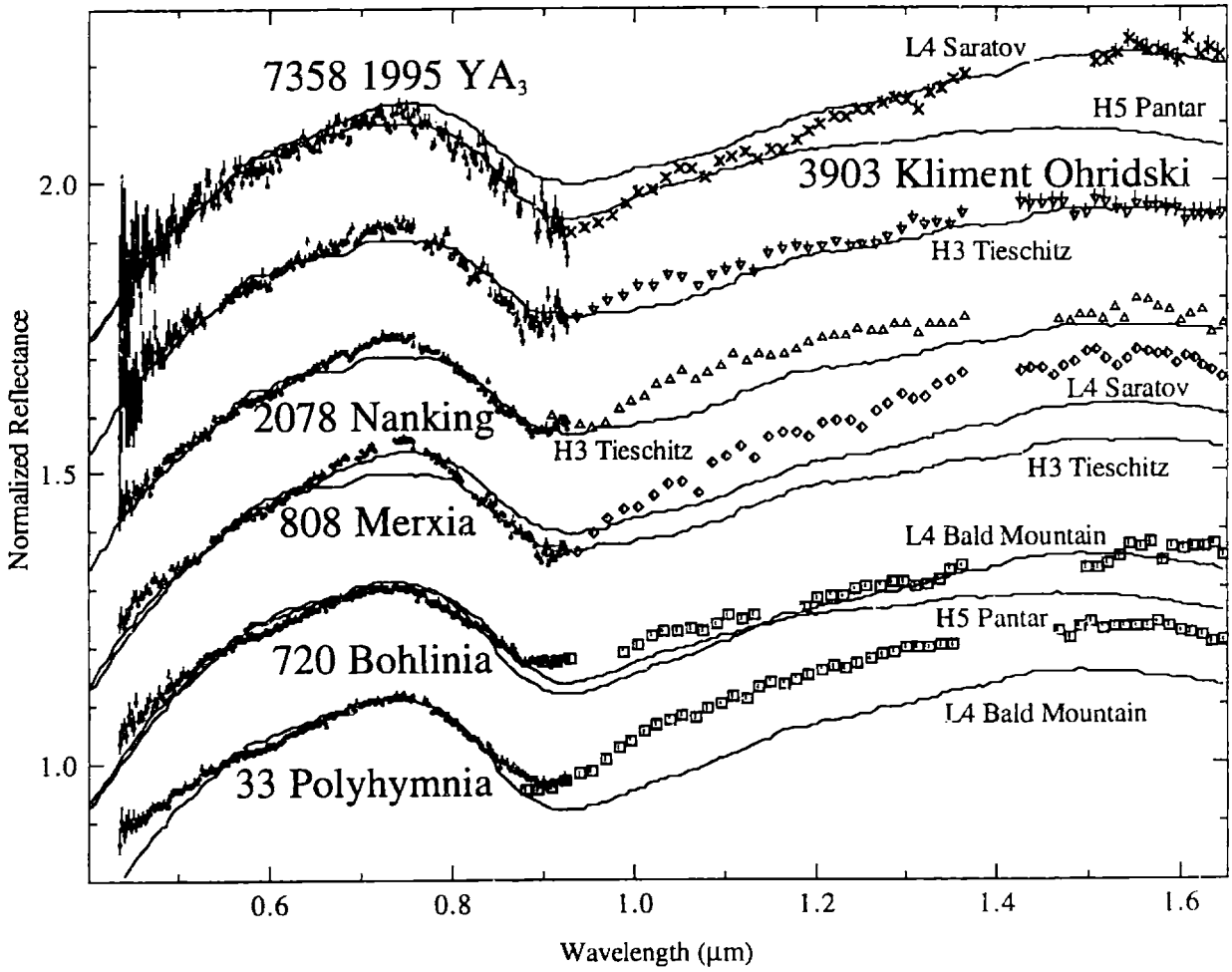

Figure 5.7.11. Reflectance spectra of pyroxene-rich Sq asteroids versus various H and L chondrites. Small dots are from SMASS II (Bus, 1999) and larger symbols are from SMASSIR. The meteorite spectra are from Gaffey (1976). All spectra are normalized to unity at 0.55 μm. All spectra are offset by 0.2 in reflectance from each other. Error bars are ±1σ.

The other pyroxene-rich object is 3376 Armandhammer (Figure 5.7.12), which is a member of the Vesta family. Armandhammer has a spectrum similar to the eucrites, with the characteristic 1 μm feature due to orthopyroxene. The weaker strength and smaller width of the 1 μm feature in the asteroid spectrum compared to the eucrite could be due to a smaller grain size on the asteroid surface and/or a higher proportion of glass. The lower surface temperature (~120 K) on this asteroid would also tend to reduce the width of the feature (by ~10%).

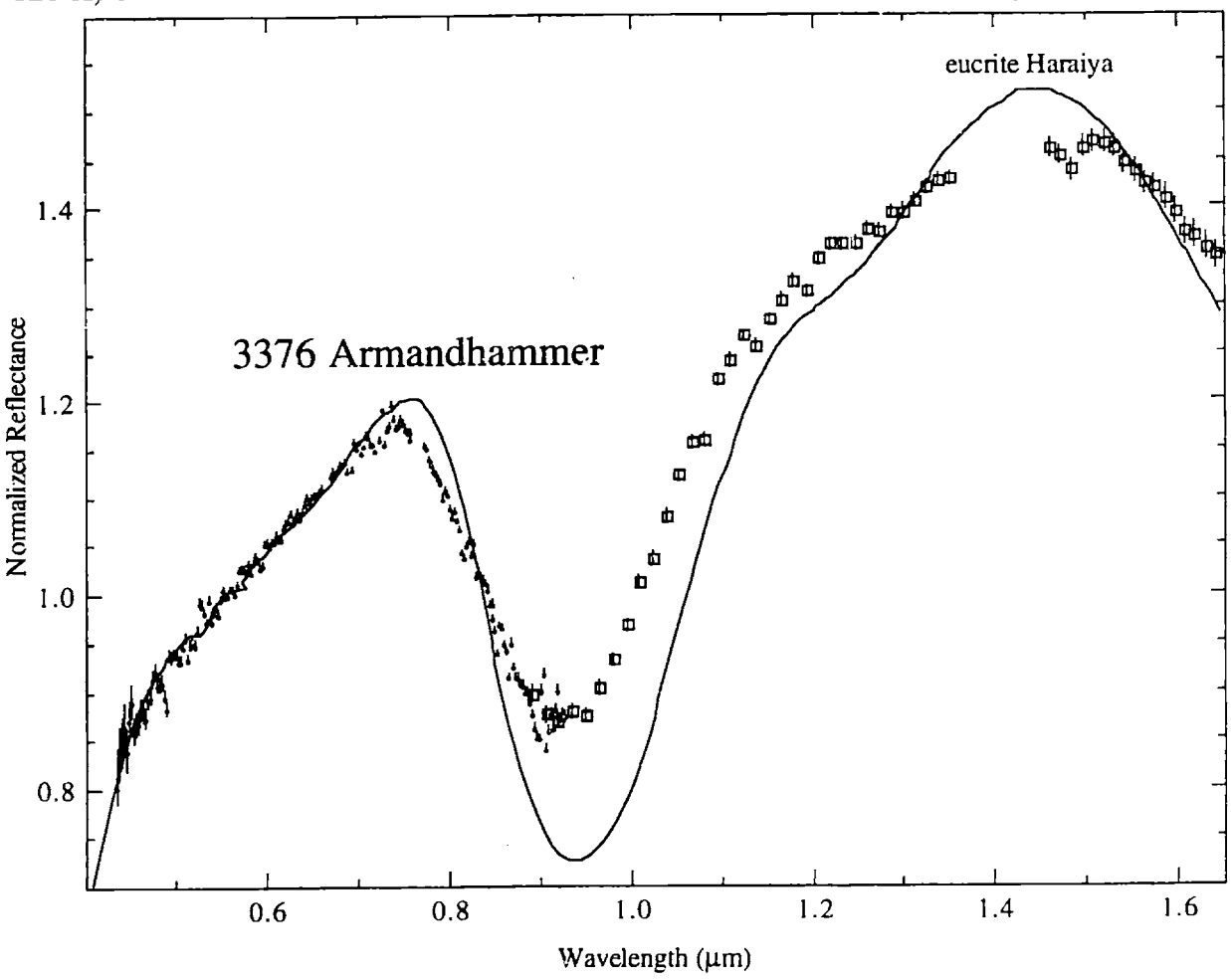

Figure 5.7.12. Reflectance spectrum of 3376 Armandhammer versus a spectrum of the eucrite Haraiya. Small dots are from SMASS II (Bus, 1999) and larger symbols are from SMASSIR. The meteorite spectrum is from Gaffey (1976). All spectra are normalized to unity at 0.55 μm. Error bars are $\pm 1\sigma$.

5.7.6.2 Olivine-Rich Sq Asteroids

The other Sq asteroids have broader 1 μm features that make them appear more olivine-rich (Figure 5.7.13); however, their UV and 1 μm features are weaker than typical olivine-dominated objects. Compared to other Sq asteroids, one possibility is that these asteroids have a higher olivine abundance plus a higher abundance of opaques, which would suppress the UV feature and the 1 μm band. All of these objects have estimated diameters smaller than 15 km. Knysna and Binzel are both in the Flora family.

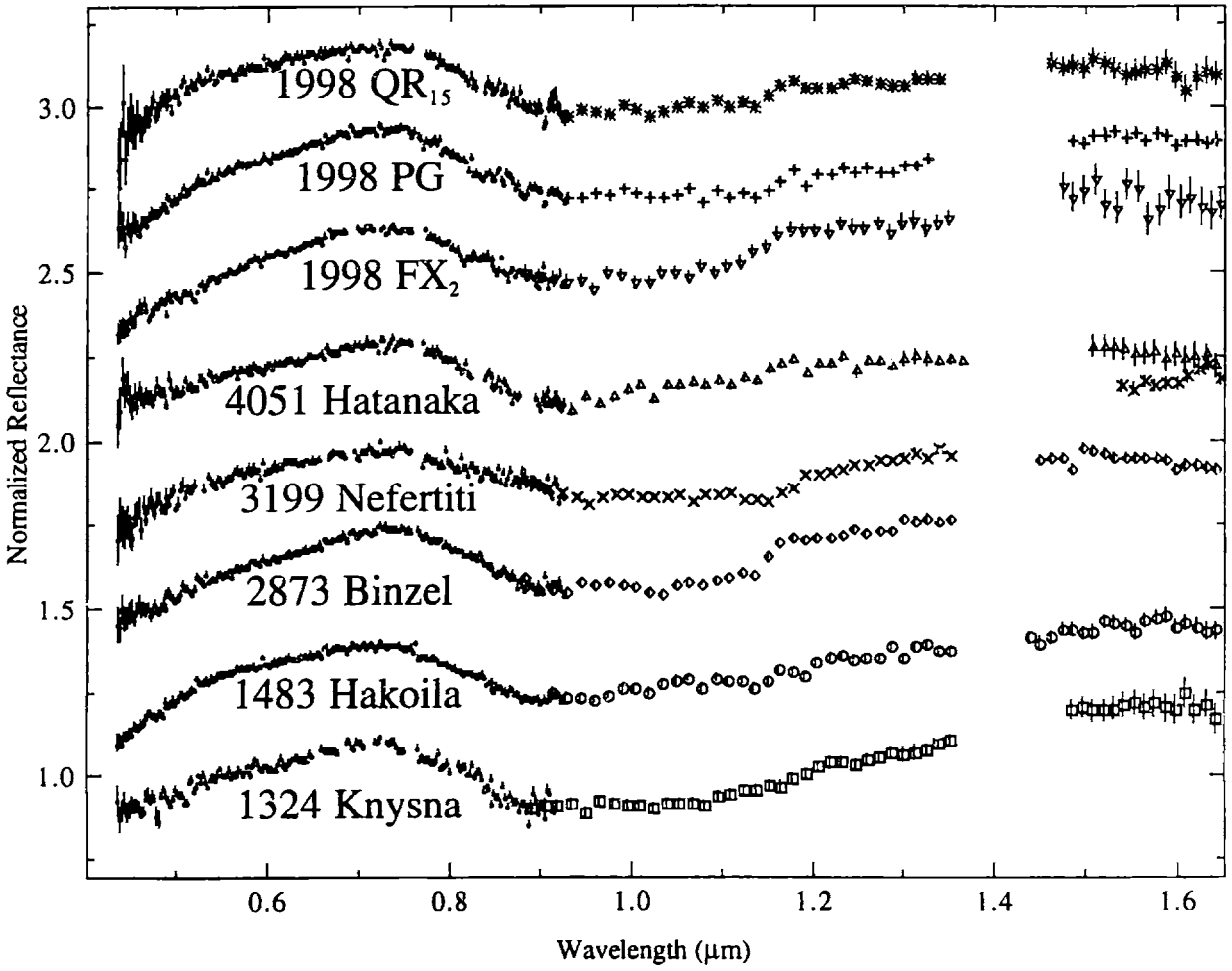

Figure 5.7.13. Reflectance spectra of olivine-rich Sq asteroids. Small dots are from SMASS II (Bus, 1999) and larger symbols are from SMASSIR. All spectra are normalized to unity at 0.55 mμ_ All spectra are offset by 0.3 in reflectance from each other. Error bars are ±1σ.

The visible spectra of these objects are somewhat similar (Figure 5.7.14) to the ureilite Novo Urei and H3 chondrite Tieschitz. Ureilites contain up to ~10% dark matrix, which tends to suppress its absorption features. Tieschitz is also relatively dark (albedo of 0.13) and also has suppressed features. Asteroid 1483 Hakoila is also a very good spectral match to the ureilite and the H3 chondrite in the near-infrared while Nefertiti and Knysna appear more olivine-rich due to their broader features. The ureilites are known to have considerable compositional variations (Mittlefehldt *et al.*, 1998). Novo Urei has a ratio of pyroxene to pyroxene plus olivine of ~0.3. This ratio varies from 0 to 0.9 for all ureilites. If these objects have compositions similar to ureilites, they would be expected to have rather low albedos (~0.08); however, the only object with a measured albedo (3199 Nefertiti) has one that is much higher (0.26 to 0.41), which implies a composition very different from the ureilites. It appears very difficult to differentiate between ureilites and "dark" ordinary chondrites in this wavelength region.

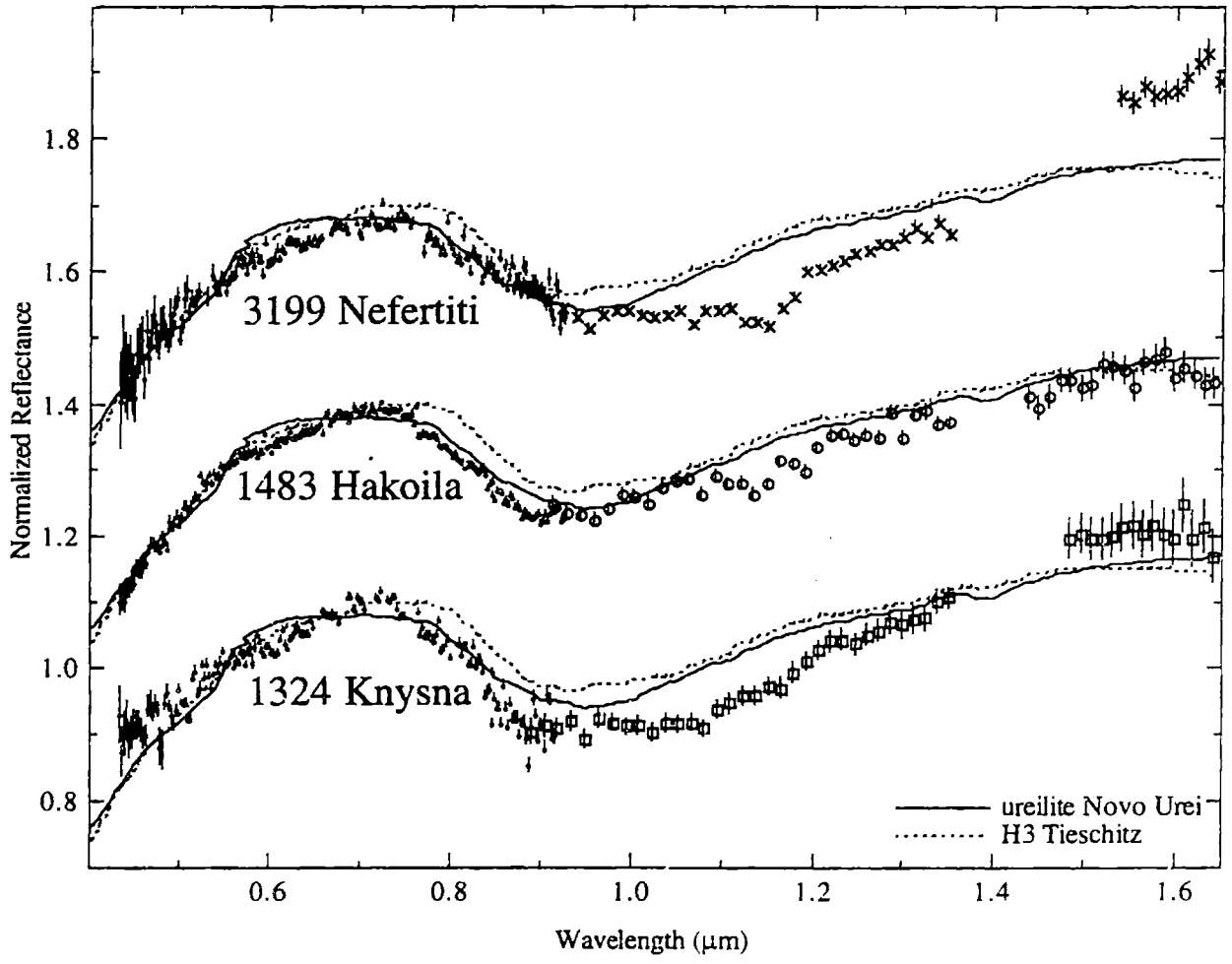

Figure 5.7.14. Reflectance spectra of 1324 Knysna, 1483 Hakoila and 3199 Wallonia versus spectra of ureilite Novo Urei and LL4 chondrite Soko Banja. Small dots are from SMASS II (Bus, 1999) and larger symbols are from SMASSIR. The meteorite spectra are from Gaffey (1976). All spectra are normalized to unity at 0.55 μm. All spectra are offset by 0.3 in reflectance from each other. Error bars are $\pm 1\sigma$.

5.7.7 Subgroup: Sr Asteroids

Two Sr asteroids (NEA 1864 Daedalus and 3819 Robinson) were observed in SMASSIR (Table 5.7.5). These two objects are relatively small with diameters less than 10 km.

Table 5.7.4. Sr asteroids observed in SMASSIR. Proper elements (a, e', sin i') are from Milani and Knezevic (1994). Osculating elements are given for the NEAS, which are from the *Ephemerides of Minor Planets* (1999). Diameters and albedos tend to be from IRAS (Tedesco, 1994) except for diameters in parentheses, which are calculated using the H magnitude with an estimated albedo of 0.25. HCM family membership is from Zappalà *et al.* (1995). SMASS II classifications are from Bus (1999). The error bars for the asteroid band positions are estimated to be ±0.02 μm for the band minima and centers. The estimated error bars for the band depths are ±5% times the depth. The band depth is calculated by dividing a linear continuum out of each spectrum.

Asteroid	a (AU)	e'	sin i'	IRAS Albedo	Diameter (km)	HCM Family	NEA	Gaffey *et al.* (1993) subclass	Minimum (μm)	Center (μm)	Depth
1864 Daedalus	1.461	0.615	0.378		(3)		Apollo		1.05	1.05	22%
3819 Robinson	2.772	0.100	0.178		(9)				1.06	1.08	41%

These two asteroids are plotted in Figure 5.7.15. Both objects appear olivine-rich; however, Robinson has a very deep feature with the three distinctive olivine bands while Daedalus has a much shallower feature. Robinson's spectrum looks like a Brachina spectrum that has been slightly reddened and whose 1 μm feature has been slightly suppressed. Robinson is the only small asteroid (diameter less than 20 km) with this distinctive olivine-dominated spectrum. Robinson is not as red (reflectance at 1.65 μm of 1.65) as the deep-featured A types (reflectances of 1.8 to 2.35). Robinson could have a surface that has been altered to a lesser extent than the deep-featured A asteroids or a metallic iron component (~25 wt.%), which should also redden the spectrum but should keep the distinctive olivine bands. Daedalus has a similar spectral slope to LL4 chondrite Soko Banja, but to appears to be more olivine-rich than this meteorite due to its broader feature with a band center at ~1.05 μm.

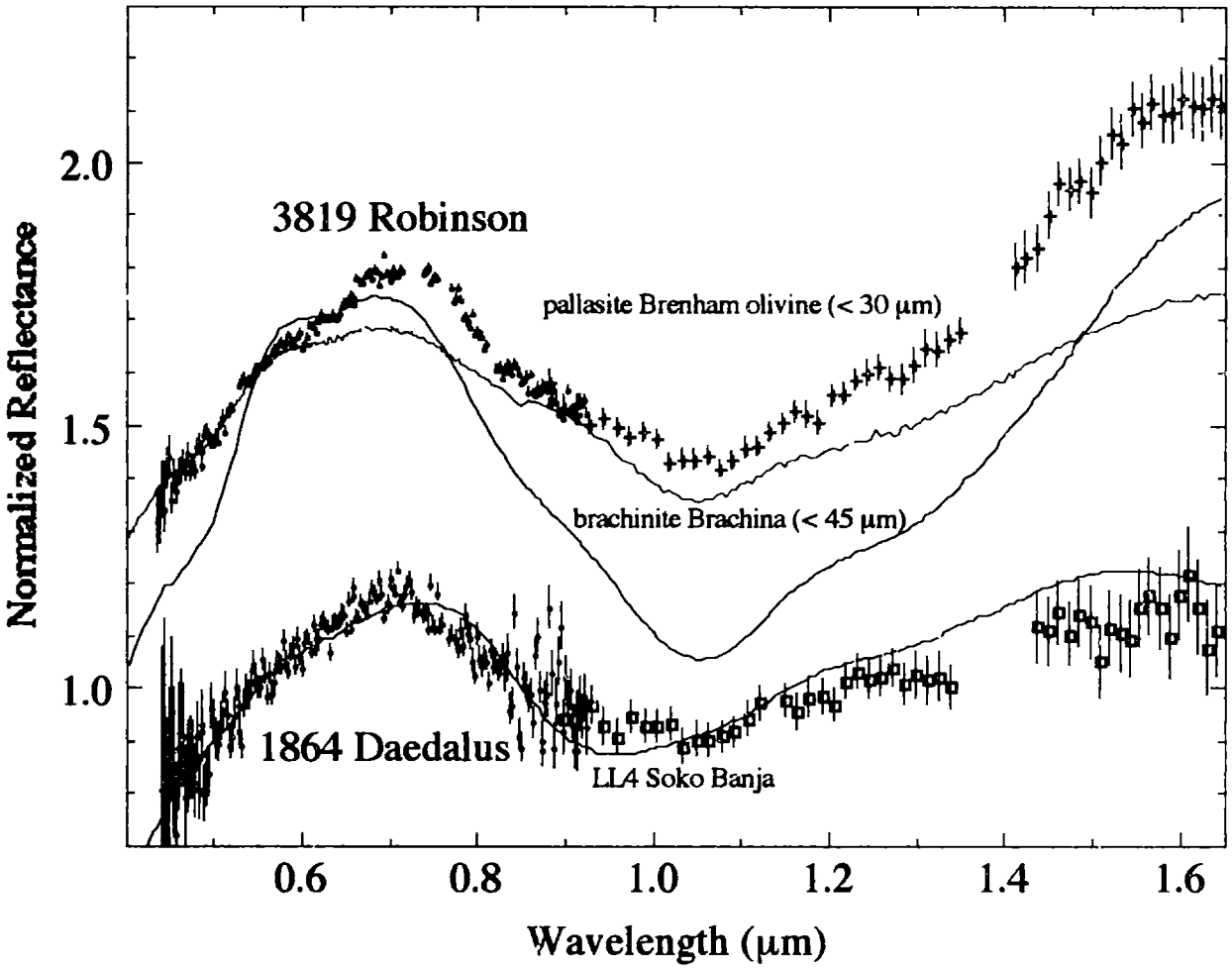

Figure 5.7.15. Reflectance spectra of Sr asteroids 1864 Daedalus and 3819 Robinson versus spectra of LL4 chondrite Soko Banja, and brachinite Brachina (particle size less than 45 μm) and pallasite Brenham olivine (pallasite less than 30 μm). Small dots are from SMASS II (Bus, 1999) and larger symbols are from SMASSIR. The Soko Banja spectrum is from Gaffey (1976). The Brachina spectrum is a RELAB spectrum from Sunshine and Hiroi (personal communication) from a sample supplied by the South Australian Museum. The Brenham olivine spectrum is from King and Ridley (1987). All spectra are normalized to unity at 0.55 μm. All spectra are offset by 0.6 in reflectance from each other. Error bars are ±1σ.

5.7.8 Subgroup: S Asteroids

Thirty-seven objects classified just as S asteroids by Bus (1999) were observed in SMASSIR (Table 5.7.6). These objects tended to be rather large with ~50% of the main-belt objects having diameters greater than 100 km. All of these asteroids will be discussed except for 675 Ludmilla, 1685 Toro and 5131 1990 PG, which are extremely noisy.

Table 5.7.6. S asteroids (Bus, 1999) observed in SMASSIR. Proper elements (a, e', sin i') are from Milani and Knezevic (1994). Osculating elements are given for the NEAS, which are from the *Ephemerides of Minor Planets* (1999). Diameters and albedos tend to be from IRAS (Tedesco, 1994) except for diameters in parentheses, which are calculated using the H magnitude with an estimated albedo of 0.25. The error bars for the asteroid band positions are estimated to be ±0.02 μm for the band minima and centers. The estimated error bars for the band depths are ±5% times the depth. The band depth is calculated by dividing a linear continuum out of each spectrum.

Asteroid	a (AU)	e'	sin i'	IRAS Albedo	Diameter (km)	HCM Family	NEA	Gaffey *et al.* (1993) subclass	Minimum (μm)	Center (μm)	Depth
5 Astraea	2.576	0.229	0.079	0.23	119				0.90	0.91	15%
6 Hebe	2.425	0.162	0.245	0.27	185			S(IV)	0.89	0.90	11%
7 Iris	2.386	0.212	0.110	0.28	200			S(IV)	0.93	0.94	15%
15 Eunomia	2.644	0.148	0.226	0.21	255	Eunomia		S(III)	1.01	1.05	15%
18 Melpomene	2.296	0.183	0.166	0.22	141			S(V)	0.88	0.88	9%
20 Massalia	2.409	0.162	0.025	0.21	146	Massalia		S(VI)	0.91	0.91	15%
25 Phocaea	2.400	0.226	0.395	0.23	75			S(IV)	0.92	0.95	19%
26 Proserpina	2.656	0.120	0.052	0.20	95			S(II)	0.90	1.03	18%
28 Bellona	2.777	0.179	0.147	0.18	121				0.92	0.93	11%
32 Pomona	2.587	0.110	0.107	0.26	81			S(IV)	0.90	0.91	14%
37 Fides	2.642	0.160	0.057	0.18	108			S(V)	0.90	0.92	12%
39 Laetitia	2.769	0.068	0.170	0.29	150			S(II)	1.05	1.05	16%
40 Harmonia	2.267	0.021	0.065	0.24	108			S(VII)	0.90	0.90	13%
57 Mnemosyne	3.154	0.097	0.265	0.21	113			S(VII)	0.90	0.91	12%
80 Sappho	2.296	0.150	0.159	0.18	78			S(IV)	0.89	0.89	15%
113 Amalthea	2.376	0.121	0.077	0.26	46			S(I)	1.06	1.07	28%
158 Koronis	2.869	0.045	0.038	0.28	35	Koronis			0.94	0.95	18%
243 Ida	2.862	0.045	0.036	0.24	28	Koronis			0.90	0.91	15%
346 Hermentaria	2.796	0.064	0.133	0.22	107				0.89	0.96	14%
374 Burgundia	2.780	0.113	0.166	0.30	45	Ceres			0.91	0.92	15%
389 Industria	2.608	0.098	0.160	0.20	79			S(V)	0.90	0.90	13%
675 Ludmilla	2.770	0.174	0.183		(71)				0.88	-	-
737 Arequipa	2.592	0.203	0.218	0.27	44				0.90	0.92	12%
825 Tanina	2.226	0.114	0.052	0.35	11	Flora			1.02	1.03	23%
1036 Ganymed	2.664	0.467	0.475	0.29	32		Amor	S(VI-VII)	0.92	0.92	21%
1627 Ivar	1.863	0.418	0.141	0.12	7		Amor		0.92	0.92	18%
1685 Toro	1.367	0.436	0.163	0.31Ø	1¡		Apollo		-	-	-
1807 Slovakia	2.226	0.144	0.073		(10)	Flora			0.91	1.03	20%
1866 Sisyphus	1.893	0.539	0.658	0.18¢	8¢		Apollo		0.92	0.93	14%
3122 Florence	1.769	0.423	0.377		(4)		Amor		0.94	1.00	18%
4954 Eric 2.001	0.448	0.300			(8)		Amor		0.92	0.92	19%
5131 1990 PG	1.486	0.570	0.593		(4)		Apollo		-	-	-
5836 1993 MF	2.444	0.532	0.140		(4)		Amor		0.89	0.90	15%
1997 BQ	1.745	0.479	0.191		(0.7)		Apollo		0.92	0.92	15%
1997 BR	1.336	0.306	0.296		(0.9)		Apollo		0.92	0.99	20%
1997 CZ_5	2.292	0.399	0.422		(5)		Mars-crosser		0.92	0.92	20%
1998 FM_5	2.265	0.555	0.199		(0.2)		Amor		0.89	1.03	15%

Ø The albedo for 1685 Toro is from Veeder *et al.* (1989).
¡ The diameter for 1685 Toro is from Ostro *et al.* (1983).
¢ The albedo and diameter for 1866 Sisyphus are from Veeder *et al.* (1989).

5.7.8.1 Pyroxene-Rich S Asteroids

Figure 5.7.16 plots the spectra of the eighteen pyroxene-rich main-belt S-asteroids. All of these objects have 1 μm features with minima at approximately the same wavelength (~0.91 μm) indicative of orthopyroxene, but have significant variations in spectral slope. These objects also have variations in the turnover position between the 1 and 2 μm features of between 1.46 and 1.62 μm, implying compositional differences (e.g., abundance of olivine, pyroxene composition) between objects. There is a wide range of spectral slopes that vary from one of the reddest ordinary chondrites (L5 chondrite Homestead) to the very-red octahedrite Butler. These asteroids tend to have band minima at slightly shorter wavelengths than Homestead (0.93 μm). All of these asteroids have band depths between 11 and 15%, except for 18 Melpomene (depth of 9%) and 25 Phocaea (depth of 19%). The reddest object (Phocaea) does have the largest band depth; however, no obvious correlation was seen between the band depth and spectral slope for the other objects. The cause of these slope differences will be discussed in Section 5.8.

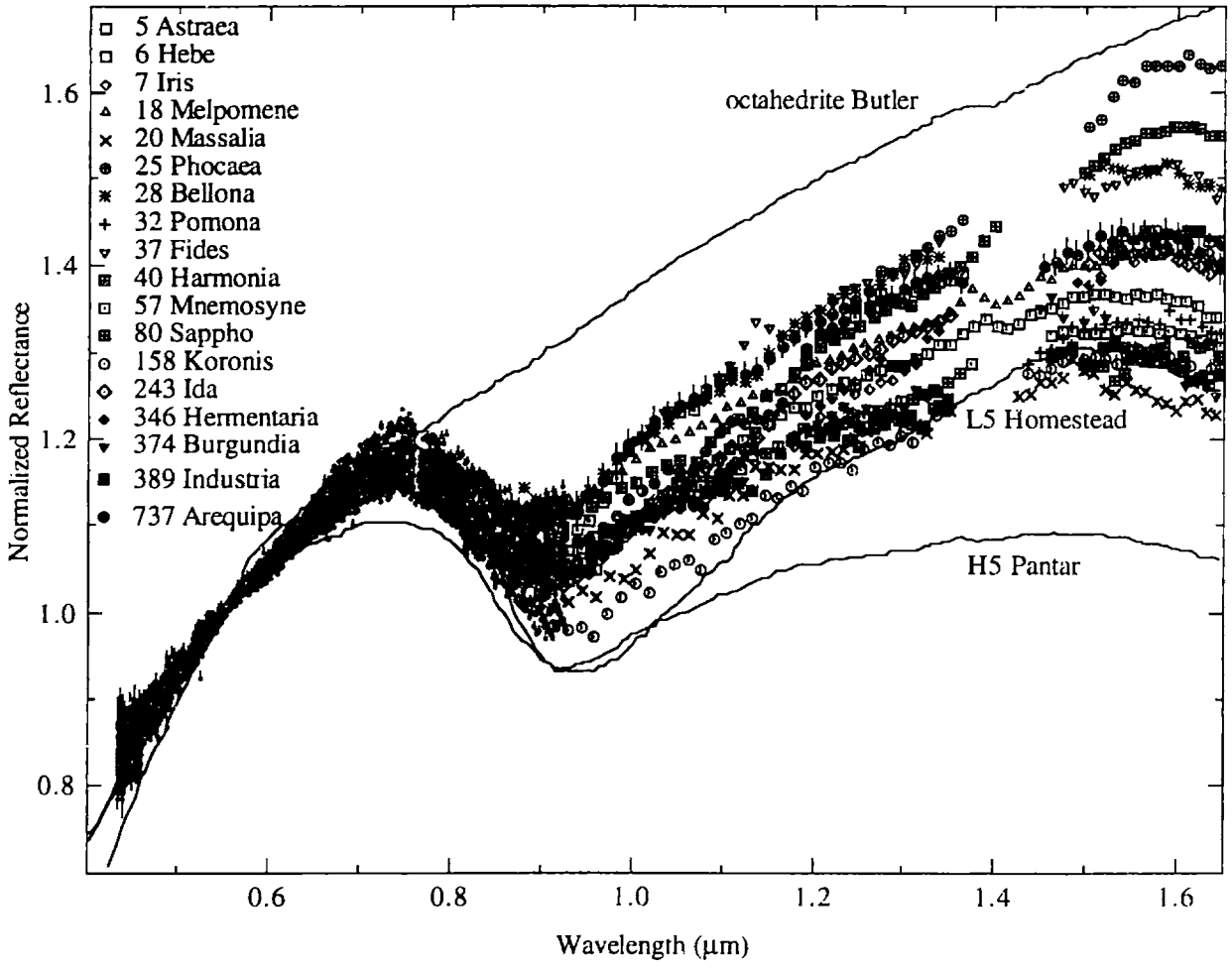

Figure 5.7.16. Reflectance spectra of large pyroxene-rich S asteroids versus spectra of H5 Pantar, L5 chondrite Homestead and octahedrite Butler. Small dots are from SMASS II (Bus, 1999) and larger symbols are from SMASSIR. All spectra are normalized to unity at 0.55 μm. Error bars are $\pm 1\sigma$.

Figure 5.7.17 plots pyroxene-rich NEAs (and the one Mars-crosser) versus H6 chondrite Lancon. These objects all have spectral slopes that range from similar to the spectrum of L5 chondrite Homestead to slightly redder.

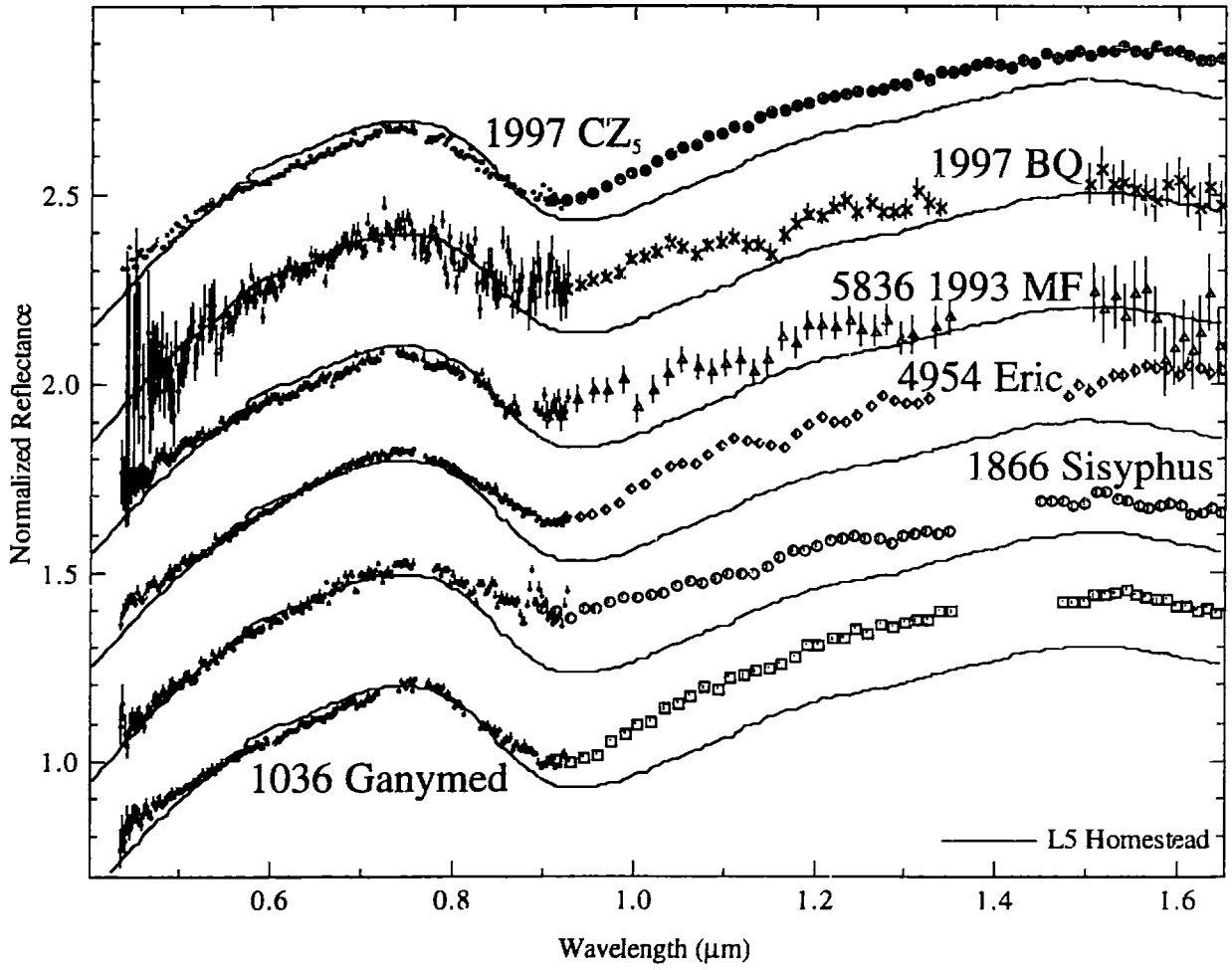

Figure 5.7.17. Reflectance spectra of pyroxene-rich S-asteroid NEAs versus a spectrum of L5 Homestead. Small dots are from SMASS II (Bus, 1999) and larger symbols are from SMASSIR. The meteorite spectrum is from Gaffey (1976). All spectra are normalized to unity at 0.55 μm. All asteroid spectra are offset by 0.3 in reflectance from each other. Error bars are ±1σ.

5.7.8.2 Olivine-Rich S Asteroids

Figure 5.7.18 plots the olivine-rich main-belt S-asteroids (except for the very olivine-rich Amalthea and the smaller-sized Flora family members 1807 Slovakia and 825 Tanina, which will be discussed later) versus LL4 chondrite Soko Banja. The three plotted objects (15 Eunomia, 26 Proserpina and 39 Laetitia) are relatively large (diameters between 95 and 255 km). Each of these asteroids has a very broad 1 μm band plus a broad feature at ~1.3 μm. Their 1 μm features tend to be flatter and broader than Soko Banja' band, which is indicating a higher olivine content for these objects than Soko Banja.

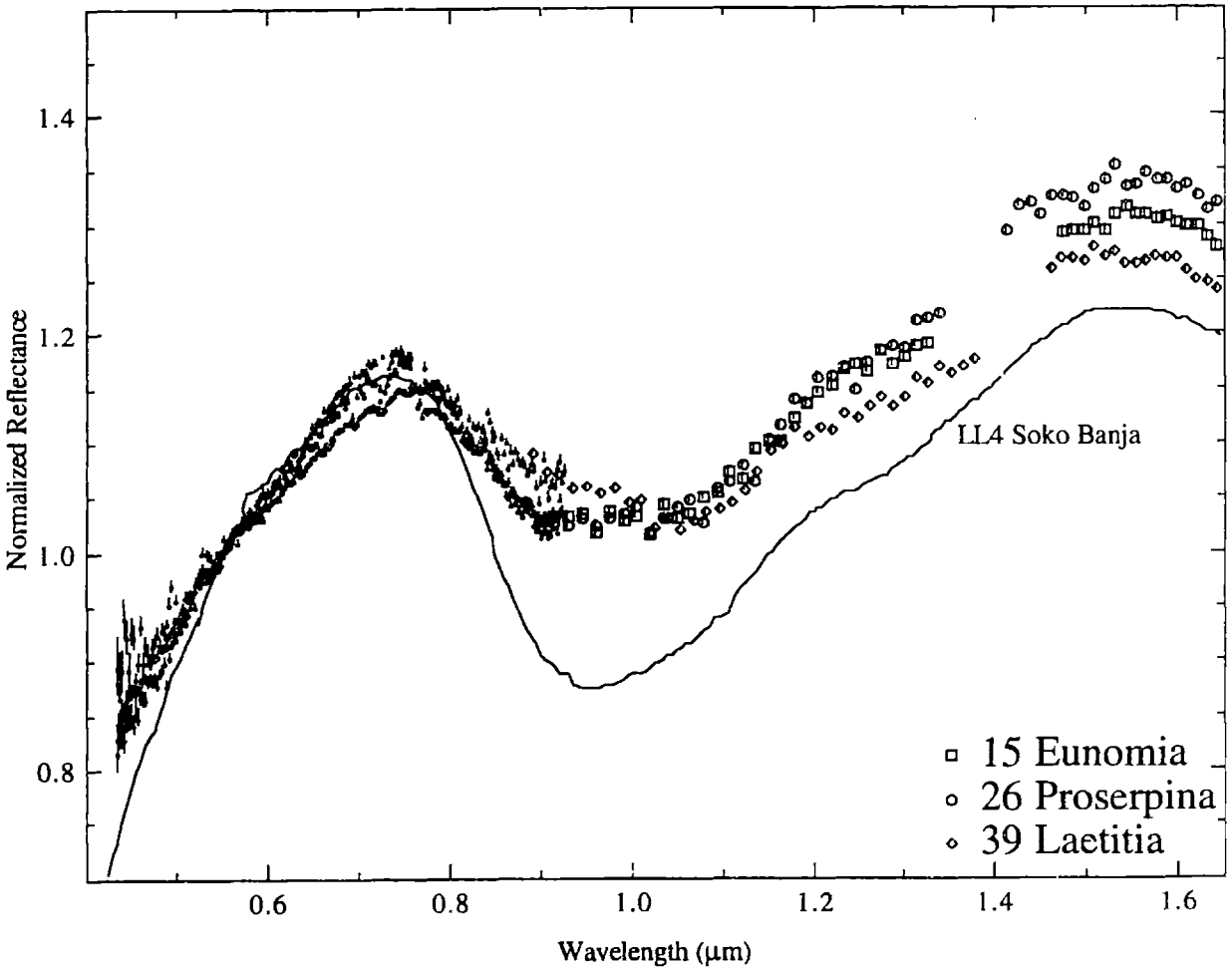

Figure 5.7.18. Reflectance spectra of large olivine-rich S asteroids versus a spectrum of LL4 chondrite Soko Banja. Small dots are from SMASS II (Bus, 1999) and larger symbols are from SMASSIR. The meteorite spectrum is from Gaffey (1976). All spectra are normalized to unity at 0.55 μm. Error bars are $\pm 1\sigma$.

Amalthea (Figure 5.7.19) appears to be very olivine-rich with a band minimum at ~1.06 μm and is plotted versus Brachina. Amalthea has more distinctive olivine bands than the other olivine-rich S asteroids. Amalthea is not as red as the deep-featured A types and could have a olivine surface composition that is not as altered as those objects or a metallic iron component (~25 wt.%), which should also redden the spectrum but keep the distinctive olivine bands.

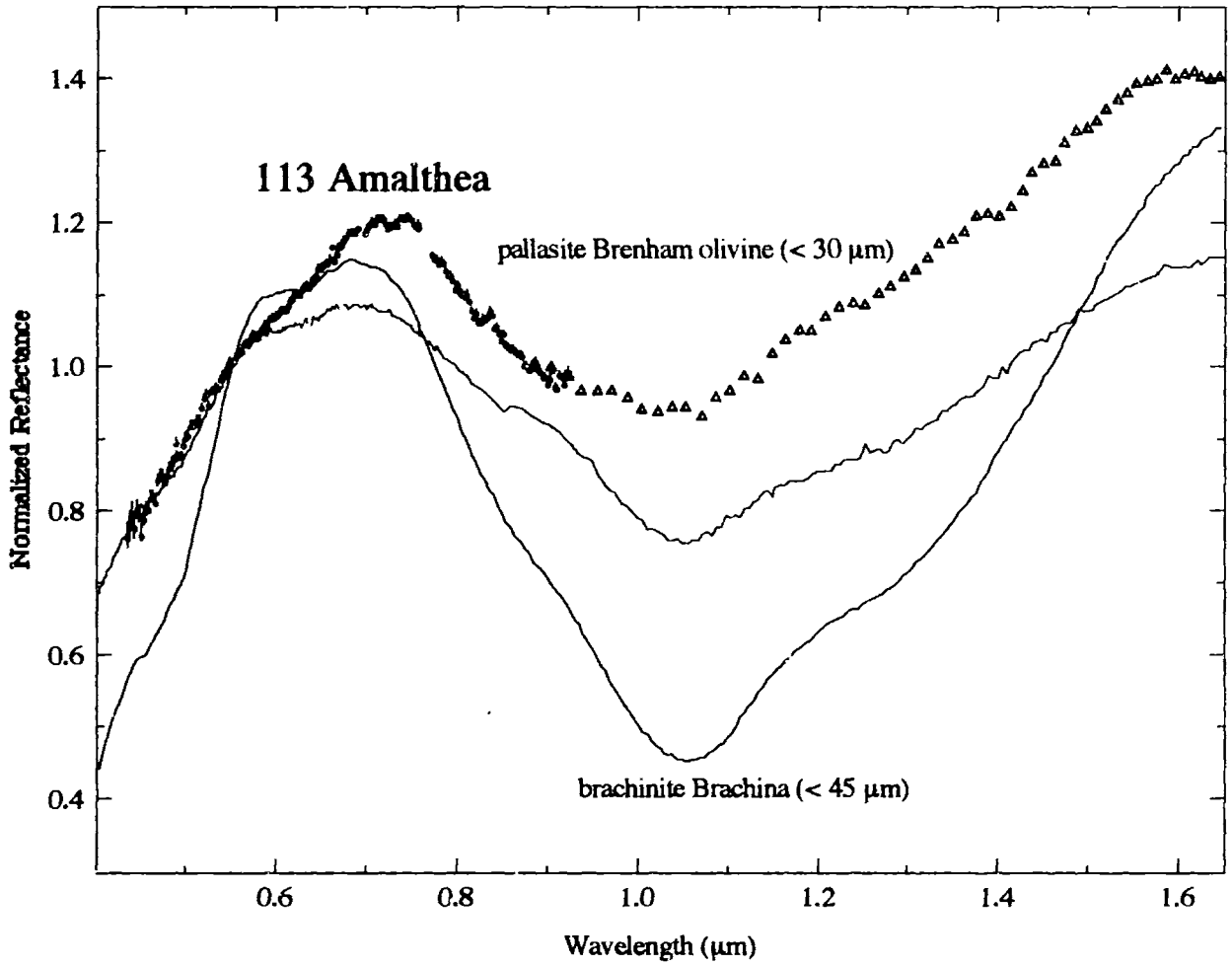

Figure 5.7.19. Reflectance spectrum of S asteroid 113 Amalthea versus spectra of brachinite Brachina (particle size less than 45 μm) (black line) and pallasite Brenham olivine (pallasite less than 30 μm) (red line). Small dots are from SMASS II (Bus, 1999) and larger symbols are from SMASSIR. The Soko Banja spectrum is from Gaffey (1976). The Brachina spectrum is a RELAB spectrum from Sunshine and Hiroi (personal communication) from a sample supplied by the South Australian Museum. The Brenham olivine spectrum is from King and Ridley (1987). All spectra are normalized to unity at 0.55 μm. Error bars are $\pm 1\sigma$.

Figure 5.7.20 plots the band depth versus reflectance at 1.65 μm for A asteroids, 42 Isis, S asteroids with very distinctive olivine bands (113 Amalthea, 354 Eleonora and 3819 Robinson) and olivine and olivine/metal mixtures. These three S asteroids tend to have much weaker features than Brachina and depths closer in strength to the pallasite olivine samples. The positions of these objects on the plot appear consistent with both a "reddened" pallasite olivine that would not have its band depth significantly changed or an "altered" brachinite sample where the band depth has been significantly weakened.

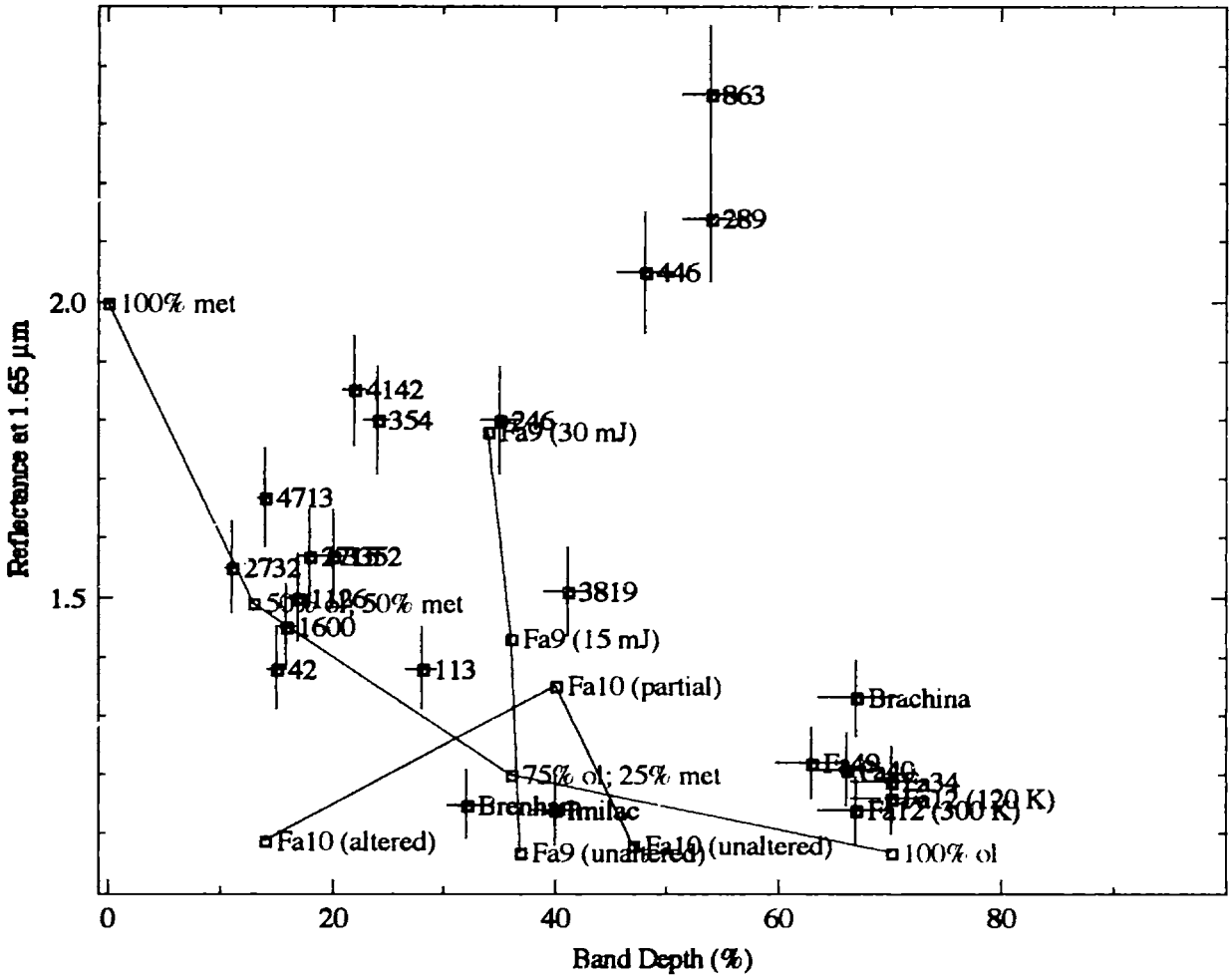

Figure 5.7.20. Band depths (%) versus reflectance at 1.65 μm for A asteroids, 42 Isis, 113 Amalthea, 354 Elonora, 3819 Robinson and olivine and olivine/metal mixtures from Table 5.1.2. Blue symbols and lines are data from Yamada *et al.* (1999), red symbols and lines are from the olivine/metal mixtures of Cloutis *et al.* (1990a) and green symbols and lines are data from Moroz *et al.* (1996). Error bars for the asteroids for the band depths and reflectances are estimated to be ±5%.

Flora family members Slovakia and Tanina are plotted versus LL4 Soko Banja in Figure 5.17.21. These two objects are approximately 10 km in diameter. Their spectra are relatively noisy, but have similar spectral properties with the larger olivine-rich main-belt S-asteroids. These objects have slightly broader 1 μm features than the LL4 chondrites and are slightly redder.

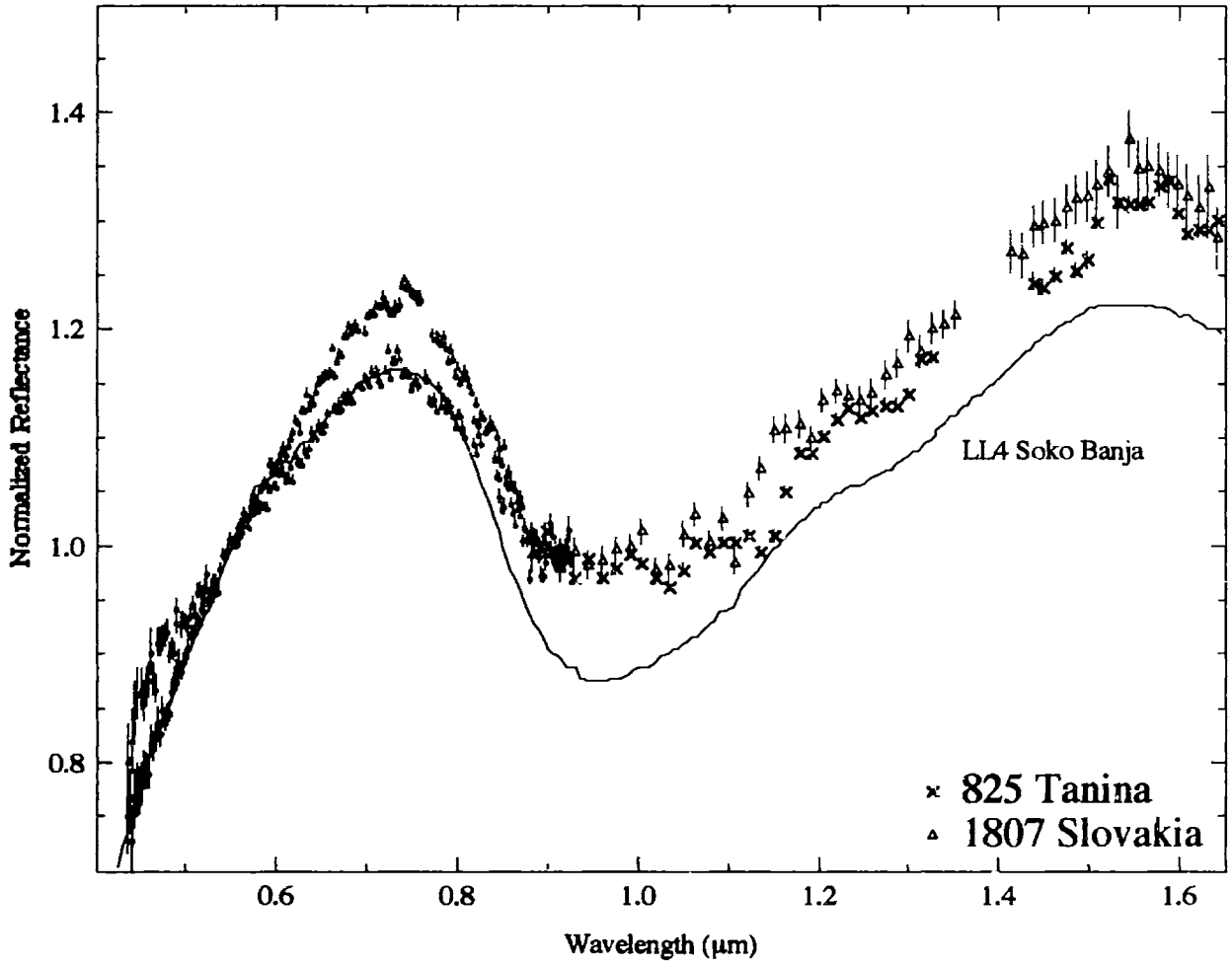

Figure 5.7.21. Reflectance spectra of small main-belt olivine-rich S asteroids versus a spectrum of LL4 chondrite Soko Banja. Small dots are from SMASS II (Bus, 1999) and larger symbols are from SMASSIR. The meteorite spectrum is from Gaffey (1976). All spectra are normalized to unity at 0.55 μm. Error bars are ±1σ.

Figure 5.7.22 plots the olivine-rich S-asteroid NEAs versus LL4 chondrite Soko Banja. These objects have similar band structures with this LL4 chondrite with minimums near ~0.95 μm; however, they all have redder spectral slopes than Soko Banja. All of these objects have diameters of 7 km or less. These NEAs appear spectrally more similar to LL4 chondrites than the olivine-rich main-belt S asteroids.

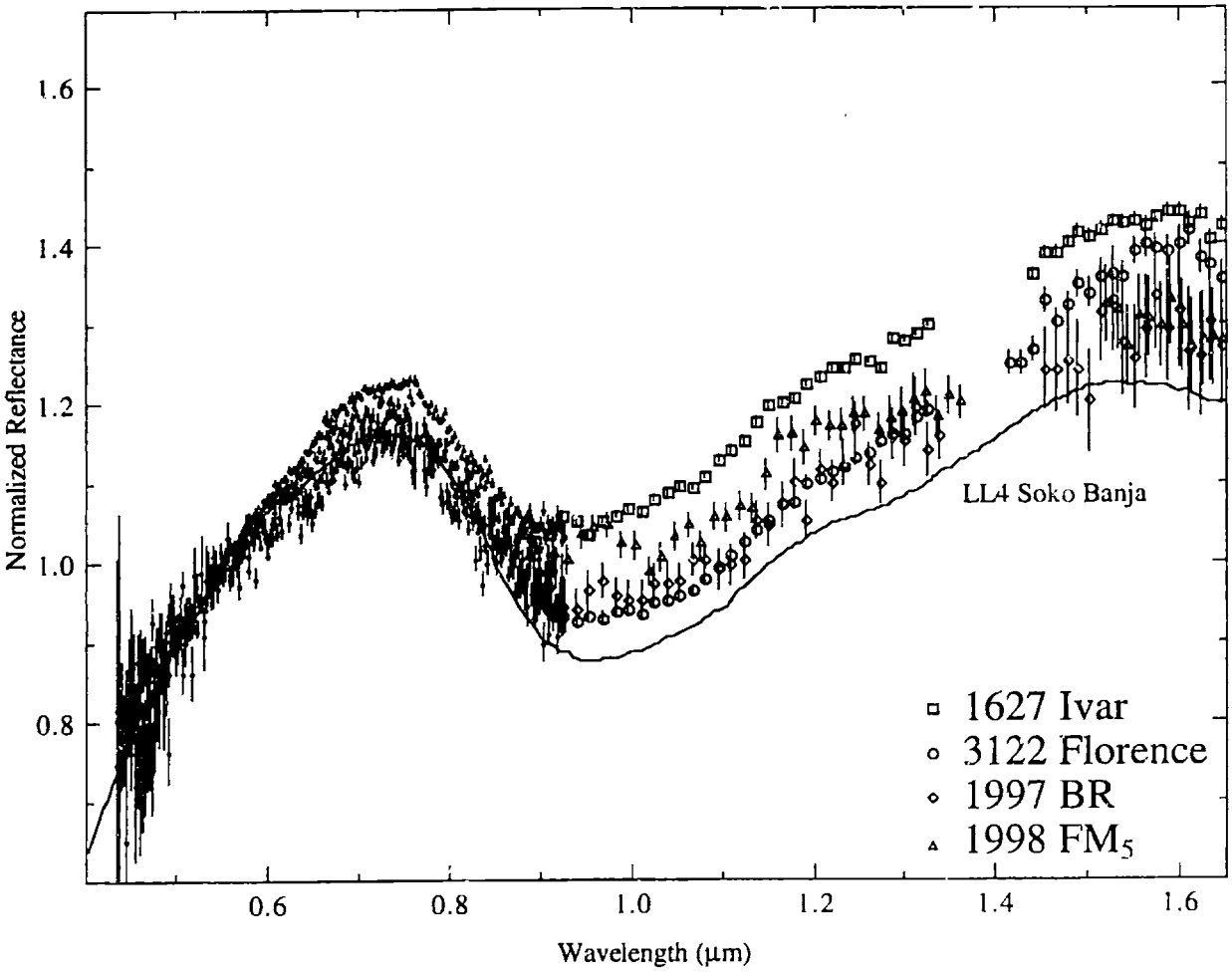

Figure 5.7.22. Reflectance spectra of olivine-rich S-asteroid NEAs versus a spectrum of LL4 chondrite Soko Banja. Small dots are from SMASS II (Bus, 1999) and larger symbols are from SMASSIR. The meteorite spectrum is from Gaffey (1976). All spectra are normalized to unity at 0.55 μm. Error bars are ±1σ.

5.7.9 Forging Spectroscopic Links to Ordinary Chondrites

As can be seen by the preceding discussion of the Bus (1999) S subclasses, the S-types appear to contain a large variety of different compositions. Objects with spectra similar to all three ordinary chondrites classes (H, L and LL) are present in the main belt and NEA S-asteroid population. However, it appears very difficult to make compelling arguments linking any particular asteroid and any ordinary chondrite since there are a large number of possible objects in the main belt and among the NEAs that could be supplying these meteorites.

Many asteroids have much redder spectra than ordinary chondrites, even though the structure of their absorption bands appear similar (e.g., Figure 5.7.15; Figure 5.7.21). These redder objects include 6 Hebe (Figures 5.7.1 and 5.7.16), which has been proposed to be the parent body of the H chondrites. As stated earlier, Gaffey (1996) and Gaffey and Gilbert (1998) propose that Hebe's redness is due to melt sheets of metallic iron on the surface.

To try to understand what might be causing the spectral differences between the ordinary chondrites and the S asteroids, the band depths versus the peak reflectances (Figure 5.7.22a) and albedos (Figure 5.7.23b) for the S asteroids, including all Bus (1999) subtypes, that have been identified as pyroxene-rich (excluding 3376 Armandhammer) plus the H and L chondrites, a ureilite and the relatively featureless iron meteorites. However, this analysis can not rule out that S asteroids have thermal histories quite different than ordinary chondrites, such as some type of differentiated or partially differentiated assemblage

As can be easily seen in the top plot, these S asteroids tend to have weaker band depths and redder spectral slopes (shown as the peak reflectance) than the ordinary chondrites. If you add metallic iron to an ordinary chondrite and measure the spectrum, the band depth and peak reflectance will fall on a straight line connecting the meteorite and iron meteorite. The position on the line will be dependent on how much metallic iron is added with the band depth decreasing and reflectance increasing with increasing amounts of iron.

All of these S asteroids appear consistent with just adding metallic iron to an ordinary chondrite surface, which would suppress the bands and redden the spectrum. The amount of metal needed would depend on which ordinary chondrite is used. Also plotted are the parameters for the altered L5 chondrite from the laser irradiation experiments of Moroz *et al.* (1996), which falls within the S asteroid field.

Figure 5.7.23b plots band depth versus albedo. There is a huge range in albedos for the S asteroids, ordinary chondrites, the ureilite and iron meteorites. As with the upper plot, if you add metallic iron to an ordinary chondrite and measure the spectrum, the band depth and peak reflectance will fall on a straight line connecting the meteorite and iron meteorite. The position on the line will be dependent on how much metallic iron is added with the band depth decreasing with increasing amounts of iron. The albedo may or may not decrease, depending whether the iron meteorite is brighter or darker. The albedos of the S asteroids appear consistent with mixtures of metallic iron and ordinary chondrite material. The altered L5 chondrite appears to be too dark to be a good analog for almost all of these S asteroids; however, this is under the assumption that the Moroz *et al.* (1996) experiments is accurately duplicating asteroidal alteration processes. The altered material tends to have significant amounts of finely dispersed opaques that lower the albedo, which is believed to be due to enrichment of iron oxide in the glass. The ureilite is also too dark to be a good analog for these S asteroids with known albedos.

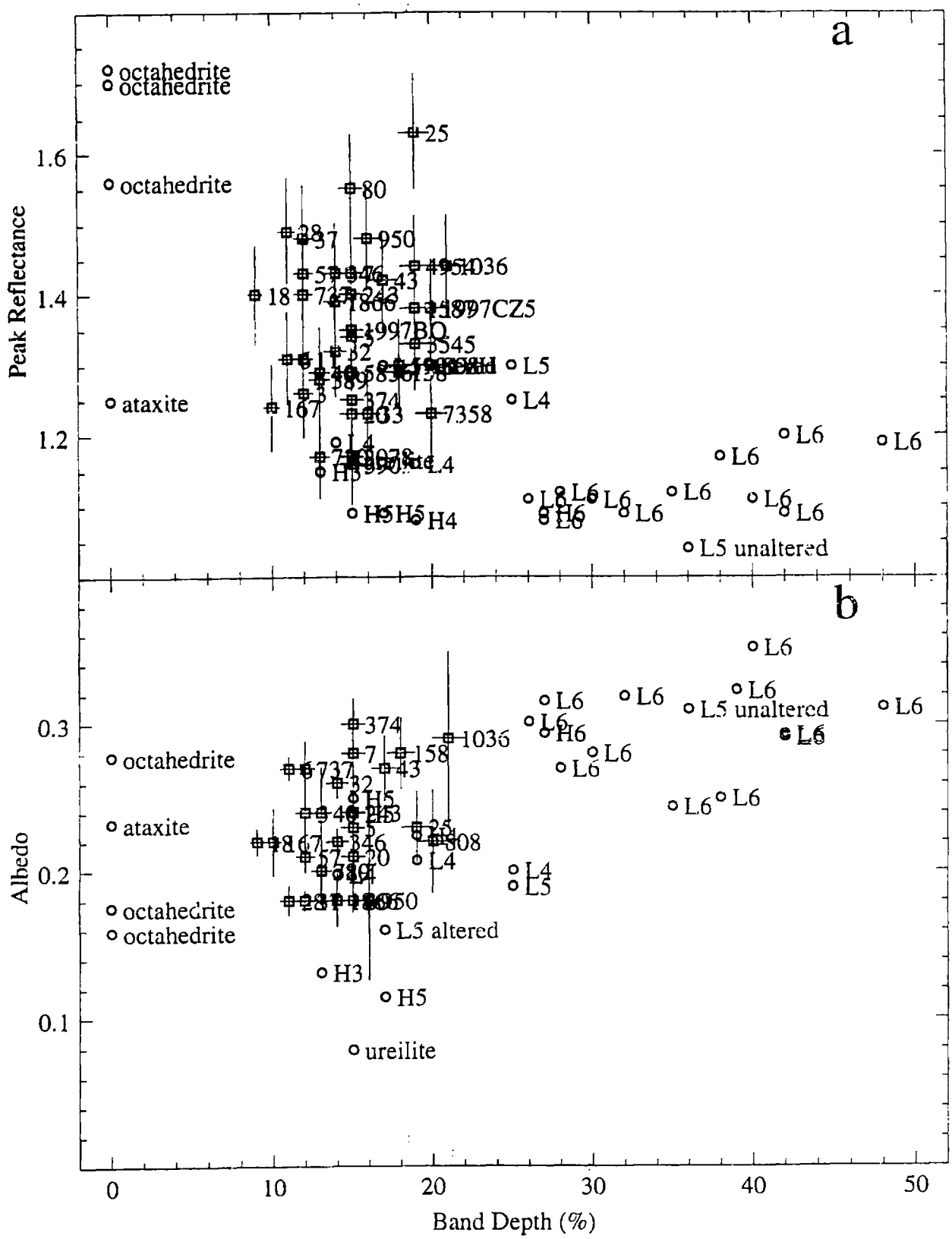

Figure 5.7.23. Plot of band depths versus (a) peak reflectance and (b) albedo for the pyroxene-rich S asteroids, H and L chondrites, a ureilite and iron meteorites. Asteroids are plotted with squares and meteorites are plotted with circles. Error bars are $\pm 1\sigma$.

The diameters of these asteroids are plotted versus the peak reflectances (Figure 5.7.24a) and band depths (Figure 5.7.24b) for these S asteroids. There appears to be no correlation between diameter and peak reflectance, but the band depth appears to be definitely increasing with decreasing diameter. These trends are consistent with either the smaller objects being less iron-rich or less altered than the larger ones.

If these asteroids have silicate compositions similar to ordinary chondrites and the reddening is due to metallic iron, two scenarios appear possible for the reddening. Either metal is being added or silicates are being subtracted from the surface. Gaffey (1996) and Gaffey and Gilbert (1998) argue that melts sheets or iron formed through impacts on the surface would increase the amounts of spectrally red metallic iron the surface. Since H chondrites contain higher amounts of metallic iron (~18 wt.%) than other ordinary chondrites, they believe that it will be easier to form melt sheets on H chondrite surfaces.

Another possibility is that impacts by micrometeorites could erode silicates from the surface, which would increase the relative amounts of metallic iron. Larger objects would tend to have longer surface ages than smaller objects and thus would be expected to have less silicates on their surfaces.

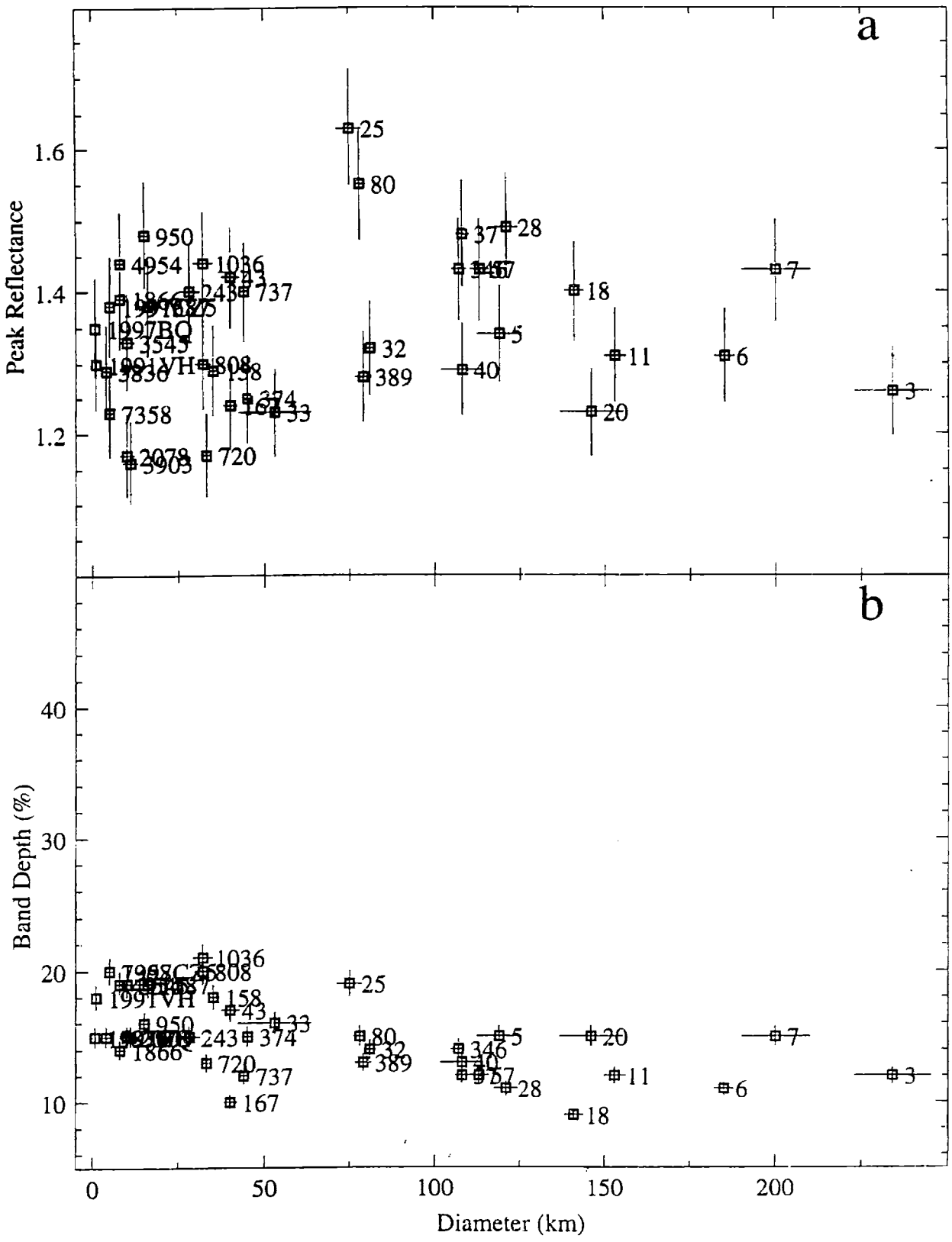

Figure 5.7.24. Plot of diameters versus (a) peak reflectance and (b) band depths for the pyroxene-rich S asteroids. Error bars are $\pm 1\sigma$.

5.7.10 Conclusions

As seen by many other researchers, the S asteroids have a diverse suite of compositions (Table 5.1.7). Almost all of the Bus (1999) subclasses appear to contain silicate compositions ranging from olivine-rich to pyroxene-rich. Near-infrared spectra are vital for determining mineralogies for the S asteroids so extreme caution needs to be used for any mineralogic interpretations based solely on visible data.

A number of S asteroids, such as the Sk objects 3 Juno, 11 Parthenope, 167 Urda and 1991 VH, have spectra very similar to ordinary chondrites. However, a considerable number of S objects, such as the pyroxene-rich S asteroids 6 Hebe and 18 Melpomene, have spectra that look like ordinary chondrite spectra that have been significantly reddened and have had their absorption bands suppressed. Adding spectrally red metal, in contrast with the spectrally neutral metal found in ordinary chondrites, appears to be the easiest way to redden a spectrum and suppress the bands. The advantage of using metal to redden an ordinary chondrite spectrum is that the metal would not decrease the albedo significantly since S asteroids (albedos usually between ~0.18 and ~0.30) tend to have comparable to slightly lower albedos than ordinary chondrites (usually between 0.25 and 0.35). Other proposed models for altering the surface such as the laser alteration experiments of Moroz *et al.* (1996) lower the albedo significantly (from 0.31 to 0.16 for the altered L5). However without knowing the actual surface compositions of these objects, it is impossible to rule out any proposed process. These objects could also have distinctly different thermal histories than ordinary chondrites.

Small asteroids tend to have stronger band depths that are more similar to ordinary chondrites. Smaller objects would be expected to be less altered than larger ones since they would be expected to have shorter surface ages. This is consistent with the results of (Binzel *et al.*, 1998), who see a similar trend based just on visible data.

Table 5.1.7. Mineralogic interpretation of S asteroids observed in SMASSIR. For NEAs, their orbital type is given instead of their semi-major axis (a). Quotation marks are used for meteoritic analogs that appear less certain.

Type	Asteroid	a (AU)	Meteoritic Analog	Mineralogic Interpretation
red-sloped Sa	63 Ausonia	2.395	none readily apparent	silicate-dominated (primarily olivine) surface assemblages as indicated by strong UV features and broad 1 μm bands; the 1 μm features appear suppressed and reddened relative to laboratory-measured samples, possibly indicating a metallic iron component and/or some type of alteration process
	625 Xenia	2.647	none readily apparent	
	913 Otila	2.198	none readily apparent	
	2038 Bistro	2.435	none readily apparent	
less red-sloped olivine-rich Sa	950 Ahrensa	2.371	"reddened" H chondrite	strong UV features and distinctive 1 μm bands due to pyroxene; redder by ~30% than H chondrites
	1587 Kaarstedt	2.545	"reddened" H chondrite	
	3545 Gaffey	2.870	"reddened" H chondrite	
less red-sloped pyroxene-rich Sa	1350 Rosselia	2.858	"reddened" LL chondrite	strong UV features and broad 1 μm bands that appear dominated by olivine; redder by ~10 to ~20% than LL chondrites
	2396 Kochi	2.794	"reddened" LL chondrite	
	3474 Linsley	2.558	"reddened" LL chondrite	
	3767 DiMaggio	2.603	"reddened" LL chondrite	
	4512 Sinhue	2.767	"reddened" LL chondrite	
Sk	3 Juno	2.669	L chondrite	visible spectra similar to L chondrites; strengths and structure of 1 μm bands also similar to L chondrites; spectral slopes range from similar to L4 chondrite Saratov to ~20% redder
	11 Parthenope	2.452	L chondrite	
	43 Ariadne	2.203	"reddened" L chondrite	
	167 Urda	2.854	L chondrite	
	1991 VH	Apollo	L chondrite	
Sl with a suppressed 1 μm feature	169 Zelia	2.358	"reddened" LL chondrite	relatively strong UV features and broad 1 μm bands that appear dominated by olivine; spectra tend to be much redder (~30 to ~40%) redder than LL chondrites
	352 Gisela	2.194	"reddened" LL chondrite	
	416 Vaticana	2.788	"reddened" LL chondrite	
	584 Semiramis	2.374	"reddened" LL chondrite	
	1980 Tezcatlipoca	Amor	"reddened" LL chondrite	
pyroxene-rich Sq	33 Polyhymnia	2.867	"pyroxene-richer" H or L chondrite	visible spectra similar to H and L chondrites; have 1 μm bands that range from similar in structure to H and L chondrites to more pyroxene-rich; spectral slopes tend to be similar to H and L chondrites
	720 Bohlinia	2.887	L chondrite	
	808 Merxia	2.745	"pyroxene-richer" H or L chondrite	
	2078 Nanking	2.369	"pyroxene-richer" H or L chondrite	
	3903 Kliment Ohridski	2.930	H chondrite	
	7358 1995 YA_3	Amor	H or L chondrite	
eucritic Sq	3376 Armandhammer	2.349	eucrite	distinctive 1 μm feature due to pyroxene that is similar in strength and structure to eucrite spectra
olivine-rich Sq	1324 Knysna	2.185	"ureilite"	relatively weak UV features compared to other S asteroids; have relatively broad 1 μm features dominated by olivine; appear spectrally similar to ureilites; however, the one object (3199 Nefertiti) with a published albedo (0.26-0.41) is not consistent with a ureilite composition
	1483 Hakoila	2.717	"ureilite"	
	2873 Binzel	2.245	"ureilite"	
	3199 Nefertiti	Amor	none readily apparent	
	4051 Hatanaka	2.790	"ureilite"	
	1998 FX_2	Amor	"ureilite"	
	1998 PG	Amor	"ureilite"	
	1998 QR_{15}	Amor	"ureilite"	

Table 5.1.7. (continued).

Type	Asteroid	a (AU)	Meteoritic Analog	Mineralogic Interpretation
S type (Sl, Sr, S) with distinctive olivine bands	113 Amalthea	2.376	"reddened" pallasite or "altered" brachinite	strong UV features; have very distinctive olivine bands; spectral slopes range from similar (113 Amalthea) to much redder (354 Eleonora) than measured olivine samples
	354 Eleonora	2.798	"reddened" pallasite "altered" brachinite	
	3819 Robinson	2.772	"reddened" pallasite or "altered" brachinite	
Sr with a suppressed 1 μm feature	1864 Daedalus	Apollo	none readily apparent	visible spectra similar to LL chondrites; has a similar 1 μm band strength to LL chondrites but slightly noisy spectrum appears more olivine-rich
pyroxene-rich S	5 Astraea	2.576	"reddened" H or L chondrite	similar visible spectra to H and L chondrites; have 1 μm features that indicate surfaces dominated by pyroxene; spectral slopes vary from similar to ordinary chondrites to much redder
	6 Hebe	2.425	"reddened" H or L chondrite	
	7 Iris	2.386	"reddened" H or L chondrite	
	18 Melpomene	2.296	"reddened" H or L chondrite	
	20 Massalia	2.409	"reddened" H or L chondrite	
	25 Phocaea	2.400	"reddened" H or L chondrite	
	28 Bellona	2.777	"reddened" H or L chondrite	
	32 Pomona	2.587	"reddened" H or L chondrite	
	37 Fides	2.642	"reddened" H or L chondrite	
	40 Harmonia	2.267	"reddened" H or L chondrite	
	57 Mnemosyne	3.154	"reddened" H or L chondrite	
	80 Sappho	2.296	"reddened" H or L chondrite	
	158 Koronis	2.869	"reddened" H or L chondrite	
	243 Ida	2.862	"reddened" H or L chondrite	
	346 Hermentaria	2.796	"reddened" H or L chondrite	
	374 Burgundia	2.780	"reddened" H or L chondrite	
	389 Industria	2.608	"reddened" H or L chondrite	
	737 Arequipa	2.592	"reddened" H or L chondrite	
	1036 Ganymed	2.664	"reddened" H or L chondrite	
	1866 Sisyphus	Apollo	"reddened" H or L chondrite	
	4954 Eric	Amor	"reddened" H or L chondrite	
	5836 1993 MF	Amor	"reddened" H or L chondrite	
	1997 BQ	Apollo	"reddened" H or L chondrite	
	1997 CZ_5	Mars-crosser	"reddened" H or L chondrite	
olivine-rich S	15 Eunomia	2.644	none readily apparent	UV features similar to LL chondrites, but 1 μm features appear broader and flatter, indicating surface assemblages that are more olivine-rich
	26 Proserpina	2.656	none readily apparent	
	39 Laetitia	2.769	none readily apparent	
	113 Amalthea	2.376	none readily apparent	
	825 Tanina	2.226	none readily apparent	
	1807 Slovakia	2.226	none readily apparent	
LL chondrite-like S	1627 Ivar	Amor	"reddened" LL chondrite	similar visible spectra to LL chondrites; have 1 μm features with similar band structures to LL LL chondrites; spectra are slightly redder (~10 to ~20%) than LL chondrites
	3122 Florence	Amor	"reddened" LL chondrite	
	1997 BR	Apollo	"reddened" LL chondrite	
	1998 FM_5	Amor	"reddened" LL chondrite	

5.8 X (E, M and P) Asteroids

5.8.1 Background

X objects are a class of asteroids defined by Tholen (1984) that have flat to slightly reddish spectra from 0.3 to 1.1 μm that appear essentially featureless at ECAS wavelengths. The X class was divided into three subclasses (E, M and P) on the basis of visual albedo. Bus (1999) did not use visual albedo in his taxonomy and labeled all of these types of asteroids as X with four subclasses: X, Xc, Xe and Xk. Xc asteroids have spectra intermediate between X and C objects while Xk asteroids have spectra intermediate between X and K objects. The Xe asteroids have an absorption feature at ~0.5 μm.

E asteroids, due to their relatively featureless spectra and high albedos (greater than 0.3), have been interpreted as having surfaces composed predominately of an essentially iron-free silicate (e.g., Zellner *et al.*, 1977; Kelley, 1999). The most obvious meteoritic analog is the aubrites (enstatite achondrites), which are igneous meteorites composed of essentially iron-free enstatite plus accessory phases such as FeNi metal, troilite, forsteritic olivine, plagioclase feldspar and diopside (Watters and Prinz, 1979). However, the identification of an absorption feature in the 3 μm wavelength region of a number of main-belt E-asteroid spectra (Rivkin *et al.*, 1995) has been interpreted as indicating hydrated minerals on the surfaces of some of these objects, which is inconsistent with an igneous origin.

The only known near-Earth E-asteroid 3103 Eger has been postulated as the source body for at least some of the aubrites (Gaffey *et al.*, 1992). Eger has a relatively featureless spectrum in the visible and near-infrared and a high albedo (0.34-0.53) (Benner *et al.*, 1997), which is unique among known NEAs and consistent with the spectra of aubrites. Aubrites tend to have the longest cosmic ray exposure ages with of all known stony meteorites with a cluster of ages around 55 million years (Graf and Marti, 1992a) and one age as long as 110-120 million years. The ordinary chondrites having an average age of ~17 million years (Graf and Marti, 1992b). These relatively long ages compared to other stony meteorites appear consistent with aubrites residing near the surface of a body with a near-Earth orbit and not with their existence as small meteoroids, which would be expected to have shorter average lifetimes in space. The aphelion of Eger's orbit falls within the Hungaria region (~1.9 AU) where a high percentage of classified asteroids are E objects (e.g., Gradie and Tedesco, 1982; Gradie *et al.*, 1989)

P asteroids have very low albedos (less than 0.07). These objects tend to be found in the outer part of the belt (past ~3.2 AU). CCD spectra of these objects (Vilas and Gaffey, 1989) tend to find no absorption features due to iron in phyllosilicates, which they believe indicates that these objects were not heated to high enough temperatures for aqueous alteration to occur.

M asteroids have moderate visual albedos (~0.10 to ~0.22). Since metallic iron has the same reflectance characteristics in this wavelength region, the M asteroids have been historically identified as the disrupted cores of differentiated objects that have had their silicates removed from their surface. Approximately forty asteroids have been classified as M types by Tholen (1989).

Radar observations are the most sensitive available indicator of metal abundance on asteroids. The radar albedo of an asteroid is a function of both the porosity and metal abundance (effective dielectric constant of the surface) (Ostro *et al.*, 1985). Since the radar albedo is a function of these two properties of the asteroid, it is not possible to unambiguously determine the metal abundance without knowing the porosity of the surface. Radar observations of some M asteroids do appear to indicate metal-rich surfaces. Asteroid 16 Psyche has the highest radar albedo of all main-belt asteroids, which is consistent with both a metallic regolith having typical lunar values of porosity (~0.5) and an enstatite chondrite-type regolith (~30% metal) with a porosity slightly below the lunar range (~0.35 to ~0.55) (Ostro *et al.*, 1985). One M-type Amor asteroid (6178 1986 DA), classified by Tedesco and Gradie (1987), exhibits the highest radar albedo (0.58 ± 0.12) of any observed asteroid, strongly implying a metallic iron surface (Ostro *et al.*, 1991).

Jones *et al.* (1990), Rivkin *et al.* (1995) and Rivkin *et al.* (2000) have observed almost 30 M asteroids in the 3 μm region. Rivkin *et al.* (2000) has found that over 35% of them have 3 μm absorption features, which implies a non-metallic surface assemblage on these objects. Asteroid Psyche has no evident 3 μm feature, which is consistent with a metallic iron surface. They have also found that large (diameters greater than 65 km) M asteroids are likely to be hydrated (~75% of observed objects) while smaller M types (diameters less than 65 km) are very unlikely to be hydrated (~10%).

Lupishko and Belskaya (1989) noted that the ECAS spectra of five M-type asteroids (16 Psyche, 21 Lutetia, 22 Kalliope, 69 Hesperia and 110 Lydia) appeared to show weak absorption features in the 0.8 to 0.9 μm range. Binzel *et al.* (1995) found no significant changes in the visible rotational spectra of Psyche, implying no large scale variations in the content of mafic silicates (if present) on the surface and a largely homogeneous surface.

The prevailing question concerning X asteroids are "what are the composition of these relatively featureless objects?" Do X asteroids with high albedos have surfaces composed of iron-free enstatite and do the X types with moderate albedos have surfaces that are predominately metallic iron?

5.8.2 Investigation of X Asteroids

Fourteen X (X, Xc, Xe and Xk) types were observed in SMASSIR. Except for the three NEAs, each of these objects tend to have very large diameters (larger than 68 km). Each of the Bus (1999) X subgroups will be discussed in separate sections.

Table . X, Xc, Xe and Xk asteroids observed in SMASSIR. Proper elements (a, e', sin i') are from Milani and Knezevic (1994) except for high-inclination objects, which are from LeMaitre (personal communication). Diameters and albedos are from IRAS (Tedesco, 1994) except for diameters in parentheses, which are calculated using the H magnitude with an estimated albedo of 0.25. Family memberships are from Zappalà *et al.* (1995).

Asteroid	a (AU)	e'	sin i'	SMASS II	IRAS Albedo	Diameter (km)	HCM Family	NEA	3 μm band depth
16 Psyche	2.922	0.103	0.044	X	0.12	253			2 ± 4% (Jones *et al.*, 1990)
21 Lutetia	2.435	0.130	0.037	Xk	0.22	96			
22 Kalliope	2.910	0.089	0.218	X	0.14	181			
44 Nysa	2.423	0.174	0.053	Xc*	0.55	71	Nysa		14 ± 5.9% (Rivkin *et al.*, 1995)
64 Angelina	2.682	0.152	0.039	Xe	0.40&	51&			5.8 ± 4.6% (Rivkin *et al.*, 1995)
65 Cybele	3.433	0.104	0.062	Xc	0.07	237			0 ± 1% (Jones *et al.*, 1990)
71 Niobe	2.755	0.170	0.419	Xe	0.31	83			
92 Undina	3.196	0.071	0.151	Xc	0.25	126			45 ± 12% (Jones *et al.*, 1990) 10 ± 2.5% (Rivkin *et al.*, 1995)
140 Siwa	2.732	0.201	0.034	Xc	0.07	110			
304 Olga	2.404	0.122	0.257	Xc	0.05	68			
336 Lacaderia	2.252	0.089	0.107	Xk	0.05	69			
2100 Ra-Shalom	0.832	0.437	0.271	Xc	0.13@	2@		Aten	
3103 Eger	1.406	0.355	0.357	Xe	0.34-0.53#	1.5-1.9#		Apollo	
1992 BF	0.908	0.271	0.127	Xc		(0.3)		Aten	

* Classification has changed from Bus (1999).
& Albedo and diameter for 64 Angelina are from Morrison (1977).
@ Albedo and diameter for 2100 Ra-Shalom are from Harris *et al.* (1998).
# Albedo and diameter range for 3103 Eger are from Benner *et al.* (1997).

5.8.3 Subgroup: X Asteroids

Two X asteroids (16 Psyche and 22 Kalliope) were observed in SMASSIR (Figure 5.8.1). Both objects have relatively featureless spectra with Psyche slightly redder than Kalliope. Their flat spectra tend to fall intermediate between an octahedrite and an ataxite. An iron meteorite with a Ni content between Chulafinee (7%) and Babb's Mill (17%) (Buchwald, 1975) would have spectral slopes similar to these asteroids.

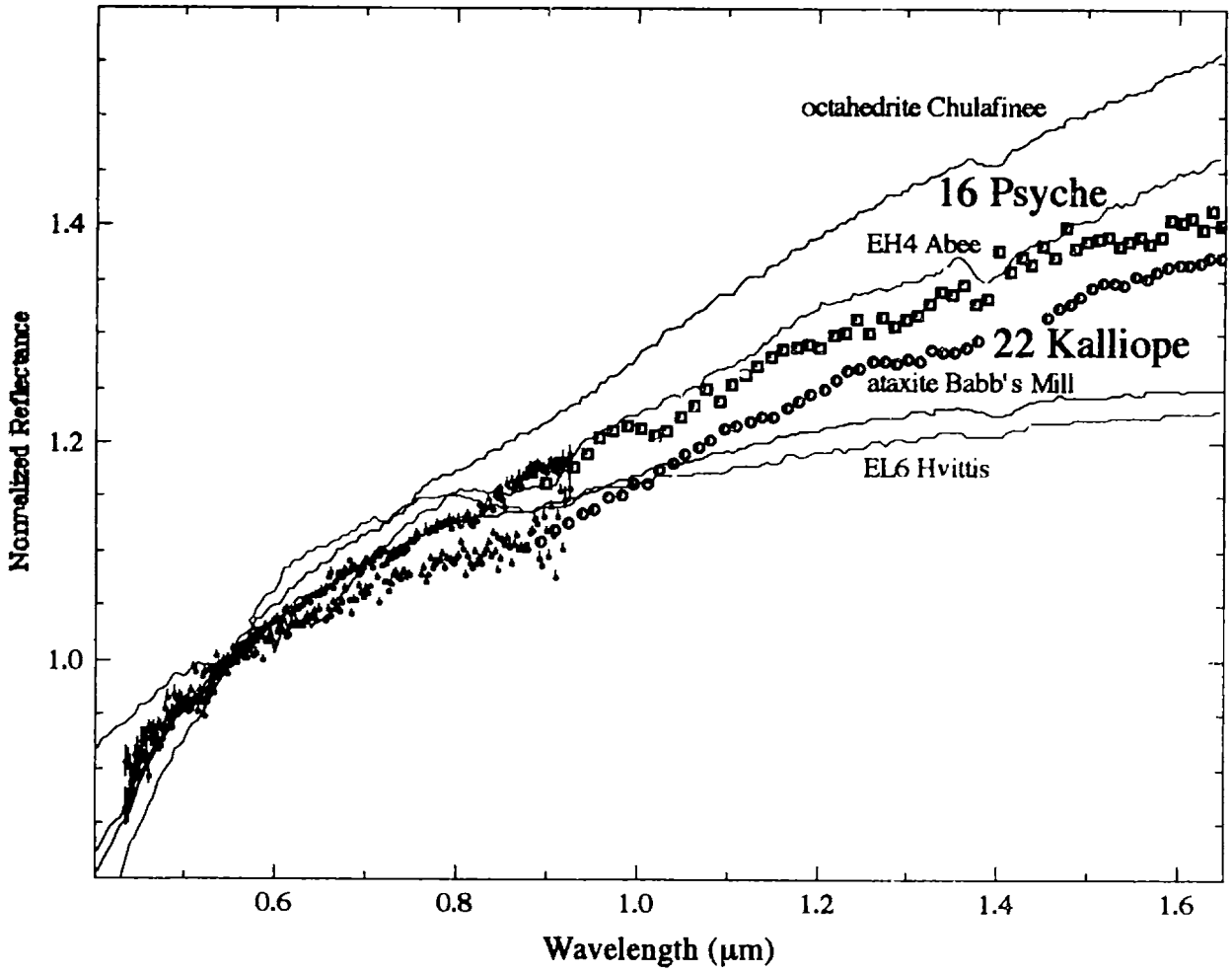

Figure 5.8.1. Reflectance spectra for X asteroids 16 Psyche and 22 Kalliope versus ataxite Babb's Mill (black line), EH4 chondrite Abee (blue line) and EL6 chondrite Hvittis (red line). Small points are from SMASS II (Bus, 1999) and larger symbols are from SMASSIR. All meteorite spectra are from Gaffey (1976). All spectra are normalized to unity at 0.55 μm. Error bars are $\pm 1\sigma$.

Also plotted are an EH4 and an EL6 chondrite. Abee (EH4) has a similar spectral slope to the asteroids; however, Abee has a slight (depth of ~2%) feature at ~0.9 μm, which is not apparent in the asteroid spectra, and a weaker UV feature. The ~0.9 μm band could be due to low-iron pyroxenes ($Fs_{1\text{-}10}$) that have been found in Abee (Mittlefehldt *et al.*, 1998) or some type of terrestrial alteration product. Abee's albedo (0.08) is slightly lower than that of Psyche (0.12

± 0.01) and Kalliope (0.14 ± 0.01). The albedos of the octahedrite (0.18) and ataxite (0.23) are slightly higher. A metallic iron surface appears to be the best "guess" for these two asteroid's compositions, but an enstatite chondrite surface can not be ruled out from the available data.

5.8.4 Subgroup: Xc Asteroids

Five main-belt Xc objects (44 Nysa, 65 Cybele, 92 Undina, 140 Siwa and 304 Olga) and two NEAs (2100 Ra-Shalom and 1992 BF) were observed in SMASSIR. Nysa and Undina have very similar spectra (Figure 5.8.2) with features at ~0.9 μm plus relatively high albedos (0.55 ± 0.07 for Nysa and 0.25 ± 0.01 for Undina). The ECAS and 52-color data for Nysa appear to confirm the presence of this feature; however, this feature is not present in the ECAS and 52-color data for Undina.

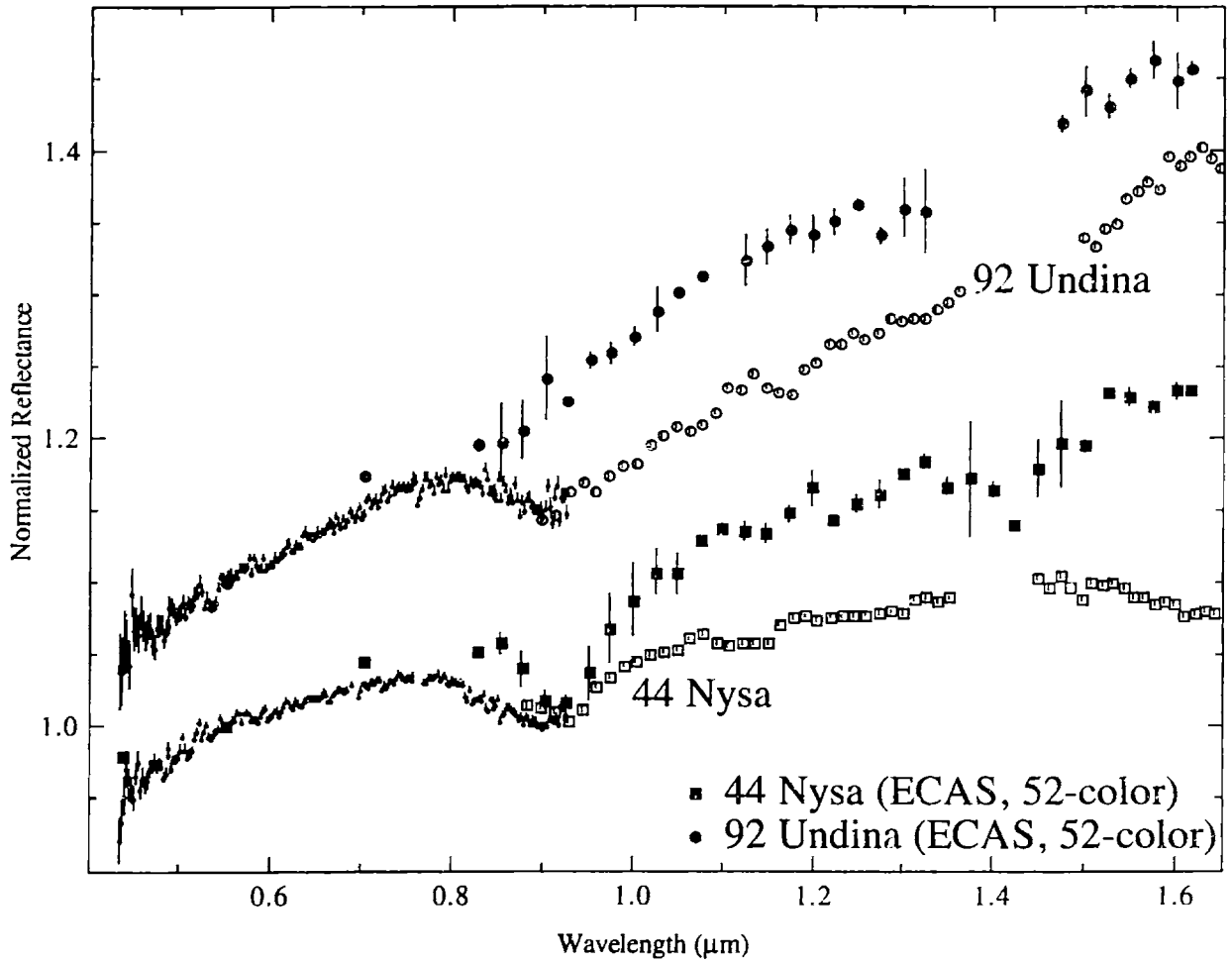

Figure 5.8.2. Reflectance spectra for Xc asteroids 44 Nysa and 92 Undina. Small points are from SMASS II (Bus, 1999) and larger symbols are from SMASSIR. Dark symbols are a combination of ECAS (Zellner *et al.*, 1985) and 52-color data (Bell *et al.*, 1988). All spectra are normalized to unity at 0.55 μm and the asteroid spectra are offset by 0.1 in reflectance from each other. Error bars are ±1σ.

It is unclear which spectrum (ECAS or SMASS) is "correct." Besides one of these observations being "wrong," another possibility is that Undina could also have substantial rotational variations. The SMASSIR spectrum for Undina has a similar spectral slope to the 52-color data and is consistent with the ECAS spectrum, which would appear to be consistent with the Bus (1999) X class.

From their SMASS and SMASSIR spectra, possible surface compositions for these objects include a low-iron pyroxene or some mixture of metallic iron and pyroxene. Both types of compositions would have suppressed 1 μm features. The high albedo of Nysa would argue for a metal-free composition for its surface, while Undina's lower albedo would argue for either composition. These objects have also been found to have 3 μm features, which is not consistent with either of these postulated surface compositions. Nysa has been found to have a feature with a strength of ~14% (Rivkin *et al.*, 1995), while Undina's feature has been measured at both ~45% (Jones *et al.*, 1990) and ~10% (Rivkin *et al.*, 1995). Carbonaceous meteorites such as CI, CM and CR chondrites have albedos too low (less than 0.07) to be plausible compositions for these objects. CO and CV chondrites contain lesser amounts of phyllosilicates, but also tend to have lower albedos (less than 0.16) than these two asteroids.

The three other main-belt Xc asteroids (Figure 5.8.3) tend to be relatively featureless in the near-infrared with very low albedos (0.05 to 0.07). Cybele and Siwa appear to be best matched by a shock-darkened L5 chondrite. The absence of any significant spectral features implies very opaque-rich surfaces so the spectral similarity to a shock-darkened ordinary chondrite probably only implies just a dark surface on these asteroids and may not imply a composition similar to ordinary chondrites.

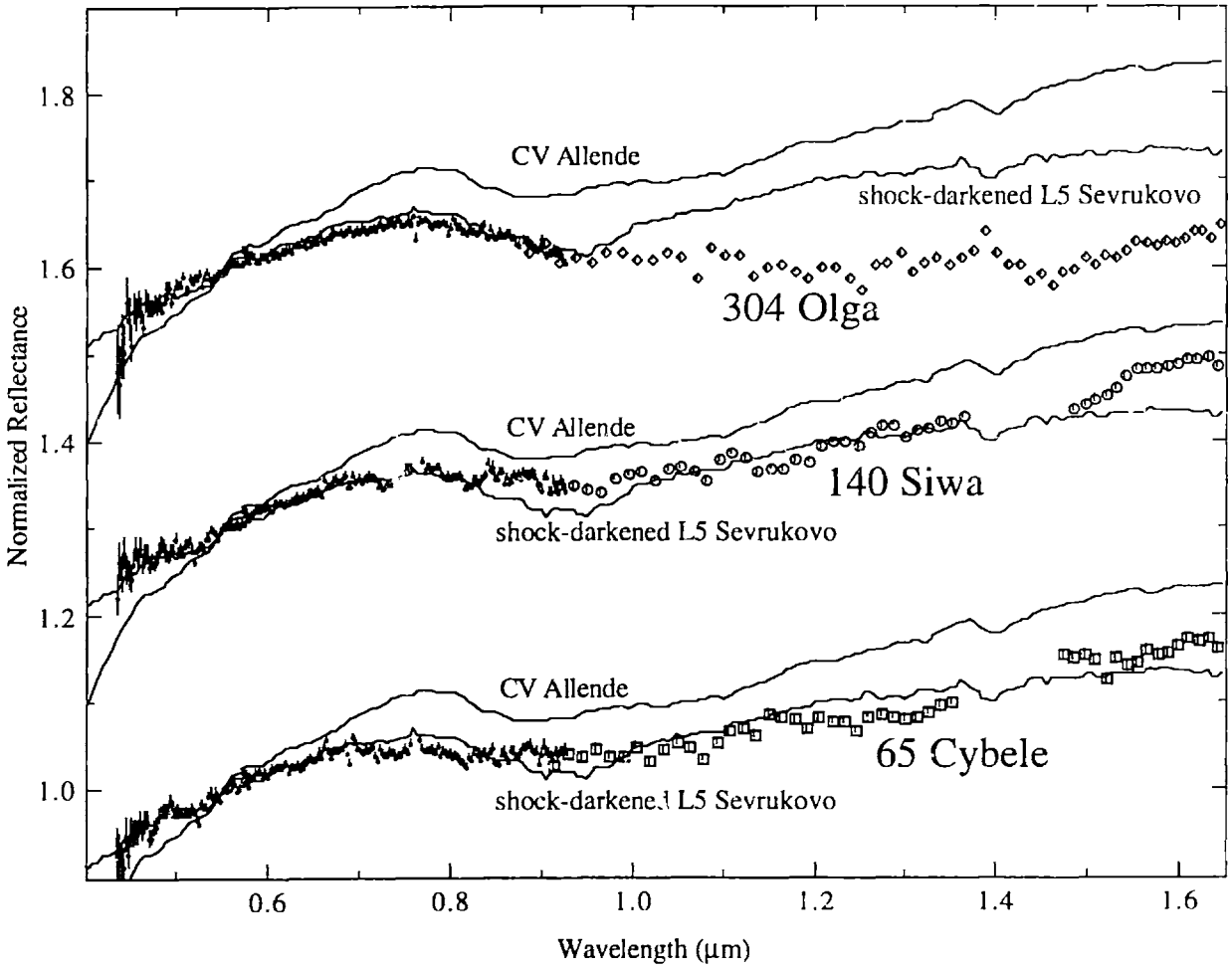

Figure 5.8.3. Reflectance spectra for Xc asteroids 65 Cybele, 140 Siwa and 304 Olga. Cybele, Siwa and Olga are plotted versus shock-darkened L5 chondrite Sevrukovo and CV chondrite Allende. Small points are from SMASS II (Bus, 1999) and larger symbols are from SMASSIR. All meteorite spectra are from Gaffey (1976). All spectra are normalized to unity at 0.55 μm and the asteroid spectra are offset by 0.3 in reflectance from each other. Error bars are ±1σ.

The spectra of the two NEAs are shown in Figure 5.8.4. Ra-Shalom has a relatively high residual absorption feature (~26%) at ~1.4 μm plus a very strong telluric feature at ~1.15 μm. The feature apparent at ~0.9 μm could also possibly be due to atmospheric water. The spectra slope of Ra-Shalom has a similar spectral slope to Olga; however, its albedo (0.13 ± 0.04) is higher than Olga's albedo (0.05 ± 0.01). The noisy spectrum (due to the faint magnitude of V17.5) of NEA 1992 BF appears more similar to an H chondrite than to the other Xc objects.

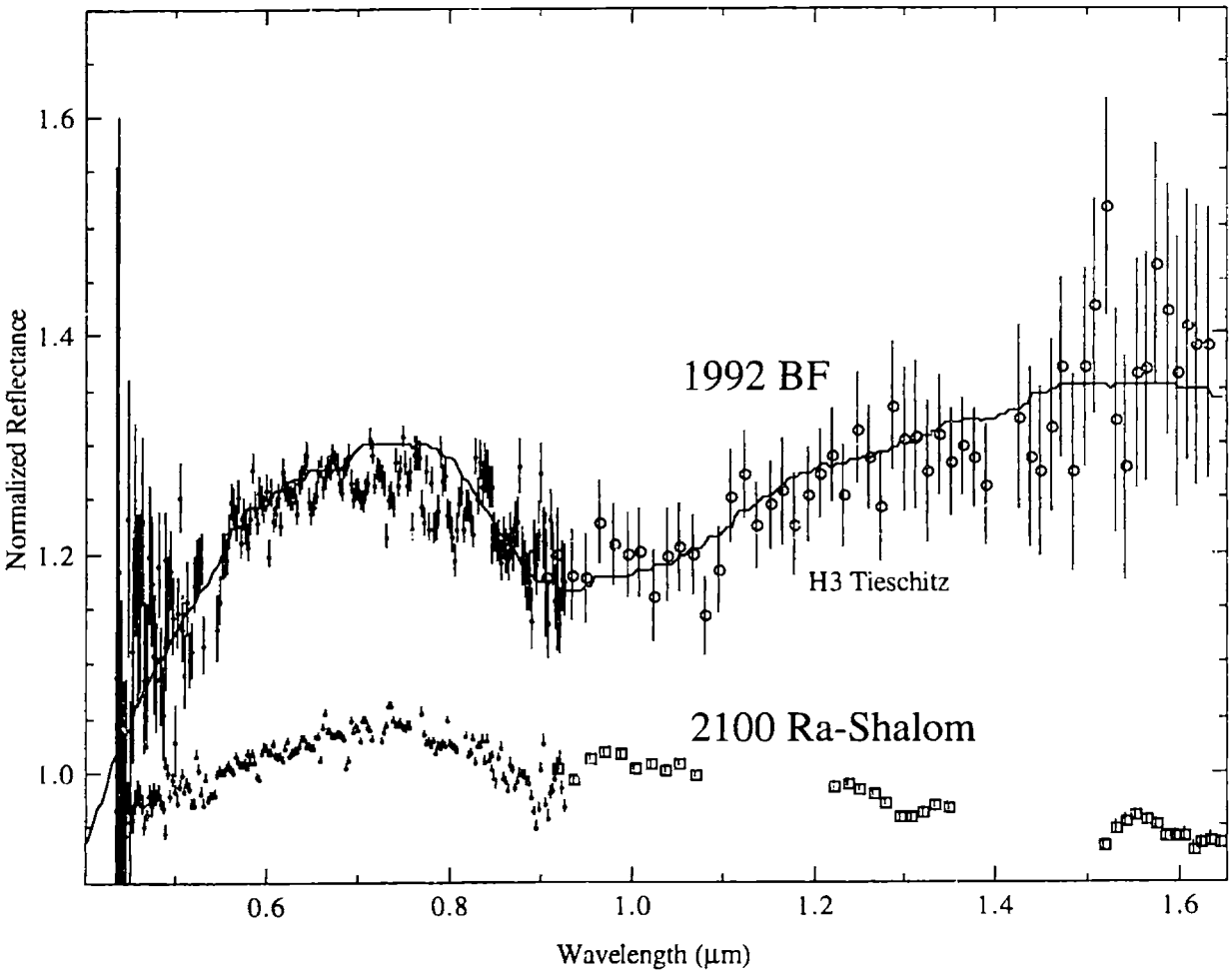

Figure 5.8.4. Reflectance spectra for Xc asteroids 2100 Ra-Shalom and 1992 BF. Asteroid 1992 BF is plotted versus H3 chondrite Tieschitz (Gaffey, 1976). Small points are from SMASS II (Bus, 1999) and larger symbols are from SMASSIR. All spectra are normalized to unity at 0.55 μm and the asteroid spectra are offset by 0.2 in reflectance from each other. Error bars are ±1σ.

5.8.5 Subgroup: Xe Asteroids

Two main-belt Xe asteroids (64 Angelina and 71 Niobe) and one NEA (3103 Eger) were observed in SMASSIR (Figure 5.8.5). The Angelina spectrum is about 10% redder than its 52-color spectrum, which is relatively noisy. Angelina and Eger both have a strong absorption feature that is centered at ~0.5 μm. This feature has also been seen in the CCD spectra of Eger by Hammergren (1998). Niobe has a much weaker feature than Angelina and Eger. These objects also have a relatively-flat red-sloped structure from ~0.55 to ~0.70 μm then have a flat to slight feature out to 1 μm. Angelina (0.40 ± 0.04), Niobe (0.31 ± 0.01) and Eger (0.34 to 0.53) all have relatively high albedos. Angelina also has a relatively weak (5.8 ± 4.6%) (Rivkin *et al.*, 1995) 3 μm feature, which is usually attributed to hydrated silicates.

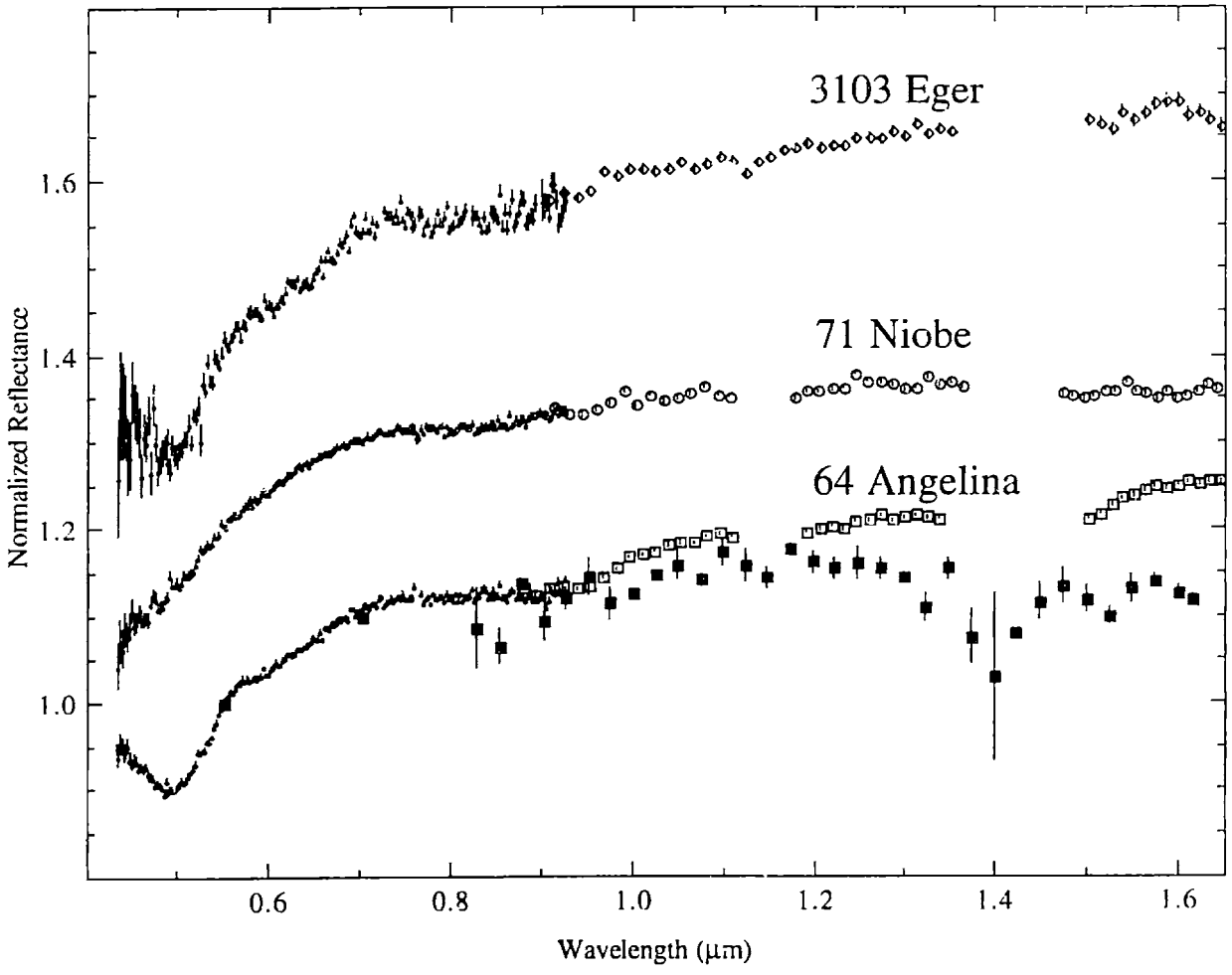

Figure 5.8.5. Reflectance spectra for Xe asteroids 64 Angelina, 71 Niobe and 3103 Eger. Small points are from SMASS II (Bus, 1999) and larger symbols are from SMASSIR. Dark squares are a combination of ECAS (Zellner *et al.*, 1985) and 52-color data (Bell *et al.*, 1988). All spectra are normalized to unity at 0.55 μm and offset by 0.2 in reflectance from each other. Error bars are ±1σ.

The high albedos of these objects are consistent with an iron-free silicate composition such as the Happy Canyon enstatite (albedo of 0.44), which is plotted in Figure 5.8.5. But the question is "what is causing the feature centered at ~0.5 μm?," which is not apparent in the enstatite spectrum. One possibility is some type of sulfide (Cloutis, personal communication). Sulfides such as pyrrhotite ($Fe_{1-x}S$) and synthetically produced troilite (FeS) have a deep feature with similar spectral characteristics to these E asteroids. This absorption feature is commonly found in sulfides and is due to a conduction band (Vaughn and Craig, 1978), such as those found in semiconductors. In these types of materials, there are two energy levels where electrons may reside (Clark, 1999). The higher level is called the conduction band where electrons move freely within the lattice and the lower level has electrons attached to individual atoms. The difference in energy between the levels is called the band gap and the resulting spectrum looks like a step function.

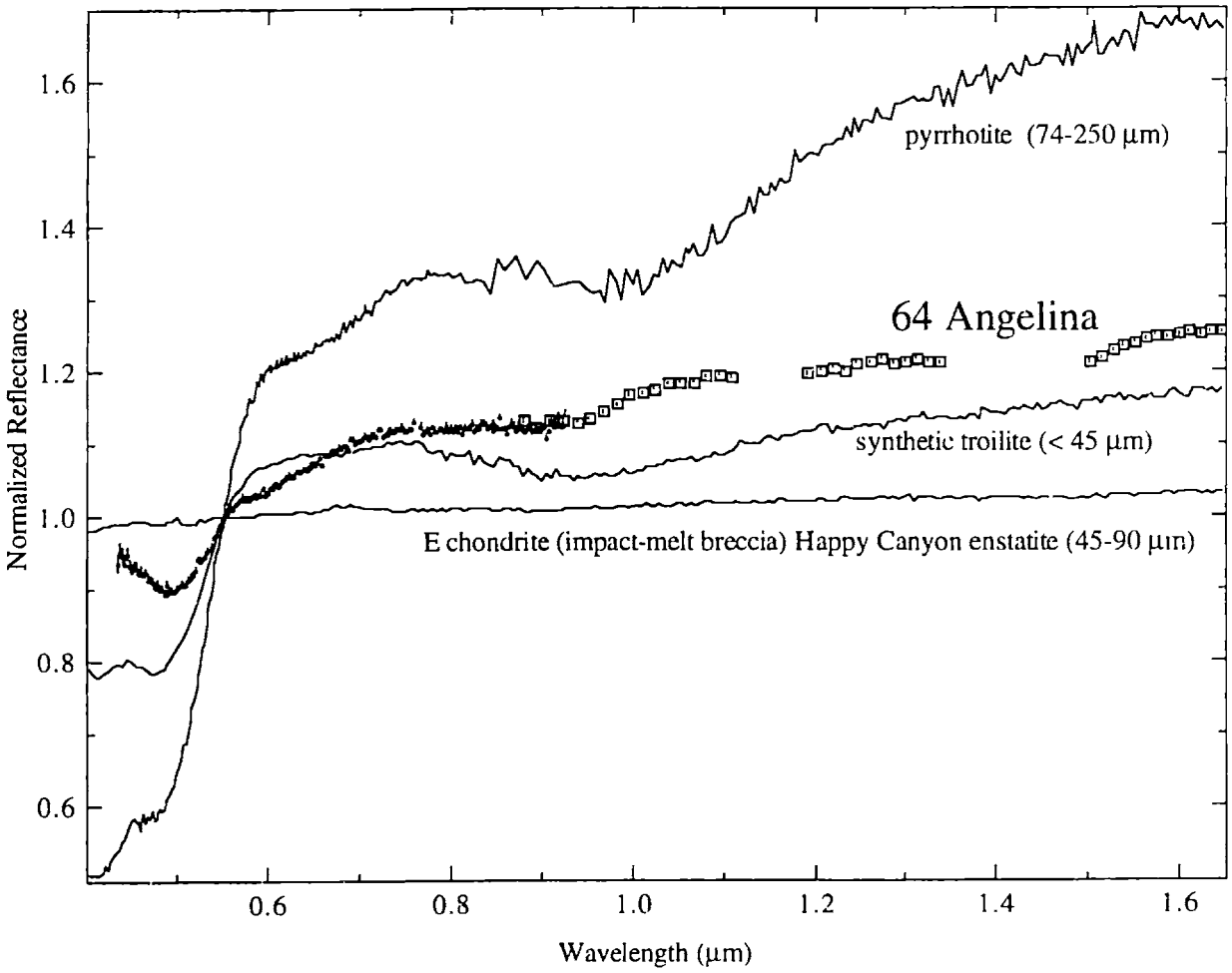

Figure 5.8.5. Reflectance spectrum for Xe asteroids 64 Angelina versus spectra of enstatite from E chondrite (impact-melt breccia) Happy Canyon (particle size between 45 and 90 μm), synthetic troilite (particle size less than 45 μm) and pyrrhotite (particle size between 74 and 250 μm). The spectra of Happy Canyon and the synthetic troilite are from Cloutis *et al.* (1993a). The spectrum of pyrrhotite is from Clark *et al.* (1993). Small points are from SMASS II (Bus, 1999) and larger symbols are from SMASSIR. All spectra are normalized to unity at 0.55 μm. Error bars are ±1σ.

Other minerals with similar absorption features include hematite (Fe_2O_3) (Clark, *et al.*, 1993) and melilite [$(Ca,Na)_2(Al,Mg)(Si,Al)_2O_7$] (Cloutis and Gaffey, 1993b) (Figure 5.8.6). These spectra are plotted as reflectance (not as normalized reflectance) due to hematite's very red spectrum. For the plot, Angelina's normalized spectrum is multiplied by 0.34 (its albedo). Hematite's absorption edge (beginning of its absorption feature) starts at a slightly longer wavelength (~0.60 μm) than Angelina's edge (~0.55 μm). Hematite is found only as a terrestrial alteration product in meteorites (Rubin, 1997). Melilite, found in high-albedo CAIs, has a similar feature centered at 0.5 μm; however, it has a very strong absorption band in the near-infrared.

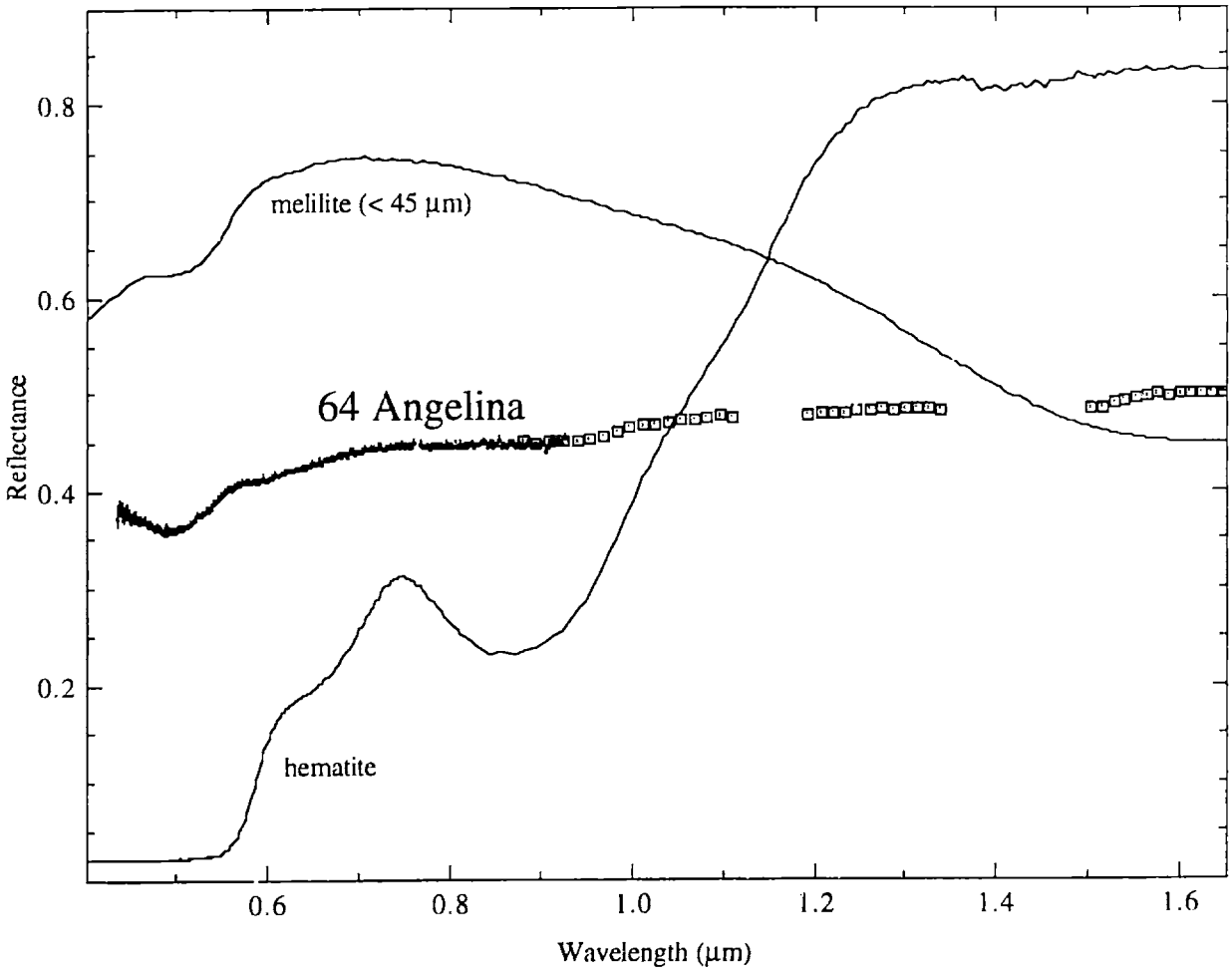

Figure 5.8.6. Reflectance spectrum for Xe asteroids 64 Angelina versus spectra of melilite (particle size less than 45 μm) and hematite. The spectra are not normalized to unity and Angelina's spectrum is multiplied by 0.40 (its albedo). The spectrum of melilite is from Cloutis and Gaffey (1993b). The spectrum of hematite is from Clark *et al.* (1993). Small points are from SMASS II (Bus, 1999) and larger symbols are from SMASSIR. Error bars are $\pm 1\sigma$.

Spectrally some type of sulfide appears to be the best match for this ~0.5 μm absorption feature and sulfides are found in aubrites; however, sulfides tend to have very low albedos (~0.05) while these asteroids tend to have rather high albedos (greater than 0.31). A linear mixture (Figure 5.8.6) of 50% pyrrhotite (chosen because of its very strong absorption band) and 50% enstatite from Happy Canyon has a ~0.5 μm feature with a slightly weaker strength than Angelina's feature plus a slightly lower albedo (~0.25) than Angelina. This mixture does not produce the feature at ~0.9 μm. However, sulfides (primarily troilite) are only found in relatively small amounts (up to 7 vol.%) in aubrites (Watters and Prinz, 1979). A linear mixture with 10% pyrrhotite only produces a very slight ~0.5 μm feature and weakens any argument that a pyrrhotite-like mineral is causing the feature.

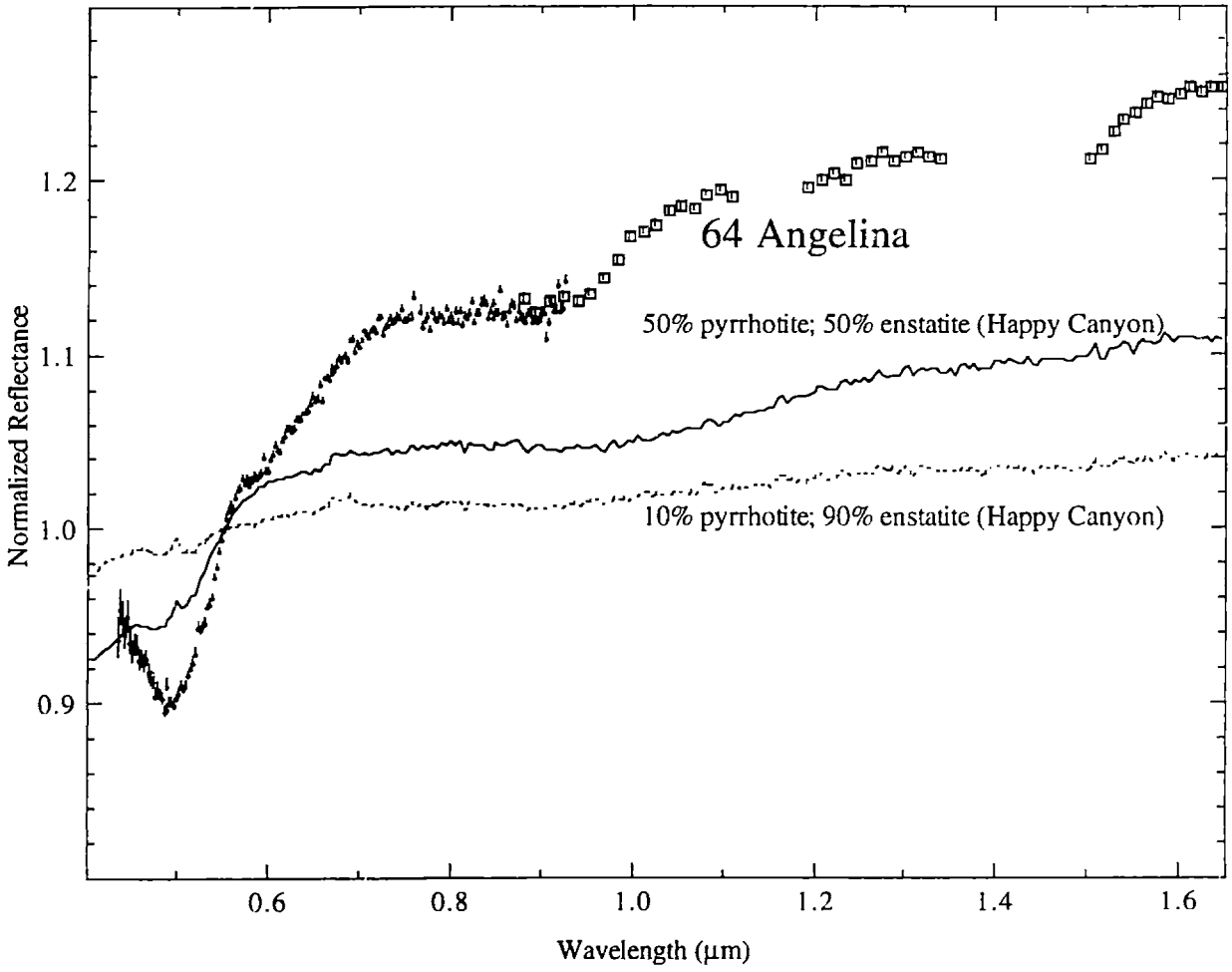

Figure 5.8.7. Reflectance spectrum for Xe asteroids 64 Angelina versus spectra of a linear mixture of 50% pyrrhotite and 50% enstatite (Happy Canyon) (dark line) and a linear mixture of 10% pyrrhotite and 90% enstatite (Happy Canyon) (dashed line). Small points are from SMASS II (Bus, 1999) and larger symbols are from SMASSIR. All spectra are normalized to unity at 0.55 μm. Error bars are $\pm 1\sigma$.

5.8.6 Subgroup: Xk Asteroids

Two Xk objects (21 Lutetia and 336 Lacaderia) were observed in SMASSIR (Figure 5.8.8). Lacaderia has a similar strength UV feature and a similar spectral slope with ataxite Babb's Mill. Lacaderia appears to be a better match with the ataxite than with the EL6, which has a stronger UV feature. However, Lacaderia has an albedo of 0.05, which is much lower than that of the ataxite (0.23) and closer to the EH4's albedo (0.08). The Lutetia spectrum matches very well its 52-color spectrum and appears not as spectrally red as the spectra of the ataxite and the EL6. Lutetia's albedo (0.22) is also more similar to the ataxite. One possible way to lower the spectral slope of the ataxite would be to increase its nickel content. As can be seen by this discussion, it is difficult to make any mineralogic assessment without distinctive absorption features.

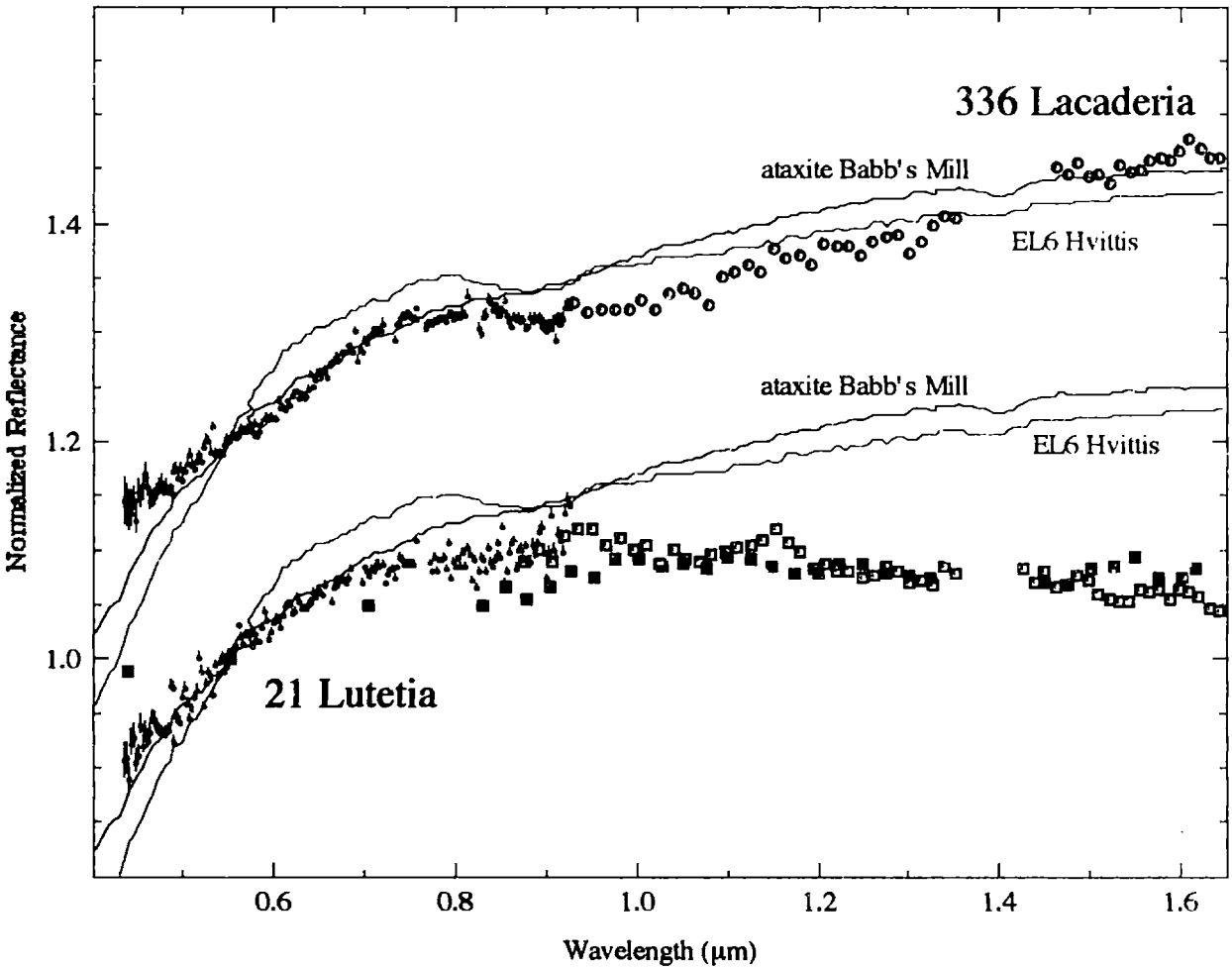

Figure 5.8.8. Reflectance spectra for Xk asteroids 21 Lutetia (squares) and 336 Lacaderia (circles) versus ataxite Babb's Mill (black line) and EL6 chondrite Hvittis (red line). Small points are from SMASS II (Bus, 1999) and larger symbols are from SMASSIR. Dark symbols for Lutetia are a combination of ECAS (Zellner *et al.*, 1985) and 52-color data (Bell *et al.*, 1988). All meteorite spectra are from Gaffey (1976). All spectra are normalized to unity at 0.55 μm. The asteroid spectra are offset by 0.2 in reflectance from each other. Error bars are $\pm 1\sigma$.

5.8.7 Conclusions

As can be seen by the preceding discussion, it is difficult to make any firm assessments (Table 5.1.3) about the X asteroids due to the lack of distinctive absorption features. For example, many of these objects (e.g., 16 Psyche, 22 Kalliope) have spectra that are similar to iron meteorites; however, other meteorite types (e.g., enstatite chondrites) can not be easily ruled out. The very distinctive ~0.5 μm feature in the Xe spectra is difficult to characterize since the abundance of low-albedo minerals (sulfides) that could cause this band are much larger than what is found in the high-albedo aubrites. Some of these objects (e.g., 44 Nysa, 92 Undina) also have 3 μm features, which apparently indicate hydrated silicates on the surfaces; however, these asteroids have albedos too high and spectra unlike any known carbonaceous chondrite.

Table 5.1.3. Mineralogic interpretation of X asteroids observed in SMASSIR. For NEAs, their orbital type is given instead of their semi-major axis (a). Quotation marks are used for meteoritic analogs that appear less certain.

Type	Asteroid	a (AU)	Meteoritic Analog	Mineralogic Interpretation
X	16 Psyche	2.922	"iron meteorite," "EH4 chondrite"	relatively featureless spectra with UV features similar in strength to iron meteorites
	22 Kailiope	2.910	"iron meteorite," "EH4 chondrite"	
High-albedo Xc	44 Nysa	2.423	none readily apparent	slight UV features; absorption feature at 0.9 μm; objects have relatively high albedos; objects also have 3 μm features, which apparently indicates hydrated silicates on the surface
	92 Undina	3.196	none readily apparent	
Low-albedo Xc	65 Cybele	3.433	"shock-darkened ordinary chondrite"	slight UV features and relatively featureless spectra in the near-infrared
	140 Siwa	2.732	"shock-darkened ordinary chondrite"	
	304 Olga	2.404	none readily apparent	
	2100 Ra-Shalom	0.832	none readily apparent	
Xe	64 Angelina	2.682	"aubrite"	spectra have a strong feature at ~0.5 μm that is similar to those found in sulfides; objects have relatively high albedos (greater than 0.3) and featureless spectra past 0.6 μm that are consistent with a silicate composition similar to aubrites
	71 Niobe	2.755	"aubrite"	
	3103 Eger	1.406	"aubrite"	
Xk	21 Lutetia	2.435	none readily apparent	tend to have stronger UV features than other X asteroids; spectra are relatively featureless in the near-infrared
	336 Lacaderia	2.252	none readily apparent	

Chapter 6
Mantle Material in the Main Belt: Battered to Bits?

6.1 Introduction

As first stated by Chapman (1986) and later discussed by Bell *et al.* (1989), one serious problem in our current understanding of the asteroid belt is the explanation for the apparent rarity of olivine-dominated metal-free silicate objects in the main belt and in our meteorite collection. Olivine-dominated objects will refer to silicate compositions that are over ~80% olivine. The complete (or near complete) differentiation of a chondritic parent body is believed to result in an object with a iron-nickel core, a thick olivine-dominated (dunite) mantle and a thin plagioclase/pyroxene crust. Kracher and Wasson (1982) argue that the differentiation of a chondritic parent body can also produce a sulfide-rich layer. The meteoritical evidence for these differentiated bodies is the existence of iron meteorites (core), pallasites (core-mantle) and HEDs (crust). However, mantle material from these differentiated bodies is apparently not present in our meteorite collection (Grady, 1995).

If some fraction of iron meteorites are fragments of the cores of these differentiated asteroids, the disruption of these bodies should produce (Granahan and Bell, 1991; Granahan, 1993) a number of Ni-rich (5-20 wt.% Ni) iron cores (historically thought to correspond to asteroids of type M), a large number of olivine-dominated metal-free asteroids (possibly corresponding to type A) and a number of pyroxene-dominated asteroids (assumed to correspond to type V or J and similar to asteroid 4 Vesta). Compositional groupings of iron meteorites imply ~70 differentiated parent bodies (Wasson, 1995). The problem with this scenario is that M asteroids are much more abundant in the main belt (~40 classified asteroids) (Tholen, 1989) than asteroids classified as A (~15 asteroids) (Bus, 1999). The abundant S-types usually have reflectance spectra that indicate surfaces containing both olivine and pyroxene (Gaffey *et al.*, 1993), which may correspond to chondritic and/or primitive achondritic assemblages. However, both olivine-dominated and pyroxene-dominated objects are also known to occur among the S-asteroid population.

Objects with "basaltic" spectra have been found to be more abundant at smaller sizes (~50 asteroids with diameters less than 10 km); however, these objects are generally believed to be fragments of one asteroid (4 Vesta) since almost all of them are located in the Vesta family or relatively near Vesta. One V asteroid has been identified past 3 AU (Lazzaro *et al.*, 1999), which is located too far from Vesta to be considered a fragment. Crustal material from differentiated asteroids is also rare in the asteroid belt and in our meteorite collection if asteroids with Vesta-like spectra and the HEDs are all fragments of Vesta or if the HEDs originate from

one other differentiated parent body that was catastrophically disrupted. Alternate views of Vesta being the HED parent body can be found in Wasson (1995).

The mechanism for differentiating these parent bodies is generally believed to be due to the short-lived radionuclide ^{26}Al (e.g., Grimm and McSween, 1993). Excesses of ^{26}Mg (the decay product of ^{26}Al) have been found in both CAIs (Lee *et al.*, 1976) and in one eucrite (Srinivasan *et al.*, 1998, 1999). The exact locations of the parent bodies of the iron meteorites are unknown, but it can probably be assumed that they formed in the inner main belt (e.g., Wasson, 1990) since the number of bodies that appear differentiated decreases with increasing heliocentric distance (e.g., Gradie and Tedesco, 1982; Gradie *et al.*, 1989).

Scott (1977a) has interpreted the relative rarity of mantle material among observed meteorite falls as being due to the fracturing of this material into centimeter-size fragments in space or during atmospheric transit and the relatively high weathering rate of this material (relative to iron meteorites). Feierberg *et al.* (1982) discussed how the mantle material could still be contained in a number of the S-types if collisional mixing produced surfaces on these asteroids that were composed of mantle and crustal material. Gaffey (1985), Chapman (1986) and Bell *et al.* (1989) have interpreted the apparent absence of metal-free olivine asteroids in the asteroid belt as being due to the grinding down of this material to sizes that are not spectroscopically observable. "Space weathering," possibly analogous to what has been proposed for S-asteroids (e.g., Wetherill and Chapman, 1988; Pieters *et al.*, 1993), may also be "hiding" the metal-free olivine-dominated asteroids.

Since these interpretations have been proposed, a considerable amount of astronomical and meteoritical research has been done that is relevant to the problem of the "missing" olivine. The astronomical work includes primarily SMASS observations by Xu *et al.* (1995) and Bus (1999). The goal of this chapter is to update the status of this problem since the time of earlier reviews (Chapman, 1986; Bell *et al.*, 1989) and to evaluate whether a more coherent picture can be formed from the now available meteoritical and asteroidal evidence, including SMASS and SMASSIR observations. A earlier version of this work was published in Burbine *et al.* (1996); however, everything has been updated to include more recent results.

6.2 Meteoritical Evidence for the Existence and Number of (Fully) Differentiated Asteroids

6.2.1 Iron Meteorites

The meteoritical evidence for the formation of metallic iron cores in asteroid and then the subsequent disruption of some of these differentiated bodies is based principally on analyses of trace element chemistry and determinations of metallographic cooling rates for iron meteorites. Based on the contents of Ni, Ga, Ge and Ir, twelve main groups with five or more members have

been established: ([IAB and IIICD], IC, IIAB, IIC, IID, IIE, IIF, IIIAB, IIIE, IIIF, IVA and IVB). Following the recommendation of Choi *et al.* (1995), the groups IAB and IIICD, which hitherto have been treated as separate groups, are now considered one group and these meteorites are referred to as IABs.

The chemical classification of twelve genetic groups has yielded much insight into the origin and formation of iron meteorites (e.g., Scott, 1972; Scott and Wasson, 1975). Small variations of Ga and Ge within ten of the groups (the so-called "magmatic" groups that includes all iron-meteorite groups except IAB and IIE) and large differences in the Ga and Ge content between these groups may reflect fractionation processes in the condensing solar nebula. Thus, the intergroup differences in Ga and Ge content supports the view that each "magmatic" group of irons formed in its own separate parent body. Refractory siderophile elements such as Ir, Pt and Au show large variations within the narrow Ni range of each magmatic group. For example, the variation of Ir content in members of the IIAB group spans a factor of 10,000 and covers the whole range of Ir in all other iron meteorites. Groups IAB (including IIICD) and IIE show no such variations and are called "non-magmatic" irons. As discussed earlier, the IIE irons have been linked with the H chondrites.

Wasson and Wetherill (1967) and Scott (1972) suggested that the strong correlations of siderophile elements with Ni in the magmatic groups were produced by fractional crystallization of a molten metallic-core magma within a small planet. The partition coefficients inferred from fractionations within the groups agree nicely with those obtained in the laboratory. This gives strong support to fractional crystallization as the common process responsible for the observed trends in iron meteorites (e.g., Jones and Drake, 1983; Jones and Malvin, 1990).

The almost complete absence of silicates in magmatic irons also speaks in favor of a core origin. Further support comes from the fact that metallographic cooling rates, determined for most magmatic groups, are low (1-500 K/million years) and seem to be constant for all members of a group. The small intergroup variations of cooling rates are consistent with the idea that each group formed in a separate parent body and the slow cooling is consistent with a completely differentiated parent body in which the metallic core was well insulated by the overlying mantle and regolith. The IVA irons, which have cooling rates that span more than two orders of magnitude (19-3400 K/million years) (Rasmussen *et al.*, 1995) are the exceptions.

6.2.2 Pallasites

As discussed earlier, pallasites (over forty known) are stony-iron meteorites containing predominately magnesian olivine and metallic iron. The millimeter to centimeter-sized single crystals or polycrystalline aggregates of olivine are set in a continuous network of metal that, where abundant, shows a well-developed Widmanstätten structure (Dodd, 1981).

Wasson (1974) and Scott (1977b) classified twenty-two of twenty-eight pallasites into a main group (nineteen members) and the Eagle Station grouplet (three members) on the basis of trace element concentrations in the metal phase and classified six other pallasites as anomalous. The main-group pallasites overlap the Ga-Ge field of IIIAB meteorites and plot close to the fields for high-Ni IIIAB meteorites for other trace elements, implying a possible relationship between the IIIAB irons and main-group pallasites (Scott, 1977b). Wasson *et al.* (1999) has also proposed a relationship between the high-Au IIIAB iron and main-group pallasites based on similarities in trace element abundances. The IIIAB irons with high-Au, high-Ni and low-Ir abundances are believed to have been crystallized relatively late since Au and Ni are incompatible elements (tend to remain in the liquid phase during crystallization) while Ir is a compatible element (tends to go into the solid phase during crystallization) for metallic melts having low to moderate sulfur contents (Wasson *et al.*, 1998). As crystallization continues, the liquid will be continually enriched in Au and Ni and depleted in Ir. Therefore, the metal that solidifies from the liquid will also be relatively enriched in Au and Ni and depleted in Ir for increasing degree of crystallization.

Recently, a third pallasite grouplet (pyroxene-pallasites) have been defined on the basis of the identification of two members (Vermillion and Y-8451) (Boesenberg *et al.*, 1995). Pallasites in this grouplet contain relatively large (millimeter-sized) pyroxene grains while pyroxenes in main group and Eagle Station pallasites are much smaller (sizes on the order of microns to tens of microns) (Buseck, 1977; Davis and Olsen, 1991).

6.2.3 Brachinites

Brachina was originally classified as a chassignite (e.g., Nehru *et al.*, 1979); however, Brachina's ~4.5 billion year age (Crozaz and Pellas, 1983) and dramatically different trace element patterns argue against any relationship to Chassigny, which is believed to be a sample of Mars (e.g., Ashwal *et al.*, 1982). The brachinites are labeled as primitive achondrites due to their near-chondritic compositions, but achondritic textures (Nehru *et al.*, 1992). Due to the high chalcophile and siderophile contents of the brachinites relative to other igneous meteorites (e.g., eucrites, Chassigny), Warren and Kallemeyn (1989) have proposed that brachinites formed on a small, slightly-differentiated asteroid (or asteroids) where sulfide and metal phases remained abundant in partially molten regions of the mantle and/or crust and did not segregate.

6.2.4 Mesosiderites

Igneous clasts in mesosiderites are known to resemble the HEDs both petrologically (Floran, 1978) and chemically (rare-earth elements) (Rubin and Mittlefehldt, 1992). However, preliminary data of Wadhwa *et al.* (1999) has shown that the ^{53}Mn-^{53}Cr systematics for silicate

clasts in the Vaca Muerta mesosiderite are different than the trends found in HEDs, implying different parent bodies for this mesosiderite and the HEDs.

The mesosiderites are generally interpreted as being the result of the impact-mixing of basaltic silicates from one differentiated asteroid and metallic iron from the core of another differentiated asteroid (e.g., Wasson and Rubin, 1985; Hassanzadeh *et al.*, 1990; Keil *et al.*, 1994). The main problem with this impact origin is the low abundance of olivine, the expected major component of the mantle in these differentiated asteroids, in mesosiderites. Other scenarios for producing mesosiderites include basaltic crust foundering and sinking through a substantially molten mantle to the core-mantle interface where it becomes impregnated with iron and forms a thin mesosiderite layer (Chapman and Greenberg, 1981).

6.2.5 HEDs

Both the eucrites (containing predominately pigeonite and plagioclase) and diogenites (containing predominately orthopyroxene) appear to be magmatic in origin; however, the specifics of the fractionation process are still under debate (Hewins and Newsom, 1988). Howardites are polymict breccias including eucritic and diogenitic material, suggesting that all three meteorite types originated on the same parent body. A small number (only two known) of olivine-rich diogenites, which contain approximately one-third olivine, are also known to exist (Sack *et al.*, 1991).

Metal segregation (and, therefore, core formation) in the HED parent body is implied by the depletion of siderophile incompatible elements (e.g., Mo, W) relative to non-siderophile incompatible elements (e.g., La) (e.g., Palme and Rammensee, 1981; Newsom, 1985; Hewins and Newsom, 1988). Since both types of elements are incompatible with respect to silicates, their depletion with respect to the assumed chondritic starting material implies metal was fractionated out of the melt. Since the HED meteorites tend to have constant ratios of incompatible siderophile and non-siderophile elements over a wide range of absolute concentrations, metal segregation is believed to have occurred before the igneous fractionation events (Hewins and Newsom, 1988).

The density of eucrites are ~3 g/cm^3 and iron meteorites are ~7.5 g/cm^3 (Consolmagno and Britt, 1998). Vesta's calculated density, determined from the mass derived from mutual perturbations, is 4.3$\pm$0.3 g/cm^3 (Hilton, 1999), which appears consistent with a silicate crust and mantle and a metallic iron core. However, other assemblages can not be ruled out.

6.2.6 Oxygen Isotopes

One useful way to identify different reservoirs of meteoritic material is through oxygen isotope analyses. Oxygen isotope diagrams (Figure 6.1) plot the isotopic composition of ^{18}O

versus ^{17}O, normalized to ^{16}O. Different meteorite classes tend to plot in specific areas of the oxygen isotope diagram. The solar nebula appears not to have been completely homgenized with respect to isotopes of oxygen prior to condensation and accretion of the planets and asteroids. Therefore, material that condensed in different regions or at different times had different oxygen isotope abundances (Clayton and Mayeda, 1978). This oxygen isotope abundance remains with the material since chemical and mass-fractionation processes only change the isotopic abundances along a straight line on the oxygen isotope diagram.

Measured HEDs, mesosiderites and main-group pallasites all have virtually indistinguishable oxygen isotope compositions (Clayton and Mayeda, 1978), which implies either that all of these meteorites came from the same oxygen isotope reservoir or two different reservoirs with the same oxygen isotope abundances. Oxygen isotopic compositions of chromite in IIIAB iron meteorites fall on the same fractionation line as the HEDs, mesosiderites and main-group pallasites and are almost identical with chromite from the Brenham pallasite (Clayton *et al.*, 1986). The oxygen isotope data imply that all of these meteorites come from the same parent body or different parent bodies that all had the same oxygen isotope abundances.

6.2.7 Other Achondritic Meteorites that May Possibly be Mantle Material

Ureilites lack plagioclase and have super-chondritic Ca/Al ratios and are depleted in incompatible lithophile elements, which indicate a high degree of igneous processing (Mittlefehldt *et al.*, 1998). However, the ureilites (olivine-pyroxene achondrites) do not appear to have resided in a body that underwent core formation due to the high abundance of siderophile elements in these meteorites relative to terrestrial and meteoritic igneous rocks (Goodrich *et al.*, 1987; Goodrich, 1992). Ureilites also plot only on the oxygen isotope nebular mixing line with carbonaceous chondritic material and contain trapped noble gases with chondritic abundances processing (Mittlefehldt *et al.*, 1998). Approximately forty ureilites are known.

The unusual olivine-rich (70 wt.% olivine) primitive achondrite Divnoe (Petaev *et al.*, 1994) has been postulated (Shukolyukov *et al.*, 1995) as possible mantle material in the eucrite parent body due to similarities between Divnoe and the diogenites in REE patterns and contents of light noble gasses. Weigel *et al.* (1996) believe that Divnoe is related to the brachinites due to similarities between the chemical abundances of the major lithophile, siderophile, refractory and volatile elements, falling on the same oxygen isotope fractionation line and Divnoe and Brachina containing the same (ordinary chondritic) trapped Xe isotopic pattern.

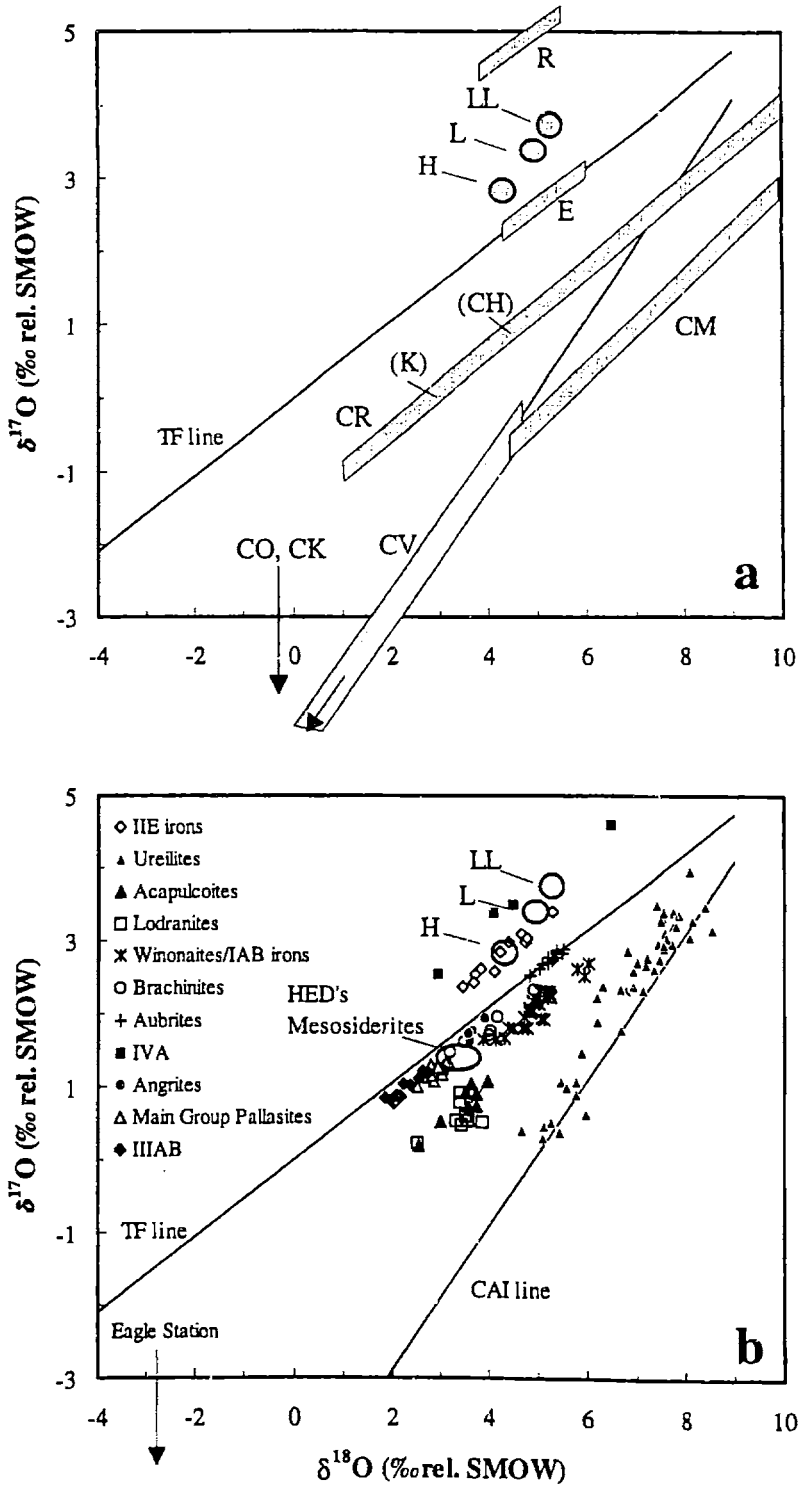

Figure 6.1. Oxygen isotope compositions (relative to standard mean ocean water or SMOW) for (a) the chondritic groups of meteorites and (b) the differentiated groups of meteorites. Figure is taken from Meibom and Clark (1999). Also plotted are the TF (terrestrial fractionation) line and the CAI (calcium-aluminum inclusion) line.

6.2.8 Meteorite Ages

The large difference in cosmic ray exposure ages between iron (200-1000 million years) (e.g., Voshage and Feldman, 1979) and stony meteorites (< 70 million years) (e.g., Crabb and Schultz, 1981; Scherer and Schultz, 2000) indicates that iron meteorites tend to survive much longer in interplanetary space than stony meteorites (Wasson, 1974). Terrestrial ages for Antarctic chondrites and achondrites from Nishiizumi *et al.* (1989) were all less than million years with the largest proportion of samples having ages less than 420,000 years. Recently, two Antarctic chondrites were found with terrestrial ages of 2 (Scherer *et al.*, 1997) and 2.35 (Welten *et al.*, 1997) million years. Three Antarctic iron meteorites had terrestrial ages of 1, 3.2 and 5 million years, respectively, but most iron meteorites also had ages less than 420,000 years (Nishiizumi *et al.*, 1989). The terrestrial ages of the stony meteorites indicate that weathering is destroying most of these samples and even our Antarctic meteorite collection is only representative of the meteorites that have fallen on the Earth for a short period of time (relative to the age of the solar system).

6.2.9 Conclusions from Meteoritical Evidence

In summary, the members of the ten magmatic groups of iron meteorites seem to have formed in the metallic cores of ten different differentiated parent bodies, which implies at least ten iron-meteorite parent bodies that were later disrupted. Adding in the number of iron meteorites that are in grouplets and that are ungrouped and also estimating that some of them are impact melts from chondritic parent bodies, Wasson (1995) guesses that there is evidence for approximately 70 differentiated parent bodies.

The basaltic achondrites appear to be from the crust of a differentiated body. Differentiated olivine-metal meteorites (pallasites) exist, which also leads to the conclusion that some asteroids did differentiate and that these samples are fragments of these core-mantle boundaries. It is unclear what the original sizes of the pallasite parent bodies are since the gravitational acceleration in larger bodies (diameters greater than 20 km) would be expected to cause a much cleaner separation of the olivine and metal (Wood, 1979). Large numbers of olivine-dominated fragments from these disrupted differentiated asteroids do not appear to exist in our present-day meteorite collection. The shorter cosmic-ray exposure of stony meteorites relative to iron meteorites implies relatively short survival times for stony meteorites in interplanetary space.

Consolmagno and Drake (1977) argue that the HED parent body is still intact due to the vastly smaller number of known differentiated olivine-dominated meteorites versus basaltic achondrites. Since the HED parent body is believed to contain substantially more olivine than HED material, more olivine-dominated meteorites would be expected in our meteorite collection

if the HED parent body disrupted. Also, the rarity of olivine-rich diogenites also implies that the HED parent body is still relatively intact (Sack *et al.*, 1991). The only known large main belt asteroid with reflectance spectra similar to the HED meteorites is 4 Vesta (e.g., McCord *et al.*, 1970).

The oxygen isotope data imply that the HEDs, main-group pallasites, mesosiderites and IIIAB iron meteorites come from the same parent body or different parent bodies that all had the same oxygen isotope abundances. The scenario that these four types of meteorites are all derived from the same parent body would suggest that this body was catastrophically disrupted, which would result in fragments from the core (IIIAB irons) and the core-mantle boundary (pallasites) and is inconsistent with the HEDs being fragments of the still-intact Vesta. A mechanism would be needed that preferentially supplied HEDs versus olivine-dominated meteorites to Earth. An example of one such scenario would be the existence of only a single HED fragment (or fragments) of the disrupted differentiated body being currently (and for the last few hundred thousand years) in a meteorite-supplying orbit (Wasson, personal communication). Even if HEDs were "luckily" originating from some other single unknown disrupted differentiated body, the "mantle" material from this disruption is still "missing."

6.3 Asteroidal Evidence for the Existence of Metal-Free Olivine-Dominated Objects

As can be seen by the discussion of different asteroid classes in Chapter 5, a significant fraction of objects (e.g., some S asteroids, Q asteroids) appear to have olivine-rich compositions Some of these asteroids appear spectrally similar to LL chondrites, which are mixtures of olivine, pyroxene and metal. Many of these objects have spectra redder than known meteorite samples, which could be consistent with some type of "altered" olivine-rich material or some mixture or differentiated or partially differentiated silicates with metallic iron.

However, only a relatively few objects (e.g., the deep-featured A-types, 42 Isis, 113 Amalthea, 354 Eleonora, 3819 Robinson) have spectra with the three distinctive absorption bands due to olivine, which should be characteristic of olivine-dominated metal-free mantle fragments. These objects have silicate compositions of almost entirely olivine since pyroxene grains tends to more absorbing then olivine and to dominate the spectral properties of any mixture. A small abundance of pyroxene will tend to suppress the distinctive olivine bands. Asteroids with these distinctive bands also tend to be relatively large (diameters between 27 and 155 km). The obvious exception is the 9-km 3819 robinson.

Almost all of the objects in the main belt with spectra similar to the HEDs are located near Vesta and are most likely fragments of this large body, making basaltic asteroids not related to Vesta apparently very rare in the belt. The SMASS survey has looked at sizable numbers of small (< 20 km) main-belt asteroids and has identified approximately fifty asteroids with basaltic

spectra similar to Vesta (almost all in the vicinity of Vesta), but very few A-type asteroids. Even the newly identified small A-types do not have the distinctive three bands due to olivine and appear to either have been heavily altered and/or contains metallic iron. The number of main-belt asteroids that have predominately silicate-free metallic surfaces is also unknown, although 16 Psyche appears to be one of the most likely candidates.

Taking the astronomical observations at face value implies large numbers of mantle fragments and basaltic crust fragments (unrelated to Vesta) are not present in the current asteroid belt. However, some process (e.g., "space weathering") could be "hiding" the distinctive spectra of the mantle and basaltic crust fragments. Observed A asteroids tend to be much redder than terrestrial and extraterrestrial olivine samples. This may indicate that an alteration process, such as the one proposed by Yamada *et al.* (1999) and Hiroi and Sasaki (2000) that reddens the spectra but keeps the distinctive olivine bands, is affecting the surface. The work of Moroz *et al.* (1996) shows that as the alteration increases, the olivine tends to melt and recrystallize with the olivine absorption bands becoming suppressed. Coating these objects with carbonaceous material will also tend to suppress the absorption bands. The amount of metallic iron on these bodies is also unknown since metallic iron does not have distinctive absorption features. The A asteroids at small sizes (diameters less than 20 km) that have been studied have less distinctive olivine bands than the larger A objects. This observation argues that an alteration process is not affecting the spectra of these olivine-dominated bodies since the larger objects would be expected, on average, to have older surfaces and appear "more weathered." However, it is impossible to completely rule out an alteration process, which is "disguising" the mantle fragments.

Only a few asteroid families have been identified as possibly being olivine-dominated mantle material. One example is the Flora family, which has a large number of olivine-rich members. Bus (1999) has observed fourteen Zappalà *et al.* (1990, 1995) families and found that all of them are relatively homogeneous spectrally. He found that four possible olivine objects (A-asteroid 2732 Witt and three Sa asteroids) are located near the Lydia family, which is composed primarily of X asteroids. Witt and Sa objects have spectra consistent with heavily-altered olivine and/or some type of olivine/metal mixture. Bus theorizes that the Lydia family may be core material of a disrupted differentiated object and the four possible olivine asteroids may be mantle material from the same body. One Williams (1979, 1989, 1992) family (#67, the Ceres family) is known to contain both an A- (446 Aeternitas) and M-type (441 Bathilde) asteroid; however, this family was not defined by the clustering methods of Zappalà *et al.* (1990, 1995).

The identification of asteroids with Vesta-like spectra in the Vesta family and between Vesta and the 3:1 resonance by Binzel and Xu (1993) is consistent with the scenario that material

can be ejected from Vesta, enter the 3:1 resonance and become a meteorite-supplying Earth-crossing asteroid. These Vesta fragments would then be the source of the HEDs that fall on Earth and explain why the HEDs sample the crust of only one parent body without also providing metal-free olivine mantle samples.

6.4 Battered to Bits: A Collisional Scenario

The lack of direct astronomical evidence and meteoritic evidence for an abundance of metal-free olivine mantle material leads us to consider a collisional scenario where this material has been substantially destroyed over the age of the solar system (Chapman, 1986; Bell *et al.*, 1989). I attempt to update and quantify this scenario based on the current meteoritic and astronomical evidence discussed earlier and with current collisional models.

A first step in the collisional scenario is to characterize the sizes of the differentiated parent bodies and estimate their collisional history. The possible metallic nature of asteroid 16 Psyche (diameter of ~260 km) and the existence of Vesta (diameter of ~500 km) suggest relatively large sizes. Recent theoretical work (Haack *et al.*, 1990), using the insulating effects of regolith and megaregolith (brecciated impact rubble) layers combined with cooling rate data, have calculated that smaller (less than 100 km) diameter objects appear to be the most plausible parent bodies. Parent body diameters calculated by Mittlefehldt *et al.* (1998), for different cooling rate estimates and for different iron meteorite groups, varied from 6 to 330 km. Rivkin *et al.* (2000) has found that relatively small (diameters < 65 km) M asteroids tend not to be hydrated and could possibly contain the parent bodies of some of the iron meteorites. Davis *et al.* (1999) believe that all this evidence argues persuasively that iron meteorite parent bodies tended to have diameters less than 100 km. However, they do not understand why two large asteroids (Vesta and the Psyche parent body) melted and differentiated with many small ones, but the melting and differentiation did not appear to affect intermediate bodies as well.

A second step is to consider the volume of the mantle material formed in a differentiated parent body. I assume core (37% total radius), mantle (47%) and crust thicknesses (6%) from Gaffey *et al.* (1993) for the differentiation of a parent body with a CV/CO chondritic composition. As an illustration, for a 100-km parent body the resulting volume of the mantle material would be 4.1×10^5 km^3, equivalent to twelve 40-km diameter asteroids or ninety-seven 20-km diameter asteroids. For a 500-km differentiated parent body, the theoretical layer thicknesses give a volume of 5.1×10^7 km^3 for the mantle material or the equivalent of 56 fragments that are 120 km (the approximate theoretical mantle radius) (in diameter), 1,523 fragments that are 40 km and 12,186 fragments that are 20 km. The total volume of mantle material must be scaled by the number of disrupted parent bodies. As stated before, the

meteoritical evidence points to about 70 such bodies, which is clearly a lower limit because our meteorite collection cannot be assumed to be fully sampling the population.

The actual distribution of sizes of the resulting fragments for catastrophically disrupted parent bodies is believed to be described by a power law, which is written as $N(> d) \propto d^{-b}$ where $N(> d)$ is the number of asteroids greater than a particular size, d is the diameter and b is the exponent (e.g., Dohnanyi, 1969; Greenberg and Nolan, 1989). Greenberg and Chapman (1983) have also discussed how impact cratering (meaning any process that launches material off the surface) might be important for stripping off the crust and mantles of differentiated parent bodies.

To try to estimate the average collisional lifetime for a given mantle fragment, I performed order-of-magnitude calculations based on the method of Namiki and Binzel (1991) and Farinella *et al.* (1992). The lifetime of a given mantle fragment against catastrophic disruption by collision will be a function of three factors (Namiki and Binzel, 1991; Farinella *et al.*, 1992): the size of the smallest body that is capable of shattering and disrupting it; the abundance of these bodies in the present belt; and the probability of collisions between the mantle fragment and other asteroids. Each of these factors has a number of variables (e.g., energy needed to shatter and disperse a body of a given size, number of asteroids at sizes less than 10 km, which can only be very roughly estimated.

There is a considerable amount of disagreement on the initial size of the asteroid belt. The asteroid belt today contains approximately one-thousandth of an Earth mass. Larger asteroid populations in the past have been suggested by models such as Chapman and Davis (1975). They estimated an initial asteroid population that is between ~30 and ~3,000 times more populous than today that stripped the crust and mantles of differentiated objects (excluding Vesta) to produce the observed number of large S-type asteroids, assumed to be the stony-iron cores of these differentiated bodies.

Assuming approximately five earth masses of material in the asteroid belt region, Chambers (1999) has simulated the removal of 50 Mars-sized bodies in one scenario and 200 smaller planetary embryos in another. He has found that these objects could be completely cleared out by resonances with the giant planets. Another effect could be due to scattered comets from the Uranus-Neptune zone, which could also affect collisional evolution in the early asteroid belt. Gil-Hutton and Brunini (1999) have modeled the effect of comets for initial asteroid populations ~1.7 to ~1000 times the current mass. Assuming different comet size distributions, they found that they were able to reproduce the mass of the current asteroid belt very quickly (~2 x 10^7 years). Their models also were all able to reproduce very well the size distribution of the present-day asteroid belt in 4.5 x 10^9 years and Vesta's intact basaltic crust.

Davis *et al.* (1985) estimated an earlier population "several" times the present-day belt which evolved to the present-day asteroid-size distribution, preserved Vesta's basaltic crust and produced at least the observed number of Hirayama families. The collisional model of Marzari *et al.* (1999), using an initial asteroid population with 400 bodies that have diameters larger than 100 km with a *b* of 3.5, a *b* of 3 for diameters less than 100 km and approximately twice the mass of the asteroid belt today, was able to duplicate very well the number of observed families (~64). Using a starting mass of approximately five times the mass of the present-day asteroid belt, Marzari *et al.* (1999) has found that number of observable families would be around 175, which is much higher than what is found today.

One additional constraint that can be used to determine which populations are "realistic" in these calculations is that collisional evolution had to be sufficient to disrupt over ~70 differentiated parent bodies so as to produce the iron meteorites (from metallic iron cores) that are found today. The impacting asteroid population must have been high enough to disrupt these larger differentiated objects in a timescale where only one asteroid with an intact basaltic crust, Vesta, is present today.

To do any modeling, the projectile-to-target diameter ratio needed to shatter a solid body needs to be calculated. This ratio is derived from the definition of Q^* (Davis, personal communication), which is the kinetic energy per unit mass of the target required to produce a barely catastrophic outcome. A barely catastrophic outcome is defined an event where the largest fragment produced from the disruption is one-half the size of the original body (Davis *et al.*, 1989). Q^* equals the energy of the impact ($1/2mv^2$) (where m is the mass of the impactor) times the partitioning of the total collisional energy between the projectile and target (usually assumed to be equally divided between both bodies, which equals a factor of 1/2) and divided by the mass of the target. Assuming similar densities for the target and the projectile so the ratio of their diameters will be equal to the cube root of the ratio of their masses, the projectile-to-target diameter ratio will be equal to $(4Q^*/v^2)^{1/3}$ (Farinella *et al.*, 1992).

To collisionally destroy a body, the impact must be energetic enough so that the resulting fragments have enough energy to escape the original parent body and not reassemble. Values for Q^* can be calculated from laboratory fragmentation experiments of representative materials for sizes usually ranging from 10 to 100 cm. There are many theories (e.g., Davis *et al.*, 1985; Housen and Holsapple, 1990; Davis *et al.*, 1994; Love and Ahrens, 1996) on how to scale Q^*s for asteroidal-sized bodies. In our calculations, Q^*s from Love and Ahrens (1996), which assume that gravity is dominating the collisions, will be primarily used since their values appear to be at the high end of the reasonable range of possible values. Q^*s from the work of Love and Ahrens (1996) vary from 20,000 J/kg for a 20-km silicate body to 600,000 J/kg for a 500-km object. The average collision velocity for main-belt asteroids between 50 and 80 km, from the

calculations of Farinella and Davis (1992) for asteroids larger than 50 km, is 5.8 km/s. For 500-, 200- and 100-km diameter differentiated objects to be catastrophically disrupted, the critical diameters for the impacting projectiles are 207, 57.5 and 22.8 km, respectively.

There are currently 23 asteroids with estimated diameters greater than 207 km in the IRAS survey and I will assume this is the present-day number of asteroids that could disrupt a 500-km differentiated body using Q^*s from Love and Ahrens (1996). The number of asteroids at small sizes (< 10 km) is believed to be roughly estimated by assuming a power law distribution (d^{-b}) for the number of asteroids [$N(> d)$] greater than a particular size. The boundary condition for the power law distribution of the present-day main belt is 682 asteroids with diameters greater than 50 km (Farinella and Davis, 1992). Values of the exponent (b) tend to be estimated from analyses of the magnitude distribution of small asteroids from the Palomar-Leiden Survey (van Houten *et al.*, 1970). The estimated value of the exponent (b) for the present-day asteroid belt is usually taken as 2.5 (Dohnanyi, 1971). In the calculations for the number of projectiles for sizes larger than a particular diameter, I will use an exponent of 2.5 except for using 23 asteroids with diameters greater than 207 km. Increasing the value of the exponent increases the number of objects that could disrupt the differentiated bodies, except for the largest size (207 km), and, therefore, decreases the average collisional lifetimes of the objects.

The number of disruptive collisions per year is $P_i(R + r)^2 n$ where P_i is the average collision probability, R is the radius of the target, r is the radius of the projectile and n is the number of bodies that could disrupt the mantle fragment. The collisional lifetime (years per disruptive collision) of an object will be the inverse of this number. P_i is calculated (Wetherill, 1967) using the orbital elements of the target and projectile by evaluating the fraction of time during which two orbiting bodies would be closer together than their collision cross-section. The average P_i, for diameters 50 km or greater, for an asteroid in the present-day main belt has been calculated to be 2.8×10^{-18} km^{-2} yr^{-1} (Farinella and Davis, 1992).

Table 6.1 details the outcome for several scenarios for asteroid collisional evolution where I use a collision velocity of 5.8 km/s (Farinella and Davis, 1992) and the Q^* model from Love and Ahrens (1996). I present as a baseline the case where the current asteroid population is assumed constant over the age of the solar system. Under this environment, the results show that differentiated bodies are not disrupted and, therefore, do not yield iron meteorites. (Of course, no mantle fragments are liberated either.)

Table 6.1. Average collisional lifetimes (years) for 20-, 40-, 100-, 200- and 500-km diameter asteroids for different average asteroid populations (times present-day). The 100-, 200- and 500-km diameters are assumed to be the possible sizes of the original differentiated parent bodies. The 20-, 40- and 100-km diameters are assumed to be the possible sizes of the mantle fragments. The average collisional lifetimes were calculated using Q^* values (kinetic energy per unit mass of the target) from Love and Ahrens (1996), an average collision velocity of 5.8 km/s from Farinella and Davis (1992) and an exponent (b) of 2.5 from (Dohnanyi, 1971) for the number of asteroids larger than a particular diameter.

Diameter (km)	Average Asteroid Population (times present-day)	Average Collisional Lifetime (years)	Viable?	Implications for Metal-Free Olivine Asteroids
20	1	2.7×10^9	No. Iron-meteorite parent bodies for sizes	None produced.
40	1	6.4×10^9	greater than 20 km would tend not to be	Parent bodies not
100	1	2.0×10^{10}	disrupted over the age of the solar system.	destroyed.
200	1	4.5×10^{10}		
500	1	1.2×10^{11}		
20	10	2.7×10^8	Yes, if iron-meteorite parent bodies were	Parent bodies must be less
40	10	6.4×10^8	less than about 100 km in diameter.	than 100 km in diameter.
100	10	2.0×10^9		
200	10	4.5×10^9		
500	10	1.2×10^{10}		
20	50	5.4×10^7	Yes, if iron-meteorite parent bodies	Survival times
40	50	1.3×10^8	have diameters less than about 500 km.	short compared to
100	50	4.0×10^8	Reasonable chance for Vesta to survive	the age of the solar
200	50	9.0×10^8	to present-day.	system.
500	50	2.4×10^9		
20	100	2.7×10^7	Yes. Iron-meteorite parent bodies of all	Survival times
40	100	6.4×10^7	assumed sizes would be disrupted in less	short compared to
100	100	2.0×10^8	than about 1 billion years. Reasonable	the age of the solar
200	100	4.5×10^8	chance for Vesta to survive to present-day.	system.
500	100	1.2×10^9		
20	200	1.4×10^7	Yes. Iron-meteorite parent bodies of all	Survival times
40	200	3.2×10^7	assumed sizes would be disrupted in less	short compared to
100	200	1.0×10^8	than about 600 million years. Less likely	the age of the solar
200	200	2.3×10^8	chance for Vesta to survive to present-day.	system.
500	200	6.0×10^8		

In Table 6.1, I also investigate the outcomes for collisional scenarios where larger early asteroid populations are assumed such that 10, 50, 100 and 200 times more collisions occur relative to the baseline case. I find that increasing the baseline by a factor of 10 will disrupt iron meteorite parent bodies if they had diameters less than about 100 km. I also find that all possible sizes of differentiated parent bodies are disrupted over the age of the solar system for a collisional environment 50 times or greater than our baseline. In all these cases where differentiated parent bodies are disrupted, I also find that the collisional lifetimes for mantle-

sized fragments (diameters less than 100 km) are short compared to the age of the solar system. The existence of Vesta sets an upper limit on the collisional environment where there must be some reasonable probability of its survival to present day.

The principal quantitative conclusion from my collisional analysis is that any collsional environment which allows for the disruption of differentiated parent bodies is also sufficient to result in the comminution of most, if not all, of the olivine-dominated metal-free mantle (and basaltic crust) material. The disruption of iron meteorite parent bodies must have occurred early in solar system history to explain the paucity of differentiated families. However, such a collisional history leads to many alternative questions. For example, "Why are C-asteroids, which are believed to be as fragile as dunite material, remaining?" and "Why did Vesta's basaltic crust survive?" An explanation for the abundant numbers of C-asteroids still remaining in the asteroid belt, as first proposed by Chapman (1976), is that the original number of these C-type asteroids must have greatly outnumbered the original number of differentiated objects. The "Vesta constraint" considered by Davis *et al.* (1985) requires that Vesta remains the sole large asteroid with a basaltic crust in the current solar system. If differentiated parent body sizes of ~100 km as suggested by Haack *et al.* (1990) were more typical than Vesta's much larger size (~500 km), than the preferential survival of Vesta becomes more likely. However, if the typical sizes of the differentiated parent bodies was 100 km or less, it is unclear why Vesta and Psyche are so much larger.

6.5 Conclusions

An updated look at the problem of the missing mantle material within our meteorite collections and within the detection limits of our current astronomical capabilities can be summarized in terms of the following evidence.

- Analyses of iron meteorites suggest that they are sampling the cores of approximately 60 differentiated parent bodies which have been catastrophically disrupted. This is a lower limit to the number of differentiated bodies that have existed in the asteroid belt.
- Only a relatively few olivine-dominated metal-free meteorites are known to exist. However, these meteorites do not appear to come from the mantle of a large fully differentiated parent body.
- Even though HEDs account for about 6% of meteorite falls, they appear to be have originated on a single parent body. Thus, there is arguably a shortage of basaltic crust material analogous to the mantle shortage.
- Pallasites appear to be from the core-mantle boundaries of differentiated asteroids, adding further evidence that substantial differentiation processes occurred.

• Iron meteorites have much longer cosmic ray exposure ages than stony meteorites indicating that they have a longer lifetime in interplanetary space and could be the longest survivors of an intense collisional history.

• Our meteorite collections represent only a snapshot of very recent solar system history. Terrestrial ages for Antarctic meteorites extend upward to a few million years. With the possible exception of some irons, older meteorites appear to have been destroyed by terrestrial weathering.

• Astronomical surveys, which can now systematically measure spectral properties of inner belt asteroids down to 10-km diameters, reveal that asteroids with distinctive olivine spectra (e.g., A-asteroids, olivine-rich S-asteroids) continue to be rare. Asteroids with distinctive basaltic spectra (Vesta-like) that are not located near Vesta are also rare.

• Asteroid families that appear to be the result of the breakup of a differentiated parent body are rare.

The current evidence remains consistent with a scenario where, with the exception of Vesta, all differentiated bodies were either disrupted or had their mantles stripped very early in the age of the solar system (Chapman, 1974). Olivine-rich metal-free fragments have been continually broken down until they all (or almost all) now fall below our current astronomical measurement limits (Gaffey, 1985; Chapman, 1986; Bell *et al.*, 1989). Crustal material from the original differentiated parent bodies was also broken down below our current observation limits. The only plausible reason that Vesta fragments would not be similarly broken down is if they were formed very recently (Pieters and Binzel, 1994; Wasson *et al.*, 1996).

Chapter 7
Conclusions

This study has produced a number of major results concerning plausible meteoritic parent bodies and the compositional structure of the asteroid belt.

- **Almost all Vestoids appear to be fragments of Vesta.**

All Vestoids (diameters less than 10 km) in the Vesta family have near-infrared spectra similar to eucrites and appear almost certainly to be fragments of Vesta. The spectral variations in continuum slope among the Vestoids appear to be primarily caused by differences in particle size as seen by spectral measurements of different HED grain sizes, which are shown to span the spectral range of the Vestoids. None of the Vestoids have spectra similar to diogenites, which leads to the conclusion that 10 km objects can not be ejected from Vesta with surfaces covered predominately with diogenite material. For Vestoids outside the Vesta family, all but one object (2579 Spartacus) has spectra similar to eucrites and howardites. Spartacus has a very broad 1 μm feature and appears to have significant amounts of olivine on its surface. Vestoids in the Vesta family have weaker band depths than those outside the Vesta family. Vestoids in the NEA population have the strongest band depths. The differences in band depths may imply a larger glass component on the Vestoids on the surfaces of Vestoids in the Vesta family, which should weaken the band intensity.

- **A asteroids appear to be evidence for a "space weathering" process in the belt.**

Deep-featured A types appear to be definitive evidence that spectral alteration processes are occurring on some asteroids. These asteroids have the distinctive absorption bands due to olivine and similar band depths to terrestrial and meteoritic olivine; however, the asteroids are significantly reddened. Reddening agents such as metallic iron tend to suppress the intensity of the band and olivine's distinctive features. The only postulated process that appears to redden the olivine band and not weaken the band depth are the pulse laser experiments of Yamada *et al.* (1999), which are hoped to duplicate the energy of micrometeorite impacts. It is very difficult to determine if this alteration process is affecting other objects due to the difficulties in determining surface compositions of asteroids by reflectance spectroscopy.

• Plausible parent bodies for a number of carbonaceous chondrite meteorites have been identified.

A number of main-belt asteroids have been identified as spectral analogs to particular carbonaceous chondrites. Ch-asteroid 19 Fortuna is spectrally very similar to CM chondrites Murchison and LEW 90500 with both types of objects having features at 0.7 μm and similar spectral slopes. Eos family members 221 Eos and 653 Berenike have similar strength UV features and have 1 μm bands with the CO chondrite Warrenton. K-asteroid 599 Luisa has a similar strength UV feature and similar near-infrared spectra with CV chondrite Mokoia. Cosmic ray exposure ages for the linked meteorites appear consistent with the orbital position of the linked asteroid. Fortuna is located near the 3:1 resonance and Luisa is located near the 5:2 resonance, which should be supplying fragments to Earth on timescales of a few million years. The meteorites (Murchison and LEW 90500) linked to Fortuna have exposure ages of less than a million years while the linked meteorite (Mokoia) with Davida has an exposure age of ~10 million years. The Eos family is located near the higher-order 9:4 resonance, which is believed to be supplying fragments to Earth on longer timescales (tens of millions of years to a billion years). The linked meteorite (Warrenton) with the Eos family has a relatively long exposure age (~34 million years).

• S asteroids are a very diverse group of objects with a number of them having spectra consistent with a mixture of ordinary chondrite material and metallic iron.

A significant fraction of S asteroids have spectral properties that range from similar to ordinary chondrites to spectra that is much redder with weaker 1 μm bands. These objects tend to have spectra consistent with a mixture of ordinary chondrite material and metallic iron that is spectrally red, in contrast to the spectrally flat metallic iron found in ordinary chondrites. Smaller objects tend to have stronger band depths that larger objects so the "alteration" process appears to have some size dependence. It appears very difficult to impossible to rule out other proposed alteration processes such as glass formation.

• Mineralogic interpretations based on visible asteroid spectra or assigned asteroid classes should be treated with caution.

Almost all of the Bus (1999) classes appear to contain at least two compositionally distinct types of objects on the basis of their near-infrared spectra. Mineralogic interpretations on the basis of just visible spectra or an assigned asteroid class may not be accurate and should be treated with extreme caution.

• Plausible asteroidal parent bodies can be assigned to a large number of meteorite groups.

A number of asteroids appear spectrally similar to specific meteorites classes. The "best" spectral matches from this study are listed in Table 7.1. Many of these objects listed in the table are Vestoids, which are all believed to be fragments of Vesta.

Table 7.1. Asteroids that appear to be the best spectral matches to specific meteorite classes. For NEAs, their orbital type is given instead of their semi-major axis (a).

Asteroid	Class	a (AU)	Diameter (km)	HCM Family	Meteoritic Analog
3 Juno	Sk	2.669	234	Juno	L chondrite
4 Vesta	V	2.362	506	Vesta	howardite
10 Hygiea	C	3.142	407	Hygiea	heated CI chondrite
11 Parthenope	Sk	2.452	153		L chondrite
19 Fortuna	Ch	2.442	225		Murchison (CM chondrite), LEW 90500 (CM chondrite)
167 Urda	Sk	2.854	40	Koronis	L chondrite
221 Eos	K	3.012	104	Eos	Warrenton (CO)
253 Mathilde	Cb	2.647	53		heated (900 °C) CM chondrite
335 Roberta	B	2.475	89		heated CI chondrite
379 Huenna	C	3.136	92	Themis	heated CI chondrite
599 Luisa	K	2.773	65		Mokoia (CV chondrite)
653 Berenike	K	3.014	39	Eos	Warrenton (CO chondrite)
702 Alauda	B	3.195	195		heated CI chondrite
1273 Anchises	V	2.394	(6)		eucrite
1862 Apollo	Q	Apollo	1		LL4-5 chondrite
1906 Naef	V	2.374	(6)	Vesta	eucrite
1929 Kollaa	V	2.363	(8)	Vesta	eucrite
1933 Tinchen	V	2.353	(5)	Vesta	eucrite
2045 Peking	V	2.380	(8)	Vesta	eucrite
2442 Corbett	J	2.388	(6)		eucrite
2590 Mourao	V	2.343	(6)		eucrite
2653 Principia	V	2.444	(8)		eucrite
2851 Harbin	V	2.478	(7)		eucrite
3268 De Sanctis	V	2.347	(4)	Vesta	eucrite
3376 Armandhammer	Sq	2.349	(9)	Vesta	eucrite
3657 Ermolova	J	2.313	(6)	Vesta	eucrite
3753 Cruithne	Q	Aten	(3)		LL6 chondrite
3903 Kliment Ohridski	Sq	2.930	(11)	Koronis	H chondrite
3908 Nyx	V	Amor	1		howardite
3944 Halliday	V	2.369	(5)	Vesta	eucrite
3968 Koptelov	V	2.322	(5)	Vesta	eucrite
4005 Dyagilev	J	2.452	(6)	Vesta	eucrite
4147 Lennon	V	2.362	(5)	Vesta	eucrite
4188 Shulnazaria	V	2.335	(6)		eucrite
4215 Kamo	J	2.417	(7)	Vesta	eucrite
4900 Maymelou	V	2.380	(5)	Vesta	eucrite
7358 1995 YA_3	Sq	Amor	(11)		H or L chondrite
7889 1994 LX	V	Apollo	(2)		howardite
1991 VH	Sk	Apollo	(1)		L chondrite
1998 KU_2	Cb	Amor	(1)		heated CI or CM chondrite

• Asteroids with distinctive olivine absorption bands are rare and are evidence that mantle material form disrupted differentiated bodies has been broken down into sizes below our current astronomical measurement limits.

Asteroids with the distinctive olivine bands appear to be relatively rare in the main belt with less than ten objects identified. Compositional groupings of iron meteorites imply ~70 differentiated parent bodies since the complete (or near complete) differentiation of a chondritic parent body is believed to result in an object with a iron-nickel core, a thick olivine-dominated mantle and a thin plagioclase/pyroxene crust. The disruption of these bodies to release iron meteorites from the core should also produce large numbers of olivine mantle fragments, which are not apparent in the belt. Mantle material from these differentiated bodies is also rare in our meteorite collection. All of the available evidence remains consistent with a scenario where, with the exception of Vesta, all differentiated bodies were either disrupted or had their mantles stripped very early in the age of the solar system. Olivine-rich metal-free fragments have been continually broken down until they all (or almost all) now fall below our current astronomical measurement limits.

• Sample return missions are needed to really understand the surface of composition of asteroids.

As can be seen by the discussion of asteroid spectra in this thesis, it is very difficult to identify meteoritic parent bodies unless the spectra tend to be relatively unusual (e.g., Vesta, the Vestoids and the HEDs) or the spectra are just "perfect" matches (e.g., CO chondrite Warrenton and the Eos family). Many have spectra that are consistent with some type of alteration process occurring on a particular meteorite; however, it is difficult to conclusively say that the differences are not due to composition and the asteroid actually has a surface very unlike the proposed meteoritic analog. Deep-featured A asteroids are the best evidence that some type of alteration is occurring on the belt since no measured olivine sample matches there spectral properties. It is harder to understand if alteration is occurring on S asteroid surfaces and what type of alteration it is since these objects tend to be olivine-pyroxene mixtures with an unknown amount of metal.

To answer the above questions, we need samples from known objects. The samples can be studied in the laboratory and we can then understand what is controlling the reflectance properties of the surface, such as what was done with the returned lunar samples. One Japanese mission (MUSES-C) (Yeomans, 1999) is being planned and plan on rendezvousing with a NEA (most likely 10302 1989 ML). The spacecraft will collect material by descending to the surface

and firing projectiles at the asteroid and collecting the ejected fragments. The spaceraft will return to Earth with a few grams of material.

However to determine the alteration processes that are occurring on asteroids, we need samples from a number of objects for a variety of different classes. This study has identified plausible meteorite parent bodies in the main belt and near-Earth population that should be prime candidates for sample return missions. Only by obtaining samples directly from asteroids will we be able to conclusively determine their compositions. I would argue that the highest priority object would be a near-Earth S-asteroid that appears to have a silicate composition similar to ordinary chondrites, but is spectrally reddened since the relationship between this object and ordinary chondrites are difficult to determine just from spectral measurements. Two NEAs observed in SMASSIR that fit this description are 7358 1995 YA_3 and 1991 VH.

References

Abell P. A. and Gaffey M. J. (1999) A preliminary investigation into the geologic composition and thermal history of mainbelt asteroid 349 Dembowska (abstract). *Asteroids, Comets and Meteors*, 101.

Adams J. B. (1974) Visible and near-infrared diffuse reflectance spectra of pyroxenes as applied to remote sensing of solid objects in the solar system. *J. Geophys. Res.* **87**, 4829-4836.

Adams J. B. and McCord T. B. (1970) Remote sensing of lunar surface mineralogy: Implications from visible and near-infrared reflectivity of Apollo 11 samples. *Proc. Apollo 11 Lunar Sci. Conf.* **3**, 1937-1945

Adams J. B. and McCord T. B. (1973) Vitrification darkening in the lunar highlands and identification of Descartes material at the Apollo 16 site. *Proc. Lunar Sci. Conf.* **4th**, 163-177.

Allègre C. J., Manhès G. and Göpel C. (1995) The age of the Earth. *Geochim. Cosmochim. Acta* **59**, 1445-1456.

Allen C. C., Morris R. V. and McKay D. S. (1995) Experimental space weathering of lunar soils (abstract). *Meteoritics* **30**, 479-480.

Ashwal L. D., Warner J. L. and Wood C. A. (1982) SNC meteorites: Evidence against an asteroidal origin. *J. Geophys. Res.* **87 (suppl.)**, A393-A400.

Asphaug E. (1997) Impact origin of the Vesta family. *Meteoritics & Planetary Science* **32**, 965-980.

Baldwin B. and Sheaffer Y. (1971) Ablation and breakup of large meteoroids during atmospheric entry. *J. Geophys. Res.* **76**, 4653-4668.

Barucci M. A., Doressoundiram A., Fulchignoni M., Florczak M., Lazzarin M., Angeli C. and Lazzaro D. (1998) Search for aqueously altered materials on asteroids. *Icarus* **132**, 388-396.

Bell J. F. (1988) A probable asteroidal parent body for the CV or CO chondrites (abstract). *Meteoritics* **23**, 256-257.

Bell J. F. (1998) The Vesta asteroid family: Fact or fiction? (abstract). *Lunar Planet. Sci.* **XXIX**, Abstract #1851.

Bell J. F., Owensby P. D., Hawke B R. and Gaffey M. J. (1988) The 52-color asteroid survey: Final results and interpretation (abstract). *Lunar Planet. Sci.* **XIX**, 57-58.

Bell J. F., Davis D. R., Hartmann W. K. and Gaffey M. J. (1989) Asteroids: The big picture. In *Asteroids II* (R. P. Binzel, T. Gehrels and M. S. Matthews, Eds.), pp. 921-945. University of Arizona Press, Tucson, Arizona.

Bell P. M., Mao H. –K. and Weeks R. A. (1976) Optical spectra and electron paramagnetic resonance of lunar and synthetic glasses: A study of the effects of controlled atmosphere, composition and temperature. *Proc. Lunar Planet Sci. Conf.* **7th**, 2543-2549.

Belton M. J. S., Chapman C. R., Veverka J., Klaasen K. P., Harch A., Greeley R., Greenberg R., Head J. W. III, McEwen A., Morrison D., Thomas P. C., Davies M. E., Carr M. H., Neukman G., Fanale F. P., Davis D. R., Anger C., Gierasch P. J., Ingersoll A. P. and Pilcher C. B. (1994) First images of asteroid 243 Ida. *Science* **265**, 1543-1547.

Belton M. J. S., Chapman C. R., Thomas P. C., Davies M. E., Greenberg R., Klaasen K., Byrnes D., D'Amario L. Synnott S., Johnson T. V., McEwen A., Merline W. J., Davis D. R., Petit J-M., Storrs A., Veverka J. and Zellner B. (1995) Bulk density of asteroid 243 Ida from the orbit of its satellite Dactyl. *Nature* **374**, 785-788.

Benner L. M., Ostro S. J., Giorgini J. D., Jurgens R. F., Mitchell D. L., Rose R., Rosema K. D., Slade M. A., Winkler R., Yeomans D. K., Campbell D. B., Chandler J. F. and Shapiro I. I. (1997) Radar Detection of Near-Earth Asteroids 2062 Aten, 2101 Adonis, 3103 Eger, 4544 Xanthus and 1992 QN. *Icarus* **130**, 296-312.

Binzel R. P. (1995) Forging new links in the asteroid-meteorite connection (abstract). *Meteoritics* **30**, 486.

Binzel R. P. and Xu S. (1993) Chips off of asteroid 4 Vesta: Evidence for the parent body of basaltic achondrite meteorites. *Science* **260**, 186-191.

Binzel R. P., Xu S., Bus S. J., Skrutskie M. F., Meyer M. R., Knezek P. and Barker E. S. (1993) Discovery of a main-belt asteroid resembling ordinary chondrite meteorites. *Science* **262**, 1541-1543.

Binzel R. P., Bus S. J., Sunshine J., Burbine T. H., Neely A. W. and Brown R. W. (1995) Rotationally resolved spectra of asteroid 16 Psyche. *Icarus* **117**, 443-445.

Binzel R. P., Burbine T. H. and Bus S. J. (1996a) Groundbased reconnaissance of asteroid 253 Mathilde: Visible wavelength spectrum and meteorite comparison. *Icarus* **119**, 447-449.

Binzel R. P., Bus S. J., Burbine T. H. and Sunshine J. M. (1996b) Spectral properties of near-Earth asteroids: Evidence for sources of ordinary chondrite meteorites. *Science* **273**, 946-948.

Binzel R. P., Gaffey M. J., Thomas P. C., Zellner B. H., Storrs A. D. and Wells E. N. (1997) Geologic mapping of Vesta from 1994 Hubble Space Telescope images. *Icarus* **128**, 95-103.

Binzel R. P., Bus S. J. and Burbine T. H. (1998) Size dependence of asteroid spectral properties: SMASS results for near-Earth and main-belt asteroids (abstract). *Lunar Planet. Sci.* **XXIX**, Abstract #1222.

Boesenberg J. S., Prinz M., Weisberg M. K., Davis A. M., Clayton R. N., Mayeda T. K. and Wasson J. T. (1995) Pyroxene pallasites: A new pallasite grouplet (abstract). *Meteoritics* **30**, 488-489.

Bottke W. F. Jr., Rubincam D. P. and Burns J. A. (1999) Delivery of meteoroids from 6 Hebe via Yarkovsky thermal drag (abstract). *Lunar Planet. Sci.* **XXX**, Abstract #1504.

Bowell E., Hapke B., Domingue D., Lumme K., Peltoniemi J. and Harris A. W. (1989) Application of photometric models to asteroids. In *Asteroids II* (R. P. Binzel, T. Gehrels and M. S. Matthews, Eds.), pp. 524-556. University of Arizona Press, Tucson, Arizona.

Brearley A. J. (1995) Aqueous alteration and brecciation in Bells, an unusual, saponite-bearing, CM chondrite. *Geochim. Cosmochim. Acta* **59**, 2291-2317.

Brearley A. J. and Jones R. H. (1998) Chondritic meteorites. In *Reviews in Mineralogy, Vol. 36, Planetary Materials* (J. J. Papike, Ed.), pp. (3-1)-(3-398). Mineralogical Society of America, Washington, DC.

Britt D. T. and Pieters C. M. (1988) Bidirectional reflectance properties of iron-nickel meteorites. *Proc. Lunar Planet Sci. Conf.* **18th**, 503-512.

Britt D. T. and Pieters C. M. (1989) Bidirectional reflectance characteristics of black chondrite meteorites (abstract). *Lunar Planet. Sci.* **XX**, 109-110.

Britt D. T. and Pieters C. M. (1991) Black ordinary chondrites: An analysis of abundance and fall frequency. *Meteoritics* **26**, 279-285.

Britt D. T., Tholen D. J., Bell J. F. and Pieters C. M. (1992) Comparison of asteroid and meteorite spectra: Classification by principal component analysis. *Icarus* **99**, 153-166.

Browning L. B., McSween H. Y. Jr. and Zolensky M. E. (1996) Correlated alteration effects in CM carbonaceous chondrites. *Geochim. Cosmochim. Acta* **60**, 2621-2633.

Buchanan P.C., Lindstrom D. J., Mittlefehldt D.W., Koeberl C. and Reimold W.U. (2000) The South African polymict eucrite Macibini. Submitted to *Meteoritics & Planetary Science*.

Buchwald V. F. (1975) *Handbook of Iron Meteorites.* University of California Press, Berkeley and Los Angeles, California. 1418 pp.

Burbine T. H. Jr. (1991) Principal component analysis of asteroid and meteorite spectra from 0.3 to 2.5 μm. M.S. Thesis, University of Pittsburgh. 155 pp.

Burbine T. H. (1998) Could G-class asteroids be the parent bodies of the CM chondrites? *Meteoritics & Planetary Science* **33**, 253-258.

Burbine T. H. and Binzel R. P. (1997) SMASSIR measurements of Vesta chips: Evidence for weathering? (abstract). *Bull. Am. Astron. Soc.* **29**, 964.

Burbine T. H., Meibom A. and Binzel R. P. (1996) Mantle material in the main belt: Battered to bits? *Meteoritics & Planetary Science* **31**, 607-620.

Burbine T. H., Binzel R. P and Bus S. J. (1998) Is Vesta the parent body of the "Vesta Chips"? Yes. (abstract). *Lunar Planet. Sci.* **XXIX**, Abstract #1459.

Burns J. A., Bottke W. F. and Rubincam D. P. (1999) Yarkovsky effect plus planetary perturbations ⇒ Tortuous meteoroid paths (abstract). *Bull. Am. Astron. Soc.* **31**, 1111.

Burns R. G. (1970) Crystal field spectra and evidence of cation ordering in olivine minerals. *Am. Min.* **55**, 1608-1631.

Burns R. G. (1993a) *Mineralogical Applications of Crystal Field Theory* (2nd Ed.). Cambridge University Press, Cambridge, England. 551 pp.

Burns R. G. (1993b) Origin of electronic spectra of minerals in the visible to near-infrared region. In *Remote Geochemical Analysis: Elemental and Mineralogical Composition* (C. M. Pieters and P. A. J. Englert, Eds.), pp. 3-29. Cambridge University Press, New York, New York.

Bus S. J. (1999) Compositional structure in the asteroid belt: Results of a spectroscopic survey. Ph.D. Thesis, Massachusetts Institute of Technology. 367 pp.

Buseck P. R. (1977) Pallasite meteorites-mineralogy, petrology, and geochemistry. *Geochim. Cosmochim. Acta* **41**, 711-740.

Buseck P. R. and Hua X. (1993) Matrices of carbonaceous chondrite meteorites. In *Ann. Rev. Earth Planet Sci.* **22**, 457-497. Annual Reviews Inc., Palo Alto, California.

Calvin W. M. and King T. V. V. (1997) Spectral characteristics of iron-bearing phyllosilicates: Comparison to Orgueil (CI1), Murchison and Murray (CM2). *Meteoritics & Planetary Science* **32**, 693-701.

Campins H. and Swindle T. D. (1998) Expected characteristics of cometary meteorites. *Meteoritics & Planetary Science* **33**, 1201-1212.

Casanova I., Graf T. and Marti K. (1995) Discovery of an unmelted H-chondrite inclusion in an iron meteorite. *Science* **268**, 540-542.

Cassidy W. A. and Harvey R. P. (1991) Are there real differences between Antarctic finds and modern falls meteorites? *Geochim. Cosmochim. Acta* **55**, 99-104.

Catalog of the Antarctic Meteorites (1995) National Institute of Polar Research, Tokyo, Japan. 230 pp.

Chambers J. (1999) Clearing planetary embryos from the asteroid belt (abstract). *Asteroids. Comets and Meteors*, 101.

Chapman C. R. (1974) Asteroid size distribution: Implications for the origin of stony-iron and iron meteorites. *Geophys. Res. Lett.* **1**, 341-344.

Chapman C. R. (1976) Asteroids as meteoritic parent-bodies: The astronomical perspective. *Geochim. Cosmochim. Acta* **40**, 701-719.

Chapman C. R. (1986) Implications of the inferred compositions of the asteroids for their collisional evolution. *Mem. Soc. Astron. Italiana* **57**, 103-114.

Chapman C. R. (1996) S-type asteroids, ordinary chondrites, and space weathering: The evidence from *Galileo*'s fly-bys of Gaspra and Ida. *Meteoritics & Planetary Science* **31**, 699-725.

Chapman C. R. and Davis D. R. (1975) Asteroid collisional evolution: Evidence for a much larger early population. *Science* **190**, 553-556.

Chapman C. R. and Gaffey M. J. (1979a) Reflectance spectra for 277 asteroids. In *Asteroids* (T. Gehrels and M. S. Matthews, Eds.), pp. 655-687, Univ. Arizona Press, Tucson, Arizona.

Chapman C. R. and Gaffey M. J. (1979b) Spectral reflectances of the asteroids. In *Asteroids* (T. Gehrels and M. S. Matthews, Eds.), pp. 1064-1089, Univ. Arizona Press, Tucson, Arizona.

Chapman C. R. and Greenberg R. (1981) Meteorites from the asteroid belt: The stony-iron connection (abstract). *Lunar Plan. Sci.* **XII**, 129-131.

Chapman C. R. and Salisbury J. W. (1973) Comparisons of meteorite and asteroid spectral reflectivities. *Icarus* **19**, 507-522.

Chapman C. R., Veverka J., Thomas P. C., Klaasen K., Belton M. J. S., Harch A., McEwen A., Johnson T. V., Helfenstein P., Davies M. E., Merline W. J. and Denk T. (1995) Discovery and physical properties of Dactyl, a satellite of asteroid 243 Ida. *Nature* **374**, 783-785.

Choi B-G., Ouyang X. and Wasson J. T. (1995) Classification and origin of IAB and IIICD iron meteorites. *Geochim. Cosmochim. Acta* **59**, 593-612.

Christophe Michel-Levy M., Bourot-Denise M., Palme H., Spettel B. and Wänke H. (1987) L'eucrite de Bouvante: Chimie pétrologie et minéralogie. *Bull. Minéral.* **110**, 449-458.

Clark B. E. (1995) Spectral mixing models of S-type asteroids. *J. Geophys. Res.* **100**, 14443-14456.

Clark B. E., Bell J. F., Fanale F. P. and O'Connor D. J. (1995) Results of the seven-color asteroid survey: Infrared spectral observations of ~50-km size S-, K-, and M-type asteroids. *Icarus* **113**, 387-402.

Clark B. E., Veverka J., Helfenstein P., Thomas P. C., Bell J. F. III, Harch A., Robinson M. S., Murchie S. L., McFadden L. and Chapman C. R. (1999) NEAR photometry of asteroid 253 Mathilde. *Icarus* **140**, 53-65.

Clark R. N., Swayze G. A., Gallagher A. J., King T.V.V. and Calvin W. M. (1993) The U. S. Geological Survey, Digital Spectral Library: Version 1: 0.2 to 3.0 microns. *U.S. Geological Survey Open File Report 93-592*. 1340 pp.

Clark R. N. (1999) Spectroscopy of rocks and minerals and principles of spectroscopy. *Remote Sensing for the Earth Sciences (Manual of Remote Sensing)* (Ed., A. N. Rencz), Third Edition, Vol. **3**), pp. 3-58. John Wiley & Sons, Inc., New York, New York. 672 pp.

Clayton R. N. and Mayeda T. K. (1978) Genetic relations between iron and stony meteorites. *Earth Planet. Sci. Lett.* **40**, 168-174.

Clayton R. N., Mayeda T. K., Prinz M., Nehru C. E. and Delaney J. S. (1986) Oxygen isotope confirmation of a genetic association between achondrites and IIIAB iron meteorites (abstract). *Lunar Plan. Sci.* **XVII**, 141-142.

Cloutis E. A. and Gaffey M. J. (1993a) Accessory phases in aubrites: Spectral properties and implications for asteroid 44 Nysa. *Earth, Moon, and Planets* **63**, 227-243.

Cloutis E. A. and Gaffey M. J. (1993b) The constituent minerals in calcium-aluminum inclusions: Spectral reflectance properties and implications for CO carbonaceous chondrites and asteroids. *Icarus* **105**, 568-579.

Cloutis E., Gaffey M. J., Jackowski T. L. and Reed K. L. (1986) Calibration of phase abundance, composition, and particle size distribution for olivine-orthopyroxene mixtures from reflectance spectra. *J. Geophys. Res.* **91**, 11641-11653.

Cloutis E. A., Gaffey M. J., Smith D. G. W. and Lambert R. St. J. (1990a) Metal silicate mixtures: Spectral properties and applications to asteroid taxonomy. *J. Geophys. Res.* **95**, 8323-8338.

Cloutis E. A., Gaffey M. J., Smith D. G. W. and Lambert R. St. J. (1990b) Reflectance spectra of mafic silicate-opaque assemblages with applications to meteorite spectra. *Icarus* **84**, 315-333.

Consolmagno G. J. and Britt D. T. (1998) The density and porosity of meteorites from the Vatican collection. *Meteoritics & Planetary Science* **33**, 1231-1241.

Consolmagno G. J. and Drake M. J. (1977) Composition and evolution of the eucrite parent body: Evidence from rare earth elements. *Geochim. Cosmochim. Acta* **41**, 1271-1282.

Crabb J. and Schultz L. (1981) Cosmic-ray exposure ages of the ordinary chondrites and their significance for parent body stratigraphy. *Geochim. Cosmochim. Acta* **45**, 2151-2160.

Crozaz G. and Pellas P. (1983) Where does Brachina come from? (abstract). *Lunar Plan. Sci.* **XIV**, 142-143.

Cruikshank D. P. and Hartmann W. K. (1984) The meteorite-asteroid connection: Two olivine-rich asteroids. *Science* **223**, 281-283.

Cruikshank D. P., Tholen D. J., Hartmann W. K., Bell J. F. and Brown R. H. (1991) Three basaltic earth-approaching asteroids and the source of the basaltic meteorites. *Icarus* **89**, 1-13.

Davis A. M. and Olsen E. J. (1991) Phosphates in pallasite meteorites as probes of mantle processes in small planetary bodies. *Nature* **353**, 637-640.

Davis D. R., Chapman C. R., Greenberg R. and Weidenschilling S. J. (1985) Collisional history of asteroids: Evidence from Vesta and the Hirayama families. *Icarus* **62**, 30-53.

Davis D. R., Weidenschilling S. J., Farinella P., Paolicchi P. and Binzel R. P. (1989) Asteroid collisional history: Effects on sizes and spins. In *Asteroids II* (R. P. Binzel, T. Gehrels and M. S. Matthews, Eds.), pp. 805-826. University of Arizona Press, Tucson, Arizona.

Davis D. R., Ryan E. V. and Farinella P. (1994) Asteroid collisional evolution: Results from current scaling algorithms. *Planet. Space Sci.* **42**, 599-610.

Davis D. R., Farinella P. and Marzari F. (1999) The missing Psyche family: Collisionally eroded or never formed? *Icarus* **137**, 140-151.

Delaney J. S., O'Neill C. and Prinz M. (1984) Two magma types in the eucrite Bouvante (abstract). *Lunar Plan. Sci.* **XV**, 210-211.

Di Martino M., Migliorini F., Cellino A. and Zappalá V. (1997) Can CO/CV meteorites come from the Eos family? (abstract). *Meteoritics & Planetary Science* **32 (suppl.)**, A35.

Dodd R. T. (1981) *Meteorites, A Petrologic-Chemical Synthesis*. Cambridge University Press, Cambridge, England. 368 pp.

Dohnanyi J. S. (1969) Collisional model of asteroids and their debris. *J. Geophys. Res.* **74**, 2531-2554.

Dohnanyi J. S. (1971) Fragmentation and distribution of asteroids. In *Physical Studies of Minor Planets* (T. Gehrels, Ed.), NASA SP-267, pp. 263-295.

Doressoundiram A., Barucci M. A., Fulchignoni M. and Florczak M. (1998) Eos family: A spectroscopic study. *Icarus* **131**, 15-31.

Ephemerides of Minor Planets (1999) Institute for Theoretical Astronomy, St. Petersburg, Russia. 800 pp.

Eugster O., Eberhardt P., Thalmann Ch. and Weigel A. (1998) Neon-E in CM-2 chondrite LEW90500 and collisional history of CM-2 chondrites, Maralinga, and other CK chondrites. *Geochim. Cosmochim. Acta* **62**, 2573-2582.

Farinella P. and Davis D. R. (1992) Collision rates and impact velocities in the main asteroid belt. *Icarus* **97**, 111-123.

Farinella P. and Vokrouhlicky D. (1999) Semimajor axis mobility of asteroidal fragments. *Science* **283**, 507-510.

Farinella P., Davis D. R., Cellino A. and Zappalà V. (1992) The collisional lifetime of asteroid 951 Gaspra. *Astron. Astrophys.* **257**, 329-330.

Farinella P., Gonczi R., Froeschlé Ch. and Froeschlé C. (1993) The injection of asteroid fragments into resonances. *Icarus* **101**, 174-187.

Farinella P., Vokrouhilicky D. and Hartmann W. K. (1998) Meteorite delivery via Yarkovsky orbital drift. *Icarus* **132**, 378-387.

Feierberg M. A., Larson H. P., Fink U. and Smith H. A. (1980) Spectroscopic evidence for two achondrite parent bodies: 349 Dembowska and 4 Vesta. *Geochim. Cosmochim. Acta* **45**, 971-981.

Feierberg M. A., Lebofsky L. A. and Larson H. P. (1981) Spectroscopic evidence for aqueous alteration products on the surfaces of low-albedo asteroids. *Geochim. Cosmochim. Acta* **44**, 513-524.

Feierberg M. A., Larson H. P. and Chapman C. R. (1982) Spectroscopic evidence for undifferentiated S-type asteroids. *Ap. J.* **257**, 361-372.

Floran R. J. (1978) Silicate petrography, classification, and origin of the mesosiderites: Review and new observations. *Proc. Lunar Planet Sci. Conf.* **9th**, 1053-1081.

Fornasier S., Lazzarin M., Barbieri C. and Barucci M. A. (1999) Spectroscopic comparison of aqueous altered asteroids with CM2 carbonaceous chondrite meteorites. *Astron. Astrophys. Suppl. Ser.* **135**, 65-73.

Gaffey M. J. (1974) A systematic study of the spectral reflectivity characteristics of the meteorite classes with applications to the interpretation of asteroid spectra for mineralogical and petrological information. Ph.D. Thesis, Massachusetts Institute of Technology. 355 pp.

Gaffey M. J. (1976) Spectral reflectance characteristics of the meteorite classes. *J. Geophys. Res.* **81**, 905-920.

Gaffey M. J. (1978) Mineralogical characterizations of asteroid surface materials: Evidence for unsampled types (abstract). *Meteoritics* **13**, 471-473.

Gaffey M. J. (1984) Rotational spectral variations if asteroid (8) Flora: I lications for the nature of the S-type asteroids and for the parent bodies of the ordinary chondrites. *Icarus* **60**, 83-114.

Gaffey M. J. (1986) The spectral and physical properties of metal in meteorite assemblages: Implications for asteroid surface materials. *Icarus* **66**, 468-486.

Gaffey M. J. (1996) Spectral identification of asteroid 6 Hebe as the main-belt parent body of the H-type ordinary chondrites (abstract). *Meteoritics & Planetary Science* **31 (suppl.)**, A47.

Gaffey M. J. (1997) Surface lithologic heterogeneity of asteroid 4 Vesta. *Icarus* **127**, 130-157.

Gaffey M. J. (1999a) Improving methodologies for quantitative interpretation of S(IV)/OC type asteroidal spectra with applications for the NEAR Eros mission (abstract). *Lunar Planet. Sci.* **XXX**, Abstract #1375.

Gaffey M. J. (1999b) Progress in the search for ordinary chondrite parent bodies in the asteroid belt (abstract). *Asteroids, Comets and Meteors*, 45.

Gaffey M. J. and Gilbert S. L. (1998) Asteroid 6 Hebe: The probable parent body of the H-type ordinary chondrites and the IIE iron meteorites. *Meteoritics & Planetary Science* **33**, 1281-1296.

Gaffey M. J., Bell J. F. and Cruikshank D. P. (1989) Reflectance spectroscopy and asteroid surface mineralogy. In *Asteroids II* (R. P. Binzel, T. Gehrels and M. S. Matthews, Eds.), pp. 98-127. University of Arizona Press, Tucson, Arizona.

Gaffey M. J., Reed K. L. and Kelley M. S. (1992) Relationship of E-type Apollo asteroid 3103 (1982 BB) to the enstatite achondrite meteorites and the Hungaria asteroids. *Icarus* **100**, 95-109.

Gaffey M. J., Bell J. F., Brown R. H., Burbine T. H., Piatek J. L., Reed K. L. and Chaky D. A. (1993) Mineralogical variations within the S-type asteroid class. *Icarus* **106**, 573-602.

Gil-Hutton R. and Brunini A. (1999) Collisional evolution of the early asteroid belt. *Planet. Space Sci.* **47**, 331-338.

Gladman B. J., Migliorini F., Morbidelli A., Zappalà V., Michel P., Cellino A., Froeschlé C., Levison H. F., Bailey M. E. and Duncan M. (1997) Dynamical lifetimes of objects injected into asteroid belt resonances. *Science* **277**, 197-201.

Goldstein R.M. (1981) Radar observations of Apollo. *Icarus* **48**, 59-61.

Goodrich C. A. (1992) Ureilites: A critical review. *Meteoritics* **27**, 327-352.

Goodrich C. A., Jones J. H. and Berkeley J. L. (1987) Origin and evolution of the ureilite parent magmas: Multi-stage igneous activity on a large parent body. *Geochim. Cosmochim. Acta* **51**, 2255-2273.

Gradie J. and Tedesco E. (1982) Compositional structure of the asteroid belt. *Science* **216**, 1405-1407.

Gradie J. C., Chapman C. R. and Tedesco E. F. (1989) Distribution of taxonomic classes and the compositional structure of the asteroid belt. In *Asteroids II* (R. P. Binzel, T. Gehrels and M. S. Matthews, Eds.), pp. 316-335. University of Arizona Press, Tucson, Arizona.

Grady M. M. (1995) Parental paradoxes. *Nature* **378**, 18-19.

Graf Th. And Marti K. (1992a) Cosmic-ray exposure history of enstatite meteorites (abstract). *Meteoritics* **27**, 227.

Graf Th. And Marti K. (1992b) On the delivery of meteorites and near-Earth asteroids (abstract). *Lunar Plan. Sci.* **XXIII**, 433-434.

Granahan J. C. (1993) Investigations of asteroid family geology. Ph.D. Thesis, Univ. Hawaii, Honolulu. 187 pp.

Granahan J. C. and Bell J. F. (1991) On the geologic reality of asteroid families (abstract). *Lunar Plan. Sci.* **XXII**, 477-478.

Greenberg R. and Chapman C. R. (1983) Asteroids and meteorites: Parent bodies and delivered samples. *Icarus* **55**, 455-481.

Greenberg R. and Nolan M. C. (1989) Delivery of asteroids and meteorites to the inner solar system. In *Asteroids II* (R. P. Binzel, T. Gehrels and M. S. Matthews, Eds.), pp. 778-804. University of Arizona Press, Tucson, Arizona.

Grimm R. E. and McSween H. Y. Jr. (1993) Heliocentric zoning of the asteroid belt by aluminum-26 heating. *Science* **259**, 653-655.

Grossman J. N. (1994) The Meteoritical Bulletin, No. 76, 1994 January: The U.S. Antarctic meteorite collection. *Meteoritics* **29**, 100-143.

Grove T. L. and Bartels K. S. (1992) The relation between diogenite cumulates and eucrite magmas. *Proc. Lunar Planet. Sci. Conf.* **22nd**, 437-445.

Haack H., Rasmussen K. L. and Warren P. H. (1990) Effects of regolith/megaregolith insulation on the cooling histories of differentiated asteroids. *J. Geophys. Res.* **95**, 5111-5124.

Hammergren M. (1998) The composition of near-Earth objects. Ph.D. Thesis, University of Washington. 109 pp.

Hanowski N. P. and Brearley A. J. (1997) Chondrule serpentinites as indicators of aqueous alteration in CM carbonaceous chondrites (abstract). *Lunar Planet. Sci.* **XXVIII**, 501-502.

Hapke B. W. (1981) Bidirectional reflectance spectroscopy 1. Theory. *J. Geophys. Res.* **86**, 3039-3054.

Harris A. W., Davies J. K. and Green S. F. (1998) Thermal infrared spectrophotometry of the near-Earth asteroids 2100 Ra-Shalom and 1991 EE. *Icarus* **135**, 441-450.

Hartmann W. K., Farinella P., Vokrouhlicky D., Weidenschilling S. J., Morbidelli A., Marzari F., Davis D. R. and Ryan E. (1999) Reviewing the Yarkovsky effect: New light on the delivery of stone and iron meteorites from the asteroid belt. *Meteoritics & Planetary Science* **34 (suppl.)**, A161-A167.

Hassanzadeh J., Rubin A. E. and Wasson J. T. (1990) Compositions of large metal nodules in mesosiderites: Links to iron meteorite group IIIAB and the origin of mesosiderite subgroups. *Geochim. Cosmochim. Acta* **54**, 3197-3208.

Hayes D. S. and Latham D. W. (1975) A rediscussion of the atmospheric extinction and the absolute spectral-energy distribution of Vega. *Astrophys. J.* **197**, 593-601.

Hewins R. H. and Newsom H. E. (1988) Igneous activities in the early solar system. In *Meteorites and the Early Solar System* (J. F. Kerridge and M. S. Matthews, Eds.), pp. 73-101. University of Arizona Press, Tucson, Arizona.

Hilton J. L. (1999) US Naval observatory ephemerides of the largest asteroids. *Astron. J.* **117**, 1077-1086.

Hinrichs J. L., Lucey P. G., Robinson M. S., Meibom A. and Krot A. N. (1999) Implications of temperature-dependent near-IR spectral properties of common minerals and meteorites for remote sensing of asteroids. *Geophys. Res. Lett.* **26**, 1661-1664.

Hiroi T. and Pieters C. M. (1997) Origin of Vestoids suggested from their space weathering trend (abstract). *Bull. Am. Astron. Soc.* **29**, 973.

Hiroi T. and Pieters C. M. (1998) Origin of Vestoids suggested from the space weathering trend in the visible reflectance spectra of HED meteorites and lunar soils. *Antarct. Met. Res.* **11**, 165-172.

Hiroi T. and Sasaki S. (2000) Compositional dependency of space weathering on the S/A/R/V asteroids. Submitted to *Meteoritics & Planetary Science.*

Hiroi T. and Takeda H. (1991) Reflectance spectroscopy and mineralogy of primitive achondrites-lodranites. *Proc. NIPR Symp. Antarct. Meteorites* **4**, 163-177.

Hiroi T., Bell J. F., Takeda H. and Pieters C. M. (1993a) Modeling of S-type asteroid spectra using primitive achondrites and iron meteorites. *Icarus* **102**, 107-116.

Hiroi T., Bell J. F., Takeda H. and Pieters C. M. (1993b) Spectral comparison between olivine-rich asteroids and pallasites. *Proc. NIPR Symp. Antarct. Meteorites* **6**, 234-245.

Hiroi T., Pieters C. M., Zolensky M. E. and Lipschutz M. E. (1993c) Evidence of thermal metamorphism on the C, G, B, and F asteroids. *Science* **261**, 1016-1018.

Hiroi T., Pieters C. M. and Takeda H. (1994) Grain size of the surface regolith of asteroid 4 Vesta estimated from its reflectance spectrum in comparison with HED meteorites. *Meteoritics* **29**, 394-396.

Hiroi T., Binzel R. P., Sunshine J. M., Pieters C. M and Takeda H. (1995) Grain sizes and mineral compositions of surface regoliths of Vesta-like asteroids. *Icarus* **115**, 374-386.

Hiroi T., Zolensky M. E., Pieters C. M. and Lipschutz M. E. (1996) Thermal metamorphism of the C, G, B, and F asteroids seen from the 0.7 μm, 3 μm, and UV absorption strengths in comparison with carbonaceous chondrites. *Meteoritics & Planetary Science* **31**, 321-327.

Howell E. S. (1995) Probing asteroid composition using visible and near-infrared spectroscopy. Ph.D. Thesis, Univ. Arizona, Tucson. 186 pp.

Howell E. S., Merényi E. and Lebofsky L. A. (1994) Classification of asteroids using a neural network. *J. Geophys. Res.* **99**, 10847-10865.

Johnson T. V. and Fanale F. P. (1973) Optical properties of carbonaceous chondrites and their relationship to asteroids. *J. Geophys. Res.* **78**, 8507-8518.

Jones J. H. and Drake M. J. (1983) Experimental investigations of trace element fractionation in iron meteorites, II. The influence of sulfur. *Geochim. Cosmochim. Acta* **47**, 1199-1209.

Jones J. H. and Malvin D. J. (1990) A nonmetal interaction model for the segregation of trace metals during solidification of Fe-Ni-S, Fe-Ni-P, and Fe-Ni-S-P alloys. *Metall. Trans. B.* **21B**, 697-706.

Jones T. D. (1988) An infrared reflectance study of water in outer belt asteroids: Clues to composition and origin. Ph.D. Thesis, Univ. of Arizona, 281 pp.

Jones T. D., Lebofsky L. A., Lewis J. S. and Marley M. S. (1990) The composition and origin of the C, P, and D asteroids: Water as a tracer of thermal evolution in the outer belt. *Icarus* **88**,172-192.

Kargel J. S. (1994) Metalliferous asteroids as potential sources of precious metals. *J. Geophys. Res.* **99**, 21129-21141.

Keil K., Haack H. and Scott E. R. D. (1994) Catastrophic fragmentation of asteroids: Evidence from meteorites. *Planet. Space Sci.* **42**, 1109-1122.

Kelley M. S. (1999) Genetic studies of the members of small dynamical asteroid families. Ph.D. Thesis, Rensselaer Polytechnic Institute. 72 pp.

Kimura M. and Ikeda Y. (1995) Anhydrous alteration of Allende chondrules in the solar nebula II: Alkali-Ca exchange reactions and formation of nepheline, sodalite and Ca-rich phases in chondrules. *Proc. NIPR Symp. Antarct. Meteorites* **8**, 123-138.

King T. V. V. (1986) Contributions toward a quantitative understanding of reflectance spectroscopy: Phyllosilicates, olivine, and shocked materials. Ph.D. Thesis, Univ. of Hawaii, 230 pp.

King T. V. V. and Clark R. N. (1989) Spectral characteristics of chlorites and Mg-serpentines using high-resolution reflectance spectroscopy. *J. Geophys. Res.* **94**, 13997-14008.

King T. V. V. and Clark R. N. (1997) The presence of a single absorption feature: What it does and doesn't imply (abstract). *Lunar Planet. Sci.* **XXVIII**, 727-728.

King T. V. V. and Ridley W. I. (1987) Relation of the spectroscopic reflectance of olivine to mineral chemistry and some remote sensing implications. *J. Geophys. Res.* **92**, 11457-11469.

King T. V. V., Clark R. N., Calvin W. M., Sherman D. M. and Brown R. H. (1992) Evidence for ammonium-bearing minerals on Ceres. *Science* **255**, 1551-1553.

Kitts K. and Lodders K. (1998) Survey and evaluation of eucrite bulk compositions. *Meteoritics & Planetary Science* **31 (suppl.)**, A197-A213.

Klein C. and Hurlbut C. S. Jr. (1993) *Manual of Mineralogy* (21th Ed.). John Wiley & Sons, Inc. New York, New York. 681 pp.

Knezevic Z. and Milani A. (1994) Asteroid proper elements: The big picture. In *Asteroids, Comets, Meteors 1993*. (A. Milani, M. Di Martino and A. Cellino, Eds.), pp. 143-158. Kluwer Academic Publishers, Dordrecht, Netherlands.

Kracher A. and Wasson J. T. (1982) The role of S in the evolution of the parental cores of the iron meteorites. *Geochim. Cosmochim. Acta* **46**, 2419-2426.

Kring D. A., Hill D. H., Gleason J. D., Britt D. T., Consolmagno G. J., Farmer M., Wilson S. and Haag R. (1999) Portales Valley: A meteoritic sample of the brecciated and metal-veined floor of an impact crater on an H-chondrite asteroid. *Meteoritics & Planetary Science* **34**, 663-669.

Krisciunas K., Sinton W., Tholen D., Tokunaga A., Golisch W., Griep D., Kaminski C., Impey C. and Christian C. (1987) Atmospheric extinction and night-sky brightness at Mauna Kea. *Pub. Astron. Soc. Pac.* **99**, 887-894.

Krot A. N., Petaev M. I., Scott E. R. D., Choi B-G., Zolensky M. E. and Keil K. (1998) Progressive alteration in CV3 chondrites: More evidence for asteroidal alteration. *Meteoritics & Planetary Science* **33**, 1065-1085.

Landolt A. U. (1973) UBV photometric sequences in the celestial equatorial selected areas 92-115. *Astron. J.* **87**, 959-1020.

Larson H. P. and Fink U. (1975) Infrared spectral observations of asteroid 4 Vesta. *Icarus* **26**, 420-427.

Lazzaro D., Michtchenko T., Carvano J. M. and Florczak M. (1999) A V-type asteroid at 3AU? (abstract). *Asteroids, Comets and Meteors*, 57.

Lebofsky L. A., Feierberg M. A., Tokunaga A. T., Larson H. P. and Johnson J. R. (1981a) The 1.7- to 4.2-μm spectrum of asteroid 1 Ceres: Evidence for structural water in clay minerals. *Icarus* **48**, 453-459.

Lebofsky L. A., Veeder G. J., Rieke G. H., Lebofsky M. T. Matson D. L., Kowal C., Wynn-Williams C. G. and Becklin E. E.(1981b) The albedo and diameter of 1862 Apollo. *Icarus* **48**, 335-338.

Lee T., Papanastassiou D. A. and Wasserburg G. J. (1976) Demonstration of ^{26}Mg excess in Allende and evidence for ^{26}Al. *Geophys. Res. Lett.* **3**, 109-112.

Lindstrom M. M. and Score R. (1994) Populations, pairing and rare meteorites in the U.S. Antarctic meteorite collection (abstract). *Workshop on Meteorites from Hot and Cold Deserts* (LPI Tech. Rept. 95-02), 43-45.

Lipschutz M. E., Zolensky M. E. and Bell M. S. (1999) New petrographic and trace element data on thermally metamorphosed carbonaceous chondrites. *Antarct. Met. Res.* **12**, 57-80.

Lodders K. and Osborne R. (1999) Perspectives on the comet-asteroid-meteorite link. In *The Composition and Origin of Cometary Materials* (K. Altwegg, P. Ehrenfreund, J. Geiss and W. Huebner, Eds.), in press. Kluwer Academic Publishers, Dordrecht, Netherlands.

Love S. G. and Ahrens T. J. (1996) Catastrophic impacts on gravity dominated asteroids. *Icarus* **124**, 141-155.

Love S. G. and Keil K. (1995) Recognizing mercurian meteorites. *Meteoritics & Planetary Science* **30**, 269-278.

Lucey P. G., Keil K. and Whitely R. (1998) The influence of temperature on the spectra of the A-asteroids and implications for their silicate chemistry. *J. Geophys. Res.* **103**, 5865-5871.

Lupishko D. F. and Belskaya I. N. (1989) On the surface composition of the M-type asteroids. *Icarus* **78**, 395-401.

Marti K. and Graf T. (1992) Cosmic-ray exposure history of ordinary chondrites. *Ann. Rev. Earth Planet. Sci.* **20**, 221-243.

Marzari F., Cellino A., Davis D. R., Farinella P., Zappalà V. and Vanzani V. (1996) Origin and evolution of the Vesta asteroid family. *Astron. Astrophys.* **316**, 248-262.

Marzari F., Farinella P. and Davis D. R. (1999) Origin, aging, and death of asteroid families. *Icarus* **142**, 63-77.

McCord T. B., Adams J. B. and Johnson T. V. (1970) Asteroid Vesta: Spectral reflectivity and compositional implications. *Science* **168**, 1445-1447.

McFadden L. A., Gaffey M. J. and Takeda H. (1981) The layered crust model and the surface of Vesta (abstract). *Lunar Planet. Sci.* **XII**, 685-687.

McFadden L. A., Gaffey M. J. and McCord T. B. (1984) Mineralogical-petrological characterization of near-Earth asteroids. *Icarus* **59**, 25-40.

McFadden L. A., Gaffey M. J. and McCord T. B. (1985) Near-Earth asteroids: Possible sources from reflectance spectroscopy. *Science* **229**, 160-163.

McSween H. Y. Jr. (1977) Petrographic variations among carbonaceous chondrites of the Vigarano type. *Geochim. Cosmochim. Acta* **41**, 1777-1790.

McSween H. Y. Jr., Bennett M. E. III and Jarosewich E. (1991) The mineralogy of ordinary chondrites and implications for asteroid spectrophotometry. *Icarus* **90**, 107-116.

Meibom A. and Clark B. E. (1999) Evidence for the insignificance of ordinary chondritic material in the asteroid belt. *Meteoritics & Planetary Science* **34**, 7-24.

Mittlefehldt D. W. (1994) ALH84001, a cumulate orthopyroxenite member of the Martian meteorite clan. *Meteoritics* **29**, 214-221.

Mittlefehldt D. W., McCoy T. J., Goodrich C. A. and Kracher A. (1998) Non-chondritic meteorites from asteroidal bodies. In *Reviews in Mineralogy, Vol. 36, Planetary Materials* (J. J. Papike, Ed.), pp. (4-1)-(4-195). Mineralogical Society of America, Washington, DC.

Miyamoto M. and Zolensky M. E. (1994) Infrared diffuse reflectance spectra of carbonaceous chondrites: Amount of hydrous minerals. *Meteoritics* **29**, 849-853.

Morbidelli A., Zappalà V., Moons M., Cellino A. and Gonczi R. (1995) Asteroid families close to mean motion resonances: Dynamical effects and physical implications. *Icarus* **118**, 132-154.

Moroz L. V., Fisenko A. V., Semjonova L. F., Pieters C. M. and Korotaeva N. N. (1996) Optical effects of regolith processes on S-asteroids as simulated by laser shots on ordinary chondrite and other mafic materials. *Icarus* **122**, 366-382.

Moroz L., Schade U. and Wäsch R. (2000) Reflectance spectra of olivine-orthopyroxene-bearing assemblages at decreased temperatures for remote sensing of asteroids. Submitted to *Icarus*.

Morrison D. (1977) Asteroid sizes and albedos. *Icarus* **31**, 185-220.

Mottola S., Erikson A., Harris A. W., Hahn G., Neukum G., Buie M. W., Sears W. D., Harris A. W., Tholen D. J., Whitely R. J., Magnusson P., Pironen J., Kwiatowski T., Borczyk W., Howell E. S., Hicks M. D., Fevig R., Krugly Yu. N., Velichko F. P., Chiorny V. G., Gaftonyuk N. M., Di Martino M., Pravec P., Sarounová L., Wolf M., Worman W., Davies J. K., Schober H. –J. and Pych W. (1997) Physical model of near-earth asteroid 6489 Golevka (1991 JX) from optical and infrared observations. *Astron. J.* **114**, 1234-1245.

Namiki N. and Binzel R. P. (1991) The surface evolution of 951 Gaspra: A pre-Galileo estimate. *Geophys. Res. Lett.* **18**, 1155-1158.

Nehru C. E., Prinz M. and Zucker S. M. (1979) Brachina: Origin, melt inclusions and relationship to Chassigny (abstract). *Meteoritics* **14**, 493-494.

Nehru C. E., Prinz M., Delaney J. S., Dreibus G., Palme H., Spettel B. and Wänke H. (1983) Brachina: A new type of meteorite, not a chassignite. *J. Geophys. Res.* **88 (suppl.)**, B237-B244.

Nehru C. E., Prinz M., Weisberg M. K., Ebihara M. E., Clayton R. N. and Mayeda T. K. (1992) Brachinites: A new primitive achondrite group (abstract). *Meteoritics* **27**, 267.

Nesvorny D. and Morbidelli A. (1998) Three-body mean motion resonances and the chaotic structure of the asteroid belt. *Astron. J.* **116**, 3029-3027.

Newsom H. E. (1985) Molybdenum in eucrites: Evidence for a metal core in the eucrite parent body. *J. Geophys. Res.* **90 (suppl.)**, C613-C617.

Nishiizumi K., Elmore D. and Kubik P. W. (1989) Update on terrestrial ages of Antarctic meteorites. *Earth Planet. Sci. Lett.* **93**, 299-313.

Ostro S. J., Campbell D. J. and Shapiro I. I. (1983) Radar observations of asteroid 1685 Toro. *Astron. J.* **88**, 565-576.

Ostro S. J., Campbell D. J. and Shapiro I. I. (1985) Mainbelt asteroids: Dual-polarization radar observations. *Science* **229**, 442-446.

Ostro S. J., Campbell D. B., Chandler J. F., Hine A. A., Hudson R . S., Rosema K. D. and Shapiro I. I. (1991) Asteroid 1986 DA: Radar evidence for a metallic composition. *Science* **252**, 1399-1404.

Ott U., Löhr H. P. and Begemann F. (1985) Noble gases and the classification of Brachina. *Meteoritics* **20**, 69-78.

Ott U., Löhr H. P. and Begemann F. (1987) Noble gases in ALH 84025: Like Brachina, unlike Chassigny (abstract). *Meteoritics* **22**, 476-477.

Palme H. and Rammensee W. (1981) The significance of W in planetary differentiation processes: Evidence from new data on eucrites. *Proc. Lunar Planet. Sci.* **12th**, 949-964.

Petaev M. I., Barsukova L. D., Lipschutz M. E., Wang M.-S., Ariskin A. A., Clayton R. N. and Mayeda T. K. (1994) The Divnoe meteorite: Petrology, chemistry, oxygen isotopes and origin. *Meteoritics* **29**, 182-199.

Pieters C. M. (1999) Resolving the many mysteries of Martian soil: Lessons learned from Apollo (abstract). *Bull. Am. Astron. Soc.* **31**, 1166-1167.

Pieters C. M. and Binzel R. P. (1994) Young Vesta (regolith)? (abstract). *Lunar Planet. Sci.* **XXV**, 1083-1084.

Pieters C. M. and McFadden L. A. (1994) Meteorite and asteroid reflectance spectroscopy: Clues to the early solar system processes. *Ann. Rev. Earth Planet. Sci.* **22**, 457-497.

Pieters C. M., Fischer E. M., Rode O. and Basu A. (1993) Space weathering on meteorite parent bodies: Issues raised by new lunar soil analyses. *J. Geophys. Res.* **98**, 20817-20824.

Powell B. N. (1971) Petrology and chemistry of mesosiderites-II. Silicate textures and compositions and metal-silicate relationships. *Geochim. Cosmochim. Acta* **35**, 5-34.

Rajan S. and Gaffey M. J. (1984) Spectral reflectance characteristics of Allende white inclusions (abstract). *Lunar Planet. Sci.* **XV**, 284-285.

Rasmussen K. L., Ulff-Møller F. and Haack H. (1995) The thermal evolution of IVA iron meteorites: Evidence from metallographic cooling rates. *Geochim. Cosmochim. Acta* **59**, 3049-3059.

Reinsch C. H. (1967) Smoothing by spline functions. *Numer. Math.* **10**, 177-183.

Rivkin A. S., Howell E. S., Britt D. T., Lebofsky L. A., Nolan M. C. and Branston D. D. (1995) 3-μm spectrophotometric survey of M and E-class asteroids. *Icarus* **117**, 90-100.

Rivkin A.S., Clark B. E., Britt D. T. and Lebofsky L. A. (1997) Infrared spectrophotometry of the NEAR flyby target 253 Mathilde. *Icarus* **127**, 255-257.

Rivkin A. S., Trilling D. E. and Lebofsky L. A. (1998) Infrared (1.65-3.5 micrometers) observations of 387 Aquitania (abstract). *Bull. Am. Astron. Soc.* **30**, 1023

Rivkin A. S., Lebofsky L. A., Clark B. E., Howell E. S. and Britt D. T. (2000) The nature of M-class asteroids from 3-μm observations. Submitted to *Icarus*.

Roush T. L. and Singer R. B. (1987) Possible temperature variation effects on the interpretation of spatially resolved reflectance observations of asteroid surfaces. *Icarus* **69**, 571-574.

Rubin A. E. (1990) Kamacite and olivine in ordinary chondrites: Intergroup and intragroup relationships. *Geochim. Cosmochim. Acta* **54**, 1217-1232.

Rubin A. E. (1997) Mineralogy of meteorite groups. *Meteoritics & Planetary Science* **32**, 231-247.

Rubin A. E. and Mittlefehldt D. W. (1992) Classification of mafic clasts from mesosiderites: Implications for endogenous igneous processes. *Geochim. Cosmochim. Acta* **56**, 827-840.

Rubincam D. P. (1995) Asteroid orbit evolution due to thermal drag. *J. Geophys. Res.* **100**, 1585-1594.

Ruzicka A., Snyder G. A. and Taylor L. A. (1997) Vesta as the howardite, eucrite and diogenite parent body: Implications for the size of a core and for large-scale differentiation. *Meteoritics & Planetary Science* **32**, 825-840.

Sack R. O., Azeredo W. J. and Lipschutz M. E. (1991) Olivine diogenites: The mantle of the eucrite parent body. *Geochim. Cosmochim. Acta* **55**, 1111-1120.

Salisbury J. W. and Hunt G. R. (1974) Meteorite spectra and weathering. *J. Geophys. Res.* **98**, 4439-4441.

Salisbury J. W., D'Aria D. M. and Jarosewich E. (1991) Midinfrared (2.5-13.5 microns) reflectance spectra of powdered stony meteorites. *Icarus* **92**, 280-297.

Sato K., Miyamoto M. and Zolensky M. (1997) Absorption bands near three micrometers in diffuse reflectance spectra of carbonaceous chondrites: Comparison with asteroids. *Meteoritics & Planetary Science* **32**, 503-507.

Scherer P. and Schultz L. (2000) Noble gas record, collisional history and pairing of CV, CO, CK and other carbonaceous chondrites. *Meteoritics & Planetary Science* **35**, 145-153.

Scott E. R. D. (1972) Chemical fractionation in iron meteorites and its interpretation. *Geochim. Cosmochim. Acta* **36**, 1205-1236.

Scott E. R. D. (1977a) Formation of olivine-metal textures in pallasite meteorites. *Geochim. Cosmochim. Acta* **41**, 693-710.

Scott E. R. D. (1977b) Pallasites-metal composition, classification and relationships with iron meteorites. *Geochim. Cosmochim. Acta* **41**, 349-360.

Scott E. R. D. and Jones R. H. (1990) Disentangling nebular and asteroidal features of CO3 carbonaceous chondrite meteorites. *Geochim. Cosmochim. Acta* **54**, 2485-2502.

Scott E. R. D. and Wasson J. T. (1975) Classification and properties of iron meteorites. *Rev. Geophys. Space Phys.* **13**, 527-546.

Sears D. W. G. (1998) The case for rarity of chondrules and CAI in the early solar system and some implications for astrophysical models. *Astrophys. J.* **498**, 773-778.

Sears D. W. G. and Dodd R. T. (1988) Overview and classification of meteorites. In *Meteoritics and the Early Solar System* (eds. J. F. Kerridge and M. S. Matthews), pp. 3-31. Univ. Arizona Press, Tucson, Arizona.

Shukolyukov Y. A., Assonov S. S., Smoliar M. I. and Kolesnikov E. M. (1995) Noble gases and strontium isotopes in the unique meteorite Divnoe. *Meteoritics* **30**, 654-660.

Singer R. B. and Roush T. L. (1985) Effects of temperature on remotely sensed mineral absorption features. *J. Geophys. Res.* **90**, 12434-12444.

Srinivasan G., Goswami J. N. and Bhandari N. (1998) Search for extinct aluminum-26 in the Piplia Kalan eucrite (abstract). *Meteoritics & Planetary Science* **33 (suppl.)**, A148-A149.

Srinivasan G., Goswami J. N. and Bhandari N. (1999) ^{26}Al in eucrite Piplia Kalan: Plausible heat source and formation chronology. *Science* **284**, 1348-1350.

Storrs A., Weiss B., Zellner B., Burleson W., Sichitiu R., Wells E., Kowal C. and Tholen D. (1999) Imaging observations of asteroids with Hubble Space Telescope. *Icarus* **137**, 260-268.

Sunshine J. M. (1994) Inferring the composition of mafic lithologies from multi- and hyper-spectral data sets: Implications for remote sensing of terrestrial bodies. Ph.D. Thesis, Brown University. 186 pp.

Sunshine J. M. and Pieters C. M. (1998) Determining the composition of olivine from reflectance spectroscopy. *J. Geophys. Res.* **103**, 13675-13688.

Sunshine J. M., Binzel R. P., Burbine T. H. and Bus S. J. (1998) Is asteroid 289 Nenetta compositionally analogous to the Brachinite meteorites? (abstract). *Lunar Planet. Sci.* **XXIX**, Abstract #1430.

Takeda H. (1997) Mineralogical records of early planetary processes on the howardite, eucrite, diogenite parent body with references to Vesta. *Meteoritics & Planetary Science* **32**, 841-853.

Takeda H. and Graham A. L. (1991) Degree of equilibration of eucritic pyroxenes and thermal metamorphism of the earliest planetary crust. *Meteoritics* **26**, 129-134.

Takeda H., Mori H. and Ogata H. (1989) Mineralogy of augite-bearing ureilites and the origin of their chemical trends. *Meteoritics* **24**, 73-81.

Taylor G. J. (1992) Core formation in asteroids. *J. Geophys. Res.* **97**, 14717-14726.

Tedesco E. F. (1994) Asteroid albedos and diameters. *Asteroids, Comets and Meteors 1993* (Eds. A. Milani, M. DiMartino and A. Cellino), 205-222. Kluwer Academic Publishers, Netherlands.

Tedesco E. F. and Gradie J. (1987) Discovery of M class objects among the near-Earth asteroid population. *Astron. J.* **93**, 738-746.

Tholen D. J. (1984) Asteroid taxonomy from cluster analysis of photometry. Ph.D. Thesis, Univ. Arizona, Tucson. 150 pp.

Tholen D. J. (1989) Asteroid taxonomic classifications. In *Asteroids II* (R. P. Binzel, T. Gehrels and M. S. Matthews, Eds.), pp. 1139-1150. University of Arizona Press, Tucson, Arizona.

Thomas P. C., Binzel R. P., Gaffey M. J., Zellner B. H., Storrs A. D. and Wells E. N. (1997a) Vesta: Spin Pole, size, and shape from HST Images. *Icarus* **128**, 88-94.

Thomas P. C., Binzel R. P., Gaffey M. J., Storrs A. D., Welis E. N. and Zellner B. H. (1997b) Impact excavation on asteroid 4 Vesta: Hubble Space Telescope results. *Science* **277**, 1492-1495.

Tomeoka K., Kojima H. and Yanai K. (1989) Yamato-82162: A new kind of CI carbonaceous chondrite found in Antarctica. *Proc. NIPR Symp. Antarct. Meteorites* **2**, 36-54.

van Houten C. J., van Houten-Groeneveld I. and Gehrels T. (1970) Minor planets and related objects. V. The density of Trojans near the preceding Lagrangian point. *Astron. J.* **75**, 651-662.

Vaughn D. J. and Craig J. R. (1978) *Mineral Chemistry of Metal Sulfides*. Cambridge University Press, Cambridge, England. 493 pp.

Veeder G.J., Hanner M. S., Matson D. L., Tedesco E. F., Lebofksy L. A. and Tokunaga A. T. (1989) Radiometry of near-Earth asteroids. *Astron. J.* **97**, 1211-1219.

Veverka J., Helfenstein P., Lee P., Thomas P., McEwen A. S., Belton M., Klaasen K., Johnson T. V., Granahan J., Fanale F., Geissler P. and Head J. W. III (1996) Ida and Dactyl: Spectral reflectance and color variations. *Icarus* **120**, 66-76.

Veverka J., Thomas P., Harch A., Clark B., Bell J. F. III, Carcich B. and Joseph J., Murchie S., Izenberg N., Chapman C., Merline W., Malin M., McFadden L. and Robinson M. (1999) NEAR encounter with asteroid 253 Mathilde: Overview. *Icarus* **140**, 3-16.

Vilas F. (1994) A cheaper, faster, better way to detect water of hydration on solar system bodies. *Icarus* **111**, 456-467.

Vilas F. and Gaffey M. J. (1989) Phyllosilicate absorption features in main-belt and outer-belt asteroid reflectance spectra. *Science* **246**, 790-792.

Vilas F. and McFadden L. A. (1992) CCD reflectance spectra of selected asteroids. I. Presentation and data analysis considerations. *Icarus* **100**, 85-94.

Vilas F. and Sykes M. V. (1996) Are low-albedo asteroids thermally metamorphosed? *Icarus* **124**, 483-489.

Voshage H. and Feldman H. (1979) Investigations on cosmic-ray produced nuclides in iron meteorites, 3. Exposure ages, meteoroid sizes and sample depths determined by mass spectrometric analyses of potassium and rare gases. *Earth Planet. Sci. Lett.* **45**, 293-308.

Wadhwa M., Shukolyukov A., Davis A. M. and Lugmair G. W. (1999) Origin of silicate clasts in mesosiderites: Trace element microdistributions and Mn-Cr systematics tell the tale (abstract). *Lunar Planet. Sci.* **XXX**, Abstract #1707.

Wahl W. (1950) The statement of chemical analyses of stony meteorites and the interpretation of the analyses in terms of minerals. *Mineral. Mag.* **29**, 416-426.

Warren P. H. and Kallemeyn G. W. (1989) Allan Hills 84025: The second brachinite, far more differentiated than Brachina, and an ultramafic achondritic clast from L chondrite Yamato 75097. *Proc. Lunar Planet Sci. Conf.* **19th**, 475-486.

Wasson J. T. (1974) *Meteorites.* Springer-Verlag, New York, New York. 316 pp.

Wasson J. T. (1990) Ungrouped iron meteorites in Antarctica: Origin of anomalously high abundance. *Science* **249**, 900-902.

Wasson J. T. (1995) Sampling the asteroid belt: How biases make it difficult to establish meteorite-asteroid connections (abstract). *Meteoritics* **30**, 595.

Wasson J. T. and Rubin A. E. (1985) Formation of mesosiderites by low-velocity impacts as a natural consequence of planet formation. *Nature* **318**, 168-170.

Wasson J. T. and Wetherill G. W. (1967) The origin of iron meteorites (abstract). *Meteoritics* **3**, 134.

Wasson J. T., Chapman C. R., Grogan K. and Dermott S. F. (1996) Possible formation of the Vesta-like family asteroids and the main IRAS dust band by an oblique impact on Vesta (abstract). *Lunar Planet. Sci.* **XXVII**, 1387-1388.

Wasson J. T., Pieters C. M., Fisenko A. V., Semjonova L. F., Moroz L. V. and Warren P. H. (1997) Simulation of space weathering of HED meteorites by laser impulse irradiation (abstract). *Lunar Planet. Sci.* **XXVIII**, 1505-1506.

Wasson J. T., Lange D. E., Francis C. A. and Ulff-Møller F. (1999) Massive chromite in the Brenham pallasite and the fractionation of Cr during the crystallization of asteroidal cores. *Geochim. Cosmochim. Acta* **63**, 1219-1232.

Watters T. R. and Prinz M. (1979) Aubrites: Their origin and relationship to enstatite chondrites. *Proc. Lunar Planet. Sci. Conf.* **10th**, 1073-1093.

Weigel A., Eugster O., Koeberl C. and Krähenbühl U. (1996) Primitive differentiated achondrite Divnoe and its relationship to brachinites (abstract). *Lunar Planet. Sci.* **XXVII**, 1403-1404.

Weisberg M. K. and Prinz M. (1998) Fayalitic olivine in CV3 chondrite matrix and dark inclusions: A nebular origin. *Meteoritics & Planetary Science* **33**, 1087-1099.

Weisberg M. K., Prinz M., Clayton R. N., Mayeda T. K., Grady M. M., Franchi I., Pillinger C. T. and Kallemeyn G. K. (1996) The K (Kakangari) chondrite grouplet. *Geochim. Cosmochim. Acta* **60**, 4253-4263.

Weisberg M. K., Prinz M., Clayton R. N. and Mayeda T. K. (1997) CV3 chondrites: Three subgroups, not two (abstract). *Meteoritics & Planetary Science* **32 (suppl.)**, A138-A139.

Welten K. C., Alderliesten C., van der Borg K., Lindner L., Loeken T. and Schultz L. (1997) Lewis Cliff 86360: An Antarctic L-chondrite with a terrestrial age of 2.35 million years. *Meteoritics & Planetary Science* **32**, 775-780.

Welten K. C., Lindner L., Alderliesten C. and van der Borg K. (1999) Terrestrial ages of ordinary chondrites from the Lewis Cliff stranding area, East Antarctica. *Meteoritics & Planetary Science* **34**, 559-569.

Wetherill G. W. (1967) Collisions in the asteroid belt. *J. Geophys. Res.* **72**, 2429-2444.

Wetherill G. W. (1987) Dynamical relationship between asteroids, meteorites, and Apollo-Amor objects. *Phil. Trans. Roy. Soc. Lond.* **A323**, 323-337.

Wetherill G. W. and Chapman C. R. (1988) Asteroids and meteorites. In *Meteorites and the Early Solar System* (J. F. Kerridge and M. S. Matthews, Eds.), pp. 35-67. University of Arizona Press, Tucson, Arizona.

Williams J. G. (1979) Proper elements and family memberships of the asteroids. In *Asteroids* (T. Gehrels, Ed.), pp. 1040-1063. University of Arizona Press, Tucson, Arizona.

Williams J. G. (1989) Asteroid family identifications and proper elements. In *Asteroids II* (R. P. Binzel, T. Gehrels and M. S. Matthews, Eds.), pp. 1034-1072. University of Arizona Press, Tucson, Arizona.

Williams J. G. (1992) Asteroid families-An initial search. *Icarus* **96**, 251-280.

Wisdom J. (1983) Chaotic behavior and the origin of the 3/1 Kirkwood gap. *Icarus* **56**, 51-74.

Wisdom J. (1985) Meteorites may follow a chaotic route to earth. *Nature* **315**, 731-733.

Wood J. A. (1979) Review of the metallographic cooling rates of meteorites and a new model for the planetesimals in which they formed. In *Asteroids* (T. Gehrels, Ed.), pp. 849-891. University of Arizona Press, Tucson, Arizona.

Xu S., Binzel R. P., Burbine T. H. and Bus S. J. (1995) Small main-belt asteroid spectroscopic survey: Initial results. *Icarus* **115**, 1-35.

Yamada M., Sasaki S., Nagahara H., Fujiwara A., Hasegawa S., Yano H., Hiroi T., Ohashi H. and Ohtake H. (1999) Simulation of space weathering of planet-forming materials: Nanosecond pulse laser irradiation and proton implantation on olivine and pyroxene samples. *Earth, Planets and Space* **51**, 1255-1265.

Yamaguchi A., Mori H. and Takeda H. (1993) Mineralogy and shock textures in the Padvarninkai eucrite (abstract). *Meteoritics* **28**, 462-463.

Yeomans D. K. (1999) MUSES-C: A near-Earth asteroid lander and sample return mission (abstract). *Asteroids, Comets and Meteors*, 60-61.

Young A. T. (1989) Extinction and transformation. In *Infrared Extinction and Standardization* (E. F. Milone, Ed.), pp. 6-14. Springer-Verlag, Berlin, Germany.

Zappalà V., Cellino A., Farinella P. and Knezevic Z. (1990) Asteroid families I. Identification by hierarchical clustering and reliability assessment. *Astron. J.* **100**, 2030-2046.

Zappalà V., Cellino A., Farinella P. and Milani A. (1994) Asteroid families. II. Extension to unnumbered multiopposition asteroids. *Astron. J.* **107**, 772-801.

Zappalà V., Bendjoya Ph., Cellino A., Farinella P. and Froeschlé C. (1995) Asteroid families: Search of a 12,487-asteroid sample using two different clustering techniques. *Icarus* **116**, 291-314.

Zellner B., Leake M., Morrison D. and Williams J. G. (1977) The E asteroids and the origin of the enstatite achondrites. *Geochim. Cosmochim. Acta* **41**, 1759-1767.

Zellner B., Tholen D. J. and Tedesco E. F. (1985) The eight-color asteroid survey: Results for 589 minor planets. *Icarus* **61**, 355-416.

Zolensky M. E. (1998) The flux of meteorites to Antarctica. In *Meteorites: Flux with Time and Impact Effects.* (Geological Society Special Publication **140**) (M. M. Grady, Hutchison R., McCall G. J. H. and Rothery D. A., Eds.), pp. 93-104. Geological Society, London, England.

Zolensky M., Barrett R. and Browning L. (1993) Mineralogy and composition of matrix and chondrule rims in carbonaceous chondrites. *Geochim. Cosmochim. Acta* **57**, 3123-3148.

Appendix A
Observational Parameters

Observational parameters are given for the SMASSIR objects. For objects with multiple spectra, an asterisk is used to indicate the spectrum deemed to be the "highest-quality" one. The "best" spectra are plotted in Appendix B. Dates and times of the observations are given in universal time (UT). If only one time is given instead of a range, only the time of the first observation was noted in the log book. The images column gives the number of exposures that were used in the reduction of the asteroid spectrum. The quoted airmass is the average airmass for the set of observations. The strength of the 1.4 μm feature is the difference from unity (given as a percentage) of the ratio of the point in the SMASSIR spectrum most affected by the telluric absorption feature and the estimated "actual" reflectance at that wavelength. The estimated error bars for the strengths of the 1.4 μm feature are ±2%.

Asteroid	Date	Time (UT)	Run	Airmass	Images	Standard Star	Airmass	Strength of 1.4 μm Feature
1 Ceres	* 9/15/98	15:25-	ir11	1.00	8	Hyades 64	1.00	6%
	9/16/98	15:38-	ir11	1.00	4	Hyades 64	1.00	20%
	9/17/98	15:31-	ir11	1.00	4	93-101	1.02	9%
2 Pallas	9/15/98	11:25-11:31	ir11	1.11	10	112-1333	1.06	15%
	* 9/18/98	09:49-09:53	ir11	1.09	10	112-1333	1.10	7%
3 Juno	2/10/97	05:13-05:19	ir7	1.21	6	Hyades 64	1.01	7%
	* 1/4/98	15:45-15:52	ir9	1.09	6	Hyades 64	1.04	6%
	4/29/98	07:01-	ir10	1.03	6	102-1081	1.07	6%
	5/1/98	07:50-07:55	ir10	1.03	6	107-998	1.06	7%
	5/2/98	07:02-	ir10	1.02	6	102-1081	1.08	15%
4 Vesta	1/30/97	14:17-14:25	ir8	1.35	7	Hyades 64	1.03	14%
5 Astraea	3/1/99	05:19-	ir13	1.06	6	Hyades 64	1.06	1%
6 Hebe	2/8/97	13:58-14:08	ir7	1.05	10	Hyades 64	1.01	17%
	4/29/98	13:16-13:22	ir10	1.08	10	102-1081	1.07	9%
	4/30/98	13:23-13:27	ir10	1.08	6	102-1081	1.11	4%
	5/1/98	13:08-13:13	ir10	1.08	6	107-998	1.06	14%
	* 5/2/98	13:24-13:30	ir10	1.09	6	107-998	1.10	2%
7 Iris	* 2/8/97	15:17-15:23	ir7	1.27	6	Hyades 64	1.01	24%
	5/1/98	14:54-15:00	ir10	1.32	6	107-998	1.06	24%
9 Metis	2/28/99	14:40-	ir13	1.14	8	Hyades 64	1.08	10%
	* 3/1/99	13:57-	ir13	1.13	8	102-1081	1.07	3%
10 Hygiea	9/29/97	15:11-15:23	ir8	1.01	8	93-101	1.13	13%
	9/30/97	15:26-	ir8	1.00	8	93-101	1.06	12%
	10/1/97	15:24-15:32	ir8	1.01	10	93-101	1.06	3%
	10/3/97	15:11-15:15	ir8	1.00	8	93-101	1.06	7%
	* 1/4/98	09:24-	ir9	1.04	10	Hyades 64	1.04	0%
	1/27/99	12:45-	ir12	1.04	8	Hyades 64	1.12	8%
11 Parthenope	10/2/97	14:20-14:28	ir8	1.14	10	Hyades 64	1.05	3%
12 Victoria	1/27/99	14:29-	ir12	1.21	10	Hyades 64	1.12	22%
15 Eunomia	* 9/16/98	14:14-	ir11	1.04	6	Hyades 64	1.00	4%
	9/17/98	13:47-13:49	ir11	1.04	6	93-101	1.02	8%
	1/27/99	06:06-	ir12	1.06	4	Hyades 64	1.12	12%
16 Psyche	4/29/98	11:21-11:26	ir10	1.20	10	102-1081	1.07	13%
	* 4/30/98	11:25-11:30	ir10	1.25	6	102-1081	1.11	1%
	5/1/98	10:45-10:50	ir10	1.20	6	107-998	1.06	14%
	5/2/98	10:55-11:02	ir10	1.19	6	102-1081	1.08	15%
18 Melpomene	2/8/97	13:46-13:52	ir7	1.06	6	Hyades 64	1.01	15%
	4/30/98	13:32-13:38	ir10	1.14	6	102-1081	1.11	4%
	* 5/2/98	13:35-13:40	ir10	1.10	6	107-998	1.10	1%
19 Fortuna	* 2/27/99	09:37-09:45	ir13	1.01	6	Hyades 64	1.01	6%
	3/1/99	10:22-	ir13	1.06	6	Hyades 64	1.06	30%
20 Massalia	* 9/16/98	14:04-	ir11	1.04	6	93-101	1.09	10%
	9/17/98	13:37-13:40	ir11	1.02	6	93-101	1.02	14%
21 Lutetia	* 1/5/98	12:04-	ir9	1.03	10	102-1081	1.20	12%
	2/28/99	14:26-	ir13	1.15	10	Hyades 64	1.08	21%
	3/1/99	13:29-13:43	ir13	1.12	6	102-1081	1.07	4%
22 Kalliope	1/4/97	09:28-09:36	ir6	1.07	10	98-978	1.11	9%
	* 2/8/97	06:26-06:32	ir7	1.03	6	Hyades 64	1.01	2%
	5/1/98	08:12-08:19	ir10	1.01	6	107-998	1.06	8%
25 Phocaea	2/8/97	08:58-09:11	ir7	1.16	10	Hyades 64	1.01	19%
26 Proserpina	3/1/99	06:00-06:06	ir13	1.03	6	Hyades 64	1.06	4%
28 Bellona	2/10/97	08:09-08:16	ir7	1.04	6	Hyades 64	1.01	11%
32 Pomona	2/8/97	06:42-06:56	ir7	1.00	10	Hyades 64	1.01	13%
	* 4/30/98	10:06-	ir10	1.22	10	102-1081	1.11	2%
33 Polyhymnia	* 2/9/97	09:48-09:59	ir7	1.04	10	Hyades 64	1.01	2%
	5/2/98	08:13-08:23	ir10	1.08	6	102-1081	1.08	13%
37 Fides	5/24/99	07:19-07:35	ir14	1.13	10	102-1081	1.09	6%
39 Laetitia	* 1/5/98	10:40-	ir9	1.07	10	102-1081	1.20	4%
	1/27/99	14:16-	ir12	1.06	6	Hyades 64	1.12	26%

Asteroid	Date	Time (UT)	Run	Airmass	Images	Standard Star	Airmass	Strength of 1.4 μm Feature
40 Harmonia	10/2/97	11:27-11:34	ir8	1.50	10	93-101	1.07	27%
42 Isis	2/9/97	15:33-15:43	ir7	1.17	10	Hyades 64	1.01	3%
43 Ariadne	2/8/97	09:28-09:39	ir7	1.01	6	Hyades 64	1.01	13%
44 Nysa	* 9/15/98	13:32-	ir11	1.06	10	93-101	1.08	5%
	9/16/98	13:51-	ir11	1.10	10	93-101	1.09	9%
57 Mnemosyne	2/8/97	15:30-15:42	ir7	1.21	10	Hyades 64	1.01	25%
63 Ausonia	2/9/97	05:31-05:37	ir7	1.11	6	Hyades 64	1.01	5%
64 Angelina	2/8/97	12:45-13:02	ir7	1.05	5	Hyades 64	1.01	14%
65 Cybele	2/28/99	06:03-	ir13	1.02	8	Hyades 64	1.08	10%
68 Leto	10/2/97	14:40-14:48	ir8	1.17	10	Hyades 64	1.05	14%
71 Niobe	9/17/98	05:36-05:47	ir11	1.34	5	112-1333	1.13	8%
80 Sappho	10/2/97	15:21-15:28	ir8	1.11	8	Hyades 64	1.05	4%
82 Alkmene	10/2/97	14:54-15:05	ir8	1.17	8	Hyades 64	1.05	7%
92 Undina	4/30/98	14:11-14:36	ir10	1.29	8	102-1081	1.11	10%
113 Amalthea	10/2/97	12:23-12:39	ir8	1.09	10	93-101	1.09	1%
140 Siwa	1/4/98	12:10-12:46	ir9	1.05	10	Hyades 64	1.05	11%
158 Koronis	1/5/98	13:44-	ir9	1.04	8	102-1081	1.20	4%
	* 5/1/98	06:25-06:33	ir10	1.02	10	107-998	1.06	3%
167 Urda	10/3/97	11:49-12:01	ir8	1.08	10	93-101	1.06	3%
169 Zelia	2/10/97	07:07-07:17	ir7	1.06	10	Hyades 64	1.01	5%
221 Eos	2/8/97	10:09-10:20	ir7	1.03	6	Hyades 64	1.01	9%
	* 4/29/98	10:43-11:01	ir10	1.06	10	102-1081	1.07	3%
	4/30/98	10:26-10:36	ir10	1.05	10	102-1081	1.11	5%
	5/1/98	10:24-10:34	ir10	1.05	8	107-998	1.06	6%
	5/2/98	09:50-09:57	ir10	1.05	6	102-1081	1.08	5%
	5/22/99	14:33-14:41	ir14	1.17	10	112-1333	1.08	30%
243 Ida	2/10/97	08:25-08:39	ir7	1.05	10	Hyades 64	1.01	8%
244 Sita	5/22/99	13:50-14:14	ir14	1.25	10	102-1081	1.25	31%
246 Asporina	10/2/97	10:30-10:41	ir8	1.35	10	93-101	1.07	3%
253 Mathilde	1/4/98	08:05-08:45	ir9	1.17	18	Hyades 64	1.04	8%
289 Nenetta	2/9/97	10:27-10:42	ir7	1.02	10	Hyades 64	1.01	1%
291 Alice	10/2/97	10:50-11:08	ir8	1.32	16	93-101	1.07	16%
304 Olga	10/3/97	13:42-13:53	ir8	1.07	10	93-101	1.06	2%
335 Roberta	10/3/97	11:18-11:27	ir8	1.26	8	93-101	1.06	25%
336 Lacaderia	2/28/99	11:01-11:09	ir13	1.09	8	Hyades 64	1.08	7%
346 Hermentaria	2/8/97	13:27-13:33	ir7	1.01	6	Hyades 64	1.01	14%
349 Dembowska	9/29/97	14:58-15:07	ir8	1.01	8	93-101	1.13	12%
	10/1/97	15:08-15:17	ir8	1.02	10	Hyades 64	1.00	11%
	10/2/97	15:33-15:38	ir8	1.03	10	Hyades 64	1.05	16%
	10/3/97	15:22-15:26	ir8	1.03	8	93-101	1.06	5%
	* 1/4/98	09:08-	ir9	1.10	10	Hyades 64	1.04	1%
352 Gisela	* 2/10/97	10:14-10:25	ir7	1.08	10	Hyades 64	1.01	4%
	5/1/98	12:02-12:14	ir10	1.35	6	107-998	1.06	18%
354 Eleonora	2/9/97	15:50-15:58	ir7	1.22	10	Hyades 64	1.01	20%
364 Isara	3/1/99	12:54-13:16	ir13	1.05	14	Hyades 64	1.06	16%
374 Burgundia	5/24/99	14:30-14:43	ir14	1.13	8	102-1081	1.09	20%
379 Huenna	3/1/99	05:39-05:53	ir13	1.06	8	Hyades 64	1.06	11%
389 Industria	10/1/97	11:42-11:53	ir8	1.15	10	93-101	1.15	11%
416 Vaticana	2/10/97	07:24-07:38	ir7	1.10	10	Hyades 64	1.01	8%
446 Aeternitas	10/1/97	13:14-13:34	ir8	1.00	10	93-101	1.06	16%
480 Hansa	10/3/97	13:21-13:32	ir8	1.10	10	93-101	1.06	3%
511 Davida	1/4/97	08:11-08:20	ir6	1.10	10	98-978	1.11	6%
	5/22/99	11:04-11:10	ir14	1.11	6	102-1081	1.28	58%
	5/23/99	10:23-10:34	ir14	1.09	8	102-1081	1.24	6%
	* 5/24/99	09:30-09:40	ir14	1.10	8	102-1081	1.09	5%
515 Athalia	3/1/99	08:48-08:58	ir13	1.02	10	Hyades 64	1.06	3%
584 Semiramis	2/9/97	5:50-5:55	ir7	1.06	6	Hyades 64	1.01	11%
599 Luisa	5/2/98	08:32-08:42	ir10	1.04	6	102-1081	1.08	4%
625 Xenia	4/30/98	08:44-09:21	ir10	1.01	20	102-1081	1.11	7%

Asteroid	Date	Time (UT)	Run	Airmass	Images	Standard Star	Airmass	Strength of 1.4 μm Feature
653 Berenike	1/4/98	13:14-13:29	ir9	1.05	10	Hyades 64	1.05	2%
675 Ludmilla	5/1/98	07:04-07:10	ir10	1.15	6	107-998	1.06	21%
702 Alauda	3/1/99	09:07-09:13	ir13	1.06	10	Hyades 64	1.06	11%
720 Bohlinia	5/2/98	13:01-13:11	ir10	1.40	8	107-998	1.10	17%
737 Arequipa	2/10/97	08:48-08:58	ir7	1.04	10	Hyades 64	1.01	16%
773 Irmintraud	2/9/97	10:55-11:07	ir7	1.01	10	Hyades 64	1.01	6%
774 Armor	9/16/98	14:27-14:40	ir11	1.00	10	Hyades 64	1.00	3%
787 Moskva	3/1/99	14:18-14:48	ir13	1.16	18	102-1081	1.07	5%
808 Merxia	10/3/97	14:18-14:28	ir8	1.01	10	93-101	1.06	7%
811 Nauheima	5/2/98	12:33-12:52	ir10	1.29	10	107-998	1.10	14%
825 Tanina	3/1/99	11:53-12:15	ir13	1.08	14	Hyades 64	1.06	22%
863 Benkoela	4/30/98	09:34-09:53	ir10	1.02	10	102-1081	1.11	4%
913 Otila	9/15/98	14:12-14:31	ir11	1.01	9	Hyades 64	1.00	2%
915 Cosette	2/28/99	07:26-07:44	ir13	1.06	12	Hyades 64	1.08	11%
918 Itha	10/2/97	13:32-13:51	ir8	1.07	10	93-101	1.07	1%
950 Ahrensa	4/29/98	13:31-14:11	ir10	1.02	20	102-1081	1.07	16%
1036 Ganymed	9/15/98	13:53-	ir11	1.13	10	112-1333	1.06	7%
1126 Otero	5/1/98	08:32-09:14	ir10	1.21	10	107-998	1.06	19%
1273 Anchises	4/30/98	10:50-11:17	ir10	1.44	14	102-1081	1.11	12%
1289 Kutaïssi	3/1/99	11:11-11:37	ir13	1.04	10	Hyades 64	1.06	23%
1324 Knysna	1/4/98	14:36-15:27	ir9	1.08	24	Hyades 64	1.04	9%
1350 Rosselia	2/28/99	09:26-09:48	ir13	1.00	10	Hyades 64	1.08	15%
1483 Hakoila	9/18/98	09:13-09:36	ir11	1.19	12	112-1333	1.10	13%
1518 Rovaniemi	2/28/99	06:26-06:48	ir13	1.04	14	Hyades 64	1.08	3%
1584 Fuji	9/18/98	05:52-06:10	ir11	1.18	10	112-1333	1.10	18%
1587 Kahrstedt	5/2/98	07:41-08:03	ir10	1.08	10	102-1081	1.08	10%
1600 Vyssotsky	5/24/99	07:48-08:08	ir14	1.03	10	102-1081	1.09	40%
1626 Sadeya	9/18/98	05:10-05:40	ir11	1.09	7	112-1333	1.10	18%
1627 Ivar	2/10/97	10:38-11:23	ir7	1.10	20	Hyades 64	1.01	7%
1658 Innes	2/10/97	13:10-13:29	ir7	1.08	10	Hyades 64	1.01	6%
1685 Toro	5/24/99	11:02-11:37	ir14	1.63	12	102-1081	1.09	56%
1807 Slovakia	1/27/99	08:40-09:21	ir12	1.01	14	Hyades 64	1.12	6%
1862 Apollo	1/4/97	05:03-07:14	ir6	1.14	45	Hyades 64	1.01	23%
1863 Antinous	2/28/99	13:02-13:40	ir13	1.14	8	Hyades 64	1.08	0%
1864 Daedalus	2/28/99	11:56-12:48	ir13	1.03	20	Hyades 64	1.08	14%
1866 Sisyphus	4/29/98	11:36-12:19	ir10	1.09	20	102-1081	1.07	12%
1892 Lucienne	9/18/98	08:51-09:00	ir11	1.03	6	112-1333	1.10	10%
1904 Massevitch	1/5/98	12:51-13:30	ir9	1.07	20	102-1081	1.20	9%
1906 Naef	9/17/98	14:51-15:23	ir11	1.02	12	Hyades 64	1.04	10%
1929 Kollaa	* 2/8/97	07:45-08:36	ir7	1.05	20	Hyades 64	1.01	9%
	5/1/98	13:28-14:36	ir10	1.41	6	107-998	1.06	35%
1933 Tinchen	5/2/98	08:57-09:26	ir10	1.06	14	102-1081	1.08	22%
1980 Tezcatlipoca	1/4/98	07:14-07:51	ir9	1.11	16	Hyades 64	1.04	6%
1981 Midas	2/27/99	12:06-12:41	ir13	1.34	16	Hyades 64	1.06	6%
2014 Vasilevskis	5/24/99	09:00-09:20	r14	1.04	10	102-1081	1.09	6%
2038 Bistro	5/1/98	11:03-11:32	ir10	1.11	6	107-998	1.06	16%
2045 Peking	2/27/99	08:43-09:25	ir13	1.01	20	102-1081	1.08	5%
2078 Nanking	1/4/97	11:42-12:52	ir6	1.03	22	98-978	1.11	40%
	* 2/10/97	09:36-09:54	ir7	1.05	10	102-1081	1.07	9%
2100 Ra-Shalom	9/30/97	11:11-11:45	ir8	1.76	20	93-101	1.06	26%
2159 Kukkamäki	1/4/97	08:33-09:17	ir6	1.03	20	98-678	1.11	18%
	* 2/10/97	06:25-06:53	ir7	1.02	12	Hyades 64	1.01	3%
	5/1/98	09:31-10:12	ir10	1.21	16	107-998	1.06	29%
2396 Kochi	3/1/99	06:12-06:53	ir13	1.02	20	Hyades 64	1.06	12%
2442 Corbett	9/16/98	06:20-06:42	ir11	1.21	10	112-1333	1.07	13%
2579 Spartacus	10/2/97	12:51-13:19	ir8	1.13	14	93-101	1.07	2%
2590 Mourão	2/9/97	08:16-08:35	ir7	1.08	10	Hyades 64	1.01	11%
2653 Principia	9/15/98	11:40-12:13	ir11	1.10	16	112-1333	1.06	8%
2715 Mielikki	10/3/97	14:36-15:03	ir8	1.00	14	93-101	1.06	4%

Asteroid	Date	Time (UT)	Run	Airmass	Images	Standard Star	Airmass	Strength of 1.4 μm Feature
2732 Witt	10/3/97	12:14-12:50	ir8	1.07	18	93-101	1.06	3%
2763 Jeans	1/27/99	11:37-12:20	ir12	1.04	14	Hyades 64	1.12	6%
2851 Harbin	3/1/99	09:21-09:39	ir13	1.05	10	Hyades 64	1.06	21%
2873 Binzel	5/24/99	08:27-08:47	ir14	1.09	10	102-1081	1.09	19%
3103 Eger	2/10/97	12:41-13:00	ir7	1.10	10	Hyades 64	1.01	6%
3122 Florence	2/10/97	11:47-12:28	ir7	1.12	20	Hyades 64	1.01	8%
3167 Babcock	1/5/98	14:27-15:00	ir9	1.01	16	102-1081	1.20	12%
3199 Nefertiti	2/10/97	13:56-14:26	ir7	1.23	12	Hyades 64	1.01	31%
3268 De Sanctis	10/1/97	12:17-12:57	ir8	1.06	13	Hyades 64	1.00	1%
3352 McAuliffe	2/27/99	06:33-07:25	ir13	1.10	18	Hyades 64	1.06	15%
3376 Armandhammer	1/4/98	11:26-11:54	ir9	1.09	14	Hyades 64	1.04	7%
3474 Linsley	5/24/99	09:50-10:17	ir14	1.19	12	102-1081	1.09	7%
3545 Gaffey	5/23/99	09:15-09:52	ir14	1.24	16	102-1081	1.18	4%
3628 Boznemcová#	2/9/97	08:51-09:35	ir7	1.16	39	Hyades 64	1.01	4%
	2/9/97	11:20-12:59	ir7	1.08	17	102-1081	1.11	
3657 Ermolva	2/9/97	07:05-07:23	ir7	1.02	12	Hyades 64	1.01	16%
3753 Cruithne	9/30/97	14:36-14:59	ir8	1.51	18	93-101	1.06	30%
3767 DiMaggio	5/24/99	13:55-14:20	ir14	1.20	12	102-1081	1.09	26%
3819 Robinson	4/29/98	09:28-10:22	ir10	1.13	20	102-1081	1.07	7%
3849 Incidentia	3/1/99	07:05-07:47	ir13	1.02	20	Hyades 64	1.06	7%
3903 Kliment Ohridski	9/29/97	11:47-12:30	ir8	1.16	20	93-101	1.13	5%
3908 Nyx	1/4/97	09:50-11:00	ir6	1.12	17	98-978	1.11	12%
3944 Halliday	5/2/98	11:11-11:44	ir10	1.22	16	102-1081	1.08	15%
3968 Koptelov	4/29/98	08:33-09:11	ir10	1.30	20	102-1081	1.07	7%
4005 Dyagilev	* 2/8/97	10:43-11:31	ir7	1.02	20	Hyades 64	1.01	8%
	5/1/98	12:23-12:57	ir10	1.29	14	107-998	1.06	14%
4051 Hatanaka	1/5/98	10:54-11:45	ir9	1.12	20	102-1081	1.20	7%
4062 Schiaparelli	3/1/99	07:55-08:36	ir13	1.02	20	Hyades 64	1.06	4%
4142 Dersu-Uzala	9/16/98	14:52-15:11	ir11	1.04	10	Hyades 64	1.00	14%
4145 Maximova	9/15/98	12:32-13:05	ir11	1.05	16	93-101	1.08	2%
4147 Lennon	4/29/98	07:24-08:08	ir10	1.14	18	102-1081	1.07	9%
4188 Shulnazaria	9/15/98	14:40-15:00	ir11	1.01	6	Hyades 64	1.01	10%
4215 Kamo	9/15/98	10:28-11:00	ir11	1.03	16	112-1333	1.06	17%
4503 Cleobulus	1/27/99	13:29-14:02	ir12	1.01	16	Hyades 64	1.12	14%
4512 Sinuhe	3/1/99	09:48-09:58	ir13	1.01	10	Hyades 64	1.06	17%
4606 Saheki	10/1/97	10:48-11:21	ir8	1.13	16	93-101	1.06	14%
4713 Steel	2/27/99	10:01-10:34	ir13	1.12	14	Hyades 64	1.06	4%
4900 Maymelou	5/23/99	13:28-14:01	ir14	1.24	14	102-1081	1.18	8%
4954 Eric	2/8/97	14:25-15:08	ir7	1.10	20	Hyades 64	1.01	10%
5131 1990 BG	1/27/99	09:49-10:10	ir12	1.16	10	Hyades 64	1.12	6%
5693 1993 EA	5/22/99	07:53-08:41	ir14	1.05	14	102-1081	1.28	23%
5836 1993 MF	10/1/97	14:25-14:58	ir8	1.04	12	93-101	1.06	21%
5840 1978 ON	9/29/97	13:48-14:26	ir8	1.02	17	93-101	1.13	19%
	* 2/28/99	09:56-10:36	ir13	1.01	10	Hyades 64	1.08	20%
6047 1991 TB_1	9/17/98	12:26-13:15	ir11	1.19	13	93-101	1.10	26%
6489 Golevka	5/22/99	11:23-11:44	ir14	1.16	10	102-1081	1.28	11%
7358 1995 YA_3	9/15/98	05:57-06:47	ir11	1.30	14	112-1333	1.06	13%
7889 1994 LX	5/2/98	14:01-14:49	ir10	1.08	22	107-998	1.10	12%
10115 1992 SK	2/27/99	13:15-13:47	ir13	1.41	16	Hyades 64	1.06	7%
11398 1998 YP_{11}	2/27/99	14:13-14:44	ir13	1.01	16	Hyades 64	1.06	9%
11405 1999 CV_3	2/27/99	10:53-11:16	ir13	1.14	16	102-1081	1.08	3%
1991 VH	2/9/97	13:42-14:14	ir7	1.02	16	Hyades 64	1.01	5%
1992 BF	1/4/98	10:01-11:11	ir9	1.25	16	Hyades 64	1.04	16%
1997 BQ	2/9/97	13:39-15:20	ir7	1.60	20	Hyades 64	1.01	25%
1997 BR	2/8/97	11:48-12:39	ir7	1.09	20	Hyades 64	1.01	16%
1997 CZ_5	2/9/97	06:26-06:40	ir7	1.02	20	Hyades 64	1.01	1%
1997 RT	9/30/97	13:22-14:02	ir8	1.26	14	93-101	1.06	14%
1998 FM_5	4/30/98	07:17-08:26	ir10	1.03	20	102-1081	1.11	13%
1998 FX_2	4/30/98	11:42-12:10	ir10	1.02	13	102-1081	1.11	16%

Asteroid	Date	Time (UT)	Run	Airmass	Images	Standard Star	Airmass	Strength of 1.4 μm Feature
1998 HT_{31}	5/2/98	10:07-10:41	ir10	1.08	16	102-1081	1.08	7%
1998 KU_2	9/16/98	05:29-06:07	ir11	1.21	30	112-1333	1.07	6%
1998 MW_5	5/23/99	10:49-11:42	ir14	1.17	22	102-1081	1.17	6%
1998 PB_1	9/15/98	07:26-07:53	ir11	1.10	14	112-1333	1.06	17%
1998 PG	9/18/98	08:05-08:42	ir11	1.05	18	112-1333	1.10	21%
1998 QR_{15}	9/18/98	06:59-07:41	ir11	1.08	16	112-1333	1.10	13%
1998 XB	1/27/99	15:06-15:39	ir12	1.07	14	Hyades 64	1.12	6%
1999 AQ_{10}	1/27/99	10:38-11:13	ir12	1.17	11	Hyades 64	1.12	9%
1999 CF_9	2/28/99	08:11-09:12	ir13	1.00	14	Hyades 64	1.08	11%
1999 DJ_4	1/27/99	15:11-15:39	ir13	1.00	16	Hyades 64	1.06	6%
1999 GK_4	5/23/99	08:02-08:32	ir14	1.07	12	102-1081	1.07	13%
1999 HF_1	5/23/99	07:20-07:49	ir14	1.28	14	102-1081	1.18	11%
1999 JD_6	5/23/99	12:22-13:03	ir14	1.21	16	102-1081	1.18	8%
1999 JV_3	5/22/99	09:48-10:43	ir14	1.10	18	102-1081	1.28	17%
1999 KU_4	5/24/99	12:17-13:15	ir14	1.43	20	102-1081	1.09	44%
1999 KW_4	5/23/99	14:12-14:41	ir14	1.02	10	102-1081	1.02	58%

The two sets of 3628 Boznemcová spectra were combined since they were taken a few hours apart on the same evening.

Appendix B
SMASSIR Spectra

Plots are presented of the "best-quality" asteroids observed in SMASSIR from 0.4 to 1.65 μm. Small dots are used for visible data from SMASS I or II. Open diamonds are used for SMASSIR data. Dark squares are a combination of ECAS and 52-color data, when 52-color data for the object were available. The near-infrared data for 3908 Nyx are from Cruikshank *et al.* (1991). If the ECAS data were not a good spectral match for the SMASS I or II data, only the 52-color data are plotted and normalized to the SMASS I or II data. Crosses are used for the Gaffey and Gilbert (1998) data for 6 Hebe and the Abell and Gaffey (1999) data for 349 Dembowska. If no visible data were available, the SMASSIR spectrum was normalized to unity at ~0.92 μm. All spectra are normalized to unity at 0.55 μm if visible data were available. If no visible data were available, the SMASSIR spectra are normalized to unity at ~0.92 μm. Error bars are $\pm 1\sigma$.

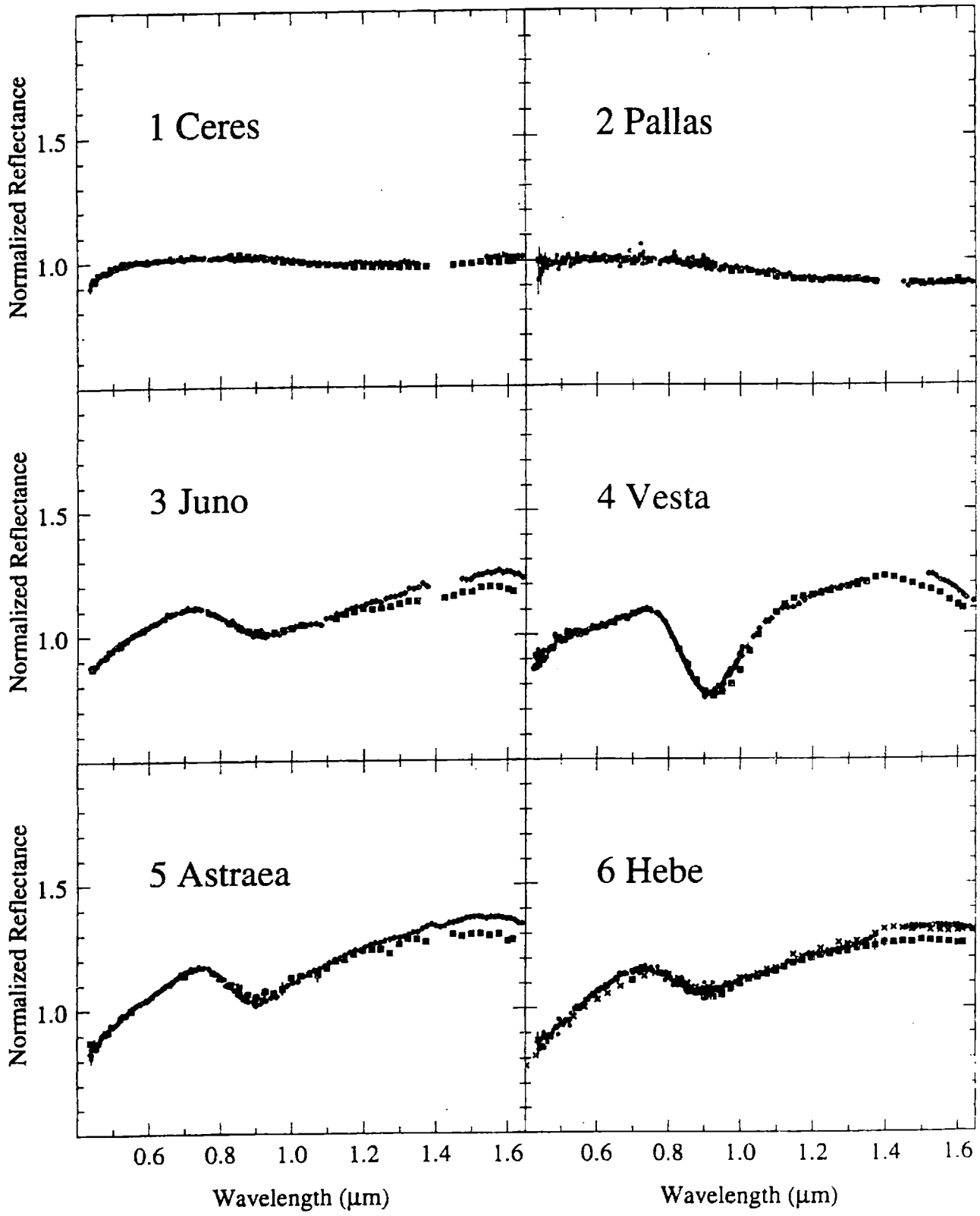
1 Ceres
2 Pallas
3 Juno
4 Vesta
5 Astraea
6 Hebe
Normalized Reflectance
1.5
1.0
0.6
0.8
1.0
1.2
1.4
1.6
Wavelength (μm)

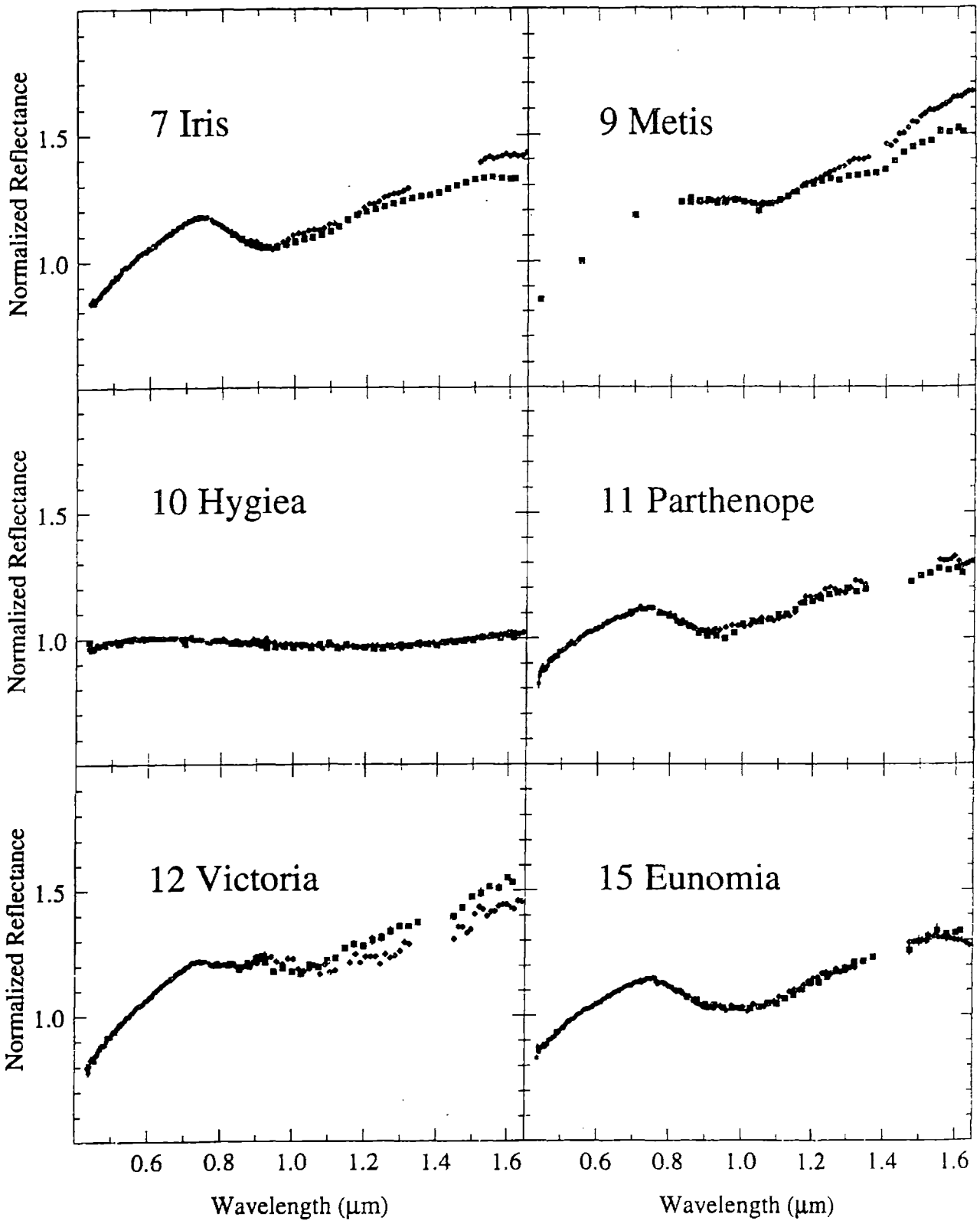
7 Iris
9 Metis
10 Hygiea
11 Parthenope
12 Victoria
15 Eunomia
Normalized Reflectance
1.5
1.0
0.6
0.8
1.0
1.2
1.4
1.6
Wavelength (μm)

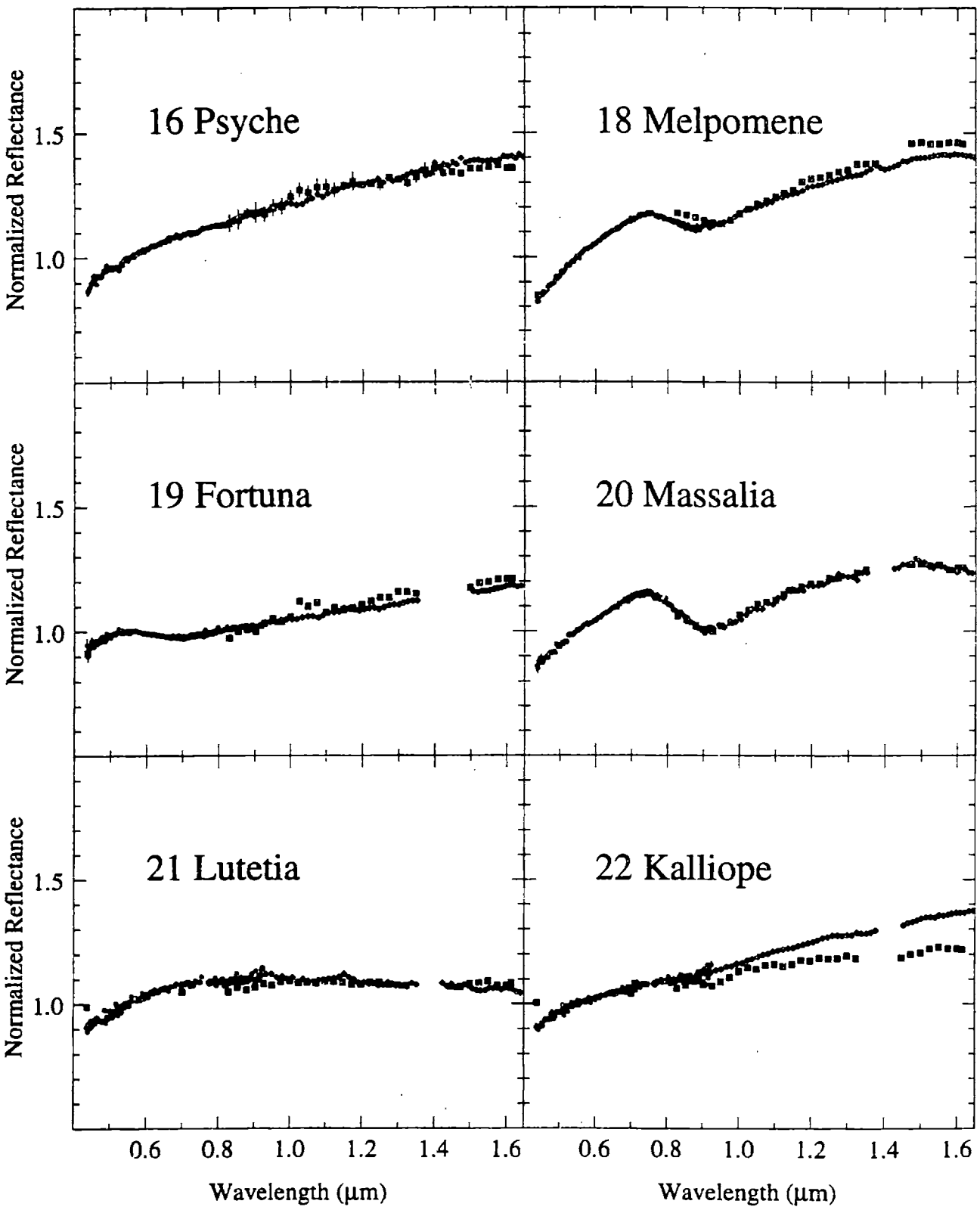
16 Psyche
18 Melpomene
19 Fortuna
20 Massalia
21 Lutetia
22 Kalliope
Normalized Reflectance
1.0
1.5
0.6
0.8
1.0
1.2
1.4
1.6
Wavelength (μm)

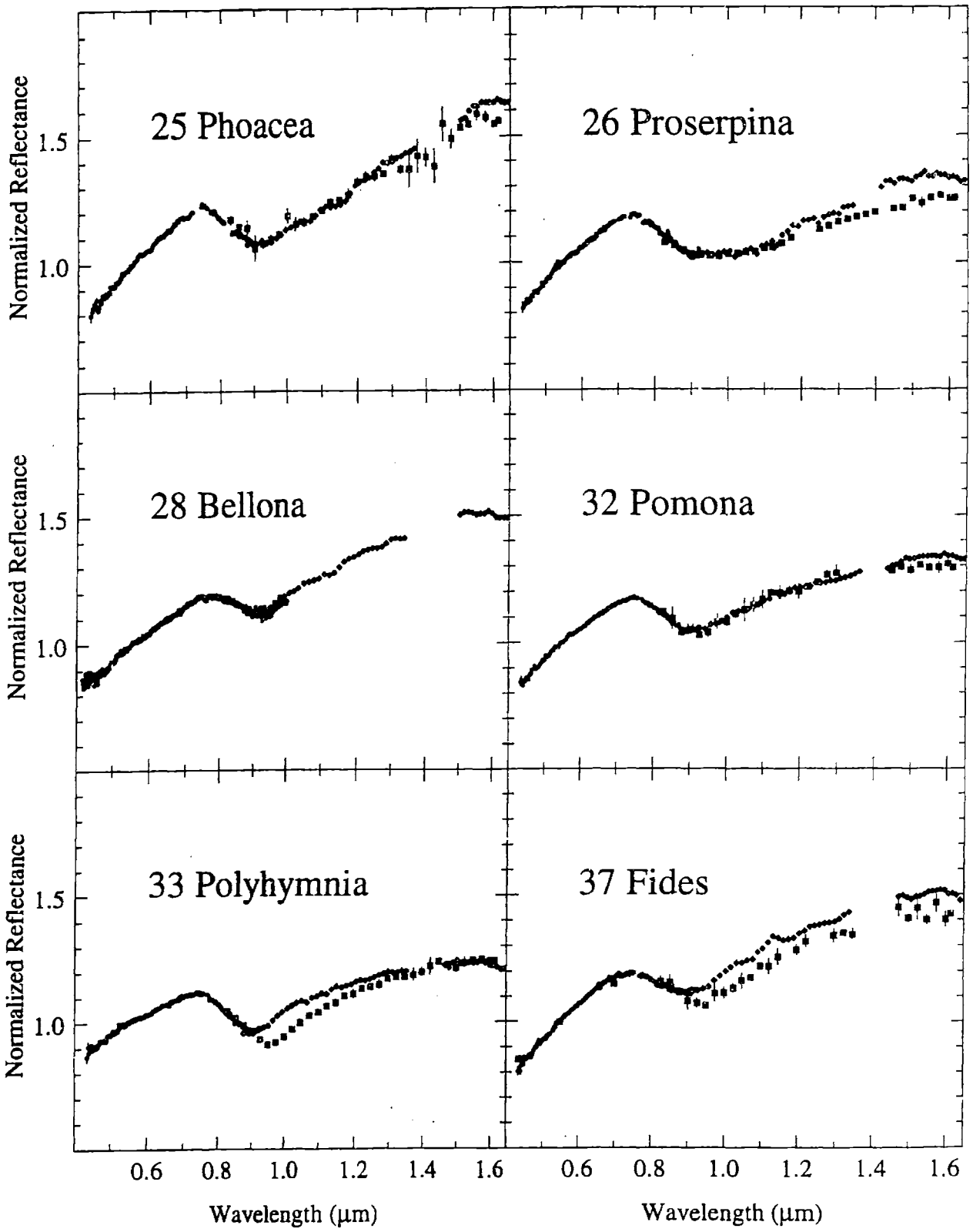
25 Phoacea
26 Proserpina
28 Bellona
32 Pomona
33 Polyhymnia
37 Fides
Normalized Reflectance
1.5
1.0
0.6
0.8
1.0
1.2
1.4
1.6
Wavelength (μm)

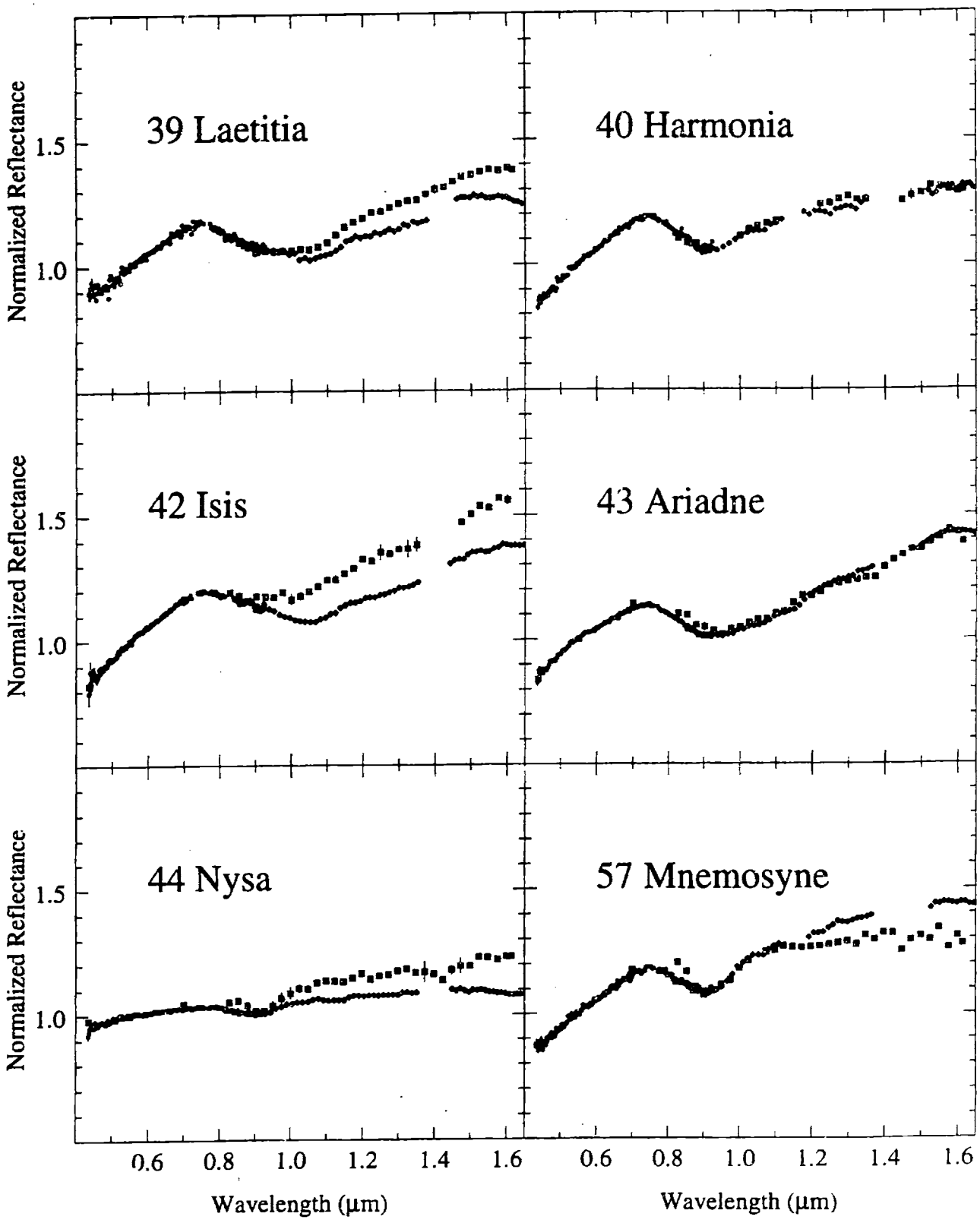
39 Laetitia
40 Harmonia
42 Isis
43 Ariadne
44 Nysa
57 Mnemosyne
Normalized Reflectance
1.5
1.0
0.6
0.8
1.0
1.2
1.4
1.6
Wavelength (μm)

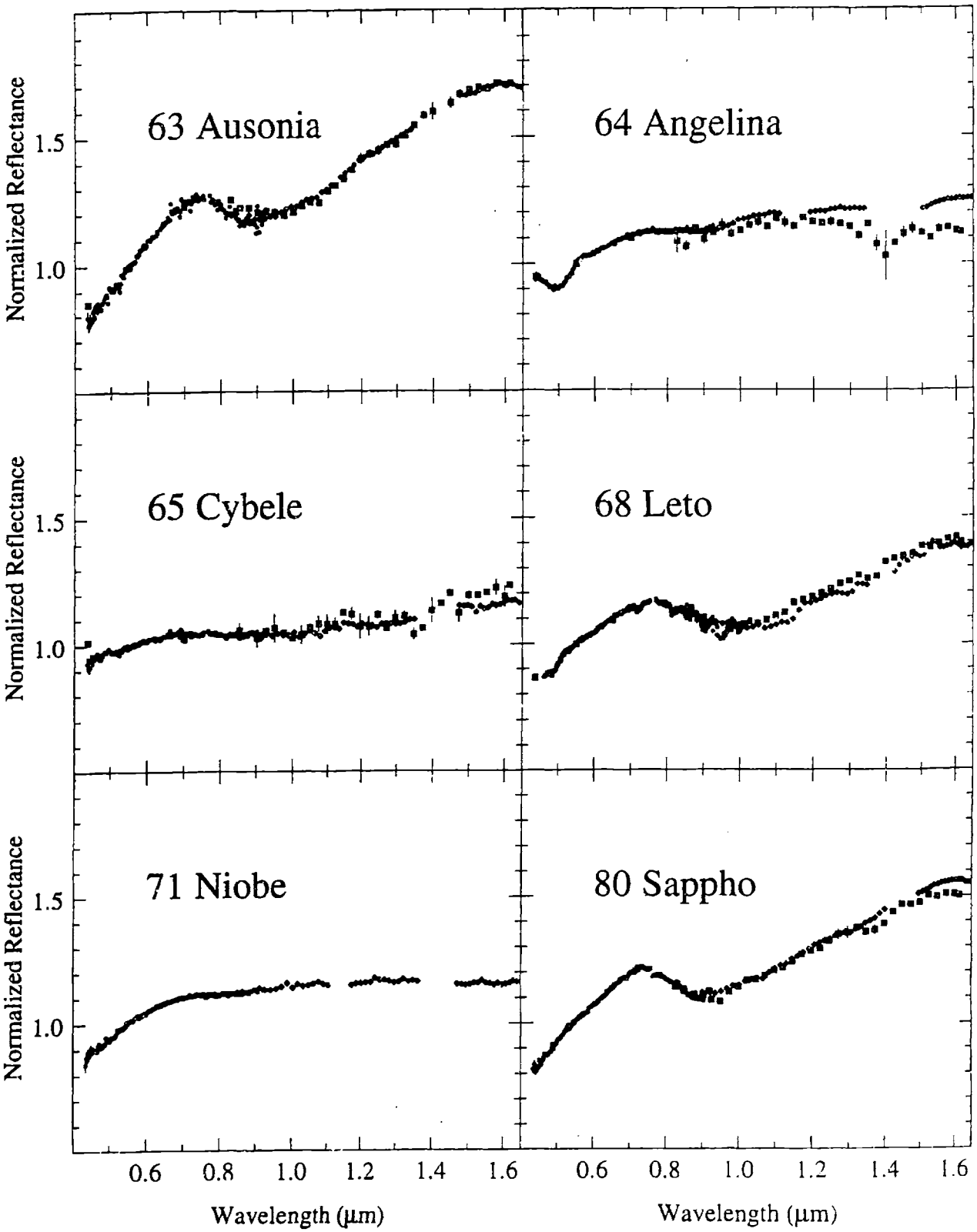
63 Ausonia
64 Angelina
65 Cybele
68 Leto
71 Niobe
80 Sappho
Normalized Reflectance
1.0
1.5
0.6
0.8
1.0
1.2
1.4
1.6
Wavelength (μm)

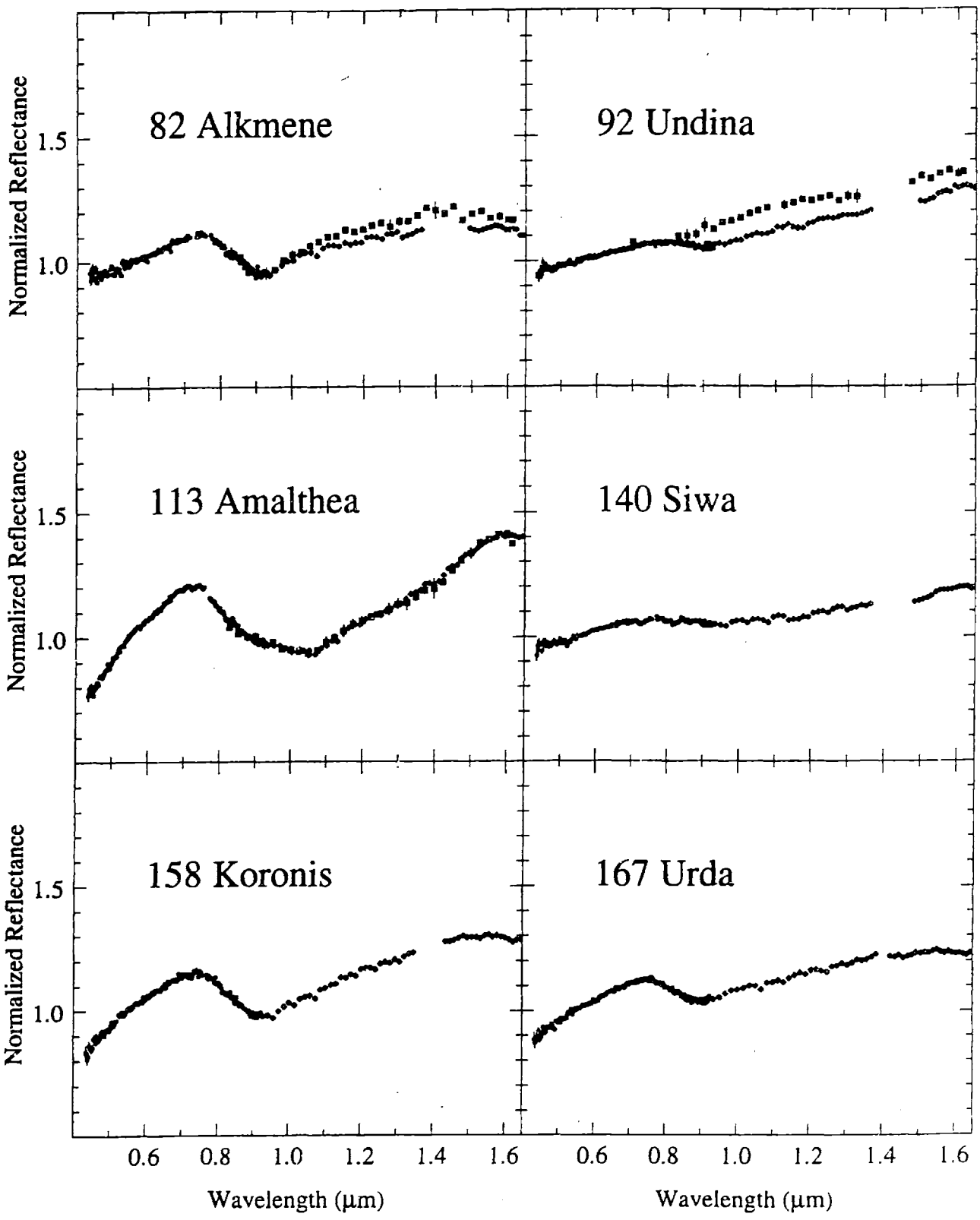
82 Alkmene
92 Undina
113 Amalthea
140 Siwa
158 Koronis
167 Urda
Normalized Reflectance
1.5
1.0
0.6
0.8
1.0
1.2
1.4
1.6
Wavelength (μm)

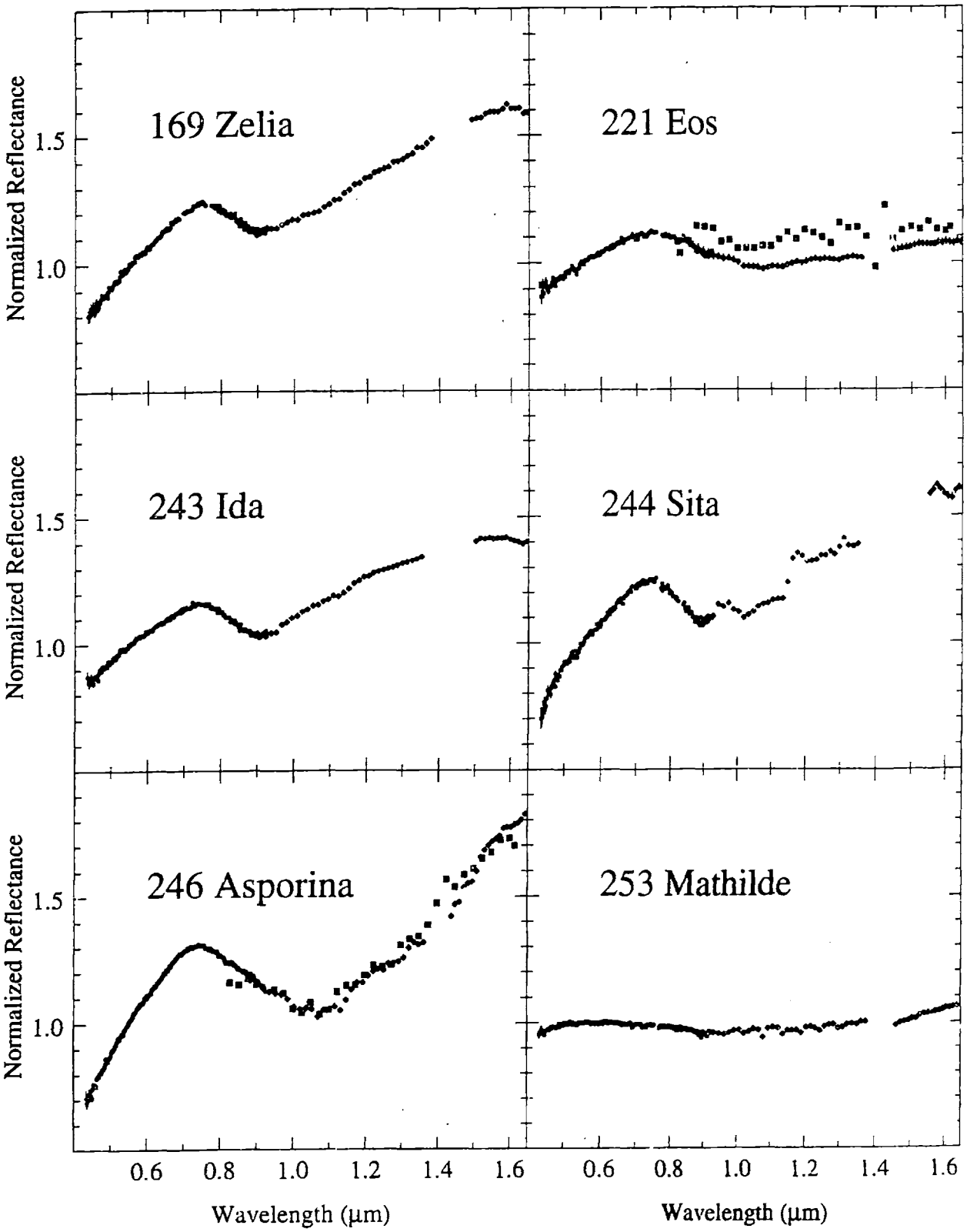
169 Zelia
221 Eos
243 Ida
244 Sita
246 Asporina
253 Mathilde
Normalized Reflectance
1.5
1.0
0.6
0.8
1.0
1.2
1.4
1.6
Wavelength (μm)

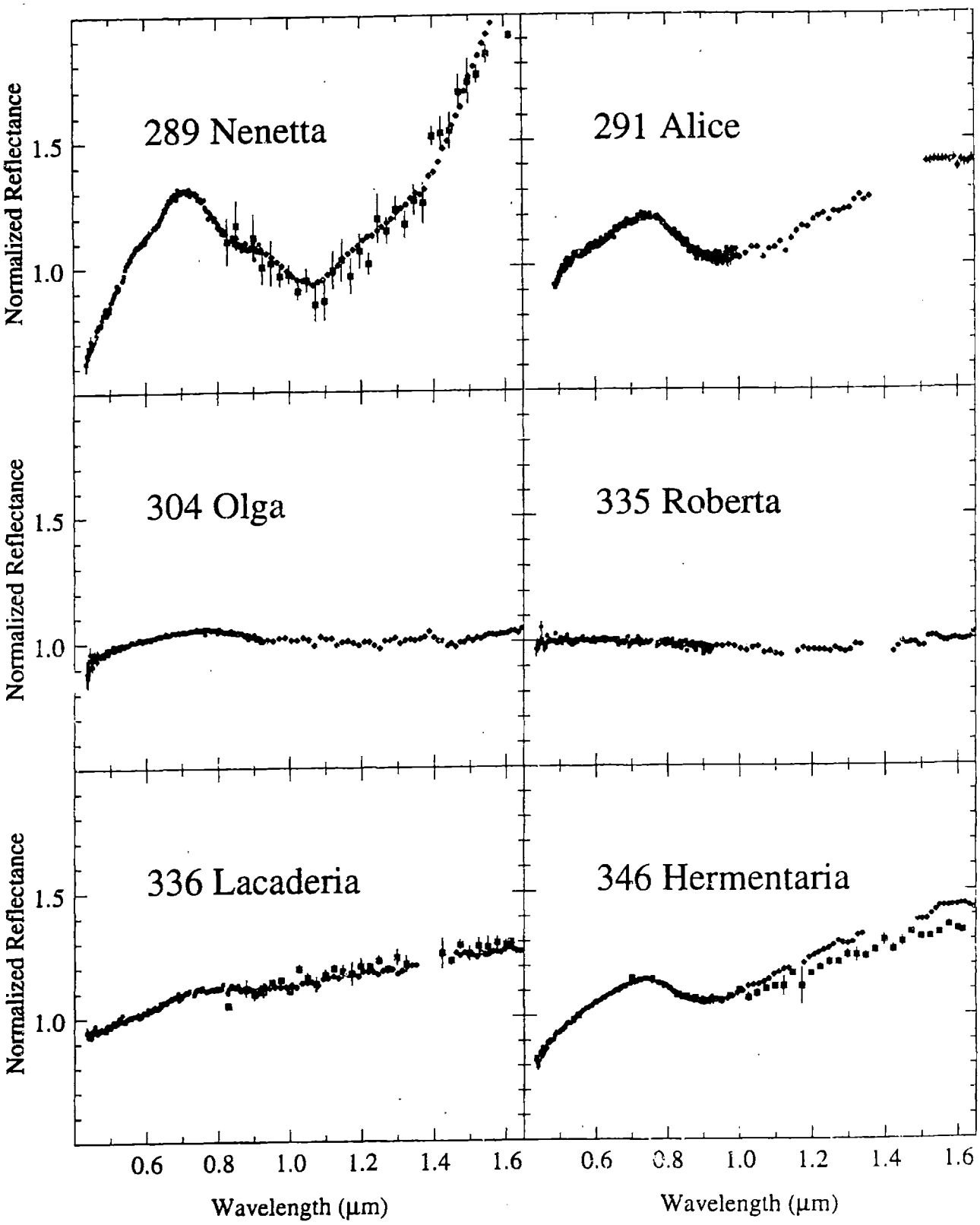
289 Nenetta
291 Alice
304 Olga
335 Roberta
336 Lacaderia
346 Hermentaria
Normalized Reflectance
1.0
1.5
0.6
0.8
1.0
1.2
1.4
1.6
Wavelength (μm)

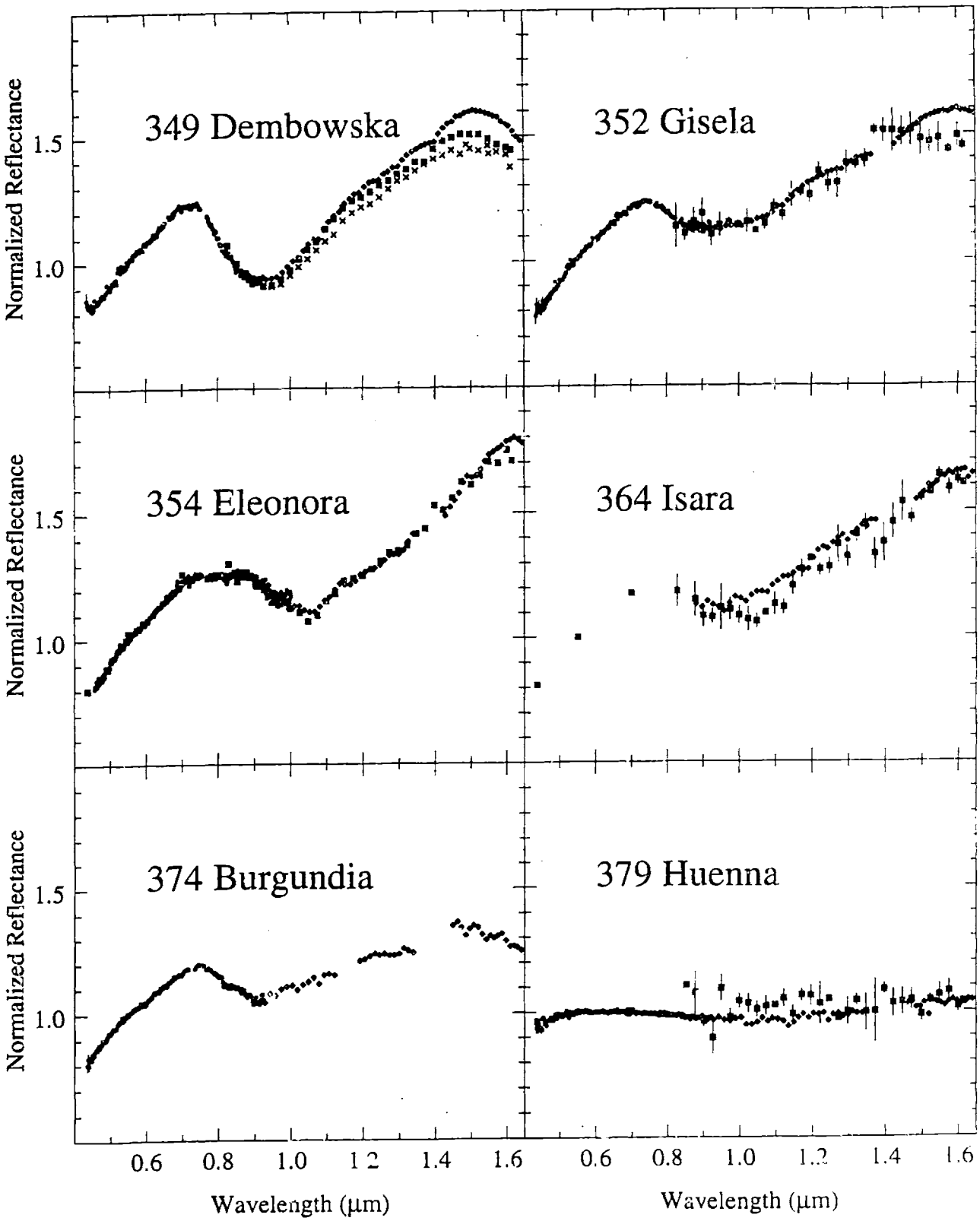
349 Dembowska
352 Gisela
354 Eleonora
364 Isara
374 Burgundia
379 Huenna
Normalized Reflectance
1.5
1.0
0.6
0.8
1.0
1.2
1.4
1.6
Wavelength (μm)

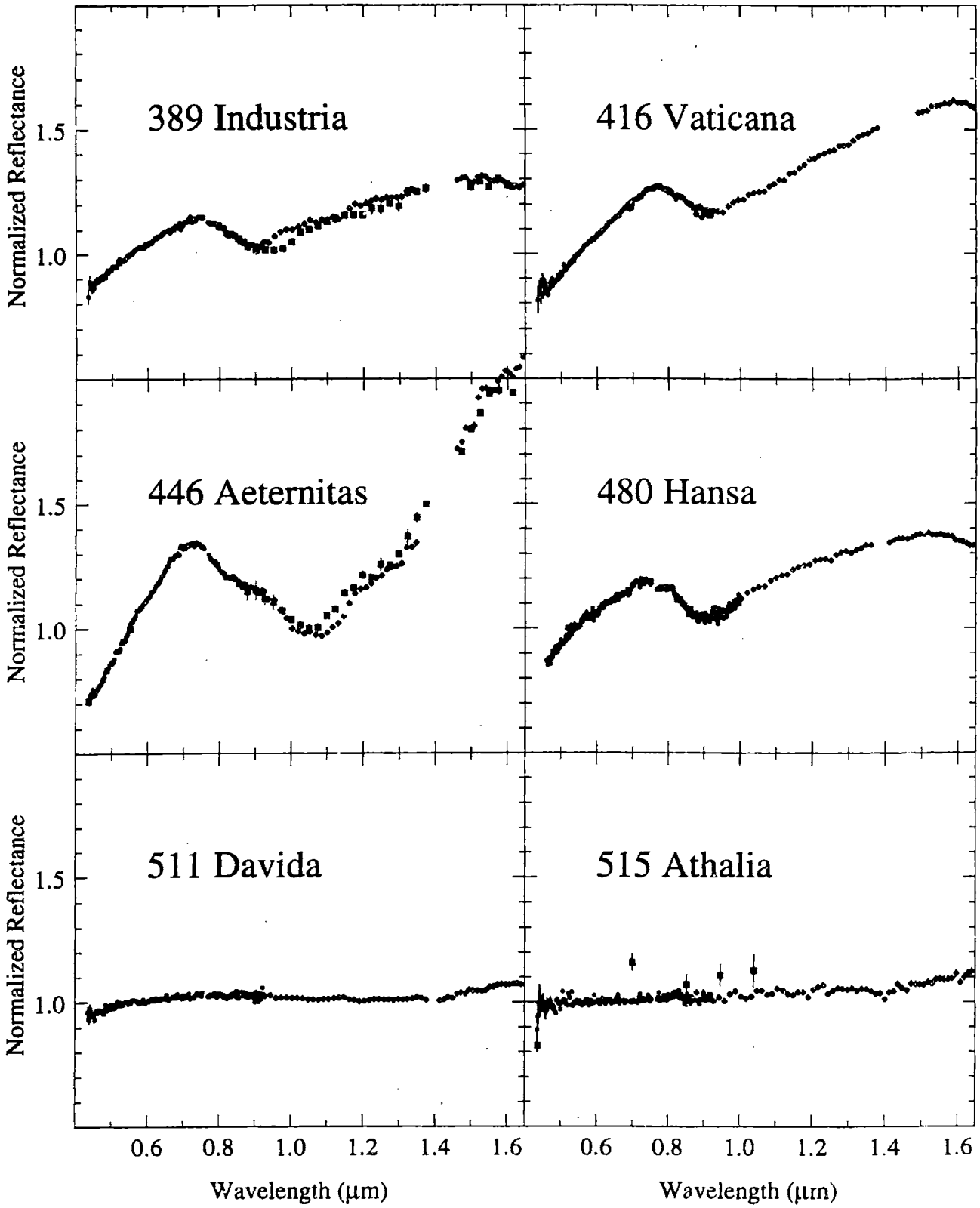
389 Industria
416 Vaticana
446 Aeternitas
480 Hansa
511 Davida
515 Athalia
Normalized Reflectance
1.5
1.0
0.6
0.8
1.0
1.2
1.4
1.6
Wavelength (μm)

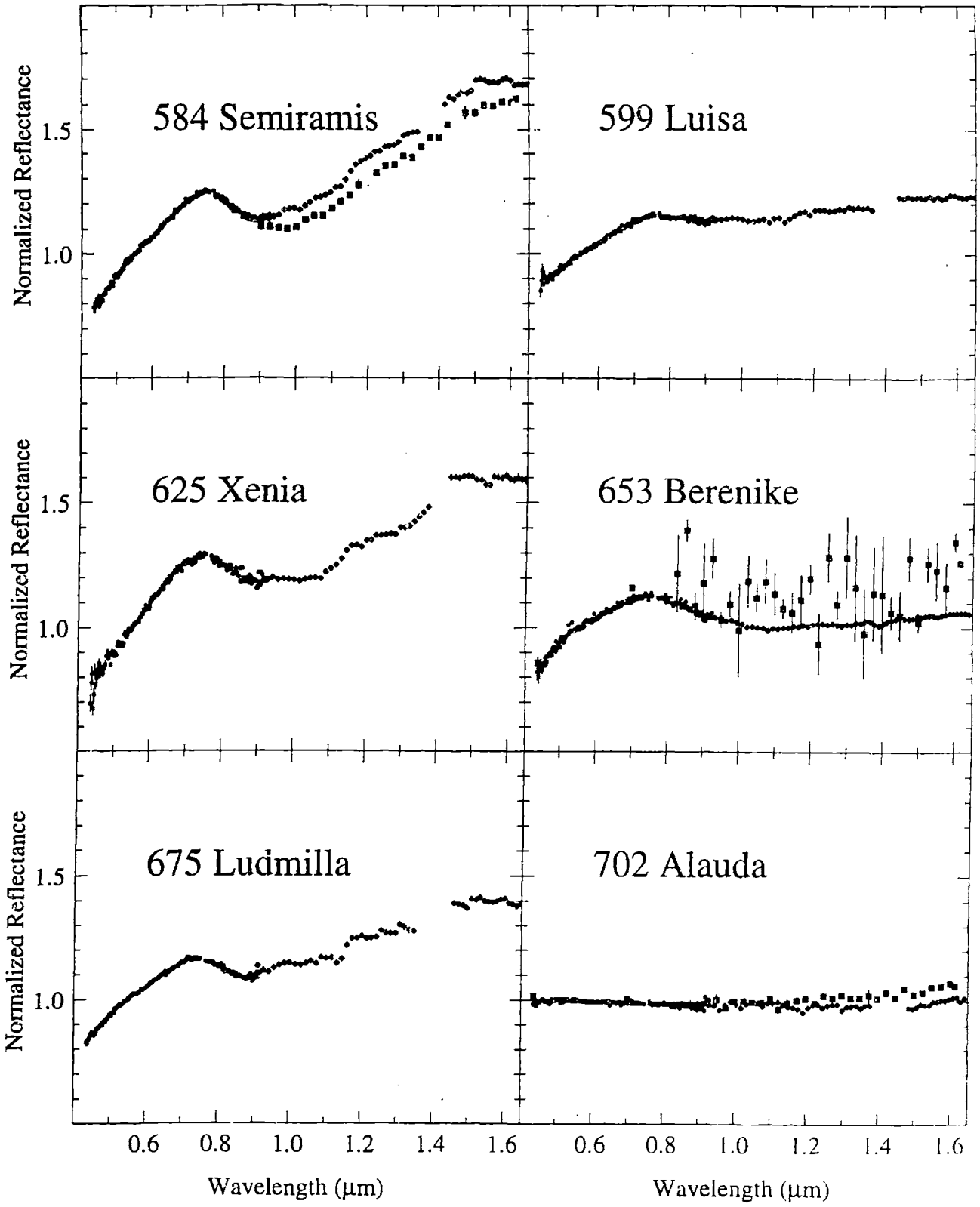
584 Semiramis
599 Luisa
625 Xenia
653 Berenike
675 Ludmilla
702 Alauda
Normalized Reflectance
1.5
1.0
0.6
0.8
1.0
1.2
1.4
1.6
Wavelength (μm)

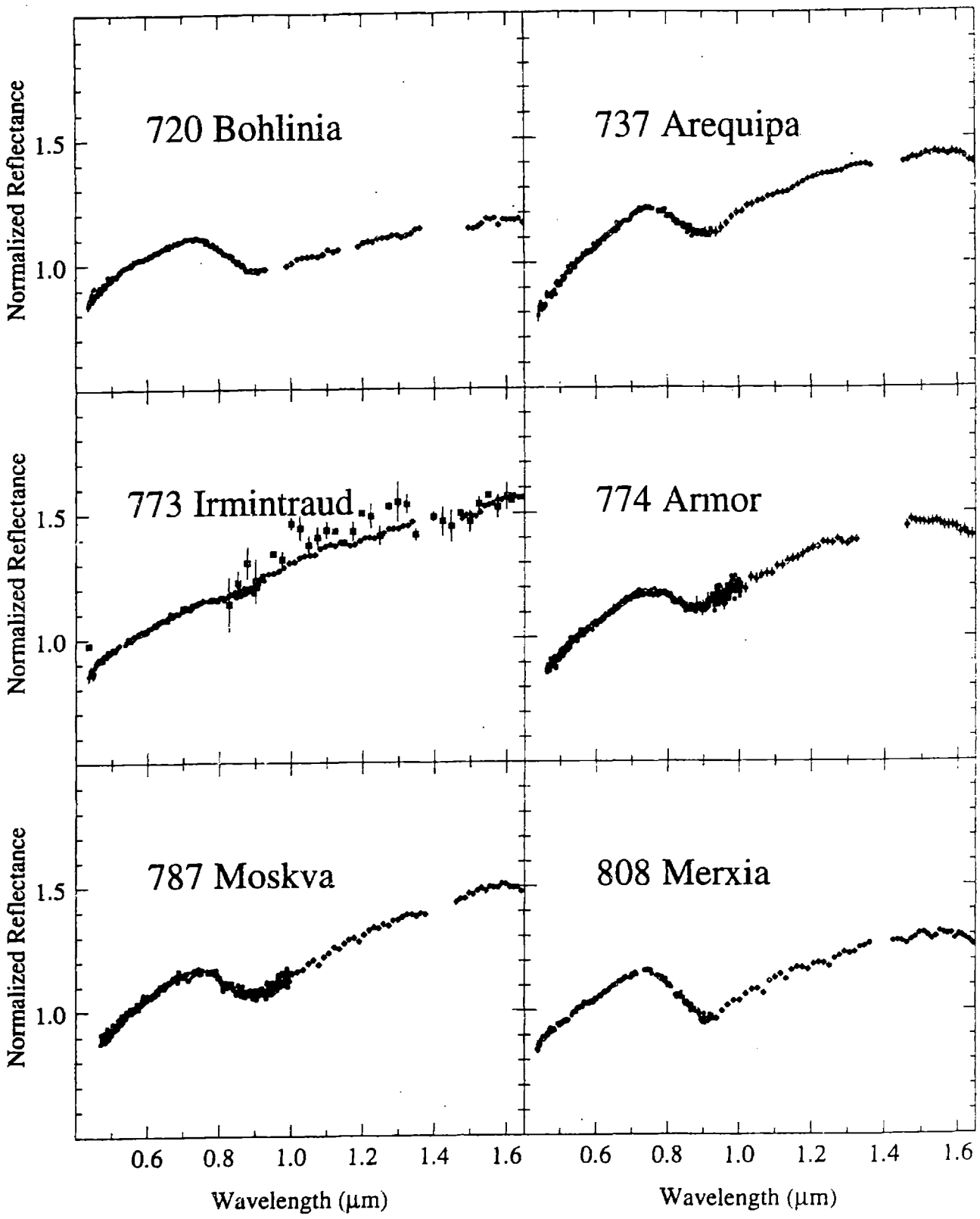
720 Bohlinia
737 Arequipa
773 Irmintraud
774 Armor
787 Moskva
808 Merxia
Normalized Reflectance
1.5
1.0
0.6
0.8
1.0
1.2
1.4
1.6
Wavelength (μm)

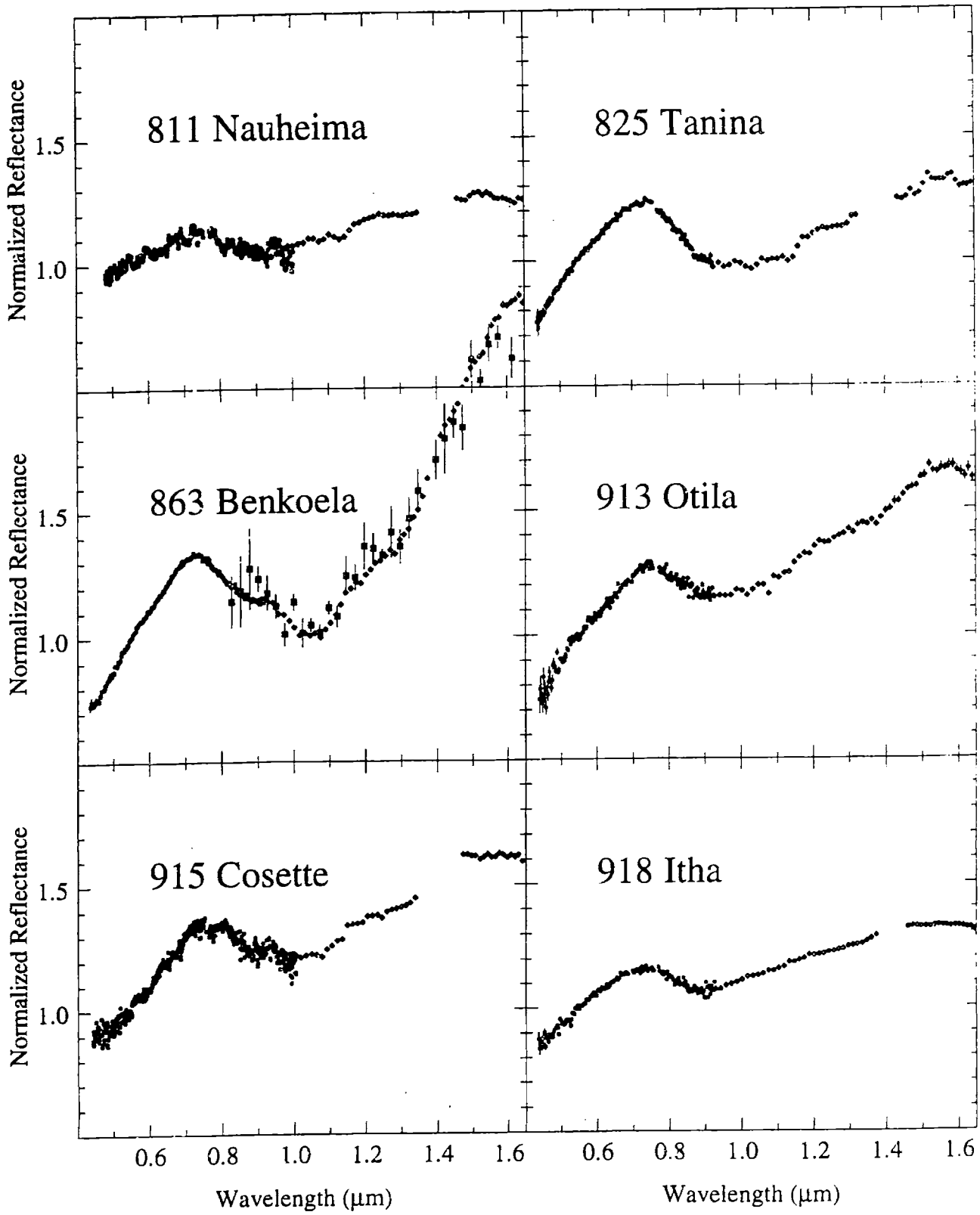
811 Nauheima
825 Tanina
863 Benkoela
913 Otila
915 Cosette
918 Itha
Normalized Reflectance
1.5
1.0
0.6
0.8
1.0
1.2
1.4
1.6
Wavelength (μm)

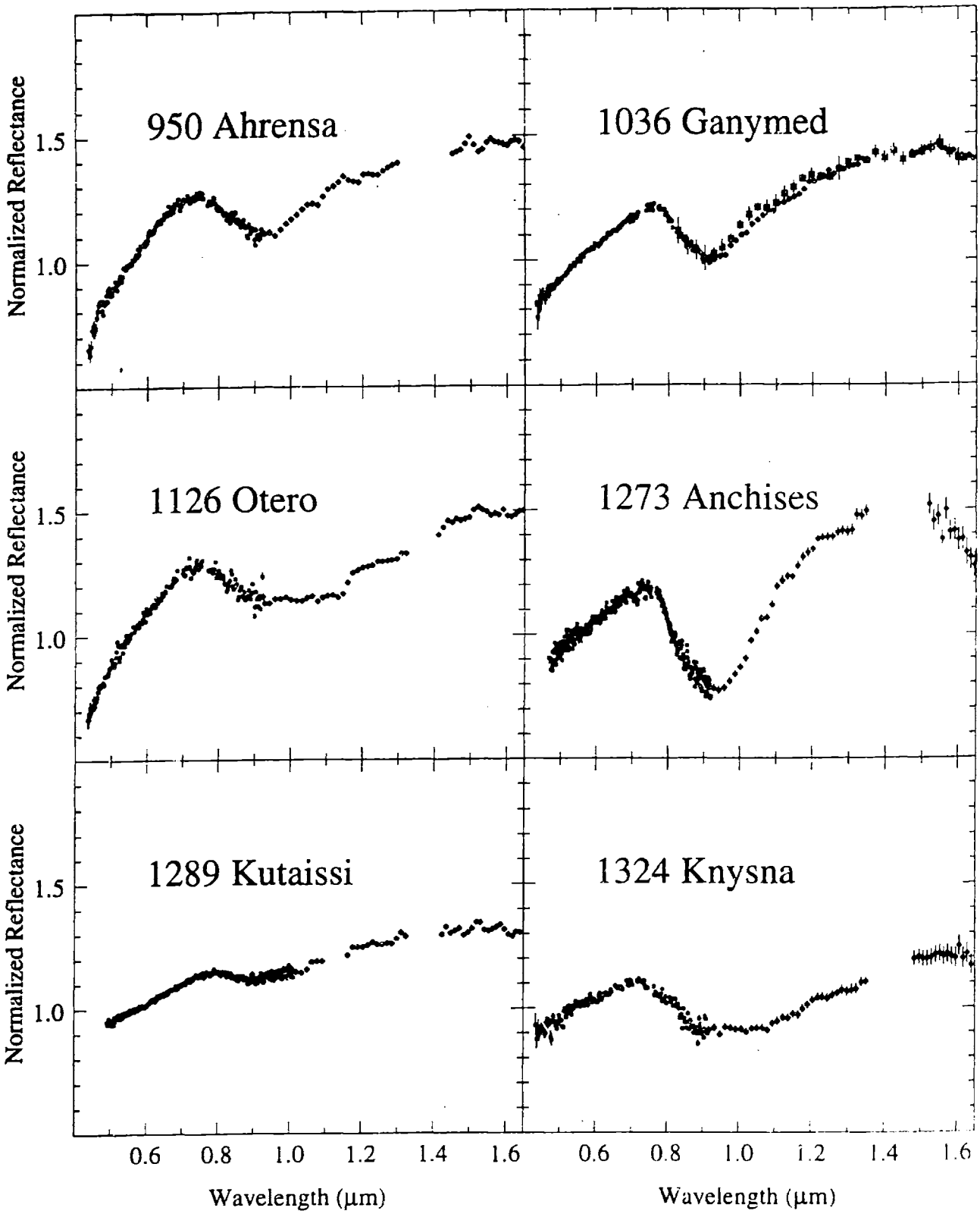
950 Ahrensa
1036 Ganymed
1126 Otero
1273 Anchises
1289 Kutaissi
1324 Knysna
Normalized Reflectance
1.5
1.0
0.6
0.8
1.0
1.2
1.4
1.6
Wavelength (μm)

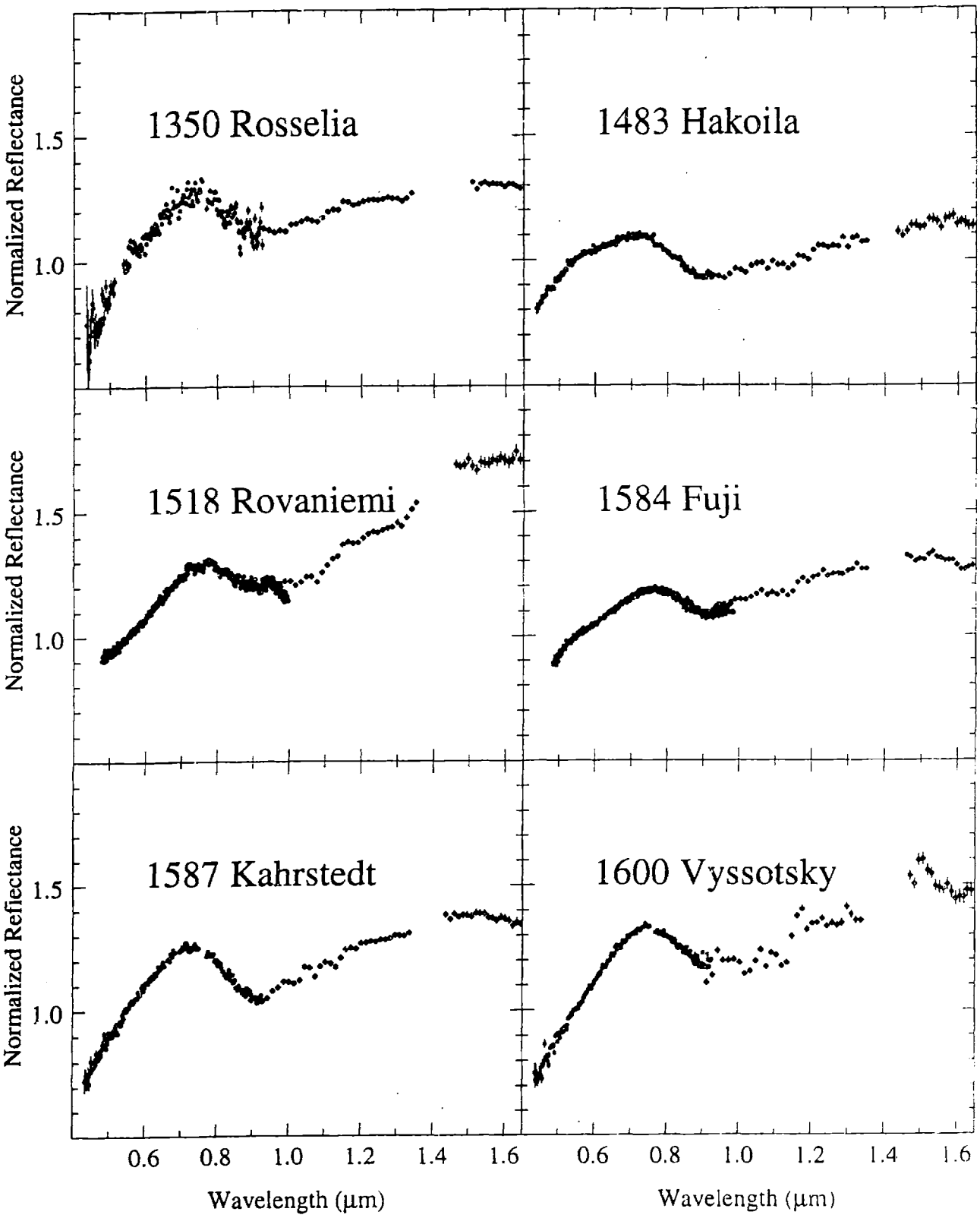
1350 Rosselia
1483 Hakoila
1518 Rovaniemi
1584 Fuji
1587 Kahrstedt
1600 Vyssotsky
Normalized Reflectance
Normalized Reflectance
Normalized Reflectance
1.5
1.0
0.6
0.8
1.0
1.2
1.4
1.6
Wavelength (μm)
Wavelength (μm)

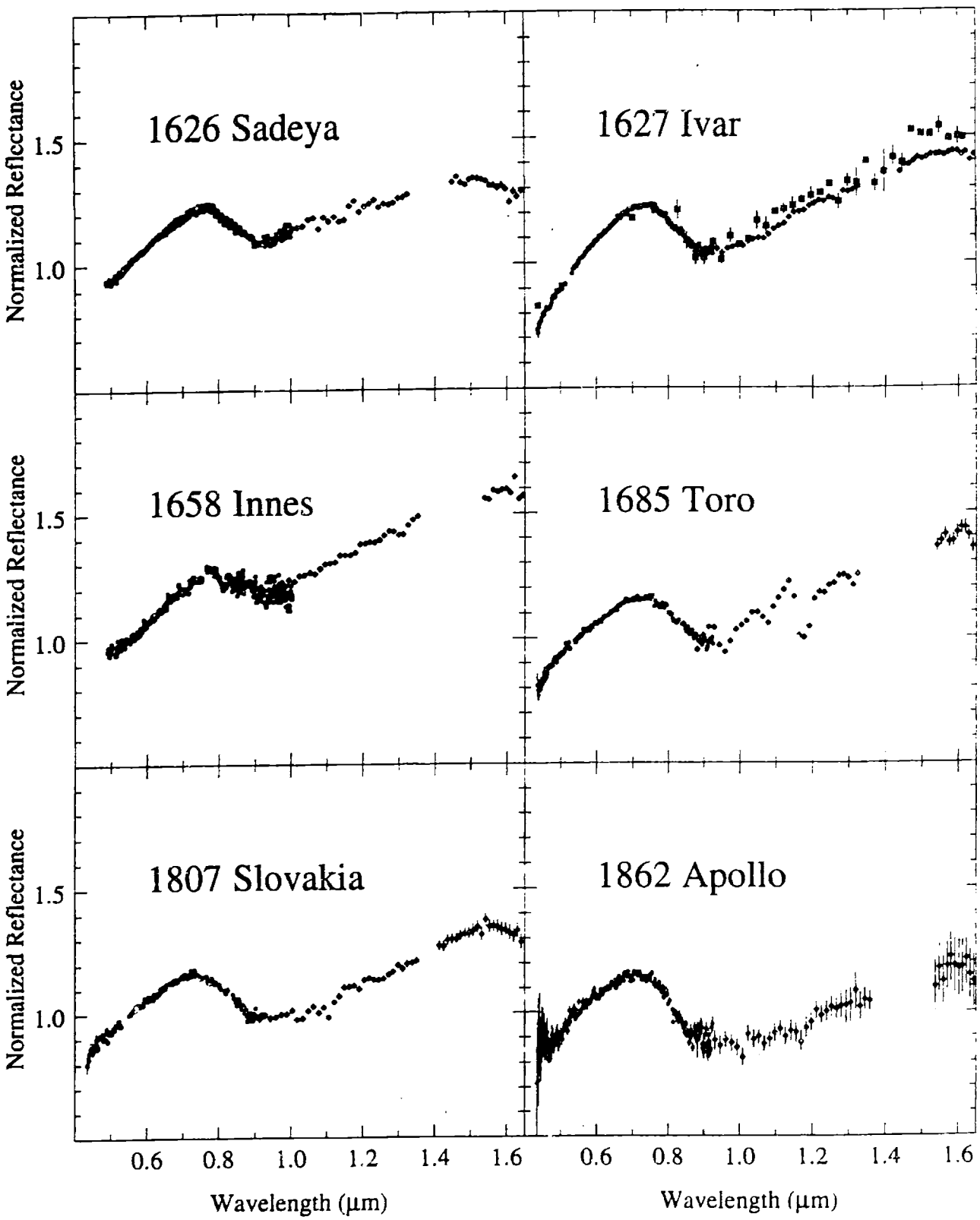
1626 Sadeya
1627 Ivar
1658 Innes
1685 Toro
1807 Slovakia
1862 Apollo
Normalized Reflectance
1.5
1.0
0.6
0.8
1.0
1.2
1.4
1.6
Wavelength (μm)

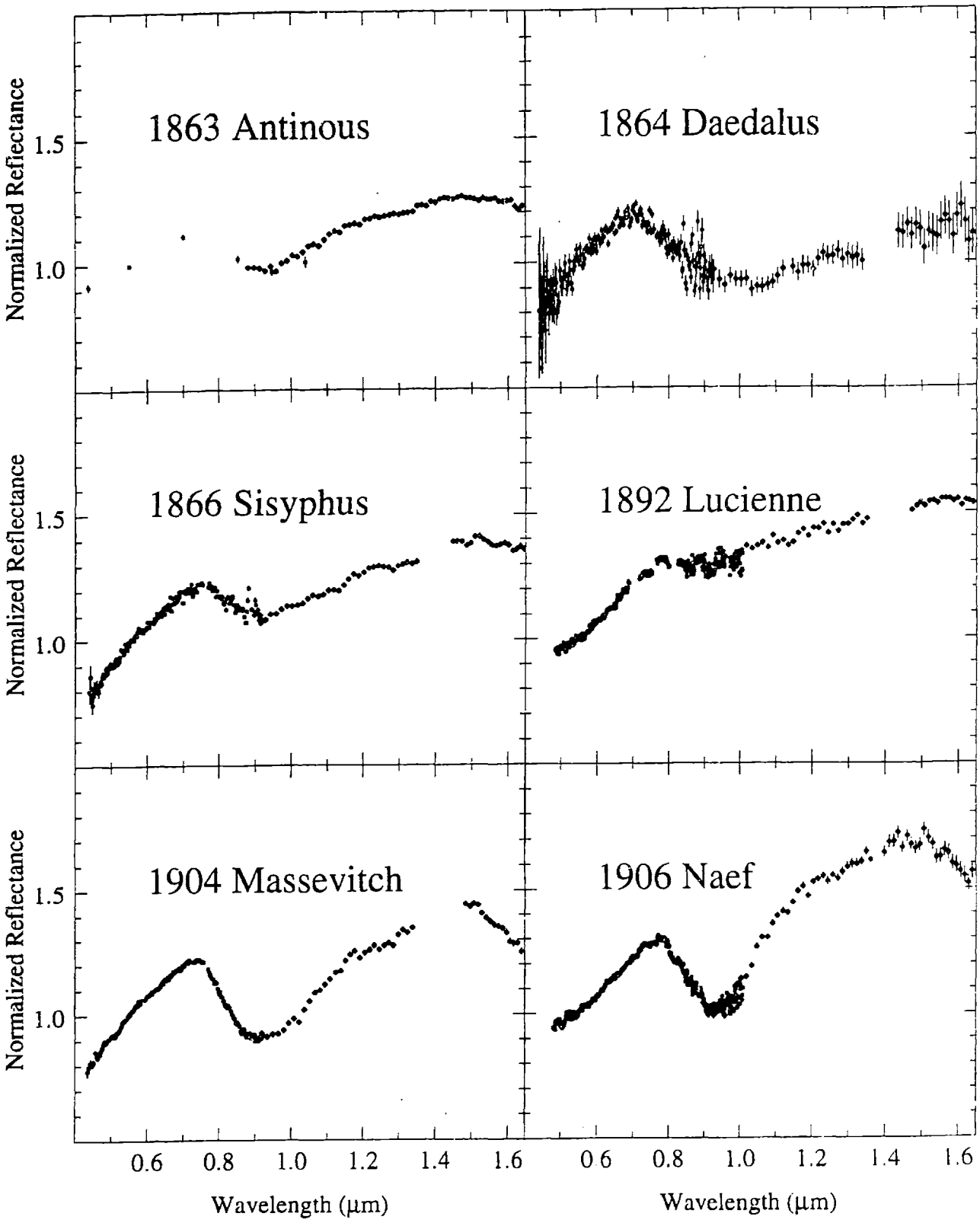
1863 Antinous
1864 Daedalus
1866 Sisyphus
1892 Lucienne
1904 Massevitch
1906 Naef
Normalized Reflectance
Normalized Reflectance
Normalized Reflectance
1.5
1.0
1.5
1.0
1.5
1.0
0.6
0.8
1.0
1.2
1.4
1.6
0.6
0.8
1.0
1.2
1.4
1.6
Wavelength (μm)
Wavelength (μm)

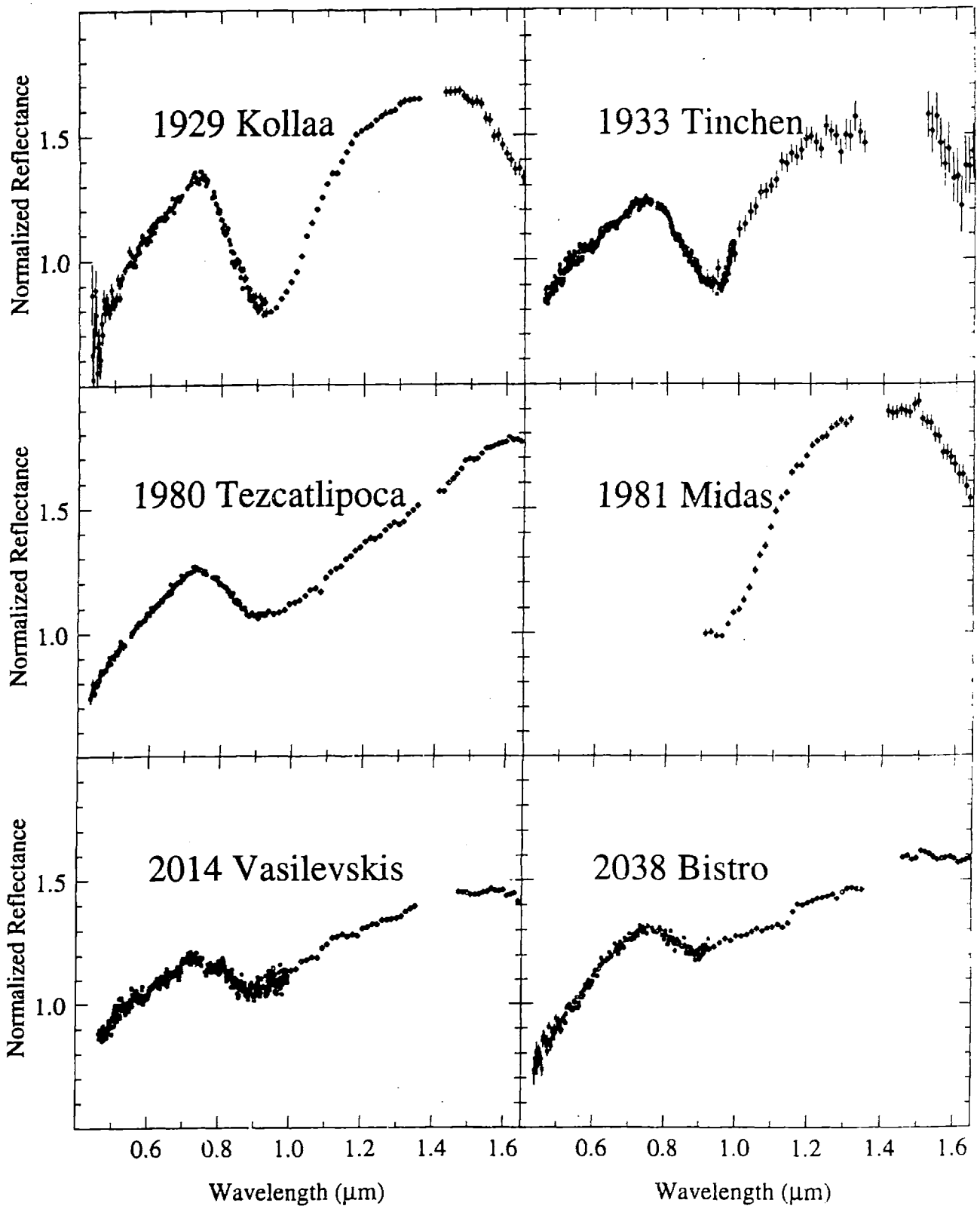
1929 Kollaa
1933 Tinchen
1980 Tezcatlipoca
1981 Midas
2014 Vasilevskis
2038 Bistro
Normalized Reflectance
1.0
1.5
0.6
0.8
1.0
1.2
1.4
1.6
Wavelength (μm)

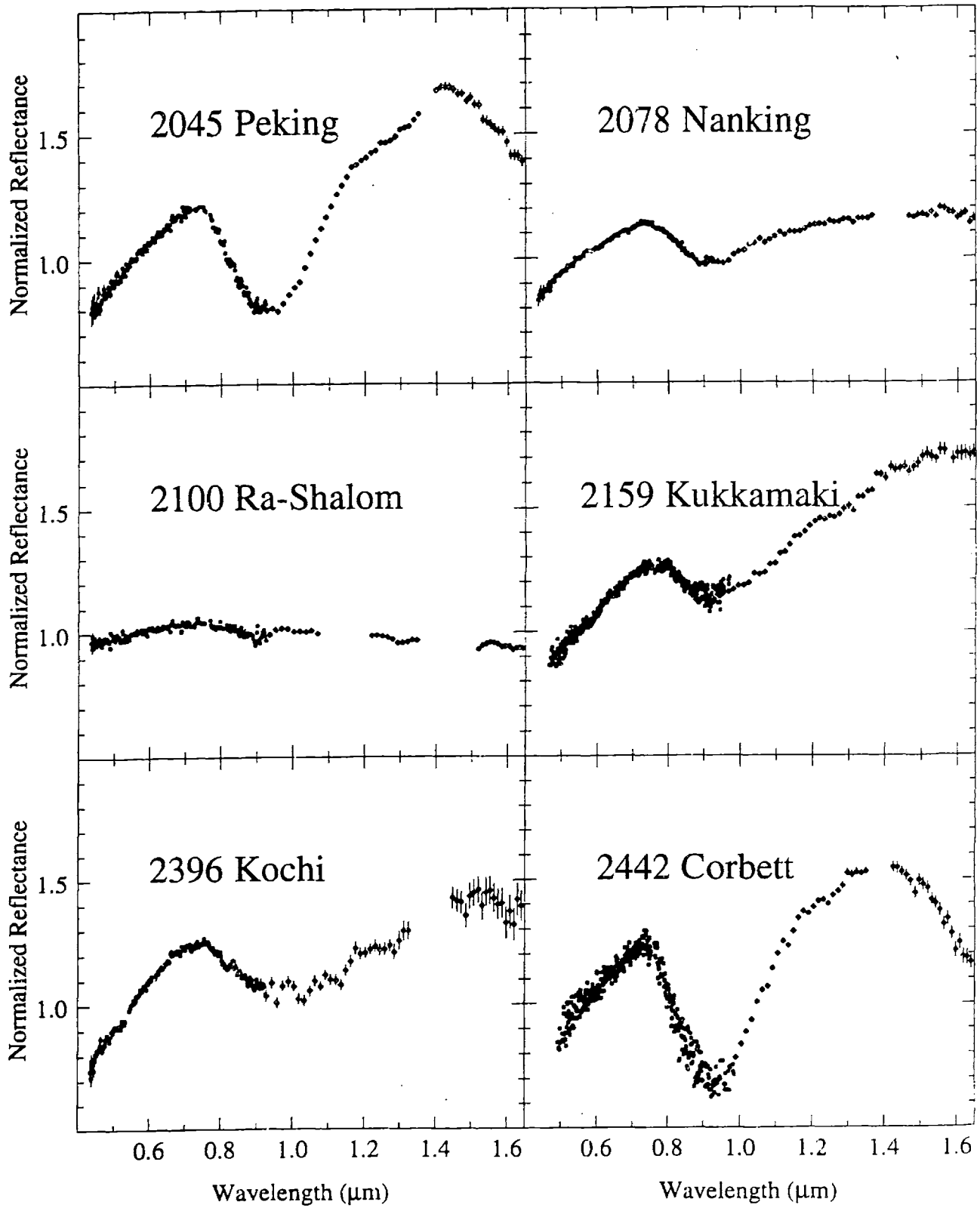
2045 Peking
2078 Nanking
2100 Ra-Shalom
2159 Kukkamaki
2396 Kochi
2442 Corbett
Normalized Reflectance
1.5
1.0
0.6
0.8
1.0
1.2
1.4
1.6
Wavelength (μm)

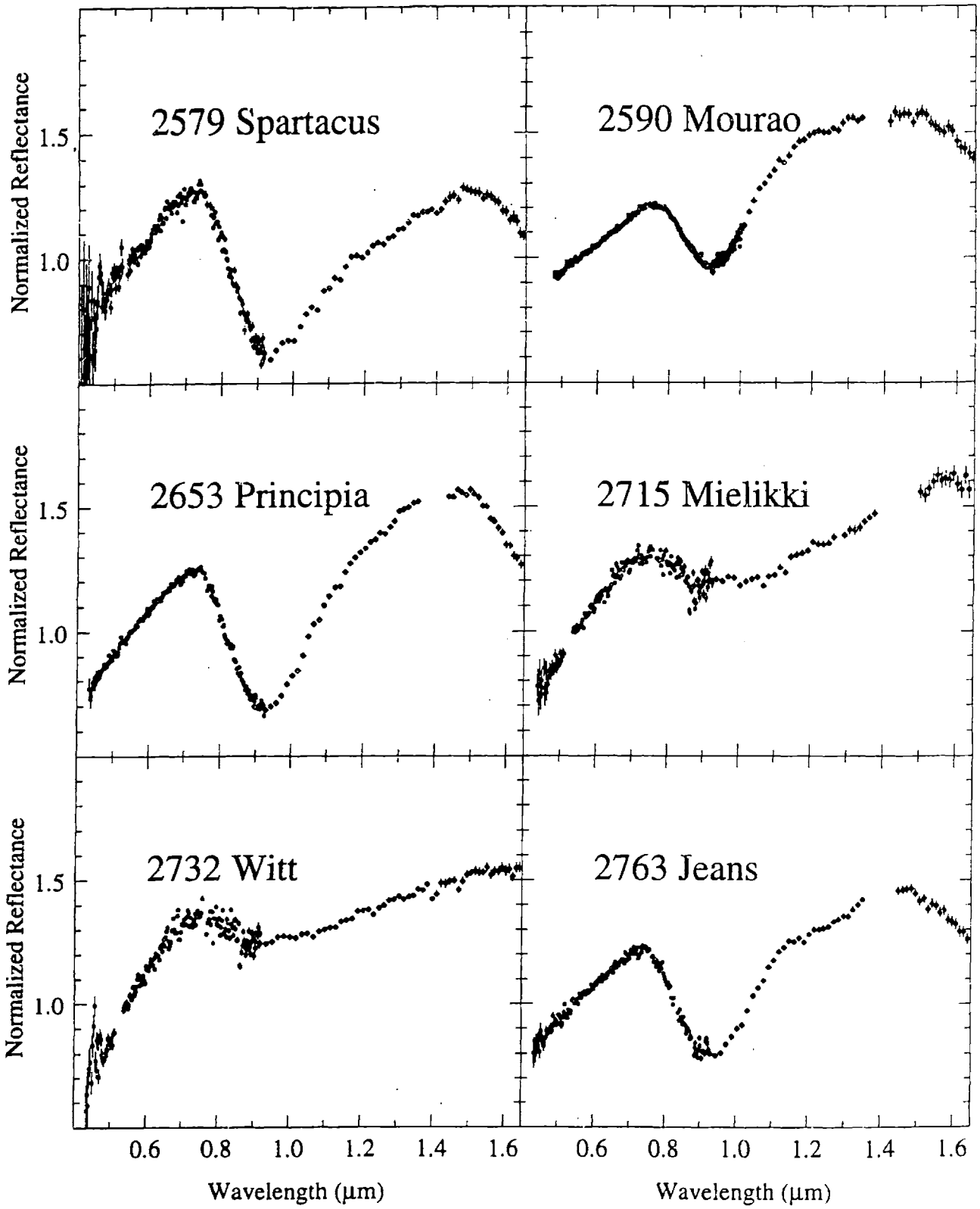
2579 Spartacus
2590 Mourao
2653 Principia
2715 Mielikki
2732 Witt
2763 Jeans
Normalized Reflectance
1.5
1.0
0.6
0.8
1.0
1.2
1.4
1.6
Wavelength (μm)

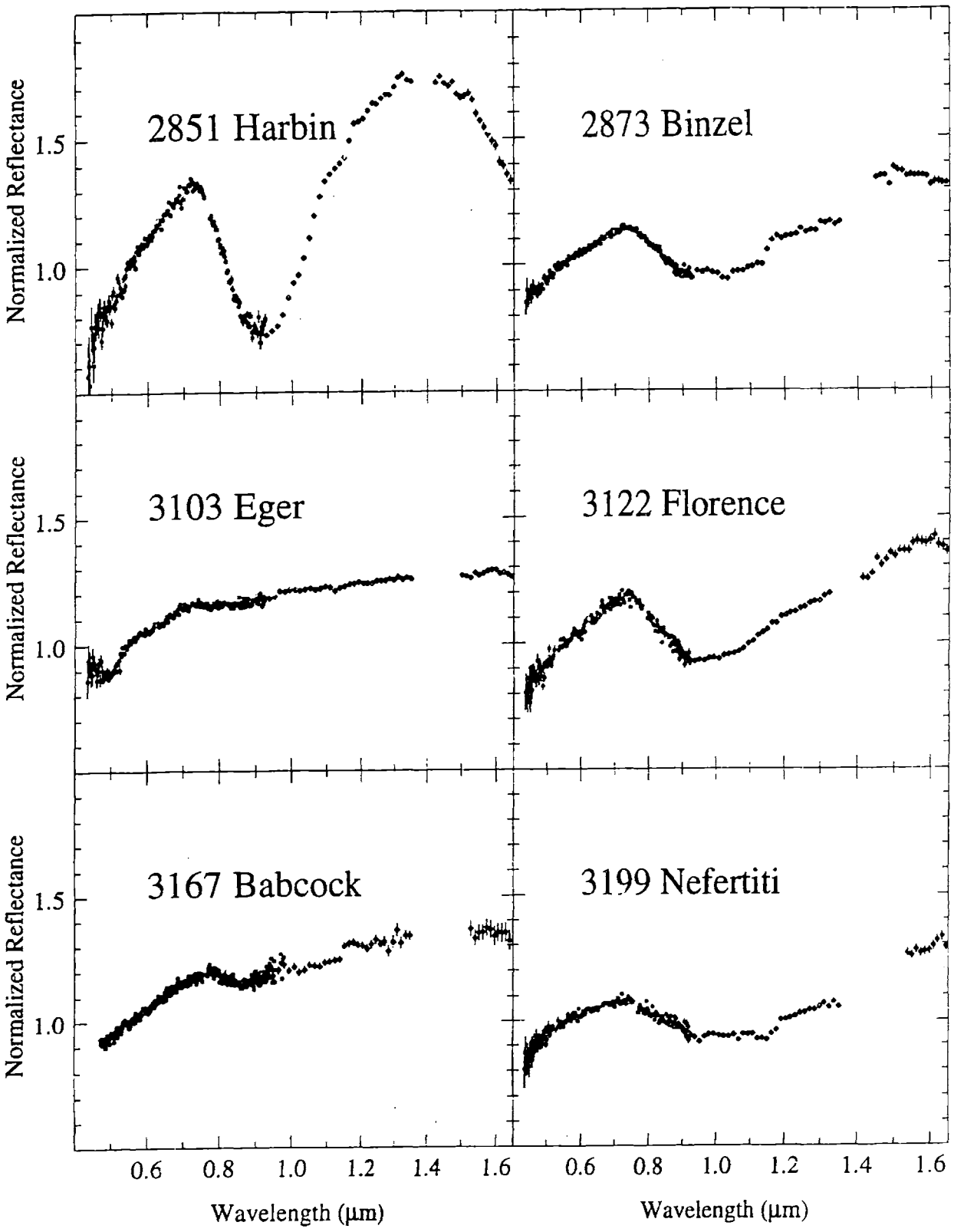
2851 Harbin
2873 Binzel
3103 Eger
3122 Florence
3167 Babcock
3199 Nefertiti
Normalized Reflectance
1.0
1.5
0.6
0.8
1.0
1.2
1.4
1.6
Wavelength (μm)

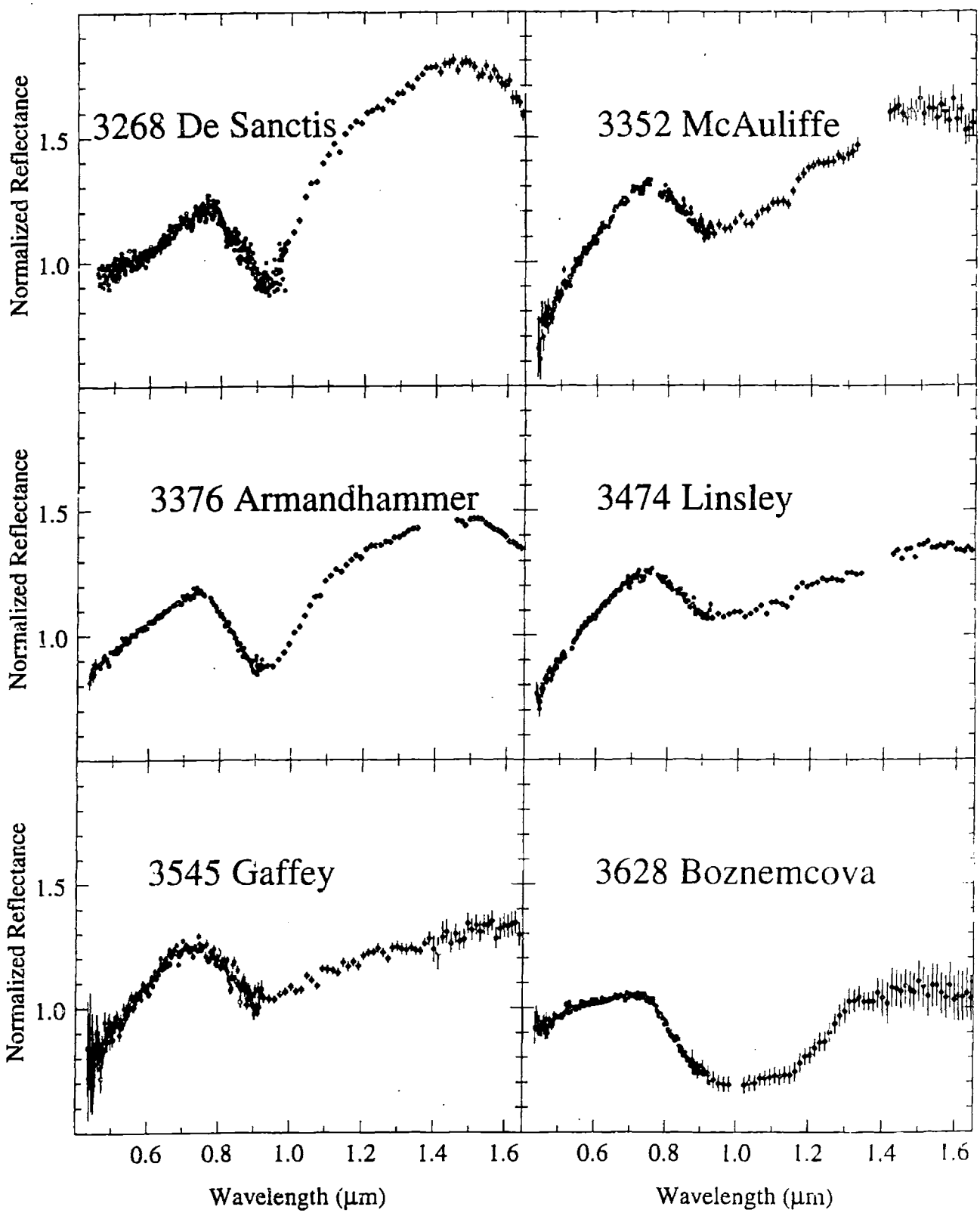
3268 De Sanctis
3352 McAuliffe
3376 Armandhammer
3474 Linsley
3545 Gaffey
3628 Boznemcova
Normalized Reflectance
1.5
1.0
0.6
0.8
1.0
1.2
1.4
1.6
Wavelength (μm)

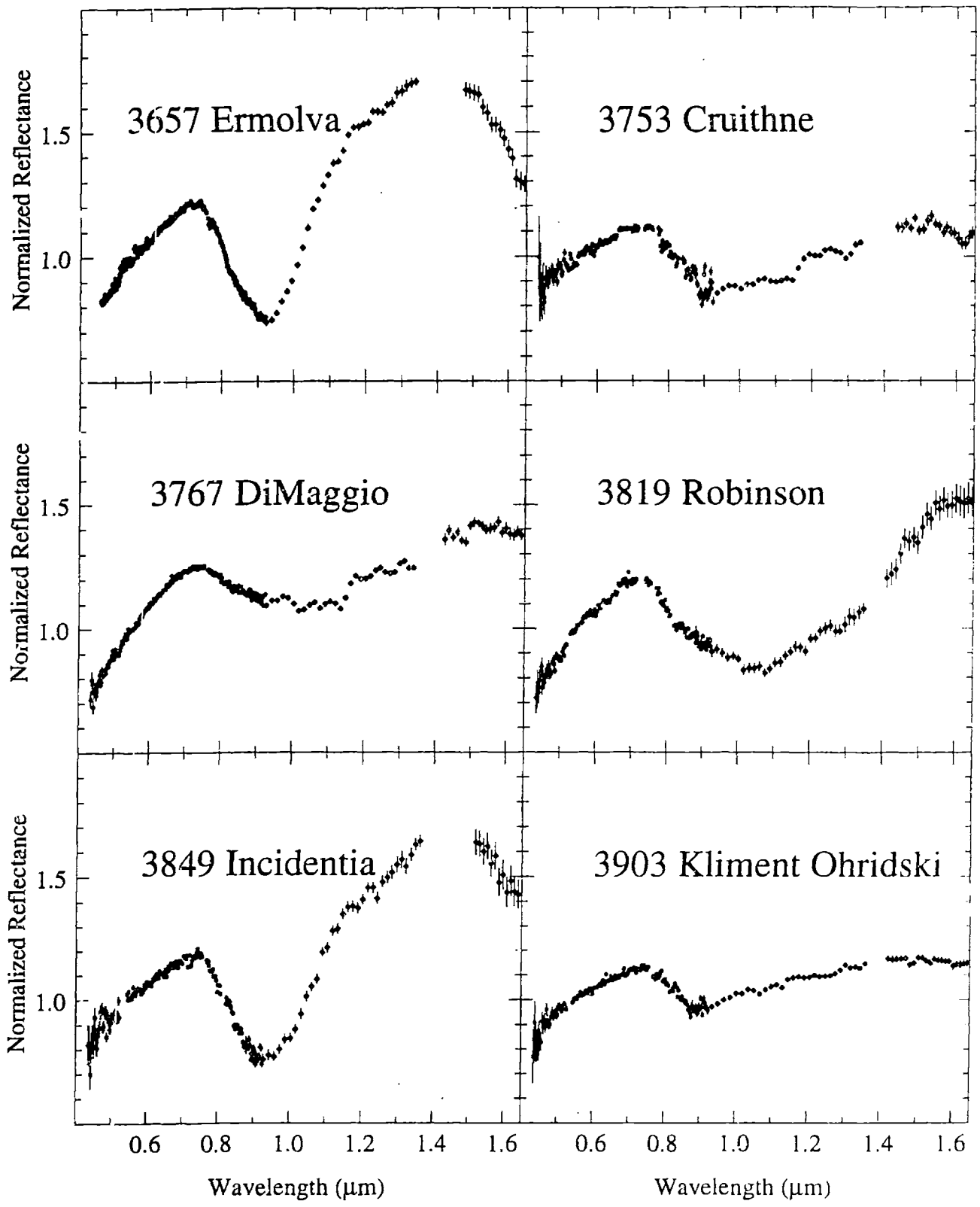
3657 Ermolva
3753 Cruithne
3767 DiMaggio
3819 Robinson
3849 Incidentia
3903 Kliment Ohridski
Normalized Reflectance
1.5
1.0
0.6
0.8
1.0
1.2
1.4
1.6
Wavelength (μm)

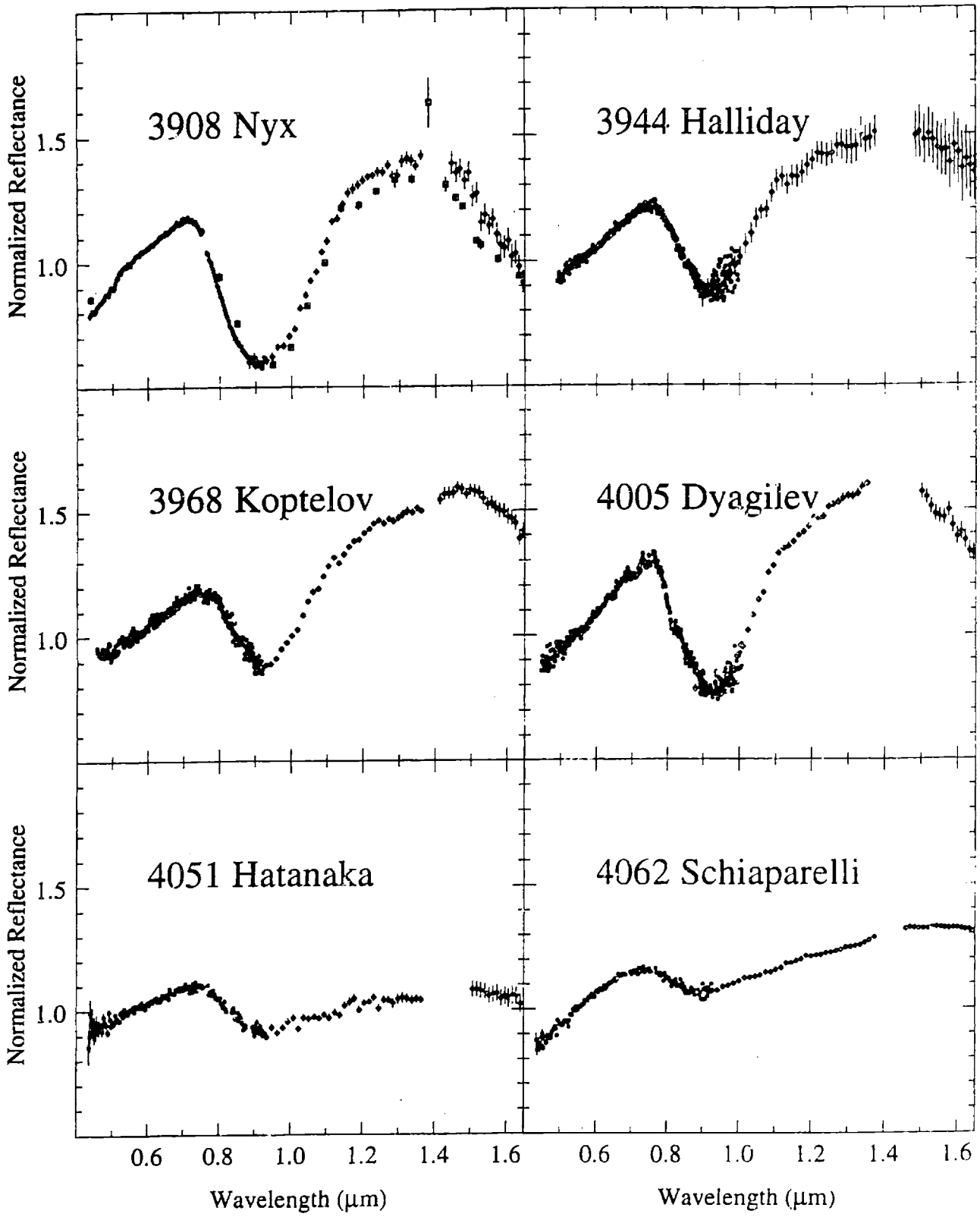
3908 Nyx
3944 Halliday
3968 Koptelov
4005 Dyagilev
4051 Hatanaka
4062 Schiaparelli
Normalized Reflectance
1.5
1.0
0.6
0.8
1.0
1.2
1.4
1.6
Wavelength (μm)

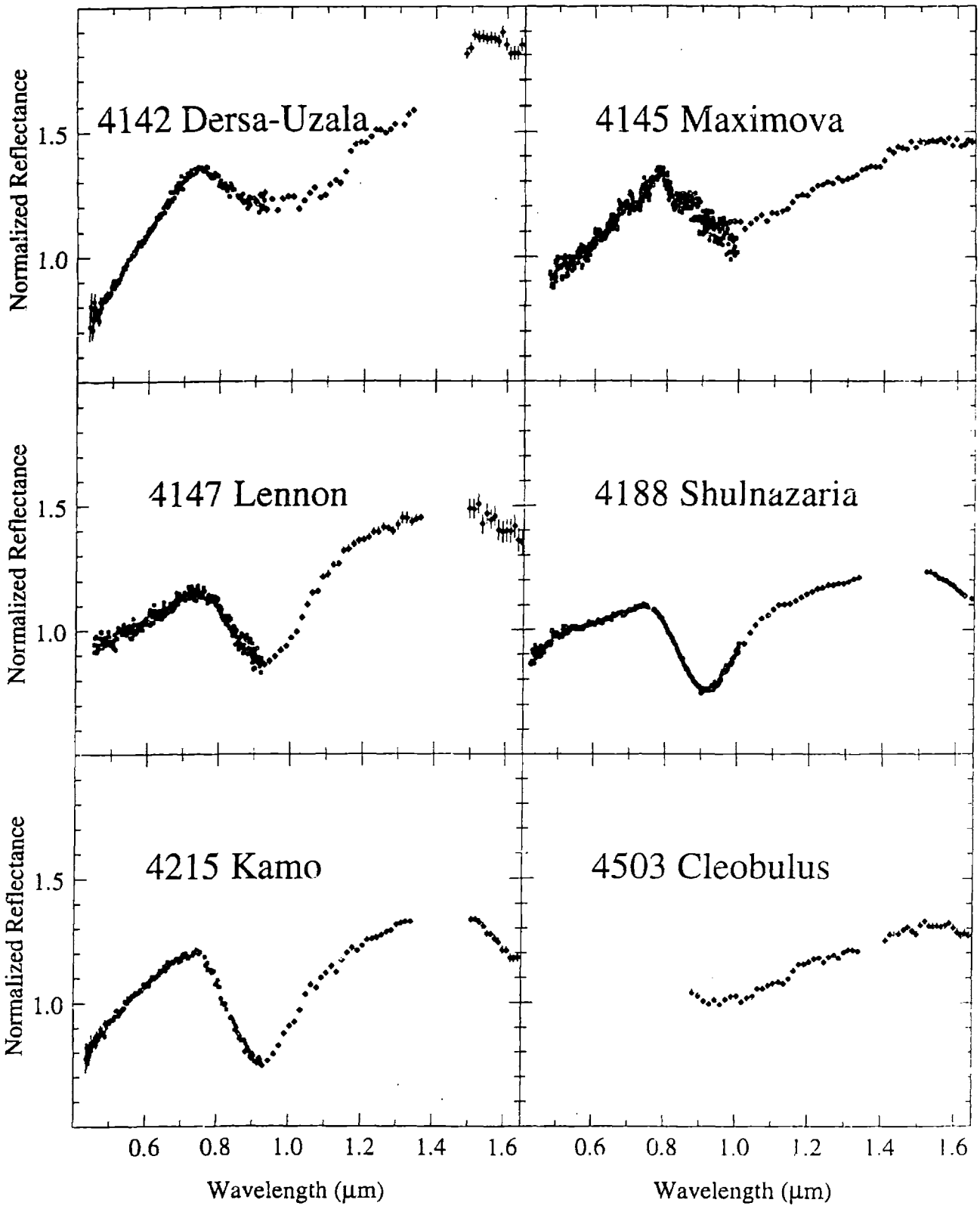
4142 Dersa-Uzala
4145 Maximova
4147 Lennon
4188 Shulnazaria
4215 Kamo
4503 Cleobulus
Normalized Reflectance
1.5
1.0
0.6
0.8
1.0
1.2
1.4
1.6
Wavelength (μm)

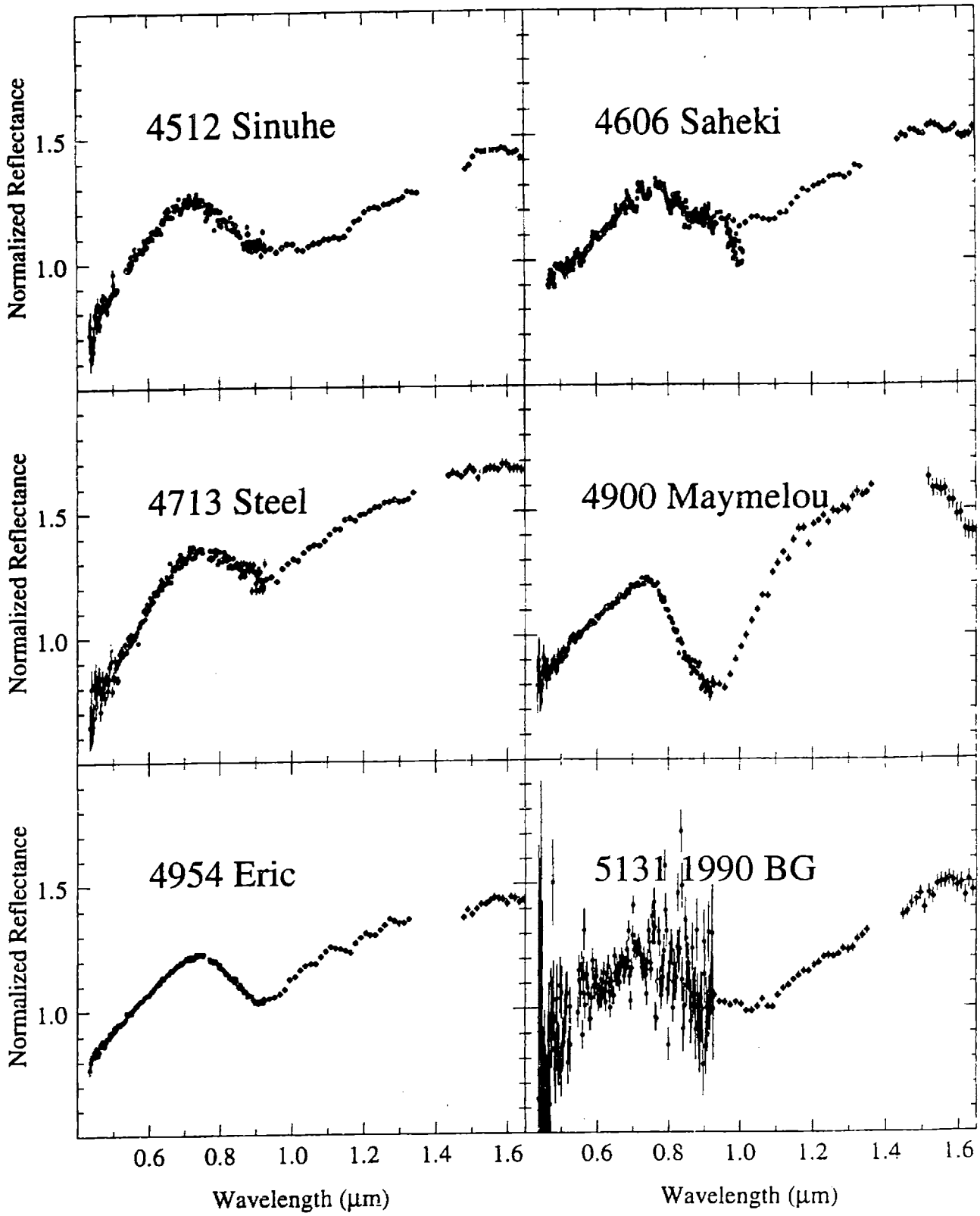
4512 Sinuhe
4606 Saheki
4713 Steel
4900 Maymelou
4954 Eric
5131 1990 BG
Normalized Reflectance
1.5
1.0
0.6
0.8
1.0
1.2
1.4
1.6
Wavelength (μm)

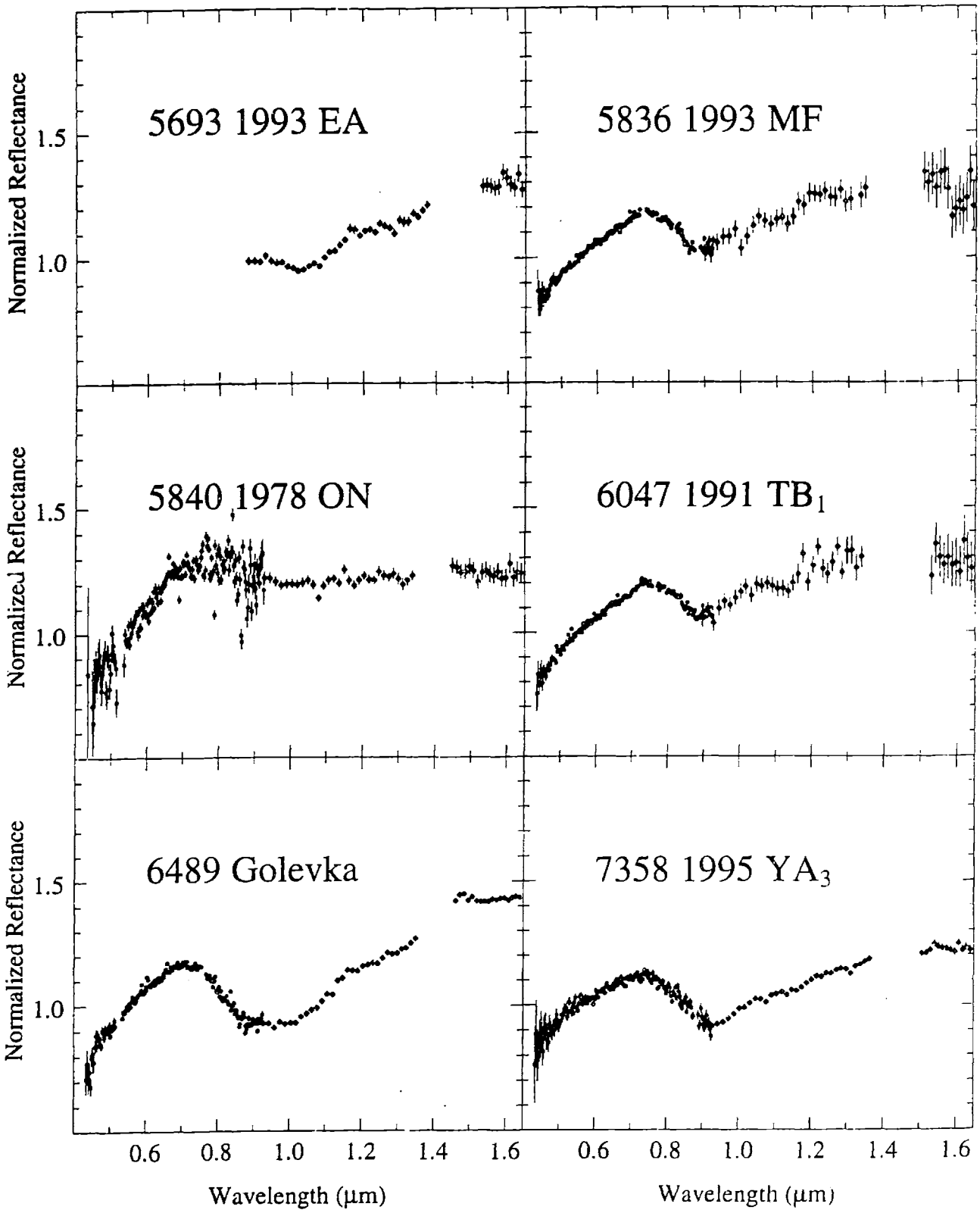
5693 1993 EA
5836 1993 MF
5840 1978 ON
6047 1991 TB1
6489 Golevka
7358 1995 YA3
Normalized Reflectance
1.5
1.0
0.6
0.8
1.0
1.2
1.4
1.6
Wavelength (μm)

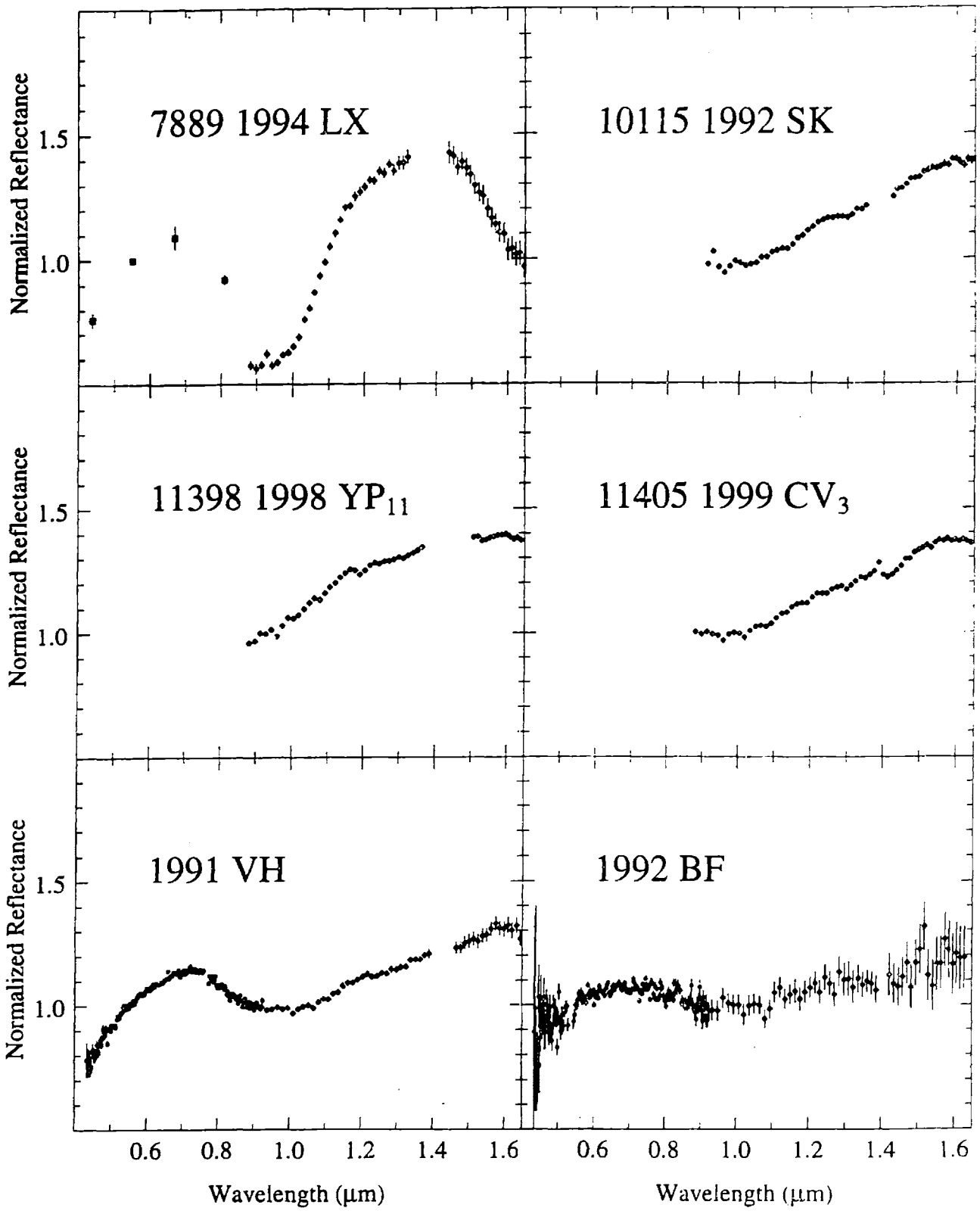
7889 1994 LX
10115 1992 SK
11398 1998 YP11
11405 1999 CV3
1991 VH
1992 BF
Normalized Reflectance
1.5
1.0
0.6
0.8
1.0
1.2
1.4
1.6
Wavelength (μm)

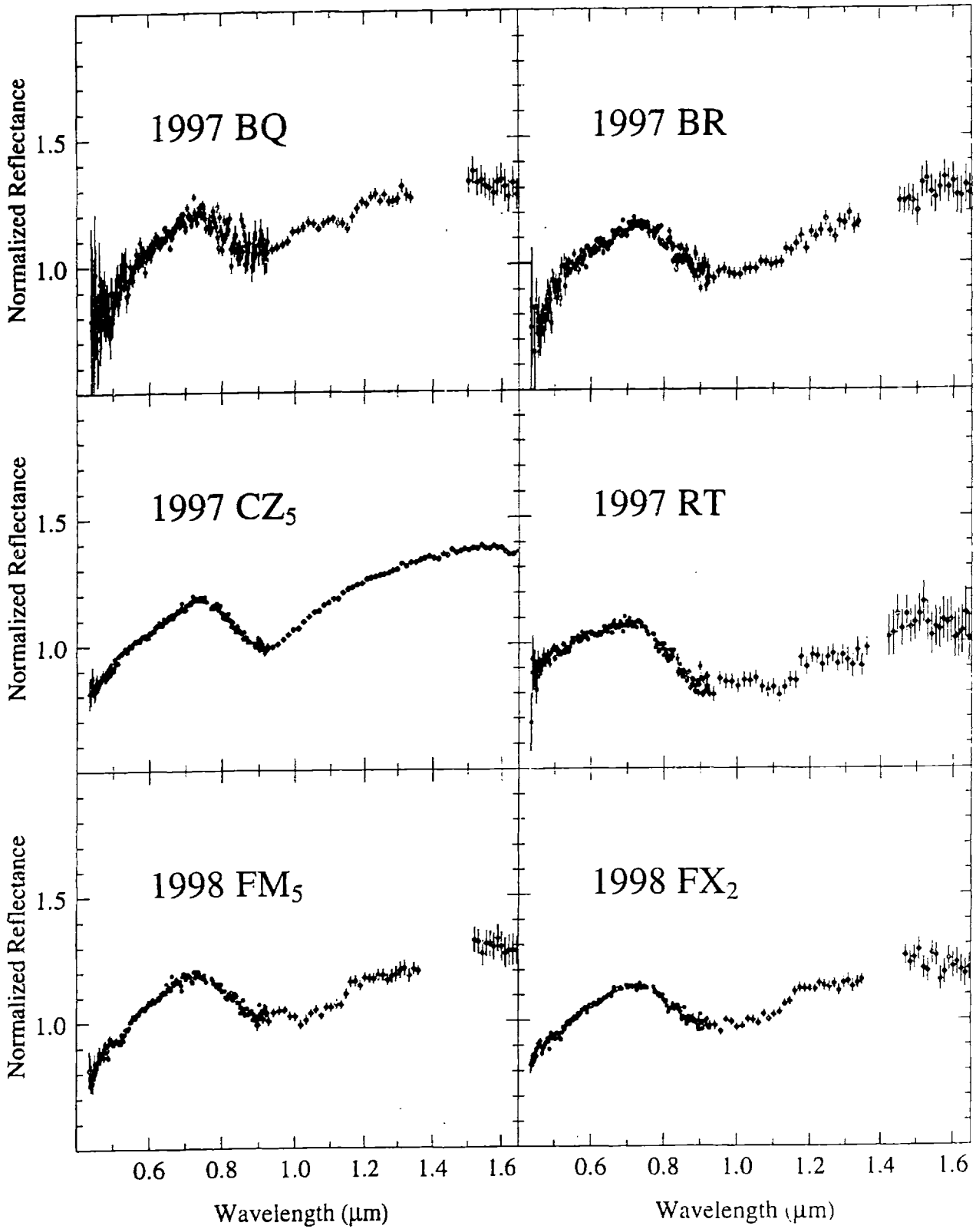
1997 BQ
1997 BR
1997 CZ5
1997 RT
1998 FM5
1998 FX2
Normalized Reflectance
1.5
1.0
0.6
0.8
1.0
1.2
1.4
1.6
Wavelength (μm)

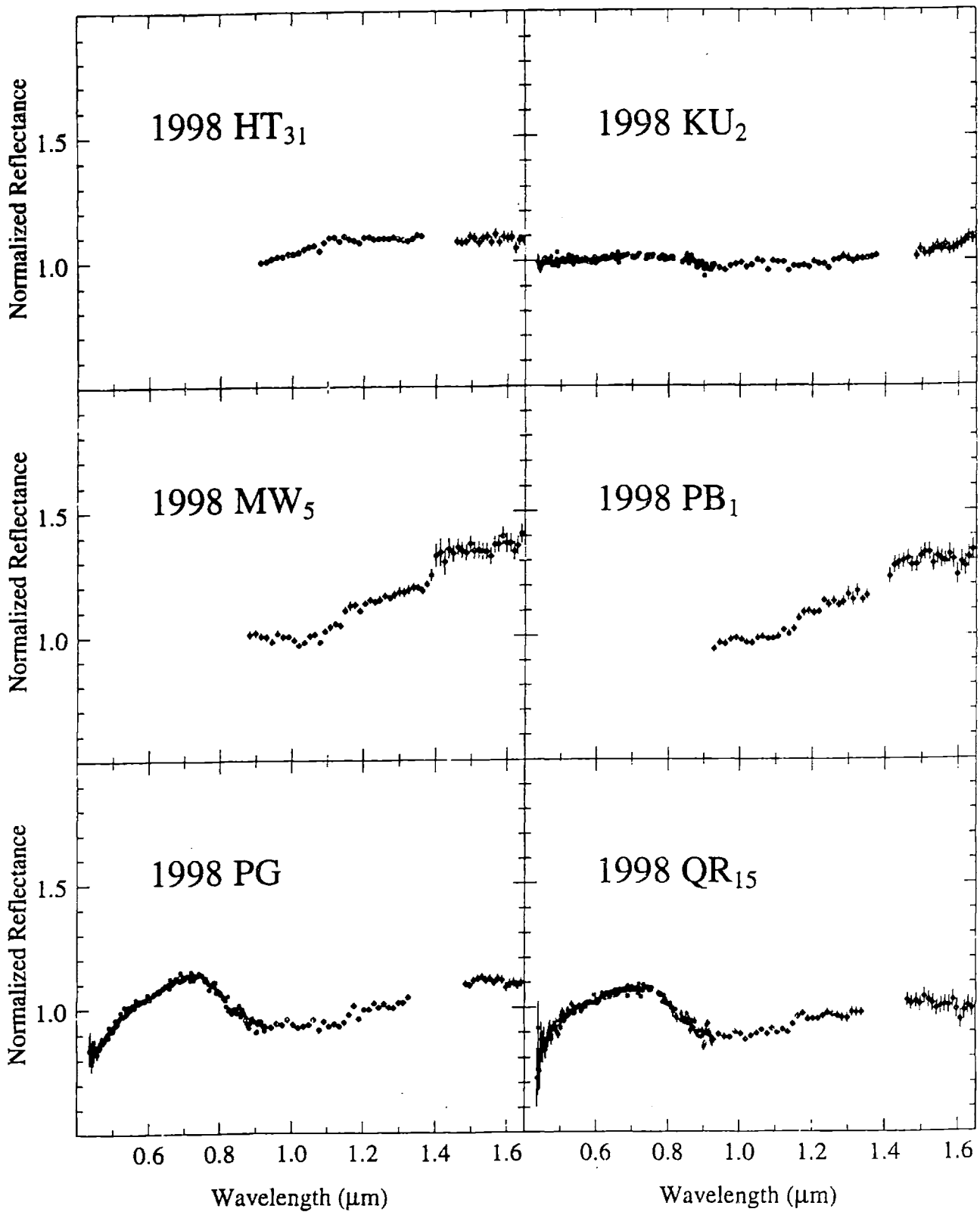
1998 HT31
1998 KU2
1998 MW5
1998 PB1
1998 PG
1998 QR15
Normalized Reflectance
1.5
1.0
0.6
0.8
1.0
1.2
1.4
1.6
Wavelength (μm)

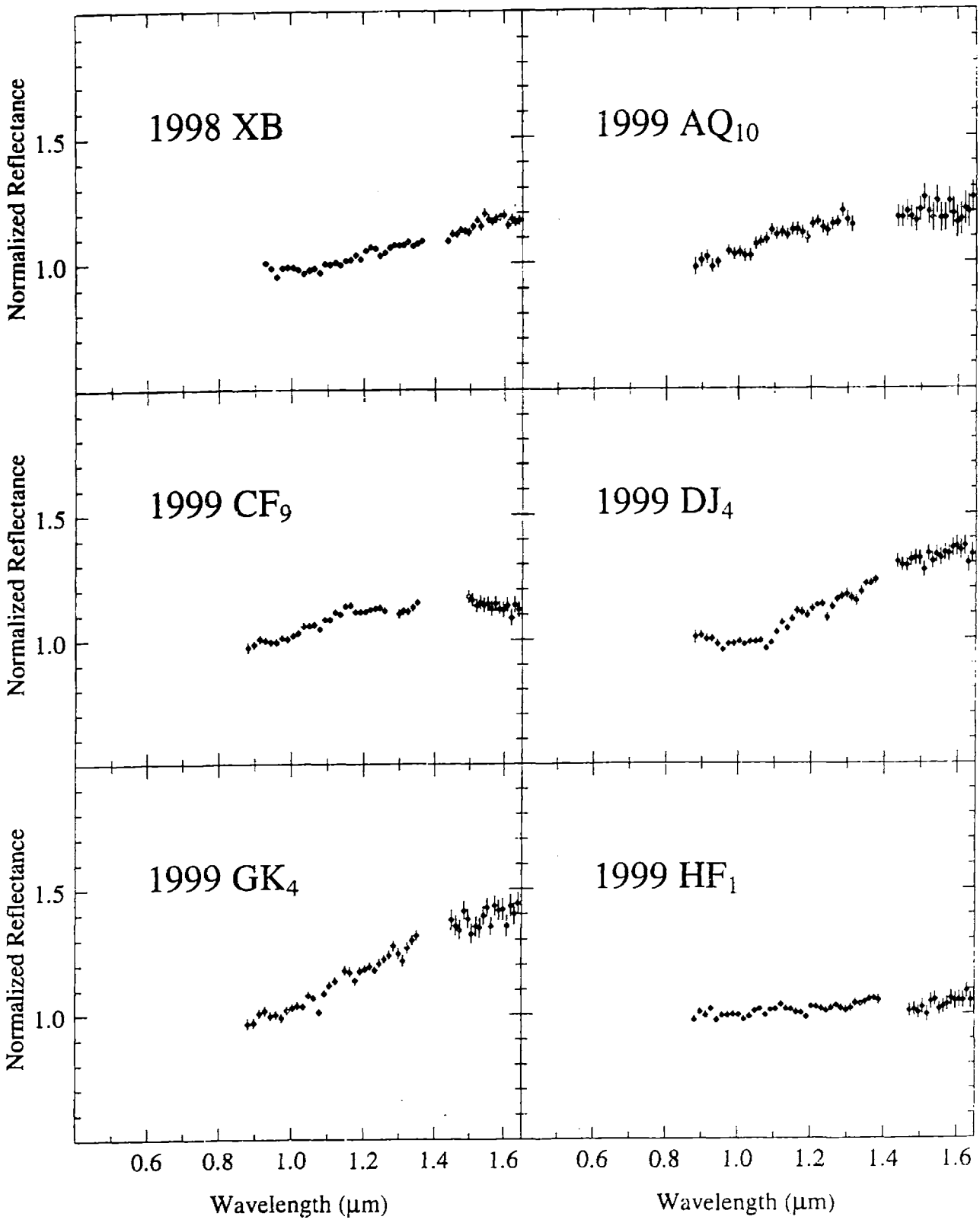
1998 XB
1999 AQ10
1999 CF9
1999 DJ4
1999 GK4
1999 HF1
Normalized Reflectance
1.5
1.0
0.6
0.8
1.0
1.2
1.4
1.6
Wavelength (μm)

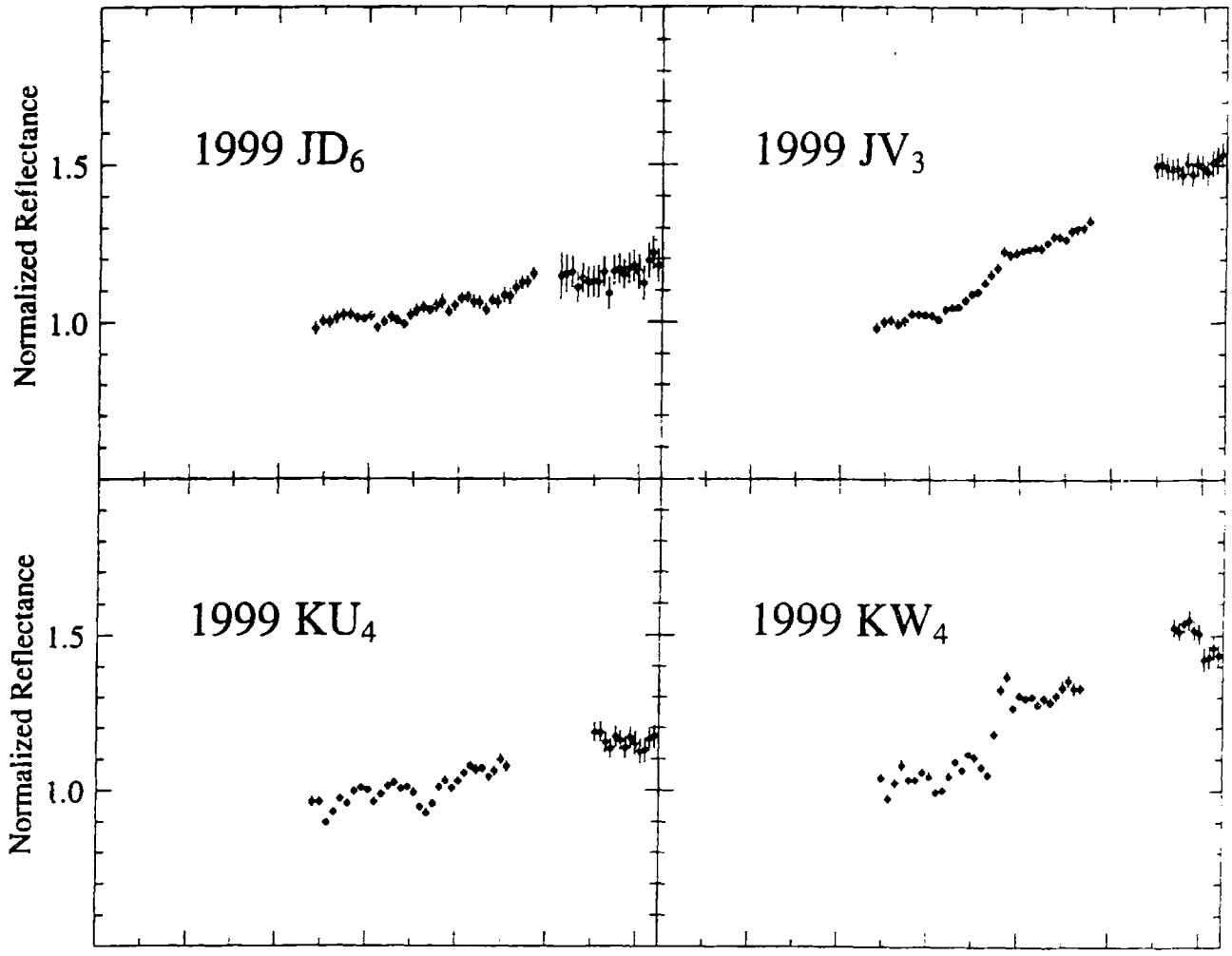
1999 JD6
1999 JV3
1999 KU4
1999 KW4
Normalized Reflectance
Normalized Reflectance
1.5
1.0
1.5
1.0

Appendix C
SMASSIR Spectra for Objects Observed Multiple Times

Plots of SMASSIR asteroids that had multiple observations. Small dots are used for visible data from SMASS I or II. Open diamonds are used for SMASSIR data. Dark squares are a combination of ECAS and 52-color data, when 52-color data for the object was available. If the ECAS data was not a good spectral match for the SMASS I or II data, only the 52-color data is plotted and normalized to the SMASS I or II data. Crosses are used for the Gaffey and Gilbert (1998) data for 6 Hebe and the Abell and Gaffey (1999) data for 349 Dembowska. All spectra are normalized to unity at 0.55 μm. Error bars are $\pm 1\sigma$.

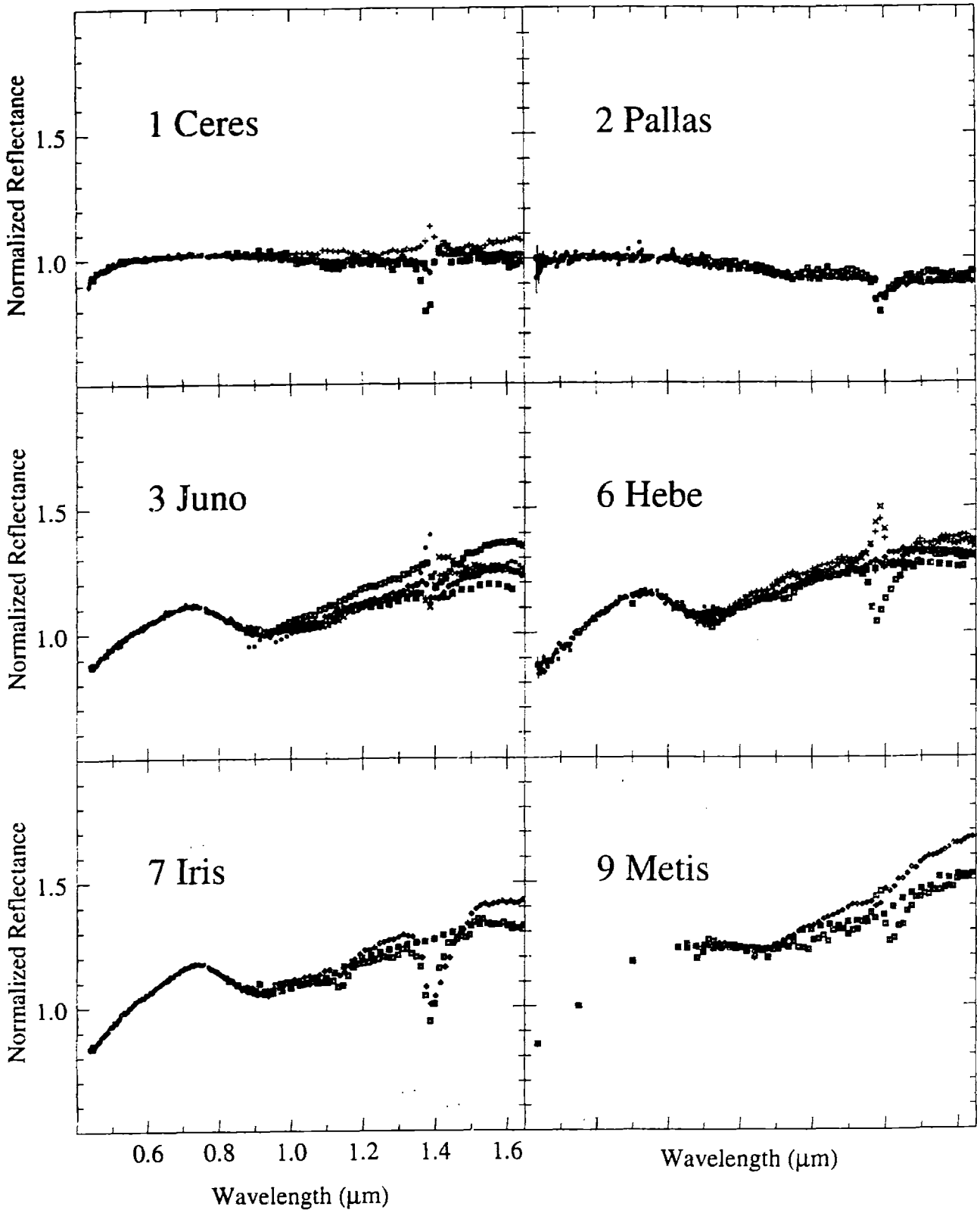
1 Ceres
2 Pallas
3 Juno
6 Hebe
7 Iris
9 Metis
Normalized Reflectance
1.5
1.0
0.6
0.8
1.0
1.2
1.4
1.6
Wavelength (μm)

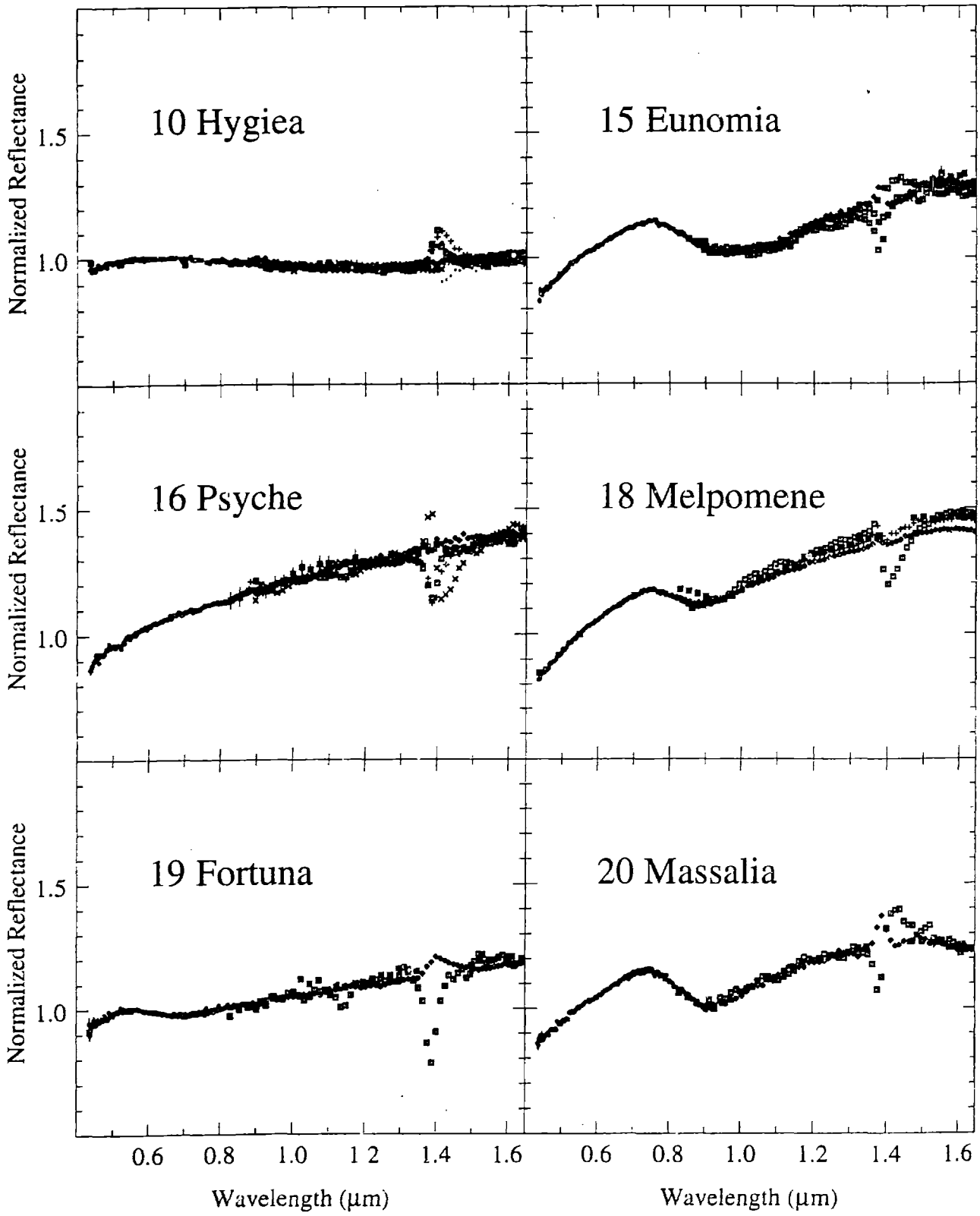
10 Hygiea
15 Eunomia
16 Psyche
18 Melpomene
19 Fortuna
20 Massalia
Normalized Reflectance
1.5
1.0
0.6
0.8
1.0
1.2
1.4
1.6
Wavelength (μm)

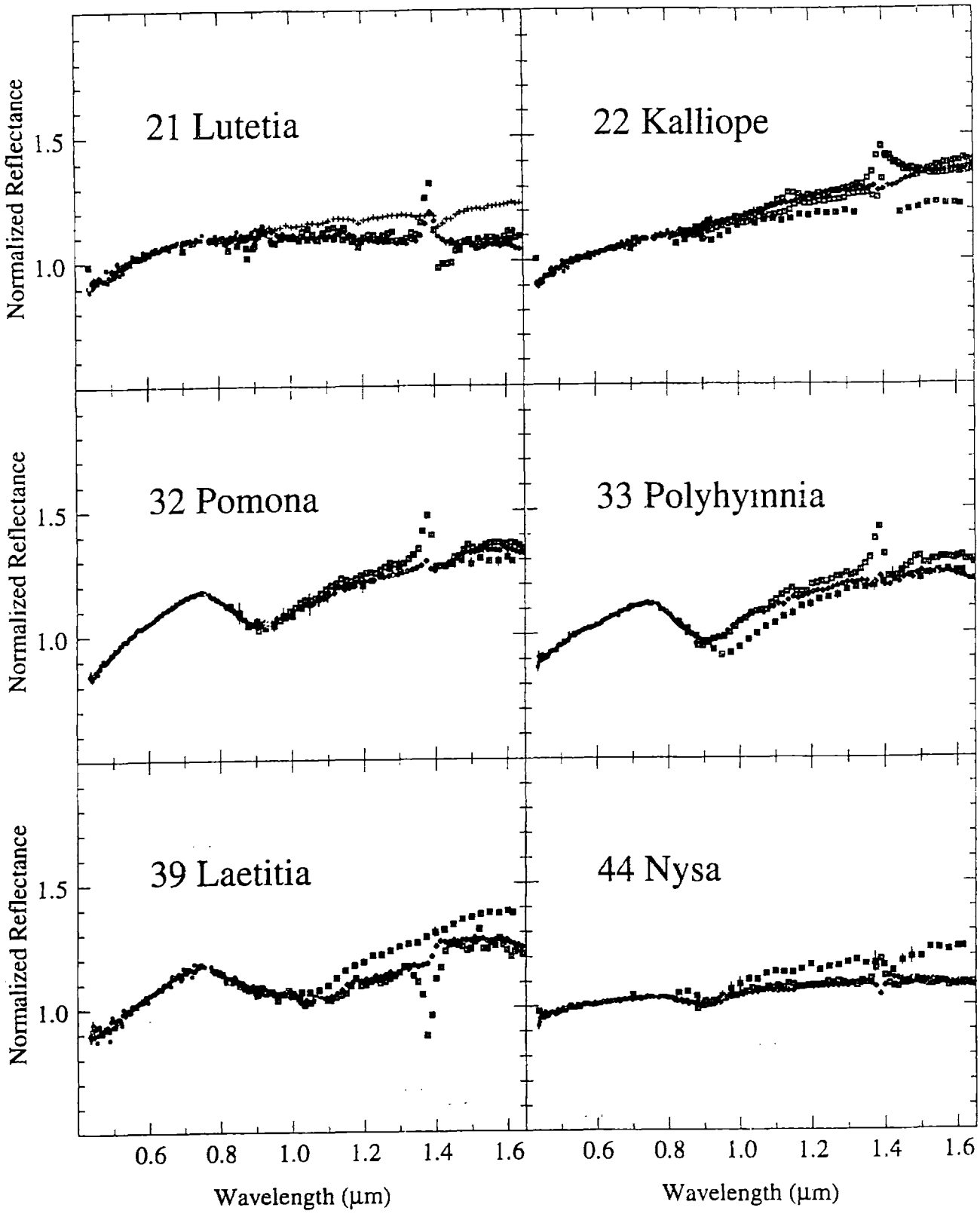
21 Lutetia
22 Kalliope
32 Pomona
33 Polyhymnia
39 Laetitia
44 Nysa
Normalized Reflectance
1.5
1.0
0.6
0.8
1.0
1.2
1.4
1.6
Wavelength (μm)

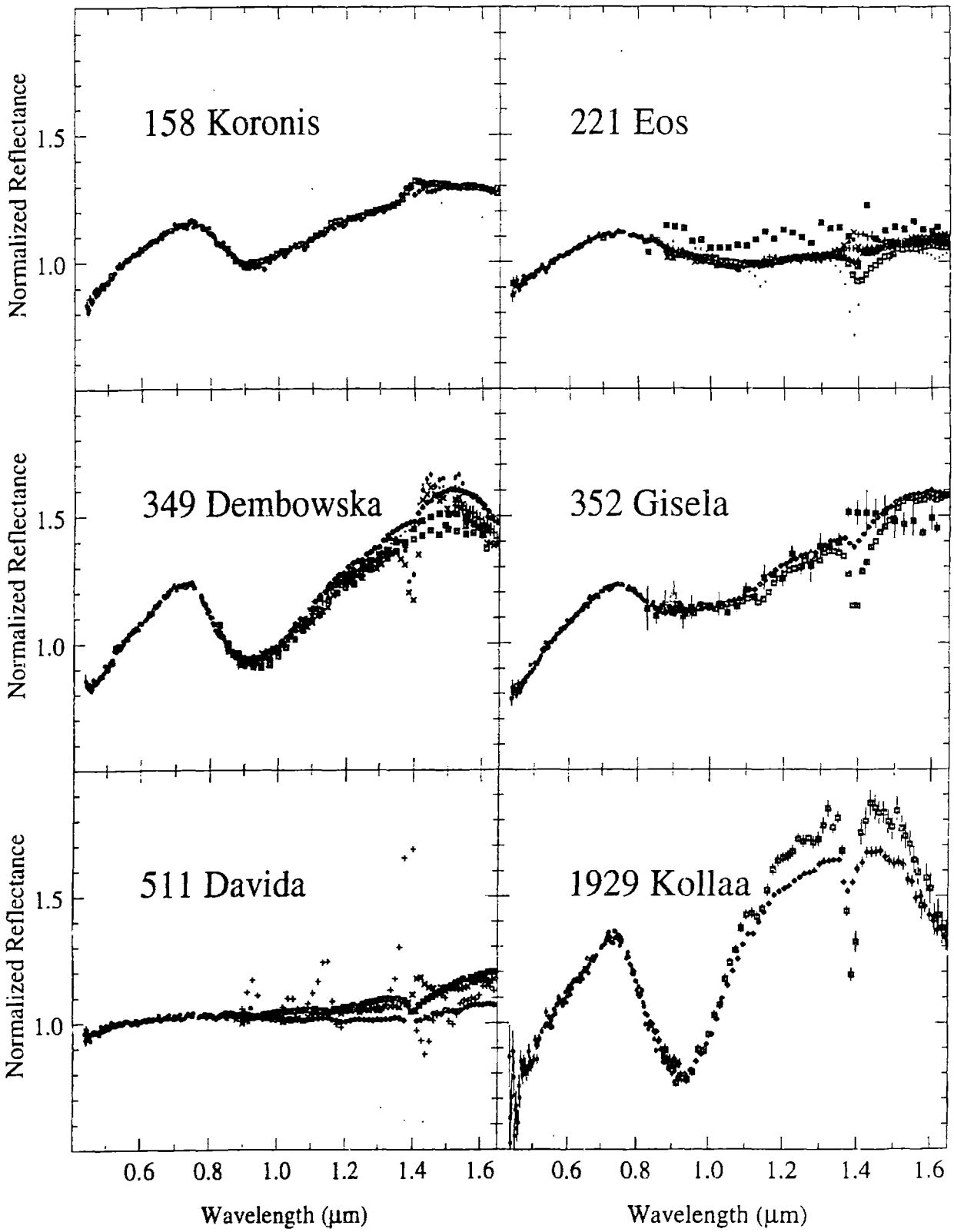
158 Koronis
221 Eos
349 Dembowska
352 Gisela
511 Davida
1929 Kollaa
Normalized Reflectance
1.5
1.0
0.6
0.8
1.0
1.2
1.4
1.6
Wavelength (μm)

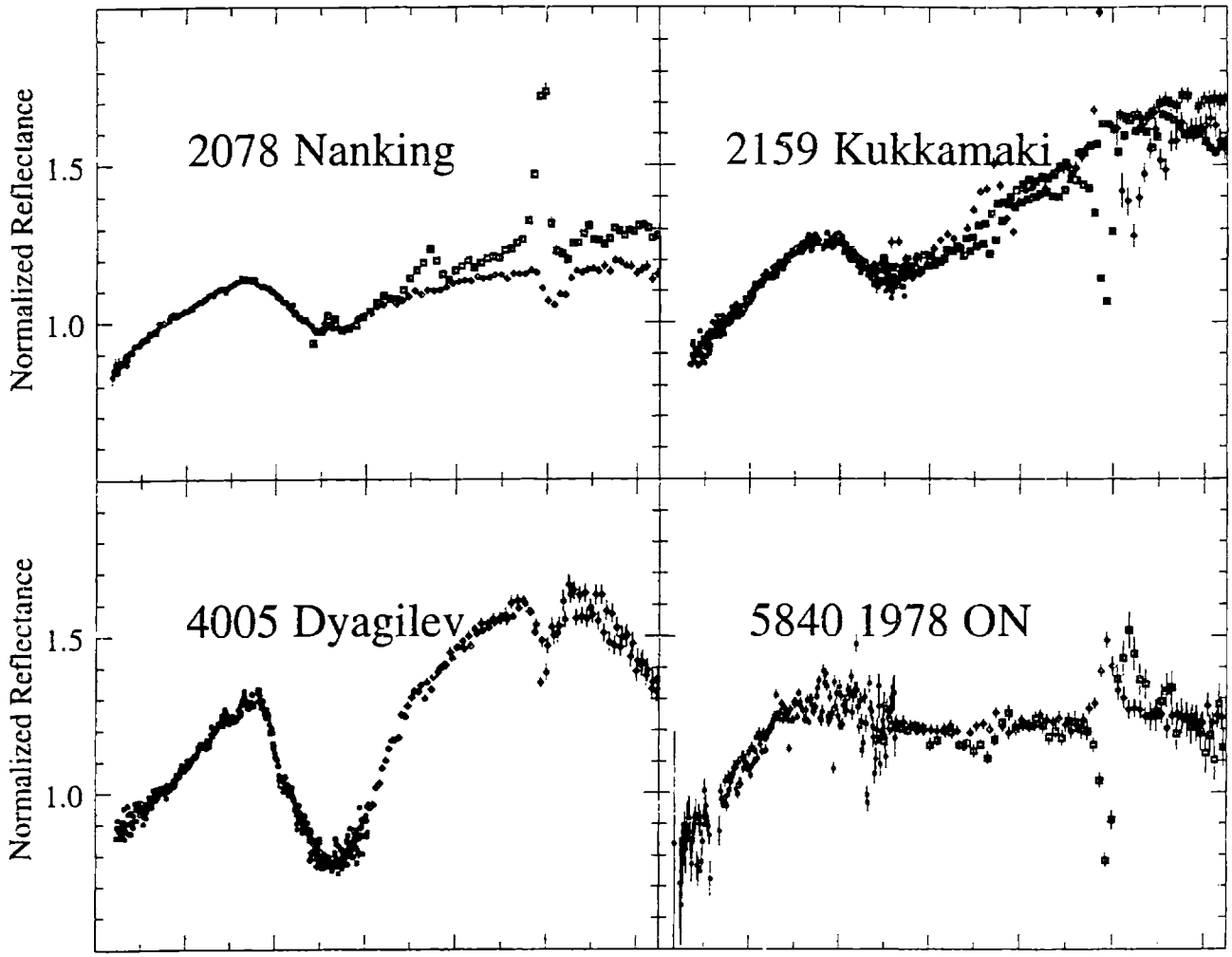
2078 Nanking
2159 Kukkamaki
4005 Dyagilev
5840 1978 ON
Normalized Reflectance
1.5
1.0
Normalized Reflectance
1.5
1.0

Appendix D
Taxonomic Classifications and Physical Parameters

Numbers, names, classes (Tholen, 1989; Xu *et al.*, 1995; Bus, 1999; Gaffey *et al.*, 1993), albedos and diameters (Tedesco, 1994) of SMASSIR objects. Bus (personal communication) has slightly revised his Bus (1999) classifications by inserting NEAs and recently observed main-belt objects into his taxonomy. Asteroids observed in SMASS II that are labeled with an asterisk (*) have had their classifications changed from those published in Bus (1999). The IRAS albedos and diameters usually have error bars of less than 10%. HCM (hierarchical clustering method) family membership is from Zappalà *et al.* (1995). NEA types (Aten, Apollo or Amor) are from the Minor Planet Center web page (http://cfa-www.harvard.edu/iau/lists/Unusual.html). Mars-crossers are also labeled. Diameters (D) in parentheses are calculated ($D = 10^{((6.259 - 0.4H - \log p)/2)}$) (Bowell *et al.*, 1989) using the H magnitude (time-averaged magnitude of an asteroid calculated at zero phase angle and unit heliocentric and geocentric distances) (H) with estimated albedos (p) of 0.25 for A, O, Q and S objects, 0.5 for E objects, 0.05 for B, C and G objects and 0.42 for V and J objects. Diameters are rounded to the nearest kilometer except for diameters under 1 km, which are rounded to the nearest tenth of a kilometer.

Asteroid	Tholen	SMASS I	SMASS II	S Subclass	Albedo	Diameter (km)	HCM Family	NEA	52-color
1 Ceres	G		C		0.11	848	Ceres		yes
2 Pallas	B		B		0.16	498			yes
3 Juno	S	S	Sk	S(IV)	0.24	234	Juno		yes
4 Vesta	V	V	V		0.42	506†	Vesta		yes
5 Astraea	S		S		0.23	119			yes
6 Hebe	S	S	S	S(IV)	0.27	185			yes
7 Iris	S	S	S	S(IV)	0.28	200			yes
9 Metis	S			----		(149)			yes
10 Hygiea	C	C	C		0.07	407	Hygiea		yes
11 Parthenope	S		Sk	S(IV)	0.18	153			yes
12 Victoria	S		L	S(II)?	0.18	113			yes
15 Eunomia	S		S	S(III)	0.21	255	Eunomia		yes
16 Psyche	M		X		0.12	253			yes
18 Melpomene	S	S	S	S(V)	0.22	141			yes
19 Fortuna	G		Ch			225‡			yes
20 Massalia	S		S	S(VI)	0.21	146	Massalia		yes
21 Lutetia	M		Xk		0.22	96			yes
22 Kalliope	M	M	X		0.14	181			yes
25 Phocaea	S	S	S	S(IV)	0.23	75			yes
26 Proserpina	S		S	S(II)	0.20	95			yes
28 Bellona	S		S		0.18	121			
32 Pomona	S	S	S	S(IV)	0.26	81			yes
33 Polyhymnia	S		Sq	S(IV)		(53)			yes
37 Fides	S		S	S(V)	0.18	108			yes
39 Laetitia	S		S	S(II)	0.29	150			yes
40 Harmonia	S		S	S(VII)	0.24	108			yes
42 Isis	S	S	L	S(I)	0.17	100			yes
43 Ariadne	S	S	Sk	S(III)	0.27	66	Flora		yes
44 Nysa	E		Xc*		0.55	71	Nysa		yes
57 Mnemosyne	S		S	S(VII)	0.21	113			yes
63 Ausonia	S		Sa	S(II-III)	0.16	103			yes
64 Angelina	E		Xe		0.40&	51&			yes
65 Cybele	P		Xc		0.07	237			yes
68 Leto	S	S		S(II)	0.23	123			yes
71 Niobe	S	S	Xe		0.31	83			
80 Sappho	S		S	S(IV)	0.18	78			yes
82 Alkmene	S	S	Sq	S(VI)	0.21	61			yes
92 Undina	X		Xc		0.25	126			yes
113 Amalthea	S		S	S(I)	0.26	46			yes
140 Siwa	P		Xc		0.07	110			
158 Koronis	S	S	S		0.28	35	Koronis		
167 Urda	S	S	Sk		0.22	40	Koronis		
169 Zelia	S	S	Sl		0.23	34			
221 Eos	S	S	K		0.14	104	Eos		yes
243 Ida	S	S	S		0.24	28	Koronis		
244 Sita			Sa		0.19	11	Flora		
246 Asporina	A		A		0.17	60			yes
253 Mathilde			Cb		0.05!	53!			
289 Nenetta	A	A	A		0.24	34			yes
291 Alice	S				0.21	15	Flora		
304 Olga	C		Xc		0.05	68			
335 Roberta	FP		B		0.06	89			
336 Lacaderia	D		Xk		0.05	69			yes
346 Hermentaria	S	S	S		0.22	107			yes
349 Dembowska	R	R	R		0.38	140			yes
352 Gisela	S		Sl		0.43	20	Flora		yes
354 Eleonora	S	S	Sl		0.19	155			
364 Isara	S			S(II)	0.26	28	Flora		yes
374 Burgundia	S	S	S		0.30	45	Ceres		
379 Huenna	B		C		0.06	92	Themis		yes

Asteroid	Tholen	SMASS I	SMASS II	S Subclass	Albedo	Diameter (km)	HCM Family	NEA	52-color
389 Industria	S		S	S(V)	0.20	79			yes
416 Vaticana	S	S	Sl		0.17	85			
446 Aeternitas	A	A	A		0.24	45			yes
480 Hansa	S	S			0.25	56			
511 Davida	C	C	C		0.05	326			
515 Athalia	I		Cb		0.04	38	Themis		
584 Semiramis	S		Sl	S(IV)	0.20	54			yes
599 LuisaS	S	K			0.14	65			
625 Xenia			Sa		0.22	28			
653 Berenike	S	S	K		0.24	39	Eos		yes
675 Ludmilla	S	S	S			(71)			
702 Alauda	C	C	B		0.06	195			yes
720 Bohlinia	S	S	Sq		0.20	33	Koronis		
737 Arequipa	S	S	S		0.27	44			
773 Irmintraud	D		T		0.04	96			yes
774 Armor		S			0.25	50			
787 Moskva		S			0.24	27	Maria		
808 Merxia		S	Sq*		0.22	32	Merxia		
811 Nauheima	S	S				(19)	Koronis		
825 Tanina	SR		S		0.35	11	Flora		
863 Benkoela	A	A	A		0.60	27			yes
913 Otila		Sa				(11)	Flora		
915 Cosette		S				(12)	Flora		
918 Itha		S			0.22	20			
950 Ahrensa			Sa		0.18	15			
1036 Ganymed	S		S	S(VI-VII)	0.29	32		Amor	yes
1126 Otero			A		0.18	12			
1273 Anchises		V				(6)			
1289 Kutaïssi	S	S			0.14	26	Koronis		
1324 Knysna			Sq			(8)	Flora		
1350 Rosselia			Sa		0.16	23	Koronis		
1483 Hakoila			Sq			(14)			
1518 Rovaniemi		S				(9)	Flora		
1584 Fuji S	S				0.20	22			
1587 Kahrstedt			Sa			(16)			
1600 Vyssotsky			A			(11)			
1626 Sadeya		S				(21)			
1627 Ivar	S		S		0.12	7		Amor	yes
1658 Innes	AS	S				(13)	Rafita		
1685 Toro			S		0.31Ø	1¡		Apollo	
1807 Slovakia			S			(10)	Flora		
1862 Apollo	Q		Q		0.21§	1*f*		Apollo	
1863 Antinous	SU					(2)		Apollo	
1864 Daedalus	SQ		Sr			(3)		Apollo	
1866 Sisyphus			S		0.18¢	8¢		Apollo	
1892 Lucienne		S				(10)			
1904 Massevitch			R		0.16	18			
1906 Naef		V				(6)	Vesta		
1929 Kollaa		V	V			(8)	Vesta		
1933 Tinchen			V			(5)	Vesta		
1980 Tezcatlipoca			Sl		0.21	4		Amor	
1981 Midas			(V) ∞			(2)		Apollo	
2014 Vasilevskis		S				(12)			
2038 Bistro			Sa		0.13	13			
2045 Peking			V			(8)	Vesta		
2078 Nanking		S?	Sq*			(10)			
2100 Ra-Shalom		C	Xc		0.13@	2@		Aten	
2159 Kukkamäki		S				(10)			
2396 Kochi			Sa			(13)			
2442 Corbett		J				(6)			

Asteroid	Tholen	SMASS I	SMASS II	S Subclass	Albedo	Diameter (km)	HCM Family	NEA	52-color
2579 Spartacus			V			(5)			
2590 Mourão		V				(6)	Vesta		
2653 Principia			V			(8)			
2715 Mielikki			A		0.18	13			
2732 Witt			A			(10)	Lydia		
2763 Jeans			V			(8)			
2851 Harbin			V			(7)			
2873 Binzel			Sq*			(7)	Flora		
3103 Eger			Xe		0.34-0.53#	1.5-1.9#		Apollo	
3122 Florence			S			(4)		Amor	
3167 Babcock		S			0.32	12	Maria		
3199 Nefertiti			Sq		0.26-0.41¿	2¿		Amor	
3268 De Sanctis		V				(4)	Vesta		
3352 McAuliffe			A			(2)		Amor	
3376 Armandhammer			Sq			(9)	Vesta		
3474 Linsley			Sa			(7)			
3545 Gaffey			Sa			(10)	Koronis		
3628 Boznemcová		O	O			(8)			
3657 Ermolva		J				(6)	Vesta		
3753 Cruithne			Q			(3)		Aten	
3767 DiMaggio			Sa			(13)	Eunomia		
3819 Robinson			Sr			(9)			
3849 Incidentia			V			(6)			
3903 Kliment Ohridski			Sq			(11)	Koronis		
3908 Nyx		V			0.23$	1$		Amor	
3944 Halliday		V				(5)	Vesta		
3968 Koptelov		V				(5)	Vesta		
4005 Dyagilev		J				(6)	Vesta		
4051 Hatanaka			Sq			(9)	Liberatrix		
4062 Schiaparelli		S				(5)	Flora		
4142 Dersu-Uzala			A			(5)			
4145 Maximova		S				(5)	Flora		
4147 Lennon		V				(5)	Vesta		
4188 Shulnazaria			V			(6)			
4215 Kamo		J	V			(7)	Vesta		
4503 Cleobulus						(2)		Amor	
4512 Sinuhe			Sa			(11)			
4606 Saheki		S				(8)			
4713 Steel			A			(7)			
4900 Maymelou			V			(5)	Vesta		
4954 Eric			S			(8)		Amor	
5131 1990 BG			S			(4)		Apollo	
5693 1993 EA								Apollo	
5836 1993 MF			S			(4)		Amor	
5840 1978 ON			Ld			(10)	Henan		
6047 1991 TB_1						(1)		Apollo	
6489 Golevka			Q		0.61∂	0.3∂		Amor	
7358 1995 YA_1			Sq			(5)		Amor	
7889 1994 LX			(V)∞			(2)		Apollo	
10115 1992 SK						(1)		Apollo	
11398 1998 YP_{11}								Amor	
11405 1999 CV_3								Apollo	
1991 VH			Sk			(1)		Apollo	
1992 BF			Xc			(0.3)		Aten	
1997 BQ			S			(0.7)		Apollo	
1997 BR			S			(0.9)		Apollo	
1997 CZ_5		S				(5)		(Mars-crosser)	
1997 RT			O			(0.3)		Amor	
1998 FM_5			S			(0.2)		Amor	
1998 FX_2			Sq			(0.6)		Amor	

Asteroid	Tholen	SMASS I	SMASS II	S Subclass	Albedo	Diameter (km)	HCM Family	NEA	52-color
1998 HT_{31}								Apollo	
1998 KU_2			Cb			(1)		Amor	
1998 MW_5								Apollo	
1998 PB_1								Amor	
1998 PG			Sq			(1)		Amor	
1998 QR_{15}			Sq			(0.7)		Amor	
1998 XB								Aten	
1999 AQ_{10}								Aten	
1999 CF_9								Apollo	
1999 DJ_4								Apollo	
1999 GK_4								Apollo	
1999 HF_1								Aten	
1999 JD_6								Aten	
1999 JV_3								Apollo	
1999 KU_4								(Mars-crosser)	
1999 KW_4								Aten	

* Classification has changed from Bus (1999).
† The diameter for 4 Vesta is from Hubble Space Telescope observations (Thomas *et al.*, 1997a).
‡ The diameter for 19 Fortuna is from Hubble Space Telescope observations (Storrs *et al.*, 1999).
& The albedo and diameter for 64 Angelina are from Morrison (1977).
! The albedo and diameter for 253 Mathilde are from the NEAR spacecraft encounter (Veverka *et al.*, 1999).
Ø The albedo for 1685 Toro is from Veeder *et al.* (1989).
¡ The diameter for 1685 Toro is from Ostro *et al.* (1983).
§ The albedo for 1862 Apollo is from Lebofsky *et al.* (1981b).
ƒ The diameter for 1862 Apollo is from Goldstein (1981).
@ The albedo and diameter for 2100 Ra-Shalom are from Harris *et al.* (1998).
# The albedo and diameter ranges for 3103 Eger are from Benner *et al.* (1997).
¢ The albedo and diameter for 1866 Sisyphus are from Veeder *et al.* (1989).
¿ The albedo and diameter for 3199 Nefertiti are from Veeder *et al.* (1989).
$ The albedo and diameter for 3908 Nyx are from Cruikshank *et al.* (1991).
∂ The diameter and albedo for 6489 Golevka are from Mottola *et al.* (1997).
∞ Asteroids 1981 Midas and 7889 1994 LX are classified as V types from their SMASSIR spectra.

Appendix E
Meteorite and Mineral Spectra

Listing of the mineral and meteorite spectra plotted in this thesis. Included are the name of the sample, particle size, temperature, RELAB ID number (if available) and figure that spectrum was used. Powders prepared by Gaffey (1976) tended to have grain sizes between 30 and 300 μm. Bulk powders were crushed, but no grain sizes were measured of the resulting particles. For the RELAB ID numbers, the middle three letters are the initials of the principal investigator who obtained each spectrum, which includes Rick Binzel (RPB), Ed Cloutis (EAC), Mike Gaffey (MJG), Taki Hiroi (TXH), Lucy-Ann McFadden (LAM), Carlé Pieters (CMP) and John Wasson (JTW).

Sample	Type	Particle Size	RELAB ID	Reference	Figure
Abee	EH4	powder	MR-MJG-020	Gaffey (1976)	5.8.1
ALHA76005	eucrite	< 250 μm	TB-RPB-024		4.8, 4.20
ALHA76005	eucrite	bulk powder	TB-RPB-023		4.7, 4.8
ALHA81011	eucrite	bulk powder	TB-RPB-013		4.7
ALH 85001	eucrite	bulk powder	TB-RPB-015		4.7
Allende	CV	bulk powder	MR-MJG-117	Gaffey (1976)	5.3.1
Augite	pyroxene	74-250 μm		Clark *et al.* (1993)	5.5.5
Aumale	L6	powder	MR-MJG-053	Gaffey (1976)	5.5.1, 5.6.1
Babb's Mill	ataxite	slab	MR-MJG-083	Gaffey (1976)	5.8.1, 5.8.8
Bald Mountain	L4	powder	MR-MJG-044	Gaffey (1976)	5.7.11
Beligica 7904	CM (unusual)	< 63 μm	MB-CMP-018	Hiroi *et al.* (1993c)	5.2.6
Bereba	eucrite	powder	MR-MJG-085	Gaffey (1976)	4.5
Bouvante	eucrite	< 25 μm	MP-TXH-090-A		4.9, 4.16, 4.18, 4.19
Bouvante	eucrite	< 250 μm	TB-RPB-028		4.9
Bouvante	eucrite	bulk powder	TB-RPB-029		4.9
Brachina	brachinite	< 45 μm	MT-TXH-049		5.1.2, 5.1.5, 5.7.15, 5.7.19
Brenham olivine	pallasite	< 30 μm		King and Ridley (1987)	5.1.2, 5.4.5, 5.7.15, 5.7.19
Butler	octahedrite	slab	MR-MJG-081		5.1.11, 5.7.16
Castalia	H5	powder	MR-MJG-029	Gaffey (1976)	5.7.5
Chassigny	chassignite	powder	MR-MJG-104	Gaffey (1976)	1.2
Chulafinee	octahedrite	slab	MR-MJG-082	Gaffey (1976)	1.2, 5.8.1
EETA79005	eucrite	< 250 μm	TB-RPB-026		4.8
EETA79005	eucrite	bulk powder	TB-RPB-025		4.7, 4.8
EET 83251	eucrite	< 63 μm (120 K)			4.13
EET 83251	eucrite	< 63 μm (300 K)			4.13
EET 83251	eucrite	bulk powder	TB-RPB-022		4.7
EET 87503	howardite	< 25 μm	MB-TXH-068	Hiroi *et al.* (1994)	4.1
EET 87503	howardite	< 63 μm (120 K)			4.14, 4.15
EET 87503	howardite	< 63 μm (300 K)			2.2, 4.14
EET 87503	howardite	106-150 μm (120 K)			4.14
EET 87503	howardite	106-150 μm (300 K)			2.2, 4.14
EET 87542	eucrite	bulk powder	TB-RPB-014		4.7, 4.12, 4.16, 4.18, 4.19
EET 90020	eucrite	bulk powder	TB-RPB-020		4.12
Fa_9	olivine	< 75 μm		Yamada *et al.* (1999)	5.1.6
Fa_9	olivine (altered) (15 mJ)	< 75 μm		Yamada *et al.* (1999)	5.1.6
Fa_9	olivine (altered) (30 mJ)	< 75 μm		Yamada *et al.* (1999)	5.1.6, 5.4.5
Fa_{10}	olivine	< 75 μm	MS-CMP-042-A	Moroz *et al.* (1996)	5.1.13
Fa_{10}	olivine (partially altered)	< 75 μm	MS-CMP-042-B	Moroz *et al.* (1996)	5.1.13
Fa_{10}	olivine (altered)	< 75 μm	MS-CMP-042-C	Moroz *et al.* (1996)	5.1.13
Fa_{12}	olivine	< 63 μm (120 K)		Hinrichs *et al.* (1999)	2.1
Fa_{12}	olivine	< 63 μm (300 K)		Hinrichs *et al.* (1999)	2.1
Frankfort	howardite	powder	MR-MJG-095	Gaffey (1976)	4.5
Gorlovka	H3-H4 (shock-darkened)		RS-CMP-O48-P1	Britt and Pieters (1989)	5.2.8
Happy Canyon	E chondrite (impact melt)	45-90 μm	SC-EAC-001	Cloutis *et al.* (1993a)	5.8.5
Haraiya	eucrite	powder	MR-MJG-089	Gaffey (1976)	4.5, 5.7.12
Hedenbergite	pyroxene	powder		Clark *et al.* (1993)	5.4.4
Hematite	oxide	powder		Clark *et al.* (1993)	5.8.6
Homestead	L5	powder	MR-MJG-048	Gaffey (1976)	5.7.16, 5.7.17
Hvittis	EL6	powder	MR-MJG-024	Gaffey (1976)	5.8.1, 5.8.8
Imilac olivine	pallasite	chip	MB-TXH-041	Hiroi *et al.* (1993b)	5.1.2
Jelica	LL6	powder	MR-MJG-072	Gaffey (1976)	5.5.8

Sample	Type	Particle Size	RELAB ID	Reference	Figure
Johnstown	diogenite	< 75 μm	MS-JTW-049-A	Wasson *et al.* (1997)	4.10
Johnstown	diogenite (partially altered)	< 75 μm	MS-JTW-049-B	Wasson *et al.* (1997)	4.10
Johnstown	diogenite (altered)	< 75 μm	MS-JTW-049-C	Wasson *et al.* (1997)	4.10
Johnstown	diogenite	powder	MR-MJG-098-P	Gaffey (1976)	1.2, 4.5, 4.18
Jonzac	eucrite	powder	MR-MJG-088	Gaffey (1976)	4.5
Juvinas	eucrite	powder	MR-MJG-091	Gaffey (1976)	4.4
Kainsaz	CO	powder	MR-MJG-113	Gaffey (1976)	5.3.1
Kakangari	K	powder	MR-MJG-011	Gaffey (1976)	5.4.7
Lancon	H6	powder	MR-MJG-033	Gaffey (1976)	5.5.1
LAP 91900	diogenite	bulk powder	TB-RPB-018		4.18, 5.7.1
Leoville	CV	powder	MR-MJG-120	Gaffey (1976)	5.4.7
Le Teilleul	howardite	powder	MR-MJG-096	Gaffey (1976)	4.5, 4.21
LEW 87004	eucrite	bulk powder	TB-RPB-019		4.7
LEW 90500	CM	< 100 μm	MB-TXH-054	Hiroi *et al.* (1993c)	5.2.10, 5.2.11, 5.2.12, 5.2.13
LEW 90500	CM	bulk powder	MC-RPB-002	Burbine (1998)	5.2.3, 5.2.12, 5.2.13
MAC 88177	lodranite	chip	MB-CMP-026	Hiroi *et al.* (1993a)	4.20
Macibini Clast 3	eucrite	< 63 μm	TB-RPB-027		4.11
Manbhoom	LL6	< 63 μm (120 K)			5.5.4
Manbhoom	LL6	< 63 μm (300 K)			5.5.4
Manbhoom	LL6	powder	MR-MJG-073	Gaffey (1976)	5.5.1, 5.5.2, 5.5.3
Melilite		< 45 μm	SC-EAC-067	Cloutis and Gaffey (1993b)	5.8.6
META78008	ureilite	chip	MP-LAM-006-C1		5.5.5
Mokoia	CV	powder	MR-MJG-121	Gaffey (1976)	5.3.2
Murchison	CM	powder	MR-MJG-109	Gaffey (1976)	1.2, 5.2.1, 5.2.10, 5.2.11
Murchison	CM (heated 900 °C)	< 63 μm	MB-TXH-064-F	Hiroi *et al.* (1993c)	5.2.8
Nobleborough	eucrite	powder	MR-MJG-093	Gaffey (1976)	4.5
Novo Urei	ureilite	powder		Gaffey (1976)	5.1.10, 5.7.14
Odessa	octahedrite	45-90 μm	SC-EAC-006	Cloutis *et al.* (1990a)	5.1.3, 5.1.10
Olivenza	LL5	powder	MR-MJG-071	Gaffey (1976)	5.5.7
Olivine		45-90 μm	SC-EAC-002	Cloutis *et al.* (1990a)	5.1.3
Olivine 25 wt.%, Odessa 75%		45-90 μm	SC-EAC-005	Cloutis *et al.* (1990a)	5.1.3
Olivine 50 wt.%, Odessa 50%		45-90 μm	SC-EAC-004	Cloutis *et al.* (1990a)	5.1.3, 5.1.11, 5.4.5
Olivine 50 wt.%, Magnetite 50%		45-90 μm	SC-EAC-027	Cloutis *et al.* (1990b)	5.1.12
Olivine 75 wt.%, Odessa 25%		45-90 μm	SC-EAC-003	Cloutis *et al.* (1990a)	5.1.3, 5.1.11
Olivine 99.5 wt.% (< 45 μm), 0.5% Carbon (< 0.023 μm)			SC-EAC-018	Cloutis *et al.* (1990b)	5.1.12
Olivine 99.5 wt.% (45-90 μm), 0.5% Carbon (< 0.023 μm)			SC-EAC-022	Cloutis *et al.* (1990b)	5.1.12
Orgueil	CI	powder	MR-MJG-105	Gaffey (1976)	5.2.1
Padvarninkai	eucrite	< 25 μm	MB-TXH-096-A		4.11
Padvarninkai	eucrite	powder	MR-MJG-086	Gaffey (1976)	4.5, 4.11
Pantar	H5	powder	MR-MJG-032	Gaffey (1976)	5.7.1, 5.7.11, 5.7.16
Pasamonte	eucrite	powder	MR-MJG-090	Gaffey (1976)	1.5, 4.5, 5.6.1
Pavlovka	howardite	powder	MR-MJG-094	Gaffey (1976)	4.1, 4.5
PCA 82501	eucrite	bulk powder	TB-RPB-012		4.7
PCA 82502	eucrite	bulk powder	TB-RPB-021		4.7
PCA 91007	eucrite	bulk powder	TB-RPB-016		4.7
Petersburg	howardite	powder	MR-MJG-097	Gaffey (1976)	4.5
Pyrrhotite	sulfide	74-250 μm		Clark *et al.* (1993)	5.8.5
Renazzo	CR	< 100 μm	MB-TXH-058	Hiroi *et al.* (1993c)	5.2.1, 5.2.3
Roda	diogenite	powder	MR-MJG-099	Gaffey (1976)	4.5, 4.21
Saratov	L4	powder	MR-MJG-046	Gaffey (1976)	5.1.10, 5.7.7, 5.7.8, 5.7.11
Saratov	L4	bulk powder	TB-RPB-017		5.7.7
Sevrukovo	L5 (shock-darkened)	powder	MR-MJG-078	Gaffey (1976)	5.8.3
Shalka	diogenite	powder	MR-MJG-101	Gaffey (1976)	4.1, 4.5

Sample	Type	Particle Size	RELAB ID	Reference	Figure
Shelburne	L5	powder	MR-MJG-050	Gaffey (1976)	1.5
Sioux County	eucrite	powder	MR-MJG-087	Gaffey (1976)	4.1, 4.5, 4.6
Soko Banja	LL4	powder	MR-MJG-070	Gaffey (1976)	5.5.2, 5.5.7, 5.7.3, 5.7.6, 5.7.9, 5.7.15, 5.7.18, 5.7.21, 5.7.22
Stannern	eucrite	powder	MR-MJG-092-P	Gaffey (1976)	4.5
Tatahouine	diogenite	powder	MR-MJG-100-P	Gaffey (1976)	4.5
Tieschitz	H3	powder	MR-MJG-039	Gaffey (1976)	5.7.11, 5.7.14, 5.8.3
Troilite (synthetic)	sulfide	< 45 μm	EA-EAC-002	Cloutis *et al.* (1993a)	5.8.5
Vavilovka	LL6	powder	MR-MJG-074	Gaffey (1976)	5.5.3, 5.5.6
Veramin	mesosiderite	slab	MR-MJG-084	Gaffey (1976)	5.1.14
Warrenton	CO	< 75 μm	MR-MJG-116-P1	Gaffey (1976)	5.3.1, 5.3.2
Warrenton	CO	75-150 μm	MR-MJG-116-P2	Gaffey (1976)	5.3.2
Y-74357	lodranite	chip	MB-TXH-037	Hiroi *et al.* (1993a)	5.1.10
Y-74442	LL4	< 25 μm	MB-TXH-086		5.7.6
Y-75011	eucrite	bulk powder	TB-RPB-008		4.7
Y-791186	eucrite	bulk powder	TB-RPB-009		4.7
Y-792510	eucrite	bulk powder	TB-RPB-007		4.7
Y-82162	CI (unusual)	< 63 μm	MB-CMP-019	Hiroi *et al.* (1993c)	5.2.2, 5.2.6, 5.2.8
Y-86720	CM (unusual)	< 63 μm	MB-CMP-020	Hiroi *et al.* (1993c)	5.2.3, 5.2.5
Zavid	L6	powder	MR-MJG-065	Gaffey (1976)	5.5.2, 5.5.3